

Applications of the novel bio-  
derived solvent Cyrene™ in polymer  
chemistry

Roxana-Alina Milescu

*PhD*

University of York

Chemistry

May 2021



This thesis is dedicated to my father, Gheorghe Milescu, whom I lost to cancer.



# Abstract

Polar aprotic solvents such as *N*-methyl-2-pyrrolidone, *N,N'*-dimethylformamide and *N,N'*-dimethylacetamide are under regulatory pressure worldwide due to their toxicity. Cyrene™, a bio-based solvent first developed by the University of York in collaboration with Circa Group made from cellulosic biomass, represents a promising alternative to polar aprotic solvents with chronic toxicity or other health-related concerns.

This thesis explores the use of Cyrene as polar aprotic solvents replacement in polymer dissolution for graffiti removal, extractions of flavonoids, dispersion of carbon nanotubes, polymerisation and/or production of poly(amide-imide) wire enamels and production of filtration membranes. Cyrene proved a good cleaning agent for acrylic and cellulose-based graffiti aerosols, giving comparable results to *N*-methyl-2-pyrrolidone, without the latter's chronic toxicity and chemical contamination concerns. Poly(amide-imide) enamels synthesised with Cyrene were chemical resistant, showed superior adhesion strength and were flexible. Cyrene showed up to ten times better extraction capacity of flavonoids (hesperidin and rutin) when mixed with water than using established ethanol-water mixtures and an increase to 91% when heated up to 65 °C. Cyrene demonstrated an efficient liquid media to disperse carbon nanotubes and reached concentrations up to 0.27 mg mL<sup>-1</sup>, which were stable for up to six months. Cyrene produced membranes tailored for applications from reverse osmosis (<0.001 µm pore size) to microfiltration (0.1-10 µm) by changing polymers employed and the viscosity of the casting solution. Cyrene-based membranes showed higher porosity than usual and formed pores without the use of additives. Hansen Solubility Parameters were employed in this work to predict polymer dissolutions and discover new viable blends of Cyrene with other green solvents for these applications.

This study has demonstrated the applicability of Cyrene across a broad range of applications involving polymer synthesis and fabrication of advanced materials, especially those which do not require rapid evaporation of the solvent or where higher viscosity is essential.



# List of contents

|   |           |
|---|-----------|
| <b>Abstract</b> .....   | <b>5</b>  |
| <b>List of contents</b> .....   | <b>7</b>  |
| <b>List of tables</b> .....   | <b>15</b> |
| <b>List of figures</b> .....  | <b>19</b> |
| <b>Acknowledgements</b> .....   | <b>29</b> |
| <b>Declaration</b> .....  | <b>31</b> |
| <b>1. Introduction</b> .....  | <b>33</b> |
| 1.1. Scope of this study .....  | 35        |
| 1.2. Green Chemistry .....  | 36        |
| 1.2.1. The 12 principles of Green Chemistry.....                      | 36        |
| 1.2.2. Modern chemical legislation.....                               | 38        |
| 1.2.3. Circular economy .....   | 39        |
| 1.2.4. Sustainability .....   | 40        |
| 1.2.5. Sustainability applied to solvents .....                       | 42        |
| 1.2.6. Solvent selection guides.....                                  | 44        |
| 1.2.7. Green metrics.....   | 45        |
| 1.3. Solvents.....  | 47        |
| 1.3.1. Definition, classification and uses of solvents .....          | 47        |
| 1.3.2. Effect of solvent on solubility.....                           | 49        |
| 1.3.3. Polar aprotic solvents solubilisation mechanism.....           | 50        |
| 1.3.4. Polymer dissolution in solvents .....                          | 50        |
| 1.4. Conventional vs. green and bio-based polar aprotic solvents..... | 53        |
| 1.4.1. Traditional polar aprotic solvents .....                       | 53        |
| 1.4.2. Green and bio-based polar aprotic solvents.....                | 57        |
| 1.5. Introduction to Cyrene.....                                      | 61        |
| 1.5.1. Synthesis of Cyrene using Furacell™ process.....               | 61        |
| 1.5.2. Characterisation of Cyrene .....                               | 64        |

|  |           |
|--|-----------|
| 1.5.2.1. Physical and chemical properties - Background .....   | 64        |
| 1.5.2.2. Viscosity .....   | 67        |
| 1.5.3. Hansen Solubility Parameters and predicted environmental impact of Cyrene .....                         | 68        |
| 1.5.3.1. Calculations of Hansen parameters of Cyrene using the Yamamoto-Molecular Breaking (Y-MB) method ..... | 68        |
| 1.5.3.2. Calculations of Hansen parameters of Cyrene using group-contribution method                           | 72        |
| 1.5.3.3. Prediction of Health, Safety and Environmental (HSE) impact of Cyrene .....                           | 74        |
| 1.5.4. Property prediction for Cyrene using COSMOtherm.....  | 75        |
| 1.5.5. Applications of Cyrene.....   | 78        |
| 1.5.6. Toxicity profile of Cyrene.....   | 80        |
| 1.5.7. Cradle-to-gate life cycle assessment (LCA) of Cyrene production .....                                   | 81        |
| <b>2. Application of Cyrene in graffiti paint removal .....</b>  | <b>85</b> |
| 2.1. Introduction.....   | 87        |
| 2.2. Graffiti removal technologies - Background.....   | 88        |
| 2.2.1. Laser technology.....   | 89        |
| 2.2.2. Mechanical techniques.....  | 90        |
| 2.2.3. Biological methods .....  | 91        |
| 2.2.4. Chemical treatment.....   | 91        |
| 2.3. Anti-graffiti coatings .....  | 92        |
| 2.4. Environmental implications and health issues generated by graffiti removal.....                           | 93        |
| 2.5. Graffiti paints and substrates .....  | 96        |
| 2.5.1. Acrylic and cellulose nitrate aerosol paints.....   | 96        |
| 2.5.2. Porous and non-porous substrates .....  | 99        |
| 2.6. HSPiP's predictive role in graffiti removal .....   | 101       |
| 2.7. Graffiti paints characterisation by infrared spectroscopy.....  | 103       |
| 2.8. Effectiveness of the cleaning tests .....   | 104       |
| 2.8.1. Chemical cleaning performance using the immersion tests .....   | 104       |
| 2.8.2. Chemical cleaning performance using poultices .....   | 107       |
| 2.8.3. Mechanism of graffiti removal from porous and non-porous substrates.....                                | 108       |



|  |            |
|--|------------|
| 2.8.4. Physico-chemical changes to the paint during the chemical removal of graffiti paint | 112        |
| 2.9. Chapter conclusion  | 115        |
| <b>3. Application of Cyrene in poly(amide-imide) (PAI) wire enamels</b>                    | <b>117</b> |
| 3.1. Introduction  | 119        |
| 3.2. Wire enamels - Background   | 121        |
| 3.3. Poly(amide-imide) synthesis pathways  | 122        |
| 3.3.1. Acid chloride route   | 122        |
| 3.3.2. Diisocyanate route  | 124        |
| 3.4. HSPiP's predictions of poly(amide-imide) solubility                                   | 125        |
| 3.5. Synthesis of PAI wire enamel using and mixtures containing Cyrene                     | 128        |
| 3.6. Dynamic viscosity of the PAI fluids   | 129        |
| 3.7. Thermal curing of poly(amide-imide) films   | 130        |
| 3.8. PAIs characterisation   | 132        |
| 3.8.1. Infrared spectroscopy   | 132        |
| 3.8.2. <sup>1</sup> H-NMR spectra of PAIs  | 133        |
| 3.8.3. Thermal properties of PAIs  | 134        |
| 3.9. Poly(amide-imide) cured films testing   | 135        |
| 3.9.1. Solvent resistance test   | 135        |
| 3.9.2. Hardness test   | 137        |
| 3.9.3. Flexibility test  | 139        |
| 3.9.4. Adhesion strength   | 139        |
| 3.10. Chapter conclusion   | 140        |
| <b>4. Extraction of bio-active compounds</b>   | <b>143</b> |
| 4.1. Introduction  | 145        |
| 4.2. Green extraction  | 146        |
| 4.3. Extraction of hesperidin and rutin - Background                                       | 148        |
| 4.4. HSPiP's predictions in flavonoids extraction  | 150        |
| 4.5. Solvent extraction of hesperidin and rutin  | 155        |

|   |            |
|---|------------|
| 4.5.1. Efficiency of a single-stage solid-liquid extraction .....                         | 155        |
| 4.5.2. Factors influencing the extraction.....  | 158        |
| 4.5.2.1. Water influence .....  | 158        |
| 4.5.2.2. Temperature influence .....  | 160        |
| 4.6. Green metrics .....  | 161        |
| 4.7. Chapter conclusion .....   | 163        |
| <b>5. Cyrene in single-walled carbon nanotubes (SWCNTs) dispersion .....</b>              | <b>165</b> |
| 5.1. Introduction.....  | 167        |
| 5.2. Methods of carbon nanotubes dispersion - Background .....                            | 169        |
| 5.2.1. Covalent methods of dispersion.....  | 169        |
| 5.2.2. Non-covalent methods .....   | 170        |
| 5.2.3. The additives used in non-covalent dispersion of carbon nanotubes.....             | 171        |
| 5.2.3.1. Surfactants.....   | 171        |
| 5.2.3.2. Polymers .....   | 173        |
| 5.3. HSPiP's predictions in carbon nanotubes dispersion .....                             | 174        |
| 5.4. Dispersion of SWCNTs using the ultrasonication technology .....                      | 175        |
| 5.4.1. Dispersion of pristine SWCNTs in neat solvents.....                                | 175        |
| 5.4.2. SWCNTs dispersion in Cyrene with the aid of Triton™ X-100.....                     | 177        |
| 5.4.3. SWCNTs dispersion in solvents with the aid of polyvinyl pyrrolidone (PVP).....     | 178        |
| 5.4.4. Overall results and mechanisms proposed .....                                      | 180        |
| 5.5. Characterisation of SWCNT dispersions by Transmission Electron Microscopy (TEM)..... | 182        |
| 5.5.1. SWCNTs dispersed in neat solvents.....   | 182        |
| 5.5.2. SWCNTs dispersed using Triton™ X-100.....  | 186        |
| 5.5.3. SWCNTs dispersed with the aid of PVP .....   | 190        |
| 5.6. Stability of SWCNTs solutions.....   | 193        |
| 5.6.1. SWCNTs dispersed in neat solvents.....   | 193        |
| 5.6.2. SWCNTs dispersed with the aid of Triton™ X-100.....                                | 195        |
| 5.6.3. SWCNTs dispersed with the aid of PVP .....   | 198        |
| 5.7. Chapter conclusion .....   | 202        |

|   |            |
|---|------------|
| <b>6. Cyrene in membrane technology .....</b>                                   | <b>205</b> |
| 6.1. Introduction .....   | 207        |
| 6.2. Filtration membranes - Background .....                                    | 207        |
| 6.2.1. Types of membranes.....  | 208        |
| 6.2.1.1. Membranes classified based on their morphology .....                   | 208        |
| 6.2.1.2. Types of filtrations based on pore size .....                          | 210        |
| 6.2.1.3. Other types of membranes .....   | 211        |
| 6.2.2. Properties of filtration membranes .....                                 | 211        |
| 6.2.2.1. High permeability and selectivity.....                                 | 211        |
| 6.2.2.2. Resistant to fouling .....   | 212        |
| 6.2.2.3. Mechanical strength .....  | 214        |
| 6.2.2.4. High temperature resistance .....                                      | 214        |
| 6.2.2.5 Manufacturing reproducibility, low price .....                          | 214        |
| 6.2.2.6. Sustainability .....   | 215        |
| 6.2.3. Membrane preparation by Non-Solvent Induced Phase Separation (NIPS)..... | 215        |
| 6.2.4. Demixing processes during NIPS.....                                      | 216        |
| 6.2.4.1. Liquid-liquid demixing.....  | 216        |
| 6.2.4.2. Solid-liquid demixing.....   | 218        |
| 6.3. Materials used in membrane technology .....                                | 218        |
| 6.3.1. Polyethersulfone (PES).....  | 219        |
| 6.3.2. Polyvinylidene difluoride (PVDF) .....                                   | 219        |
| 6.3.3. Polysulfone (PSf) .....  | 220        |
| 6.3.4. Cellulose acetate (CA) .....   | 220        |
| 6.3.5. Polyimide (PI) .....   | 221        |
| 6.4. Solvents and mixtures of solvents used to produce membranes.....           | 221        |
| 6.4.1. Cyrene and NMP .....   | 221        |
| 6.4.2. Cygnet 0.0-Cyrene mixture (Cg:Cy) .....                                  | 222        |
| 6.4.3. Cygnet 0.0 .....   | 222        |
| 6.4.4. <i>N,N'</i> -Dimethyl- <i>N,N'</i> -dibutylsuccinamide (MBSA).....       | 223        |

|   |     |
|---|-----|
| 6.4.5. $\gamma$ -Valerolactone (GVL).....   | 223 |
| 6.4.6. Cyclopentanone (CP) .....  | 223 |
| 6.5. Additives used in membranes preparation .....  | 223 |
| 6.5.1. Polyvinyl pyrrolidone (PVP) .....  | 223 |
| 6.5.2. Single-walled carbon nanotubes (SWCNTs) .....  | 224 |
| 6.5.3. Natural polysaccharides .....  | 225 |
| 6.5.4. Polysaccharides-based Starbon™ materials .....   | 226 |
| 6.6. Polyethersulfone (PES) membranes .....   | 227 |
| 6.6.1. HSPiP's predictive role in polymer dissolution .....   | 227 |
| 6.6.2. Polyethersulfone (PES) membranes preparation .....   | 229 |
| 6.6.2.1. PES membranes using Cyrene (PES/C) and NMP (PES/N) as solvents.....  | 229 |
| 6.6.2.2. PES membranes using Cyrene (PES/C), 50 wt% Cygnet 0.0-Cyrene blend (PES/Cg-Cy) and pure Cygnet 0.0 (PES/Cg)..... | 230 |
| 6.6.2.3. PES membranes prepared with <i>N,N'</i> -dimethyl- <i>N,N'</i> -dibutylsuccinamide (PES/MBSA).....               | 231 |
| 6.6.2.4. PES membranes prepared with Cyrene or NMP and carbon nanotubes .....   | 232 |
| 6.6.2.5. PES membranes prepared with Cyrene and Starbon™ materials as a bio-based additive .....                          | 233 |
| 6.6.3. Viscosity of PES/C and PES/N casting solutions.....  | 233 |
| 6.6.4. Scanning Electron Microscopy (SEM) analyses of PES membranes .....   | 235 |
| 6.6.4.1. SEM analyses of PES/C and PES/N membranes.....   | 235 |
| 6.6.4.2. SEM analyses of PES/Cyrene, PES/Cg:Cy and PES/Cygnet membranes .....   | 240 |
| 6.6.4.3. SEM analysis of PES/MBSA membranes.....  | 241 |
| 6.6.4.4. SEM of membranes using single-walled carbon nanotubes (SWCNTs) .....   | 243 |
| 6.6.4.5. SEM images of PES/C/S300 membranes .....   | 246 |
| 6.6.4.6. Influence of membranes thickness on morphology .....   | 248 |
| 6.6.5. Porosity of PES membranes.....   | 249 |
| 6.6.5.1. Mercury Intrusion Porosimetry (MICP) analysis of PES/C and PES/N membranes .....                                 | 249 |
| 6.6.5.2. Gravimetric determination of the porosity of PES/C and PES/N membranes ....                                      | 251 |

|   |            |
|---|------------|
| 6.6.6. PES membranes characterisation by infrared spectroscopy .....                          | 252        |
| 6.6.7. Thermal stability of PES membranes .....   | 253        |
| 6.6.7.1. Thermal stability of PES/C and PES/N membranes.....                                  | 253        |
| 6.6.7.2. Thermal stability of PES/C, PES/Cg:Cy and PES/Cg membranes .....                     | 254        |
| 6.6.8. Surface wetting property of PES membranes.....   | 255        |
| 6.6.9. Pure water permeability of PES/C and PES/N.....  | 256        |
| 6.7. Polyvinylidene difluoride (PVDF) filtration membranes .....                              | 257        |
| 6.7.1. HSPiP's predictive role in polymer dissolution .....                                   | 257        |
| 6.7.2. Preparation of PVDF membranes .....  | 259        |
| 6.7.3. SEM images of PVDF membranes .....   | 261        |
| 6.8. Polysulfone (PSf), cellulose acetate (CA), and polyimide (PI) filtration membranes ..... | 264        |
| 6.8.1. Preparation of PSf, CA and PI membranes.....   | 264        |
| 6.8.2. SEM analyses of the produced membranes .....   | 265        |
| 6.8.3. Thermal stability of the produced membranes .....                                      | 268        |
| 6.9. Chapter conclusion .....   | 270        |
| <b>7. Conclusion and further work .....</b>   | <b>273</b> |
| 7.1. Conclusion.....  | 275        |
| 7.2. Further work .....   | 276        |
| <b>8. Experimental section.....</b>   | <b>279</b> |
| 8.1. Chemicals .....  | 281        |
| 8.1.1. Chemicals - Chapter 2 .....  | 281        |
| 8.1.2. Chemicals - Chapter 3 .....  | 281        |
| 8.1.3. Chemicals - Chapter 4 .....  | 282        |
| 8.1.4. Chemicals – Chapter 5.....   | 282        |
| 8.1.5. Chemicals - Chapter 6 .....  | 282        |
| 8.2. Experimental – Chapter 1 .....   | 283        |
| 8.3. Experimental – Chapter 2 .....   | 283        |
| 8.4. Experimental – Chapter 3 .....   | 287        |
| 8.5. Experimental – Chapter 4 .....   | 289        |

|   |            |
|---|------------|
| 8.6. Experimental – Chapter 5 .....                           | 291        |
| 8.7. Experimental – Chapter 6 .....                           | 293        |
| 8.8. Computational methodologies .....                        | 299        |
| 8.8.1. Hansen Solubility Parameters in Practice (HSPiP) ..... | 299        |
| 8.8.2. COSMOtherm modelling .....                             | 302        |
| 8.8.3. CHEM21 green metrics toolkit .....                     | 307        |
| <b>Appendix A .....</b>                                       | <b>309</b> |
| <b>Appendix B .....</b>                                       | <b>337</b> |
| <b>Appendix C .....</b>                                       | <b>351</b> |
| <b>Abbreviations .....</b>                                    | <b>355</b> |
| <b>References .....</b>                                       | <b>359</b> |

# List of tables

|  |     |
|--|-----|
| Table 1: Twelve principles of Green Chemistry by Anastas and Warner .....  | 37  |
| Table 2: Twelve criteria of Gu and Jerome that a green solvent needs to meet.....  | 43  |
| Table 3: Types of solvents based on their polarity .....   | 48  |
| Table 4: Applications of commonly used polar aprotic solvents .....  | 53  |
| Table 5: Classification of the hazards of polar aprotic solvents used in this study .....  | 54  |
| Table 6: Classification of the hazards of green and bio-based polar aprotic solvents used in this study, including Cyrene.....   | 58  |
| Table 7: Physico-chemical properties of Cyrene in comparison with the traditional polar aprotic solvents used in this study .....  | 65  |
| Table 8: Viscosity of Cyrene samples of different purities measured at 25 °C.....  | 68  |
| Table 9: Predicted Hansen Solubility parameters (HSPs) for Cyrene compared to traditional polar aprotic solvents.....  | 71  |
| Table 10: Applications of Cyrene .....   | 78  |
| Table 11: Toxicological and ecotoxicological information .....   | 80  |
| Table 12: Inductively Coupled Plasma-Mass Spectrometer analysis of ceramic tiles .....   | 100 |
| Table 13: Hansen Solubility Parameters of different solvents and RED calculated for acrylic graffiti paint .....   | 102 |
| Table 14: Hansen Solubility Parameters of different solvents and RED calculated for cellulose-based graffiti paint.....  | 103 |
| Table 15: Vapour pressure and surface tension of the tested solvents .....   | 110 |
| Table 16: Inorganic content of the residues obtained after the acrylic paint dissolution in NMP and Cyrene .....   | 114 |
| Table 17: Hansen solubility parameters, the scores given and relative energy distance (RED) of the neat solvents used for Torlon AI10 dissolution .....                    | 126 |
| Table 18: Hansen solubility parameters, the scores given and relative energy distance (RED) of the neat solvents and solvent systems used for Torlon AI10 dissolution..... | 127 |
| Table 19: Composition of poly(amide imide) solutions .....   | 128 |
| Table 20: Thermal properties of PAI films produced with Cyrene, NMP, 51% EC-49% Cyrene, 75% EC-25% Cyrene and 51% DMSO-49% Cyrene cured at 240 °C.....                     | 134 |
| Table 21: Six principles recommended by Chemat for a green extraction.....   | 147 |
| Table 22: Distance from the position of the individual solvents to the centre of the sphere centre ( $R_s$ ) calculated for both hesperidin and rutin .....                | 154 |

|   |     |
|---|-----|
| Table 23: Concentration of Cyrene, water and geminal diol found in the mixtures Cyrene-water used in this study (30% Cyrene-70% H <sub>2</sub> O, 50% Cyrene-50% H <sub>2</sub> O and 70% Cyrene-30% H <sub>2</sub> O)..... | 155 |
| Table 24: Comparative results of the new and the older extraction methods. ....   | 161 |
| Table 25 The concentration (mg mL <sup>-1</sup> ) of single-walled carbon nanotubes in the solution after dispersion and 6-month stability.....   | 201 |
| Table 26: Hansen Solubility Parameters of different solvents and RED calculated for PES polymer .....   | 228 |
| Table 27: Hansen Solubility Parameters of different solvents and RED calculated for PES3020 dissolution .....   | 228 |
| Table 28: Composition of casting solutions (wt%) .....  | 229 |
| Table 29: Composition of casting solutions of PES/C, PES/Cg:Cy and PES/Cg (wt%) .....   | 230 |
| Table 30: Composition of casting solutions of PES/MBSA and the non-solvents used.....   | 231 |
| Table 31: Casting solution composition (wt%) of PES membranes produced with carbon nanotubes and NMP or Cyrene .....  | 232 |
| Table 32: Composition of casting solutions (wt%) .....  | 233 |
| Table 33: The density of the solvents used in PES membranes cast using MBSA as solvent and water, TMO and hexane as non-solvents.....   | 243 |
| Table 34: Thermogravimetric (TGA) analysis measurements of PES membranes produced with Cyrene (PES/C) and NMP (PES/N).....  | 253 |
| Table 35: Thermogravimetric (TGA) and differential thermogravimetric (DTG) analyses measurements of PES membranes.....  | 254 |
| Table 36: Solvents predicted by HSPiP as good solvents for PVDF dissolution and their Hansen Solubility Parameters.....   | 258 |
| Table 37: Composition of the casting solutions (%w/v) of PVDF membranes produced with different solvents.....   | 260 |
| Table 38: Casting solutions of CA, PSf and PI membranes produced using Cyrene, pure Cygnet 0.0 and 50% Cyrene-50% Cygnet (wt%) .....  | 264 |
| Table 39: TGA and DTG measurements of PSf, CA and PI membranes.....   | 269 |
| <br>  |     |
| Table A 1: Greener solvents used in this work .....   | 309 |
| Table A 2: Hansen solubility parameters, the scores given, relative energy distance (RED) and molar volume of the solvents used to test acrylic graffiti paint dissolution .....  | 310 |
| Table A 3: Hansen solubility parameters, the scores given, relative energy distance (RED) and molar volume of the solvents used for the cellulose-based paint dissolution.....  | 311 |



|   |     |
|---|-----|
| Table A 4: Hansen solubility parameters, the scores given, relative energy distance (RED) and molar volume of neat solvents and Cyrene-water mixtures used to test acrylic graffiti paint dissolution .....   | 312 |
| Table A 5: Hansen solubility parameters, the scores given, relative energy distance (RED) and molar volume of neat solvents and Cyrene-water mixtures used to test cellulose-based graffiti paint dissolution.....                                  | 313 |
| Table A 6: Hansen solubility parameters, the scores given, relative energy distance (RED) and molar volume of the neat solvents used for Torlon AI10 dissolution.....   | 314 |
| Table A 7: Hansen solubility parameters, the scores given, relative energy distance (RED) and molar volume of the neat solvents and solvent systems used for Torlon AI10 dissolution .....  | 315 |
| Table A 8: Solvents employed in the extraction of hesperidin and rutin and their classification according to Chem21 green solvent guide. <sup>38</sup> .....  | 316 |
| Table A 9: Hansen solubility parameters, the scores given, relative energy distance (RED) and molar volume of the solvents used to test hesperidin dissolution.....   | 317 |
| Table A 10: Hansen solubility parameters, the scores given, relative energy distance (RED) and molar volume of the solvents used to test the dissolution of rutin .....   | 318 |
| Table A 11: Binary mixtures and their optimized $R_a$ and composition for hesperidin and rutin .  | 319 |
| Table A 12: Tertiary mixtures with Cyrene and their optimized $R_a$ and composition .....   | 320 |
| Table A 13: Hansen solubility parameters, the scores given and relative energy distance (RED) of the pure solvents, mixtures, and Cyrene's geminal diol used to test the dissolution of hesperidin .....  | 321 |
| Table A 14: Hansen solubility parameters, the scores given and relative energy distance of the pure solvents, mixtures, and Cyrene's geminal diol used to test the dissolution of rutin.....  | 323 |
| Table A 15: Hansen solubility parameters, the scores given and relative energy distance (RED) of the pure solvents, mixtures, Cyrene's geminal diol and ternary Cyrene/geminal diol/water mixtures used to test the dissolution of hesperidin ..... | 325 |
| Table A 16: Hansen solubility parameters, the scores given and relative energy distance (RED) of the pure solvents, mixtures, Cyrene's geminal diol and ternary Cyrene/geminal diol/water mixtures used to test the dissolution of rutin .....      | 327 |
| Table A 17: Solubility of polyvinyl pyrrolidone PVP K90 in various solvents .....   | 328 |
| Table A 18: Concentrations, average and standard deviation of single-walled carbon nanotubes (SWCNTs) dispersed in pure solvents (Cyrene and NMP) and with the aid of additives (Triton X-100 and PVP).....   | 329 |
| Table A 19: Hansen solubility parameters, the scores given and relative energy distance (RED) of the solvents used to test the dissolution of PES3020.....  | 332 |

|  |     |
|--|-----|
| Table A 20: Hansen solubility parameters, the scores given, and relative energy distance (RED) of the solvents and Cygnet-Cyrene mixtures proposed to dissolve polyethersulfone PES3020..... | 333 |
| Table A 21: Overall porosity (%) and pore diameter ( $\mu\text{m}$ ) of PES membranes prepared with Cyrene (PES/C) and NMP (PES/N).....  | 334 |
| Table A 22: Gravimetric analysis of PES membranes prepared with Cyrene (PES/C) and NMP (PES/N).....  | 334 |
| Table A 23: Static contact angle of PES/C and PES/N membranes.....   | 335 |
| Table A 24: Pure water permeability of membranes casted from cold and hot casting solutions .....  | 335 |
| Table A 25: Hansen solubility parameters, the scores given and relative energy distance (RED) of the solvents used to test the dissolution of PVDF 5130.....                                 | 336 |

# List of figures

|  |    |
|--|----|
| Figure 1: Closing the loop for a circular economy. Adapted from reference. <sup>11</sup> .....   | 40 |
| Figure 2: Venn diagram of economic, environmental, and social sustainability content. Adapted from reference. <sup>15</sup> .....  | 41 |
| Figure 3: Solvent use by sector. Adapted from reference. <sup>47</sup> .....   | 47 |
| Figure 4: Electronegativities for atoms commonly involved in the structure of polar aprotic solvents and polarisation of the carbonyl group. ....  | 50 |
| Figure 5: Surface layer formation process. Adapted from reference. <sup>53</sup> .....   | 51 |
| Figure 6: Synthesis of <i>N</i> -methyl-2-pyrrolidone from fossil resources <sup>87</sup> .....  | 55 |
| Figure 7: (a) Synthesis of <i>N,N'</i> -dimethylformamide from methyl formate and dimethylamine and (b) from dimethylamine, carbon dioxide and hydrogen.....                                       | 56 |
| Figure 8: (a) Synthesis of <i>N,N'</i> -dimethylacetamide synthesis from dimethyl amine with acetic acid and from (b) dimethyl amine with methyl acetate.....                                      | 56 |
| Figure 9: (a) Synthesis of dimethyl sulfoxide from Kraft process of from (b) dimethyl sulfide. ....  | 57 |
| Figure 10: Synthesis schemes of (a) dialkyl and (b) cyclic carbonates.....   | 59 |
| Figure 11: Synthesis scheme of <i>N,N'</i> -dimethyl- <i>N,N'</i> -dibutylsuccinamide from succinic acid and <i>N</i> -methyl-1- <i>n</i> -butylamide. Adapted from reference. <sup>39</sup> ..... | 59 |
| Figure 12: Synthesis of $\gamma$ -Valerolactone from biomass <i>via</i> levulinic acid. <sup>107</sup> .....   | 60 |
| Figure 13: Synthesis of cyclopentanone from furfural. <sup>108</sup> .....   | 60 |
| Figure 14: Molecular structures of (a) Cyrene, (b) dairy lactone and (c) 5-hydroxymethyl-2(5h)-furanone.....   | 61 |
| Figure 15: Synthesis of Cyrene from cellulose <i>via</i> levoglucosenone (Furacell™ process). Adapted from reference. <sup>115</sup> .....   | 62 |
| Figure 16: (a) Sample of Cyrene and (b) the FC5 commercial demonstration plant in Tasmania, Australia. ....  | 62 |
| Figure 17: Products and by-products formed from cellulose pyrolysis in Furacell™ process. Adapted from reference. <sup>111</sup> .....   | 63 |
| Figure 18: Self-aldol condensation of Cyrene in the presence of bases.....   | 64 |
| Figure 19: Nomenclature of Cygnet molecules. Adapted from reference. <sup>126</sup> .....  | 66 |
| Figure 20: Synthesis of Cygnet 0.0 from Cyrene and 1,2-ethanediol. ....  | 66 |
| Figure 21: Cygnet 0.0 as a solvent in (a) Heck and (b) fluorination reactions. ....  | 66 |
| Figure 22: Cyrene hydration reaction. ....   | 67 |
| Figure 23: Dynamic viscosity of Cyrene samples of 99.2% (a), 99.48% (b) and 99.71% (c) as a function of temperature. ....  | 67 |

|   |     |
|---|-----|
| Figure 24: The structure and SMILES notation obtained for Cyrene.....   | 69  |
| Figure 25: InChi input of Cyrene. <sup>141</sup> .....  | 70  |
| Figure 26: Y-MB method used to calculate Hansen Solubility Parameters of Cyrene using descriptors SMILES. <sup>142</sup> .....  | 71  |
| Figure 27: Joback method to calculate the heat of vaporization for Cyrene. <sup>143</sup> .....   | 72  |
| Figure 28: Health, Safety and Environmental impact of Cyrene (left) and NMP (right) with predictive role only. <sup>142</sup> .....   | 74  |
| Figure 29: COSMO-RS (real solvation) of cellulose nitrate using various solvents, including Cyrene. ....  | 75  |
| Figure 30: $\delta$ -potentials of cellulose nitrate and polar aprotic solvents. Name "nitrocellulose" was given by the software. Cyrene and NMP were created manually, hence the labels "BCONF_102" and "BCONF_99" .....   | 76  |
| Figure 31: (a) Chemical equilibrium between the keto and enol forms of Cyrene and their (b) $\delta$ -potentials (green for the ketone and red for the enol).....   | 77  |
| Figure 32: Life cycle assessment of Cyrene's production using Furacell™ process. Adapted from reference. <sup>166</sup> .....   | 82  |
| Figure 33: Footprint of Cyrene (IPCC 2013 Impact Assessment Method) was realised in the context of NMP's, which was realised by Argonne National Laboratory (ANL), Ecoinvent database version 3.1 and GaBi life cycle assessment. Adapted from reference. <sup>166</sup> .....                                | 83  |
| Figure 34: Molecular structures of monomers used in acrylate polymers: (a) acrylic acid, (b) methyl acrylate, (c) butyl acrylate, (d) methyl methacrylate and (e) butyl methacrylate. ....  | 96  |
| Figure 35: Synthesis of cellulose nitrate.....  | 97  |
| Figure 36: (a) Acrylic aerosols paints and (b) cellulose nitrate used to (c) spray paint the porous and non-porous substrates .....   | 98  |
| Figure 37: (a) Aluminium foil and (b) ceramic tile used in this work.....   | 99  |
| Figure 38: Acrylic paint (a) and cellulose (b) paints in Hansen sphere. Only the good solvents (blue spheres) are named here. ....  | 102 |
| Figure 39: (a) Infrared spectra of acrylic and (b) cellulose nitrate-based graffiti paints.....   | 103 |
| Figure 40: (a) Immersion tests result of the coated tiles with acrylic and (b) cellulose nitrate paint after cleaning using different solvents. An original painted tile is shown for comparison. ....  | 105 |
| Figure 41: (1a) Top view of a pristine aluminium slide, (2a) cross-sectional optical microscope image of untreated ceramic tile and the cleaning results of both painted substrates using (b) Cyrene and (c) NMP. The grey colour from 2b is due to the light, no changes in the material were observed. .... | 106 |
| Figure 42: (a) Pristine tile, (b) acrylic and (c) cellulose-based graffiti paint removal from porous ceramic tiles using 75% Cyrene-25% H <sub>2</sub> O mixture (% v/v).....   | 106 |

|   |     |
|---|-----|
| Figure 43: (a) Results of the poultice test of acrylic graffiti paint removal from the glazed side using NMP and (b) Cyrene. A porous tile was stained using (c) acrylic and (d) cellulose-based graffiti and the spots cleaned using various solvents, including Cyrene.....   | 107 |
| Figure 44: Mechanism proposed to explain the graffiti removal from the (1a) non-porous and (2a) porous substrate using pure, individual solvents and poultices. (1b) The results of graffiti removal from a non-porous substrate and (2b) of a porous substrate using pure, individual solvents and poultices.....  | 109 |
| Figure 45: (a, c) Mechanism of acrylic and (b, d) cellulose-based graffiti paint using (a, b) Cyrene and (c, d) NMP. ....   | 110 |
| Figure 46: (a) Stages of the acrylic graffiti paint dissolution in NMP from red to dark-red. (b) Pure NMP on the left followed by none successive washings and the last vial is the resulted residue and clean solvent, (c) shows pure Cyrene on the left followed by none successive washings and the last vial is the resulted residue and clean solvent (d) the residues after washing alongside the dried paint. .... | 112 |
| Figure 47: Infrared spectra for the red acrylic paint cleaned by (in red) Cyrene and (in blue) NMP. Two acrylic resins (in green and magenta) are shown here for comparison.....  | 113 |
| Figure 48: Chemical structure of the poly(amide imide) (PAI) monomeric unit. ....   | 119 |
| Figure 49: Synthesis of PAI from aromatic diamines and aromatic acid chloride anhydrides (acid chloride route) <i>via</i> poly(amic acid) intermediate. ....  | 123 |
| Figure 50: Synthesis of PAI from TMA and 4,4-MDI (diisocyanate route). ....   | 124 |
| Figure 51: (a) Position of pure solvents and (b) solvent systems in Hansen space for Torlon AI10. Only the good solvents (blue spheres) are named here.....   | 125 |
| Figure 52: Dynamic viscosity of PAI/Cyrene, PAI/NMP, PAI/51% EC-49% Cyrene and PAI/51% DMSO-49% Cyrene fluids as a function of shear rate.....  | 129 |
| Figure 53: Thermal cross-linking of PAI enamels.....  | 131 |
| Figure 54: Infrared spectroscopy of PAIs synthesised from NMP, Cyrene, 51% ethylene carbonate-49% Cyrene, 75% ethylene carbonate-25% Cyrene and 51% DMSO-49% Cyrene. ....   | 132 |
| Figure 55: <sup>1</sup> H-NMR spectrum of PAI/Cyrene.....   | 133 |
| Figure 56: (a) Solvent resistance test of the poly(amido-imide) resins produced from Cyrene, (b) NMP, (c) 51% EC-49% Cyrene, (d) 75% EC-25% Cyrene and (e) 51% DMSO-49% Cyrene cured at 220 °C. ....  | 135 |
| Figure 57: (a) Chemical resistance to NMP of the poly(amido-imide) resins produced from NMP, (b) 51% EC-49% Cyrene, (c) 75% EC-25% Cyrene and (d) 51% DMSO-49% Cyrene cured at 240 °C. ....   | 136 |
| Figure 58: (a) Preliminary results of the hardness test of 9H pencil passed once onto the coated PAI/NMP, and ten times for (b) PAI/Cyrene and (c) PAI/NMP. ....  | 137 |

|  |     |
|--|-----|
| Figure 59: (a) Pristine aluminium slide and the results of the hardness test of cured (b) PAI/Cyrene, (c) PAI/NMP and (d) PAI/51% EC-41% Cyrene.....   | 138 |
| Figure 60: (a) Flexibility test of PAI/Cyrene, (b) PAI/NMP and (c) PAI/51% EC-49% Cyrene.....  | 139 |
| Figure 61: (a) Adhesion strength test of PAI produced with Cyrene, (b) NMP and (c) 51%EC-49% Cyrene (1) before and (2) after the test. ....  | 140 |
| Figure 62: Hesperidin extraction from orange peel and its chemical structure.....  | 148 |
| Figure 63: Rutin extraction from black tea leaves and its chemical structure. ....   | 149 |
| Figure 64: Recommended solvents mapped in Hansen space with solubility sphere of hesperidin (a) and rutin (b). Only the good solvents (blue spheres) are named here. ....  | 151 |
| Figure 65: (a) New Hansen spheres of hesperidin and (b) rutin when adding the new mixtures of solvents (% v/v). (c) Cyrene's geminal diol (hydrate) was plotted with Cyrene-water mixtures separately for hesperidin and (d) rutin to observe their distinct positions in Hansen space. (e) New ternary mixtures of Cyrene/geminal diol/water (obtained from the same Cyrene-water mixtures from (c) and (d) have been included in Hansen sphere for hesperidin and (f) rutin dissolution. All mixtures are expressed in % v/v. Only the good solvents (blue spheres) are named here. .... | 153 |
| Figure 66: Extraction yield of hesperidin ( $\text{mg g}^{-1}$ ) from RT, hot and fast hot extraction, determined using UHPLC compared to the "standard" (70% EtOH-30% H <sub>2</sub> O in light-green column). All extractions are executed in one stage. The binary and ternary solvent systems were predicted by HSPiP.....   | 156 |
| Figure 67: Concentration of rutin ( $\text{mg g}^{-1}$ ) from room temperature (RT) extraction, "hot extraction" (65 °C) and "fast hot" extraction determined using UHPLC. All extractions were realised in one stage. The binary and ternary solvent systems were predicted by HSPiP .....  | 157 |
| Figure 68: (a) Influence of water on dissolution and extraction of hesperidin and (b) rutin using Cyrene.....  | 159 |
| Figure 69: (a) Structures of single- and (b) multi-walled carbon nanotubes. Adapted from reference. <sup>444, 445</sup> .....  | 167 |
| Figure 70: (a) Molecular structure of the cationic surfactant (CTAB), (b) anionic (SDS) and (c) nonionic surfactant (Triton™ X-100). ....  | 172 |
| Figure 71: (a) Structure of PVP and its possible wrapping arrangements around CNT tubes. Adapted from reference. <sup>562</sup> .....  | 173 |
| Figure 72: Single-walled carbon nanotubes dispersed in neat Cyrene and NMP using 1-, 5-, 10- and 20-hour sonication. ....  | 176 |
| Figure 73: Single-walled carbon nanotubes dispersed in Cyrene and NMP in the presence of Triton™ X-100, using 10- and 20-hour sonication. ....   | 177 |
| Figure 74: Single-walled carbon nanotubes dispersed in Cyrene and NMP in the presence of PVP, using 1-, 5-, 10- and 20-hour sonication.....  | 179 |

|   |     |
|---|-----|
| Figure 75: Dispersion of single-walled carbon nanotubes in neat solvents (Cyrene and NMP) and in presence of additives (Triton and PVP). Error bars were not added. ....  | 180 |
| Figure 76: (a) Residues after sonication, centrifugation and filtration of SWCNTs in Cyrene and (b) NMP, with or without additives. ....  | 182 |
| Figure 77: (1, 2) TEM images of 0.1 mg mL <sup>-1</sup> and (3, 4) 1.25 mg mL <sup>-1</sup> SWCNT dispersed in neat Cyrene at (a) low resolution and (b) high resolution after (1, 3) one hour and (2, 4) 20 hours of sonication. ....              | 183 |
| Figure 78: (1, 2) TEM images of 0.1 mg mL <sup>-1</sup> and (3, 4) 1.25 mg mL <sup>-1</sup> SWCNT dispersed in neat NMP at (a) low resolution and (b) high resolution after (1, 3) one hour and (2, 4) 20 hours of sonication. ....                 | 185 |
| Figure 79: (1, 2) TEM images of 0.1 mg mL <sup>-1</sup> and (3, 4) 1.25 mg mL <sup>-1</sup> SWCNT dispersed in Cyrene and Triton™ X-100 at (a) low resolution and (b) high resolution after (1, 3) one hour and (2, 4) 20 hours of sonication. .... | 187 |
| Figure 80: (1, 2) TEM images of 0.1 mg mL <sup>-1</sup> and (3, 4) 1.25 mg mL <sup>-1</sup> SWCNT dispersed in NMP and Triton™ X-100 at (a) low resolution and (b) high resolution after (1, 3) one hour and (2, 4) 20 hours of sonication. ....    | 189 |
| Figure 81: (1, 2) TEM images of 0.1 mg mL <sup>-1</sup> and (3, 4) 1.25 mg mL <sup>-1</sup> SWCNT dispersed in Cyrene and PVP at (a) low resolution and (b) high resolution after (1, 3) one hour and (2, 4) 20 hours of sonication. ....           | 191 |
| Figure 82: (1, 2) TEM images of 0.1 mg mL <sup>-1</sup> and (3, 4) 1.25 mg mL <sup>-1</sup> SWCNT dispersed in NMP and PVP at (a) low resolution and (b) high resolution after (1, 3) one hour and (2, 4) 20 hours of sonication. ....              | 192 |
| Figure 83: (a) Stability studies of SWCNTs dispersed in neat Cyrene at the start and after (b) one day, (c) 8 days, (d) 20 days and (e) 30-day stability test. ....   | 194 |
| Figure 84: (a) Stability studies of SWCNTs dispersed in neat NMP at the start and after (b) one-day stability test. ....  | 195 |
| Figure 85: (a) Stability studies of SWCNTs dispersed in Cyrene with the aid of Triton™ X-100 as dispersant at the start and after (b) one day, (c) 8 days, (d) 20 days and (e) 30-day stability test. ....  | 197 |
| Figure 86: (a) Stability studies of SWCNTs dispersed in NMP with the aid of Triton™ X-100 as dispersant at the start and after (b) one-day stability test. ....   | 198 |
| Figure 87: (a) Stability studies of SWCNTs dispersed in Cyrene with the PVP as dispersant at the start and after (b) one day, (c) 8 days, (d) 20 days and (e) 30-day stability test. ....   | 199 |
| Figure 88: (a) Stability studies of SWCNTs dispersed in NMP with the aid of PVP as dispersant at the start and after (b) one-day stability test. ....   | 200 |
| Figure 89: Cyrene-based fluids with six-month stability test. ....  | 201 |

|  |     |
|--|-----|
| Figure 90: Symmetrical membranes: (a) microporous, (b) nonporous dense and (c) electrically charged. Asymmetrical membranes: (d) Loeb-Sourirajan structure, (e) thin-film composite and (f) supported liquid. Adapted from reference. <sup>591</sup> .....   | 208 |
| Figure 91: Electrically charged membranes packed in an electro dialysis system. Adapted from reference. <sup>609</sup> .....   | 209 |
| Figure 92: Types of filtration membranes based on size of the analyte. Adapted from reference. <sup>612</sup> .....  | 210 |
| Figure 93: Membranes fouling phenomenon. Adapted from reference. <sup>615</sup> .....  | 212 |
| Figure 94: Schematic non-solvent induced phase separation process. ....  | 216 |
| Figure 95: Chemical structure of polyethersulfone.....   | 219 |
| Figure 96: Chemical structure of polyvinylidene difluoride. ....   | 219 |
| Figure 97: Chemical structure of polysulfone. ....   | 220 |
| Figure 98: Chemical structure of cellulose acetate. ....   | 220 |
| Figure 99: Synthesis of polyimide membranes from a diamine and a dianhydride. Adapted from reference. <sup>360</sup> .....   | 221 |
| Figure 100: Mixtures of Cg:Cy at different concentrations and pure Cygnet 0.0. ....  | 222 |
| Figure 101: (a) Low and (b) high magnifications of top surface SEM images of a Bucky paper obtained from single-walled carbon nanotubes dispersed in Cyrene. ....  | 225 |
| Figure 102: (a) Neat solvents used to dissolve the polymer PES3020 and (b) mixtures of Cygnet in Cyrene were mapped in Hansen space with solubility sphere for PES3020. Hansen solubility parameters are given here in units of MPa <sup>1/2</sup> . Only the good solvents (blue spheres) are named here..... | 227 |
| Figure 103: (a) Variation of the dynamic viscosity versus shear rate of polyethersulfone casting solutions in Cyrene and (b) NMP.....  | 234 |
| Figure 104: Detail of cross-sectional SEM images of (a) PES/C0.1 and (b) PES/N0.1.....   | 236 |
| Figure 105: Cross-sectional SEM images of PES membranes produced from Cyrene and different concentrations of PVP: (1) 0%, (2) 0.1%, (3) 0.5%, (4) 1%, (5) 5% and (6) 10% in cold (a) and hot solutions (b). All membranes have a thickness of 500 μm.....  | 237 |
| Figure 106: Cross-sectional SEM images of PES membranes produced from NMP and different concentrations of PVP: (1) 0%, (2) 0.1%, (3) 0.5%, (4) 1%, (5) 5% and (6) 10% in cold (a) and hot solutions (b). All membranes have a thickness of 500 μm.....   | 239 |
| Figure 107: Cross-sectional SEM images of PES membranes using Cyrene and cast from a gel at (a) room temperature and from (b) a hot gel, using (c) Cygnet 0.0/Cyrene blend at room temperature and (d) hot solution and from (e) pure Cygnet 0.0. All membranes have a thickness of 200 μm. ....               | 240 |



|  |     |
|--|-----|
| Figure 108: Scanning Electron Microscopy images of (a) cross-section, (b), top side and (c) bottom side of PES membranes using MBSA as solvent and (1) water, (2) TMO and (3) hexane as non-solvent. All membranes have a thickness of 150 $\mu\text{m}$ . .....   | 242 |
| Figure 109: Scanning Electron Microscopy images of (a) cross-section, (b), top side and (c) bottom side of membranes of (1) PES and Cyrene, (2) PES, Cyrene and 3% PVP and (3) PES, Cyrene and 5% PVP and (4) NMP. All membranes contain 0.1% single-walled carbon nanotubes (SWCNTs) and a thickness of 150 $\mu\text{m}$ . ..... | 244 |
| Figure 110: Stereo (optical) microscope images of (a) the top surface and (b) bottom surface of a PES membrane produced with (1) Cyrene, (2) Cyrene and 5% PVP or (3) NMP. All membranes contain 0.01% SWCNT.....  | 245 |
| Figure 111: Scanning Electron Microscopy images of (a) cross-section, (b) top side and (c) bottom side of membranes produced from (1) pristine PES, (2) PES and 1% PVP and (3) PES and 1% S300. All membranes have been produced using Cyrene as a solvent and have a thickness of 150 $\mu\text{m}$ . .....                       | 247 |
| Figure 112: Influence of the thickness of flat sheet membrane on PES membranes morphology with a thickness of (a) 150, (b) 200 and (c) 500 $\mu\text{m}$ . .....   | 248 |
| Figure 113: (a) Overall porosity and (b) pore size distribution of PES membranes prepared with Cyrene (in blue) and NMP (in orange). .....   | 249 |
| Figure 114: (a) Pore size distribution of PES produced with Cyrene and (b) NMP using relaxation NMR. ....  | 251 |
| Figure 115: Gravimetric analysis of PES/C (in blue) and PES/N (in orange). ....  | 251 |
| Figure 116: Infrared spectra of PES/C0 and PES/C10. ....   | 252 |
| Figure 117: (a) Static water contact angle and (b) the time-dependent values for a sessile drop spreading over a range of PES membranes produced with Cyrene. ....   | 255 |
| Figure 118: (a) Pure water permeability of membranes cast from cold (room temperature) and (b) hot casting solution.....   | 256 |
| Figure 119: Recommended solvents mapped in Hansen space with solubility sphere for PVDF polymer. Only the good solvents (blue spheres) were named here. ....   | 258 |
| Figure 120: PVDF dissolution in (a) Cyrene, (b) NMP, (c) DMSO, (d) GVL and (e) CP at the beginning of stirring.....  | 259 |
| Figure 121: PVDF dissolution in (a) Cyrene, (b) NMP, (c) DMSO, (d) GVL and (e) CP at the end of casting gel producing. NMP and DMSO solutions are viscous liquids, while GVL, Cyrene, and CP form strong gels. ....  | 260 |
| Figure 122: SEM micro-images of cross-section (a), top side detail of the same cross-section (b) and the top surface of membranes produced from Cyrene (1), NMP (2), DMSO (3), GVL (4) and CP (5), All membranes were cast at 500 $\mu\text{m}$ . .....  | 262 |

|  |     |
|--|-----|
| Figure 123: Scanning electron microscopy images of membranes produced from (1) polysulfone, (2) cellulose acetate and (3) polyimide using Cyrene (a,b), Cg:Cy (c,d) and pure Cygnet 0.0 (e) as solvents. The membranes were cast from solutions at room temperature (a, c) and from a hot solution at 100 °C (b, d, e). All membranes have a thickness of 200 µm. .... | 267 |
| Figure 124: (a) Painted aluminium slides and (b) ceramic tiles using different colours from both acrylic and cellulose-based graffiti aerosols. ....   | 283 |
| Figure 125: Red graffiti paint removal from non-porous aluminium slides. (a) The slides were painted using graffiti aerosol and left to dry and (b) immersed in beakers containing different solvents. ....  | 284 |
| Figure 126: (a) Pristine and painted tiles, (b) dip-in test of graffiti paint removal from the stained ceramic tiles using (c) Stuart rollers. ....  | 285 |
| Figure 127: Poultice test: (a) the stained surface was covered by (b) poultices made of solvent and talc and covered using plastic foil. After 24 hours, (c) the plastic foil was removed, and results were assessed. ....   | 285 |
| Figure 128: Cross-sectional optical microscope image of a ceramic tile cleaned by Cyrene. ....   | 286 |
| Figure 129: Schematic diagram of PAIs curing system. ....  | 287 |
| Figure 130: (a) Hardness tester and (b) the pencils used in the abrasion test of PAI wire enamels. ....  | 289 |
| Figure 131: UH-PLC chromatogram of hesperidin standard. ....   | 290 |
| Figure 132: UH-PLC chromatogram of hesperidin extracted by 70% Cyrene-30% H <sub>2</sub> O mixture. ....   | 291 |
| Figure 133: The description of the single-walled carbon nanotubes (SWCNTs) dispersion in Cyrene, NMP and ethanol used in this project. ....  | 292 |
| Figure 134: The schematic illustration of membrane preparation using NIPS process. ....  | 294 |
| Figure 135: MIP and NMR methods of porosity using a PES/C5. ....   | 295 |
| Figure 136: A schematic diagram of the frontal filtration equipment. (1) nitrogen cylinder, (2) valve, (3) pressure sensor, (4) water bath, (5) membrane cell, (6) magnetic stirrer, (7) electronic balance, (8) PC. ....  | 297 |
| Figure 137: <sup>1</sup> H-NMR Spectra of Cygnet 0.0 and the reactants leading to its formation ....   | 298 |
| Figure 138: <sup>1</sup> H-NMR spectrum of Cg:Cy from the reaction between Cyrene and ethylene glycol ....   | 299 |
| Figure 139: (a) Hansen Solubility Parameters 3D diagram and (b) an example from the present work with R <sub>0</sub> (interaction radius) and R <sub>a</sub> (Hansen distance). R <sub>a1</sub> and R <sub>a2</sub> are examples of Hansen distances between the solute and a good and a bad solvent, respectively. ....   | 301 |
| Figure 140: (a) Cosmo geometry, (b) δ-surface, (c) δ-profile and (d) δ-potential of Cyrene. ....   | 303 |
| Figure 141: COSMOconfX interface. ....   | 304 |
| Figure 142: List of compounds and polymer selected for a property calculation. ....  | 306 |

|  |     |
|--|-----|
| Figure 143: Composition of COSMOtherm system.....  | 306 |
| Figure B 1: Scores from 1 (good cleaning) to 5 (no change) given to the cleaned tiles of (1) acrylic and (2) cellulose nitrate paint.....  | 337 |
| Figure B 2: (a) Porous and non-porous substrates were painted on <i>approx.</i> 70% of the surface, (b) were dried and immersed in (b, c) beakers or (d) vials containing individual solvents. ....  | 338 |
| Figure B 3: Results of the graffiti cleaning from the aluminium slides using (1) Cyrene, (2) NMP and (3) DMF of cleaning (1a, 2b, 3a) acrylic and (1b, 2a, 3b) cellulose-based paints.....   | 338 |
| Figure B 4: Effect of NMP on cellulose and acrylic paint. (a) A yellow residue can be seen onto aluminium slide, (b) ceramic tile and (c) on the bottom of the vial. ....  | 339 |
| Figure B 5: (a) Solvent residues from acrylic and (b) cellulose nitrate graffiti removal by various polar aprotic solvents, including Cyrene. THF has evaporated after a while. ....   | 339 |
| Figure B 6: (a) DMF reagent of 99% purity and (b) DMF anhydrous (99.8%) used as cleaning agent for acrylic and cellulose-based paints.....   | 339 |
| Figure B 7: (a) Solutions of PAIs produced using NMP, Cyrene and mixtures of Cyrene with EC or DMSO and (b) PAIs resins. ....  | 340 |
| Figure B 8: PAI/Cyrene cured at 220 °C. ....   | 340 |
| Figure B 9: (a) <sup>1</sup> H-NMR spectra of PAI/NMP, PAI/51% EC-49% Cyrene, PAI/75% EC-49% Cyrene and PAI/51% DMSO -49% Cyrene. All PAIs were cured at 240 °C. (b) <sup>13</sup> C NMR spectrum of PAI/Cyrene. ....  | 341 |
| Figure B 10: (a) Thermogravimetric analysis (TGA) and differential scanning calorimeter (DSC) measurements of (b) PAI/Cyrene, (c) PAI/NMP, (d) PAI/51% EC-49% Cyrene, (e) PAI/75% EC-49% Cyrene and (f) PAI/51% DMSO - 49% Cyrene. All PAI films were cured at 240 °C..... | 342 |
| Figure B 11: (a) Partial solubility parameters of hesperidin and (b) rutin calculated using DIY 5.03 version of Hansen Solubility Parameters in Practice (HSPiP). ....   | 343 |
| Figure B 12: In vitro dissolution test of hesperidin and the scores given by visual inspection. ...  | 343 |
| Figure B 13: (a) Dissolution of hesperidin in Cyrene (red circle) at room temperature (b) and at 65 °C.....  | 343 |
| Figure B 14: (a) Forced fit for hesperidin using HSPiP and (b) the new RED values of the solvents after the changes in software. ....  | 344 |
| Figure B 15: (a) Hansen Solubility Parameters (HSPs) calculated for (b) Cyrene's hydrate using DIY 5.03 version of HSPiP. ....   | 344 |
| Figure B 16: (a) Solution of 1.25 mg mL <sup>-1</sup> SWCNTs dispersion on ethanol, (b) NMP and (c) Cyrene after shaking the tube for 10 seconds and left to settle for one hour.....  | 345 |

|  |     |
|--|-----|
| Figure B 17: (a) Solution of 1.25 mg mL <sup>-1</sup> SWCNTs in NMP and Cyrene after 10 hours of sonication and centrifugation at 10°C and (b) 20 °C immediately after sonication. ....            | 345 |
| Figure B 18: (a) Miscibility of MBSA and water 1:1 after 1 hour and (b) after 3 days.....  | 345 |
| Figure B 19: (a) Miscibility of MBSA and excess of water after 1hour and (b) after 3 days.....   | 346 |
| Figure B 20: Change in viscosity with temperature of PAI/C10 and PES/N10 casting solutions. .  | 346 |
| Figure B 21: Casting bath in which the PES membrane was produced with MBSA (PES/MBSA) and casted in hexane. The red rails are showing the residue of PES remaining after the casting process. .... | 346 |
| Figure B 22: Cross-sectional SEM figure of PES membranes produced using Cyrene and 5% PVP and 0.1% SWCNTs.....   | 347 |
| Figure B 23: (a) Coagulation bath of PES/PVP membranes in Cyrene and (b) NMP after membrane casting. (c) shows PES membranes produced with Cyrene and S300 after casting. ....                     | 347 |
| Figure B 24: Pore diameters of Cyrene-based PES membranes.....   | 347 |
| Figure B 25: Pore diameter of NMP-based PES membranes.....   | 348 |
| Figure B 26: (a-b) Thermogravimetric analysis (TGA) and differential thermogravimetric (DTG) measurements of PES/C and (c-d) PES/N membranes.....  | 348 |
| Figure B 27: (a) Thermogravimetric (TGA) and (b) differential thermogravimetric (DTG) measurements of PES-based membranes and pure Cyrene and Cygnet 0.0.....                                      | 349 |
| Figure B 28: (a) Thermogravimetric (TGA) and (b) differential thermogravimetric (DTG) measurements of Cyrene and Cygnet 0.0. ....  | 349 |
| Figure B 29: PES/C1 membrane cast using different thickness: (a) 500 µm and (b) 250 µm.....  | 349 |
| Figure B 30: (a) Thermogravimetric (TGA) and (b) differential thermogravimetric (DTG) measurements of PSf (1), CA (2) and PI (3)-based membranes and neat Cyrene and Cygnet 0.0 ....               | 350 |
| <br>   |     |
| Figure C 1: Summary of first pass metrics toolkit “baseline” for old method of extraction using a mixture between ethanol and water. ....  | 352 |
| Figure C 2: Summary of first pass metrics toolkit using a mixture between Cyrene and water. .  | 354 |

# Acknowledgements

My biggest thanks go to Professor James Hanley Clark for this considerable opportunity I received from him and for his belief in me and all the doors he opened for me. I would like to thank Tony Duncan from CIRCA Group for such a fantastic opportunity to work on the novel solvent, Cyrene. Being part of RenewChem was invaluable as a student and working with industry was very helpful on such a novel project.

I would also like to thank Doctor Con Robert McElroy for his excellent supervision, support, discussions, and challenges throughout my research. I would like to thank Doctor Thomas Farmer for his comprehensive understanding of my project and discussions.

I would like to thank Doctor Richard Gammons, Surajana Bose, Doctor Tabitha Petchey and Paul Elliott for their assistance and detailed analytical equipment experience; Katy Brooke, Sophie Palmer, Doctor Hannah Briers and Carla Nunes Vital for their support within secretarial matter; Doctor Meg Stark and Karen Hodgkinson from Bioscience Technology Facility, Biology Department, the University of York for helping me with the SEM and TEM analyses. I want to thank Professor Duncan MacQuarrie, Doctor Katie Lamb, and Rebecca Donovan, who took the time to review sections of this thesis.

Additionally, I extend my thanks to INGE.BASF for providing Ultrason E3020 P and PVP Luvitek K-90 used in this project; SOLVAY for Torlon AI10; Allnex, Germany for Viacryl SC 134/50WS165 and Viacryl SC 166/45BAC. I would also like to thank Doctor Carlos Grattoni from the School of Earth and Environment, Leeds University, for the mercury porosimetry analyses, and Doctor Paul M. Williams and Matthew J. Walters from the University of Swansea for their help with membranes casting and water filtration experiments.

I would also thank Professor Cristian Boscornea and Doctor Cristina Ott from the Faculty of Applied Chemistry and Materials Science, Polytechnic University of Bucharest, Romania, who supported me in this journey.

By no means least, I would like to thank my family, especially my sister Olivia Apostu, and friends for their support and patience whilst I wrote this thesis.



# Declaration

I declare that this thesis is a presentation of original work and I am the sole author. This work has not previously been presented for an award at this, or any other, University. All sources are acknowledged as References.

All additional contributions to the research by collaborators and co-workers are fully acknowledged in each chapter.





# Chapter I

## 1. Introduction<sup>1</sup>

---

<sup>1</sup> Life Cycle Assessment of Cyrene production was obtained from Circa Group.



## 1.1. Scope of this study

The overall ambition of this project was to demonstrate the use of the bio-based solvent Cyrene as a replacement for conventional polar aprotic solvents in polymer dispersion for coating, cleaning, membrane applications, solvent extraction of natural products, and carbon nanotubes dispersion. Each of these applications are currently served from common polar aprotic solvents, but these incumbent solvents are under every increasing scrutiny and restriction linked to their toxicity.

In Chapter 2, a simple strategy was used to facilitate safe and effective chemical cleaning of graffiti paint using Cyrene. Nowadays, graffiti is removed from surfaces with cleaning products, solvents, lasers, mechanical abrasion, or biological technologies. Typically, these technologies are not effective, are expensive or damage the substrate. Chemical cleaning of graffiti is at risk due to the toxicity of the solvents involved and the negative environmental impact of huge wastes generated.

Chapter 3 describes the use of Cyrene in the preparation of poly(amide imide) enamels (PAIs). Currently polar aprotic solvents NMP, DMF or DMAc are used. NMP and given six-year deferral period (until 9 May 2024) for wire coatings sector, when the producers must find a replacement. DMF was proposed at the end of the year 2019 to be restricted and the list of polar aprotic solvents for PAI synthesis is thus getting slimmer.

In Chapter 4, Cyrene has been used to extract hesperidin and rutin from orange peel and tea leaves, commonly conducted in large amounts of ethanol or methanol.

In Chapter 5, Cyrene has been used to disperse single-walled carbon nanotubes, which are commonly obtained in NMP, ethanol or water with the aid of surfactants. The aim of this study was to unzip individual nanotubes and obtain stable solutions, which are critical conditions for most of the applications.

In Chapter 6 Cyrene was employed as solvent in the fabrication of flat sheet membranes from polyethersulfone, polyvinylidene fluoride, cellulose acetate, polysulfone and polyimide. This application is at risk due to most of the solvents being restricted (NMP) or about to be banned (DMF and DMAc) in many countries due to environmental and health issues. The ketal derivative of Cyrene, Cygnet 0.0 was used in membrane technology on its own or in mixture with Cyrene to cast. Additives such as carbon nanotubes (single-walled carbon nanotubes, assisted by Chapter 5) and polysaccharides were employed in the membrane's preparation, to improve their properties such as hydrophilicity, anti-fouling, selectivity, chemical resistance and porosity. Other green

solvents, such as cyclopentanone,  $\gamma$ -butyrolactone and *N,N'*-dimethyl-*N,N'*-dibutylsuccinamide were employed in the fabrication of filtration membranes for comparative purposes.

Finally, in Chapter 8, the key findings of this study are presented with the recommendations for future research in the areas of paint strippers, poly(amide imide) synthesis, carbon nanotubes dispersion, extraction of natural flavonoids and membrane science.

## **1.2. Green Chemistry**

### **1.2.1. The 12 principles of Green Chemistry**

The term "Green chemistry" was first developed by Paul Anastas and John Warner and reflects the efforts undertaken by chemistry research, manufacturing, and policy to advance sustainability and contribute towards a green economy.<sup>1</sup> The 12 principles of Green Chemistry have influenced the way chemistry and chemical processes are designed (Table 1).<sup>2 3</sup>

Table 1: Twelve principles of Green Chemistry by Anastas and Warner

| Principle                            | Definition   |
|--------------------------------------|--|
| 1. Prevention                        | It is better to prevent waste than to treat or clean up waste after it has been created.   |
| 2. Atom economy                      | Synthetic methods should be designed to maximize the incorporation of all materials used in the process into the final product.  |
| 3. Less hazardous chemical syntheses | Wherever practicable, synthetic methodologies should be designed to use and generate substances that possess little or no toxicity to human health and the environment.  |
| 4. Designing safer chemicals         | Chemical products should be designed to preserve the efficacy of function while reducing toxicity.   |
| 5. Safer solvents and auxiliaries    | The use of auxiliary substances ( <i>e.g. solvents, separation agents, etc.</i> ) should be made unnecessary wherever possible and innocuous when used.  |
| 6. Design for energy efficiency      | Energy requirements of chemical processes should be recognized for their environmental and economic impacts and should be minimised. If possible, synthetic methods should be conducted at ambient temperature and pressure. |
| 7. Use of renewable resources        | A raw material of feedstock should be renewable rather than depleting wherever technically and economically practicable.   |
| 8. Reduce derivatives                | Unnecessary derivatization should be minimized or avoided if possible because such steps require additional reagents and can generate waste.   |
| 9. Catalysis                         | Catalytic reagents (as selective as possible) are superior to stoichiometric reagents.   |
| 10. Design for degradation           | Chemical products should be designed so that at the end of their function they break down into innocuous degradation products and do not persist in the environment.   |
| 11. Pollution prevention             | Analytical methodologies need to be further developed to allow for real-time, in-process monitoring and control prior to the formation of hazardous substances.  |
| 12. Accident prevention              | Substances and the form of a substance used in a chemical process should be chosen to minimize the potential for chemical accidents, including releases, explosions, and fires.  |

Green chemistry has received increasing attention over recent decades due to the chemical industries relationship with the environment. The transition to a green economy is happening and the chemists are working to build a bio-refinery where the petroleum refinery is replaced with a bio-based platform to overcome social and environmental challenges. The known petroleum

resources are becoming exhausted, and many solvents have been discovered to expand the range and number of bio-based solvents. The aim of green chemistry is to improve chemical products and processes to reduce negative impact to humans and the environment.<sup>4</sup> The concept of green chemistry represents “design of chemical products and processes to reduce or eliminate the use and generation of hazardous substances”.<sup>1, 2</sup> Risk is controlled by reducing the exposure of chemicals to the operators, but where exposure is likely (*i.e.*, with solvent use in graffiti cleaning) then safer solvents (reduced hazard) must be used. Generally, the chemical industry therefore defines the risk as a function of hazards and exposure:<sup>2</sup>

$$\text{Risk} = f(x(\text{hazard} \times \text{exposure})) \quad (\text{eq.1})$$

The “hazards” are represented by chemicals and processes, while the “exposure” is the contact of a person with those particular hazards. When the hazard is high and the exposure is not controlled, the risk of an injury and even death can become very high. The risk can be limited by simply minimising the hazards, as it is easier to be controlled than the exposure (*i.e.*, for graffiti removal). In this case, the spillages or accidents do not represent as severe problem, though should nevertheless be avoided. Minimising the hazards can be achieved by designing safer chemicals and therefore, limits the risk of accidents with harmful consequences.

### 1.2.2. Modern chemical legislation

Legislative requirements are indicated as the primary driver of solvent replacement; however, other factors such as economic considerations, social responsibility, internal chemical management policies, consumers’ demands, and users’ safety were also indicated as important factors. The central role of legislation is to protect humans, animals, and environment from the negative effects of harmful solvents. The needs of modern society are protected by chemical legislation such as:

- Registration, Evaluation, Authorisation and Restriction of Chemicals (REACH).
- Control of Substances Hazardous to Health (COSHH),
- Classification, Labelling and Packaging of substances and Mixtures (CLP),
- Chemicals (hazard information and packaging for supply) (CHIP),
- Control of Lead at Work Regulations 2002 (CLAW),
- The Dangerous Substances and Explosive Atmospheres Regulations 2002 (DSEAR),
- European Directives for controlling explosive atmospheres (ATEX),
- EU Pesticides or Plant Protection Products (PPP).

These legislations are managed in the UK by Health and Safety Executive (HSE) and European Chemical Agency (ECHA). ECHA assures the safety use of chemicals on EU's territory, whilst HSE is an UK agency involved in regulation and enforcement of workplace health, safety, and welfare, and for research into occupational risks in Great Britain. REACH is a regulation of the European Union (EC) No. 1907/2006 of the European Parliament and of the Council on the (REACH) is EU legislation designed to identify and restrict the toxic or environmentally hazardous substances and promotes alternatives to reduce animal tests.<sup>5</sup> It forces manufacturers and importers to register every chemical (produced or imported at more than 1 tonne/year) and evaluate its health and environmental risks. The CLP legislation ensures classification and labelling of chemicals, and their clear exposure to workers and consumers in the EU.<sup>6</sup> ECHA named classified endocrine disruptors (ED), carcinogens, mutagens, substances toxic for reproduction (CMR), sensitizers (skin sensitizers and respiratory sensitizers) as substance of very high concern (SVHC).<sup>5</sup> REACH can restrict these SVHCs, banning them completely from use or conditions can be placed on their uses. For example, SVHC solvents such as DMF and DMAc require an authorisation from REACH to be used in the EU. Also, REACH regulation defines the Derived No-Effect Levels (DNELs) limits the exposure to a substance above which humans should not be exposed.

United Kingdom (England, Scotland and Wales) has left European Union in 2016 and this decision has impacted the management of chemicals.<sup>7</sup> From 1<sup>st</sup> January 2021, the companies based in UK, do not comply to the EU chemical legislation including REACH, CLP or PPP anymore. From January 2021, UK REACH operates in GB, while some of the present principles of the present EU REACH Regulation will remain. Both EU and UK REACH will operate independently after Brexit.<sup>8</sup> Northern Ireland still complies to the EU Regulations after Brexit. However, the Health and Safety Executive (HSE) remains the national regulator for the entire UK.

### **1.2.3. Circular economy**

The aim of circular economy is to recirculate the elements so that the need for virgin material can be avoided.<sup>9</sup> In a circular economy the end-of-life of a product needs to be balanced against its performance and its timeframe for use.<sup>10</sup> The initial design of a product is crucial in order to create an effective material recirculation with zero waste. For an effective recirculation, a product should be reused, recycled or renewed rather than sent to landfill or incinerated (Figure 1):<sup>11</sup>

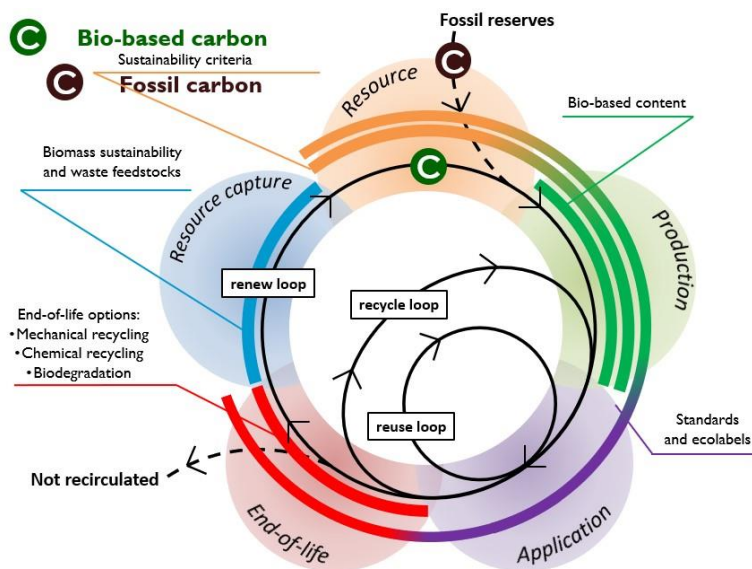


Figure 1: Closing the loop for a circular economy. Adapted from reference.<sup>11</sup>

To achieve a circular economy, resources are chosen to convert into target chemicals and bio-products. Also, the use of waste as feedstock should be prioritised.<sup>12</sup> Biorefineries offer a sustainable way to convert waste into marketable bioproducts and bioenergy, and are seen as comparable to petrochemical refineries. To achieve a maximum material recirculation, it is required to increase the recycling capacity and a stronger market for the secondary materials necessary. In a circular economy, clean synthetic methods must become compatible with sustainable global development goals and innovation in chemical design should be made to find replacements for the current toxic chemicals and to ensure the harmful compounds are not released into the environment (*i.e.*, during the renew loop).<sup>13</sup>

## 1.2.4. Sustainability

Common public conception is that “chemical” is associated with “dangerous and toxic”. Nowadays, this is changing and the concept of “green chemistry” is covering all areas of chemistry and demanded by today’s society. Sustainability is critical in modern society and it is expressed by “meeting the needs of the present without compromising the ability of future generations to meet their own”.<sup>14</sup> Triple bottom line (TBL) is a sustainability-related construct created by Elkington<sup>15</sup> which is based on the integration of the social, environmental, and economic dimensions to evaluate the performance of a process in a broader perspective to create greater value. In brief, sustainability implies minimising the negative environmental impact, while trying to maintain a balance between all three “pillars” (Figure 2):



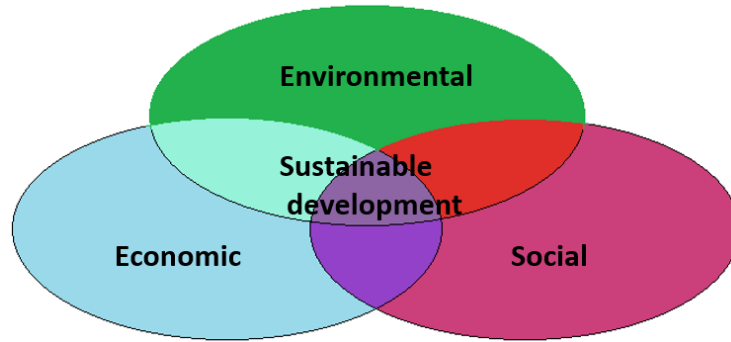


Figure 2: Venn diagram of economic, environmental, and social sustainability content. Adapted from reference.<sup>15</sup>

Environmental sustainability is defined by the use of natural resource, biodiversity and pollution prevention, not relying on the fossil resources. Social sustainability was defined to protect, improve human health and to promote sustainable living. Finally, economic sustainability refers to reusing of goods and application of waste as a resource. However, a product or process cannot be considered sustainable without comprehensive data. Quantitative datasets against benchmarks, establishing requirements must be met for social, economic, and environmental sustainability. The pursuit of these targets would ideally generate a “green economy”, which means “low-carbon, resource-efficient and socially inclusive”.<sup>16</sup>

### 1.2.5. Sustainability applied to solvents

Current regulations are urging industries to use bio-based solvents because they have a low toxicity, are environmentally friendly and are biodegradable. The “bio-refinery” concept is widely accepted as the use of natural resources, combining the biomass (any organic matter which is not food) conversion and simple processes to produce bio-based chemicals and fuels.<sup>17</sup> According to European Committee for Standardisation (CEN) the definition of a bio-based product is “wholly or partly derived from biomass, such as plants, trees or animals (the biomass can have undergone physical, chemical or biological treatment)”.<sup>18</sup> Bio-based solvents derived directly (bio-based) or synthesised (bio-derived) from natural materials are being developed to become benign replacements for petroleum-based solvents.<sup>19</sup> The cycle of bio-based carbon closes when a bio-based solvent is used: at the end of its life, this solvent is incinerated or lost in atmosphere as carbon dioxide, which is then fixed during photosynthesis, allowing for the carbon to be reincorporated back into bio-based solvents (the renew loop in Figure 1).<sup>11</sup> The utilisation of biomass in this process ensures a more sustainable life cycle and reduces the carbon footprint of the solvent. Solvents should be sustainable from an economic, social and environmental perspective and compete with the traditional ones concerning the cost of their production and the land used for their production should not replace the land for food production.<sup>20</sup> The term “green solvent” is commonly accepted that their production, use and disposal as related to the 12 principles of green chemistry; hence Gu and Jerome suggested 12 criteria that a green solvent need to meet (Table 2):<sup>21</sup>

Table 2: Twelve criteria of Gu and Jerome that a green solvent needs to meet

| Principle           | Definition  |
|---------------------|---|
| 1. Availability     | A green solvent needs to be available on a large scale, and the production capacity should not greatly fluctuate in order to ensure a constant availability of the solvent on the market. |
| 2. Price            | Green solvents have to be not only competitive in terms of price but also their price should not be volatile during time in order to ensure sustainability of the chemical process.       |
| 3. Recyclability    | In all chemical processes, a green solvent has to be fully recycled, of course using eco-efficient procedures.  |
| 4. Grade            | Technical grade solvents are preferred in order to avoid energy-consuming purification processes required to obtain highly pure solvents.   |
| 5. Synthesis        | Green solvents should be prepared through an energy-saving process and the synthetic reactions should have high atom-economy.   |
| 6. Toxicity         | Green solvents have to exhibit negligible toxicity in order to reduce all risks when manipulated by humans or released in nature when used for personal and home care, paints, etc.       |
| 7. Biodegradability | Green solvents should be biodegradable and should not produce toxic metabolites.  |
| 8. Performance      | To be eligible, a green solvent should exhibit similar and even superior performances (viscosity, polarity, density, etc.) compared to currently employed solvents.                       |
| 9. Stability        | For use in a chemical process, a green solvent has to be thermally and (electro) chemically stable.   |
| 10. Flammability    | For safety reasons during manipulation, a green solvent should not be flammable.  |
| 11. Storage         | A green solvent should be easy to store and should fulfil all legislations to be safely transported either by road, train, boat or plane.   |
| 12. Renewability    | The use of renewable raw materials for the production of green solvents should be favoured with respect to the carbon footprint.  |

Capello defined a green solvent as a solvent having a lower environmental, health and safety (EHS) impact and energy demand during its LCA compared to conventional solvents.<sup>22</sup> In order to assess the greenness of a solvent, various aspects need to be taken into consideration such as environmental impacts starting from the early stages of production until the end; recycling and disposal; using the feedstock as raw material is preferred; and formation of waste should be

avoided.<sup>23</sup> This way, organic solvents including some ionic liquids and supercritical CO<sub>2</sub> were considered as “green solvents”. For over 20 years, ionic liquids (ILs) were considered as green solvents because they are not volatile at ambient conditions (avoiding VOC emissions) and non-flammable, are thermally and chemically stable. They are used in many applications, from synthetic chemistry to extractions, catalysis, electrochemistry and pharmaceutical industry.<sup>24-29</sup> However, commonly used ILs have poor degradability, are difficult to remove from products, and are toxic, hence they are no longer widely considered as green and their use in pharmaceutical and food applications remains limited.<sup>26, 30</sup> Subsequently a new generation of ILs are being developed, so called “deep eutectic solvents” (DESs), with higher melting points than of ILs which have been used in the extraction of bio-active compounds from plants, organic reactions, electrochemistry and enzyme reactions.<sup>31-34</sup> An ideal green solvent must first have low human safety concerns, linking back to the earlier discussion of risk. In addition, green solvents should be produced from renewable resources, be easily degradable, low/no environmental toxicity, low/no VOCs and easy to recover and recycle. Economically, a green solvent should be cheap, widely available and simple equipment involved in the process of synthesis. When defining “greenness” of a solvent, the environmental, health and safety (EHS) characteristics are considered and the life cycle assessment (LCA) is quantified by associating the environmental impact with all the stages from production to disposal of a chemical or process.<sup>22</sup>

### 1.2.6. Solvent selection guides

Various solvent selection guides are currently available, these being valuable tools for green-minded chemists. GlaxoSmithKline proposed a list of solvents and their properties in 2011, this guide being seen as one of the most influential.<sup>35</sup> The solvents are scored on a scale of 1 (red) to 10 (green), based on data. The American Chemical Society subsequently listed the main solvents used in chemical reactions and extraction processes, scored on a scale 1 (green) -10 (red), where the higher the number, the more toxic is the solvent.<sup>36</sup> Sustainable Solvent Selection Service (S4),<sup>37</sup> developed by the Green Chemistry Centre of Excellence at the University of York, offers advice and scientific expertise regarding solvents and their use, using computational modelling (with no experimental work) of solvent properties (physical, safety and regulatory concerns) to predict useful solvents and their materials compatibility. The performance of the solvents selected using the above criteria are assessed in the lab, and environmental and economic concerns are applied to determine the ideal candidate for a specific application. By this approach, S4 has recently focused on hydrocarbons and polar aprotic solvents and launched the bio-based Cyrene to replace

toxic polar aprotic solvents and 2,2,5,5-tetramethyloxolane (TMO) to replace toluene and tetrahydrofuran (THF). Green solvents were considered for binary solvents with Cyrene for PAI, PES, PVDF and graffiti applications. Table B1 shows a list of greener solvents from CHEM21 Solvent Selection Guide<sup>38</sup> (where green means “recommended” and yellow is attributed to “problematic”) or obtained at GCCE, University of York and tested in this work.<sup>39, 40</sup> CHEM21 is a public-private partnership between six pharmaceutical companies, ten universities and five enterprises which uses a methodology based on health, safety and environment criteria, aligned with the Global Harmonized System (GHS) and European regulations and ranks the solvents in three categories: recommended, problematic and hazardous.<sup>38</sup>

### 1.2.7. Green metrics

Green metrics are used to assess the greenness of a chemical process by quantifying its efficiency and environmental performance. The first general metric for green chemistry, E-factor focuses on the waste generation in a process<sup>3</sup> and is the simplest green metric to use at industrially scale. E-factor is described as the ratio of the mass of waste per mass of product:

$$E - \text{factor} = \frac{\text{mass of waste (kg)}}{\text{mass of product (kg)}} \quad (\text{eq. 2})$$

E-factor is the amount of waste produced (considered “everything but the desired product”) and more waste means higher environmental impact. Hence, the ideal E-factor is zero, highlighting the first Green Chemistry principle (Table 1). This is useful for large industry scale where can facilitate a holistic assessment of a complete process, but at smaller scale use (*i.e.*, in pharmaceutical syntheses), where the quality is very important, the same E-factor is disadvantageous. In this case, E-factor could be helpful when associated with a yield, stoichiometry and solvent usage. E-factor and atom economy (AE, defined as molecular weight of the desired product divided by the sum of the molecular weights of all substances produced) (equation 3) were introduced in the early 1990s and have been used worldwide and refined.<sup>41</sup> Trost used AE to compare the efficiency of synthetic routes to a target molecule and became a framework for the chemists<sup>42</sup> to pursue greener chemistry:

$$AE = \frac{\text{molecular weight of product}}{\text{total molecular weight of reactants}} \times 100 \quad (\text{eq.3})$$

However, AE does not consider solvents and auxiliary chemicals and can be used to predict and evaluate the amount of waste. A refined AE was defined by GlaxoSmithKline (GSK) as reaction mass efficiency (RME):<sup>42</sup>

$$\text{RME} = \frac{\text{mass of isolated product (kg)}}{\text{total mass of reactants (kg)}} \times 100 \quad (\text{eq. 4})$$

DOZN™ from Merck evaluates green chemicals based on 12 Principles of Green Chemistry.<sup>43</sup> The aim of this green metric is to improve the resource use, more efficient use of energy, and minimising human and environmental hazards. However, this approach lacks in used of the lifecycle impacts of raw materials and considers instead their hazards and efficient use.

Mass intensity (MI) compares the total mass of materials going into a reaction to the mass of product coming out:

$$\text{MI} = \frac{\text{total mass of reactants (kg)}}{\text{mass of product (kg)}} \quad (\text{eq. 5})$$

MI incorporates solvents and auxiliaries but does not take into account their recycling, similarly to E-factor. Hence, either E-factor or MI do not represent the process efficiency.

Many other green metrics are available, and it is the user's choice when assessing the greenness of a process, but many times, they do not include all the factors. In this regards, the CHEM21 toolkit ensures a holistic approach to metrics, permitting direct comparison of processes or syntheses.<sup>44</sup> The key parameters of CHEM21 toolkit are life cycle assessment (LCA), solvents, renewability, health and safety, critical elements, catalysis, chemical of concern, waste, efficiency and energy. This toolkit has been fully described in Section 7.8.3. of this thesis and has been used to assess the greenness of flavonoids extractions in Chapter 4.

## 1.3. Solvents

### 1.3.1. Definition, classification and uses of solvents

Solvents are liquids used as dissolving media for applications in cleaning, extracting and purifying products, and the modification of materials.<sup>45</sup> International Union of Pure and Applied Chemistry (IUPAC) defined a solvent as one component of a solution.<sup>46</sup> Almost half of the global solvents are used for paints and coatings industry (Figure 3), where solvent represents the major ingredient in the total weight of the paint.<sup>22</sup> Other applications include pharmaceutical, inks, personal care and household, cleaning products, chemical synthesis (for polymers and other chemicals), biotechnology, metal and wood industry, food industry and medical applications.

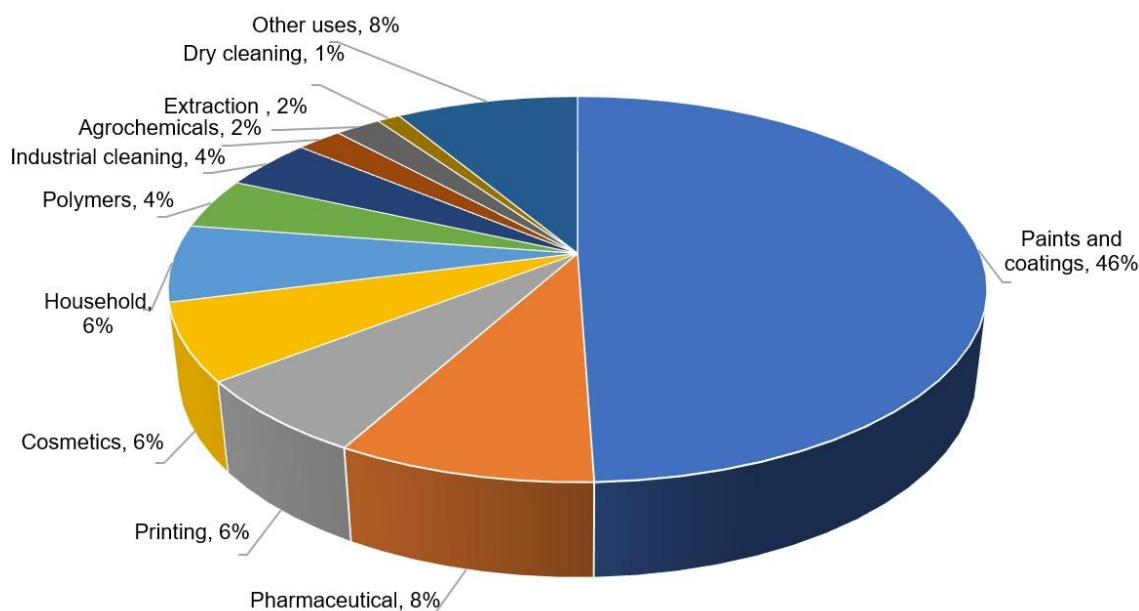
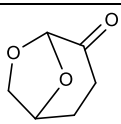
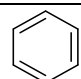
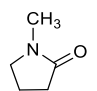
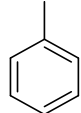
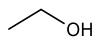
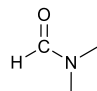
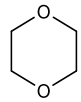
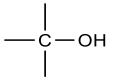
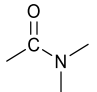
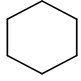
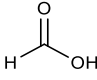
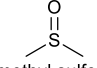
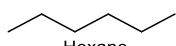
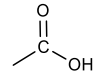
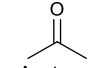
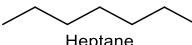
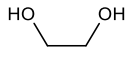
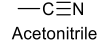
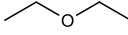
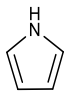
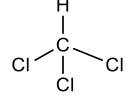


Figure 3: Solvent use by sector. Adapted from reference.<sup>47</sup>

In general, solvents are classified into three categories; a few examples from each class are presented in Table 3:

Table 3: Types of solvents based on their polarity

| Polar protic solvents  | Polar aprotic solvents  | Non-polar solvents   |
|--|---|--|
| $\text{H}_2\text{O}$<br>Water  | <br>Cyrene                         | <br>Benzene         |
| $\text{—OH}$<br>Methanol   | <br><i>N</i> -Methyl-2-Pyrrolidone | <br>Toluene         |
| <br>Ethanol           | <br><i>N,N'</i> -dimethylformamide | <br>1,4-Dioxane     |
| <br><i>t</i> -Butanol | <br><i>N,N'</i> -Dimethylacetamide | <br>Cyclohexane     |
| <br>Formic acid       | <br>Dimethyl sulfoxide            | <br>Hexane          |
| <br>Acetic acid       | <br>Acetone                      | <br>Heptane        |
| <br>Ethylene glycol | <br>Acetonitrile                 | <br>Diethyl ether |
| <br>Pyrrole         |   | <br>Chloroform    |

A polar protic solvent molecule contains a source of protons. They are favourable for the unimolecular nucleophilic substitution reactions ( $\text{S}_{\text{N}}1$ ). Polar protic solvents dissolve substances with the same polarity based on the idea that "like dissolves like".

A dipolar aprotic solvent molecule possesses large dipole moment, but does not contain labile protons and so, are not capable of hydrogen bond donating; they can only accept hydrogen bonds. They lack O-H, N-H and F-H bonds. They have intermediate dielectric constant and are more suitable for the bimolecular nucleophilic substitution reactions ( $\text{S}_{\text{N}}2$ ).

A non-polar solvent molecule typically has charges evenly distributed and a low dielectric constant. These solvents are not a proton source and only exhibit weak intermolecular forces. Non-polar solvents are hydrophobic (immiscible with water) and dissolve non-polar substances.



### 1.3.2. Effect of solvent on solubility

The term miscibility is defined by IUPAC as “capability of a mixture to form a single phase over certain ranges of temperature, pressure, and composition”, while solubility represents “The analytical composition of a saturated solution, expressed in terms of the proportion of a designated solute in a designated solvent”.<sup>48</sup> Miscibility refers to solubility of liquid solutes and solubility to the ability of a substance (solute) to dissolve in a liquid. The importance of solubility goes beyond traditional branches of chemistry and is extended to pharmacology, engineering and environmental applications.<sup>49</sup> Solubility is the ability of solid, liquid or gaseous solutes to dissolve in a solvent to form a solution and is affected by several factors:

- Solute-solvent interaction. A strong solvent-solute interaction means a greater interaction of a solute in a solvent, while a weak interaction between the two means a low solubility or insolubility (“like dissolves like” principle).
- Temperature affects the solubility of a solid solute in liquid. The effect of temperature depends on the type of reaction: endothermic or exothermic.<sup>50</sup> In an endothermic reaction, a high temperature generates a stress on the reactants side and the system shifts toward the product side. In an exothermic reaction, heat is consumed “in the reverse” reaction and more of the starting material is produced.
- Concentration. Adding more starting material to a reaction, the equilibrium will shift to the right, where more product can form.
- Solvent composition. There is no definite trend for solvent composition in solubility process of a solute. In some cases pure solvents dissolve better than when mixed with other solvents.<sup>51</sup> In other cases when two or more solvents mixed, a new solvent with distinct properties is obtained and the solubility of a solute may be greater than in individual solvents.<sup>52</sup>
- Pressure. For majority of solid solutes, pressure does not affect solubility.
- Molecular size of the solute. The bigger the molecule, the more difficult is to dissolve in a solvent, but given enough time, even large particles will eventually dissolve.
- Stirring increases the speed of a solvent to dissolve a solute. This mechanical process increases the motion of the solvent around the solute, exposing the solute to fresh portions of solvent and enables the solubility.

### 1.3.3. Polar aprotic solvents solubilisation mechanism

The solubility of a solute in a solvent is based on the physical and chemical properties of both solvent and solute and physical conditions (concentration, temperature, and pressure).<sup>53</sup> Generally, solvents dissolve a species depending on the hydrogen bonding, polarity and van der Waals forces (Section 8.8.1). Hence, solubility parameters are extensively used in industry to predict the compatibility of various species with different solvents and their physical properties and solubility performance. In hydrogen bonding, polar aprotic solvents can only act as proton acceptors (Section 1.5.4.). In some cases, the solvent dissolves and reacts with the solute, leading to the formation of new covalent bonds between the two (Section 1.5.5.). Carbonyl bonds from a polar aprotic solvent are highly polar due to the large electronegativity difference between carbon and oxygen, where the carbonyl carbon is positively charged, and the carbonyl oxygen is negatively charged (Figure 4):

| Electronegativity | Atom |
|-------------------|------|
| H                 | 2.2  |
| C                 | 2.55 |
| S                 | 2.58 |
| N                 | 3.04 |
| O                 | 3.44 |

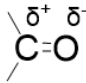


Figure 4: Electronegativities for atoms commonly involved in the structure of polar aprotic solvents and polarisation of the carbonyl group.

In solubilisation, the electronegative centre of a polar aprotic solvent (larger due to the excess of electrons) attracts positively charged species. The positively polarised part (their electron cloud is close to the nuclei and are smaller) interact with anions in a much weaker way.

### 1.3.4. Polymer dissolution in solvents

Polymers dissolution in solvents is very important for applications such as coatings, membrane science, plastics recycling, drug delivery and tissue engineering.<sup>53</sup> Knowing the dissolution capacity helps to find the most suitable solvent and hence optimize a process in these areas. In membrane science, the dissolution of the polymer determines the final structure of the membrane. During the phase inversion, a polymer solution from a polymer/additives and a solvent is cast onto a substrate and immersed in a coagulation bath containing a non-solvent where solvent/non-

solvent exchange and the polymer precipitates.<sup>54</sup> In recycling plastics, a mixture of different polymers, can be selectively dissolved by a single solvent when changing its temperature (different polymer dissolves at a different temperature).<sup>55</sup>

The dissolution of a polymer is a complex process and is controlled by the disentanglement of the polymer chains or by the solvent diffusion into polymer-solvent interface. This process of dissolution implies a solvent diffusing into the polymer when a gel is formed with two separate interfaces, one between the polymer and the gel and one between the gel and the solvent.<sup>53</sup> Once some of the gel-like layer is formed, the solvent pushes portions of this towards the bulk solvent, diluting the gel-like phase and slowly passing to the bulk solvent until all the polymer is dissolved. The surface layers of glassy polymers which can be observed during dissolution can be seen in Figure 5:<sup>56</sup>



Figure 5: Surface layer formation process. Adapted from reference.<sup>53</sup>

The steps between the pure polymer and pure solvent are as follow:

- In the infiltration layer, the glassy polymer which contains molecular size voids is penetrated by the solvent, which fills these holes and starts the diffusion.
- In a solid swollen layer, a polymer-solvent system is formed. The polymer is still in the glassy state.
- The gel layer is formed when the polymer starts swelling in a rubber-like state.
- The liquid layer, where any solid is surrounded by liquid.

The above mechanism is considered a "normal dissolution", where all the layers described are formed. However, in some cases, the polymer cracks and no gel-like layer is formed (*i.e.*, poly(methyl methacrylate) (PMMA) cracks when is dissolved below its glass transition temperature).<sup>57</sup>

The dissolution rate of a polymer is influenced by several factors:

- The molecular weight of the polymer and dispersity<sup>58</sup>

Polydisperse samples dissolved faster than monodisperse ones of the same molecular weight.<sup>59</sup> Larger molecular weights disentangle slower and present a higher degree of swelling.

- Chain chemistry, composition, and conformation of the polymer

A isotactic polymer (in which all the repeating units have the same stereochemical configuration) dissolves faster than a syndiotactic polymer (the repeating units have alternating stereochemical configurations) and atactic stereoisomers.<sup>60</sup>

- Effects of solvents and additives on polymer dissolution

A polymer is likely to dissolve faster in a smaller solvent than a bulky one because of generally higher diffusion rates and swelling power of smaller solvent molecules.<sup>61</sup> A low concentration of a non-solvent added to a good solvent can improve the solubility of a polymer due to the "plasticisation" of the polymer films by the non-solvent molecules. In high concentration, the non-solvent can swell the polymer.<sup>62</sup>

- Temperature and stirring

The dissolution rate increases with the stirring frequency of the solvent because the surface layer decreases its thickness and the dissolution rate increases.<sup>56</sup> A higher temperature can be beneficial in polymer dissolution where the solvent-polymer interactions dominate over the polymer-polymer interactions.<sup>63</sup>

## 1.4. Conventional vs. green and bio-based polar aprotic solvents

### 1.4.1. Traditional polar aprotic solvents

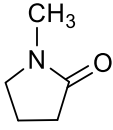


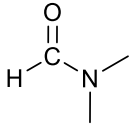



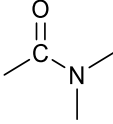


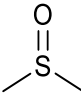

Polar aprotic solvents are vital to the chemical industry, they dissolve a wide range of chemicals with different polarities and stabilise the transition states of reactions with polar transition states, increasing the rate of reaction. They are commonly used in applications listed in Table 4:

Table 4: Applications of commonly used polar aprotic solvents

| Applications of polar aprotic solvents    | Reference |
|---|-----------|
| Organic synthesis                         | 64, 65    |
| Graphene dispersion/exfoliation           | 66-69     |
| Polymer production                        | 70-72     |
| Membrane technology                       | 73-75     |
| Metal-organic frameworks (MOFs) synthesis | 76        |
| Cleaning                                  | 77        |
| Pharmaceutical and medicine               | 78, 79    |
| Extraction and purification               | 80-82     |

Conventional polar aprotic solvents are associated with several serious problems associated with their use (Table 5): toxicity, non-green synthesis and all contain nitrogen or sulphur, so their incineration at the end of their use generates nitrogen and sulphur oxides ( $\text{NO}_x$  and  $\text{SO}_x$ ).

Table 5: Classification of the hazards of polar aprotic solvents used in this study

| Solvent   | Harmonised classification and labelling (CLP)   | Description of hazard  |
|---|---|--|
| <br>N-Methyl-2-pyrrolidone   | <br>  | <ul style="list-style-type: none"> <li>• Restricted by REACH in May 2018 by issuing Commission Regulation (EU)2018/588.</li> <li>• Entry 71: Less than 0.3% by weight as a substance or in a mixture after 9 May 2020 to be used in the EU, unless manufacturers and users take the appropriate risk management measures and provide appropriate operational conditions to the workers involved. Derived No-Effect Levels (DNELs) relating to the exposure of workers of 14,4 mg/m<sup>3</sup> for exposure by inhalation and 4,8 mg/kg/day for dermal exposure.</li> <li>• 6-year deferral for wire coatings (9 May 2024)<sup>83</sup></li> </ul> |
| <br>N,N'-Dimethylformamide | <br><br> | <ul style="list-style-type: none"> <li>• SVHC list candidate Regulation (EC) No 1272/2008 shows that the substance meets the criteria for classification as toxic for reproduction in accordance with Article 57(c) of REACH.</li> <li>• Toxic for reproduction (Article 57c).</li> <li>• Italy has proposed to restrict DMF on its own or in mixtures in a concentration equal or greater than 0.3 % in Sept 2019 (ECHA/NR/19/32)<sup>84</sup></li> </ul>   |
| <br>N,N'-Dimethylacetamide | <br>  | <ul style="list-style-type: none"> <li>• SVHC list candidate as reprotoxic ED/77/2011, article 57C.</li> <li>• SVHC due to CMR properties (carcinogenic, mutagenic or reprotoxic) (EC number: 204-826-4)<sup>85</sup></li> </ul>   |
| <br>Dimethyl sulfoxide     |    | <ul style="list-style-type: none"> <li>• No hazards<sup>86</sup></li> </ul>  |

Traditional polar aprotic solvents are linked to health and environmental hazards. They are carcinogens or reprotoxic, corrosive, flammable and present acute toxicity. The European Union regulation Registration, Evaluation, Authorisation and Restriction of Chemicals (REACH) restricted the use of NMP, regarding the reproductive effects of this solvent. DMF and DMAc are added to SVHC list as toxic for reproduction due to reproductive toxicity (may damage the unborn child). Moreover, DMF was proposed to be restricted.<sup>84</sup>

**N-Methyl-2-pyrrolidone (NMP)** is industrially manufactured by a typical ester-to-amide conversion, by treating  $\gamma$ -butyrolactone with methylamine (Figure 6):

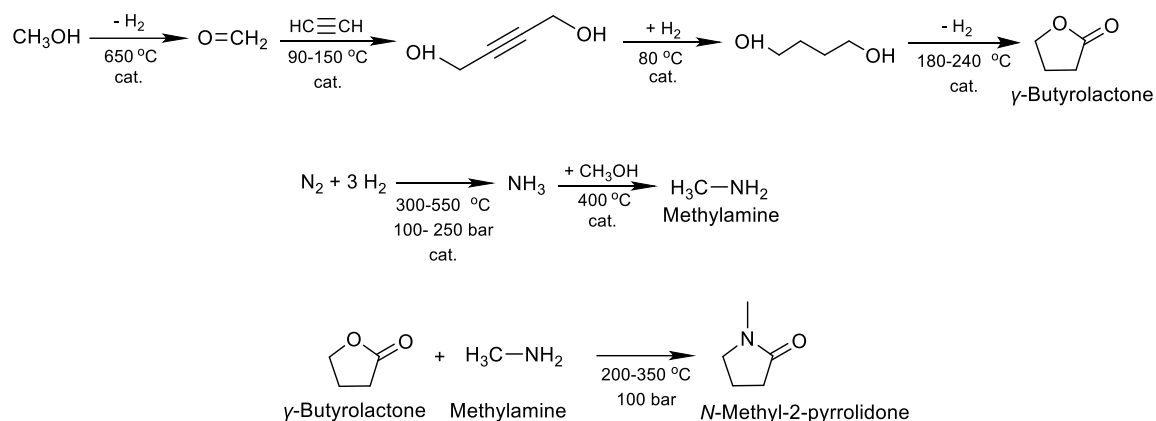


Figure 6: Synthesis of *N*-methyl-2-pyrrolidone from fossil resources<sup>87</sup>

***N,N'*-Dimethylformamide (DMF)** is obtained in two steps from methyl formate (prepared separately) and dimethylamine and no catalyst<sup>88</sup> (Figure 7a) or from dimethylamine, carbon dioxide and hydrogen under pressure at high temperatures and in the presence of Cu/ZnO in a solventless system (Figure 7b):<sup>89</sup>

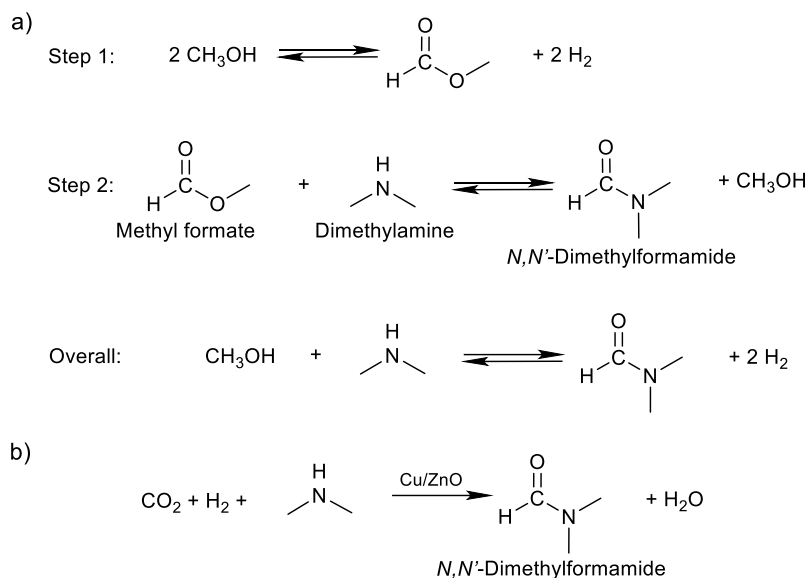


Figure 7: (a) Synthesis of *N,N'*-dimethylformamide from methyl formate and dimethylamine and (b) from dimethylamine, carbon dioxide and hydrogen.

***N,N'*-Dimethylacetamide (DMAc)** is manufactured from dimethylamine with acetic acid (Figure 8a) or dimethylamine<sup>90</sup> and with methyl acetate (Figure 8b):<sup>91</sup>

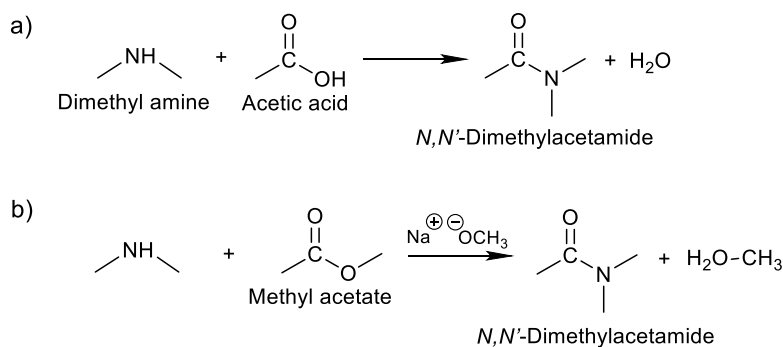


Figure 8: (a) Synthesis of *N,N'*-dimethylacetamide synthesis from dimethyl amine with acetic acid and from (b) dimethyl amine with methyl acetate.

**Dimethyl sulfoxide (DMSO)** is not toxic itself and it is used in the pharmaceutical industry for its property to transport other chemicals through the skin. However, this can also mean transport of toxic solutes into humans. DMSO is a by-product from Kraft process in the production of paper (Figure 9a), but can also be industrially synthesised from the oxidation of dimethyl sulphide with oxygen at 105 °C (Figure 9b).<sup>92</sup>



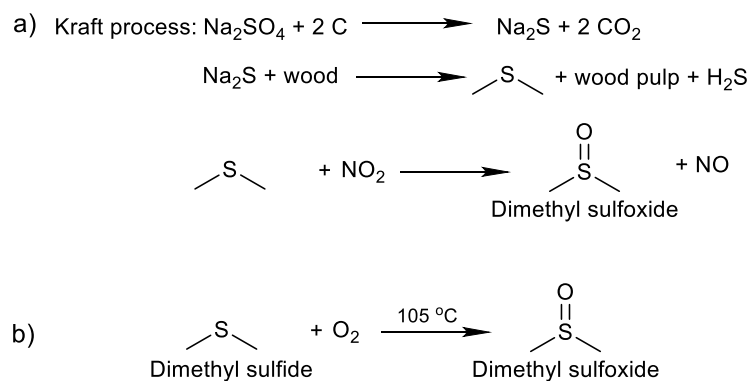


Figure 9: (a) Synthesis of dimethyl sulfoxide from Kraft process of from (b) dimethyl sulfide.

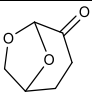

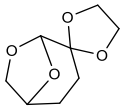
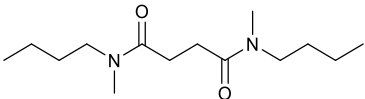

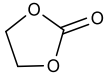
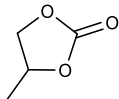

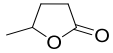
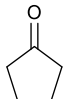


DMSO is stable at room temperature but undergo thermal decomposition at elevated temperatures into many volatile decomposition products (*e.g.* formaldehyde, dimethyl sulfide, disulfide, or bis(methylthio)methane) leading to explosions.<sup>93</sup> Though the unpleasant smell of DMSO (due to the presence of traces of dimethyl sulphide) made it less used in the industry, recently a pleasant-smelling version of it was used in PES membranes preparation<sup>94</sup> and it has partially solved the polar aprotic solvents issues in some of the application, later discussed.

Traditional polar aprotic solvents are obtained from un-green and complicated syntheses and present health issues that need to be urgently addressed.

### 1.4.2. Green and bio-based polar aprotic solvents

Currently, the solvent sector is dominated by petroleum-derived products.<sup>47</sup> It is expected that bio-based solvents will register significant growth in near future.<sup>95</sup> Solvents generally account for 50-80% of a standard reaction,<sup>96</sup> and the pressure of replace the existent toxic, volatile, highly flammable solvents is enormous. Green and sustainable chemistry attracts huge interest because of the high concerns over human health, environment preserving, safety and energy conservation. The hazards associated with the use of green and bio-based polar aprotic solvents used in this work can be seen in Table 6:

Table 6: Classification of the hazards of green and bio-based polar aprotic solvents used in this study, including Cyrene

| Solvent   | Harmonised classification and labelling (CLP)  | Description of hazard  |
|---|--|--|
| <br>Cyrene                                       |   | <ul style="list-style-type: none"> <li>Eye irritation (GHS07)<sup>97</sup></li> </ul>  |
| <br>Cygnet 0.0                                   |  | <ul style="list-style-type: none"> <li>Not known</li> </ul>  |
| <br>N,N'-Dimethyl-N,N'-dibutylsuccinamide (MBSA) |   | <ul style="list-style-type: none"> <li>The <i>in vitro</i> tests suggested no alarming indications of toxicity. The <i>in silico</i> approach based on QSAR model-based predictions for C (carcinogenicity), M (mutagenicity), R (reprotoxicity) and S (skin sensitization) endpoints predicted no activity.<sup>39</sup></li> </ul> |
| <br>Ethylene carbonate                         |  | <ul style="list-style-type: none"> <li>No harmonised classification</li> <li>Chronic exposure can cause kidney damage<sup>98</sup></li> </ul>  |
| <br>Propylene carbonate                        |   | <ul style="list-style-type: none"> <li>Causes serious eye irritation<sup>99</sup></li> </ul>   |
| <br>$\gamma$ -Valerolactone                    |  | <ul style="list-style-type: none"> <li>No harmonised classification<sup>100</sup></li> <li>very low toxicity (LD50 oral rats 8800 mg/kg)<sup>101</sup></li> </ul>  |
| <br>Cyclopentanone                             | <br> | <ul style="list-style-type: none"> <li>Flammable liquid and vapour</li> <li>Causes eye and skin irritation<sup>102</sup></li> </ul>  |

**Carbonates** have been used in this work in the preparation of poly(amide imide) enamels due to their biodegradability, low toxicity, high boiling point and high solubility.<sup>103</sup> Alkyl carbonates are converted by the oxidative carbonylation of water, alcohols or polyols (Figure 10).<sup>104-106</sup>

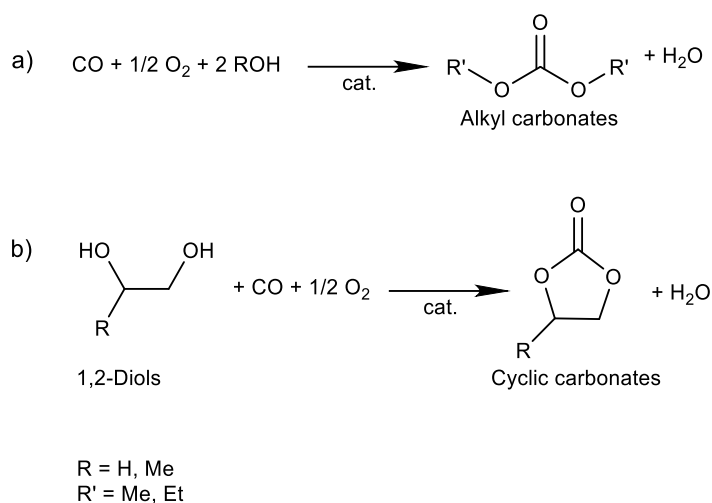


Figure 10: Synthesis schemes of (a) dialkyl and (b) cyclic carbonates.

Oxidative carbonylation is preferred to the phosgene route for the formation of carbonates because it respects some of the green chemistry requirements: avoids the waste formation, avoids the use of toxic chemicals, produces compounds that are biodegradable, uses eco-compatible solvents (water, alcohols or CO<sub>2</sub>), uses renewable materials, and uses catalysts rather than stoichiometric reagents. Ethylene, propylene, diethyl and dimethyl carbonates have been used in blending with Cyrene in PAI applications (Chapter 3).

***N,N'*-Dimethyl-*N,N'*-dibutylsuccinamide (MBSA)** was recently developed at GCCE, University of York and was obtained from *N*-methylbutylamine and succinic acid (Figure 11).<sup>39</sup>

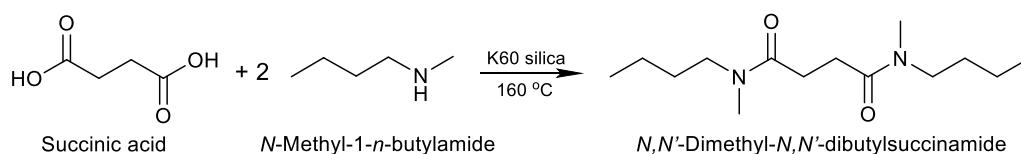


Figure 11: Synthesis scheme of *N,N'*-dimethyl-*N,N'*-dibutylsuccinamide from succinic acid and *N*-methyl-1-*n*-butylamine. Adapted from reference.<sup>39</sup>

MBSA showed low reprotoxicity due to the presence of *N*-butyl alkyl chains. MBSA has a higher boiling point than traditional polar aprotic solvents, of >250 °C, a density close to of water (0.99 g mL<sup>-1</sup>) and it is not miscible with water, unusual for such polar aprotic solvents. MBSA has attracted

the attention in this study due to the ability of dissolving polyethersulfone (PES) thermoplastic polymer and was used as a solvent to fabricate filtration membranes (Section 6.6.2.3.).

**$\gamma$ -Valerolactone (GVL)** can be synthesised from cellulose waste, is water-miscible and has very low toxicity.<sup>101</sup> GVL is obtained from biomass (poplar sawdust, paper mill sludge, tobacco chops, wheat straw, olive tree pruning) *via* levulinic acid, which is hydrogenated to the final product (Figure 12):<sup>107</sup>

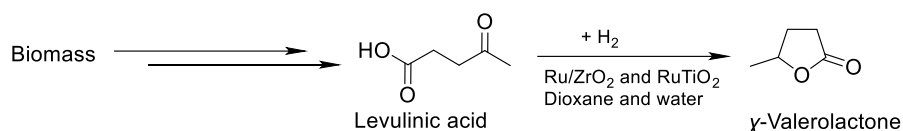


Figure 12: Synthesis of  $\gamma$ -Valerolactone from biomass *via* levulinic acid.<sup>107</sup>

**Cyclopentanone (CP)** is obtained by hydrogenation of furfural (Figure 13) which is obtained from the dehydration of C5-sugars found in the hemicellulose portion of lignocellulosic biomass.<sup>108</sup> The synthesis can take place in biphasic solvent system:

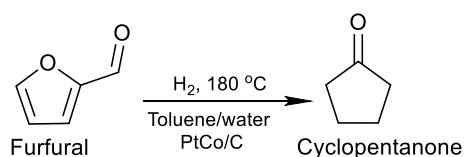


Figure 13: Synthesis of cyclopentanone from furfural.<sup>108</sup>

Water and catalysts based on  $Ru/C$  and  $Al$  or using a  $Ni-Cu$  under  $H_2$  atmosphere have been used to synthesise CP with high yield.<sup>109</sup> GVL and CP were used to produce polyvinyl difluoride flat sheet membranes (Section 6.7. ).

## 1.5. Introduction to Cyrene

### 1.5.1. Synthesis of Cyrene using Furacell™ process

In the UK, a report names 10 specific bio-based chemicals and steps to ensure that the UK moves from research to commercial products and levoglucosenone, lactic acid, 1,3-butanediol, and *n*-butanol were named.<sup>110</sup> Circa Group produce three high-value speciality chemicals from levoglucosenone: dihydrolevoglucosenone (Cyrene), dairy lactone and 5-hydroxymethyl-2(5h)-furanone (Figure 14):<sup>111</sup>

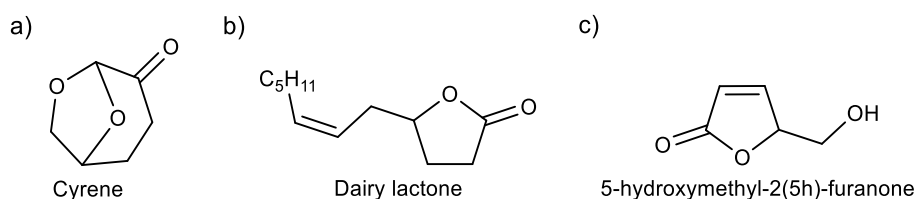


Figure 14: Molecular structures of (a) Cyrene, (b) dairy lactone and (c) 5-hydroxymethyl-2(5h)-furanone.

Made from sawdust or other bio-wastes by the company Circa Group, Cyrene started life in the virtual space, where its molecular structure was predicted to give similar key properties to many useful but toxic solvents including some amides.<sup>112</sup> The first reports of dihydrolevoglucosenone<sup>113</sup> being synthesised from levoglucosenone using elemental hydrogen for the reduction did not appear until the 1990's despite a strong precedent for the chemistry of levoglucosenone established in the 1970's.<sup>114</sup> Cyrene was first reported as a solvent in 2014<sup>112</sup> as an alternative for dipolar aprotic solvents and is produced mostly from cellulose, *via* levoglucosenone (Figure 15) using the highly selective Furacell™ process:

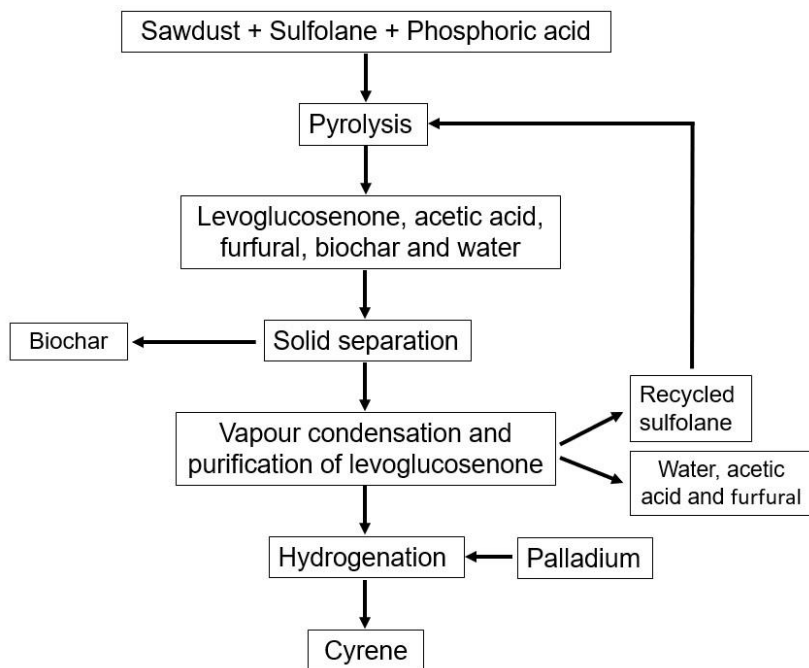


Figure 15: Synthesis of Cyrene from cellulose *via* levoglucosenone (Furacell™ process). Adapted from reference.<sup>115</sup>

The Furacell™ process has now been scaled-up to a 100 tonnes/year demonstration plant (Figure 16b) associated with a paper mill in Tasmania, Australia<sup>116</sup> and a sample of the solvent is shown in Figure 16a:



Figure 16: (a) Sample of Cyrene and (b) the FC5 commercial demonstration plant in Tasmania, Australia.

Moreover, a 1000 tonnes/year plant will be built in France as part of ReSolute project.<sup>117</sup> The Furacell™ process requires the sawdust feedstock to be shredded, and the cellulose must be swollen by using a solvent. The process respects several Green Chemistry rules: safety, use of renewable feedstocks, reduction of derivatives, waste prevention and not persistent in the environment, energy efficiency<sup>2</sup> and production of minimal by-products, reducing downstream

separation processes. The conversion of cellulose to levoglucosenone requires sulfolane as a solvent and phosphoric acid (2–3% by weight of solvent) at a temperature of 430 °C, resulting in the desired dehydration reaction *via* levoglucosan and intermediates such as 5-hydroxymethyl furfural (HMF) and levulinic acid (Figure 17):

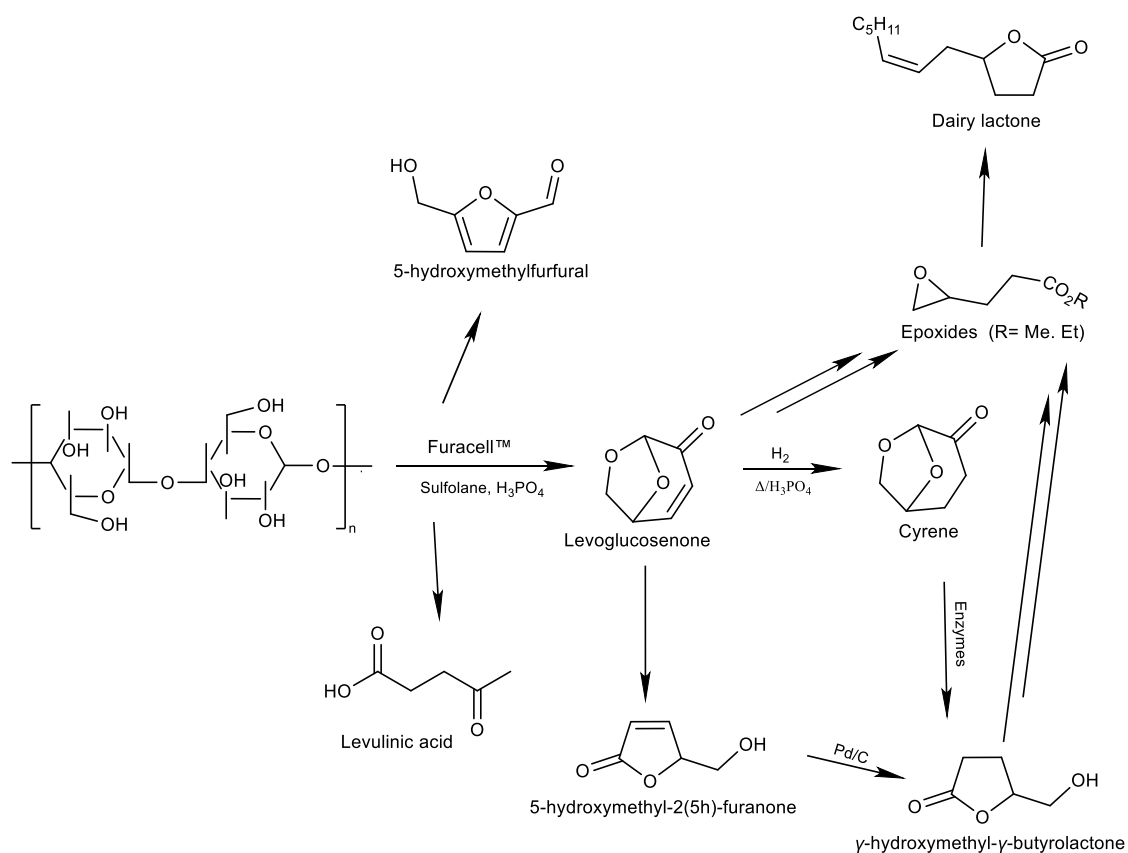


Figure 17: Products and by-products formed from cellulose pyrolysis in Furacell™ process. Adapted from reference.<sup>111</sup>

To distribute the catalyst and adequately swell the entirety of the raw material, temperatures of 150–170 °C are used when the catalyst solution is applied. The actual reaction occurs in an extruder at 430 °C, over a duration of 5 minutes. The cellulose component of the feedstock produces levoglucosenone in up to 40% of the theoretical molar yield, along with traces of HMF and levulinic acid. The carbonaceous char obtained as by-product can be used advantageously to power the Furacell™ process, resulting in overall renewable energy. The volatile products of the reaction are separated from the solid char, and fractional distillation isolates the levoglucosenone (>90% purity). When Cyrene synthesis is complete in the presence of the solvent, a small amount of ethyl acetate is needed (the molar ratio of ethyl acetate to LGO was 3:1) in the presence of 0.5 mol% of palladium (Pd/C) as a catalyst. Recent methods have used ethyl acetate as a solvent,<sup>118, 119</sup> but a solvent-less system is preferable. Recently, the conversion of levoglucosenone to Cyrene up to 100% was previously realised by the hydrogenation of LGO over a palladium catalyst under

mild conditions<sup>120, 121</sup> or through an enzymatic process involving the Old Yellow Enzyme 2.6 (OYE 2.6).<sup>122</sup>

## 1.5.2. Characterisation of Cyrene

### 1.5.2.1. Physical and chemical properties - Background

Cyrene is a pale-yellow liquid with a boiling point of 227 °C and a higher density than the other polar aprotic solvents (Table 5). Cyrene is highly dipolar, like NMP, because of its cyclic structure and the way the acetal and ketone functionalities in Cyrene are arranged. Cyrene has been classed as a dipolar aprotic solvent, similar to the reprototoxic amide solvents it seeks to replace. Cyrene has been tested in two types of nucleophilic substitution reaction, a typical application of NMP and other highly dipolar aprotic solvents.<sup>112</sup> Cyrene is susceptible to degradation in the presence of nucleophiles (attack at the carbonyl group) and bases (deprotonation of the  $\alpha$ -position of the ketone).<sup>123</sup> In the presence of certain bases, an aldol condensation product was isolated (Figure 18), causing issues for use in some reaction conditions but also offering another pathways to potentially valuable chemicals.<sup>124</sup>

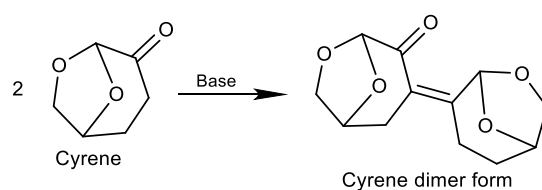


Figure 18: Self-aldol condensation of Cyrene in the presence of bases.

The physical and chemical properties of Cyrene are compared to the conventional polar aprotic solvents and can be seen in Table 7:



Table 7: Physico-chemical properties of Cyrene in comparison with the traditional polar aprotic solvents used in this study

| Solvent property                                   | Cyrene   | NMP       | DMAc      | DMF       | DMSO     |
|--|----------|-----------|-----------|-----------|----------|
| Molecular weight [g/mol]                           | 128.13   | 99.13     | 87.12     | 73.09     | 78.13    |
| Relative density [g/mL at 20-25 °C]                | 1.25     | 1.028     | 0.937     | 0.948     | 1.1      |
| Molar volume [cm <sup>3</sup> /mol]                | 102.50   | 96.43     | 92.98     | 77.10     | 71.03    |
| Boiling point [°C]                                 | 227      | 202       | 164.5-166 | 153       | 189      |
| Melting/freezing point [°C]                        | <-19.99  | -24       | -20       | -60.99    | 19       |
| Flash point [°C]                                   | 108      | 91        | 64        | 58        | 87       |
| Surface tension [mN/m at 22 °C]                    | 72.5     | 40.4      | N/A       | N/A       | 43.5     |
| Vapour pressure [hPa at 20-25 °C]                  | 0.28     | 0.39-0.43 | 2         | 3.60-5.16 | 0.55     |
| Vapour density (Air=1)                             | N/A      | 3.42      | 3.01      | 2.52      | 2.70     |
| Hansen dispersion $\delta_D$ [MPa <sup>1/2</sup> ] | 18.9     | 18        | 16.8      | 17.4      | 18.4     |
| Hansen polarity $\delta_P$ [MPa <sup>1/2</sup> ]   | 12.4     | 12.3      | 11.5      | 13.7      | 16.4     |
| Hansen H-bonding $\delta_H$ [MPa <sup>1/2</sup> ]  | 7.1      | 7.2       | 9.4       | 11.3      | 10.2     |
| Water miscibility at 20 °C                         | Miscible | Miscible  | Miscible  | Miscible  | Miscible |

\*Data collected from Sigma-Aldrich (Merck).<sup>125</sup> Hansen solubility parameters were obtained from HSPiP 5<sup>th</sup> Edition 5.0.03.

There is potential to expand the class of levoglucosenone-derived solvents through simple, high yielding reactions. The synthesis of Cyrene takes only one step, whilst Cygnet, a new class of molecules, only two steps from LGO and three steps from the raw feedstock (cellulose). Each Cygnet has a numerical designation based on the substitution pattern of the dioxolane ring, which depends on the choice of glycol reactant. Cyrene forms Cygnet 0.0, Cygnet 1.0, Cygnet 1.1, Cygnet 2.0 and Cygnet 4.0 when reacting with 1,2 ethandiol (ethylene glycol), propylene glycol, 2,3 butanediol, 1,2 butanediol and 1,2 hexanediol respectively (Figure 19):

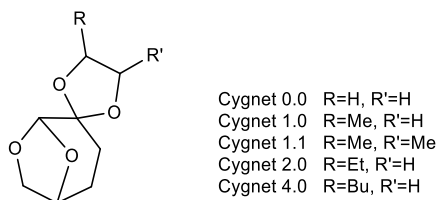


Figure 19: Nomenclature of Cygnet molecules. Adapted from reference.<sup>126</sup>

One example converts the ketone moiety of Cyrene into a ketal (Cygnet 0.0) by reaction with 1,2-ethanediol (Figure 20):<sup>126</sup>

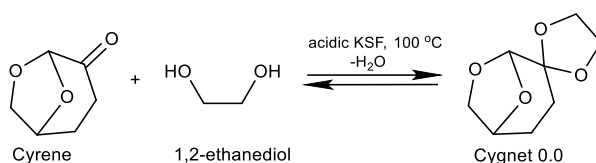


Figure 20: Synthesis of Cygnet 0.0 from Cyrene and 1,2-ethanediol.

The use of Cygnet as a solvent was demonstrated in two pharmaceutical syntheses: Heck reaction and fluorination (Figure 21):<sup>126</sup>

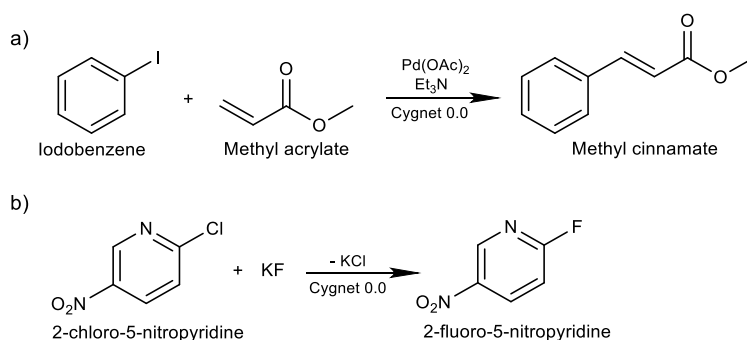


Figure 21: Cygnet 0.0 as a solvent in (a) Heck and (b) fluorination reactions.

In case of a nucleophilic fluorination reaction (2-chloro-5-nitropyridine with potassium fluoride in the presence of Cygnet 0.0 to form 2-fluoro-5-nitropyridine), Cygnet 0.0 showed similar results as DMF and superior to NMP and acetonitrile. In Heck reaction, both Cygnet 0.0 and Cyrene were comparable to NMP and DMSO. Generally, polar aprotic solvents are miscible with water, predominantly led by hydrogen bonding. Interestingly, Cyrene additionally hydrates reversibly in contact with water through its ketone group (Figure 22):

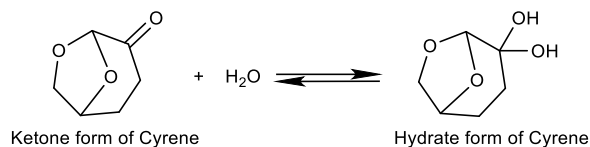


Figure 22: Cyrene hydration reaction.

By mixing water with Cyrene therefore gives a ternary system with the presence of some geminal diol hydrate. This new solvent system was used to dissolve organic compounds such as caffeine, salicylic acid, ibuprofen, aspirin, ferulic acid and mandelic acid.<sup>52</sup>

### 1.5.2.2. Viscosity

In addition to the data presented in Table 7, dynamic viscosity of Cyrene was tested in this work. A sample of 99.2% from Sigma Aldrich (Merck) and two samples of different concentrations from Circa Group (99.48 and 99.71%) were analysed (Figure 23):

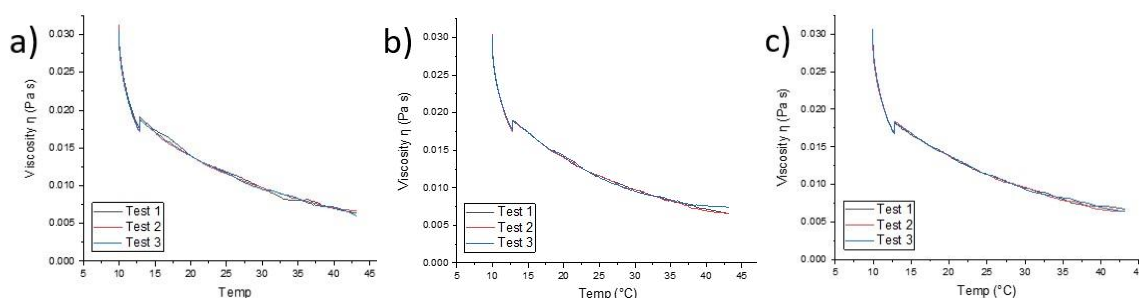


Figure 23: Dynamic viscosity of Cyrene samples of 99.2% (a), 99.48% (b) and 99.71% (c) as a function of temperature.

The samples of Cyrene were used as received. A curve at around 12 °C is due to the equilibrium of the system and can be observed for all tests. As seen in Figure 23, the viscosity of Cyrene decreases with temperature. Hence, as temperature increases, the average intermolecular forces decrease, reducing the viscosity. The viscosity vs temperatures were registered from 10 to 50 °C and the results can be seen in Table 8:

Table 8: Viscosity of Cyrene samples of different purities measured at 25 °C

| Solvent       | Viscosity at 25 °C (mPa s) |        |       |         |
|---------------|----------------------------|--------|-------|---------|
|               | Test 1                     | Test 2 | Test3 | Average |
| Cyrene 99.2%  | 11.76                      | 11.64  | 11.62 | 11.67   |
| Cyrene 99.48% | 11.64                      | 11.62  | 11.47 | 11.58   |
| Cyrene 99.71% | 11.40                      | 11.38  | 11.40 | 11.39   |

The results from Table 8 show a decrease in viscosity with purity, which means that a highly pure solvent might be easier to process in some applications. However, the impurities from the samples have not been determined in this work, it is the subject of a future research project (ReSolute).

### 1.5.3. Hansen Solubility Parameters and predicted environmental impact of Cyrene

#### 1.5.3.1. Calculations of Hansen parameters of Cyrene using the Yamamoto-Molecular Breaking (Y-MB) method

Hansen Solubility Parameters (HSPs) have been used in scientific and industrial fields including polymer materials, coatings, membranes filtration, pigments and nanomaterials dispersibility, pharmaceutical technology, drug-nail affinity, swelling, solvent diffusion, and permeation, drug-DNA interaction and more.<sup>127-138</sup> Hansen Solubility Parameters in Practice (HSPiP) is a software which can predict the molecular affinities, solubility, and solubility-related phenomena of solutes in different solvents by mapping the three values (dispersion interactions  $\delta_D$ , dipolarity  $\delta_P$  and hydrogen bonding ability  $\delta_H$ ) in a three-dimensional "Hansen space".<sup>139</sup>

The experimental HSPs of a new solvent can be determined by three methods: 1) dissolution of a wide range of polymers from database in the solvent and the creation of a sphere based on the given scores; 2) using Quantitative Structure Property Relationships (QSPR) and 3) group contributions. The first method has its limitations; the polymers from database are not real and one polymer from different producers has different properties. The QSPR method outperforms the group contribution methods and is based on the actual 3D structure of the solvent, not only the chemical groups. In this work, the Hansen Solubility Parameters of Cyrene were determined using the QSPR and group contribution methods.

Hansen solubility parameters can be calculated using several methods, but Yamamoto-Molecular Breaking (Y-MB) and Stefanis/Panayiotou are mostly used.<sup>139</sup> In this work, Hansen solubility

parameters of Cyrene have been calculated using Yamamoto Molecular Breaking (Y-MB) method, with HSPiP 5<sup>th</sup> edition 5.0.03 software in two steps:

**Step 1** - Firstly, a) Simplified Molecular-Input Line-Entry system (SMILES) notation and b) International Chemical Identifier (InChi) are created for Cyrene. The information derived from SMILES strings allow for computing  $\delta_D$ ,  $\delta_P$ ,  $\delta_H$ , Antoine parameters, relative melting and boiling points, density, and information about the Health, Safety and Environmental (HSE) of the solvent. Both SMILES and InChi are created:

a) For the existing solvents, Y-MB uses the estimation schemes from Pirika Technologies<sup>140</sup> (which provides a number of useful apps for calculation) and brings the molecular descriptors SMILES into corresponding functional group via Neural Network algorithm, using literature data for each of the parameters. As Cyrene is a new molecule and cannot be found in HSPiP database, SMILES notation was created for Cyrene in Figure 24, where black ring represents the whole molecule, while the second ring is seen covered in red dots:

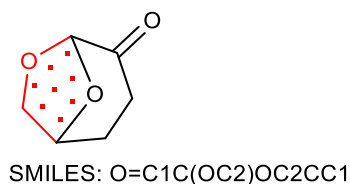


Figure 24: The structure and SMILES notation obtained for Cyrene.

b) InChi input for Cyrene was created in this work using InChi software version 1.04 (Figure 25). InChi is a unique label for well-defined chemical substances given by IUPAC, generated by converting an input chemical structure to a unique and predictable series of American Standard Code for Information Interchange (ASCII) characters. The InChiKey (as 'WHIRALQRTSITMI-UJURSFKZSA-N' for Cyrene) is a hashed version of full InChi and it's the downloadable version of it. InChi differs from CAS registry numbers (*i.e.*, 53716-82-8) in three aspects: it is free to use, it can be computed from structural information and the info is readable. They have been created to facilitate the search for molecular information in databases and on the web and they use SHA-256 algorithm. The InChi inputs are created with "No stereochemistry" option, so they are the simplest possible outputs; and the bigger the structure, the bigger the InChi. In case of isomers, the info differs in their final +/- in their InChi's). They are expressed as simple text and every structure has a unique InChi string, which is accounted for a vapour pressure and viscosity at 25 °C.

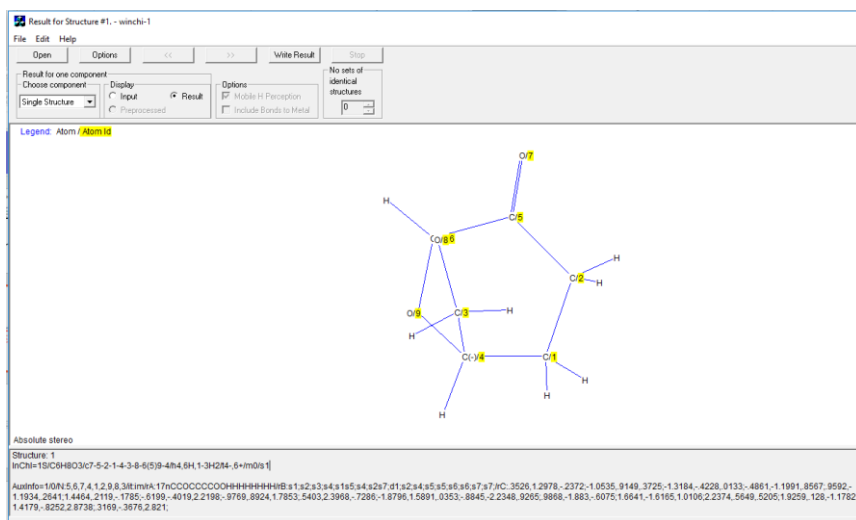


Figure 25: InChi input of Cyrene.<sup>141</sup>

As seen in Figure 25, the InChi string of Cyrene in shows the information which can be easily readable: InChI=1S/C6H8O3/c7-5-2-1-4-3-8-6(5)9-4/h4, 6H,1-3H2/t4-,6+/m0/s1. The InChi string is formed from layers, which are meant to be discussed here: “S” means standard, “1” means Identifier version number, “C6H8O3” is the chemical formula. The next series of numbers “c7-5-2-1-4-3-8-6(5)9-4” is the connectivity of main atoms in skeleton, “h4, 6H,1-3H2” are the hydrogens, “t4-,6+” represents t (stereo: sp<sup>3</sup>)4-,6+ (InChi neutralises charge on input structure by (de)protonation). The last information gives information about the stereochemistry of a compound, with “m0” m (stereo: sp<sup>3</sup>: inverted) 0 and it is present only in case of absolute configuration and “s1” s (stereo:type (1=absolute stereo, 2=relative, 3=racemic))<sup>1</sup>. Other softwares provide the facility to generate InChi’s: cactus, chemSpider, acdlabs.com, pubchem.

**Step 2** - After plotting SMILES or InChi using Y-MB method of calculation, the  $\delta_D$ ,  $\delta_P$ ,  $\delta_H$ ,  $\delta_{Tot}$ , Antoine parameters, melting point, boiling point and density are created, as seen in Figure 26:

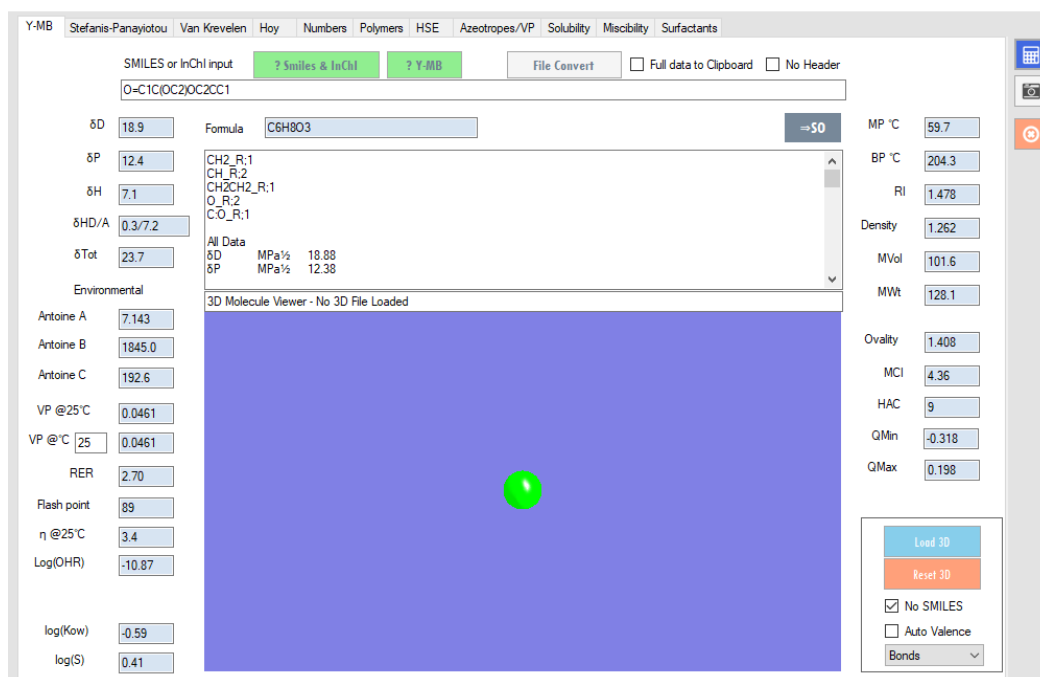


Figure 26: Y-MB method used to calculate Hansen Solubility Parameters of Cyrene using descriptors SMILES.<sup>142</sup>

The molecular formula and molecular weight are calculated, together with the estimated melting and boiling points, refractive index, densities, which are calculated via a Neural Network algorithm using literature data for each of parameters. The Hansen Solubility Parameters of Cyrene and common polar aprotic solvents are summarised in Table 9:

Table 9: Predicted Hansen Solubility parameters (HSPs) for Cyrene compared to traditional polar aprotic solvents

| Solvent                         | $\delta_D$ | $\delta_P$ | $\delta_H$ |
|---------------------------------|------------|------------|------------|
| Cyrene                          | 18.9       | 12.4       | 7.1        |
| <i>N</i> -Methyl-2-pyrrolidone  | 18         | 12.3       | 7.2        |
| Dimethyl sulfoxide              | 18.4       | 16.4       | 10.2       |
| <i>N,N'</i> - Dimethylformamide | 17.4       | 13.7       | 11.3       |
| <i>N,N'</i> - Dimethylacetamide | 16.8       | 11.5       | 9.4        |
| Dichloromethane                 | 17.0       | 7.3        | 7.1        |

*Hansen solubility parameters of traditional polar aprotic solvents are sourced from HSPiP database. HSP values are in units of MPa<sup>1/2</sup>.*

As seen in Table 9, Cyrene presents a dispersion parameter ( $\delta_D$ ) close to DMSO, polarity ( $\delta_P$ ) value close to of NMP and hydrogen-bonding ( $\delta_H$ ) identical to DCM's and close to NMP.

### 1.5.3.2. Calculations of Hansen parameters of Cyrene using group-contribution method

“Numbers” method is a complementary approach used in addition to Y-MB and calculate Heat of vaporisation “ $H_v$ ” at boiling point instead of Critical Temperature “ $T_c$ ” using the Functional Groups Contribution method and Joback Method (Figure 27):

www.pirika.com

Calc. Clear BP (exp) 0.0 K

Vc=318.5cm<sup>3</sup>/mol  
 Melting Point  
 Tm=307.58K  
 Heat of Formation (Ideal Gas, 298 K)  
 Hf=-435.59KJ/mol  
 Gibbs Energy of Formation (Ideal Gas, 298 K)  
 Gf=-197.89KJ/mol  
 Heat of Fusion  
 Heat of Fusion=18.83KJ/mol  
 Heat of Vaporization at Normal Boiling Point  
 Hv=42.39KJ/mol

Figure 27: Joback method to calculate the heat of vaporization for Cyrene.<sup>143</sup>

Joback method can predict boiling and melting points, critical temperature, volume and pressure, heat of formation, Gibbs’ energy of formation and heat capacity of ideal gas, heat of vaporisation at normal boiling point, heat of fusion and dynamic viscosity of a liquid. Joback method assumes that there are no interactions between the groups and only uses additive contributions of the groups. This method is easy to use, but it is not accurate.<sup>144</sup>

The heat of vaporisation ( $\Delta H_{vap}$ ) can be calculated using Joback method or using Pirika program, both resulting in similar values: 41.369 KJ/mol calculated using Joback method and 42.39 KJ/mol, when is calculated using Pirika. The calculation of heat of vaporisation of Cyrene was calculated in this study using Joback method as an example:



$$\Delta H_{\text{vap}} = 15.30 + \Sigma H_{\text{vap},i} \quad (\text{eq. 6})$$

$$\text{where } 3 \times \text{CH}_2 \quad 3 \times 2.223=6.678 \quad (\text{eq. 7})$$

$$2 \times \text{CH} \quad 2 \times 1.691=3.382 \quad (\text{eq. 8})$$

$$1 \times \text{C=O} \quad 6.645 \quad (\text{eq. 9})$$

$$2 \times \text{O} \quad 2 \times 4.682=9.364 \quad (\text{eq. 10})$$

The sum of groups from equations 7-10 is:

$$\Sigma H_{\text{vap},i} = 26.069 \quad (\text{eq. 11})$$

The heat of vaporisation is calculated from equations 6 and 11:

$$\Delta H_{\text{vap}} = 15.30 + 26.069 = 41.369 \text{ KJ/mol} \quad (\text{eq. 12})$$

### 1.5.3.3. Prediction of Health, Safety and Environmental (HSE) impact of Cyrene

HSE tool was found to be important for coating and painting industry and estimates vapour pressure at 25 °C; however, is only predictive. In this project Cyrene and NMP were taken in consideration and the results compared. The SMILES of the two were introduced manually and the results produced by the software displayed, as seen in Figure 28:

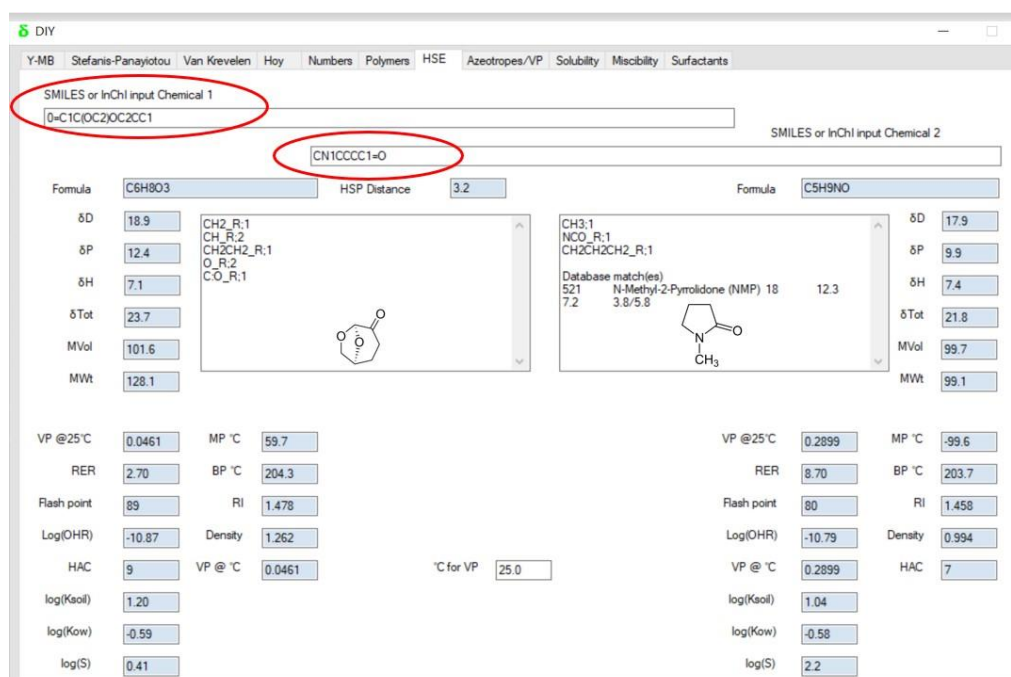


Figure 28: Health, Safety and Environmental impact of Cyrene (left) and NMP (right) with predictive role only.<sup>142</sup>

As seen in Figure 28, RER for Cyrene is 2.70, while NMP a higher value, of 8.70, which suggests the latter is likely to evaporate faster than the former, potentially leading to higher health, fire and/or explosion risks. Boiling points are predicted close to one another with a BP 204.3 °C for Cyrene and 203.7 °C. however, in fact, the difference between their boiling points is bigger: 227 °C for Cyrene and 202 °C for NMP. “Log (k<sub>soil</sub>), (k<sub>ow</sub>) and (s)” are correlated to soil/water partition coefficients. Log (s) is a measure of the amount of chemical substance that can dissolve in water at a specific temperature. This value is higher for NMP, meaning that a bigger amount of NMP is dissolving in water. Hazardous Area Classification (HAC) was given the value 7 for NMP and 9 for Cyrene. While looking to set a score for water, the same program gave a value of 1. Cyrene inaccurately received a higher HAC than NMP, however HSPiP tool has only a predictive role. In reality, NMP has been restricted by REACH, while Cyrene has been given only minimal ecotoxicity and a hazard warning for being an eye irritant.<sup>83, 97</sup>

### 1.5.4. Property prediction for Cyrene using COSMOtherm

COSMOtherm is a tool used to predict thermodynamic properties of a solvent or mixture of solvents. Solubility of liquids, gases and solids can be predicted, as well as free energies of solvation, multiphase liquid partitioning (extraction), conformer population in mixtures, interfacial tension, adsorption, and many environmental properties. In this work, Cyrene's ability to dissolve various polymers was studied. At the end of calculations, generally, a value closer to "0" predicts a good solvent. As the results are similar for all the polymers tested, in this thesis, only one example was used: cellulose nitrate paint dissolution in various solvents, including Cyrene (Figure 29):

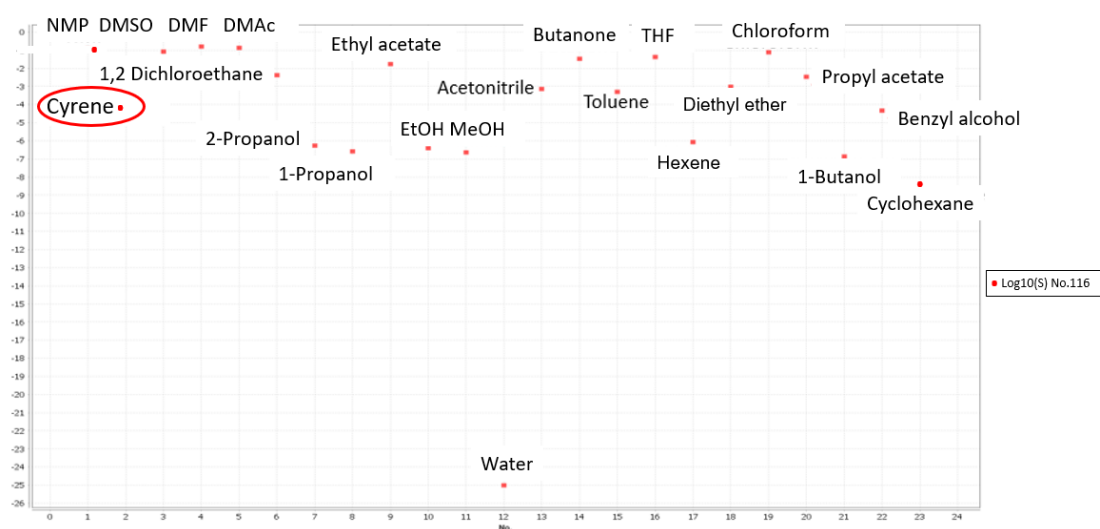


Figure 29: COSMO-RS (real solvation) of cellulose nitrate using various solvents, including Cyrene.

As shown in Figure 29, a relative lower position for Cyrene was given in comparison to the polar aprotic solvents, suggesting a lower efficiency of the solvent in cellulose nitrate graffiti paint dissolution and removal. However, when assessing the potential of Cyrene to dissolve and detach the cellulose nitrate paint from a substrate (Chapter 2), the solvent showed comparable results to NMP, DMAc and DMSO and better results than DMF. COSMOtherm has its limitations: the system contains incompressible liquids, the chemical potential is only valid for ideal gases, the long-range interactions of ions are missing (Debye-Hückel) and the polymers can only be predicted as solvents. Also, the swelling is not taken in consideration. The chemical potential of a polymer is calculated as a solvent of repeat units and COSMOtherm calculates the activity coefficients and solubilities of gaseous and liquid compounds in polymers, only available for non-crystalline polymers.

Polar aprotic solvents possess an oxygen or nitrogen atom, exhibiting a lone pair of electrons and its S-shape is negative for  $\delta < 0$  and positive for  $\delta > 0$ .<sup>145</sup> Figure 30 shows the  $\delta$ -potentials of cellulose nitrate and polar aprotic solvents. The steeper S-shape, the more polar is the molecule. DMSO was predicted to have the highest affinity for cellulose nitrate paint, having the best proton acceptor affinity for this polymer (very steep curve, Figure 30 in purple). Cyrene presents a less dramatic drop at positive  $\delta$ , hence it was predicted not as good solvent as other polar aprotic solvents (Figure 30, in blue):

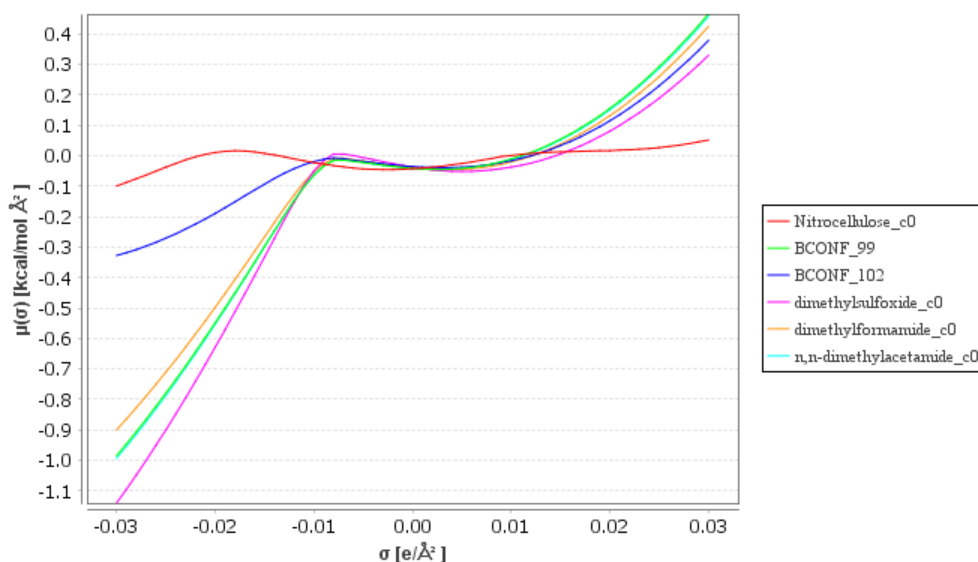


Figure 30:  $\delta$ -potentials of cellulose nitrate and polar aprotic solvents. Name “nitrocellulose” was given by the software. Cyrene and NMP were created manually, hence the labels “BCONF\_102” and “BCONF\_99”.

Figure 31 shows different  $\delta$ -potentials for the keto and enol forms of Cyrene’ hence, they have different physico-chemical properties, which can influence the predictive role of COSMOtherm.<sup>146</sup> The  $\Pi$ -shaped  $\delta$ -potential curve of Cyrene-enol (Figure 31b, in red) is negative, which corresponds to the hydrogen bond acceptor and hydrogen bond donor characters. Cyrene-keto form (Figure 31b, in green) possesses only one hydrogen acceptor group due to its  $sp^2$ -oxygen atom and its S-shape is negative for  $\delta < 0$  and positive for  $\delta > 0$ . Hence, the ketone form of Cyrene can only act as hydrogen bond acceptor, while the enol form can be both hydrogen bond acceptor and donor.

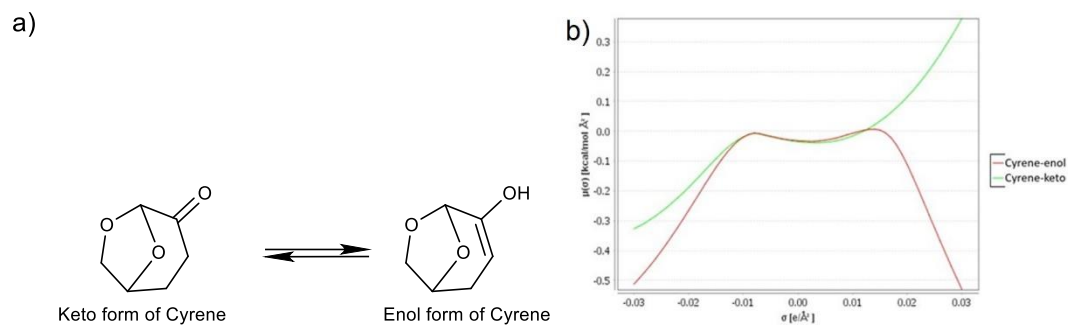


Figure 31: (a) Chemical equilibrium between the keto and enol forms of Cyrene and their (b)  $\delta$ -potentials (green for the ketone and red for the enol).

The results from the present study showed that Cyrene has ultimately not been predicted accurately in graffiti paint dissolution and removal because no conformers were calculated for the enol form of Cyrene. However, this software is a powerful tool in predicting solubility of a compound in a liquid solvent; however more parameters should be considered in the case of complex molecules for future uses.

### 1.5.5. Applications of Cyrene

Cyrene has proven to be bio-based, non-toxic, non-persistent and biodegradable, and subsequently gained great attention from scientists, being tested as a solvent for a multitude of applications.<sup>63, 147-149</sup> A summary of the key studies is reported in Table 10:

Table 10: Applications of Cyrene

| Applications of Cyrene                  | Reference                         |
|---|-----------------------------------|
| Organic synthesis                       | 147, 149-152                      |
| Graphene dispersion/exfoliation         | 148                               |
| Polymer production                      | 153, 154                          |
| Membrane technology                     | 63, 155, 156 (this work included) |
| Metal-organic framework (MOF) synthesis | 124                               |
| Biomass pre-treatment                   | 157                               |
| Solid-liquid extraction                 | 158 (this work included)          |
| Liquid-liquid extraction                | 159                               |
| Carbon nanotubes dispersion             | 160 and this work                 |
| Conductive inks                         | 161                               |
| Coatings                                | 162 and this work                 |
| Paint stripping                         | This work                         |

As seen in Table 10, Cyrene has been used as reagent and solvent in many applications since its discovery and was the subject of some reviews.<sup>163, 164</sup> These studies have also highlighted some drawbacks in use of Cyrene: it is unstable to acids and bases, has a high boiling point which involves high energy recovery (distillation) and its ketone moiety is very reactive, which represents a disadvantage in certain applications. Higher viscosity of Cyrene compared to the traditional polar aprotic solvents made it ideal for graphene exfoliation.

This thesis explores essential industrial chemical processes of neat Cyrene, its derivative or various solvent systems involving Cyrene. Neat Cyrene was not employed prior to this work in pristine carbon nanotubes dispersions, graffiti paint removal, or flavonoid extractions. Cyrene was used in poly(amide imide) wire enamels synthesis and for fabrication of filtration membranes; however novel solvent systems and casting membranes methodology were developed in this thesis for wire enamels and membranes fabrication, respectively. Also, new polymers have been used to prepare membranes using Cyrene for the first time (polysulfone, cellulose acetate and polyimide). Cyrene's

simplest derivative, Cygnet 0.0, is solid at room temperature, an unusual characteristic for an industrial solvent; however, mixing Cygnet 0.0 with Cyrene lead to a novel binary solvent system, which is a liquid at room temperature and makes it industrially useful. The use of a 50 wt% Cygnet-Cyrene mixture made a practical difference in solvent behaviour with polymers to produce flat sheet membranes from polyimide, polysulfone, polyethersulfone and cellulose acetate using non-solvent induced phase separation process (Chapter 6). Various mixtures of Cyrene with other solvents have been tested in this work, especially Cyrene-water blend. Different concentration of Cyrene mixtures in water and their dissolution ability has been tested and reported for the organic compounds.<sup>52</sup> The dissolution of these compounds was influenced by the Cyrene/water/geminal diol ratios found in the mixtures Cyrene-water. Mixtures of Cyrene in water were further used in this work to extract natural flavonoids from orange peel and tea leaves (Chapter 4).<sup>158</sup>

## 1.5.6. Toxicity profile of Cyrene

The chemical safety report for Cyrene has been submitted to ECHA with its technical dossier and the information on the environmental and human health hazard (including the exposure and risk) properties of the solvent are presented in Table 11:<sup>165</sup>

Table 11: Toxicological and ecotoxicological information

| Toxicological information |   |  |   |
|---------------------------|---|--|---|
|                           | Type of test  | Test guideline   | Results   |
| Acute toxicity            | Acute toxicity: oral                                | OECD 423 (Acute Oral Toxicity - Acute Toxic Class Method)  | No mortalities, toxicity or adverse necropsy findings. LD50>2000 mg/kg bw.  |
|                           | Acute toxicity: inhalation                          | OECD 436 (Acute Inhalation Toxicity)   | One male animal died at 120 minutes following exposure. LC50>5.16 mg/L.   |
| Irritation/corrosion      | Skin irritation                                     | OECD 404 (Acute Dermal Irritation/Corrosion)   | No evidence of skin irritation  |
|                           | Eye irritation                                      | OECD Guideline 437 (Bovine Corneal Opacity and Permeability Test)  | No corrosive/severe irritant properties.  |
| Sensitisation             | Skin sensitisation                                  | OECD 429 (Skin Sensitisation)  | Not sensitising to skin.  |
| Repeated dose toxicity    | Repeated dose toxicity: oral                        | OECD 422 (Combined Repeated Dose Toxicity Study with the Reproduction / Developmental Toxicity Screening Test) | NOAEL for systemic toxicity set to 1000 mg/kg bw/day. No systemic toxicity.   |
| Genetic toxicity          | In vitro  | OECD 471 (Bacterial Reverse Mutation Assay)  | Negative for mutagenicity to bacteria under the conditions of the test.   |
| Toxicity to reproduction  | Screening for reproductive / developmental toxicity | OECD 422 (Combined Repeated Dose Toxicity Study with the Reproduction / Developmental Toxicity Screening Test) | No systemic toxicity. The NOAEL for reproduction toxicity was established at the dose level of 1000 mg/kg bw/day.                   |
|                           | Developmental toxicity / teratogenicity             | OECD 422 (Combined Repeated Dose Toxicity Study with the Reproduction / Developmental Toxicity Screening Test) | No toxicologically significant differences. NOAEL for developmental toxicity was established at the dose level of 300 mg/kg bw/day. |



| Ecotoxicological information |  |  |               |                    |  |
|------------------------------|--|--|---------------|--------------------|--|
| Hazard for aquatic organisms | Acute toxicity to fish                               | OECD (Fish, Test)                      | Guideline 203 | Acute Toxicity     | No mortality or sub lethal effects of exposure observed in the test.               |
|                              | Acute toxicity to aquatic invertebrates (crustacean) | OECD (Daphnia sp. Immobilisation Test) | Guideline 202 | Acute              | No immobilized test organisms were observed over the test period of 48 hours.      |
|                              | Toxicity to aquatic algae and cyanobacteria          | OECD (Alga, Test)                      | Guideline 201 | Growth Inhibition  | Stable in the test media over the test period of 72 hours.                         |
|                              | Toxicity to microorganisms                           | OECD (Activated Respiration Test)      | Guideline 209 | Sludge, Inhibition | The 3 hours of 2–25 mg/L, confirming the suitability of the activated sludge used. |

Data sourced from ECHA<sup>2</sup>

All organisms have been exposed to geminal diol during the tests of Cyrene in aqueous media. As seen in Table 11, Cyrene was found un-harmful to aquatic life, having low eco-toxicity and no mutagenicity.<sup>115, 124</sup> Also, Cyrene is biodegradable in water 99% in 14 days. It was found that this bio-based solvent is eye irritant (H319) and has received ECHA level 7 certification (GHS07).<sup>97</sup>

### 1.5.7. Cradle-to-gate life cycle assessment (LCA) of Cyrene production

When considering sustainability, Life Cycle Assessment (LCA) and its parameters must also be considered: energy requirements, greenhouse gas emissions, ozone creation, total organic carbon, elements taken from the earth, eutrophication, and acidification. LCA is a process to evaluate the environmental burdens associated with the starting material acquisition, production, distribution, until the disposal associated with a process. LCA consists of an inventory (energy, raw material requirements and all emissions to the environment), an impact on the human and ecological health and the improvement assessment. Life cycle assessment of the production of Cyrene from cradle to factory gate was carried out by an industry association, one of the world's

<sup>2</sup> OECD- Organization for Economic Cooperation and Development. LC50-lethal concentration that kills 50% of the test animals during the observation period. NOAEL-no-observed-adverse-effect level is expressed in mg/kg bw/day (mg per kg body weight per day).

leading environmental and health consultancies “Ramboll”. LCA enabled understanding of overall carbon footprint of bio-based solvent along with primary drivers of the footprint.<sup>166</sup> LCA of Cyrene production process in Australia, from Ecoinvent database can be seen in Figure 32:

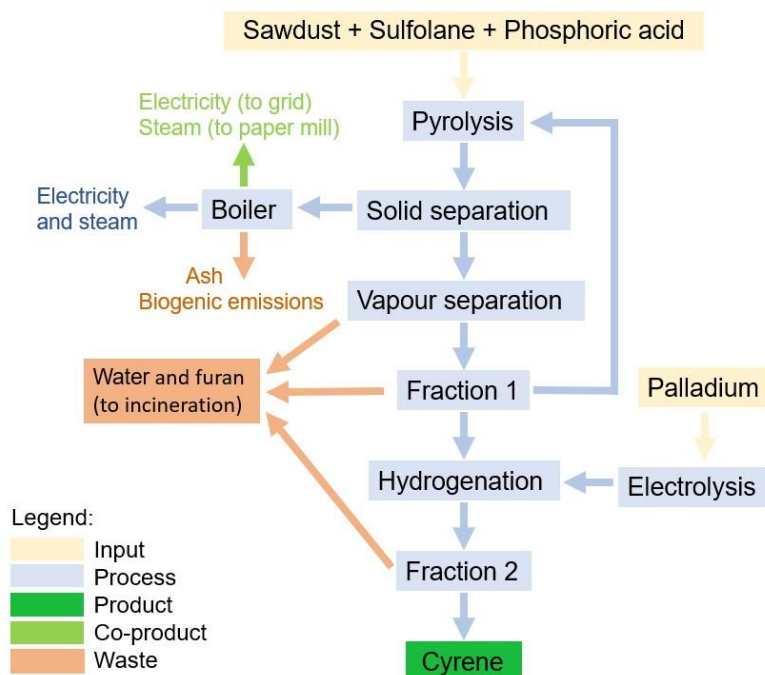


Figure 32: Life cycle assessment of Cyrene’s production using Furacell™ process. Adapted from reference.<sup>166</sup>

The life cycle inventory for obtaining 1 tonne of solvent were: sawdust (~30,000 kg), phosphoric acid (~1,000 kg), sulfolane (~30 kg), catalyst (<<1 kg), train transport (~6,000 t-km), sea transport (~200 t-km), start-up electricity (~5 kWh), waste water (~16,000 kg), boiler ash (~600 kg), waste solvent incineration (~20 kg), boiler CO<sub>2</sub> (36,000 kg), excess steam (~8,000 kWh), excess electricity (~7,000 kWh). The Furacell™ process was designed to operate using different feedstocks, including wastes, depending on what is available (geographic location and seasonality). The demonstration plant is limited in size and resides in an existing pulp and paper facility neighbouring a managed forest is helpful in limiting its environmental impact and achieving the aims of sustainability. The solvent, sulfolane, is recycled and used again, the char co-product has a calorific value that meets the energy demand for the process and used as a carbon sequestering agent.<sup>167</sup> The phosphoric acid was decided on the primary basis that it is a strong, dehydrating acid, but also it means the char can be used as a fertiliser. The start-up electricity and the wastewater are also considered in LCA. To evaluate LCA, Global Warming Potential (GWP) and biogenic greenhouse gas (GHG) emissions were analysed, and the main sources of environmental burdens identified. The Greenhouse gases (GHGs) absorb energy and do not let escape to space, warming the Earth. Different gasses give different effects of insulating the Earth. The GWP compares the global

warming impacts of different gases, using CO<sub>2</sub> as reference (GWP of 1). GWP is measures how much energy the emissions of 1 ton of a gas will absorb over a given period of time, compared to the emissions of 1 ton of carbon dioxide.<sup>168</sup> When accounting biogenic GHG emissions, general considerations for bio-based products were considered: carbon fixation rate of the feedstock, avoided emissions from natural decomposition or burning, harvesting effects on soil carbon, mineral carbon, below-ground biomass, land use change, effects outside the system boundary (e.g. increased demand for one feedstock may reduce demand for another), biomass losses in supply chain, carbon embodied in final product. In this study, the boiler emissions from the biochar are biogenic and some carbon is sequestered in the product, though due to many applications its final fate is unknown. However, ISO 14067 standard suggests that GHG emissions from combustion of biogenic carbon to be excluded (with some exceptions). In addition, GHG Protocol Product Life Cycle Accounting Standard implies that biogenic (from natural sources) and non-biogenic emissions (CO<sub>2</sub> from combustion) and uptake should be presented separately. The resulting environmental profile of Cyrene production through the Furacell™ process was compared to production of NMP and showed a more favourable profile than the latter. As shown in Figure 33, the carbon footprint of Cyrene production is much smaller than NMP.

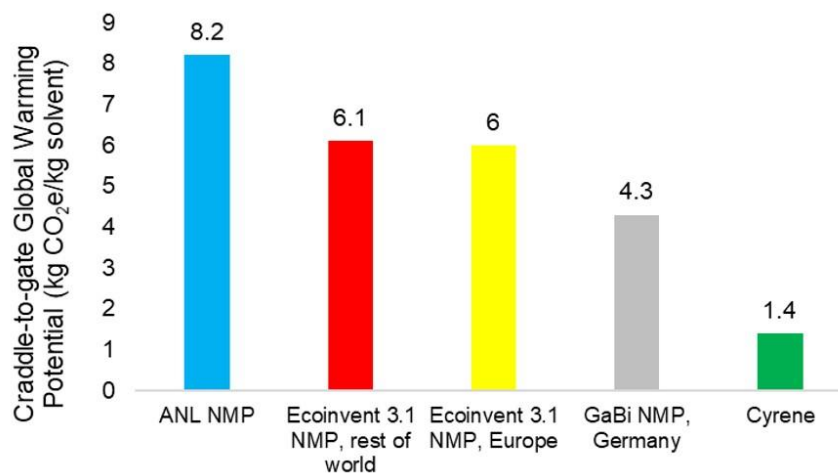


Figure 33: Footprint of Cyrene (IPCC 2013 Impact Assessment Method) was realised in the context of NMP's, which was realised by Argonne National Laboratory (ANL), Ecoinvent database version 3.1 and GaBi life cycle assessment. Adapted from reference.<sup>166</sup>

Process emissions from NMP manufacturing plants has had less impact in developed countries than rest of the world. It is most important that the sustainability of the manufacturing process of Cyrene is scrutinised, and improvements are still to be made in collaboration with suppliers to achieve a sustainable process.



# Chapter II

## 2. Application of Cyrene in graffiti paint removal<sup>3,4</sup>

---

<sup>3</sup> This chapter was adapted from the article "*Cyrene™, a sustainable solution for graffiti paint removal*", manuscript in preparation.

R.A. Milescu performed the cleaning experiments under the supervision of Dr C.R. McElroy. Dr J. Sherwood has provided the training on HSPiP. Dr T. J. Farmer, Dr. J. Sherwood, Dr C.R. McElroy and Prof J.H. Clark participated to writing of the article.

<sup>4</sup> This chapter was adapted from the article "*Solvent applications of short-chain oxymethylene dimethyl ether oligomers*", published in ACS Sustainable Chemistry & Engineering.

R.A. Milescu performed the dissolution of polyvinylpyrrolidone, poly(amide imide), polyethersulfone and polystyrene in oxymethylene dimethyl ethers (OME<sub>3-5</sub>) and removal of acrylic and cellulose nitrate-based graffiti paint from ceramic tiles.



## 2.1. Introduction

Graffiti (plural form of Italian “graffito”, meaning “scratch”) have existed as long as human civilisation with the first wall drawings appearing in caves thousands of years ago. They were simple sketches, symbols of animals or symbols of a hand or a foot, describing the life and hunting expeditions of the prehistoric men. Later, more complex drawings appeared on the walls, *e.g.* Jesus Christ with a donkey head meant to insult Christians.<sup>169</sup> Graffiti have changed over time in their visual appearance, types and motivation.<sup>170</sup> This phenomenon escalated at the start of 1970s in the wake of hip-hop culture when “graffiti art” became popular mostly in many cities. Modern graffiti is constantly progressing, and the public knows the name of some graffiti artists such as Banksy (UK), Cornbread and Daze (USA), Lady Pink (Ecuador), Millo (Italy), Smug (Scotland), Amara (Sweden), Okuda (Spain) or Saddo and Pren (Romania).<sup>171</sup> Some of them expose their artwork in galleries, museums, and special allocated street walls around the world, where artists go by their nicknames, so that they are easy for the public to remember and generate a bit of “mystery”. In Romania, the graffiti movement was prohibited by the communist leader Nicolae Ceausescu and the first graffiti appeared after the collapse of the Communism in 1989. Nowadays, there are street art exhibitions in Bucharest, where graffiti artists from around the world can paint freely on specially designated street walls.<sup>172</sup> Many examples of graffiti are illicitly sprayed without any artistic intention, during public events where monuments, buildings and vehicles are vandalised and are often associated with social decline.<sup>173, 174</sup> They often contain offensive remarks, hate statements and politically or racially insulting language. Spraying graffiti is generally seen as socially dangerous, moreover criminal, an offence under the Criminal Damage Act of England and Wales (1971).<sup>175</sup> In the UK and USA it is prohibited to sell aerosols to anyone under the age of 16, as part of graffiti abatement programs.

The invention of aerosol spray paints encouraged proliferation of graffiti drawings and are widely used due to their visual impact, quick application, availability and low price.<sup>176</sup> The large variety of graffiti formulations and brands of commercial paints has enabled graffiti artists to produce long-lasting work. Due to a current lack of knowledge of how these particular paints behave during cleaning process, these longer-lasting paints present a considerable challenge for those wishing to remove this graffiti. For effective removal of the graffiti paint, knowledge of the composition is an important factor. However, this information is commonly unknown to the user and cleaner due to many complex formulations remaining classified. Traditionally, graffiti is removed from buildings and monuments as soon as their presence is acknowledged. However, on some occasions graffiti is removed after long periods of environmental exposure (*e.g.* UV light, rain, atmospheric pollutants such as SO<sub>2</sub>, SO<sub>3</sub>, NO<sub>x</sub>, extreme conditions) or human intervention

(unsuitable cleaning or restorations techniques) when the paint interacts with these cleaning agents and with the substrate, accelerating the ageing of the paint products.<sup>177, 178</sup> Paintings and statues from museums and storage premises in particular are easily affected by interior light, humidity, inorganic pollutants, volatile organic compounds and temperature, putting their integrity and preservation at risk.<sup>179</sup> After ageing, graffiti paints changes physically and chemically (*i.e.*, crosslinking), becoming difficult to remove and leaving more residue behind.<sup>180, 177, 181, 182</sup>

Traditional methodologies of graffiti removal, such as laser technology, mechanical and chemical methods described are often ineffective for graffiti removal. Solvents are not always effective in graffiti removal due to the insolubility of graffiti paint or the chemical contamination of the substrate treated; they also pose health risks and environmental problems with their disposal. As many environmentally friendly graffiti removing techniques do not provide satisfactory performance, there is an increasing consumer demand to develop both effective and environmentally friendly cleaning products. Therefore, this study proposes a simple strategy to facilitate a safe and effective chemical cleaning procedure, using Cyrene. Cyrene is safe to use as a solvent, with no other known health issues than eye irritation (Section 1.5.6.).

## 2.2. Graffiti removal technologies - Background

Graffiti cleaning is usually fairly expensive and difficult to perform successfully. Graffiti removal from public spaces and cultural heritage represents nowadays a priority area and novel methodologies of graffiti removal are continuously developed.<sup>176, 183</sup> The use of lasers to remove graffiti is the most active research area (accounting for *approx.* 50% of research papers), followed by chemical, mechanical (water pressure washer, blade and brush scraping, sandblasting) and biological technologies.<sup>176, 184</sup> These methodologies are generally expensive, demand high energy, damage the substrate and are toxic. It is also common for graffiti to reappear after the surface is cleaned attracting more graffiti artists; hence removal of the paint is only temporary.<sup>185</sup>

The negative environmental impact of wastes generated during graffiti cleaning also need to be evaluated as large amounts of toxic solvents are released into the environment without proper disposal. In selecting the most optimum cleaning method, the type of staining agent (chemical composition) and substrate that has been vandalized (wood, metal, stones with different porosities) need to be considered. There is no single or universal removal technique that will effectively remove all graffiti paint worldwide. Consequently, different methods need to be available. In some cases, different technologies can be used together for effective graffiti



removal.<sup>186, 187</sup> In the following sections, a review of different methodologies for graffiti removal from different substrates will be discussed.

### 2.2.1. Laser technology

Laser cleaning is the most commonly used technology in paint removal as it can be used on expensive and sensitive substrates, where often the value of the artwork or monument and the environmentally friendly effects are more important than the cost of the technology.<sup>188</sup> Consequently, graffiti from cultural heritage objects are usually removed *via* laser to avoid damaging the surface.<sup>189, 190</sup> Laser cleaning works *via* ablation, where beam irradiation (pulse or continuous wave laser) breaks down the matrix of the paint so that it can be easily removed physically.<sup>191</sup> Laser removal presents advantages compared to the other methodologies:

- The process of cleaning is controllable and secure, offering localised action, feedback and identification of the substrate when combined with analytical techniques,<sup>192</sup>
- Selective removal of the material (each substance absorbs light at different wavelengths),<sup>193, 194</sup>
- A rapid and clean method,
- No solvents are used and thus this method is more environmentally friendly.

The effectiveness of laser removal depends on the nature of the substrate (roughness and porosity),<sup>195</sup> the optical properties of the pigment and resin,<sup>196</sup> the type of laser employed (*i.e.*, pulse length and wavelength)<sup>194</sup> and the depth of paint penetration.<sup>196</sup> The colour of pigments presents in the paint affects the results of laser-based graffiti removal. White paint is easily extracted by laser from stone, whereas black, blue, green and red paints are more difficult to clean and leave yellow stains.<sup>190</sup> Silver paint is the most difficult to clean *via* this method, due to its reflective aluminium-rich composition and ability to form a translucent film rich in aluminium particles.<sup>196</sup> The type of laser used can influence graffiti removal. The Nd:YVO4 ultraviolet laser at 355 nm can efficiently remove red and blue acrylic-based graffiti.<sup>187</sup> It has also been demonstrated that the third harmonic ( $\lambda=355$  nm UV), when combined with the solid-state of a Nd:YAG ultraviolet laser detaches the pigment and the resin base without damaging the substrate, while the second ( $\lambda=532$  nm) removes the pigment but leaves some acrylic resin behind.<sup>193</sup> Similar results were obtained using a 308 nm XeCl excimer laser which removed the paint completely, whereas at 1064 nm infrared Nd:YAG laser could eliminate the pigment but left some resin behind and contaminated the substrate.<sup>194</sup>

However, this technology of graffiti paint removal present disadvantages:

- The process is generally expensive,
- Mineralogical alterations caused by the surface ablation damage, generating hazardous micro powders and toxic substances,<sup>184, 189</sup>
- Laser irradiation affects the inorganic pigments, changing the crystalline phase or chemical composition.<sup>197</sup>
- The “yellowing” (or ghosting) caused by the migration of the discoloured pigments, chemical agents, solid residues resulted from the ablation of some elements (*i.e.*, iron) present in the substrate.<sup>197, 198 197</sup>

### 2.2.2. Mechanical techniques

Mechanical methods are economical, easy to use, but are often too abrasive, leading to substrate damage, as well as generating pollutants through the release of solvent, paint residues and fine blasted portions of the substrate. The mechanical technology overall acts on the surface of a substrate and only detaches small portions of graffiti at the time.<sup>184</sup> The type of resin and pigments are not the important factors in mechanically removing graffiti, but the porosity of the substrate. The porosity influences the depth of the paint penetration and hence the removability from the surface of the substrate. High-pressure washing and mechanical methods (*i.e.*, abrasive brushing and sandblasting) are used to remove graffiti from highway structures, where graffiti is a significant hazard to road safety.<sup>199, 200</sup> In this case, high pressures are needed to aggressively blast away the paint. The pressure and the particles from sandblasting have an abrasive effect and irreversibly damage valuable surfaces. A pressure washer can be expensive and hazardous due to the high temperatures and pressure employed. To minimise these effects, micro-blasting and low-pressure steam are used. A gentle micro-blasting method using a mixture of air, water and abrasive SiO<sub>2</sub> microparticles (called “Hydrogommage”) at low-pressure was found to be effective in the extraction of polyethylene silver paint, alkyd and polyester-based red, black and blue paints.<sup>187</sup> This method however is still abrasive and increases the roughness of stones.

### 2.2.3. Biological methods

Biological methods succeed where traditional methods fail, in terms of selectivity and provide a selective and safe technology for both the environment and humans.<sup>201, 202</sup> This method uses living microorganisms (*e.g.* bacteria, yeasts) to remove or cover paints through biodegradation and bioremediation respectively.<sup>203, 204</sup> The mechanism of biological cleaning consists of ester group hydrolysis into carboxylic groups, making the resins more hydrophilic and ultimately, easier to remove *via* aqueous cleaning systems containing active microorganisms.<sup>202, 205</sup> The biological method has its limitations; the type of resin used in graffiti paint dictates the removability of the paint. Acrylic resin does not degrade by the action of enzymes or some bacteria, whilst alkyd resins are biodegradable.<sup>206</sup> Bioremediation uses bacteria to generate a protective calcium carbonate layer, in order to preserve historical monuments or buildings, but risks posed by aesthetic and mineral changes are yet to be addressed. Yeasts accelerate coating deterioration and produce non-toxic metabolites and are therefore considered more environmentally friendly and safe to use.<sup>207, 208</sup>

### 2.2.4. Chemical treatment

Chemical cleaning of graffiti targets the paint directly leading to its dissolution and extraction. This method is an economical solution and uses neat solvents or their mixtures, gels and poultices.<sup>173, 209, 210</sup> The mechanism of chemical cleaning consists of weakening the adhesion between the paint and the substrate (using solvents such as acetone and DCM) or breaking down the alkyd-based paints through saponification (*e.g.* caustic alkali).<sup>184, 211</sup>

The advantages of this method are displayed below:

- This method is cited as one of the easiest to use and most economical,
- No additional roughness is induced in the substrate,<sup>187</sup>
- Quick application and action on large areas,<sup>184</sup>
- This method does not induce melting and detaching of biotite grains in granite,<sup>187, 212, 213</sup>
- The chemical agents do not decompose the calcite in marble,<sup>214</sup>
- Yellowing by discolouration of pigments or formation of by-products was not reported when using chemicals<sup>187, 197, 213, 215</sup>

Irritant effects of chemical cleaners cannot be ignored. Solvents used in graffiti removal commonly pose health risks and environmental issues associated with their disposal. Approximately half of

the solvents used globally are in the coatings and paints sector<sup>47</sup> and many of them are toxic and classified as substances of very high concern, through the EU's REACH regulations. In a sustainable world, the graffiti remover should contain no substances, which are toxic or present long-term health or environmental problems. The demands for greener cleaner products indicate the chemical paint removers should contain low VOC concentrations, fast performance across a wide range of coatings on different substrates, cheap raw materials, avoid damaging the substrate, and contain safer chemicals for the human health and the environment. Alternative halogen-free stripping formulations often have the disadvantage that they require relatively long action times, they only strip one layer of paint at time and hence require multiple applications for efficient cleaning.

Solvents are not always effective in graffiti removal because of the insolubility of the graffiti paint, or the chemical contamination of the substrate treated (related to paint residues and the dissolved materials entering the pores of a substrate). Solvent application can also result in chemical agents remaining in the substrate along with the dissolved materials which is considered a potential risk to human health.<sup>216</sup> The chemical methods using pure solvents can cause irreversible damages to the paints (*i.e.*, cross-linked polymers originated from the chemical change of the aged paints) which then can penetrate into the substrate, resulting in a "ghosting" effect.<sup>184</sup> This phenomenon makes the removal more difficult; in this case, lifting the paint off is desirable. There are anti-ghosting products specially designed for cleaning the chemically contaminated substrates and are based on harsh lightening and bleaching agents.<sup>217</sup> The effective solvents and poultices may discolour stone in some cases, leave tide marks or harmful salt residues behind.<sup>218</sup> As current environmentally friendly graffiti removers do not provide satisfactory performance, there is an increasing consumer demand to develop improved and more benign cleaning products.

### 2.3. Anti-graffiti coatings

One method that has been developed to prevent graffiti are the use of anti-graffiti coatings (often used as gels or peelable sheets). These are designed to prevent damages caused by the use of graffiti by preventing the paint from entering the substrate's system in the first place by: forming a protective barrier against the graffiti.<sup>174, 219</sup> They are based on waxes<sup>220</sup> and polyurethane<sup>221</sup> polysaccharides, fluorine,<sup>220</sup> silicon-based resins<sup>222</sup> and organic-inorganic hybrids,<sup>223</sup> nanocomposite materials.<sup>224</sup> These particular gels are used to increase the stability and life expectancy of murals and represent new tools to artists, conservators and authorities to face the challenge of graffiti vandalism. Anti-graffiti coatings in the form of peelable sheets, often used as

“zero tolerance” policy can be applied for example onto windows in public transportation but are expensive and inefficient in some cases. The pore size and the voids from a substrate dictate the way the paint penetrates through the protective anti-graffiti coatings and ultimately, dictate the cleaning effectiveness.<sup>184</sup> Micro-cracks generated from their application can inadvertently enable graffiti paint to penetrate deeper into the protected substrate, resulting in more difficult paint removal, even when applied in a thicker layer.<sup>225</sup> Paint can also penetrate through anti-graffiti coatings, due to the low glass transition temperature.<sup>220</sup> An un-cured protective coating allows the paint to penetrate more easily to the substrate than a cured coating. This feature is very important, and it is decisive in the resistance of a protective coating.

## **2.4. Environmental implications and health issues generated by graffiti removal**

In the majority of cases, cleaning agents are highly volatile, flammable or corrosive. In order to limit the risks associated with the cleaning processes, the harmful potential of the cleaning agents needs to be evaluated and the cleaning process involved further optimised. Where possible, toxic agents should also be replaced with safer counterparts, ideally without a drop in paint removal efficiency. Many chemical agents are based on volatile organic compounds (VOCs) which has been linked to ozone formation and pose a health risk to the user. These often include aromatics (toluene, xylene), amides (NMP and other pyrrolidones, DMAc, DMF), ethers (THF, dioxane), esters (carboxylic esters such as  $\gamma$ -butyrolactone (GBL)), halogenated hydrocarbons (DCM), alcohols or ketones (acetone, cyclohexanone).<sup>177, 226-231</sup> The agents used to clean graffiti are often irritants to the skin and eyes and are transport through the skin into internal organs, through inhalation, ingestion and skin absorption.<sup>226, 232-237</sup> Most of the time they are highly volatile, flammable or corrosive and pose a risk to the environment and have a limited effect on the removal of certain paints. DCM has been widely used for paint/graffiti removal. However, in 1990 this solvent was recognised as highly toxic and was suspected a potential carcinogen. NMP was found to be “less toxic and biodegradable” and replaced DCM in some paint strippers.<sup>238</sup> In 2017, both DCM and NMP present in paint strippers were associated with deaths in the USA and were finally prohibited from these products.<sup>239</sup> NMP was finally restricted by REACH in 2018, according to Commission Regulation (EU)2018/588, stating that paint removers should not consist of more than 0.3% by weight of NMP after 9 May 2020 in the EU, unless appropriate measures are taken to protect the workers involved.<sup>103</sup> The REACH regulation of Derived No-Effect Levels (DNELs)

limits the exposure of workers to only 14.4 mg/m<sup>3</sup> NMP by inhalation and 4.8 mg/kg/day for dermal exposure.<sup>240</sup> DCM is classed by Classification, Labelling and Packaging regulation (CLP) as a carcinogen category 2 chemical and is fairly volatile (with a B.P. of 39.8 °C and vapour pressure 584 hPa at 25 °C) and therefore can easily be released into the air. Consequently, DCM use in paint stripping formulations was restricted to ≤0.1% by weight for general consumers in 2010 and was extended to “professionals” in 2012. DMF and DMAc are also toxic to the reproductive system. Moreover, DMF has been recently proposed to be added to the EU’s REACH’s restricted substances list.<sup>84</sup>

The agents used to clean graffiti are often associated with reports of headache, fatigue and eyes, nose, or skin irritation. Increased contact time with these agents can lead to more damage and in some cases chronic symptoms and even death. Three potential routes of exposure to the solvent are possible during the graffiti removal: inhalation, ingestion and absorption through the skin of the volatile organic solvents among them industrially important compounds such as DMAc,<sup>233</sup> DMF<sup>234</sup> and glycol ethers.<sup>232, 235-237</sup> Eight-hour work shift experiments were created to evaluate the level of exposure to organic solvents of graffiti removers.<sup>232</sup> NMP is a mild irritant in short time exposure (8-hour exposure to 50 mg m<sup>-3</sup>).<sup>232, 241</sup> After a longer time exposure to NMP (2 days) the effects are mild to severe with irritant effects for eyes and skin.<sup>242</sup> Studies on animal high level exposure of NMP lead to repro-toxic effects such as malformations and resorption.<sup>243</sup> Use of protective mask and gloves showed reduced NMP uptake, while protective clothing showed a slight increased uptake due to the constant dermal exposure with the solvent soaked in the clothing.<sup>232</sup> NMP is mildly irritating to the eyes, the skin and the mucous membranes and has shown reprotoxic effects in rats.<sup>244, 245</sup> As dermal exposure of liquid NMP was faster than inhalation of airborne NMP, percutaneous uptake (dermal route) is the more relevant risk. Generally, percutaneous and absorption of solvent vapours from ambient air are the most significant route of exposure particularly for amphiphilic compounds with a low vapour pressure.<sup>246, 247</sup>

In the case of the mechanical methods, the harm consists of from the pressure jets containing water, chemicals, and sand particles, which can be very dangerous if not properly used. Working with lasers can cause damage to the eyes and skin.<sup>248</sup> Lasers in the ultraviolet spectrum can cause damage to the cornea and eye lens and cause retinal damage. A Q-switched Nd:YAG laser beam is especially dangerous because the beam is invisible and as the retina does not contain pain nerves, the damage can go undetected for years. For safe use of laser in graffiti cleaning, laser cleaning must take place with extraction equipment. To avoid inhalation of residues, shields and protective glasses need to be worn.

The negative environmental impact of wastes generated during graffiti cleaning also need to be evaluated. Large amounts of toxic solvents and removed paint are often released in the

environment, presenting a hazard to animals and humans. Spills caused by graffiti cleaning (from laser, mechanical and chemical methods) irreversibly endangers the environment and clean-up operations are expensive. As a result, more environmentally friendly paint-stripping solutions must be found and taken into consideration to prevent toxic chemical spillages occurring in the first place. To replace NMP, structurally similar solvents such as 1-ethyl-2-pyrrolidone and *N*-methylcaprolactam have been used in formulations. But *N*-methylcaprolactam is also toxic, causing skin and eye irritation. However, 1-ethyl-2-pyrrolidone is less toxic than NMP. Caustic paint strippers such as sodium, calcium and magnesium hydroxide in basic water-based solutions exhibit health issues such as severe skin burns and lung irritation. These products have also negative effects on the substrate, darkening the wood and increasing the grain size. Dimethyl carbonate is also used as a green solvent and has been incorporated into hybrid silica gels to clean graffiti.<sup>209</sup> Mixtures of  $\gamma$ -valerolactone (GVL)/water or  $\gamma$ -valerolactone/ $\gamma$ -butyrolactone/water have been used to clean paint, varnish and lacquer film from metal, wood, wool and textiles.<sup>249</sup> A low-toxic solvent ternary mixture formed from ethyl alcohol, acetone and iso-octane has been used in combination with laser for a low or medium-risk cleaning procedure for removing graffiti from monuments and heritage architecture.<sup>250</sup> Environmentally-friendly graffiti removal compositions commonly contain DMSO and biodegradable esters for paint and graffiti removal<sup>251</sup> or esters of soybean oil fatty acids<sup>252</sup>, dicarboxylic acid diester (such as Rhodiasolv Iris)<sup>253</sup> or dibasic esters.<sup>254</sup> DMSO is a safe solvent, compared to NMP, DMF and DMAc, but should be avoided when in composition with toxic solvents, as it can transport toxic solvents through the skin into internal organs.<sup>255, 256</sup> Dibasic esters (DBE), which are mixtures of dimethyl adipate, succinate and glutarate, are non-flammable, biodegradable, non-corrosive and non-irritant solvents, which can soften paint, thus minimising the destructive effect on the substrate itself during the scrapping procedure.<sup>257</sup> The toxic solvents used in paint stripping are currently replaced with a safer alternative, but some issues still remain; their efficiency in dissolving and extracting the paint off a substrate is still to be addressed.

## 2.5. Graffiti paints and substrates

### 2.5.1. Acrylic and cellulose nitrate aerosol paints

Paints usually consist of synthetic polymers such as acrylics, alkyds and a cellulose nitrate binder (used as a matrix for the adhesion of the paint on a surface), pigments (to give the colour of paint), a solvent (for easy spreading), and additives. The additives provide great adhesive properties, roughness in the film, water resistance, UV stability, increase bulk in the coating and reduces the cost of the paint).<sup>258</sup> In some cases, large size pigments are used as extenders (to reduce the amount of expensive binder required). Acrylic paints have been used since the 1930s and are the most used product in coatings. They are mostly based on poly-acrylate binders consisting of acrylate, methacrylate, styrene and their copolymers.<sup>259</sup> The modern paints are required to use a minimum amount of solvent or to be solventless for environmental considerations. For a solventless system, the thermoplastic powder coatings can be adjusted by adding water or be crosslinked during their application to make up for lack of solvent. The main monomers used are acrylic acid, acrylates (methyl, ethyl or butyl), methacrylate (methyl or butyl) (Figure 34) and styrene (not pictured).

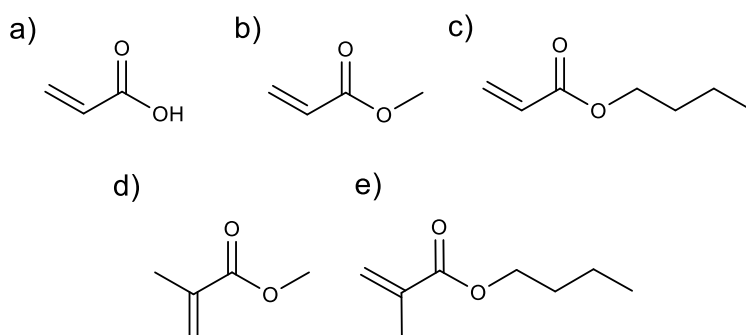


Figure 34: Molecular structures of monomers used in acrylate polymers: (a) acrylic acid, (b) methyl acrylate, (c) butyl acrylate, (d) methyl methacrylate and (e) butyl methacrylate.

Acrylic monomers (Figure 34) are used in paint formulations, based on their suitability for different applications. Methyl methacrylate is used for its weather resistance, hardness, gloss, and gloss retention. On the other side, styrene reduces gloss retention, but increases hardness and is chemically resistant. Alkyl acrylates and methacrylates are flexible and hydrophobic, whilst acrylic acid and methacrylic acid increase adhesion to metals. Compared to the other types of paint binders, acrylate resins present several advantages:

- High chemical resistance,



- Suitability under numerous weather conditions and outdoor conditions,
- High stability under UV radiation and resistance to hydrolysis,
- They display a special gloss and gloss retention.

The paints are produced through emulsion polymerisation of one or more acrylic monomers in the presence of water and a surfactant.<sup>260</sup> The water evaporates and the remaining molecules lock the pigment into a solid, stable film. The solvent-borne coatings are preferred in humid environments as they evaporate faster. However, the solvent-borne paints are less environmentally friendly due to the VOC-generating solvents used, which are traditionally petroleum-based, but must be used in difficult conditions.

Cellulose nitrate, another type of resin used in paint, is the nitrate ester of cellulose, synthesised by treating cellulose to nitric and sulfuric acids (Figure 35):<sup>261</sup>

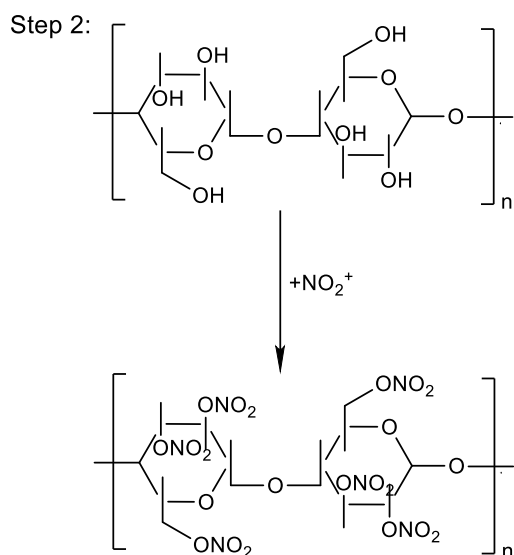
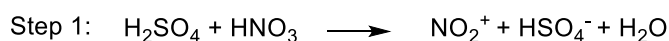


Figure 35: Synthesis of cellulose nitrate.

Cellulose nitrate as a resin is highly flammable with a low auto-ignition point. When burned, it does not leave a residue, but releases nitrogen dioxide gas, which is very toxic. The properties of cellulose nitrate resins differ depending on the amounts of reagents and conditions. The amount of nitrogen present in the compound dictates the stability and solubility in different solvents. A "high nitrogen" (nitrate content) form is less stable (used mostly in explosives) and it is less soluble in conventional solvents. A "low-nitrogen" amount (one-two nitrate groups per glucose repeat unit) is more stable and has a greater solubility in many solvents and is therefore used in household and commercial applications.<sup>262</sup> The solvents used in cellulose nitrate resins need to

evaporate easily and they need to be the same for all the raw materials. Esters (ethyl, butyl, or propyl acetate) and ketones (acetone, MEK) are mostly used for this purpose and sometimes alcohols for a cheaper price.<sup>262</sup>

The aerosol paints used in this work were acrylic and cellulose nitrate-based and are from a sealed, pressurised can and are released when a valve button is depressed, releasing the paint in a smooth and even coat. These spray paint are portable, cheap, and easy to store and apply on surfaces. Graffiti medium is widely used as a medium for these aerosols due to their speed, portability, and permanence. The acrylic and cellulose-based graffiti aerosols used in this study are seen in Figure 36:



Figure 36: (a) Acrylic aerosols paints and (b) cellulose nitrate used to (c) spray paint the porous and non-porous substrates

Both acrylic and cellulose nitrate paints are cleaned from porous and non-porous substrates differently when using different technologies, no method is perfect for a single type of binder. Acrylic paint was found to be removed successfully from marble when using an ultraviolet laser.<sup>184</sup> The cellulose nitrate paint graffiti was previously removed using chemical and laser methodologies. A mixture of ethanol, acetone and xylene (components normally found in their formulation), ultraviolet and infrared lasers removed cellulose-based paints from limestone and sandstone.<sup>210</sup> Previously, both acrylic and nitrocellulose graffiti paints were found to be soluble in polar solvents, widely used as paint strippers.<sup>210</sup> In this work, Cyrene was assessed in a chemical cleaning of these graffiti aerosols from a non-porous and a porous substrate and compared to the commonly used polar aprotic solvents. Also, Cyrene was found to be less hazardous than NMP or DCM and its use in paint removal could be an essential step in more environmentally friendly paint removal.

## 2.5.2. Porous and non-porous substrates

In this work, two types of substrates, a smooth non-porous aluminium foil (Figure 37a) and a porous ceramic tile (Figure 37b) are used in graffiti cleaning by chemical procedures. The American Society for Testing and Materials (ASTM) defines a ceramic material as “an article having a glazed or unglazed body of crystalline or partly crystalline structure, or of glass, which body is produced from essentially inorganic, non-metallic substances and either is formed from a molten mass which solidifies on cooling or is formed and simultaneously or subsequently matured by the action of the heat”.<sup>263</sup> Ceramic Tile Institute of America (CTIOA) defines ceramic as “an inorganic, non-metallic solid prepared by the action of heat and subsequent cooling”.<sup>264</sup>

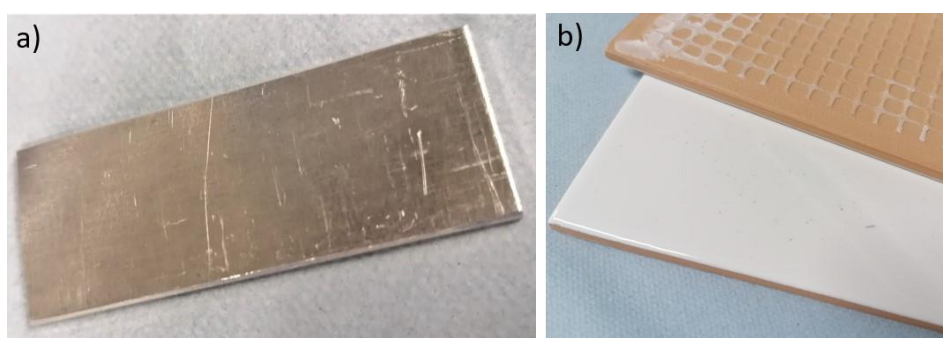


Figure 37: (a) Aluminium foil and (b) ceramic tile used in this work.

Ceramic materials can be partly/fully crystalline or amorphous (glass). Most common ceramics are crystalline, hence their definition is often restricted to inorganic crystalline materials, as opposed to the non-crystalline glasses.<sup>264</sup>

Ceramic materials are classified into three categories:

- Oxides (aluminium oxide, zirconium oxide),
- Non-oxides (carbides, borides, nitrides and composed of silicate and atoms such as tungsten, magnesium, platinum, titanium), and
- A combination of oxides and non-oxides.<sup>265</sup>

Ceramic tiles used for decoration, are generally made from natural clay, sand, feldspar, quartz, and water, and covered in decorative, waterproof, paint-like glazes. Ceramics contain  $\text{SiO}_2$  in largest proportion, metal oxides, C, N and S.<sup>266</sup> The stoneware ceramic such as wall, floor tiles and sanitary ware are produced from white and red calcined-clay wastes resulted from the ceramic industry.<sup>267</sup> Ceramic tiles used in this study were analysed by an Inductively Coupled Plasma-Mass Spectrometer (ICP-MS) and the results shown in Table 12:

Table 12: Inductively Coupled Plasma-Mass Spectrometer analysis of ceramic tiles

| Element | Concentration (%) |
|---------|-------------------|
| Al      | 5                 |
| Ca      | 2.9               |
| Fe      | 0.9               |
| Na      | 0.7               |
| Mg      | 0.2               |
| K       | 0.1               |
| P       | 0.03              |
| Zn      | 0.008             |
| Mn      | 0.008             |
| Cr      | 0.005             |
| Ba      | 0.004             |
| Ni      | 0.002             |
| Pb      | 0.0007            |
| Cu      | 0.0006            |
| Se      | 0.0003            |
| Co      | 0.0003            |
| As      | 0.0002            |
| Sn      | 0.00008           |
| Cd      | 0.00003           |
| Sb      | 0.000005          |

As seen in Table 12, Al and Ca, the ceramic tiles used in this work could indicate the oxide and non-oxide nature of the ceramic material used. The results indicate the presence of toxic elements such as Ba, As, Pb and Cd.

## 2.6. HSPiP's predictive role in graffiti removal

Hansen Solubility Parameters (HSPs) have been used to predict the dissolution of polymeric coatings in solvents and find new suitable candidates for their removal from porous and non-porous substrates. Two sets of cleaning tests were performed: immersing and poultice tests. Previously, a ternary fractional parameter solubility diagram (Teas graph) based on dispersion, hydrogen bonding and polar forces of the solvents was used to report the effectiveness of the individual or mixtures of solvents.<sup>250, 268</sup> In this study, we use HSPs to predict the dissolution of polymeric graffiti paint in pure solvents.<sup>127, 139</sup> The interaction between the solvents and both acrylic and cellulose graffiti paint was initially investigated by immersing the coated porous ceramic tiles in vials containing different individual solvents. Ranking scores were given by naked eye (Figure B 1 in Appendix B). Polar protic, polar aprotic (including Cyrene) and non-polar solvents were used to remove graffiti paint from non-porous and porous substrates. OME<sub>3-5</sub> (a mixture of oxymethylene dimethyl ethers)<sup>269</sup> and TMO (2,2,5,5-tetramethyloxolane) were tested for graffiti removal due to their low toxicity. OME<sub>3-5</sub> (with the formula H<sub>3</sub>CO-(CH<sub>2</sub>O)<sub>n</sub>-CH<sub>3</sub>, where n=3-5) has solvation properties similar to 1,4-dioxane, is water insoluble, presents less peroxide formation and may replace polar aprotic solvents in applications such as polymer recycling, or cleaning applications.<sup>269</sup> TMO is a non-peroxide forming ether which replaces common hydrocarbons such as toluene.<sup>40</sup>

In the case of acrylic paint (Figure 38a), the software predicted Cyrene, NMP, DMF, DMAc, DMSO and THF as the best solvents, with a relative energy difference (RED) smaller than 1 (Table 13). Cyrene has the smallest RED, which makes it the best solvent in this case too. Toluene and acetone have bigger RED, but they proved to be good solvents in practice, with a score of 2. DMAc, DMSO and THF have RED <1, but reality shows a lower solubility capacity of this paint. However, HSPiP software has only a predictive role in material dissolution in another, forming a solution.

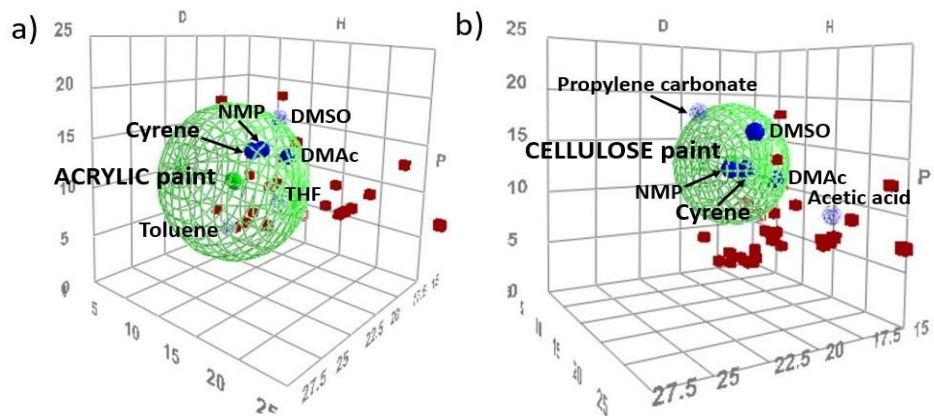


Figure 38: Acrylic paint (a) and cellulose (b) paints in Hansen sphere. Only the good solvents (blue spheres) are named here.

Table 13: Hansen Solubility Parameters of different solvents and RED calculated for acrylic graffiti paint

| Solvent                        | $\delta_D$ | $\delta_P$ | $\delta_H$ | Score | RED    |
|--------------------------------|------------|------------|------------|-------|--------|
| Cyrene                         | 18.9       | 12.4       | 7.1        | 1     | 0.546  |
| <i>N</i> -Methyl-2-pyrrolidone | 18         | 12.3       | 7.2        | 1     | 0.722  |
| <i>N,N'</i> -Dimethylacetamide | 16.8       | 11.5       | 9.4        | 2     | 0.984  |
| Dimethyl sulfoxide             | 18.4       | 16.4       | 10.2       | 2     | 1.014* |
| Tetrahydrofuran                | 16.8       | 5.7        | 8          | 2     | 1.051* |
| Toluene                        | 18         | 1.4        | 2          | 2     | 1.347* |

\* Wrongly predicted position of the solvents in Hansen space ( $RED > 1$ ). Only the good solvents are shown in this table. Hansen solubility parameters of the solvents are sourced from HSPiP database and expressed in  $MPa^{1/2}$ .

The polar protic and non-polar solvents removed partially or did not remove the graffiti, including ether solvents OME<sub>3-5</sub> and TMO. However, toluene was more efficient than its safer counterpart, TMO. Toluene has proven to be a compatible solvent for dissolution of acrylic paint, due to its low polarity but high polarisability, which allows it to respond to the higher polarity of the acrylic polymer. Based on the three Hansen parameters and scores given after the immersion test (visual test), the software predicted Cyrene, NMP, DMAc, DMF, DMSO, propylene carbonate (PC) and acetic acid as the best solvents in cellulose-based paint dissolution (Figure 38b and Table 14), with a  $RED < 1$ .

Table 14: Hansen Solubility Parameters of different solvents and RED calculated for cellulose-based graffiti paint

| Solvent                        | $\delta_D$ | $\delta_P$ | $\delta_H$ | Score | RED    |
|--------------------------------|------------|------------|------------|-------|--------|
| <i>N</i> -Methyl-2-pyrrolidone | 18         | 12.3       | 7.2        | 1     | 0.422  |
| Cyrene                         | 18.9       | 12.4       | 7.1        | 1     | 0.528  |
| <i>N,N'</i> -Dimethylacetamide | 16.8       | 11.5       | 9.4        | 1     | 0.855  |
| Dimethyl sulfoxide             | 18.4       | 16.4       | 10.2       | 1     | 0.903  |
| Propylene carbonate            | 20         | 18         | 4.1        | 2     | 0.983  |
| Acetic acid                    | 14.5       | 8          | 13.5       | 2     | 1.991* |

\* *Wrongly predicted positions of the solvents in Hansen space. Only the good solvents are shown in this table. Hansen solubility parameters of the solvents are sourced from HSPiP database and expressed in MPa<sup>1/2</sup>.*

As seen in Table 14, comparing the RED of NMP and Cyrene, a smaller relative energy difference makes Cyrene the best solvent (the smaller RED, the better solvent) for cellulose-based aerosol. Propylene carbonate has a small RED, but the practice showed that it is not as efficient as DMSO, DMAc or DMF.

## 2.7. Graffiti paints characterisation by infrared spectroscopy

The acrylic and cellulose nitrate graffiti paints infrared spectra (Figure 39) are difficult to interpret due to the presence of the binder, pigments and possibly additives in the aerosol paints.<sup>270</sup>

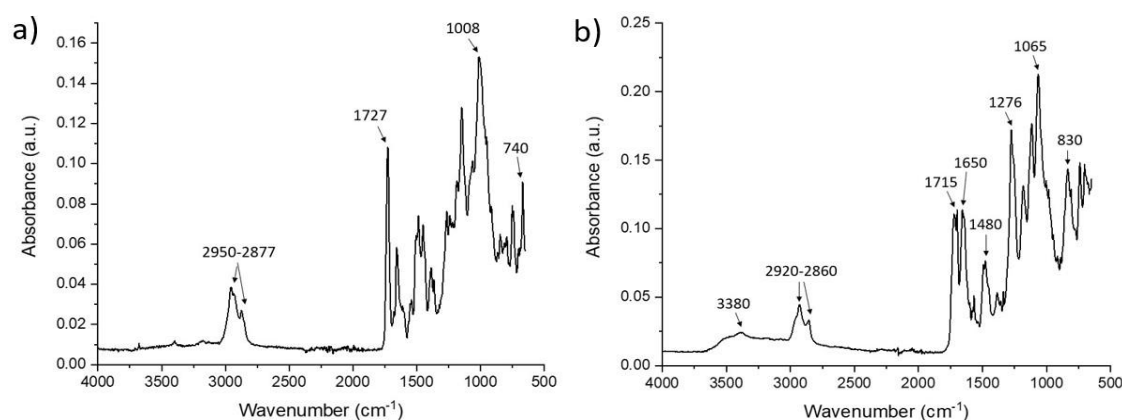


Figure 39: (a) Infrared spectra of acrylic and (b) cellulose nitrate-based graffiti paints.

The detected signals from acrylic graffiti paint (Figure 39a) indicates the presence of C-H asymmetric stretching vibrations ( $2960\text{--}2870\text{ cm}^{-1}$ ). The C-O-C stretching vibration of esters can be observed in both paints at  $1008\text{ cm}^{-1}$  for acrylic paint and  $1065\text{ cm}^{-1}$  for cellulose nitrate paint (Figure 39b). The strong bands are present around  $1700\text{ cm}^{-1}$  attributed to C=O stretching vibration and present in both paints. The presence of carbonyl group in cellulose nitrate paint can be related to its presence in paint additives or from the oxidation of cellulose (nitration step is strongly oxidising). The peak at  $740\text{ cm}^{-1}$  is attributed to primary alcohols groups. The strong peaks at  $1650$ ,  $1276$  and  $830\text{ cm}^{-1}$  of the cellulose nitrate graffiti paint show vibrations of  $\text{NO}_2$  group.<sup>271</sup>

## 2.8. Effectiveness of the cleaning tests

### 2.8.1. Chemical cleaning performance using the immersion tests

Initially, three colours of acrylic and cellulose nitrate graffiti paints were used in this study: white, red and black (Figure B 2). One layer of paint was used to stain the pieces of aluminium slides onto 60% of their surface and left to dry for a week (Figure B 2a). Ceramic tiles were only painted on their glazed surface (Figure B 2b) for a quick immersion test (one hour). The results of the dissolutions were very similar for all three colours. In order to minimise the amount of solvent used, also time and energy, smaller ceramic tiles and less solvent were used. The colour red was chosen to be used further due to its widespread use by graffiti artists and its increased difficulty of removal compared to other colours.<sup>272</sup> This paint colour has attracted much attention from researchers in their attempts to remove it from different substrates.<sup>176, 270, 273</sup> Dissolution of both cellulose and acrylic paints from aluminium slides (Figure B 3) occurred very fast in NMP. In Cyrene, the paint has swollen, and it has been gently removed, using wiping paper towel. Red graffiti was previously removed using pure solvents such as ketones, alcohols, esters, carbonates, aromatics and alkanes with the best results from acetone and methyl ethyl ketone (MEK).<sup>268</sup> In the same study, the orange paint was difficult to remove and was only partially removed. As seen in Figure B 1 in Appendix B, the dissolution of acrylic and cellulose graffiti paint from a porous substrate shows different results. At the first look, NMP cleaned the paint efficiently from the porous side of the ceramic tile. However, the solvent residue left after the acrylic graffiti cleaning process using NMP showed a yellow colour (Figure 40a), which indicated changes of the paint from red-orange to a yellow colouration of the solvent. A new ceramic tile was immersed in NMP and tapped using a soft tissue; a yellow layer can be observed on the surface of the porous substrate (Figure 40a).



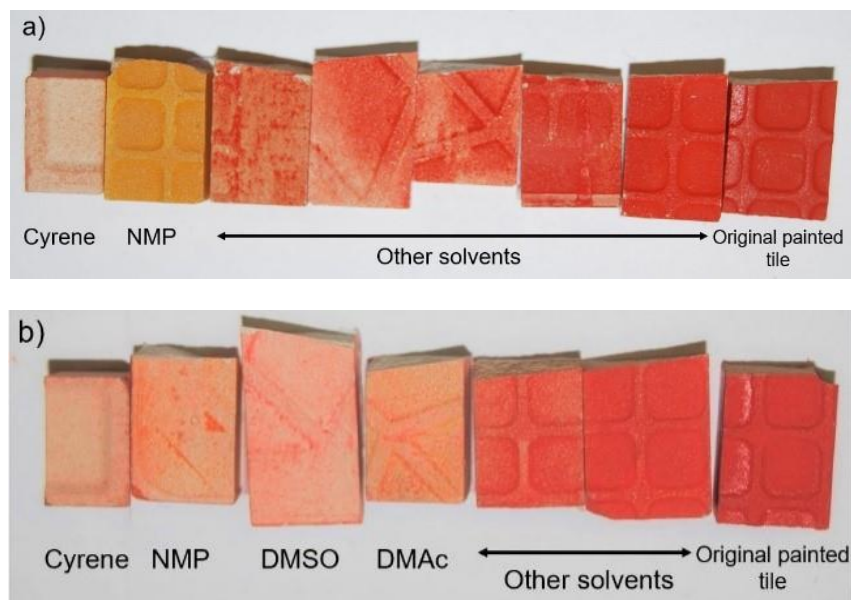


Figure 40: (a) Immersion tests result of the coated tiles with acrylic and (b) cellulose nitrate paint after cleaning using different solvents. An original painted tile is shown for comparison.

When cleaning a cellulose-based aerosol paint, NMP and DMAc also left the substrate partly yellow (Figure 40b). When the yellow layer is removed, the tiles exhibit “shadowing”, phenomenon seen on highly porous surfaces after laser and chemical cleaning.<sup>198</sup> Interestingly, DCM did not dissolve acrylic nor cellulose graffiti paints used in this work, which was widely used in the past. DCM’s poor performance may be attributed to the more complex formulation of the modern aerosols. The acrylic graffiti was mostly detached from the porous substrate only by Cyrene; however, traces of red pigments can still be seen on the surface of the ceramic tile. A clear solution and a yellow solid residue can be observed after chemical cleaning of the acrylic aerosol by DMAc, NMP and THF (Figure B 5a). The tiles cleaned by DMAc and THF still contain red pigments and are not labelled in Figure 40a. The yellow residue could represent the discoloration of red pigments which have partially dissolved in the solvent during the rolling process and was further analysed.

A Leica S6D Microscope was employed to visualise the shadowing effect after the acrylic paint removal using Cyrene and NMP. As seen in Figure 41 1b and 2b, Cyrene cleaned the paint of both porous (ceramic tile) and non-porous substrates (aluminium slide) without paint discoloration. However, when using NMP to clean a painted surface, yellow residues on both surfaces can be observed (Figure 41 1c and 2c):

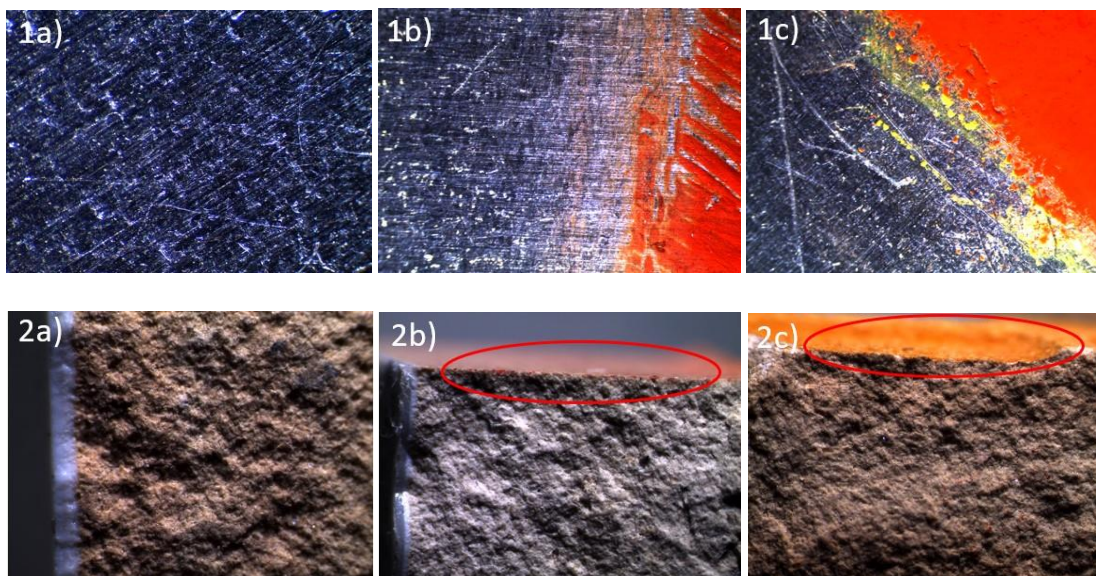


Figure 41: (1a) Top view of a pristine aluminium slide, (2a) cross-sectional optical microscope image of untreated ceramic tile and the cleaning results of both painted substrates using (b) Cyrene and (c) NMP. The grey colour from 2b is due to the light, no changes in the material were observed.

Water-based stripping formulations where water accounted for 50-70% were reported in mixtures with DCM, NMP, dibasic esters, benzyl alcohol and other polar solvents.<sup>274-276</sup> However, these solvents are toxic, and a safer water-based formulation for paint removal would be beneficial for the user and environment. As Cyrene has cleaned the graffiti paint from both porous and non-porous substrates but water has proved to be inefficient in paint removal, a mixture of 75% Cyrene-25% H<sub>2</sub>O was tested in this work. HSPiP predicted this mixture as good solvent system for acrylic and cellulose-based graffiti paint cleaning (Table A 4 and Table A 5 in Appendix A). However, as seen in Figure 42, the acrylic graffiti aerosol (Figure 42b) was removed better by the new solvent mixture than the cellulose-based paint (Figure 42c). The tiles were still wet, hence the yellow colour seen in Figure 42b.

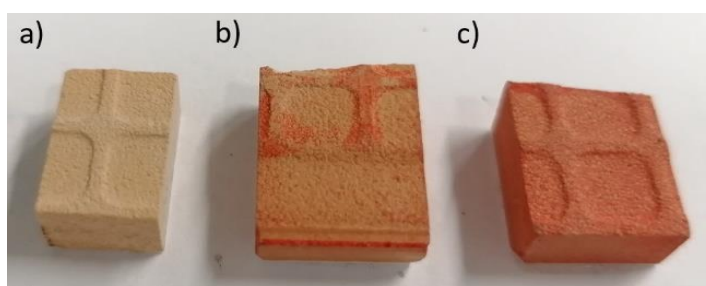


Figure 42: (a) Pristine tile, (b) acrylic and (c) cellulose-based graffiti paint removal from porous ceramic tiles using 75% Cyrene-25% H<sub>2</sub>O mixture (% v/v).

For future work, other mixtures of Cyrene and water are considered for a more detailed study of new water-based graffiti paint removal formulations. Moreover, HSPiP could be used in future work to create other binary and even ternary solvent systems suitable for graffiti paint removal.

## 2.8.2. Chemical cleaning performance using poultices

This testing method shows the best reality of cleaning materials, using a poultice formed out of absorbent material and solvents, followed by scraping this off after drying.<sup>209</sup> This method is used to prevent solvents from penetrating the substrate with any paint residues and permanently discolouring or staining the stoned substrates (“ghosting effect”). Retaining of solvents in gel matrices presents several advantages comparing to a using liquid cleaning agents:<sup>204</sup>

- This method detaches the graffiti paint without direct contact or the operator with solvents, which are often toxic,
- Less solvent is left in the underlying layer, which minimises the health effect on the user,
- The spills of pure toxic solvents are avoided.

In many cases, commercially available cleaning compositions are not able to penetrate micrometre-sized pores of fine-pored stone tiles and thus dissolve and remove dyes’ particles. Hydrogels and nanofluids, such as micelles or micro-emulsions, on the other hand, are found to be effective in selective removals.<sup>173, 183, 277</sup> In this work, in case of graffiti removal using poultices, the paste can dry and the resin is drawn into the poultice by capillary action. The paint residues were scraped off a non-porous substrate easily with the poultice when using both NMP and Cyrene leaving behind a clean surface (Figure 43 a and b):

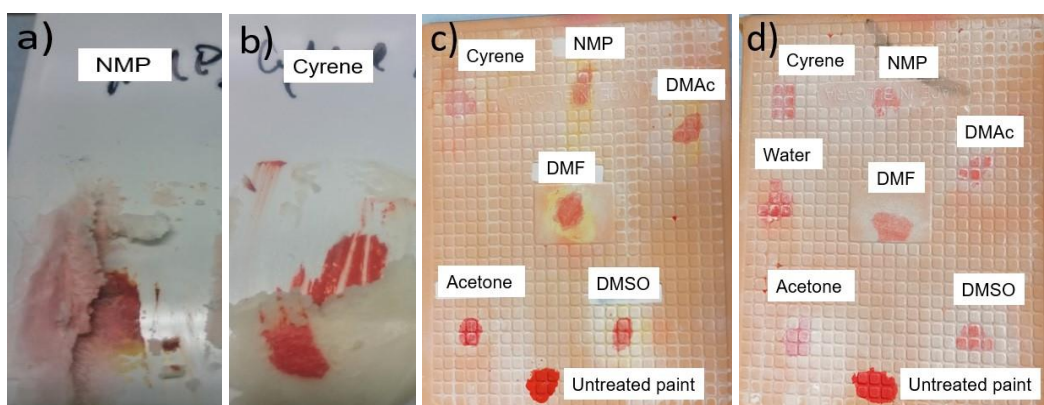


Figure 43: (a) Results of the poultice test of acrylic graffiti paint removal from the glazed side using NMP and (b) Cyrene. A porous tile was stained using (c) acrylic and (d) cellulose-based graffiti and the spots cleaned using various solvents, including Cyrene.

However, a porous substrate is more difficult to clean due to the porosity and void connectivity which determine the extension and depth of this shadowing generated by the solvents (Figure 43 c and d).<sup>187</sup> Generally, the shadows are further cleaned by an anti-ghosting product for better results; but these bleaching products are harsh to the substrate and can be environmentally damaging. Therefore, a selection of solvents which minimise the use of these agents can be very beneficial. As seen in Figure 43, NMP, DMF, DMAc all left a shadow after the acrylic graffiti paint removal; Cyrene removes the paint, without yellowing the substrate. This is likely because the first group of solvents dissolves the red pigment and extracts it from the pores but does not dissolve the yellow pigment, leaving this as a residue or discolouring the red pigments. DMSO left a wet spot for longer due to its high boiling point (189 °C) unlike acetone, which evaporates rapidly (with a boiling point of 56 °C). Acetone was more efficient than other solvents in the dissolution and removal of cellulose-based paint as part of a poultice (Figure 43d). Generally, smaller solvent molecules, such as acetone, penetrate rapidly into the coating, but in most cases, they also evaporate rapidly, which could be disadvantageous in some applications. However, acetone is a cheap and relatively green solvent and is widely used in paints removal. Larger solvent molecules often require considerably more application time and often lead to swelling of the paint/coating, which can then be rubbed off mechanically from the substrate more easily. Evaporation time possibly explains why NMP poultice colours red during the process (NMP evaporates faster) than Cyrene-based poultice which appears coloured at the interface with the paint only (Figure 127c in Section 7.3.).

### **2.8.3. Mechanism of graffiti removal from porous and non-porous substrates**

During the painting process, the molecules in the paint wet the substrate and are adsorbed onto surface forming interfacial bonds (attractive van der Waals forces) with the surface.<sup>278</sup> Generally, when wetting occurs, the paint fills any gaps or holes and is held mechanically when the paint hardens (*aka* mechanical interlocking). When a good wetting occurs between the substrate and paint, adhesive bridges over the surface irregularities are formed and the interfacial flaws are minimised or even eliminated. In some cases, when the paint is compatible with the substrate (*i.e.*, when paint contains reactive functional groups, such as hydroxyl or carbonyl), chemical bonds are formed at the interface between paint and the substrate. By chemical cleaning, the graffiti acts directly on the paint and leads to its dissolution and extraction. In the process of graffiti dissolving in a solvent, the cohesive forces in the paint break down and affect not only the inner

strength of a material, but the adhesive strength between the paint and substrate too, ultimately leading to both dissolving and lifting off the paint film.

Mechanisms of graffiti removal are proposed herein in Figure 44:

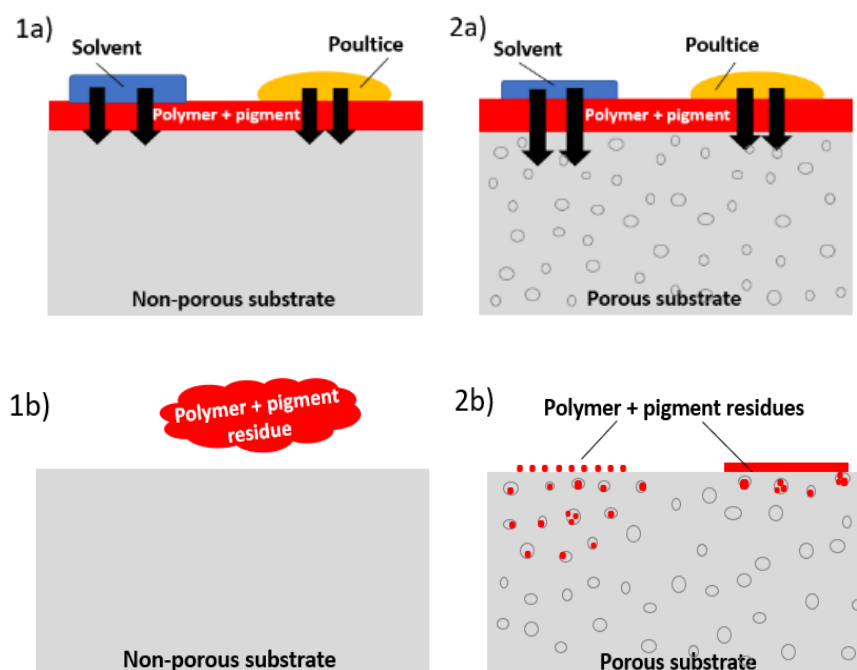


Figure 44: Mechanism proposed to explain the graffiti removal from the (1a) non-porous and (2a) porous substrate using pure, individual solvents and poultices. (1b) The results of graffiti removal from a non-porous substrate and (2b) of a porous substrate using pure, individual solvents and poultices.

Solvents are generally efficient on smooth areas, but are less effective when used on porous substrates, often with the “ghosting” effect occurring and chemically contaminating the substrates. In these cases, the cleaning only occurs partially. The removal of graffiti gives the same good results for pure solvents as poultice from a non-porous substrate (Figure 44 1b). In case of a porous substrate, the pure neat solvents migrate through the polymer deeper and faster detaching the polymeric graffiti from a porous substrate (Figure 44 2b), causing chemical contamination of the substrate. A poultice is less efficient in removing the paint from a porous substrate, but also the chemical contamination is less visible, as the solvent is less prone to migrate into the pores.

The cleaning of acrylic and cellulose-based graffiti paint by NMP and Cyrene differs in the way the dissolution occurs. NMP detaches both paints from the substrate and dissolves it after one minute of rolling or shaking the vial (Figure 45c and d). Fast lifting off observed for NMP is explained by the slightly higher value of vapour pressure (Table 15). Cyrene needed a longer time,

one hour when using the rollers or 20 minutes of continuous shaking before the solvent started dissolving the acrylic paint layer by layer (Figure 45a). The same amount of time is needed by Cyrene to lift off the cellulose-based paint, in large pieces, from the substrate before dissolving (Figure 45b).

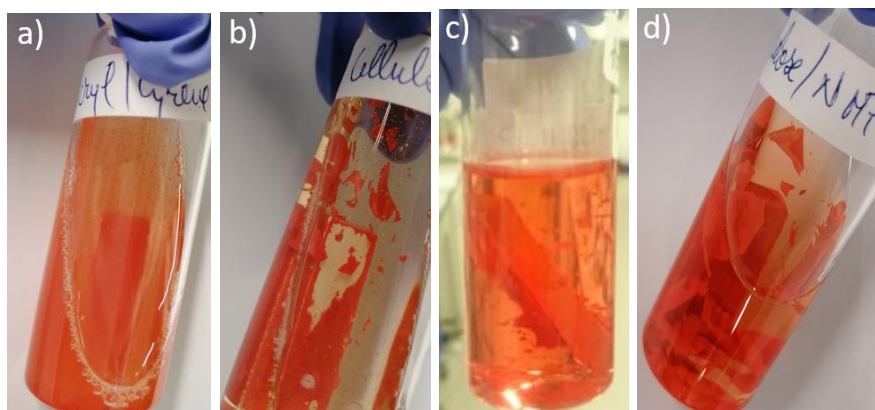


Figure 45: (a, c) Mechanism of acrylic and (b, d) cellulose-based graffiti paint using (a, b) Cyrene and (c, d) NMP.

In some cases, this phenomenon of lifting off is desirable in order to avoid the chemical contamination of the substrate (*e.g.* wood, art objects) and using Cyrene in these applications could represent a facile method of controlled cleaning. Cyrene lifts off and dissolves the paint after 1 hour (using rollers) which could allow paint removal whilst, avoiding the solvent and any residues from entering the pores of the substrate. This process of dissolution was associated with the vapour pressure and surface tension of the solvents used to remove graffiti paint (Table 15):

Table 15: Vapour pressure and surface tension of the tested solvents

| Solvent | Concentration (%) | Vapour pressure (hPa) | Reference temperature (°C) | Surface tension (mN/m) at 17-22 °C |
|---------|-------------------|-----------------------|----------------------------|------------------------------------|
| Cyrene  | 99.0              | 0.28                  | 25                         | 72.5                               |
| NMP     | 99.0              | 0.32                  | 20                         | 40.4                               |
| DMSO    | 99.0              | 0.55                  | 20                         | 43.5                               |
| DMAc    | 99.5              | 2.00                  | 22                         | 36.0*                              |
| DMF     | 99.8              | 3.80                  | 20                         | 37.0*                              |
| Acetone | 99.8              | 245.00                | 20                         | 23.2                               |
| DCM     | 99.5              | 584.00                | 25                         | 26.5                               |

Data was collected from Sigma Aldrich (Merck) and \*reference<sup>279</sup>

After penetrating the paint, highly volatile solvents lift the paint as they flashback through the paint film and affects paint removability. DCM performance in graffiti removal has been associated in the past with its vapour pressure: extremely fast evaporation rate which shortens its work life and was better than NMP.<sup>280</sup> In this study, the vapour pressure influenced the removability of the paint when using poultices. As seen in Table 15, Cyrene has a slightly lower vapour pressure than NMP, explaining the longer time needed to dissolve and lift the paint. The trade-off is one of stripping speed versus the toxicity of the solvent inhaled. NMP works faster but is reprotoxic, while Cyrene needs a longer time to strip off the paint and it is an irritant to eyes. Acetone, however, has a high vapour pressure, which was associated with an immediate effect on lifting the superior layer of the paint. However, this phenomenon of fast lifting could be disadvantageous in a thick layer of paint, and repetitive application of solvent onto stain could be necessary for a more effective cleaning. Surface tension influences the speed of paint stripping; a fluid with low surface tension can lift off the paint faster than a high surface tension-based solvent.<sup>281</sup> As seen in Table 15, Cyrene has almost twice the surface tension of NMP and almost three times of DCM, which could explain the lower stripping speed of Cyrene. Generally, the surface tension can be lowered by adding a surfactant or increasing of temperature; however, is not a common practice in paint stripping.

## 2.8.4. Physico-chemical changes to the paint during the chemical removal of graffiti paint

Acrylic paint removal by NMP showed a yellow residue; Cyrene, however, did not exhibit this colouration of the substrate at the end of the procedure of graffiti removal. Hence, both acrylic (Figure 46a) and cellulose-based paint (Figure 46b) were further analysed for their solubility in NMP and Cyrene:

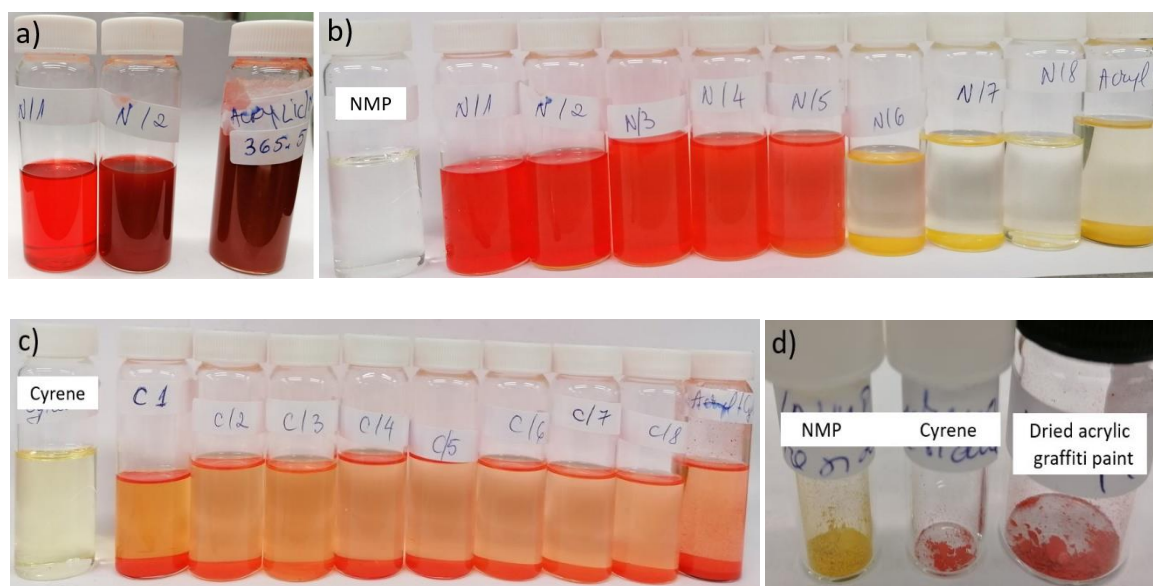


Figure 46: (a) Stages of the acrylic graffiti paint dissolution in NMP from red to dark-red. (b) Pure NMP on the left followed by none successive washings and the last vial is the resulted residue and clean solvent, (c) shows pure Cyrene on the left followed by none successive washings and the last vial is the resulted residue and clean solvent (d) the residues after washing alongside the dried paint.

After dissolution, the solution was decanted, and the residue was further washed with pure solvent. After 8 repeated dissolutions and decanting the solvent, yellow and red residues remained using NMP and Cyrene (Figure 46c). Figure 46a shows how NMP discolours the pigments in the acrylic paint, from bright red to dark red (Figure 46a), and back to red, then to orange and ultimately to yellow. It is possible that NMP selectively dissolves the red pigments while the yellow pigments remain unaffected at the end of the process. However, a temporary change of colour followed by returning to its initial colour has been previously reported for Pb, Co and Fe-based pigments during laser cleaning and is related to pigment decomposition and change in mass of the inorganic material.<sup>282</sup> Cyrene does not selectively dissolve the pigments, as both acrylic- and cellulose-based paints are dissolved effectively.



In order to analyse the differences between the residue from acrylic paint removal using NMP and Cyrene, the infrared spectra of both samples were compared to the original acrylic paint (Figure 47):

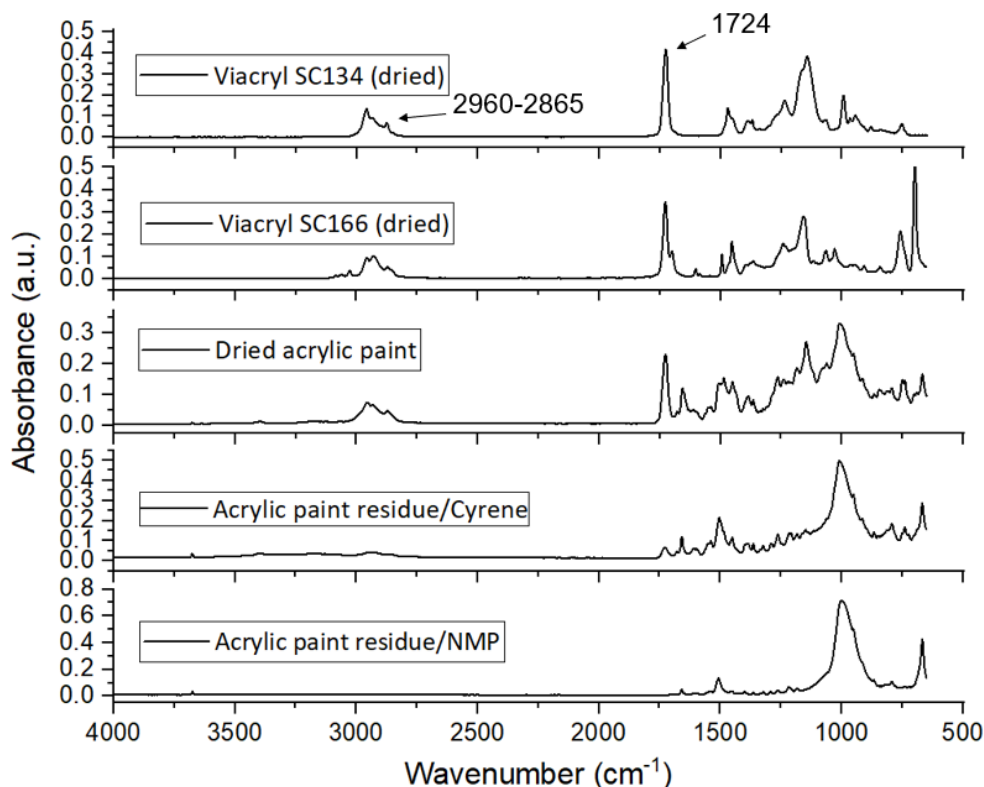


Figure 47: Infrared spectra for the red acrylic paint cleaned by (in red) Cyrene and (in blue) NMP. Two acrylic resins (in green and magenta) are shown here for comparison.

The broad band  $2960\text{-}2865\text{ cm}^{-1}$  is attributed to C-H stretching and the peak at  $1726\text{ cm}^{-1}$  is attributed to C=O stretching in ester vibration and are visible in two acrylic resins (Viacryl SC134 and Viacryl SC166) and in the Kobra acrylic paint. These bands are much weaker for Cyrene or have even disappeared for NMP. This means that the acrylic resin from the paint has partially dissolved in Cyrene and has fully dissolved in NMP. The broad band around  $1000\text{ cm}^{-1}$  could be related to a metal oxide ( $\text{SiO}_2$ ,  $\text{Al}_2\text{O}_3$ ,  $\text{TiO}_2$ ). However, the solid residue generated by the chemical cleaning of graffiti aerosol was further analysed by ICP-MS. In this work, the inorganic material from the paint and the solid residue generated by the acrylic graffiti paint removal by NMP was analysed by ICP-MS and the results can be seen in Table 16:

Table 16: Inorganic content of the residues obtained after the acrylic paint dissolution in NMP and Cyrene

| Element | Dried acrylic paint (%) | Solid residue resulted from cleaning using Cyrene | Solid residue resulted from cleaning using NMP |
|---------|-------------------------|---|--|
| Mg      | 1                       | 2.3   | 3.5  |
| Ca      | 0.3                     | 0.14  | 0.59   |
| Al      | 0.2                     | 0.5   | 0.9  |
| P       | 0.14                    | 0.07  | 0.11   |
| Fe      | 0.08                    | 0.2   | 0.3  |
| Ba      | 0.05                    | 0.1   | 0.2  |
| Na      | 0.04                    | 0.0026  | 0.0024   |
| K       | 0.023                   | 0.027   | 0.05   |
| Ti      | 0.013                   | <0.001  | 0.079  |
| Zn      | 0.003                   | 0.006   | 0.02   |
| Mn      | 0.003                   | 0.004   | 0.01   |
| Cr      | 0.0003                  | 0.0007  | 0.001  |
| Pb      | 0.0003                  | 0.0001  | 0.0006   |
| Ni      | 0.0003                  | 0.0007  | 0.0008   |
| Sn      | 0.00017                 | 0.0023  | 0.0004   |
| Cu      | 0.0001                  | 0.001   | 0.004  |
| Se      | 0.00005                 | <0.0000005  | 0.00008  |
| Cd      | 0.000035                | 0.000026  | 0.00005  |
| Co      | 0.00003                 | 0.00007   | 0.0001   |
| As      | 0.000027                | 0.000034  | 0.0001   |

The differences in the amount of inorganic material between the acrylic paint Kobra and the residues of chemical cleaning using NMP could suggest a discolouration of the pigment and ultimately their physical and chemical change. The discolouration of the pigments has been previously covered by studies concerning laser cleaning of graffiti.<sup>197, 198</sup> It was previously shown that Pb, Co and Fe-based pigments decomposed under laser ablation and oxidised to black oxides, regaining their colour after a while when the oxidation was reversed.<sup>282</sup> A change in colour of the acrylic paint in NMP (Figure 46a), where NMP discoloured the acrylic paint and then reversed it to red colour. Also, an increase in the inorganic mass in the residue can be observed in Table 16).

This could indicate the decomposition of the pigments in NMP. The acrylic graffiti aerosol used in this study is red orange. Red pigments contain cadmium (Cd), mercury (Hg), arsenic (As), iron (Fe), silicon (Si), aluminium (Al), zinc (Zn), bromine (Br), titanium (Ti), calcium (Ca), chlorine (Cl).<sup>270</sup> Ti-based pigment, TiO<sub>2</sub>, is a white pigment, but it is widely used in paint formulations to inhibit photocatalysis processes and to make the colours more pronounced.<sup>210</sup> Additionally, the yellow and orange pigments possibly contained in the aerosol contain Mg, Cd, Ca, Ba, K, chromium (Cr) and tin (Sn). Magnesium (Mg) pigments are yellow-green and it is mainly used in paint for the corrosion protective role, similar to Zn and Cr.<sup>283</sup> Sulphur is usually mixed with metallic pigments such as arsenic (As), cadmium, Hg, Cr and lead and it is guilty of blackening them. As and Hg are poisonous and not used nowadays, however, As is present in small amount in the acrylic aerosol used in this work (Table 16).

## 2.9. Chapter conclusion

Cleaning of city infrastructure and cultural heritage offers many challenges for scientists and conservators because of its irreversibility leading to lasting modifications and damages of the art materials. Chemical methods of graffiti paint removal are among the most economical cleaning technologies; however, they can penetrate and damage the substrate and are toxic to the user. To answer to these needs, a safer and efficient solvent was sought. A series of systematic tests were performed, comparing a range of solvents for cleaning several substrates and investigating two different red paints, acrylic and cellulose-based. The cleaning efficiency of Cyrene was studied in this work and compared to the commonly used solvents in this application. Aluminium foil and ceramic tile substrates were coated with two polymers, one acrylic and one cellulosic. Over thirty solvents were studied, each applied either as a neat solvent solution or as a poultice. The films formed from solvent solutions either have swelled or were dissolved by the solvents and easily detached from the substrate, meaning that the cleaning solvent has induced the loss of adhesion of the paint to the substrate. Proof of principle for using the sustainable polar aprotic solvent Cyrene in this application under laboratory scale and conditions has been demonstrated. Cyrene proved to be a good solvent for graffiti cleaning from both non-porous (aluminium foil and glazed ceramic tile) and porous (back of ceramic tile) materials. Moreover, compared to previously widely utilised polar aprotic solvents such as NMP and DMAc, Cyrene offers reduced harm to the user and the environment, and its disposal is not harmful to aquatic life. The high porosity of the substrate influenced the cleaning efficiency; penetration of the paint and the stain inside the pores made the graffiti removal very difficult. Chemical cleaning by NMP involved fast dissolution but

ghosting resulted from the solvent and paint residues remaining in the substrate. Cyrene, however, removed the graffiti more slowly but also in a more controllable way, lifting off the paint and significantly reducing this ghosting effect. Hansen Solubility Parameters were used to predict the removal of graffiti paint from porous substrate and could be used to predict various solvent systems for this application. Hansen Solubility Parameters have been employed to predict Cyrene-water mixtures in this work for cleaning graffiti paint. A blend of 75% Cyrene-25% H<sub>2</sub>O has been tested in this work and has shown promising results, which could facilitate the synthesis of new and sustainable paint stripping formulations. Moreover, Hansen solubility Parameters can be used to predict performance into new areas and potentially generate blends of Cyrene with other green solvents to address other opportunities in future work.

## Chapter III

### 3. Application of Cyrene in poly(amide-imide) (PAI) wire enamels



### 3.1. Introduction

Poly(amide-imide) (PAI) resins (Figure 48) are a class of polyimide (PI) which have attracted much attention recently due to their high thermal, mechanical and chemical stability.<sup>284</sup>

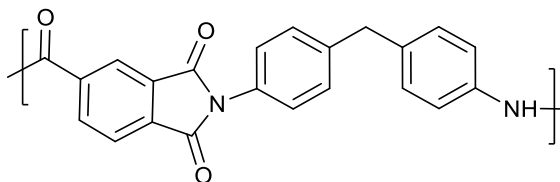


Figure 48: Chemical structure of the poly(amide imide) (PAI) monomeric unit.

These properties make this class of polymers excellent in applications such as insulating material for electrical wiring, aerospace applications, automotive, infrastructure, biomedical, flame-retardants, magnetic shielding and membrane technology (gas separation, solvent pervaporation, nanofiltration and osmose).<sup>162, 285-295</sup> The first aliphatic PAI resins were first reported in 1942 by Frosch and they were produced from 1,2,3-benzene tricarboxylic acid and aliphatic diamines leading to poly(amic acid), followed by its thermal cyclisation.<sup>292</sup> These PAIs had a low thermal resistance due to the aliphatic diamine precursors and could not be commercialised. DuPont introduced aromatic PAIs in 1945,<sup>296</sup> while in 1979 Amoco Chemicals produced Torlon from trimellitic anhydride chloride (TMAc) and 4,4'-diaminodiphenylmethane, which had high mechanical strength and stiffness alongside deformation resistance and good performances at high temperatures.<sup>297</sup> PAIs are manufactured by Solvay,<sup>293</sup> Toyobo, Quadrant (Mitsubishi) under different names such as Vylomax, Duratron, and Torlon. Torlon is owned by Solvay Advanced Polymers L.L.C. and is most used commercial PAI. Torlon PAIs are generally sold in solvent-based solutions (*e.g.* 50-50 or 80-20 NMP/aromatic hydrocarbon) and molecular weight which varies depending on the application and the methodology used.<sup>298</sup> PAIs are important for their dielectric constant (electron movement resulting in polarisation within the material on exposure to an external electric field.),<sup>299</sup> assuring good insulation and exhibit a low thermal expansion coefficient (relative expansion or strain with temperature).<sup>300, 301</sup> Traditional polyimides are brown-yellow transparent; their transparency is due to the formation of a strong charge transfer complex in or between molecular chains.<sup>302, 303</sup> The formation of charge transfer complex can be inhibited by introducing high electronegative, trifluoromethyl group (CF<sub>3</sub>), flexible ether bond, sulfone group, and amide groups into molecular structure.<sup>304, 305 300</sup> The hydrogen bonds produced by amide groups can improve intermolecular interaction, as well as impart good transparency and thermal properties of the polymer.<sup>306, 307</sup>

PAIs are generally expensive wire enamels compared to polyester or polyesterimide-based enamels and are used in applications where their outstanding properties are required.<sup>308</sup> PAIs are generally used as enamelled wire insulation operating up to 250 °C due to their good heat-resistance.<sup>299</sup> However, its heat-resistance is lower than a polyimide resin (e.g. Kapton) and its moisture absorption is not as low as that for other plastics.<sup>309</sup> PAIs exhibit high bend and tensile strength, are not readily flammable and have a high glass transition temperature ( $T_g$ ) up to 441 °C.<sup>300</sup> PAIs are also resistant to UV radiation, have excellent processability due to their flexibility and can be applied as thermoplastics used in harsh environments, where they can resist high stress with little/no creep (deformation). Mechanical properties of PAIs are related to the amide groups and the high stability is due to the imide ring.<sup>284</sup> In some cases, improved physical properties of PAIs resins and performed using curing, imidisation or additives (e.g. carbon nanotubes) are performed at high temperatures (PAI has a high glass transition temperature) for a long time.<sup>310-312</sup> Reducing crystallinity and melt point have been realised by incorporating flexible groups (-O- and -SO<sub>2</sub>-)<sup>313</sup>, cardo groups (e.g. fluorene, phthalide or phthalimidine group),<sup>314</sup> cinnamoyl and azobenzene,<sup>315</sup> phenoxy phenylene,<sup>316</sup> methoxy-substituted triphenylamine,<sup>317</sup> pendent groups<sup>318</sup> in the PAI backbone between the amide and imide groups. They are generally chemically resistant to solvents such as water, methanol, acetone, chloroform, cyclohexane but can easily degrade in polar aprotic solvents.<sup>162, 319</sup> This represents one of PAIs limitations; in order to become more chemically resistant or stronger, they need to be crosslinked.

Currently, all PAIs are produced and processes using a limited number of solvents and systems. Many of them present limitations such as product isolation or toxicity of the reagents. The solvents used for PAI synthesis are the polar aprotic solvents (NMP, DMSO, DMF and DMAc), mixtures of solvents (e.g. 3:2 acetic acid and either pyridine or *N*-methylimidazole (MI)).<sup>162, 320-322</sup> NMP has been restricted by REACH and given a 6-year deferral for wire coatings (9 May 2024).<sup>83</sup> Also, no more than 0.3% should be used on its own or in mixture after 9 May 2020, unless appropriate risk management measures and special work conditions are taken into consideration. Therefore, there is a need to develop an environmentally friendly, cost and effective method to produce PAIs while maintain performance. MI is a tertiary amine and was used as alternative solvent to more toxic NMP for more environmentally PAI systems.<sup>320</sup> In this work, with the aid of HSPiP, new green solvent systems have been developed and tested to synthesise and process PAIs for application as enamels.



## 3.2. Wire enamels - Background

In electrical engineering, the term "enamelled wire" represents a metal wire which has been insulated by a thin layer of hard baked lacquer.<sup>323</sup> Enamelled wires are used for applications requiring tight coils, such as inductors and electrical motors.<sup>324</sup> Enamel lacquer is widely used as insulating material for copper wires due to its excellent electrical resistance, low moisture absorption and for its good mechanical and chemical resistance. However, the first form of insulation was based on textiles. Rubber was used later for insulation, but thicker layers were needed. Cotton and silk were also used in this application, but more expensive. As cheaper alternatives, a thin layer of lacquer or varnish was used for the first time in America, around 1900,<sup>323</sup> but they were not satisfactory. Black enamels based on "asphalt" were trialed but found not to be chemically resistant; being soluble in oil.<sup>323</sup> The first insulated copper wires for machines and transformers were created in Germany in 1906 from cellulose acetate and an enamel lacquer. New enamelled wires covered in oil lacquers consisting of mixtures between resins and drying oils (*e.g.* wood oil, linseed oil).<sup>325</sup> These enamels conferred elasticity and chemical resistance. Lacquers were added to wires by dip-coating between 6 to 30 times until the desired thickness was reached. The wire was covered by a layer of lacquer, then "baked" (thermally polymerised) and covered with a new layer of lacquer, followed by baking and so on. The application of enamelled wires is broad, with everything from thin wires (25-40  $\mu\text{m}$  diameter) to thick (3 mm diameter) used in transformers, cables and electric, motors and electrical devices.

Modern enamelled wires are of significant interest and are undergoing continual improvement. They consist of films formed from polymeric materials, such as polyimide, polyamide imide, polyurethane, polyester or combinations of them.<sup>326, 327</sup> Modern enamelled wires have thin insulation which can suffer from electrical, mechanical and thermal stresses. To resolve these issues, scientists developed a new generation of polymer nanocomposites for high voltage applications.<sup>324</sup> Nanocomposites, which consist of dispersed nanoparticles in a base polymer provide superior thermal, electrical, chemical and mechanical properties compared to their conventional counterparts.<sup>324, 328</sup> Breakdown strength and partial discharges have been some of the major concerns of the insulation in conventional enamelled wires.<sup>327</sup> The presence of fast rising or falling voltages can lead to over-voltages and consequently to the starting of partial discharge activity; layered silicate used as additive gave encouraging inception voltages.<sup>329</sup> Electrical performance was improved by mixtures with 3 wt%  $\text{Al}_2\text{O}_3$  for inception and extinction voltages, while 2 wt%  $\text{ZrO}_2$  nanoparticles presented the highest breakdown strength.<sup>330</sup> Aromatic PAI-silica hybrid films seem to have a better heat and abrasion resistance, yet flexible when compared to conventional PAI insulation.<sup>331</sup> Carbon nanotubes have been incorporated into PAI

matrix to improve the mechanical and conductive properties.<sup>332</sup> The nanocomposites offer new ways of solving insulation challenges, but defects and problems still remain. Their lifetime, the influence of various types of applied voltages, their way of preparation and the optimum percentage of nanoparticles need to be addressed in future research.

### **3.3. Poly(amide-imide) synthesis pathways**

Poly(amide-imide) (PAI) wire enamels are commonly prepared using one of two methods: trimellitic acid chloride and diisocyanate route developed by Hitachi.<sup>308, 319, 333, 334</sup>

#### **3.3.1. Acid chloride route**

This method uses aromatic diamines and aromatic acid chloride anhydrides to synthesise poly(amide-imide) enamels and takes place in polar aprotic solvents with release of HCl and H<sub>2</sub>O.<sup>308, 333</sup> This method is based on the a) addition of an aromatic diamine (4,4'-methylenedianiline (MDA)) to a trimellitic acid chloride (TMAC) in a polar aprotic solvent and b) cyclisation of the amic acid groups to form imide rings at high temperature (Figure 49):<sup>290, 308</sup>

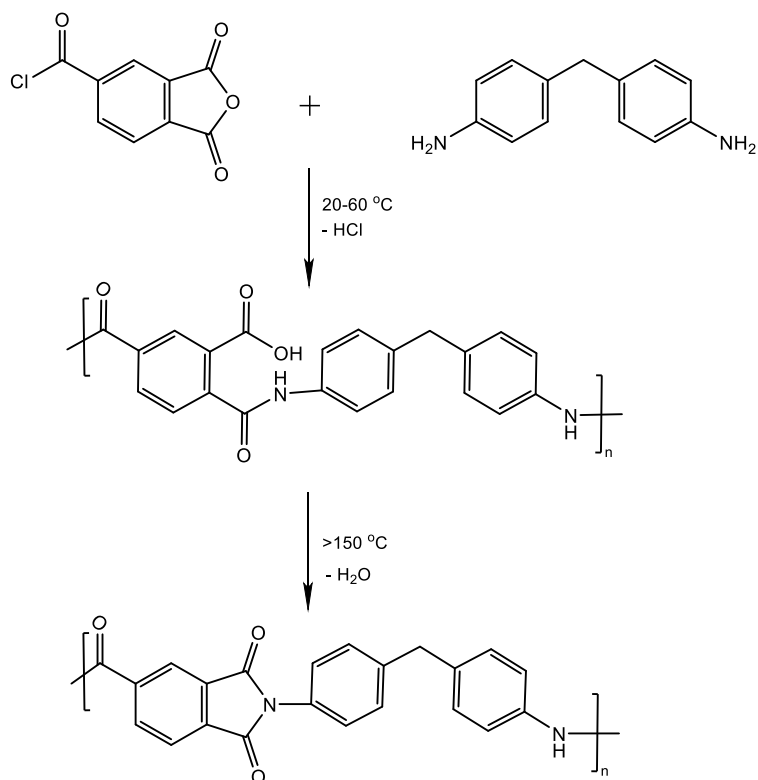


Figure 49: Synthesis of PAI from aromatic diamines and aromatic acid chloride anhydrides (acid chloride route) *via* poly(amic acid) intermediate.

Firstly, TMAC is added to MDA in a polar aprotic solvent and polymerisation occurs at ambient temperature or with mild heating to give the intermediate polyamic acid. In the next step, conversion of the amic acid groups to the imides takes place *via* intramolecular cyclisation at high temperatures, leading to the formation of the desired polymer and water as by-product. Hydrogen chloride formed as a by-product in the first step can corrode the copper wire surface upon enamelling if still present within the polymer, leading to poor adhesion. Hence, HCl needs to be neutralised (*e.g.* by using tertiary amines)<sup>335</sup> or removed by washing or by adding ethylene or propylene oxide which reacts with HCl to form the respective chloroalcohol which in turn, evaporates from the reaction. In the second step, the moisture from the hydrolysis of TMAC is kept at a low level to avoid chain termination and to generate high molecular weight polymers.<sup>290</sup> This route is used by Solvay to synthesise Torlon resins. However, this method presents drawbacks such as their high price and the toxicity of the chemicals employed. TMAC causes severe skin and eye damages and create breathing difficulties if inhaled,<sup>336</sup> while MDA is carcinogenic.<sup>337</sup> The polar aprotic solvents used in PAIs synthesis are also toxic (Section 1.4.1).

### 3.3.2. Diisocyanate route

This route is the one most extensively employed in PAI manufacturing.<sup>308, 319, 334</sup> The common poly(amido-imide)s are prepared through a polycondensation reaction between of acid anhydride such as trimellitic anhydride (TMA) and isocyanates such as 4,4'-methylenediphenyl diisocyanate (4,4'-MDI) in *N*-methyl-2-pyrrolidone (NMP) at high temperature<sup>299, 291</sup> This process is a two-step synthesis: 1) addition of an anhydride to a diisocyanate followed by decarboxylation at high temperatures resulting in an acid terminated imide and 2) the reaction of the residual isocyanate groups with the acid functionalities at high temperature (Figure 50):

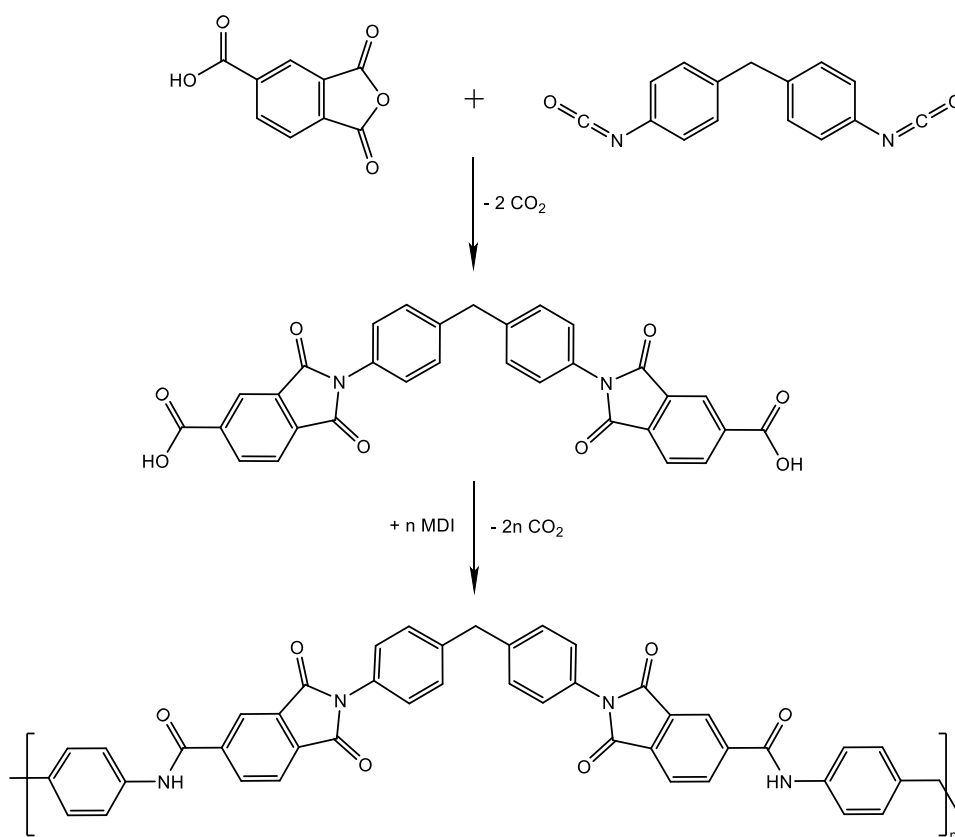


Figure 50: Synthesis of PAI from TMA and 4,4-MDI (diisocyanate route).

The viscosity of the solution is built by carbon dioxide elimination during the condensation reaction.<sup>308</sup> This route can produce high molecular imidised polymer, but is sensitive to water and hence, anhydrous conditions are required. Also, the solvents and carbon dioxide need to be eliminated prior curing to generate high performance properties.

However, any change in the structure of the monomers (the ratio and the flexibility of the groups, the presence of the bulky side groups) has effects on the chain stiffness and chain-chain interactions of the final polymer PAI. Traditional PAIs contain a diamine (diisocyanate), TMA and

a di/polyfunctional acid. Blocking agents such as phenol or chlorophenol<sup>338, 339</sup> are often added to moderate the exothermic reaction between isocyanate and acid groups. Fluorinated monomers<sup>340, 341</sup> and silicon groups<sup>342</sup> have been incorporated in PAIs used in aggressive gas separations (CO<sub>2</sub>, H<sub>2</sub>S, CH<sub>4</sub>)<sup>343</sup> and long-life wire enamels respectively.<sup>285</sup> This method is extensively used to prepare PAIs, but the toxicity of the monomers and solvents used are problematic. The monomers used in PAI synthesis are most of the time toxic. Trimellitic anhydride (TMA) was recently added to SVHC list, due to allergy or asthma symptoms present when inhaled and may cause respiratory irritation.<sup>344</sup> Methylene diphenyl diisocyanate (MDI) is suspected to be carcinogenic and it has been restricted from some products with its isomers 2,2'-MDI, 2,4'-MDI, and 4,4'-MDI (Annex XVII of EC 1907/2006, Entry 56) since 2010.<sup>345</sup> MDI is produced from phosgene and 4,4'-Methylenedianiline (MDA), which is also hepatotoxic and a carcinogen.<sup>346, 347</sup> A less toxic replacement for MDA was produced from *p*-cymene (4,4'-methylenebis-(5-isopropyl-2-methylaniline) (CDA))<sup>348</sup> or from Japanese Knotweed (named "Resveratrol" with high glass transition temperature).<sup>349</sup> Resveratrol has proven to be a sustainable replacement for BPA and MDA.<sup>350</sup> This route also uses traditional polar aprotic solvents.

### 3.4. HSPiP's predictions of poly(amide-imide) solubility

HSPiP was employed to predict dissolution commercial PAI (Torlon AI10) in various solvents for use in both application and synthesis of the polymer. The full data is presented in Table A 6. and Table A 7 (Appendix A) and summarised in Figure 51a and b:

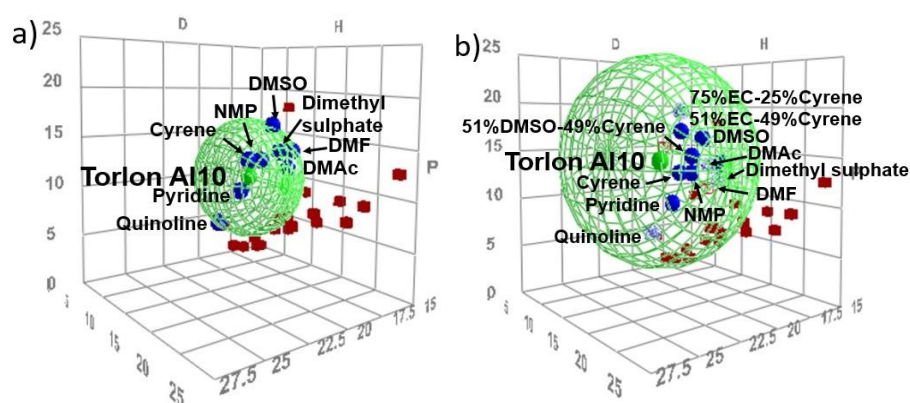


Figure 51: (a) Position of pure solvents and (b) solvent systems in Hansen space for Torlon AI10. Only the good solvents (blue spheres) are named here.

Table 17: Hansen solubility parameters, the scores given and relative energy distance (RED) of the neat solvents used for Torlon AI10 dissolution

| Solvent                        | $\delta_D$ | $\delta_P$ | $\delta_H$ | Score | RED   |
|--------------------------------|------------|------------|------------|-------|-------|
| Cyrene                         | 18.9       | 12.4       | 7.1        | 1     | 0.337 |
| Pyridine                       | 19         | 8.8        | 5.9        | 1     | 0.500 |
| <i>N</i> -Methyl-2-pyrrolidone | 18         | 12.3       | 7.2        | 1     | 0.505 |
| <i>N,N'</i> -Dimethylacetamide | 16.8       | 11.5       | 9.4        | 1     | 0.822 |
| <i>N,N'</i> -Dimethylformamide | 17.4       | 13.7       | 11.3       | 1     | 0.899 |
| Dimethyl sulphate              | 16.5       | 13         | 7          | 2     | 0.976 |
| Dimethyl sulfoxide             | 18.4       | 16.4       | 10.2       | 1     | 0.982 |
| Quinoline                      | 20.5       | 5.6        | 5.7        | 2     | 0.996 |

*Only the good solvents are listed here. Hansen solubility parameters of the solvents are sourced from HSPiP database and expressed in MPa<sup>1/2</sup>.*

As seen in Table 17, the program predicted Cyrene, pyridine, NMP, DMF, DMAc, DMSO, dimethyl sulphate, and quinoline as good solvents (Figure 51a) with the smallest relative energy difference for Cyrene (RED=0.337). The sphere has a diameter of 6.3, a Core=  $\pm[0.45, 0.80, 1.30]$ , and Hansen parameters  $\delta_D=19.30$ ,  $\delta_P=10.81$ ,  $\delta_H=8.25$  MPa<sup>1/2</sup>. A data fit of 1.0 and small values of the core are ideal.<sup>351</sup> The core values represent the  $\pm$  values for the  $\delta_D$ ,  $\delta_P$  and  $\delta_H$  parameters around the best fit which are considered "close" to the best fit.<sup>139</sup> The core values attempt to show how much the centre of the sphere can move in different directions without incurring high penalties. A good fit is considered  $\pm 0.25$  in all three Hansen parameters, while a bad one at least  $\pm 0.75$ . In this work,  $\delta_P$ ,  $\delta_D$  and  $\delta_H$  have values higher than 0.25; hence the core needed to be improved. The improvement of the core can be realized by adding more solvents. Green solvents were also considered as blends to create new solvent systems which would be viable in replacing in PAI syntheses. As seen in Tables 15, both Cyrene and DMSO are considered both good and green solvents for Torlon dissolution. Other green solvents were also investigated as multi component systems, combining carbonates and DMSO with Cyrene. Mixtures of 51 wt% ethylene carbonate, propylene carbonate, diethyl carbonate, methylene carbonate and DMSO with 49% Cyrene were tested for dissolving commercial Torlon. Only 51 % DMSO-49% Cyrene and 51% ethylene carbonate-49% Cyrene showed good performance. As ethylene carbonate is a bulk solvent with very low cost, a higher loading was also trialled in interests of giving a more commercially viable system. 75% ethylene carbonate-25% Cyrene binary system has dissolved Torlon at 100 °C, but it crystallised when cooled to ambient conditions. This is as a result of ethylene carbonate loading

which itself is solid at room temperature. The mixtures tested were added to the initial data containing neat solvents and a new Hansen sphere generated (Table 18):

Table 18: Hansen solubility parameters, the scores given and relative energy distance (RED) of the neat solvents and solvent systems used for Torlon AI10 dissolution

| Solvent                | $\delta_D$ | $\delta_P$ | $\delta_H$ | Score | RED    |
|------------------------|------------|------------|------------|-------|--------|
| Cyrene                 | 18.9       | 12.4       | 7.1        | 1     | 0.454  |
| 51% DMSO-49% Cyrene    | 18.6       | 14.4       | 8.7        | 1     | 0.514  |
| N-Methyl-2-pyrrolidone | 18         | 12.3       | 7.2        | 1     | 0.662  |
| Dimethyl sulfoxide     | 18.4       | 16.4       | 10.2       | 1     | 0.711  |
| Pyridine               | 19         | 8.8        | 5.9        | 1     | 0.732  |
| 51% EC-49% Cyrene      | 18.4       | 17.1       | 6.1        | 1     | 0.799  |
| N,N'-Dimethylformamide | 17.4       | 13.7       | 11.3       | 1     | 0.86   |
| N,N'-Dimethylacetamide | 16.8       | 11.5       | 9.4        | 1     | 0.959  |
| Quinoline              | 20.5       | 5.6        | 5.7        | 2     | 0.994  |
| Dimethyl sulphate      | 16.5       | 13         | 7          | 2     | 1.027* |
| 75% EC-25% Cyrene      | 18.2       | 19.4       | 5.6        | 1     | 1.055* |

\* *Wrongly positioned solvents in/out of the Hansen space. Only the good solvents are listed here. All mixtures are expressed in wt% and their Hansen solubility parameters were calculated based on their parameters as neat solvents sourced from HSPiP database. HSP values are in units of MPa<sup>1/2</sup>.*

As seen in Figure 48, the sphere has changed, getting larger due to the addition of new solvent systems. In this case, the revised sphere has a Radius=10.8, a Core=  $\pm[0.10, 0.35, 0.55]$ , a fit of 0.783 and Hansen parameters  $\delta_D=21.99$ ,  $\delta_P=14.34$ ,  $\delta_H=11.44$  MPa<sup>1/2</sup>. By adding more solvents to the initial sphere (containing pure solvents), the values of the Core have been improved, but the fit has changed to a smaller value. As seen in Table 16, Cyrene was again predicted the best solvent to dissolve Torlon AI10, with the smallest RED (a bigger value of RED, of 0.454, due to the modification of the sphere (bigger sphere, larger RED). The mixture of Cyrene with DMSO was predicted as the second-best, followed by NMP, pure DMSO, pyridine and the 51% EC-49% Cyrene. A mixture containing more ethylene carbonate (75% EC-25% Cyrene) is predicted as a bad solvent, with RED>1. However, in reality, this solvent system dissolved Torlon and further used in this work to produce a PAI enamel, alongside 51% DMSO-49% Cyrene and 51% EC-49% Cyrene. The 51-49% mixtures were chosen based on the replacement of neat Cyrene in accordance with the Huntsman patent.<sup>162</sup>

### 3.5. Synthesis of PAI wire enamel using and mixtures containing Cyrene

In this work, PAIs were produced in a one-pot high-temperature polycondensation at 145 °C for 4 h (diisocyanate method).<sup>162</sup> 5 polymers were produced with the only difference being the solvent employed: 2 pure solvents (Cyrene and NMP) and 3 solvent systems (51% ethylene carbonate (EC)-49% Cyrene, 75% EC-25% Cyrene and 51% dimethyl sulfoxide (DMSO)-49% Cyrene). The obtained PAI were coded as shown in Table 19:

Table 19: Composition of poly(amide imide) solutions

| PAI code                   | Solvent/mixture solvents<br>(wt%)          | Solvent or mixture<br>of solvent (g) | TMA<br>(g) | MDI<br>(g) |
|----------------------------|--|--------------------------------------|------------|------------|
| PAI/Cyrene                 | Cyrene                                     |                                      |            |            |
| PAI/NMP                    | NMP  |                                      |            |            |
| PAI/51% EC-49% Cyrene      | 51% ethylene carbonate (EC)-<br>49% Cyrene | 7.98                                 | 0.841      | 1.097      |
| PAI/75% EC-25% Cyrene      | 75% ethylene carbonate (EC)-<br>25% Cyrene |                                      |            |            |
| PAI/51% DMSO-49%<br>Cyrene | 51% dimethyl sulfoxide-49%<br>Cyrene       |                                      |            |            |

As discussed in Section 3.4., the mixtures of Cyrene with EC and DMSO were predicted to be good candidates for PAI solubility and synthesis. All solvents and solvent systems are used in this work as a greener replacement of toxic NMP. The produced polymers are dark brown in colour (Figure B 7a in Appendix B). When precipitated in ethanol, the colour changes into nude (Figure B 7b).



### 3.6. Dynamic viscosity of the PAI fluids

The effective dynamic viscosity of PAI solutions was conducted at room temperature for the prepared PAI using neat Cyrene, NMP, and mixtures of Cyrene with ethylene carbonate or DMSO (Figure 52). The viscosity of PAI/75% EC-25% Cyrene solution was not determined due to the presence of crystallised ethylene carbonate at room temperature which resulted in inconsistent data.

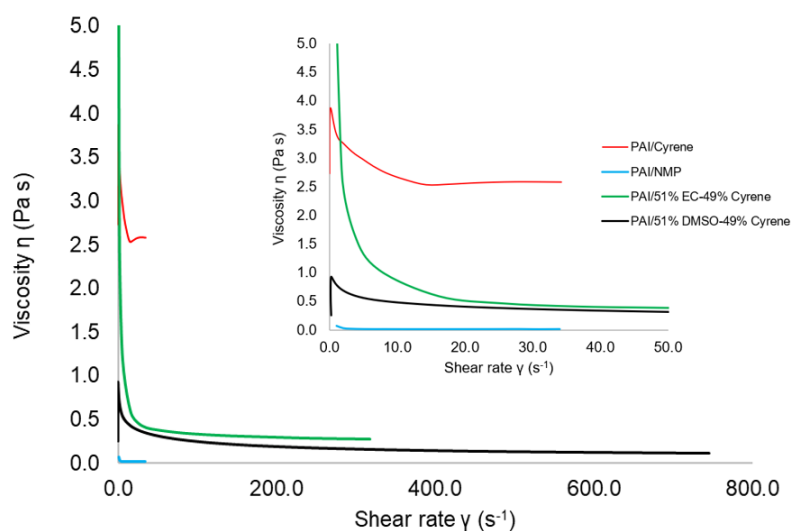


Figure 52: Dynamic viscosity of PAI/Cyrene, PAI/NMP, PAI/51% EC-49% Cyrene and PAI/51% DMSO-49% Cyrene fluids as a function of shear rate.

Figure 52 shows how the dynamic viscosity decreases with shear rate increasing in the PAI fluids for different solvents/mixtures used. All the fluids act as non-Newtonian fluids: shear thinning can be observed at low shear rates, followed by reaching a constant dynamic viscosity at high shear rates.<sup>352</sup> The shear-thinning behaviour is explained by the disentanglement of macromolecules or their orientation in the shear direction due to the shear load which lowers their flow resistance.<sup>353</sup>  
<sup>354</sup> The fluids register high values for viscosity at a low shear rate because the fluid does not have enough time to respond; the measurement is occurring in the transitional zone and not at a steady state. The non-Newtonian character of PAIs is different, depending on the solvent/solvent system used as follow: the flow curve for PAI/51% EC-49% Cyrene is very sharp, followed by PAI/Cyrene and PAI/51% DMSO-49% Cyrene, while PAI/NMP has a very low decreasing in viscosity with the shear rate. The dynamic viscosity of PAI/51% EC-49% Cyrene has a slightly higher curve than of PAI/51% DMSO-49% Cyrene, but a much steeper decrease at a low shear rate because of the presence of solvent (ethylene carbonate is solid at room temperature) which has formed agglomerations in the nanofluids at room temperature. A larger stress is necessary to destroy the

aggregates under shear at a lower shear; hence, a more pronounced viscosity decrease can be observed in PAI/51% EC-49% Cyrene.<sup>354</sup>

### 3.7. Thermal curing of poly(amide-imide) films

There are numerous curing processes which are of great academic and industrial interest. The main curing mechanisms can be split into two broad curing technologies: radiation curing ( $\gamma$ -ray, X-ray, ultraviolet, accelerated electron beams) and thermal curing (convection and conduction, induction, ultrasonic, resistance heating and with the aid of additives).<sup>355</sup> The selection of the curing method is influenced by the material used, applicability and cost. Autoclaves are widely used for thermal curing, but the process is very long, energy intensive, the curing is non-uniform and the polymer undergoes large thermal stresses. Convection heating involves gases and liquids circulating between surfaces; the curing process is long because of the low heat conductivity of polymers. Resistance heating is based on electrical resistance effect of a heating element (steel mesh, copper electrical connectors) after application of electric current, which heats up the coating and forms bonds between materials.<sup>356</sup> Conduction curing uses a hot gas heating the material from the polymer surface similar to convection heating, making the curing non-uniform and long.<sup>357, 358</sup> A very efficient curing process is based on ultrasonic heat generation which converts the high-frequency mechanical vibrations into heat and produces short welding times.<sup>359</sup> During the curing, two processes can occur: 1) the solvent evaporates, leaving a hard film or 2) the coating crosslinks, where the polymer reacts to form a dry film. Crosslinked materials are usually solvent resistant.

In this work, the PAIs were cured at 220 °C for 2h, using a hot plate system (described in Section 7.3.). Both fast ramp rate (10 °C min<sup>-1</sup>) and slow ramp rate (2 °C min<sup>-1</sup>) curing was investigated. Thermal cross-linking of PAI occurs at 220-240 °C, when bonds between the amine groups of monomer chains within these materials are formed (Figure 53).<sup>360</sup>

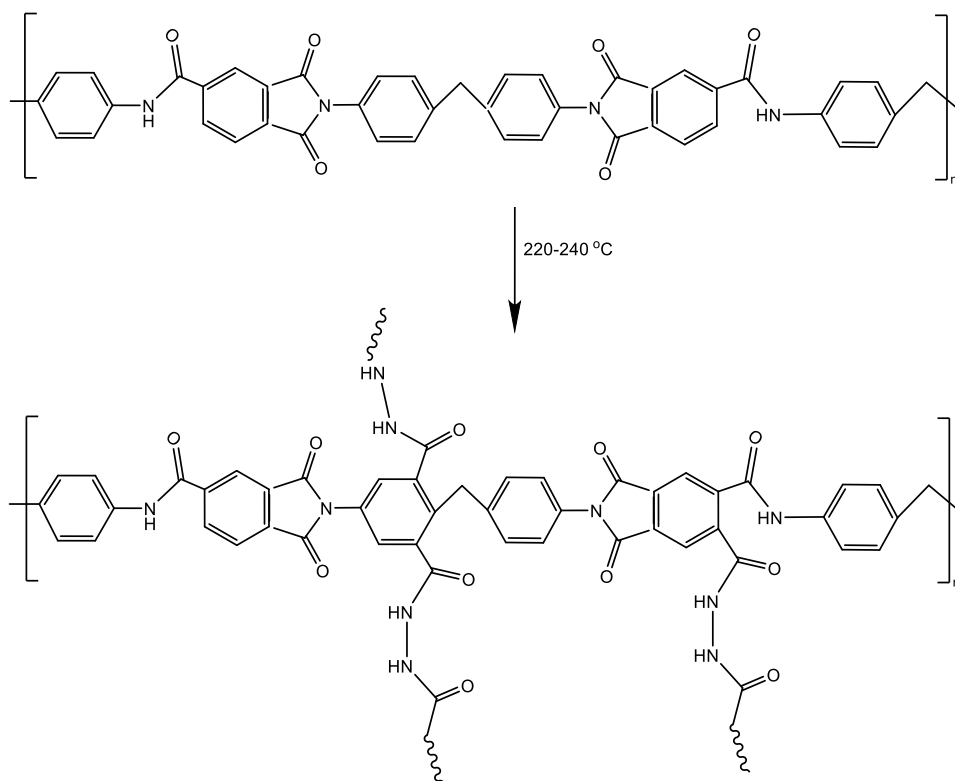


Figure 53: Thermal cross-linking of PAI enamels.

During curing of PAI in Cyrene at a high rate of temperature ( $10\text{ }^{\circ}\text{C min}^{-1}$ ), bubbles were present due to Cyrene degradation after  $140\text{ }^{\circ}\text{C}$  (Figure B 8). Hence, a slow increase of temperature was gradually applied ( $2\text{ }^{\circ}\text{C min}^{-1}$ ) from  $100\text{ }^{\circ}\text{C}$  to  $220\text{--}240\text{ }^{\circ}\text{C}$ . During the curing process, imidisation is promoted, leading to the formation of a material with higher mechanical strength and heat resistance. At high temperatures, the solvent evaporates and permanent chemical bonds are formed.<sup>361</sup> Thermal imidisation of PAI films was confirmed from their infrared spectra (Section 3.8.1.).

## 3.8. PAIs characterisation

### 3.8.1. Infrared spectroscopy

Complete imidisation of PAI films PAIs produced using NMP, Cyrene and the mixtures of Cyrene with ethylene carbonate or DMSO (wt%) and cured at 240 °C can be confirmed from their infrared spectra (Figure 54). The new PAIs are coded based on the solvent used: "PAI/NMP" is the PAI produced with NMP while "PAI/ 51% EC-49% Cyrene" represents the one with a mixture of 51% ethylene carbonate and 49% Cyrene wt%.

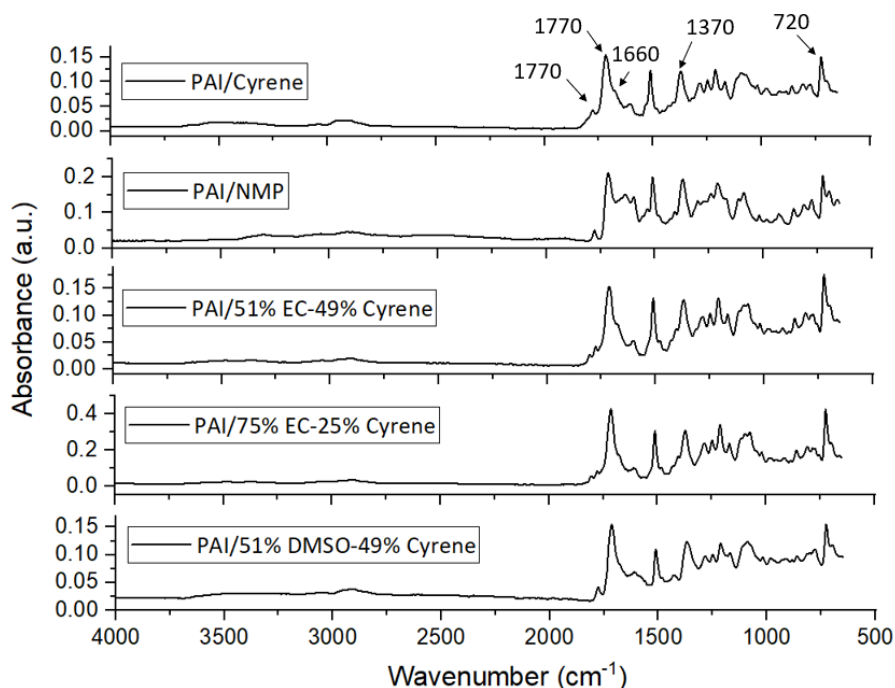


Figure 54: Infrared spectroscopy of PAIs synthesised from NMP, Cyrene, 51% ethylene carbonate-49% Cyrene, 75% ethylene carbonate-25% Cyrene and 51% DMSO-49% Cyrene.

Carbonyl peaks are overlapped at 1770, 1710 (asymmetric and symmetric imide C=O) and 1660  $\text{cm}^{-1}$  (amide C=O).<sup>301, 362</sup> Peaks between 1600-1400  $\text{cm}^{-1}$  correspond to aromatic C=C of amide groups. Absorptions at 1370 and 725-720  $\text{cm}^{-1}$  corresponded to the imide C-N and imide ring respectively.<sup>363</sup> All produced PAIs present an absorption band of amide N-H shifted to 3350-3300  $\text{cm}^{-1}$  indicating the presence of hydrogen bonding between the amide structures.<sup>364</sup> The absorption peaks at 3044-3035  $\text{cm}^{-1}$  are related to the aromatic C-H stretching, while the band at 2920-2900  $\text{cm}^{-1}$  corresponds to the aliphatic C-H stretching.

### 3.8.2. $^1\text{H}$ -NMR spectra of PAIs

$^1\text{H}$ -NMR of PAI obtained using diisocyanate route shows peaks that confirms its chemical structure (Figure 55). Due to the complexity of the composition of PAIs, the corresponding  $^1\text{H}$ -NMR spectra are composed of many signals with different intensities in the aromatic region.  $^1\text{H}$ -NMR spectrum of PAI/Cyrene can be seen in Figure 55, while NMR spectra of PAI/NMP, PAI/51% EC-49% Cyrene, PAI/75% EC-25% Cyrene and PAI/51% DMSO-49% Cyrene are seen in Figure B 9a (Appendix B).

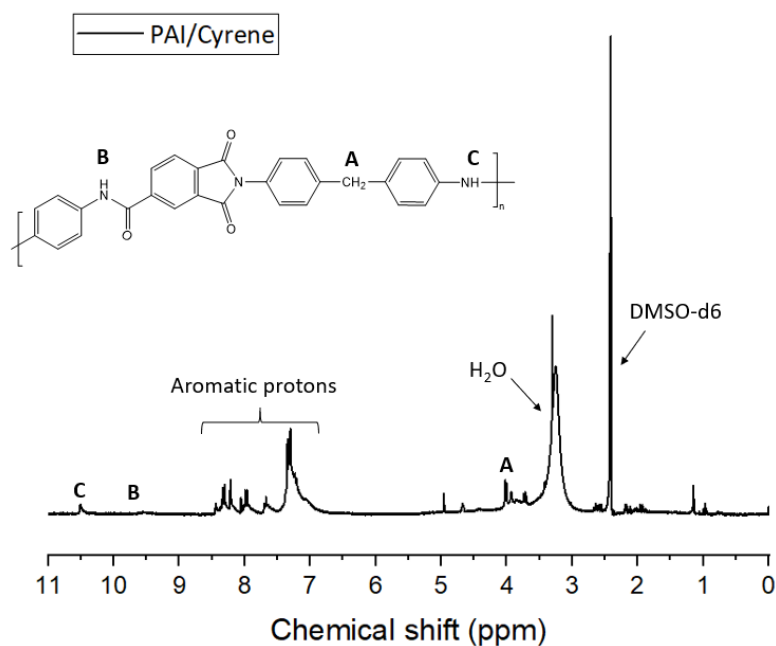


Figure 55:  $^1\text{H}$ -NMR spectrum of PAI/Cyrene

While it is very difficult to identify the components in the aromatic region, the signals between 7 ppm to 8.5 ppm are assigned to the aromatics. The aromatic protons appeared in the region of 7–8.5 ppm as follow: peaks at 7 and 7.5 ppm are assigned to MDI ring and peaks at 8.2-8.6 corresponds to TMA ring protons.<sup>319</sup> Peaks between 9.5 and 10.5 ppm are related to N-H amide groups in the main chain of polymer.<sup>288</sup> Aromatic bridging methylene protons (Ar-CH<sub>2</sub>-Ar) is observed in the range of 3.5-4.5 ppm.  $^{13}\text{C}$  NMR (DMSO- $d_6$ ,  $\delta$  ppm): 167.03, 166.99, 166.54, 155.49, 153.20, 142.60, 138.30, 137.17, 136.10, 135.55, 132.72, 130.18, 129.86, 129.75, 129.66, 129.55, 128.05, 127.95, 124.42, 123.99, 119.01, 118.94 ppm (Figure B 9b).  $^1\text{H}$  NMR and  $^{13}\text{C}$  NMR spectra were affected by the low purity of the monomers and water impurities in DMSO, which exhibited low chemical shifts ( $\delta$  between 1 and 5 ppm and 18-40 ppm respectively).

### 3.8.3. Thermal properties of PAIs

Thermal stability and decomposition behaviour of PAIs films cured at 240 °C were investigated by thermogravimetric analysis (TGA) in a nitrogen atmosphere at a heating rate of 10 °C/min (Table 20). Glass transition temperatures of the PAIs are obtained *via* differential scanning calorimeter (DSC)<sup>299</sup> (Figure B 10) while the char yield percentage at 625 °C are obtained from the TGA curves. However, the determination of the glass transition temperature ( $T_g$ ) of cured PAI-resins is not an easy task; post-curing reactions occur at high temperatures and eliminate reaction by-products.<sup>320</sup>

Table 20: Thermal properties of PAI films produced with Cyrene, NMP, 51% EC-49% Cyrene, 75% EC-25% Cyrene and 51% DMSO-49% Cyrene cured at 240 °C

| PAI film type           | Glass transition temperature ( $T_g$ ) | Decomposition temperature (°C) |             | Char yield (%) |
|-------------------------|--|--------------------------------|-------------|----------------|
|                         |  | $T_{d5\%}$                     | $T_{d10\%}$ |                |
| PAI/Cyrene              | 311                                    | 290.29                         | 326.37      | 49.41          |
| PAI/NMP                 | 301                                    | 234.88                         | 256.43      | 43.98          |
| PAI/51% EC-49% Cyrene   | 302                                    | 288.24                         | 322.78      | 43.97          |
| PAI/75% EC-25% Cyrene   | 308                                    | 307.05                         | 346.72      | 46.88          |
| PAI/51% DMSO-49% Cyrene | 282                                    | 291.48                         | 337.48      | 59.32          |

<sup>a</sup> Temperature at which 5% and 10% weight loss were recorded by TGA at 10 °C/min under nitrogen atmosphere. <sup>b</sup> Weight percentage of char obtained after TGA analysis at 625 °C under nitrogen atmosphere.

All PAIs register their first weigh loss at around 100 °C, which corresponds to moisture loss. The polymer dissolution solvent is removed at around 200-250 °C. The temperature at which 5% and 10%-weight loss are usually defined as the respective degradation temperatures ( $T_{d5\%}$  and  $T_{d10\%}$ ).<sup>365</sup> The 5% weight loss temperatures ( $T_{d5\%}$ ) for PAIs in nitrogen were observed in the range of 233-307 °C, while  $T_{d10\%}$  varied between 256 and 346 °C, depending on the solvent used. It was previously reported in literature that PAIs exhibit different thermal stability depending on the monomers used, when the solvent or curing conditions were changed.<sup>366 299 320</sup> In this work, the PAIs cured at the same temperature (240 °C) exhibit different  $T_g$ , which varies with the solvent used in the process. PAI/Cyrene showed the highest  $T_g$ , while PAI/51% DMSO-49% Cyrene. PAI/Cyrene and both 51%- and 75% EC-based PAIs showed melting points ( $T_m$ ) at around 400 °C (Figure B 10b, d, e) after crystallisation.<sup>367</sup> The crystallinity of these PAI could be the result of

thermal treatment. However, PAI/NMP and PAI/51% DMSO-49% Cyrene do not exhibit melting points, hence they are amorphous. In addition, all PAIs exhibited high char yields (>40%), suggesting a high heat resistance attributed to their high aromatic content.<sup>368</sup> Also, this phenomenon could make PAIs good candidates for the preparation of carbon materials.<sup>290</sup> PAI/51% DMSO-49% Cyrene showed the highest heat resistance, registering a char yield of 59.32%, while PAI/51% EC-49% Cyrene and PAI/NMP the lowest heat resistance, with 44% resulted char.

## 3.9. Poly(amide-imide) cured films testing

### 3.9.1. Solvent resistance test

For this test, the PAIs produced using NMP, Cyrene, 51% ethylene carbonate-49% Cyrene, 75% ethylene carbonate-25% Cyrene and 51% DMSO-49% Cyrene were one-coated and cured on tin foil to assess the chemical resistance of PAI enamels in NMP (Figure 56).<sup>162</sup>

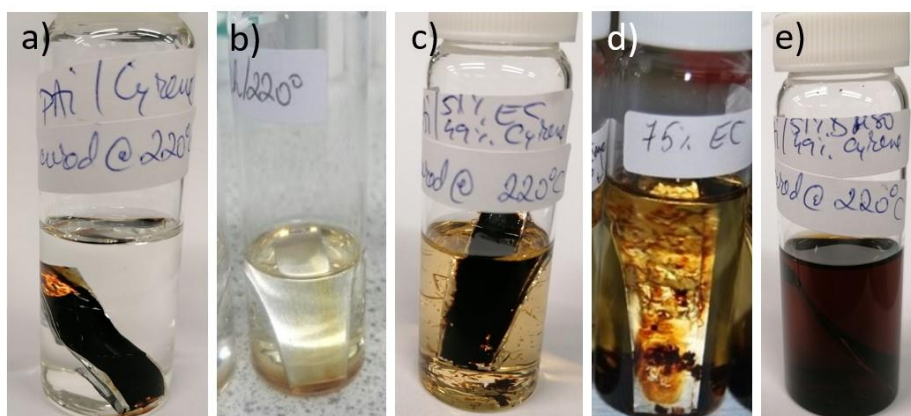


Figure 56: (a) Solvent resistance test of the poly(amido-imide) resins produced from Cyrene, (b) NMP, (c) 51% EC-49% Cyrene, (d) 75% EC-25% Cyrene and (e) 51% DMSO-49% Cyrene cured at 220 °C.

PAI/NMP (Figure 56 b), PAI/51% EC-49% Cyrene (Figure 56c), PAI/75% EC-25% Cyrene (Figure 56d), PAI/51% DMSO-49% Cyrene (Figure 56e) failed the test when they were cured at 220 °C. However, the solubility of 51% and 75% of ethylene carbonate-based PA was slow and not fully achieved (Figure 56c, d). PAI/Cyrene cured at the same temperature has shown solvent resistance to NMP (Figure 56a). The lower solubility of Cyrene- and ethylene carbonate-based PAI in solvent could be related to their higher molecular weight or their semicrystalline character.<sup>369</sup>

PAI solvent system cured at 220 °C, which failed the solvent resistance test were prepared again but at a higher curing temperature. The solvent resistance test was then repeated. When cured at 240 °C, only PAI/51% EC-49% Cyrene (Figure 57b) has shown a positive result, being chemically resistant when exposed to NMP. PAI/NMP (Figure 57a), PAI/75% EC-25% Cyrene (Figure 57c) and PAI/51% DMSO-49% Cyrene (Figure 57d). PAI/75% EC-25% Cyrene performed better when cured at 240 °C, its dissolution in solvent was not fully achieved.

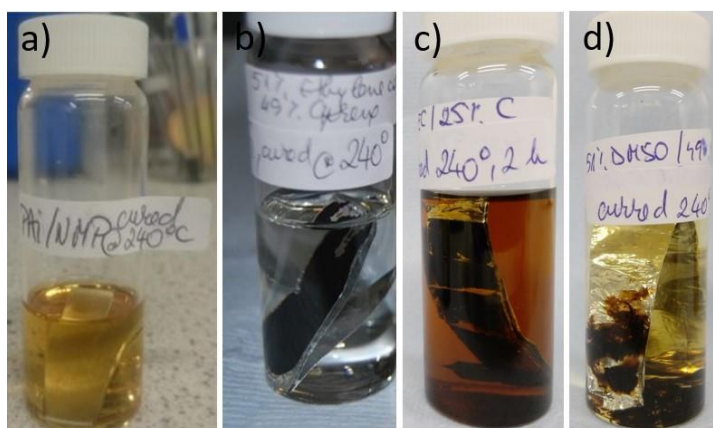


Figure 57: (a) Chemical resistance to NMP of the poly(amido-imide) resins produced from NMP, (b) 51% EC-49% Cyrene, (c) 75% EC-25% Cyrene and (d) 51% DMSO-49% Cyrene cured at 240 °C.

Cyrene and Cyrene-ethylene carbonate have proven good solvent and binary solvent system respectively to produce new poly(amido-imide) wire enamels. However, PAI/75% EC-25% Cyrene resin showed clumps of resin at room temperature due to the presence of crystalline ethylene carbonate in this solvent system. PAI/51% DMSO-49% Cyrene, however, is a viscous solution at room temperature, but presents a strong odour. DMSO is stable at room temperature but undergoes thermal decomposition at its boiling point (189 °C) because of the formation of non-condensable gases, which could be problematic when curing a PAI film at 220-240 °C. Moreover, dimethyl sulphide is a highly flammable liquid with a boiling point of 37 °C, corrosive, producing toxic fumes or SO<sub>2</sub>; its vapour/air mixtures are explosive and carries compounds across skin barrier. The temperature of decomposition can become lower in the presence of certain chemicals (*e.g.* halides, metals, electrophiles, oxidants, and reductants) through autocatalytic behaviour.<sup>93</sup> As a desired system has to be effective, easy to use and safe, PAI/75% EC-25% Cyrene and PAI/51% DMSO-49% Cyrene will not be considered further. Only three systems PAI/NMP, PAI/Cyrene and PAI/51% EC-49% Cyrene were considered for further testing. PAI/NMP was used as baseline.



### 3.9.2. Hardness test

Hardness is the capacity of a coating to resist scratching or gouging. Pencil hardness is an inexpensive and quick test to quantitatively determine such a property. Gauging hardness this way has been employed in the coatings and paint industry since 1923 and is validated as ASTM (American Society for Testing and Materials) Test Method D 3363 (Standard Test Method for Film Hardness by Pencil Test).<sup>370</sup> Due to the limited size and number of aluminium slides involved in this work, only three class of pencil were used: softest (9B), intermediate (F) and hardest (9H). A preliminary test was conducted onto cured PAI/NMP with the hardest pencil 9H pushed once forward against the film using a 1 kg hardness tester (Figure 58a).

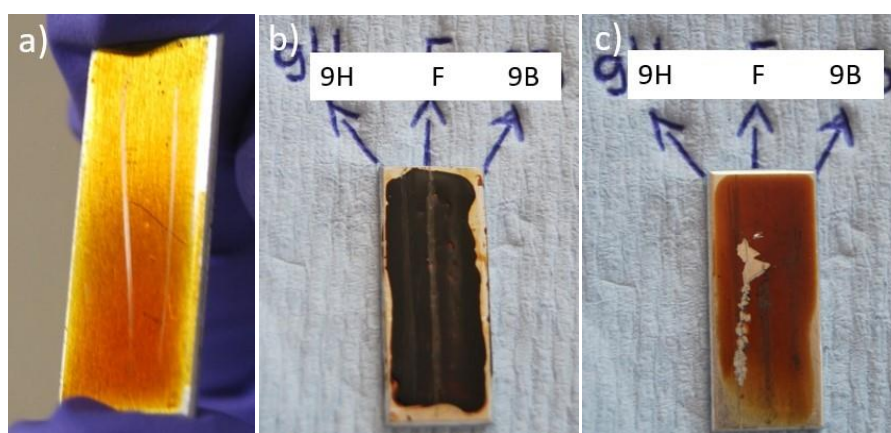


Figure 58: (a) Preliminary results of the hardness test of 9H pencil passed once onto the coated PAI/NMP, and ten times for (b) PAI/Cyrene and (c) PAI/NMP.

The test was performed twice on the same slide as a benchmark. The test then proceeded to repeat the test ten times (Figure 58 b and c). As seen in Figure 58c, PAI/NMP failed when 9H pencil was used 10 times but was resistant to F and 9B pencils. PAI/Cyrene was resistant to all pencils when used 10 times, which makes Cyrene ideal for this type of enamels (Figure 58b). The thickness of the coating played a significant role in this test. During the scratching test, a thin film is more likely to be gauged than a thick film. Moreover, stronger intermolecular bonds within polymer chain makes the coating stronger. This could explain why semicrystalline PAI/Cyrene passed the scratching test, remaining unaffected, while PAI/NMP was less resistant to scratching, failing under hardest pencil. For clearer observation, a Leica S6D Microscope was used to assess how deep the scratches were for PAI/NMP (b) and PAI/Cyrene (c) and PAI/51% EC-49% Cyrene (d) (Figure 59):

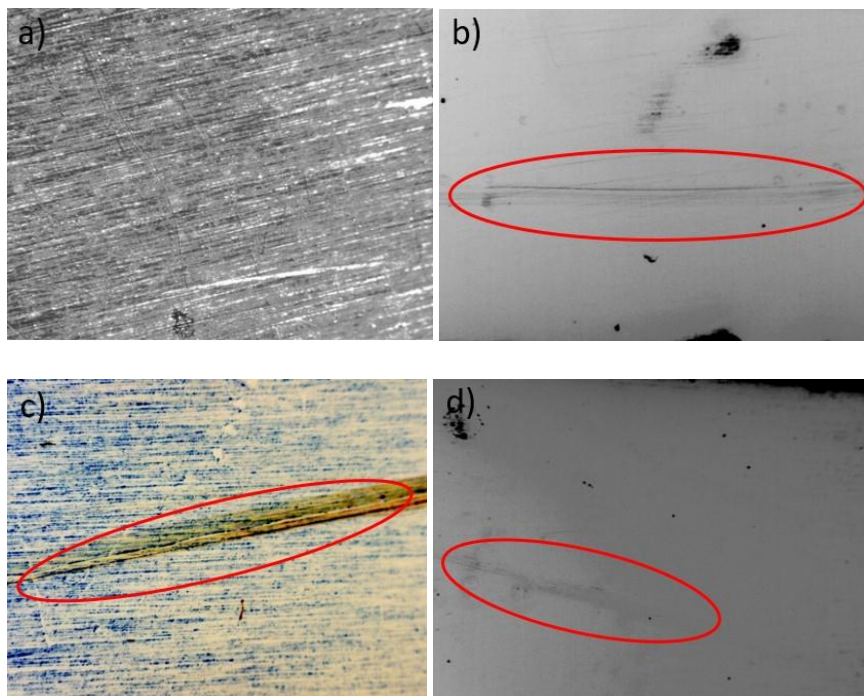


Figure 59: (a) Pristine aluminium slide and the results of the hardness test of cured (b) PAI/Cyrene, (c) PAI/NMP and (d) PAI/51% EC-41% Cyrene.

For PAI/NMP (Figure 59b), the 9H pencil gouged into coating, reflecting the light from the microscope; hence the dark yellow lines (red circle) observed in Figure 59. PAI/Cyrene (Figure 59c) and PAI/51% EC-49% Cyrene (Figure 59) give coatings which are dark brown to black. The coatings were not penetrated by any of the pencils, but 9H did mark, but not gouge the aluminium. A less obvious mark is seen for PAI/51% EC-49% Cyrene (Figure 59d) and could be caused by either a) the more resistant coating produced with this solvent system or b) a thicker coating obtained on the area with no visible scratch. The pencil rating is the level of hardness which does not scratch the surface. For this limited test, in Cyrene's-based PAIs is 9H and for NMP, F. The test is not very accurate due to the limited number of pencil hardness used, as well as the quantity and uniformity of the coating applied onto the aluminium surface before curing.

### 3.9.3. Flexibility test

Flexibility is an important test for wire coatings, permitting them to bend without breaking. The stability of enamelled wires depends on its crosslinking; hence a non-crosslinked materials can lose its elasticity over time.<sup>323</sup> A failed wire coating has severe consequences on electrical performance and safety. PAI resin was one-coat cured on a flexible aluminium foil, to easily assess their flexibility (Figure 60):

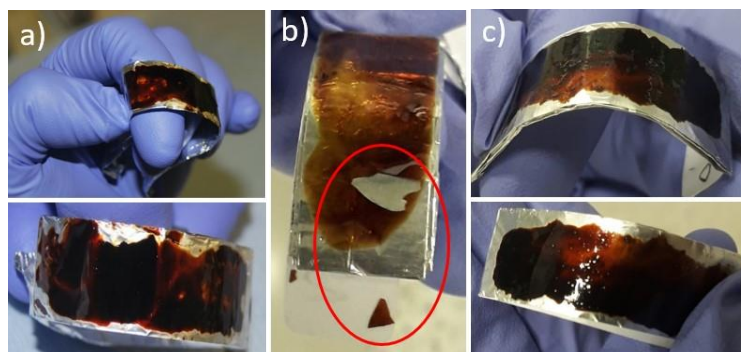


Figure 60: (a) Flexibility test of PAI/Cyrene, (b) PAI/NMP and (c) PAI/51% EC-49% Cyrene.

As shown in Figure 60a, PAI/NMP failed this test, the coating breaking into small pieces. PAI/Cyrene (Figure 60b) and PAI/51% EC-49% Cyrene (Figure 60c) were not brittle and have passed this test.

### 3.9.4. Adhesion strength

According to the ASTM definition (D907-70), adhesion is the “condition in which two surfaces are held together by interfacial forces which may consist of valence forces or interlocking forces, or both”.<sup>371</sup> The forces holding two surfaces together are Van der Waals forces, electrostatic forces or chemical bonding across the coating/substrate interface. The separation of a layer separates from a substrate is called “delamination” and occurs when debonding (breaking the adhesion forces) is driven by mechanical or thermal stress, shock waves, corrosion, electrostatic forces.<sup>372</sup> Generally, the defects occurring in adhesive bonds are incorrect curing, porosity, cracks and voids. During adhesive failures from a peeling test of adhesive tests, cohesive and interfacial failures can occur.<sup>373</sup> Generally, the thicker the coating, the larger the peeling strength is. Cohesive failures become predominant for thick coatings, while interfacial failures (delamination) are observed in case of thin adhesive layers.

In this work, the adhesion of a coating to a substrate was tested using a tape test, currently validated by ASTM Test Method D3359 (Test Methods for Measuring Adhesion by Tape Test) (Figure 61):

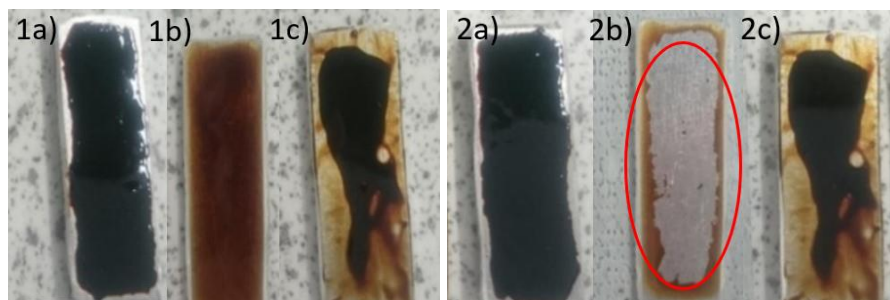


Figure 61: (a) Adhesion strength test of PAI produced with Cyrene, (b) NMP and (c) 51%EC-49% Cyrene (1) before and (2) after the test.

As seen in Figure 61b, PAI/NMP failed the test, the coating being almost completely removed. However, PAI/Cyrene (Figure 61a) and PAI/51% EC-49% Cyrene (Figure 61c) have passed the adhesion strength test and the adhesion between the coating and the substrate has remained intact; the adhesive forces have not been affected. This means that both PAI in Cyrene and in Cyrene-ethylene carbonate mixture represent good options for enamels with good adhesion properties.

### 3.10. Chapter conclusion

Poly(amide-imide) coatings are used in applications where a high thermal stability, physical and thermal resistance are most desired. In PAI production, there is a need for cost-effective, technologically effective, and environmentally friendly method to produce coatings with high thermal, mechanical, chemical, corrosion and wear resistance. In this work, the results of Cyrene were sought in comparison with the traditionally used solvent NMP and other candidates. For this purpose, HSPiP has been used in this work to predict new green solvent systems for the synthesis of PAI enamels. Based on a small-scale concept, the experiments were realised in duplicate to provide an intuitive understanding of PAI synthesis using new solvents. Cyrene has been successfully used in this application on its own and in blends with carbonates to replace their toxic counterparts. HSPiP facilitated the prediction of blends from Cyrene and other friendly solvents and particularly, a blend of Cyrene with ethylene carbonate was found to be a potential replacement for traditional NMP in this process. PAIs manufactured using Cyrene and Cyrene with 51% EC demonstrated higher resistance to solvent, were more flexible, had better adhesion

strength and abrasion resistance than the traditional PAI in NMP. This could result from a more viscous coating solutions and higher molecular weight of Cyrene and ethylene carbonate-based PAIs. Also, a small amount of solvent was still present in the polymer post-curing, which could be why they showed more elasticity than NMP-based cured enamels. Thermal analyses of PAIs showed the presence of solvent residue after curing in all cases, which influenced the properties of the enamels. However, when 75% EC-25% Cyrene and 51% DMSO-49% Cyrene were used, the films were not easily applied or presented a pungent smell. PAI/Cyrene had the highest glass transition temperature ( $T_g=311\text{ }^\circ\text{C}$ ), while PAI/51% DMSO-49% Cyrene had the lowest  $T_g$  ( $282\text{ }^\circ\text{C}$ ). PAI/51% EC-49% Cyrene had a  $T_g$  comparable to PAI/NMP with  $T_g$  of  $302$  and  $301\text{ }^\circ\text{C}$ , respectively. PAI/Cyrene had a superior degradation temperature when compared to PAI/NMP ( $290.29$  vs  $234.88\text{ }^\circ\text{C}$ ), but lower than of PAI/75% EC-25% Cyrene ( $307.05\text{ }^\circ\text{C}$ ) and comparable to PAI/51% DMSO-49% Cyrene ( $291.48\text{ }^\circ\text{C}$ ). PAI/Cyrene, PAI/51% EC-49% Cyrene and PAI/75% EC-25% Cyrene showed crystallinity with  $T_m$  at around  $400\text{ }^\circ\text{C}$ , which would increase closer chain interactions and superior properties. All the PAIs generated high yield in char, over 40%, suggesting a high heat resistance attributed to their high aromatic content. PAI/51% DMSO-49% Cyrene showed the highest heat resistance, registering a char yield of 59.32%, followed by PAI/Cyrene with 49.41% char, while PAI/51% EC-49% Cyrene and PAI/NMP the lowest heat resistance, with 44% resulted char. However, this preliminary investigation carries some limitations: uniformity and thickness of the film could not be controlled, and higher purity ( $>99\%$ ) of the monomers needs to be considered for PAI synthesis.

In conclusion, proof of principle for using greener solvents for PAI synthesis has been demonstrated. Application of Cyrene in poly(amide-imide) coatings has facilitated rapid curing and provided solvent resistant coatings and adhesion strength while still both hard and flexible. Cyrene and mixtures of Cyrene with other green solvents could represent the future replacement to the toxic counterparts.



# Chapter IV

## 4. Extraction of bio-active compounds<sup>5</sup>

---

<sup>5</sup> This chapter is adapted from the research paper “ *Sustainable single-stage solid-liquid extraction of hesperidin and rutin from agro-products using Cyrene*” submitted to ACS Sustainable Chemistry & Engineering.

R.A. Milescu has performed the solvent selection, HSP prediction and solvent system selection, solid-liquid extractions and wrote the corresponding sections together with the introduction and conclusion. Mateus L. Segatto has performed UH-PLC analysis and wrote the corresponding section. Aylon M. Stahl performed the Excel calculations for the new solvent systems. Dr C. Robert McElroy and Vânia G. Zuin supervised the work and provided the feedback. J.H. Clark assured the collaboration between the University of York and UFSCar, Brasil. All authors contributed to the writing of the article.





## 4.1. Introduction

Plants have been used for their nutritional purposes since the start of mankind. They were valued for their medicinal, cosmetics or preserving applications and first mentioned in Egyptian papyruses.<sup>374</sup> Chinese manuscripts describe over two thousand plants and a thousand of herbal plants were described during Greek and Roman period, for their use for the essential oils content.<sup>375</sup> Romanians living north of the Danube river have mentioned herbs for their medicinal purpose since 5<sup>th</sup> century B.C, (Herodotus) but used them long before. The first alcohol-based extract from rosemary was called "Hungarian water" and used as perfume or to treat headaches since 1380 in Europe.<sup>376</sup> The willow bark was used to relieve pain, fever and inflammations since 4<sup>th</sup> century and was found to contain salicylic acid, precursor of aspirin. However, its synthetic version, called acetylsalicylic acid was discovered in 1800s and used extensively today.<sup>377</sup> In 16<sup>th</sup> century, Paracelsus, a Swiss physician and alchemist introduced healing herbal "hot baths", where he added aromatic and medicinal herbs for medicinal purposes (still in use today in Romania). The first herbal products were included in the Romanian pharmacopoeia in the 19<sup>th</sup> century, and the first institute of medicinal herbs opened in Cluj in the 20<sup>th</sup> century.<sup>376</sup>

The interest in medicinal and aromatic herbs, and easily accessible wastes from agri-food processing, has revived with discovering new phenolic compounds and their applications in the last decade. Currently, plants are used for nutritional purpose, synthesis of medicinal compounds, perfumes, or aromatherapy. In this study, black tea leaves and orange skin were used as raw material to extract bio-active compounds from. Green and black tea crops consist 98% of *Camellia sinensis*, a species that contain compounds such as catechins, quinic acid, kaempferol and derivatives of quercetin, like rutin.<sup>378</sup> Rutin is useful in the treatment of vascular diseases (*e.g.* haemorrhoids, internal bleedings and varicose veins) and has potential to act as an antioxidant and as a potential SARS-CoV-2 inhibitor.<sup>379-381</sup> Hesperidin can be found in a higher concentration in the citrus peels more than in juice or seeds<sup>382, 383</sup> and presents inhibitory effect against the development of neurodegenerative diseases such as Parkinson's, Alzheimer's, Huntington's diseases,<sup>384, 385</sup> cardiovascular diseases and others, due to its anti-inflammatory, antioxidant, lipid-lowering and insulin-sensitizing properties.<sup>386, 387</sup> Hesperidin has a strong affinity to the main viral and cellular targets outperforming antiviral drugs chloroquine (relatively toxic in high doses) and hydroxychloroquine (less toxic than chloroquine, but presents side effect of retinopathy).<sup>388</sup> Quinine, an extract from the cinchona tree, also has been shown antiviral activity against COVID-19.<sup>389</sup> However, quinine has been linked to serious side effects such as thrombocytopenia (low platelet levels that can cause excessive bleeding in case of injuries) and multiorgan failure.<sup>390, 391</sup> Moreover, hesperidin showed a good safety profile, which could indicate it as a very promising

prophylaxis and treatment drug for COVID-19 and its mutations, attracting a lot of recent interest with rutin, naringenin and quercetin.<sup>388, 392-396</sup>

Extraction yield of any substance depends on solubility, therefore the choice of solvents used in extraction experiments must be performed according to analyte's physical-chemical properties. Ethanol and methanol are most frequently used in organic solid-liquid extractions of hesperidin and rutin due to their availability and low cost.<sup>397-400</sup> Ethanol is highly flammable, volatile and causes serious eye irritation. Methanol is also volatile and flammable yet more toxic than ethanol, causing kidney failure, permanent blindness by destructing the optic nerve and even death.<sup>401</sup> Using the CHEM21 green solvent guide, methanol is ranked by CHEM21 as "recommended", despite its health issues, because the current occupational exposure limits for methanol are relatively high.<sup>38</sup> Ethanol and methanol are ranked as "problematic" when they were scored for their safety, both of them being highly flammable. However, a "recommended" overall score was given when the other scoring systems (health and environment) were considered. Cyrene is ranked as "problematic" due to its high boiling point which means that Cyrene's recycling is energy intensive, but is good in other respects including high biodegradability, low persistence, and no toxicity (it is REACH approved). The aim of this work is to apply the concept of chemical valorisation in the context of a circular economy, by using agro-industrial waste and bio-based alternatives to traditional solvents which are often of environmental concern. The bio-based and biodegradable solvent Cyrene was for the first time used in a solid-liquid extraction of hesperidin and rutin from citrus waste and tea leaves. *In silico* prediction of bioactive solubility using the established model of Hansen Solubility Parameters (HSPs) was validated by the *in vitro* test sets. In this study, a minimum amount of 5 mL solvent or mixture of solvents have been used with the possibility of its purification and reuse.

## 4.2. Green extraction

There are several extraction methodologies for the extraction of bio-active compounds from agri-food wastes and many of them are high energy consuming or uses high amount of solvent.<sup>402</sup> However, there is an increasing need for green and sustainable approaches leading to bio-active compounds with low environmental impact. Food residues contain several substances that can be used within or exterior to the food chain, especially biopolymers, platform chemicals and bioactive compounds.<sup>403</sup> Currently, food waste is either used as animal feed, ploughed back into the land, incinerated, composted, sent to anaerobic digestion and/or fermentation or disposed of in the landfill in many countries.<sup>404</sup> Simply disposing of food waste is neither green nor sustainable nor

is it an efficient way to manage this resource.<sup>405</sup> Nowadays food-associated industries are challenged to be more ecological, economical and innovative. The scale on which the food loss takes place is dependent on several factors that are individual to each country, region, and type of agro-product. While in developed countries, food residues are caused mainly by commercial and consumer behaviour, agriculture-based countries such as Brasil have a substantial fraction of losses generated in food production, much of which consists of unavoidable waste.<sup>406</sup> Considering the movement towards sustainable development, led by UN's Sustainable Development Goals, informed and monitored by Green and Sustainable Chemistry,<sup>407</sup> potential arises from the use of unavoidable food residues in a sustainable chemical environment.<sup>408</sup> The concept of waste biorefineries integrated into food processing factories to increase value within the food supply chain is one that is gaining interest. The Circular Economy Action Plan of European Commission proposes to revise the EU waste directive to better reflect the requirements of a circular economy and establish a waste hierarchy: prevention, reuse, recycling, recovery and disposal.<sup>11</sup> The extraction and formulation of natural bioactive compounds from readily exploitable waste biomass has gained huge attention due to an increase in the demand on novel health-enhancing products, as well as biopesticides, preservatives for food and packaging industries.<sup>409</sup> The Green Chemistry principles<sup>1</sup> and the Principles of Green Natural Product Extraction (Table 21)<sup>17</sup> promote the use of renewable feedstocks and bio-solvents in sustainable extractions. Such principles and activities aid in meeting the challenges of the 21<sup>st</sup> century, to protect both the environment and consumers.

Table 21: Six principles recommended by Chemat for a green extraction

| Principle number | Definition   |
|------------------|--|
| 1                | "Innovation by selection of varieties and use of renewable plant resources."                 |
| 2                | "Use of alternative solvents and principally water or agro-solvents."                        |
| 3                | "Reduce energy consumption by energy recovery and using innovative technologies."            |
| 4                | "Production of co-products instead of waste to include the bio- and agro-refining industry." |
| 5                | "Reduce unit operations and favour safe, robust and controlled processes."                   |
| 6                | "Aim for a non-denatured and biodegradable extract without contaminants."                    |

"Green extraction is based on the discovery and design of extraction processes which will reduce energy consumption, allow the use of alternative solvents and renewable natural products, and

ensure a safe and high-quality extract/product”.<sup>17</sup> The authors have sought to define the green extract as “obtained in such a way to have the lowest possible impact on the environment and whose eventual recycling would have been planned for (co-products, biodegradability)”.<sup>17</sup>

### 4.3. Extraction of hesperidin and rutin - Background

Brasil is the world leader in citrus production, with a corresponding associated citrus waste of 9.4 million tons per annum.<sup>410</sup> This is principally from activities such as juicing the fruit, resulting in at least 50 wt% waste.<sup>411</sup> Citrus peel waste represents a renewable feedstock for chemicals such as the solvents *d*-limonene and *p*-cymene, as well as pectin, cellulose, bio-oil, sugars and flavonoids, such as hesperidin or naringin. Hesperidin (Figure 62) is one of the major phenolic compounds found in citrus peel,<sup>382</sup> but also found in tomatoes or mint<sup>412</sup> and contain various glycosides of three main aglycones: hesperitin (4'-methoxy-3',5,7-trihydroxyflavanone), naringenin (5,7,4'-trihydroxyflavanone) and eriodictyol (5,7,3',4'-tetrahydroxyflavanone).<sup>413</sup> Hesperidin can be found in a higher concentration in the citrus peels more than in juice or seeds.<sup>382, 383</sup>

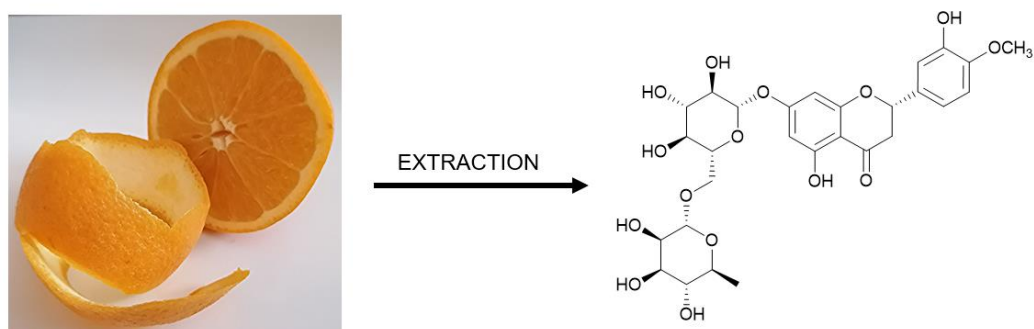


Figure 62: Hesperidin extraction from orange peel and its chemical structure.

Like citrus juices, another globally consumed agro-product is tea, which had total worldwide production of 6.3 Mtons (2018).<sup>414</sup> Green and black tea crops consist 98% of *Camellia sinensis*, a species that have compounds such as catechins, quinic acid, kaempferol and derivatives of quercetin, like rutin (Figure 63):<sup>378</sup>



Figure 63: Rutin extraction from black tea leaves and its chemical structure.

The major drawback associated with both hesperidin and rutin is their poor bioavailability because of their low aqueous solubility, limited membrane permeability or poor stability in an acidic environment.<sup>397, 415</sup> Extracting hesperidin and rutin from plant sources has been demonstrated by conventional methods such as solid-solvent extraction,<sup>398, 416-418</sup> or Soxhlet extraction<sup>419,420</sup> and non-conventional extraction procedures: microwave-assisted extraction,<sup>421 422</sup> ultrasound-assisted extraction,<sup>423</sup> solar hydro-distillation,<sup>424</sup> enzymes,<sup>425</sup> deep eutectic solvents<sup>402</sup> or sCO<sub>2</sub>.<sup>426, 427</sup> Among these processes, solid-liquid extraction is most common and is generally used as a reference against which to benchmark newly developed methodologies. Solid-liquid extraction represents the process where a solute is extracted using a liquid (maceration). The liquid is enriched with active compounds (based on osmosis) which disperses into the liquid *via* diffusion.<sup>428</sup> The main objective of a solid-liquid extraction is to extract the maximum amount of the active compounds in the minimal volume of solvent. Generally, a single-stage extraction cannot meet these conditions and a repeated (multi-stage) extraction is used.<sup>429</sup> In many cases, large amounts of solvent are needed in multi-stage extractions and the yields of bioactive products obtained are low.<sup>430</sup> One of the goals to increase the extraction yield is raising the solvent capacity to dissolve the compound of interest by changing temperature or mixing solvents.

In this work, hesperidin and rutin were extracted from orange peel and tea leaves using a single-stage solvent extraction.

## 4.4. HSPiP's predictions in flavonoids extraction

Thirty solvents (Table A 8 in Appendix A) were classified following the Chem21 green solvent guide and used in this work.<sup>38</sup> Once the leading greener solvents were identified, HSPiP 5<sup>th</sup> Edition 5.0.03 was used to find the best solvents to dissolve hesperidin and rutin based on their theoretical solubility parameters, with a predictive role only. Hansen Solubility Parameters (HSP) were chosen to predict the solubility of hesperidin and rutin in different solvents by mapping the three values (dispersion interactions  $\delta_D$ , dipolarity  $\delta_P$  and the hydrogen bonding ability  $\delta_H$ ) in a three-dimensional "Hansen space".<sup>135, 139</sup> The partial solubility parameters of the two bioactive compounds were created using the molecular descriptor SMILES and converted to HSP using the software HSPiP version 5.0.03 (Figure B 11). The parameters obtained for hesperidin and rutin were calculated as  $\delta_D=19.6$ ,  $\delta_P=10.3$ ,  $\delta_H=13.9$  MPa<sup>1/2</sup> and  $\delta_D=19.6$ ,  $\delta_P=10.6$ ,  $\delta_H=10.4$  MPa<sup>1/2</sup> respectively.

To test the solubility of hesperidin and rutin, 1 mL of each solvent was used to dissolve 1 mg of each compound (analytical standard). To calculate the empirical Hansen solubility parameters, scores from 1 to 5 were given based on the dissolution of the standards by visual comparison (Figure B 12). Solvents were given the score "1" and "2" when they showed a good solubility of the solute; scores "3" and "4" when they partially solubilised the solute and "5" when they did not dissolve the solute. The obtained scores were inserted into the HSPiP software, and an empirical Hansen Solubility Parameters sphere generated for each analyte, and their  $R_0$ ,  $\delta_D$ ,  $\delta_P$  and  $\delta_H$  are calculated. This spherical model (Hansen solubility sphere) defined by good solvents, leaving out the ones which did not dissolve the analyte. Therefore, it is possible to predict new solvents or mixtures, based on their Hansen parameters, which can dissolve the analytes (inside the sphere).

The candidate solvents from Table A 8 were mapped in a tri-dimensional Hansen space after they were assigned scores based on *in vitro* test and the HSP spheres were calculated using HSPiP software (Figure 64a and b). Full data can be found in Table A 9 and Table A 10 in Appendix A. The hesperidin sphere calculated after mapping the solvents (Figure 64a) and the scores has the core values  $\pm[1.25, 0.65, 0.50]$  and a fit of 0.956 and empirical Hansen parameters of  $\delta_D=17.3$ ,  $\delta_P=21.2$  and  $\delta_H=18.1$  MPa<sup>1/2</sup>. DMSO has the smallest distance from the solute in the Hansen space (RED value of 0.713), suggesting the greatest affinity for hesperidin, followed by DMF, methanol, DMAc, ethylene glycol and formic acid. Although methanol and ethanol are widely used for the extractions, it is for the most part the polar aprotic solvents that come closest in proximity. Cyrene partially dissolved hesperidin at room temperature (red circle in Figure B 13a), but fully dissolved

it at 65 °C (red circle in Figure B 13b), showing a clear solution. Ethanol is widely used to extract hesperidin and multiple stages of extraction are generally used, due to the partial solubility of hesperidin in this solvent. In the present study, “good solvents” were considered to be only those which completely dissolved the analytical standards. Ethanol partially dissolves the analytical standards at room temperature or when heated up to 65 °C (Figure B 13b) and the solution shows high turbidity.

The Hansen sphere calculated for rutin (Figure 64b) has a fit= 0.995 and the core values  $\pm[0.30, 0.85, 0.35]$ . The Hansen parameters of the solute, rutin, in this case, are  $\delta_D=20.3$ ,  $\delta_P=13.5$  and  $\delta_H=18.3$  MPa<sup>1/2</sup>. In this case, HSPiP predicted DMF as the best solvent to dissolve rutin, with the smallest RED value (0.768), followed by DMSO, ethanol, ethylene glycol, DMAc, Cyrene, butanol and methanol (Table A 10).

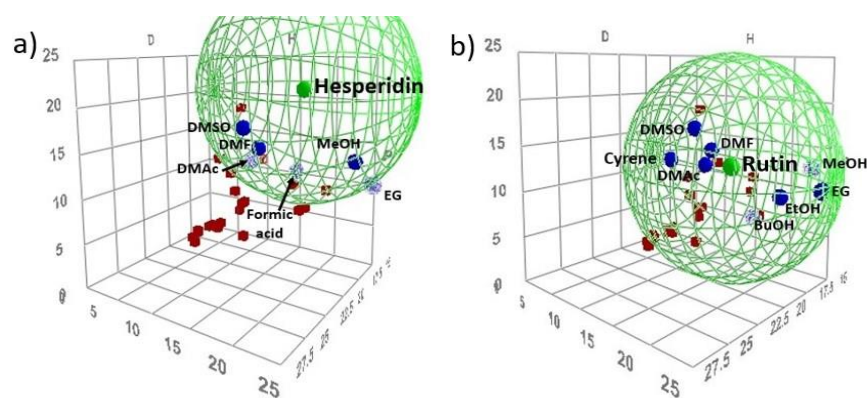


Figure 64: Recommended solvents mapped in Hansen space with solubility sphere of hesperidin (a) and rutin (b). Only the good solvents (blue spheres) are named here.

Both 0.956 and 0.995 are reasonable fit values for hesperidin and rutin. The fit for hesperidin is bad with a large value ( $\pm 1.20$ ) of dispersion cohesion solubility parameter ( $\delta_D$ ). This means that the number of test solvents did not cover a wide-enough range in that parameter. A data fit could be improved to 1.0 (with the good solvents are included in the sphere and all the bad ones are outside of it) by using the MVol correction. For hesperidin’s case, an MVol of 102.5 for Cyrene was manually introduced (Cyrene is not present in the actual data set) and the fit forced in the software. The value “limit” 7 was the best in this case with a core  $\pm[0.4, 0.65, 0.35]$  but with a worse fit, only 0.727 and a smaller sphere. The newly created sphere (Figure B 14a) results in a number of good solvents outside the sphere (Figure B 14b).

Being limited in the number of available solvents, another approach was explored. To improve the values of the core and the fit and find solvents with higher theoretical solubility for both analytes, mixtures of solvents primarily selected from the initial list were trialed. HSP was used to

predict solvation behaviour for varying ratios of chosen solvents to find blends with high potential for this application. Binary and ternary systems were tested and added to the initial sphere. The full table of binary solvent systems and their optimal composition with their calculated  $R_a$  can be seen in Table A 11. For the tertiary mixtures, those with Cyrene were preferred to test this unusual solvent ability combined with other compounds to give interesting solvent properties (Table A 12). A new sphere (Figure 65a) has been created for hesperidin when the new binary solvent systems were added with new parameters  $\delta_D= 15.54$ ,  $\delta_P=17.12$ ,  $\delta_H=13.66 \text{ MPa}^{1/2}$ . For rutin (Figure 65b), the new sphere including binary solvent system has the following parameters  $\delta_D= 21.74$ ,  $\delta_P=13.48$ ,  $\delta_H=19.70 \text{ MPa}^{1/2}$ . The new created sphere has a core of  $\pm[0.35, 1.15, 0.80]$  and 14.4 radius.



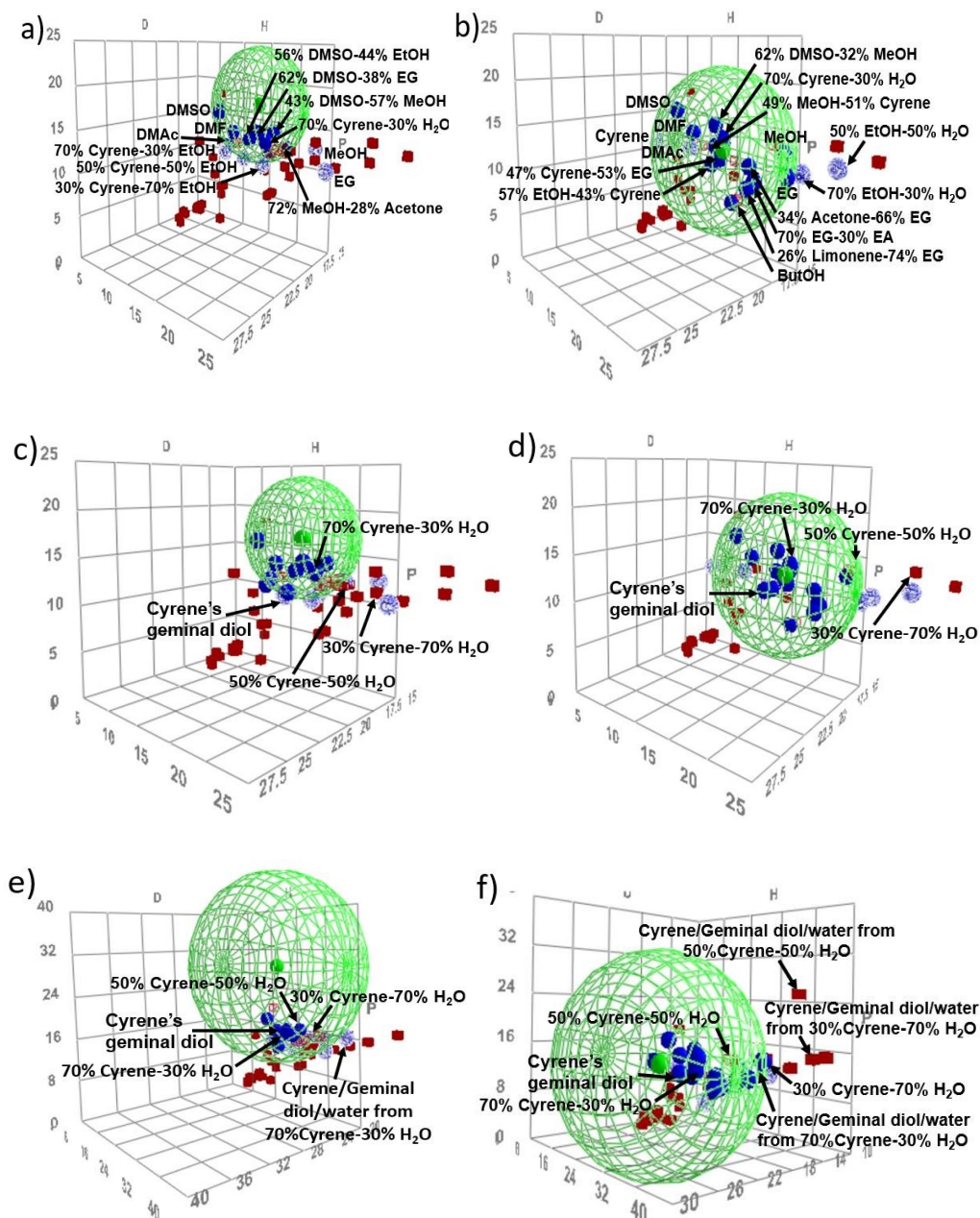


Figure 65: (a) New Hansen spheres of hesperidin and (b) rutin when adding the new mixtures of solvents (% v/v). (c) Cyrene's geminal diol (hydrate) was plotted with Cyrene-water mixtures separately for hesperidin and (d) rutin to observe their distinct positions in Hansen space. (e) New ternary mixtures of Cyrene/geminal diol/water (obtained from the same Cyrene-water mixtures from (c) and (d) have been included in Hansen sphere for hesperidin and (f) rutin dissolution. All mixtures are expressed in % v/v. Only the good solvents (blue spheres) are named here.

In this study, the mixtures of Cyrene and water were calculated as mixtures of the two individual solvents (Figure 65a and b). However, Cyrene's geminal diol (hydrate) is produced when Cyrene reacts with water, hydrating the ketone.<sup>52</sup> The new resulting geminal diol has its own place in the Hansen sphere (Figure 65c and d), different than Cyrene-water mixtures calculated previously. HSPs of geminal diol was calculated using "DIY" (Do It Yourself) tool of the same version of HPSiP (Figure B 15). After introducing its SMILES string, the software calculated the Hansen parameters

as:  $\delta_D=19.4$ ,  $\delta_P=11.2$  and  $\delta_H=15.9$  MPa<sup>1/2</sup>. The  $R_a$  distance between the individual solvents and the sphere's centre for hesperidin ( $\delta_D=17.3$ ,  $\delta_P=21.2$  and  $\delta_H=18.1$  MPa<sup>1/2</sup>) and rutin's ( $\delta_D=20.3$ ,  $\delta_P=13.5$  and  $\delta_H=18.3$  MPa<sup>1/2</sup>) from Figure 65 are presented in Table 22:

Table 22: Distance from the position of the individual solvents to the centre of the sphere centre ( $R_a$ ) calculated for both hesperidin and rutin

| Hesperidin                      |                | Rutin                           |                |
|---------------------------------|----------------|---------------------------------|----------------|
| Solvent                         | $R_a$ distance | Solvent                         | $R_a$ distance |
| DMSO                            | 9.5            | Cyrene's geminal diol (hydrate) | 3.78           |
| Cyrene's geminal diol (hydrate) | 11.07          | DMSO                            | 9.41           |
| MeOH                            | 11.13          | EtOH                            | 10.21          |
| EtOH                            | 12.82          | Ethylene glycol                 | 10.45          |
| Ethylene glycol                 | 12.92          | Cyrene                          | 11.6           |
| Cyrene                          | 14.45          | MeOH                            | 11.95          |
| Acetic acid                     | 15.06          | Acetic acid                     | 13.71          |
| Acetone                         | 15.9           | Acetone                         | 15.1           |
| MEK                             | 18.02          | MEK                             | 16.38          |
| Ethyl acetate                   | 19.51          | Ethyl acetate                   | 16.48          |
| <i>d</i> -Limonene              | 23.81          | <i>d</i> -Limonene              | 19.27          |
| H <sub>2</sub> O                | 25.01          | H <sub>2</sub> O                | 25.97          |

Table 22 shows only the chosen greener solvents used in this study. The smallest  $R_a$  values for hesperidin are of DMSO, followed by Cyrene's geminal diol. For rutin's case, Cyrene's geminal diol (hydrate) has the smallest distance, having the potential of being the best to dissolve rutin.

HSPiP software can calculate fractions of different solvents in a mixture but does not predict the reactivity of the two individual molecules to generate a new one, hence different parameters and positions in Hansen sphere for mixtures of Cyrene-water and the geminal diol (Figure 65c and d). The mixtures Cyrene-water contain a mixture of pure Cyrene, pure water and newly formed geminal diol (hydrate), as a result of the reaction between the Cyrene and water (Section 1.5.2.1.). The resulting ternary mixtures contain different concentrations of the three components (Table 23), as a function of the amount of water and Cyrene present in the mixture:

Table 23: Concentration of Cyrene, water and geminal diol found in the mixtures Cyrene-water used in this study (30% Cyrene-70% H<sub>2</sub>O, 50% Cyrene-50% H<sub>2</sub>O and 70% Cyrene-30% H<sub>2</sub>O).

| %V/v Cyrene<br>in water | Wt% Cyrene<br>in water | Mol %<br>Cyrene | Mol %<br>Geminal diol<br>(hydrate) | Mol %<br>H <sub>2</sub> O |
|-------------------------|------------------------|-----------------|------------------------------------|---------------------------|
| 30                      | 34.9                   | 0.74            | 6.79                               | 92.47                     |
| 50                      | 55.6                   | 2.8             | 13.17                              | 84.03                     |
| 70                      | 74.5                   | 17.54           | 17.54                              | 64.91                     |

*The values are calculated based on the data from reference.<sup>52</sup>*

The density of the geminal diol is unknown; we attempt to calculate the Hansen Solubility Parameters from the mole fraction of the constituents in the ternary mixture from Table 23 and the known Hansen parameters of Cyrene, water and geminal diol. As seen in Figure 65e and f, when the new ternary mixtures are added, new spheres (with different scale) have been created for both, hesperidin and rutin, with bigger cores and new RED values for all the solvents and mixtures involved. A small sphere can be obtained if a "limit" is applied; however, a larger sphere is advantageous if the user wants to find other viable solvents for hesperidin and rutin dissolution and extraction (bigger Hansen sphere, more solvents can fit inside of it). For rutin, the newly created sphere predicts geminal diol as the best solvent for its dissolution, with the smallest value RED (Table A 14), while for hesperidin the DMSO-EG remains the best-predicted mixture (Table A 13). The Hansen parameters created for the three new ternary systems of Cyrene/geminal diol/water can be seen in Table A 15 and Table A 16. From all the shown solvent systems, the best pure, binary, and tertiary solvents were tested further as extraction media for hesperidin from orange waste and rutin from black tea sample.

## 4.5. Solvent extraction of hesperidin and rutin

### 4.5.1. Efficiency of a single-stage solid-liquid extraction

The single-stage extraction experiments to obtain the selected bioactive compounds were performed using green candidates from neat solvents and their mixtures. All the concentrations are expressed in % v/v. The results of the extractions of hesperidin from orange waste are shown in Figure 66. Ethanol-water mixture and Cyrene-water 70-30% were used in this study for comparative purpose.

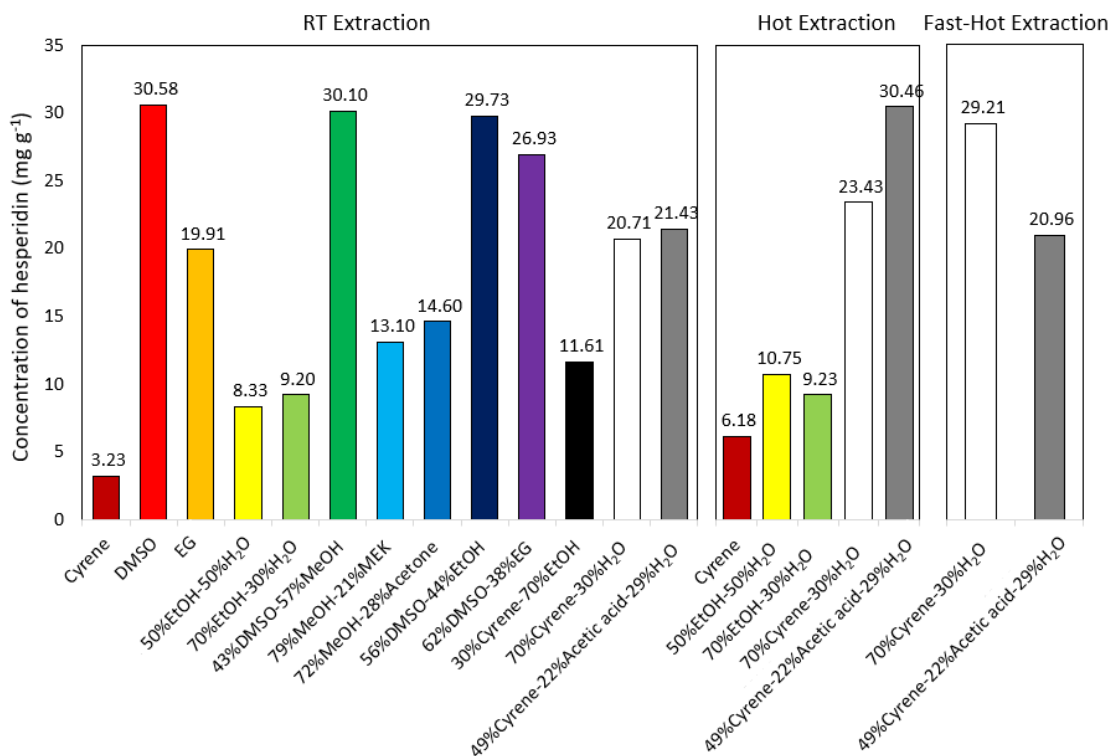


Figure 66: Extraction yield of hesperidin ( $\text{mg g}^{-1}$ ) from RT, hot and fast hot extraction, determined using UHPLC compared to the “standard” (70% EtOH-30% H<sub>2</sub>O in light-green column). All extractions are executed in one stage. The binary and ternary solvent systems were predicted by HSPiP.

As seen in Figure 66, all Cyrene-H<sub>2</sub>O mixtures out-performed the 70% EtOH-30% H<sub>2</sub>O mixture, at room temperature and at 65 °C, up to three times. In a previous study, a 60-40% EtOH-H<sub>2</sub>O mixture showed a much lower yield of hesperidin, of only 2.7  $\text{mg g}^{-1}$  after a solid-liquid extraction performed at 50 °C.<sup>431</sup> The optimal hesperidin extracting experiments at room temperature are pure DMSO (30.58  $\text{mg g}^{-1}$ ) and the mixtures MeOH-DMSO (30.10  $\text{mg g}^{-1}$ ,  $R_a=7.48$ ), DMSO-EtOH (29.73,  $R_a=9.01$ ), followed by DMSO-EG (26.93,  $R_a=7.2$ ), Cyrene-Acetic Acid-H<sub>2</sub>O (21.43,  $R_a=9.37$ ) and 70% Cyrene-30% H<sub>2</sub>O (20.71,  $R_a=7.7$ ). It was previously reported that DMSO showed three times higher yield than methanol and six times higher than ethanol from a solvent extraction process.<sup>399</sup> The smaller the value of  $R_a$  was theoretically expected to be the solvent with the best result. Other factors contribute to the solubilization/extraction of the analyte, however,  $R_a$  values can be used to guide the search for efficient extracting media, as can be seen in results mentioned above.

Cyrene has showed a low extraction capacity, with only 3.23  $\text{mg g}^{-1}$ , due to its higher viscosity. The viscosity of Cyrene is lowered by increasing the temperature (hot extraction and fast hot extraction methods) and mixing it with other solvents (Section 4.4.2.2.). The selected solvents for this test were pure Cyrene, EtOH-H<sub>2</sub>O, Cyrene-H<sub>2</sub>O and Cyrene-H<sub>2</sub>O-acetic acid. By increasing the

temperature (hot extraction method), all the yields showed improvement (except for 70% EtOH-30% H<sub>2</sub>O discussed in Section 4.4.2.2.), with an increment of 91.3% for Cyrene, 42.1% for Cyrene-H<sub>2</sub>O-acetic acid, 29.1% for 50% H<sub>2</sub>O-50% EtOH and 13% for Cyrene-H<sub>2</sub>O when the process was carried out at room temperature. To enhance the energy efficiency of hot extractions, the two-best hot-methodology experiments were selected for investigating a reduced time and energy-consuming method, named fast-hot extractions. For 70% Cyrene-30% H<sub>2</sub>O mixture, this method presented even better results showing that the extraction phenomena are not time-dependent for the solvent. Differently, Cyrene-H<sub>2</sub>O-acetic acid mixture decreased extraction yield compared to the two-hour experiment. The result for Cyrene-H<sub>2</sub>O mixture is comparable with pure DMSO and suggests that the latter pure solvent could easily be replaced by a mixture of another solvent with water. Moreover, when mixing Cyrene and water a new solvent system is generated (discussed in Section 4.4.2.1.) with improved properties than of pure Cyrene. The results for rutin extraction from black tea are shown below (Figure 67):

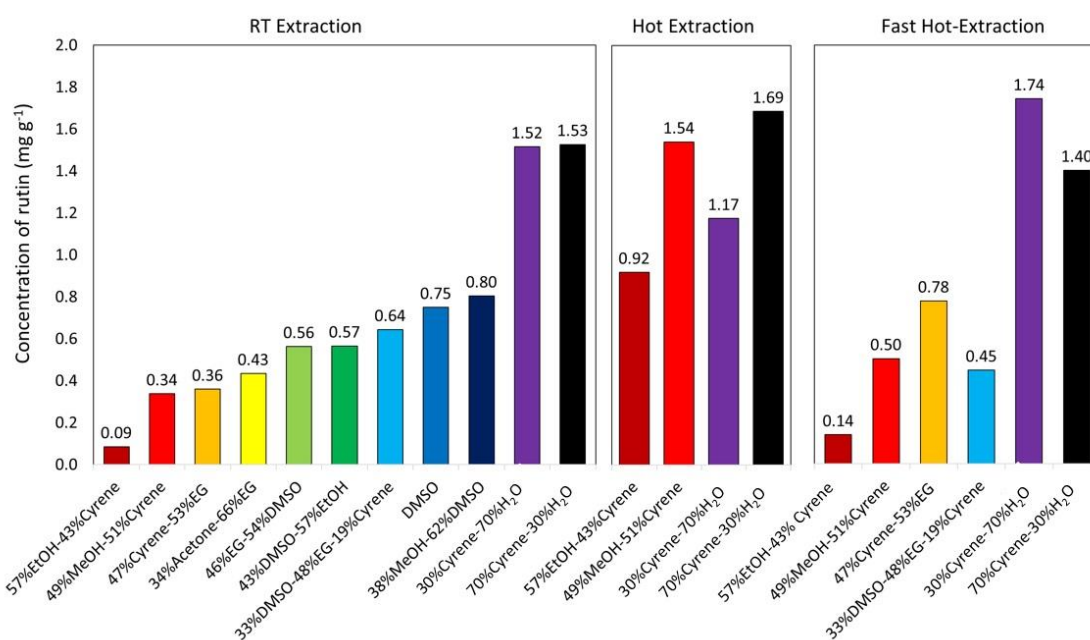


Figure 67: Concentration of rutin (mg g<sup>-1</sup>) from room temperature (RT) extraction, “hot extraction” (65 °C) and “fast hot” extraction determined using UHPLC. All extractions were realised in one stage. The binary and ternary solvent systems were predicted by HSPiP

The best yields at room temperature are seen with Cyrene-water mixtures: 30% H<sub>2</sub>O-70% Cyrene (1.53 mg g<sup>-1</sup>, R<sub>a</sub>= 4.87) and 70% H<sub>2</sub>O-30% Cyrene (1.52 mg g<sup>-1</sup>, R<sub>a</sub>= 15.49). Interestingly, the mixture 30% H<sub>2</sub>O-70% Cyrene did not dissolve the rutin standard, gaining a score of 5 in Hansen space, but has proved to be efficient in extraction from the dried tea leaves, probably due to the slightly

heating of the sample during the homogenisation, which enhanced the dissolution of flavonoid in solution. It has been observed that rutin (standard) dissolves easily at a higher temperature (65 °C). The minimum yields achieved for this test are 63% EG-34% Acetone (0.43,  $R_a= 8.18$ ), Cyrene-MeOH (0.34,  $R_a= 7.95$ ) and EtOH-Cyrene (0.09,  $R_a= 8.22$ ). The contrasts between the yield and  $R_a$  values can be seen in rutin's case too. The biggest difference can be seen in the case of Cyrene-water mixtures due to the formation of different geminal diols with distinct properties.<sup>33</sup>

Similar to hesperidin, hot and fast-hot procedures were employed for rutin extraction from black tea. Mixtures of Cyrene with MeOH, EtOH and H<sub>2</sub>O were investigated. At room temperature the mixtures Cyrene-H<sub>2</sub>O did not show differences in the extraction process (70% Cyrene-30% H<sub>2</sub>O with 1.53 mg g<sup>-1</sup>, as compared to 30% Cyrene-70% H<sub>2</sub>O with 1.52 mg g<sup>-1</sup>). On the contrary, increasing Cyrene's content within a mixture in hot extraction results in increasing yield when Cyrene is in a higher amount than water (70% Cyrene-30% H<sub>2</sub>O with 1.69 mg g<sup>-1</sup>, as compared to 30% Cyrene-70% H<sub>2</sub>O with 1.17 mg g<sup>-1</sup>). This could result in the two-hour maceration time when the viscosity of Cyrene lowers down and the diffusion of the bioactive compounds into the 70% Cyrene in water is superior that in 30% Cyrene in H<sub>2</sub>O. This means that Cyrene is a better solvent than water in this case. When heating the same Cyrene-water mixtures in a fast-hot extraction, the inverse trend is observed, with 30% Cyrene-70% H<sub>2</sub>O with 1.74 mg g<sup>-1</sup> superior to as compared to 70% Cyrene-30% H<sub>2</sub>O with 1.40 mg g<sup>-1</sup>. In this procedure, the maceration time is of only 2 minutes, when the bioactive compounds do not have enough time to diffuse from the solid into the mostly Cyrene mixture. In this case, the 70% H<sub>2</sub>O-30% Cyrene is showing superior extracting capacity than 70% Cyrene-30% H<sub>2</sub>O.

## 4.5.2. Factors influencing the extraction

### 4.5.2.1. Water influence

When water is added to Cyrene, the extraction is improved for hesperidin and rutin (Figure 68). Improved dissolution properties Cyrene-water systems were previously reported for organic compounds such as caffeine, salicylic acid, ibuprofen, aspirin, ferulic acid and mandelic acid.<sup>52</sup> In such systems, it has been shown that water reacts with Cyrene, in a readily reversible manner to form a geminal diol (hydrate).<sup>52</sup> In the present study, the Cyrene/water/geminal diol mixtures created a continuum of green solvents with controllable solubilisation properties for hesperidin and rutin. The mixtures of Cyrene and water extracted up to three times more hesperidin than pure Cyrene (Figure 68a). With rutin, a comparison could not be made due to the high viscosity of

pure Cyrene, which did not filtrate through the membrane. However, both 30% and 70% Cyrene in water systems gave the extraction yields for rutin (Figure 68b).

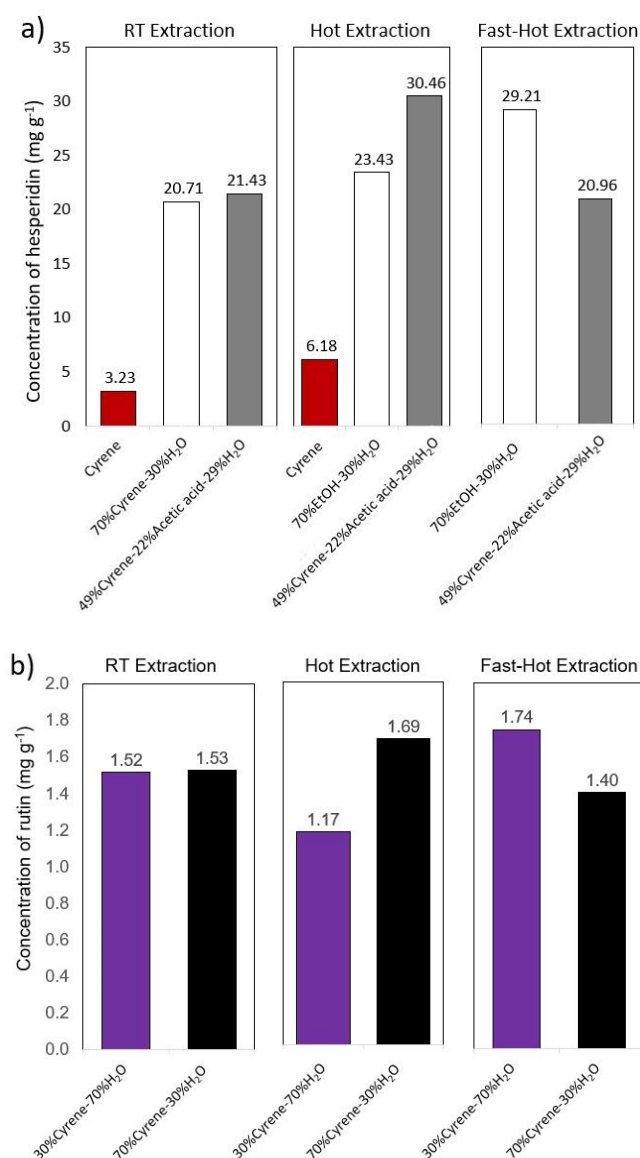


Figure 68: (a) Influence of water on dissolution and extraction of hesperidin and (b) rutin using Cyrene.

As stated, the mixtures of Cyrene and water also contain geminal diol (hydrate) and new ternary solvent systems in different proportions are formed (Table 23). As such, these different ternary systems affect the dissolution and extraction of flavonoids dramatically. The 70% Cyrene-30% H<sub>2</sub>O mixture dissolved and extracted hesperidin up to ten more times than pure Cyrene, which means that geminal diol formed in the solution is a better solvent than pure Cyrene. For rutin's case, no massive difference is spotted between 30% Cyrene-70% H<sub>2</sub>O and 70% Cyrene-30% H<sub>2</sub>O at room temperature, which could mean that a maximum of 30% Cyrene in water is necessary to dissolve rutin. After this concentration, lowering the viscosity with increasing the temperature improves

the extraction results. Based on the published results, the geminal diol formation decreases with the increasing of temperature<sup>52</sup> and Cyrene is favoured in a solution at 65 °C.

#### 4.5.2.2. Temperature influence

To study the effect of higher temperatures in extraction yields of hesperidin from orange waste, a temperature of 65 °C was considered suitable for altering important physical-chemical properties of the solvents such as viscosity, miscibility, and surface tension. The need for a higher temperature to dissolve hesperidin has been noted before.<sup>81, 398, 432</sup> The solubility of bio-active compound hesperidin was found to increase with temperature in all the solvents investigated.

For mixtures involving ethanol and water, only 50-50% shows a slight increase in hesperidin extraction upon heating. For Cyrene, heating gives twice the yield than that at room temperature (Figure 66). The Cyrene-water mixtures dissolve and extract the hesperidin from orange peel waste differently, depending on the amount of the two, with 70-30% Cyrene-H<sub>2</sub>O extracting the almost double amount of the hesperidin at room temperature (95.7% increase). The same Cyrene-H<sub>2</sub>O mixture is two times better than EtOH-H<sub>2</sub>O mixture when using the same concentration and temperature conditions. Cyrene-H<sub>2</sub>O improved the extraction capacity from 20.71 mg g<sup>-1</sup> to 23.43 and 29.21 mg g<sup>-1</sup> at higher temperature processes (Figure 66). Ethanol-H<sub>2</sub>O showed an insignificant increase of yield from 9.20 to 9.23 mg g<sup>-1</sup> at a higher temperature. This proves that the temperature has a superior impact on a mixture containing Cyrene due to its higher density than ethanol. This can be translated as lowering the viscosity with the increasing of temperature of Cyrene makes it a better solvent than ethanol. Decreasing the viscosity of Cyrene with temperature enhanced the diffusion and hence, the mass transfer from the sample to the solution, improving the extraction efficiency. Temperature-dependent solubility of bioactive compound rutin shows a similar trend as hesperidin, where the increased temperature improves the extraction capacity for mixtures where Cyrene is involved (Figure 67). The Cyrene mixtures with water, ethanol and methanol have shown up to eleven times better extraction capacity when heated up. The results obtained in the current study could be useful in greener crystallisation/purification methodologies and formulation development of bioactive compounds hesperidin and rutin.



## 4.6. Green metrics

CHEM21 metrics toolkit was used to measure the sustainability of the present method of extracting natural flavonoids. As ethanol has shown poor extraction ability in the present study, a previous environmentally friendly methodology using a mixture of ethanol and water (60-40% v/v)<sup>431</sup> has been used as baseline here to direct comparison of the proposed method used in this study. After showing potential at Zero Pass, the new method using Cyrene-water for hesperidin extraction, "first pass" was used.<sup>44</sup> The experimental of the baseline method and the method used in this study are shown in the Appendix C and the results are listed in Table 24:

Table 24: Comparative results of the new and the older extraction methods.

|  | Baseline method          | New method                   |
|--|--------------------------|------------------------------|
| Type of solvent                              | Ethanol-water 60-40%     | Cyrene-water mixture 70-30%  |
| Raw material used                            | Wet lime peel            | Dried orange peel            |
| Sample mass (g)                              | 5                        | 0.25                         |
| Solvent quantity (mL)                        | 50                       | 5                            |
| Solid-solv ratio (SSR) (g mL <sup>-1</sup> ) | 0.1                      | 0.05                         |
| T °C/time extraction                         | 50 °C/4 h                | 65 °C/2 h                    |
| Power extraction                             | 4 hours at 120 rpm       | 2 minutes at 14,450 rpm      |
| RME (%)                                      | 0.27                     | 2.92                         |
| Extraction yield (mg g <sup>-1</sup> )       | 2.7                      | 29.21                        |
| PMI (g g <sup>-1</sup> )                     | 3607.4                   | 839                          |
| PMI biomass                                  | 370.4                    | 34.2                         |
| PMI solvents                                 | 3237                     | 804.8                        |
| Product mass (g)                             | 0.0135                   | 0.0073                       |
| Type of extraction                           | Single-stage (duplicate) | Single-stage (single result) |

Many of the metrics applied were designed for reaction chemistry, thus did not generate meaningful data. However, as the new method of extraction of hesperidin from orange peel uses minimum quantities of dried sample and solvent compared to the established methodology, this was reflected in a number of metrics. The extraction method of flavonoids using a solid-liquid extraction is not a classical chemical reaction, hence the yield, conversion, selectivity, and atom economy (AE) cannot be calculated here.

The dried sample of orange peel used in this work was compared to a wet lime peel sample in a solid-liquid extraction using different solvent mixtures; the moisture from the latter one affected the yield of the extraction. However, the difference between the two samples was significant; the moisture from the wet lime sample did not make a big difference in the extraction process. The difference between both samples was related to the solvent mixture used in the process.

A mass-based yield was determined from the reaction mass efficiency (RME) which is 0.27% for the "baseline" method which uses ethanol-water mixture as extractor, compared to 2.92% for the new method using a mixture of Cyrene with water, making the newly discovered solvent mixture more efficient in flavonoids extraction. This is also born out by the PMI which shows a significantly lower mass input per g of hesperidin isolated for this method ( $805 \text{ g g}^{-1}$ ) as compared to the base line ( $3237 \text{ g g}^{-1}$ ).

Traditionally PMI is broken down to show the impact of reactants, reagents, and catalysts as one grouping (PMI reaction) and solvents as a second (PMI reaction solvents). In the case of extractions, this is displaying an overall mass input per gram of hesperidin isolated. The solvent PMI indicates that, unsurprisingly, solvents dominate the mass input in solvent extraction.

**LCA process** - LCA has been used to evaluate the quantity impact over the solvent's life cycle. The Furacell™ process to produce Cyrene presents a global warming potential lower than NMP synthesis and is leading towards being greenhouse gas neutral (Section 1.5.7.).<sup>166</sup> Circa Group has won the prestigious Environmental Leader award, top product 2019 for its bio-based and biodegradable solvent. Cyrene "replaces an otherwise toxic substance with a natural, gentler alternative without compromising quality or function. This product has the potential to change the solvent landscape for the better".<sup>433</sup>

**Solvents** - They are a critical issue as they constitute a large mass input in the process. In the current method only  $5 \text{ cm}^3$  Cyrene-water mixture was used. Coupled with improved extraction yield, this represents a significant reduction in process mass intensity (PMI) (Table 24 and Appendix C).

**Renewability** - Solvent recovery and recycling can have a positive effect on the environment and a single solvent systems is favoured in this case.<sup>434</sup> In the old method, ethanol can be easily recovered through a rotary evaporatioyn.<sup>431</sup> Cyrene and water can be easily separated. However, the distillation of Cyrene is energy intensive and requires the application of significant reduced pressure to allow distillation at a low enough temperature to ensure thermal decomposition does not take place.

**Health and safety** - It is mandatory under European law to assess for any explosion risk and classify the work area.<sup>435</sup> Ethanol is widely used in many applications, but it is highly flammable liquid and vapour (H225) and causes serious eye irritation. Also, ethanol is listed as T2 temperature class by ATEX (European Directives for controlling explosive atmospheres) (“an explosive atmosphere is not likely to occur in normal operation but, if it does occur, will persist for a short period only”).<sup>435</sup> The solvent used in this study, Cyrene is 99% biodegradable, non-flammable, it has low toxicity, no mutagenicity, although does cause eye irritation.<sup>115, 124</sup> Water, however, is non-toxic.

**Waste** - The wet waste can be reused to extract other chemicals after both extractions.

**Efficiency and energy** - In this study a mildly heating of Cyrene-water mixture led to a higher efficiency in extractions of flavonoids (up to eleven times than the baseline method). Recovery through distillation however will result in increased energy demands.

As seen in Table 24, the raw material used in the ethanol-water method uses 5 g per extraction, while in this work, a small amount of 250 mg raw material was used. The higher power used for homogenisation in the case of Cyrene-water extraction process of 14,450 rpm combined with a very short time used (2 minutes) is more advantageous than a lower power for a longer time used in an old method (120 rpm for 4 hours). The drawback of using Cyrene in the extraction of hesperidin and rutin in this study is the increase of temperature to 65 °C and the time needed to heat up the solvents or the mixture of sample with solvents to this temperature. However, less time would be more advantageous and taken into consideration for future extractions. As with all green metrics analysis, the impacts of different methodologies need to be examined holistically. Although energy requirements are greater with Cyrene-water systems, the quantity of solvent used (PMI) renewability, waste and health and safety considerations for this process suggests it is greener than the current baseline. The use of the bio-derived Cyrene for extraction and water for analysing in the process is an important step towards improving the sustainability of the process.

## 4.7. Chapter conclusion

Based on the circular bio-economy concept, this work aimed at finding new paths towards the development of new methods for the analysis and extraction of valuable bioactive compounds present in plant-derived materials as agro-industrial waste, focusing on bio-based, more efficient, sustainable and greener solvents. A new and simple process with a minimum amount of solvent in one-stage extraction was used in this work, resulting in a high-quality extract. To evaluate the sustainability of the proposed methodology, CHEM21 metric tools were used in this study. The

new single-stage extraction using Cyrene and mixtures with Cyrene showed up to three times better extraction capacity than using ethanol-water mixtures at the same conditions and up to eleven times when compared to an older methodology using ethanol-water mixture (29.2 mg g<sup>-1</sup> for 70% Cyrene-30% H<sub>2</sub>O at 65 °C compared to 9.2 mg g<sup>-1</sup> for 70% EtOH-30% H<sub>2</sub>O at RT or 65 °C and only 2.7 mg g<sup>-1</sup> for a 60% EtOH-40% H<sub>2</sub>O at 50 °C). When using mixtures Cyrene and water, the results show an increase to ten times than using pure Cyrene the capacity due to the formation of geminal diols (hydrates) with distinct properties. A mildly increased temperature of pure Cyrene improved the capacity of extracting these bioactive compounds to 91%, due to changes in viscosity and matrix accessibility. Although, improving the energy efficiency of the process and reducing energy consumption are currently being considered. In this study, Hansen's solubility parameters have proved to be a useful tool to predict optimum solvents and mixtures of solvents for the solubilisation of natural products and their extraction from complex matrices, as orange waste and black tea. As a novel bio-solvent, Cyrene shows more than promising features useful for designing greener and more sustainable methods for crystallisation, purification, extraction and formulation of bioactive compounds from natural sources. As aimed, the application of HSP combined with the use of bio-based solvents as an alternative to replacing petroleum-based solvents and further experimental validation offered important advantages such as simplicity, rational use of time and resources, contributing to materialising a circular economy model in chemistry, keeping processes as simple as possible as well as promoting a reflection about the role of waste as starting material in the current and future industrial processes.

## Chapter V

### 5. Cyrene in single-walled carbon nanotubes (SWCNTs) dispersion<sup>6</sup>

---

<sup>6</sup> TEM analysis from this chapter was realised by Dr Meg Stark and Karen Hodgkinson from Bioscience Technology Facility, Biology Department, University of York, UK.



## 5.1. Introduction

Carbon nanotubes (CNTs) are an extremely attractive material due to their electronic, mechanical, and thermal properties. It is believed that the discovery of CNTs has initiated the era of nanotechnology and has become of keen interest to materials scientists.<sup>436</sup> They contain one or several concentric graphite-like layers with diameters ranging from a few angstroms up to tens of nm and were discovered by Iijima in 1991.<sup>436-438</sup> SWCNTs are synthesised by three main methods such as chemical vapour deposition, arc discharge and laser ablation.<sup>439-442</sup> Carbon nanotubes are mainly categorised by the numbers of layers: a) single-walled carbon nanotubes (SWCNTs) consist of a single graphene layer with a diameter of less than 2 nm and b) multi-walled carbon nanotubes (MWCNTs) having two or more cylinders of graphene sheets with diameters 2-25 nm and wall-to-wall distance of 0.36 nm (Figure 69).<sup>443, 444</sup>

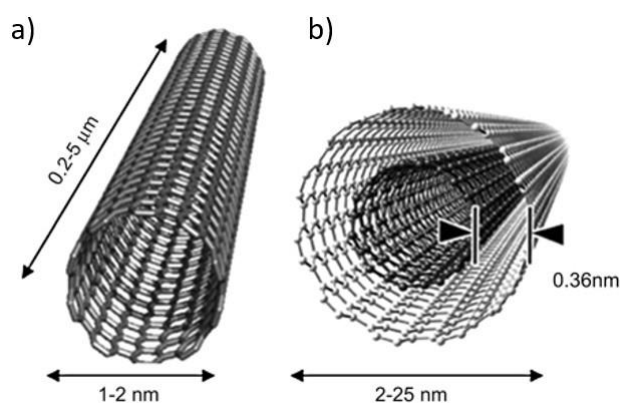


Figure 69: (a) Structures of single- and (b) multi-walled carbon nanotubes. Adapted from reference.<sup>444, 445</sup>

Carbon nanotubes (CNTs) have gained huge attention since their discovery due to their superior and tunable electrical and thermal properties, enormous surface area and low density, strength, high chemical resistance to chemical degradation and temperature resistance (low thermal expansion).<sup>446, 447</sup> However, carbon nanotubes tend to be entangled together and their poor dispersion in solvents and polymers limits their chemical modifiability and applicability.<sup>448-458</sup> However, heavily entangled and disordered SWCNT networks do not have the optimum mechanical, thermal, and electronic properties of individual SWCNTs.<sup>455-458</sup> Carbon nanotubes tend to form ropes or bundles due to van der Waals interactions and  $\pi - \pi$  interactions among inter-tubes which can aggregate further in aqueous solution forming entangled networks.<sup>459-461</sup> When dispersed in solvents and polymers, carbon nanotubes interact with the media *via* van der Waals interactions,  $\pi - \pi$  stacking, covalent and non-covalent interaction, hydrophobic

interactions, hydrogen bonding, electrostatic interaction, hydrophobic interaction and CH- $\pi$  interactions.<sup>453, 462</sup> The SWCNTs present a perfect  $sp^2$  backbones of SWCNTs, when compared to MWCNT, leading to a more hydrophobic tubular surface and the worse processability.<sup>463</sup> Individually dispersed or small bundles of carbon nanotubes in solutions are desirable for many applications such as composites for energy storage (*e.g.* hydrogen storage, fuel cells, and the lithium battery), coatings, electronic devices, sensors, transistors, integrated circuits, near-infrared detectors, filtration membranes, biological and biomedical applications.<sup>464-474</sup> The dispersion and arrangement of carbon nanotubes in the composite matrix hold a central role in controlling the properties of the resulting composites.<sup>475</sup> In membranes technology, they are mainly used for their conductivity, antimicrobial and antifouling properties.<sup>467, 468, 476, 477</sup> Short individual carbon nanotubes can puncture the microorganisms (cells lose their cellular integrity) and SWCNTs are more effective in this role than MWCNTs due to their thin end. However, in a liquid media, longer CNTs form aggregates that act like needles surrounding the cells and kill them. CNTs absorb near-infrared (NIR between 700-1100 nm) photons, generating heat or emitting light, making them efficient photothermal and imaging agents for killing the cancer cells.<sup>478</sup>

Carbon nanotubes are commonly processed by dispersing them in liquid media and numerous strategies of de-bundling of CNTs have been reported this way to prepare stable dispersions of SWCNTs in different solvents.<sup>68, 69, 454, 479-485</sup> Nanotubes do not disperse in neat solvents and the aqueous suspensions of non-functionalized CNTs are known to be unstable. However, amide solvents such as DMF and NMP have been reported as good solvents for CNTs dispersions.<sup>68, 69, 485-489</sup> These solvents have health and environmental problems; hence non-toxic methods to disperse carbon nanotubes has motivated scientists to investigate various candidates. Large-scale de-bundling of single-walled nanotubes has been demonstrated by dilution of nanotube dispersions in less toxic solvents such as 1-benzyl-2-pyrrolidinone, which forms stable solutions for a few weeks.<sup>490</sup>

Cyrene, an alternative to the toxic polar aprotic solvents, has been previously reported in a non-covalent dispersion of multi-walled carbon nanotubes with the aid of electron-deficient acceptors which had the role to interrupt the inter-CNTs  $\pi - \pi$  interactions *via* a donor-acceptor interaction mechanism, permitting the debundling and dispersion of individual MWCNTs and inhibiting their re-agglomeration.<sup>160</sup> Moreover, Cyrene was used as a dispersing medium for MWCNT-based supercapacitors electrodes, giving stable suspensions of relatively high concentration nanotubes without the need of a surfactant; the results showed that concentrations of 1-3 mg mL<sup>-1</sup> MWCNT in Cyrene are stable for two months.<sup>491</sup> In this work, non-covalent dispersion of pristine single-walled carbon nanotubes was performed using Cyrene on its own or



with the aid of a surfactant (Triton™ X-100) and a polymer (polyvinyl pyrrolidone). SWCNTs were dispersed in a solution by ultrasonication, followed by low centrifugation.

## 5.2. Methods of carbon nanotubes dispersion - Background

### 5.2.1. Covalent methods of dispersion

The covalent approach alters the structure and intrinsic properties of carbon nanotubes. The covalent bonding happens by the attachment of long alkyl chains<sup>492</sup> and polymers,<sup>493</sup> fluorination,<sup>486</sup> and radical reactions<sup>494</sup> to the end of the nanotubes or their sidewall, leading to relatively soluble materials. During chemical processes, the carbon-carbon double bond which makes up the skeleton of the tubes breaks down, disrupting the  $sp^2$  network and leading to a partial loss of conjugation and formation of defects. These defects affect the electrical and mechanical properties of the functionalised carbon nanotubes. The nanotubes have defects at the end caps where highly reactive fullerene-like hemispheres can be found or they present sidewalls defects,  $sp^3$ -hybridised defects, and vacancies in the nanotube lattice.<sup>445, 495</sup> During the chemical functionalisation, covalent bonds between the carbon form of CNTs from the end caps of nanotubes or at their defected sidewalls and various functional groups. During the covalent sidewall functionalisation, a change of hybridization from  $sp^2$  to  $sp^3$  takes place and a simultaneous loss of  $p$ -conjugation system on the graphene layer. Highly reactive molecules (fluorine) are reacted with the sidewalls, which are considered inert.<sup>496, 497</sup> The fluorinated CNTs have C-F bonds weaker than in alkyl fluorides<sup>498</sup> but can provide substitution sites for additional functionalisation<sup>499</sup> of fluorine atoms by amino, alkyl and hydroxyl groups,<sup>500</sup> as well as addition of dichlorocarbene,<sup>501</sup> chlorination, bromination<sup>502</sup> and hydrogenation.<sup>503</sup> During the purification of carbon nanotubes to remove the metals and amorphous carbon resulted from their synthesis, strong acids are used (nitric and sulfuric acid); oxidative damage to the nanotube framework can occur leaving holes functionalised with oxygenated functional groups.<sup>504, 505</sup> Similar effects can occur when carbon nanotubes are treated with strong oxidants such as  $KMnO_4$ , ozone or plasma.<sup>506-508</sup> The tubes suffer oxidative damage generating oxygenated functional groups such as carboxylic acid, ketone, alcohol and ester groups, which are precursors for further chemical reactions at the end of the tubes or defected sides.<sup>509-511</sup> The resulting functionalised carbon nanotubes with more polar groups can easily disperse in various organic solvents without the need for additives. However, most of the covalent methods use toxic solvents and generate defective

nanotubes. Covalent surface functionalisation of carbon nanotubes improves their dispersibility in neat solvents; however, it creates other problems, such as the disturbance to some extent of their graphitic structure of the walls, problem which then need to be rectified.

## 5.2.2. Non-covalent methods

In 2002, carbon nanotubes have been dispersed for the first time with the aid of surfactants. The dispersion of SWCNTs in deionised water was realised by sonication followed by ultracentrifugation and using sodium dodecyl sulphate (SDS) surfactant and poly(vinylpyrrolidone) (PVP), which eliminated the hydrophobic interface between CNTs and their aqueous medium.<sup>512</sup> Since then, many efforts have been realised to find optimum surfactants and polymers for nanotubes dispersions.<sup>481, 513-516</sup> The non-covalent functionalisation of the carbon nanotubes can be realised through the absorption of various surfactants and polymers.<sup>463, 517-524</sup> During the non-covalent functionalisation, carbon nanotubes can form  $\pi - \pi$  interaction with aromatic compounds through the graphitic sidewalls without significant change of the electronic properties of CNTs.<sup>525</sup> The non-covalent methods are advantageous in nanotubes processing due to their role in preserving the nanotubes conjugated  $\pi$  system and their electrical properties, but excessive dispersant residue can still be present in the solution at the end of the process, which can be difficult to be completely removed. Moreover, the stability of the suspension of non-covalently functionalized CNTs was found to depend on the type of dispersant<sup>515, 526</sup> and their concentration,<sup>527</sup> or the length of the nanotubes.<sup>528</sup>

Generally, the mechanical dispersion of carbon nanotubes can either take place by ball milling, bead milling or ultrasonication.<sup>529-531</sup> Ultrasonic treatment is mostly used in dispersing carbon nanotubes, for their functionalisation or nanocomposite and nanomaterials formulations.<sup>530, 531</sup> The ultrasonic dispersion is commonly performed in solvents such as water, ethanol or polar aprotic solvents, with/no aid of dispersants.<sup>453, 529</sup> Ultrasonication is based on ultrasound waves and cavitation phenomena.<sup>532</sup> Cavitation refers to the formation, growth and collapse of vapour or gas bubbles under the influence of ultrasound. The bubbles can undergo a single growth followed by their collapse or oscillatory motion for several acoustic cycles, depending on the frequency and intensity of the ultrasound waves. The acoustic emission spectrum with water as medium is based on pressure due to the ultrasound waves, with the pressure pulses due to bubble oscillation/collapse superimposed on it.<sup>532</sup> Water is mostly used as cavitation media; cavitation does not occur in the silicon oil because the amplitude of the ultrasound waves in the bath is below the cavitation threshold for silicon oil.<sup>532</sup> Cavitation can be: a) stable, leading to chemical

modification of the surface of the CNTs or b) inertial, which favours CNT exfoliation and length reduction.<sup>533</sup> During the growth and collapse phases in a high-intensity ultrasound (*i.e.*, with an ultrasonic probe), sonochemical effects occur, causing an unintentional physical and chemical modification of the carbon nanotubes. A higher amplitude of waves generates high frequencies (20 kHz-1 MHz), leading to molecular dissociation, void creation, and the rapid formation of bubbles. Continued interaction between bubbles and the acoustic field can result in their growth and violent bubble collapse creating a high local temperature.<sup>534</sup> The shock waves derived from bubble collapse can cause physical modifications to CNTs, whilst gas- or solution-phase chemistry can occur inside or outside the bubbles.<sup>535</sup> A high-intensity ultrasound has been used in organic synthesis, nanomaterials, organometallic chemistry, and industrial manufacturing processes.<sup>535, 536</sup> During the chemical syntheses, the cavitation makes available energies that are not available from any other source.<sup>537</sup> It accelerates a chemical reaction and allows less severe forcing conditions; the number of steps in synthesis can be reduced and even switch the reaction pathway. However, one of the drawbacks of ultrasonic baths is the inability to obtain uniform energy intensity and cavitation conditions in the bulk volume of the reactor. That means that different positions in the ultrasonic bath have different cavitation results which will ultimately affect the dispersion of SWCNT in solutions. Moreover, ultrasonication is often related to a certain degree of damage to the CNTs which results in their breakage and introduction of defects to their sidewall structure.<sup>538, 539</sup> Therefore, efforts are being made to minimise the defects that occur during ultrasonication by applying milder sonication intensity or by adding surfactants to the solution containing carbon nanotubes.<sup>540</sup>

### **5.2.3. The additives used in non-covalent dispersion of carbon nanotubes**

#### **5.2.3.1. Surfactants**

Surfactants are amphiphilic molecules containing both hydrophilic and hydrophobic parts and are used in carbon nanotubes dispersal because they are easily available and low-cost. Surfactants are usually involved as de-bundling agents, but their removal can be difficult because the surfactants are adsorbed at CNT's junctions and difficult to remove completely. The hydrophobic part of the surfactants can prevent tubes from aggregation, while the hydrophilic part can introduce the dispersing system in an aqueous medium.<sup>463</sup> Surfactants such as sodium dodecyl sulfonate (SDS), sodium tetradecylsulfate (STDS), Triton™ X-100, Igepal DM-970, Pluronic (F127, F108, F98), dodecyltrimethylammonium bromide (DTAB), cetyltrimethylammonium bromide (CTAB), Tween

20, Tween 80 are widely used to disperse nanotubes.<sup>519-524</sup> Ionic (anionic SDS, STDS, and cationic CTAB, DTAB) and non-ionic (Triton, Pluronic, Igepal) surfactants disperse SWCNTs in aqueous solution and stabilise them by electrostatic repulsion and by steric repulsion respectively.<sup>482, 541</sup> The structures of the cationic surfactant CTAB, anionic (SDS) and non-ionic surfactant Triton™ X-100 are seen in Figure 70:

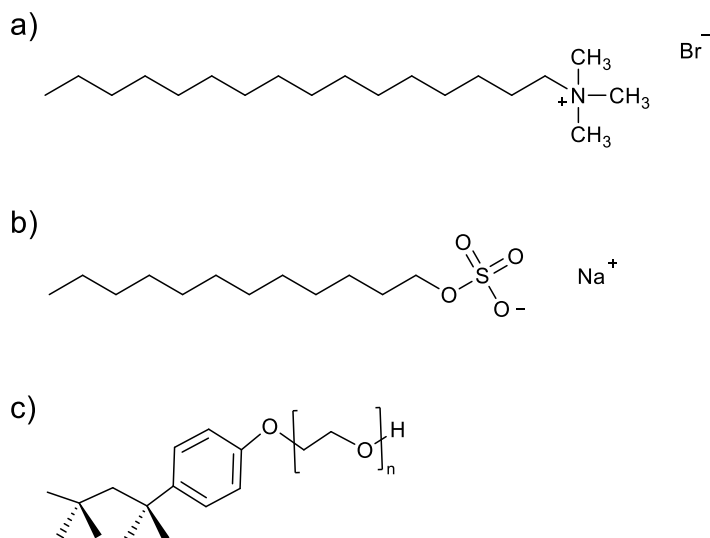


Figure 70: (a) Molecular structure of the cationic surfactant (CTAB), (b) anionic (SDS) and (c) nonionic surfactant (Triton™ X-100).

The surfactant used in this work, Triton™ X-100 (2-[4-(2,4,4-trimethylpentan-2-yl)phenoxy]) is a non-ionic surfactant with a hydrophilic polyethylene oxide chain and an aromatic hydrocarbon lipophilic or hydrophobic group (Figure 70c). Triton is a clear viscous fluid (relative density 1.065g/cm<sup>3</sup> at 20 °C) and it exhibits strong hydrogen bonding with water in which it easily dissolves. It is widely used in isolation and solubilisation of protein, DNA extraction and emulsification and as a dispersant for carbon nanotubes dispersions in water, ethanol or polar aprotic solvents.<sup>519, 520, 542, 543</sup> Their good nanotube separation and stabilisation capabilities are superior to pure solvents or other surfactants such as dodecyl sulfate (SDS) or Tween 20 or Tween 80.<sup>519, 520, 543</sup> However, the stability of this suspension using Triton™ X-100 or SDS was been previously reported to be no longer than 1 week.<sup>544</sup> The mechanism of interaction between Triton and carbon nanotubes is based on  $\pi$ -stacking.<sup>544</sup> However, Triton™ X-100 is classified as a substance of very high concern (SVHC) because it is endocrine-disrupting, causes serious eye damage, is corrosive and very toxic to aquatic life with long-lasting effects. ECHA listed this surfactant in "Authorisation list (Annex XIV) and needs to be replaced from 4 January 2021 with less toxic substances."<sup>545</sup>

### 5.2.3.2. Polymers

Polymer/CNT composites have attracted great attention due to improved mechanical, thermal and electrical properties.<sup>546</sup> However, CNTs are easy to agglomerate, leading to many defect sites in the composites, and limiting the efficiency of CNTs on polymer matrices.<sup>547</sup> Polymer structure, its molecular weight, skeleton structure can influence the dispersion efficiency of CNTs.<sup>463, 548, 549</sup> Conjugated polymers (whose backbone is made of alternating single and double bonds), including polyfluorene, polythiophene, polycarbazone disperse the carbon nanotubes and sort them simultaneously by wrapping around the nanotube through  $\pi - \pi$  interactions. However, the conjugated polymers wrapped SWCNTs may be strongly be influenced by solvent polarity and quantity and characteristics of the polymer.<sup>463</sup> The non-conjugated polymers (containing repeating non-conjugated structural units, such as polyethylene glycol, polyvinyl pyrrolidone (PVP), polyacrylonitrile, polysaccharides, cellulose) involve specific wrapping around the CNTs.<sup>521, 522</sup> PVP (Figure 71a), is a synthetic polymer consisting of linear 1-vinyl-2-pyrrolidone groups. PVP is non-toxic, chemically inert, temperature-resistant, pH-stable, and mostly used in pharmaceutical and medicine, membranes for water purification, food processing and gas separation, adhesives, paper products, cosmetics and toiletries, and carbon nanotubes dispersion.<sup>522, 550-554</sup> PVP has an affinity to complex both hydrophobic and hydrophilic substances.<sup>555</sup> PVP is a good alternative to surfactants which can be toxic and are widely used in the solubilisation of carbon nanotubes even though they did not show a better dispersion efficiency.<sup>454, 556-561</sup> Typical wrappings of a polymer, PVP in this case, around a CNT rope is shown in Figure 71b. This shows possible wrapping of PVP around a CNT tube by double helix (top), triple helix (middle) and multiple parallel wrapping strands from the same polymer chain due to the backbone bond rotations (down).<sup>562</sup>

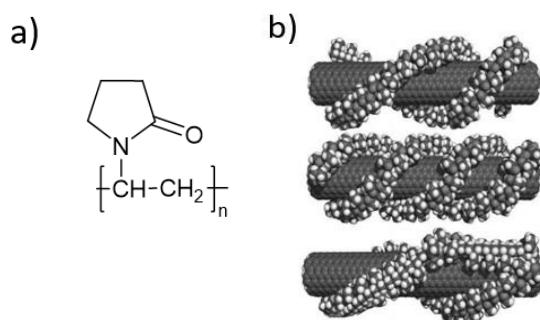


Figure 71: (a) Structure of PVP and its possible wrapping arrangements around CNT tubes. Adapted from reference.<sup>562</sup>

PVP was used in this work as a dispersant for single-walled carbon nanotubes in Cyrene for comparison with dispersions using neat solvents and surfactant/solvent media. As seen in Table A 17, PVP is soluble in a wide range of solvents including water, ethanol, Cyrene and NMP.

#### 5.2.3.3. Other additives

Graphene oxide (GO) has surfactant-like characteristics such as great water solubility and strong  $\pi - \pi$  conjugated interactions with other  $sp^2$  networks and was used to disperse carbon nanotubes, fullerenes and graphene.<sup>563</sup> Bile acid salts (BAS) is soluble in water and used to disperse CNTs in aqueous solutions and outperform various commercial surfactants.<sup>564</sup> BAS adsorption on CNT is mainly based on hydrophobic interactions which allowed efficient dispersion of CNT in aqueous suspensions.<sup>35, 137</sup> Organic dyes show strong adsorption on CNT due to their polyaromatic structure, which allow enhanced hydrophobic or  $\pi - \pi$  interactions and were used to disperse CNTs in water and organic solvents.<sup>464</sup> However, organic dyes are toxic, limiting their applications. Nanosilicas have been efficient in SWCNTs dispersions in aqueous solution; they insert into the inter-tubes *via* Van der Waals force for de-bundling SWCNTs.<sup>565</sup> Other dispersants consist of saccharides and polysaccharides,<sup>566-568</sup> proteins<sup>569</sup> and DNA.<sup>480, 570</sup>

### 5.3. HSPiP's predictions in carbon nanotubes dispersion

Hansen Solubility Parameters were employed by Ham *et al.* to correlate the degree of dispersion of single-walled carbon nanotubes in solvents and aqueous surfactant emulsions.<sup>138</sup> They found that the solvents dispersion parameter ( $\delta_D$ ) plays an essential role in dispersing nanotubes in solvents and found DMF, chloroform and NMP (with  $\delta_D$  between 17.4 and 18) to be most suitable for this role. In the same study, carbon nanotubes have swollen in solvents with  $\delta_D$  between 15.8-17 or 18-19  $MPA^{1/2}$  (DMSO, THF, DCM, benzene, toluene) and precipitated in solvent candidates with  $\delta_D$  values in the range 13-16.4  $MPA^{1/2}$  (acetone, water, methanol, hexane). Hansen Solubility parameters have not been used in this work to predict carbon nanotubes dispersion. Hence,  $\delta_D$  for Cyrene was found to be 18.9  $MPA^{1/2}$  (HSPiP 5.0.03 version), this could mean that the nanotubes should be swollen in the solution, similar to DMSO ( $\delta_D=18.4$ ). However, the "swollen" nanotubes have not been showcased in the research paper. Moreover, Ham *at al.* explained the degree of dispersion of nanotubes purely from Hansen Solubility Parameters perspective; other variables (*e.g.* viscosity, temperature) have not been considered.

## 5.4. Dispersion of SWCNTs using the ultrasonication technology

### 5.4.1. Dispersion of pristine SWCNTs in neat solvents

The single-walled carbon nanotubes used in this project were kindly offered by OCSiAL Tuball. Pristine SWCNTs were first dispersed in three different solvents: ethanol, NMP and Cyrene using ultrasonication followed by centrifugation and decanting the supernatant (Figure 133). In this work, an ultrasonic frequency of 40 kHz was used to avoid the chemical effects on CNTs and walls destruction. At a first look, a few seconds of manual shacking of  $1.25 \text{ mg mL}^{-1}$  of SWCNTs was followed by 1 hour of resting the tubes. Figure B 16 (Appendix B) shows the nanotubes freely floating in the entire amount of Cyrene, while in NMP or ethanol they settled at the bottom of the tube. That means that Cyrene is a better dispersant and stabilisation media than NMP and ethanol. NMP, however, dispersed a relatively higher number of nanotubes than of ethanol, the solution being stable after one hour. After sonication, centrifugation, and filtration of the supernatant of a solution containing SWCNTs dispersed in ethanol, very little amount was collected from three samples, which means a large amount of solvent is needed for this type of solvent. Hence, only Cyrene and NMP were further used in the dispersion of  $0.1$  and  $1.25 \text{ mg mL}^{-1}$  SWCNTs in solvent, using 1, 5, 10 and 20 hours of sonication. Neat Cyrene and NMP were used to disperse pristine SWCNTs, using different times of sonication (Figure 72). Each experiment was done up to five replications, depending on the experimental errors. The samples were coded based on the solvent used and the initial concentration of SWCNTs. "C1.25" represents a sample containing  $1.25 \text{ mg}$  SWCNT dispersed in  $1 \text{ mL}$  of Cyrene while "N0.1" means  $0.1 \text{ mg}$  SWCNT dispersed in  $1 \text{ mL}$  of NMP and using 20 hours of sonication.

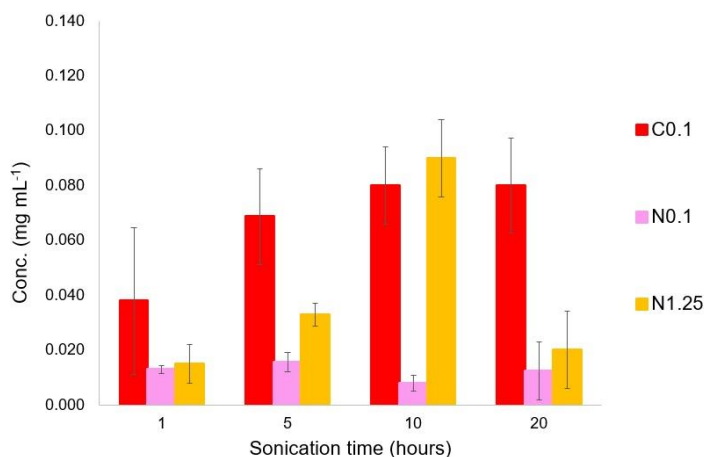


Figure 72: Single-walled carbon nanotubes dispersed in neat Cyrene and NMP using 1-, 5-, 10- and 20-hour sonication.

Full data can be found in Table A 18. It has been previously reported that different positions in the ultrasonic bath have different cavitation results conditions, which affected the dispersion of SWCNT in solutions.<sup>571</sup> That means that optimum results can be obtained if the conditions are controlled by finding the optimum point in the ultrasonic bath which can displace the highest amount of nanotubes from the bundles from a Cyrene-based solution. The standard deviation of C1.25 sonication results registered high values and did not have a statistical significance; hence they have not been included in Figure 72. Standard deviation and Z-scores were calculated from equations 16 and 17 for C0.1, N0.1 and N1.25 using 1-, 5-, 10- and 20-hour sonication. The highest standard deviation was registered by C0.1, 1h samples with  $\sigma=0.027$ , while the smallest value was registered by N0.1, 1h with  $\sigma=0.001$ . This demonstrates that the inhomogeneity of sonication had a higher impact when a higher amount of nanotubes was dispersed in a solution. Moreover, the amount of SWCNTs dispersed in N0.1, 1h was approximately three times lower than C0.1, 1h ( $0.013 \text{ mg mL}^{-1}$  compared to  $0.038 \text{ mg mL}^{-1}$ ). The highest concentration of SWCNTs was achieved in NMP solutions (N1.25, 10h), with a mean  $0.09 (\pm 0.637) \text{ mg mL}^{-1}$ , followed by C0.1, 10h, C0.1, 20h with  $0.08 (\pm 0.041 \text{ and } \pm 0.099) \text{ mg mL}^{-1}$  and C0.1, 5h with  $0.069 (\pm 0.051) \text{ mg mL}^{-1}$ . Both N1.25, 10h and C0.1, 10h had the lowest standard deviations, with  $\sigma=0.014$ ; however, a small amount of starting material (SWCNT) was needed to be dispersed in Cyrene ( $0.1 \text{ mg mL}^{-1}$  SWCNTs) than in NMP ( $1.25 \text{ mg mL}^{-1}$ ) for fairly similar final concentrations achieved. Z-scores for the lowest (0.07) and highest (0.1) values for C0.1, 10h data set are  $-0.714$  and  $1.428$  standard deviations below and above the mean, respectively. For N1.25, 10h, Z-scores lie between  $-0.714$  and  $0.714$  standard



deviations below and above the mean. C0.1, 10h samples have shown more variations between the tests than of N1.25, 10h, with the latter more reliable than the former.

Generally, a higher sonication time showed more consistency in the results. Moreover, high sonication times (10 and 20 hours) could potentially break down more nanotubes, but the solution can become saturated with the little ropes which then can re-agglomerate and interact with each other *via*  $\pi - \pi$  stacking and removed by centrifugation.

#### 5.4.2. SWCNTs dispersion in Cyrene with the aid of Triton™ X-100

The samples were coded based on the solvent used, the initial concentration of SWCNTs used and the surfactant used. "C1.25, Triton" represents a sample containing 1.25 mg SWCNT dispersed in 1 mL of Cyrene and Triton as surfactant, while "N0.1, Triton" means 0.1 mg SWCNT dispersed in 1 mL of NMP and Triton. Additionally, the sonication time was added to the initial name, *i.e.*, "C0.1, 10h, Triton" means a solution of 0.1 mg SWCNTs and Triton per mL was sonicated for 10 hours. Triton™ X-100 was chosen for its superior de-bundling and stable solutions of carbon nanotubes. In this work, Triton has been shown to produce optimal SWCNTs dispersion in Cyrene-based solutions (Figure 73):

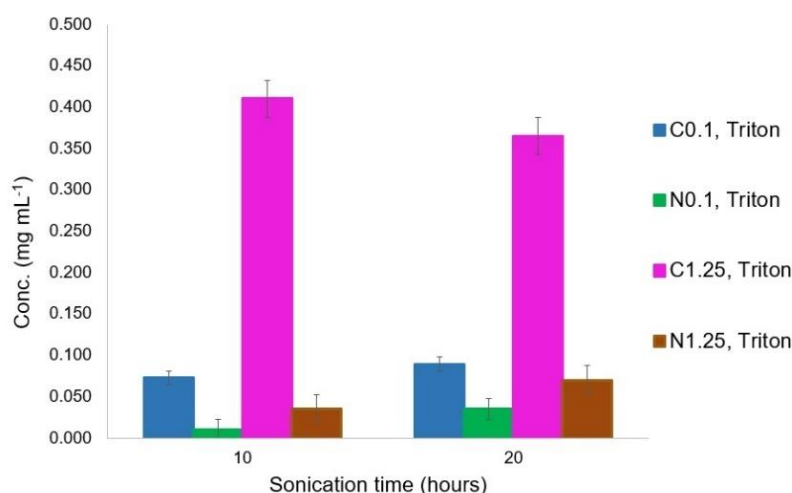


Figure 73: Single-walled carbon nanotubes dispersed in Cyrene and NMP in the presence of Triton™ X-100, using 10- and 20-hour sonication.

The standard deviation of "1" and "5 hours" sonication results is high and does not have a statistical significance; hence they have not been included in Figure 73. Bundles of SWCNT and Triton are formed in Cyrene-based solution by  $\pi$ -stacking<sup>544</sup> and removed by centrifugation;

however more short ropes of SWCNT are expected to form in C1.25, Triton when sonicated for 10 and 20 hours and left floating in the solution after centrifugation. Samples of N0.1, 10h, Triton and N1.25, 20h, Triton have shown standard deviation identical to the mean; with no limits for the confidence level for mean. This demonstrates the reliability in the sample dispersion in NMP at these conditions. Z-scores of C1.25, 10h, Triton are -0.707 and 0.707 standard deviations away from the mean, while C1.25, 20h, Triton presents Z-scores between -0.700 and 0.700 standard deviations below and above from the mean. As the values of Z-scores are similar, the standard errors of the mean can differentiate the samples. Both C1.25, 10h, Triton and C1.25, 20h, Triton have shown highest values for the level of confidence, with mean of 0.410 ( $\pm 8.912$ ) and 0.365 ( $\pm 2,228$ ), respectively. This means that Cyrene has not shown consistency in dispersing SWCNT in high concentration using Triton. When using NMP, N1.25, 10h, Triton has a lower mean 0.035 ( $\pm 1.591$ ) and a lower standard deviation 0.035 and Z-scores of -0.714 and 0.714 standard deviations below and above from the mean, only slightly further away from the mean than its counterpart C1.25, 10h, Triton. However, Cyrene disperse more SWCNTs than NMP, with a mean concentration of 0.410 mg mL<sup>-1</sup>, compared to 0.035 mg mL<sup>-1</sup> NMP. N1.25, Triton, 20 hour-sonication showed similar results to C0.1, Triton, 10 hour-sonication and lower results than C0.1, Triton, 20 hours. which means that the highest concentration of SWCNT combined with the longest time of sonication (20 hours) gives similar results to a low initial concentration of SWCNTs dispersed in Cyrene for lower sonication time (10 hours) and inferior results to an even shorter time of sonication in Cyrene and Triton.

### **5.4.3. SWCNTs dispersion in solvents with the aid of polyvinyl pyrrolidone (PVP)**

The samples were coded based on the solvent used, the initial concentration of SWCNTs used and the surfactant used. "C0.1, PVP" represents a sample containing 0.1 mg SWCNT dispersed in 1 mL of Cyrene and PVP as dispersant, while "N1.25, PVP" means 1.25 mg SWCNT dispersed in 1 mL of NMP and PVP. Additionally, the sonication time was added to the initial name, *i.e.*, "C0.1, PVP, 10 hours" means a solution of 0.1 mg SWCNTs and PVP per mL was sonicated for 10 hours. The standard deviation of the results of C1.25, PVP and N0.1, PVP dispersed using 1, 5, 10 and 20 hours do not have a statistical significance; hence they have not been included in Figure 74:

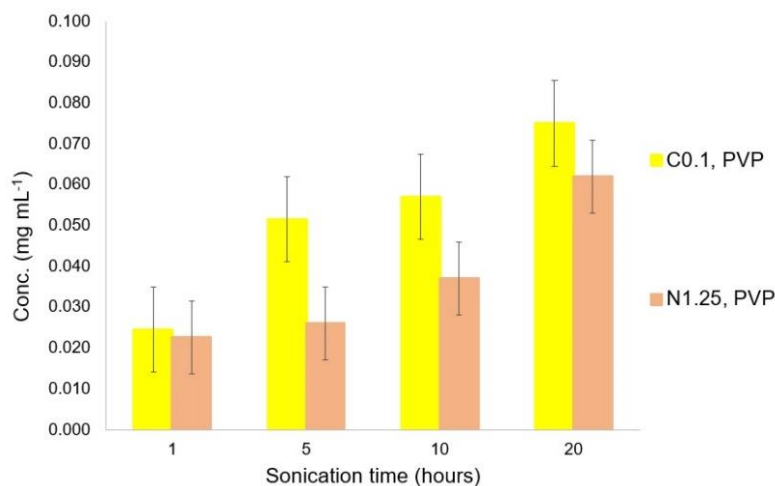


Figure 74: Single-walled carbon nanotubes dispersed in Cyrene and NMP in the presence of PVP, using 1-, 5-, 10- and 20-hour sonication.

C0.1, PVP and N1.25, PVP increased with sonication; however, the former solution showed superior debundling of SWCNTs than the latter for all sonication times. C0.1, 20h, PVP showed the highest concentration of SWCNTs dispersed in the solution, with  $0.075 (\pm 0.318)$  mg mL<sup>-1</sup> and a standard deviation  $\sigma=0.007$ , followed by N1.25, 20h, PVP with  $0.062 (\pm 0.509)$  mg mL<sup>-1</sup> and a standard deviation  $\sigma=0.011$ . Z-scores of C0.1, 20h, PVP lie between -0.714 and 0.714, not very different from N1.25, 20h, PVP with Z-scores between -0.727 and 0.727 standard deviations below and above the mean. The results showed that a lower amount of SWCNTs is needed to disperse in Cyrene, yielding a higher concentration in the fluid after 20-hour sonication in the presence of PVP. Moreover, the results from C0.1, 20, PVP are more reliable than of NMP-based solutions. C0.1, 5h, PVP showed the highest standard deviation in the PVP-based fluids, with  $\sigma=0.040$  and a mean of  $0.052 (\pm 1.814)$  mg mL<sup>-1</sup>, and Z-values of -0.725 and 0.700 standard deviations below and above the mean. In contrast, N1.25, 10h, PVP registered the lowest standard deviation,  $\sigma=0.004$  and a mean of  $0.037 (\pm 0.191)$  mg mL<sup>-1</sup>, and Z-values of -0.75 and 0.75 standard deviations below and above the mean. These results demonstrate lower reliability in the experiments using a concentration of nanotubes of 0.1 mg mL<sup>-1</sup> in Cyrene and 5-hour sonication, compared to NMP-based fluids, with a concentration of 1.25 mg mL<sup>-1</sup>, sonicated for 10 hours in the presence of PVP.

## 5.4.4. Overall results and mechanisms proposed

Overall, Cyrene was a better media to disperse carbon nanotubes than NMP, in the pure state or in the presence of a non-ionic surfactant or a polymer (Figure 75):

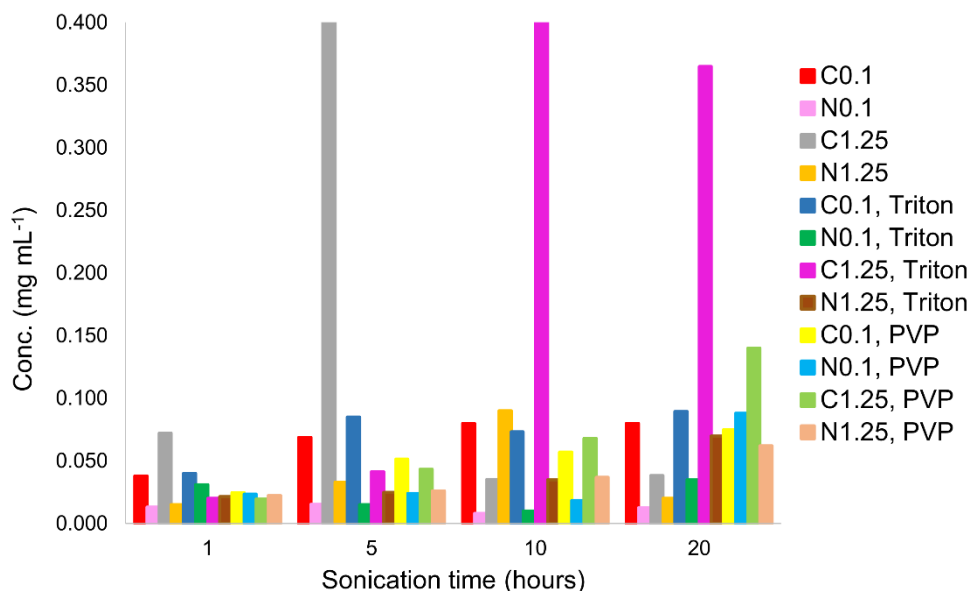


Figure 75: Dispersion of single-walled carbon nanotubes in neat solvents (Cyrene and NMP) and in presence of additives (Triton and PVP). Error bars were not added.

The maximum concentration of nanotubes in the solvent can be seen to be reached in Cyrene, probably due to the higher viscosity of the solvent. The viscosity of NMP at 25 °C is 1.66 mPa s,<sup>572, 573</sup> while Cyrene has a higher value, of 11.67 mPa s at the same temperature (Section 1.5.2.2.). Sedimentation velocity of a material during centrifugation depends on the dispersing conditions, concentration of particles in solution, as well as the density and the viscosity coefficient of the solution medium.<sup>574</sup> The main external influence on CNTs suspended in a fluid is the Buoyant force,<sup>574</sup> which is expressed as:

$$F_b = -m_0 \omega^2 r \quad (\text{eq. 13})$$

Where  $m_0$  is the mass of displaced solution and can be calculated for a solution from:

$$m_0 = V \rho_m \quad (\text{eq.14})$$

Where, V is the volume of the fluid and  $\rho_m$  is the density of the fluid.

It was reported that the sedimentation velocity of CNTs during centrifugation increased when the viscosity of the solution decreases.<sup>574</sup> In this work, this will explain why the sedimentation of SWCNT is faster in NMP than in Cyrene while the latter gives a more stable system.

Supernatants of pure solutions of SWCNTs contain most of the amorphous carbon, which has very high solvent stability,<sup>575</sup> defective nanotubes, metals and surfactant, which can be detrimental to many applications.<sup>514</sup> Pristine SWNTs are generally contaminated with amorphous carbon (AC), catalysts (Ni, Fe, Co, Mg), and graphitic carbon (from defective nanotubes).<sup>576-578</sup> The catalysts are removed from SWCNTs by thermal treatment above the melting temperature, strong acid treatment ( $\text{H}_2\text{SO}_4/\text{HNO}_3$  (3:1)) or a combination of the two.<sup>579-581</sup> AC can be removed using low-speed centrifugation, where it is suspended in aqueous media and separated from the SWNTs by decantation.<sup>582</sup> Pure Cyrene has shown the best dispersion of SWCNT. Interactions solvent-solvent or between solvent and CNTs have been reported and they involved van der Waals dispersion interactions as well as weak polar forces such as dipole- $\pi$ , C-H $\cdots$ O and C-H $\cdots\pi$  hydrogen bonds.<sup>453</sup> However, the  $\pi - \pi$  stacking was found to be stronger than C-H $\cdots\pi$  bonds.<sup>513</sup> Triton has shown similar dispersion of SWCNTs to pure Cyrene (up to  $0.4 \text{ mg mL}^{-1}$ ) and four times higher values than Cyrene/PVP-based solutions (up to  $0.1 \text{ mg mL}^{-1}$ ). This could indicate that by  $\pi$ -stacking behaviour between the SWCNTs in pure Cyrene or between SWCNTs and surfactant in Cyrene/Triton solutions<sup>544</sup> has a greater influence than the polymer wrapping mechanism related to Cyrene/PVP-based dispersion.<sup>583</sup> In the case of NMP, dispersions in NMP/PVP- and NMP/Triton-based solutions have shown greater dispersion efficiency (up to  $0.09 \text{ mg mL}^{-1}$ ) than in neat solvent (up to  $0.01 \text{ mg mL}^{-1}$ ). In this case, the polymer wrapping of PVP and  $\pi$ -stacking have significantly improved the dispersion of SWCNTs in these solutions. After sonication, centrifugation and filtration of the supernatant through a  $0.22 \mu\text{m}$  filter, bundles of short carbon nanotubes can be seen in the solutions containing neat Cyrene and Cyrene with PVP or Triton; while no SWCNT bundles can be seen in NMP-based solutions (Figure 76):

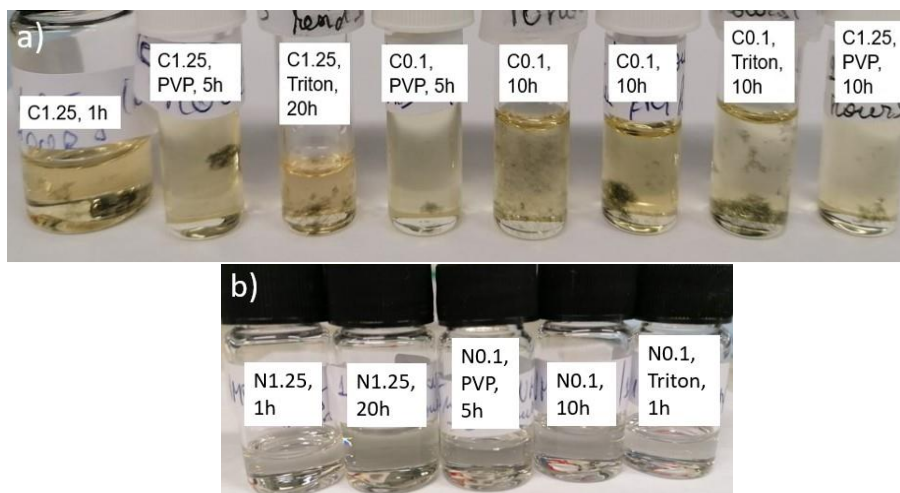


Figure 76: (a) Residues after sonication, centrifugation and filtration of SWCNTs in Cyrene and (b) NMP, with or without additives.

Figure 76 shows that more CNTs ropes break during sonication in Cyrene and leave the solution as the filtrate through a 0.22  $\mu\text{m}$  filter. Ultrasonication disperses the CNTs by the formation and collapse of cavitation bubbles which pulls apart the CNTs and cut them in shorter lengths.<sup>475, 584</sup> Short carbon nanotubes have been reported previously to form by ultrasonication and bullet blender in presence of Triton, polyethylene glycol (PEG) 4000 and SDS.<sup>585</sup> They have the advantages of not forming big bundles, do not cause clogging and they disperse easily in solutions and polymers. Hence, they are used in drug delivery systems, antibacterial membranes, biomedical applications, Li-ion batteries (higher current density).<sup>586</sup> In this thesis, Cyrene showed nanotubes breaking into small ropes during sonication, promoting this solvent as a possible source for short nanotubes synthesis.

## 5.5. Characterisation of SWCNT dispersions by Transmission Electron Microscopy (TEM)

### 5.5.1. SWCNTs dispersed in neat solvents

To characterise the dispersion of carbon nanotubes in solvents, 6  $\mu\text{L}$  of solution of solvent/SWCNT or solvent/additive/SWCNTs was applied onto a grid and left to evaporate completely before the sample was introduced into a transmission electron microscope (TEM). After 1 hour of sonication in Cyrene, a small number of nanotube aggregates can be seen in the TEM micrographs, indicating

their successful exfoliation in the solvent. The nanotubes in Cyrene suspensions are highly exfoliated at both low and concentrations ( $0.1$  and  $1.25$   $\text{mg mL}^{-1}$ ) (Figure 77)

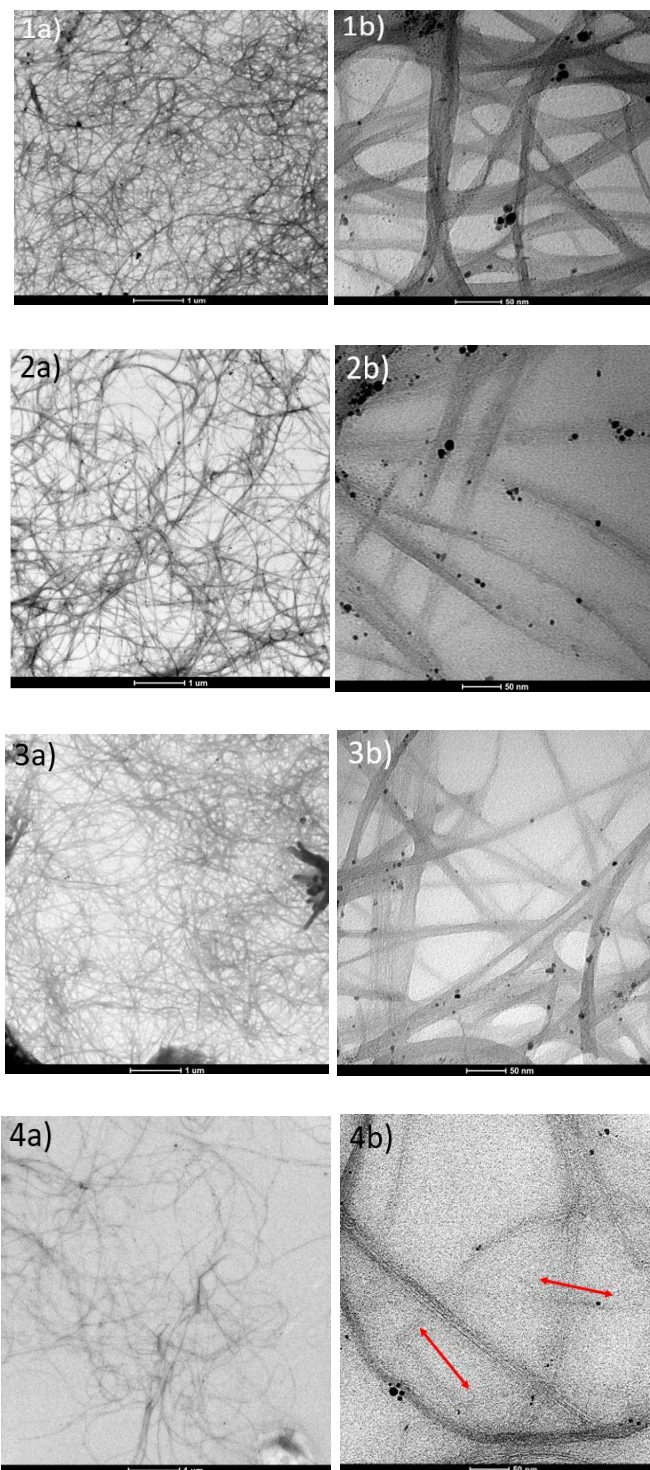


Figure 77: (1, 2) TEM images of  $0.1$   $\text{mg mL}^{-1}$  and (3, 4)  $1.25$   $\text{mg mL}^{-1}$  SWCNT dispersed in neat Cyrene at (a) low resolution and (b) high resolution after (1, 3) one hour and (2, 4) 20 hours of sonication.

High-resolution TEM images (Figure 77 4b) show that SWCNT dispersed in Cyrene after 20 hours of sonication has broken into smaller pieces and dispersed uniformly into the solution after a long time of sonication. Also, when dispersed in Cyrene, the metal catalyst particles, such as Fe, Co and Ni, are dispersed uniformly or in small aggregates.

After 20 hours of sonication, it can be seen how the carbon nanotubes dispersed in NMP are still long and entangled (Figure 78 1a,). When dispersed in NMP, the big bulky metals groups can be seen in-between the tangled nanotubes. Carbon nanotubes are randomly entangled in NMP, which does not create a good dispersion.



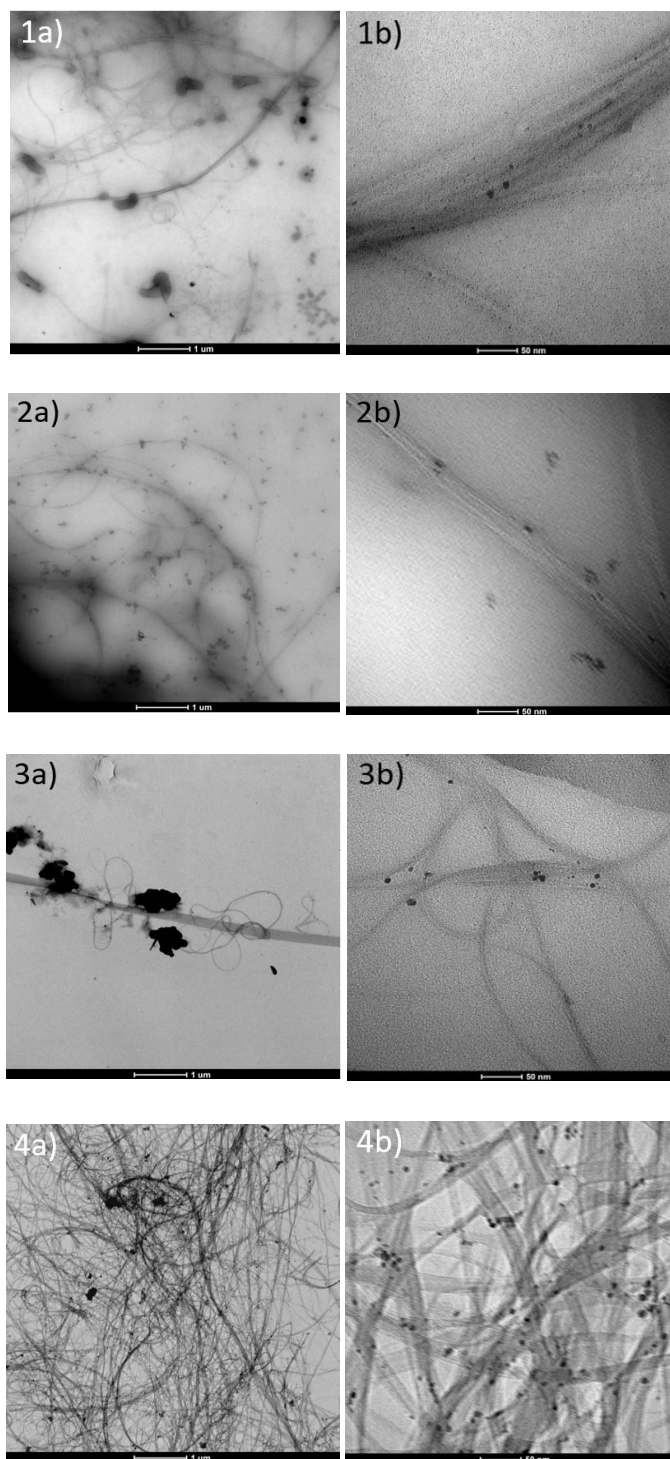


Figure 78: (1, 2) TEM images of  $0.1 \text{ mg mL}^{-1}$  and (3, 4)  $1.25 \text{ mg mL}^{-1}$  SWCNT dispersed in neat NMP at (a) low resolution and (b) high resolution after (1, 3) one hour and (2, 4) 20 hours of sonication.

N0.1 and N1.25 solutions did not show a uniform dispersion of the carbon nanotubes; hence the space from the surface of the grids (Figure 78 1-3). Only N1.25 dispersed using 20 hours exhibited a relative uniform dispersion of individual nanotubes (Figure 78 7 4).

## 5.5.2. SWCNTs dispersed using Triton™ X-100

When Triton is used in Cyrene-based solutions, uniformly dispersed nanotubes can be observed in C1.25, Triton, 1 hour and C0.1, Triton, 20 hours and C1.25, Triton, 20 hours (Figure 79 2-4).

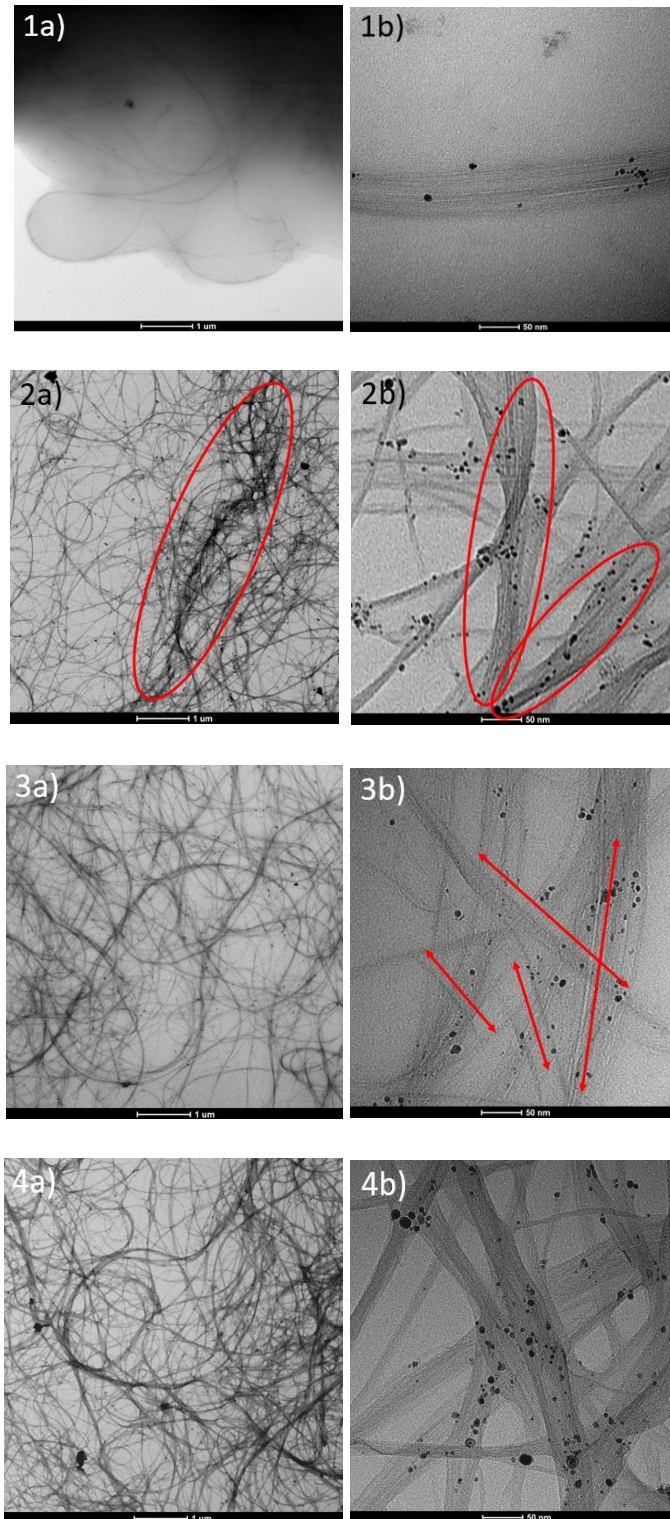


Figure 79: (1, 2) TEM images of  $0.1 \text{ mg mL}^{-1}$  and (3, 4)  $1.25 \text{ mg mL}^{-1}$  SWCNT dispersed in Cyrene and Triton™ X-100 at (a) low resolution and (b) high resolution after (1, 3) one hour and (2, 4) 20 hours of sonication.

However, in C0.1, Triton, 1 hour (Figure 79 1) was not sufficient to disperse individual CNTs, the solution presenting small bangles dispersed in a large amount of solvent. Pictures taken at high resolution show that the CNTs are detached from one another at a sonication time of 20 hours

(Figure 79 3b and 4b), a phenomenon less clear at 1-hour sonication (2b). However, a low concentration of CNTs is better detached (Figure 79 1b and 3b) than in a concentrated solution (Figure 79 2b and 4b).

For NMP-based solutions, Triton dispersed carbon nanotubes uniformly and small bundles can be observed (Figure 80) for three solutions: 1) N0.1, 1hour, Triton, 2) N0.1, 20hours, Triton and 3) N1.25, 20hours, Triton. On the grid containing N1.25, 1hour, Triton (Figure 80 2) space can be observed, with no visible nanotubes. This means that in this solution, the small number of carbon nanotubes re-aggregated easily into small bundles and left uncovered over a big part of the grid.

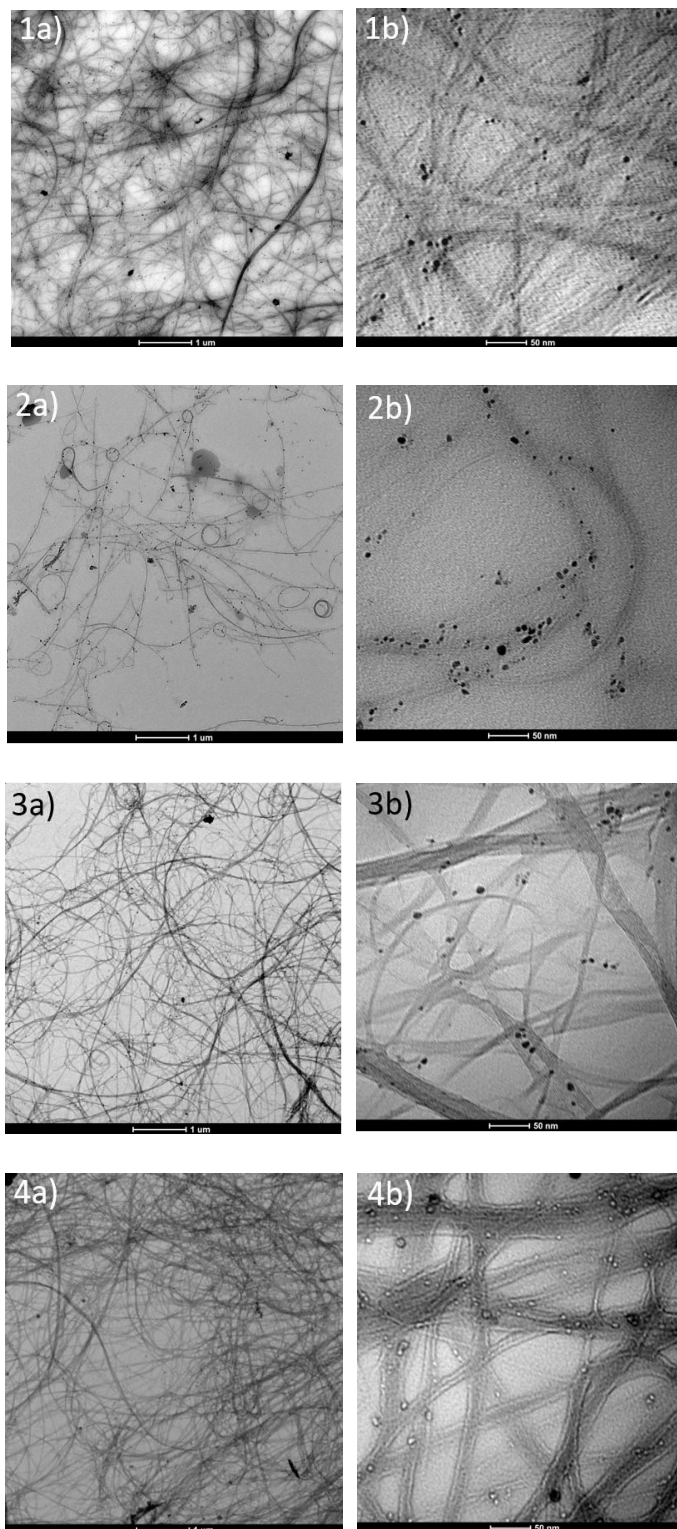


Figure 80: (1, 2) TEM images of  $0.1 \text{ mg mL}^{-1}$  and (3, 4)  $1.25 \text{ mg mL}^{-1}$  SWCNT dispersed in NMP and Triton™ X-100 at (a) low resolution and (b) high resolution after (1, 3) one hour and (2, 4) 20 hours of sonication.

### 5.5.3. SWCNTs dispersed with the aid of PVP

The wrapping effect of PVP round SWCNTs in this work has been shown to be efficient in a solution based on Cyrene, yielding highly dispersed nanotubes, which increases with the sonication time and initial concentration. As seen in Figure 81, C0.1, 1 hour, PVP (Figure 81 1a, b) and C1.25, 1 hour, PVP (Figure 81 3a, b), fewer nanotubes can be observed on the surface of the grid. However, they are well dispersed. Solutions of C0.1, 20 hours, PVP (Figure 81 2a, b) and C1.25, 20 hours, PVP (Figure 81 4a, b), a higher concentration of dispersed nanotubes can be seen, in accordance with the high initial concentration in nanotubes used. When using PVP, the time of sonication and concentration have a great impact on the dispersion efficiency.

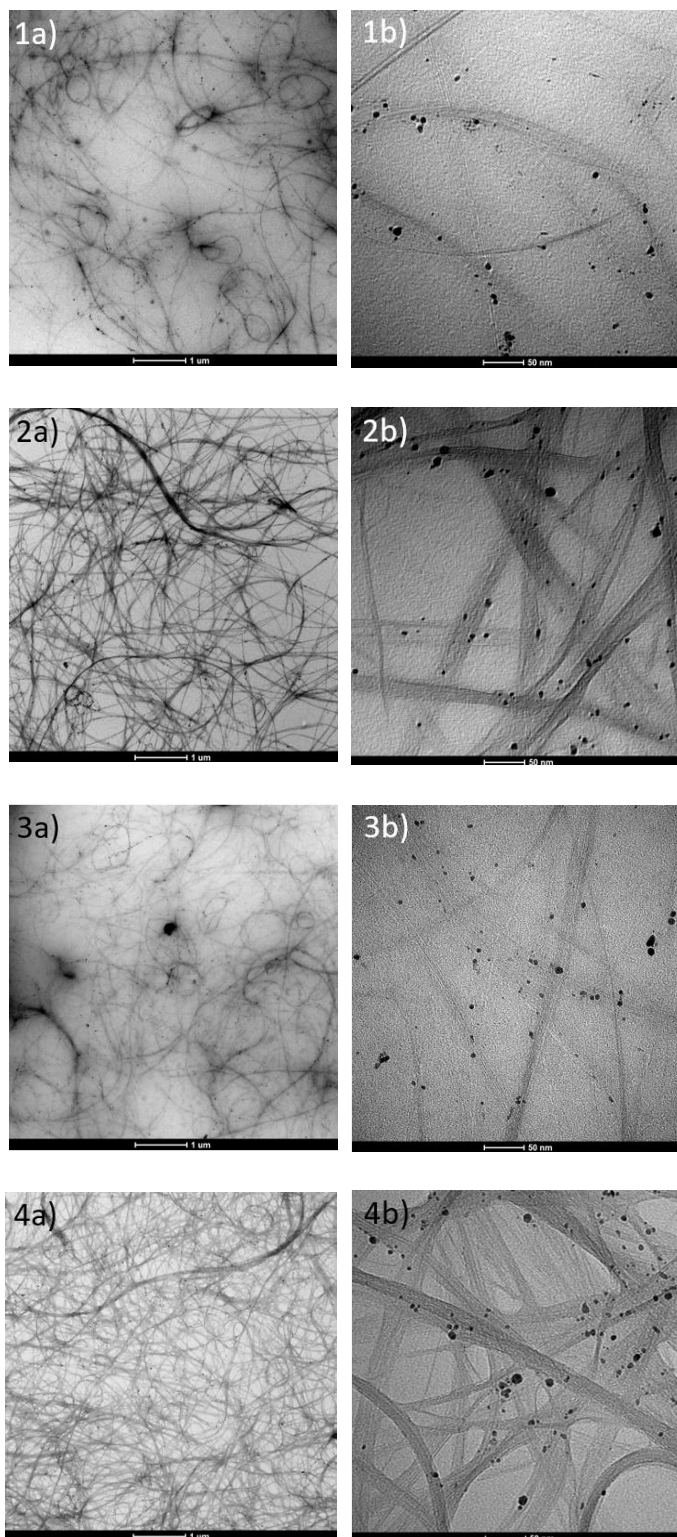


Figure 81: (1, 2) TEM images of  $0.1 \text{ mg mL}^{-1}$  and (3, 4)  $1.25 \text{ mg mL}^{-1}$  SWCNT dispersed in Cyrene and PVP at (a) low resolution and (b) high resolution after (1, 3) one hour and (2, 4) 20 hours of sonication.

All solutions show a good dispersion of nanotubes when PVP was applied as a dispersant of SWNT in NMP (Figure 82). However, a low concentration of SWCNT ( $0.1$ , 1 hour, PVP) showed bigger bundles than the other solutions due to insufficient time (1 hour) of sonication, probably

not enough to unzip the nanotubes into individual ropes (Figure 82 1). Twenty hours of sonication allowed carbon nanotubes to be efficiently dispersed in both solutions of N0.1, 20hours, PVP and N1.25, 20hours, PVP (Figure 82 2 and 4).

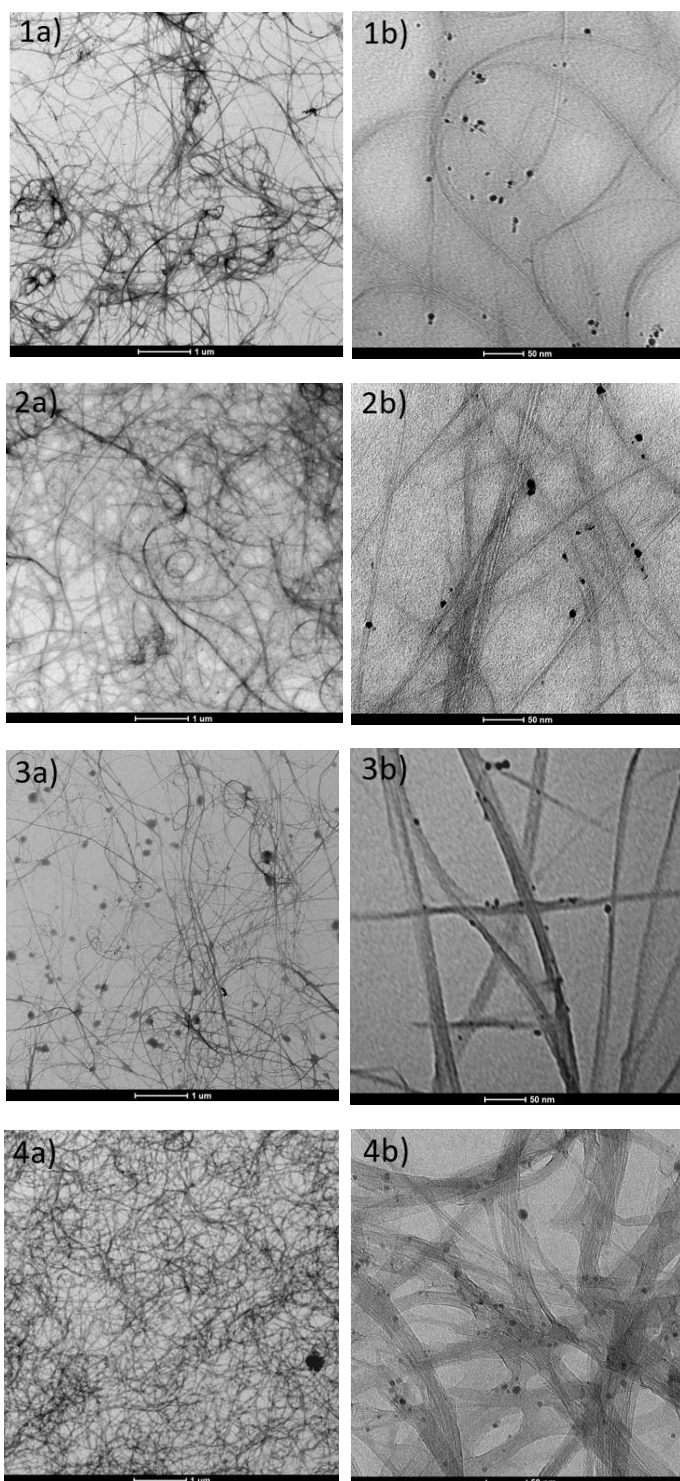


Figure 82: (1, 2) TEM images of  $0.1 \text{ mg mL}^{-1}$  and (3, 4)  $1.25 \text{ mg mL}^{-1}$  SWCNT dispersed in NMP and PVP at (a) low resolution and (b) high resolution after (1, 3) one hour and (2, 4) 20 hours of sonication.



## **5.6. Stability of SWCNTs solutions**

### **5.6.1. SWCNTs dispersed in neat solvents**

The samples were coded based on the solvent used, the initial concentration of SWCNTs used, time of sonication and the surfactant used. "C1.25, 5h" represents a sample containing 1.25 mg SWCNT dispersed in 1 mL of Cyrene, using 5 hours of sonication while "N0.1, 1h" means 0.1 mg SWCNT dispersed in 1 mL of NMP and using 1-hour sonication. As seen in Figure 83, the SWCNTs dispersed in pure Cyrene have sedimented slowly. The slow sedimentation and the higher surface tension of Cyrene might explain why the individual SWCNTs float freely into the viscous solvent.<sup>587</sup>

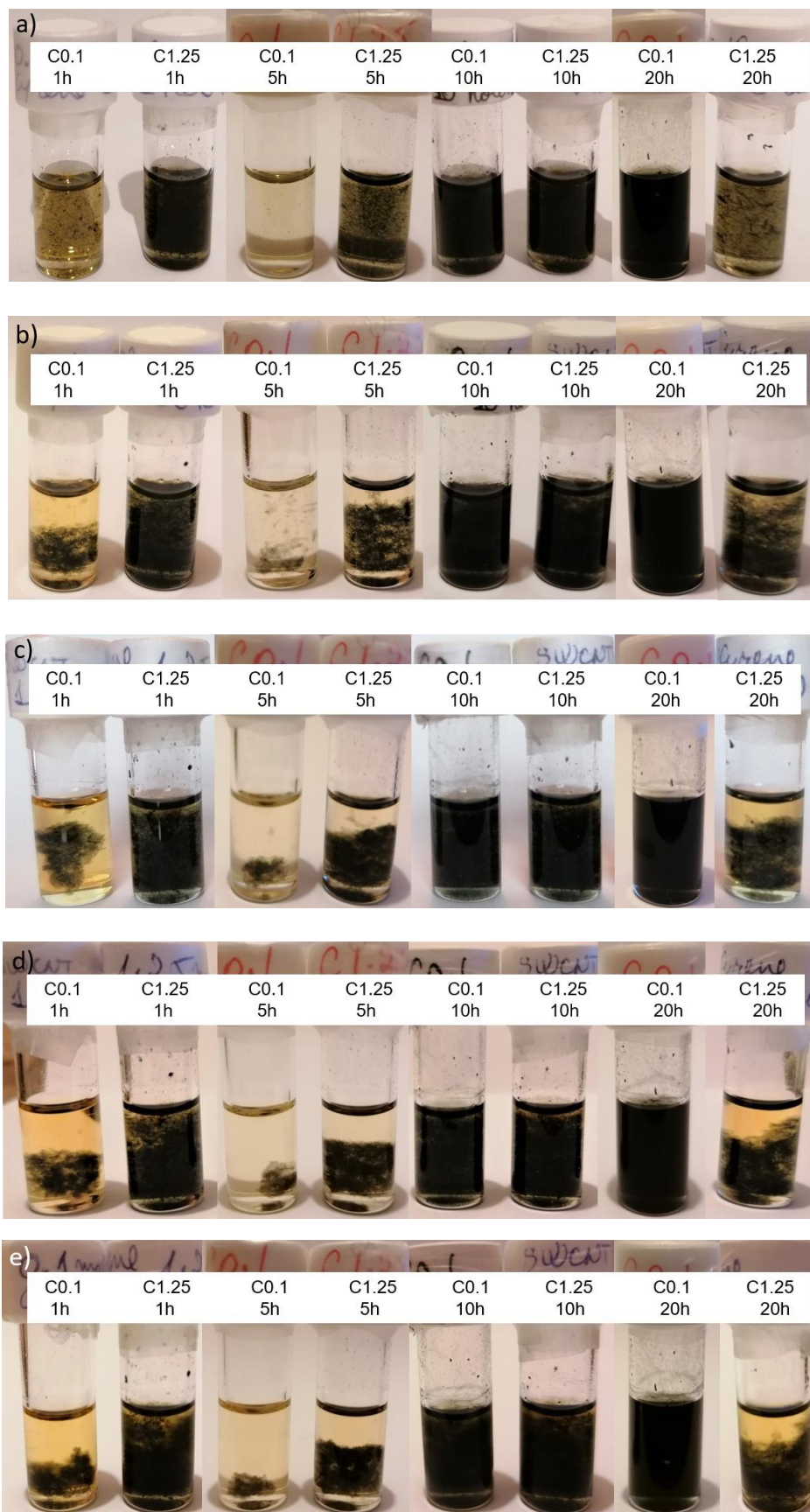


Figure 83: (a) Stability studies of SWCNTs dispersed in neat Cyrene at the start and after (b) one day, (c) 8 days, (d) 20 days and (e) 30-day stability test.

The results of stability studies show that the CNTs dispersed in pure solvent tend to re-agglomerate faster than in the highly concentrated solutions. The most stable solutions were C0.1, 10h; C1.25, 10h and C0.1, 20h, with the highest concentration of nanotubes in solution (Figure 83,). A solution of C1.25, 1h was less stable, but the sedimentation velocity of CNTs increased in this case, where a lower viscosity is predicted.<sup>574</sup>

The re-aggregation and sedimentation following dispersion in NMP are very high and the solutions were not stable after one day. Generally, the dispersions of pristine SWCNTs in pure NMP are not stable, they tend to re-agglomerate if they are not functionalised (visible large bundles or red circles in Figure 84):

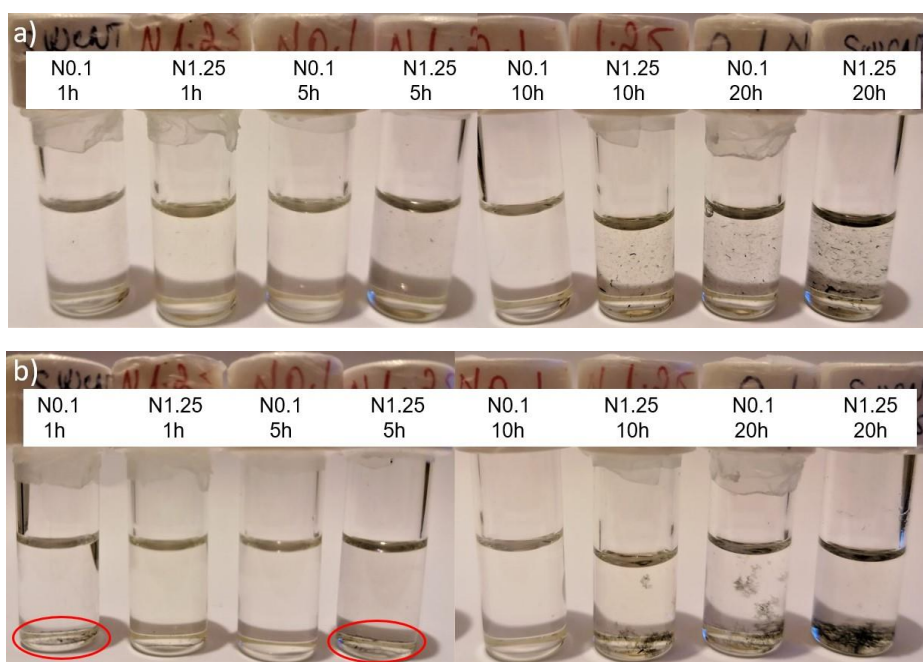


Figure 84: (a) Stability studies of SWCNTs dispersed in neat NMP at the start and after (b) one-day stability test.

### 5.6.2. SWCNTs dispersed with the aid of Triton™ X-100

It was demonstrated in a previous study that 95 % of Triton is removed by centrifugation and decanting steps, the remainder of the Triton molecules is likely randomly adsorbed onto the surface of the nanotubes.<sup>519</sup> In a previous work, a mixture of acetone and isopropyl alcohol was used to remove the residual Triton.<sup>588</sup>

In the present work, the filtered carbon nanotubes were washed with ethanol and acetone. The samples were coded based on the solvent used, the initial concentration of SWCNTs used, time of sonication and the surfactant used. “C1.25, 5h, Triton” represents a sample containing 1.25 mg

SWCNT dispersed in 1 mL of Cyrene and Triton as dispersant, using 5 hours of sonication while "N0.1, 1h, Triton" means 0.1 mg SWCNT dispersed in 1 mL of NMP and Triton using 1-hour sonication. The SWCNTs dispersed in Cyrene with Triton (Figure 85) dispersant showed a similar behaviour as when pure Cyrene was used. A low concentration of SWCNTs dispersed in solutions tend to re-aggregate faster than the concentrated, black solutions.

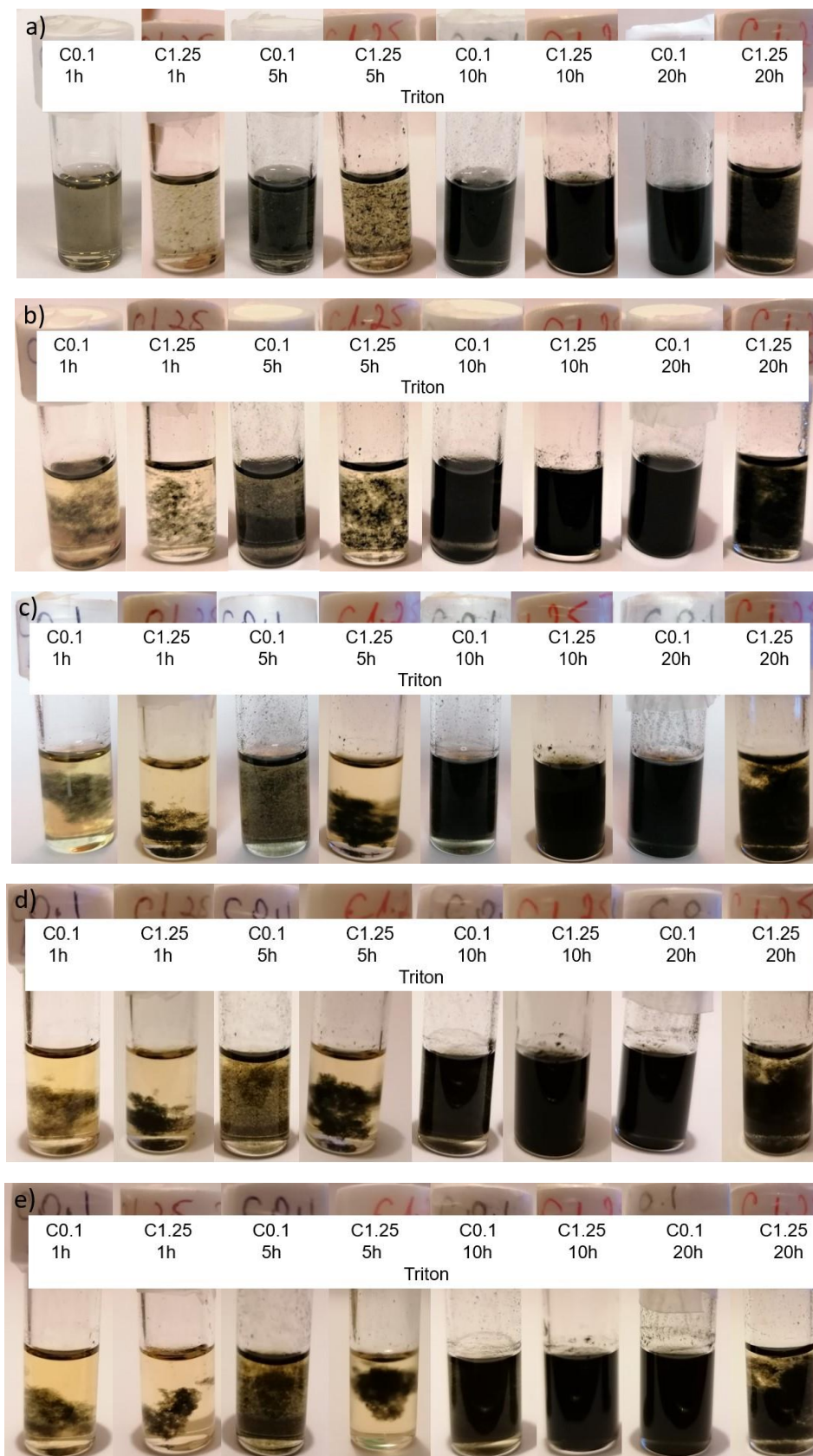


Figure 85: (a) Stability studies of SWCNTs dispersed in Cyrene with the aid of Triton™ X-100 as dispersant at the start and after (b) one day, (c) 8 days, (d) 20 days and (e) 30-day stability test.

The NMP/Triton-based solutions were not stable, the nanotubes sedimented and re-bundled in less than one day (Figure 86):

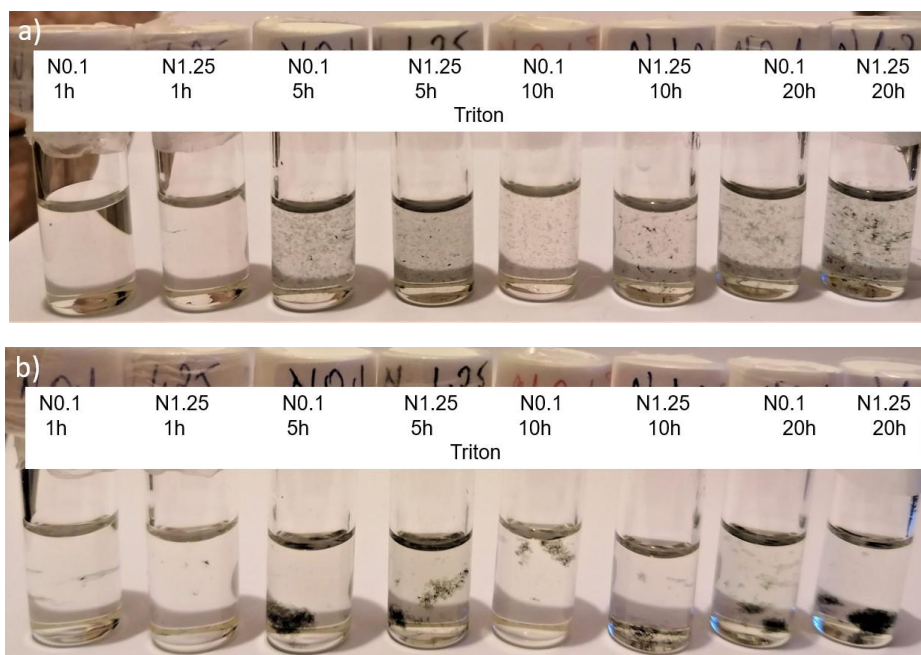


Figure 86: (a) Stability studies of SWCNTs dispersed in NMP with the aid of Triton™ X-100 as dispersant at the start and after (b) one-day stability test.

Previously, the stability of this suspension using Triton™ X-100 was reported to be no longer than 1 week.<sup>544</sup> In this work, a solution of SWCNTs dispersed in NMP and Triton was short-lived, of only one day.

### 5.6.3. SWCNTs dispersed with the aid of PVP

The samples were coded based on the solvent used, the initial concentration of SWCNTs used, time of sonication and the surfactant used. "C1.25, 5h, PVP" represents a sample containing 1.25 mg SWCNT dispersed in 1 mL of Cyrene and PVP as a dispersant, using 5 hours of sonication while "N0.1, 1h, PVP" means 0.1 mg SWCNT dispersed in 1 mL of NMP and PVP using 1-hour sonication. The SWCNTs dispersed in Cyrene with Triton (Figure 87) dispersant showed a similar behaviour as when pure Cyrene was used. A low concentration of SWCNTs dispersed in solutions tends to re-aggregate faster than the concentrated, black solutions.

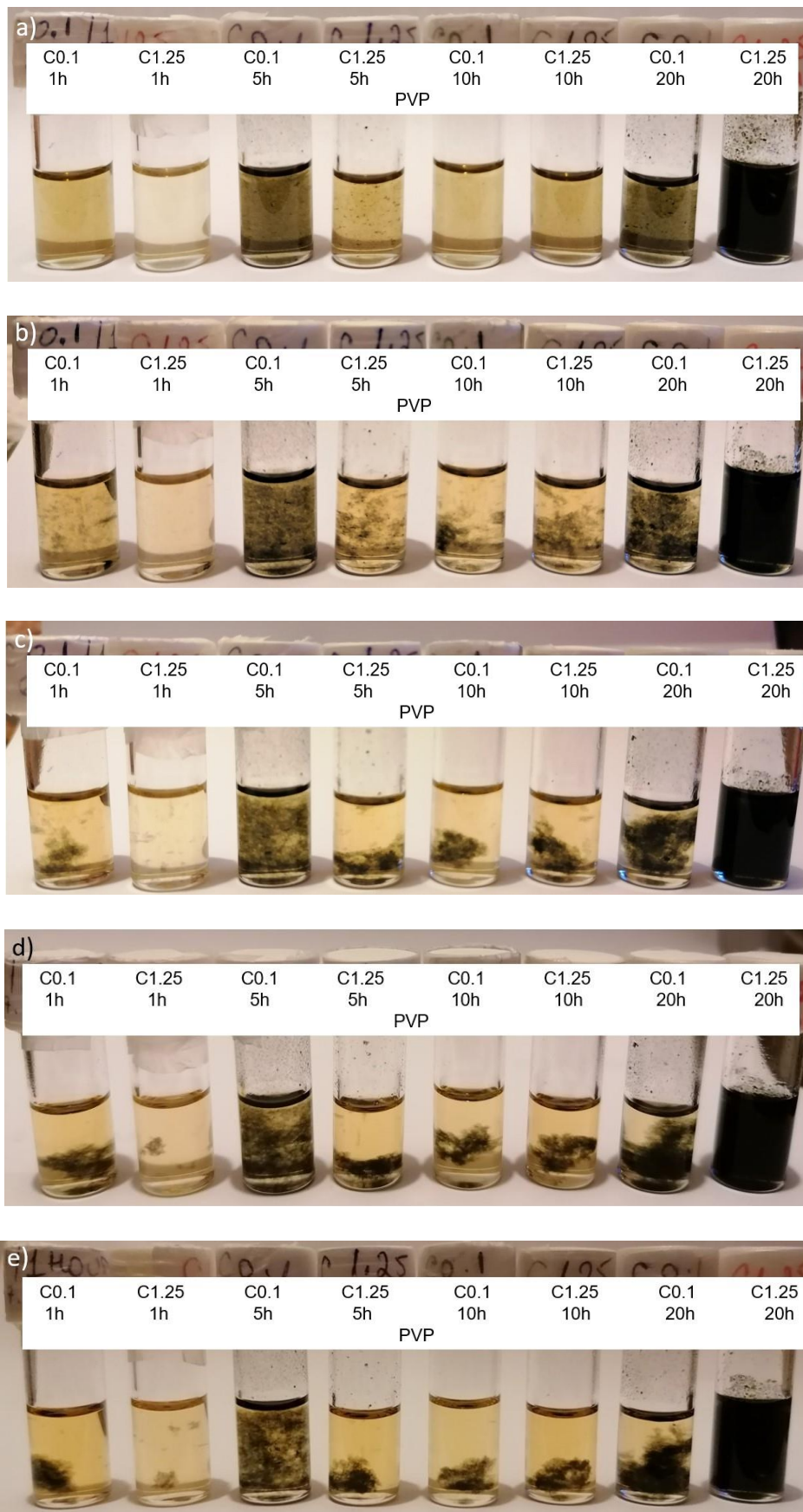


Figure 87: (a) Stability studies of SWCNTs dispersed in Cyrene with the PVP as dispersant at the start and after (b) one day, (c) 8 days, (d) 20 days and (e) 30-day stability test.

However, fewer nanotubes can be observed when they were dispersed in PVP (Figure 87) than in the presence of Triton (Figure 85). The solutions containing NMP and PVP get darker with the concentration of dispersed SWCNTs and sonication time. All solutions were not stable for more than one day (Figure 88):

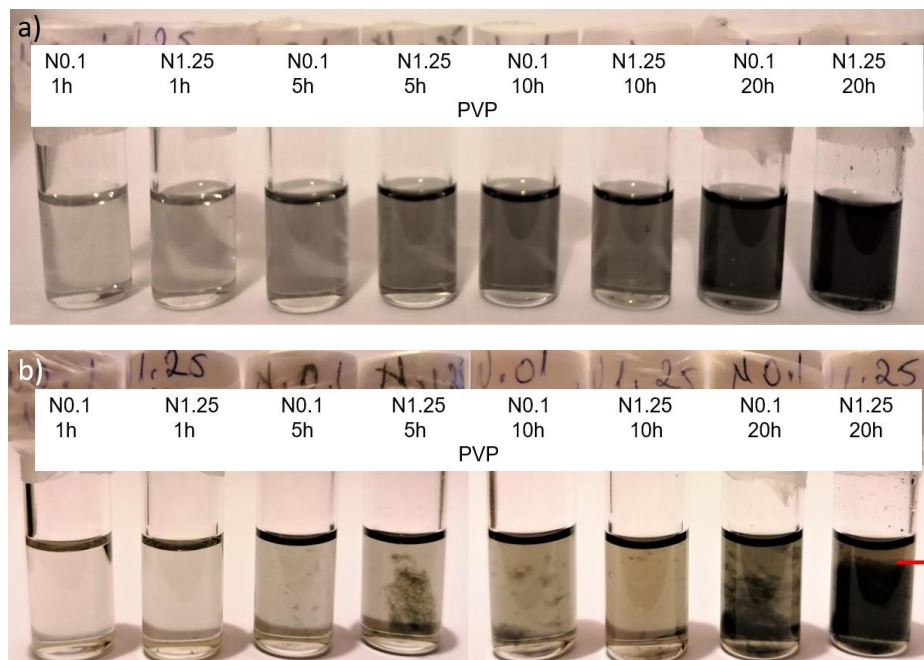


Figure 88: (a) Stability studies of SWCNTs dispersed in NMP with the aid of PVP as dispersant at the start and after (b) one-day stability test.

Interestingly, two distinct layers can be seen in NMP/PVP-based solutions (red line), which became more visible with increasing of the SWCNTs concentration in solution and sonication time. This could be the result of the dissolved amorphous carbon (AC), which has very high solvent stability.<sup>575</sup> It was previously found that more de-bundled CNTs were found in the precipitate and not present in the supernatant.<sup>519</sup> In concentrated solutions, where the two layers are more distinct (N0.1, 20h and N1,25, 20h), the sedimentation velocity is lower, probably due to the more stable SWCNTs fluids containing NMP, PVP and a higher concentration of AC.

After one month of measuring the stability of Cyrene-based fluids, only the stable fluids were left for a longer time (Figure 89). The Cyrene-based solutions seen in the figure are stable for 6 months.



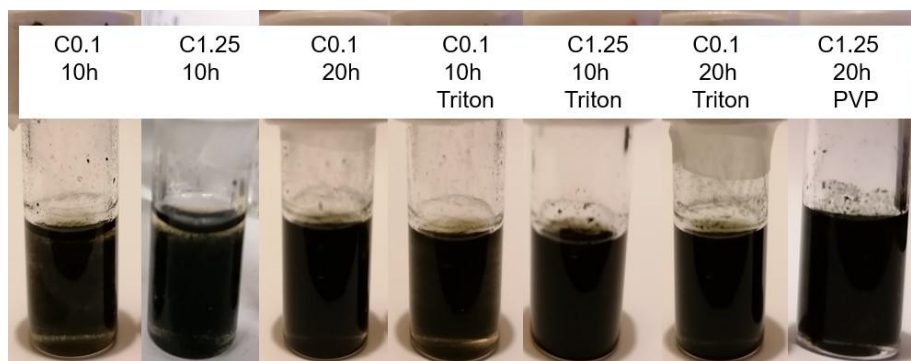


Figure 89: Cyrene-based fluids with six-month stability test.

In order to determine at what concentration Cyrene-based solutions become stable for a long time, the most stable solutions tested for stability were filtrated and the nanotubes weighed,

Table 25:

Table 25 The concentration ( $\text{mg mL}^{-1}$ ) of single-walled carbon nanotubes in the solution after dispersion and 6-month stability.

| Sample             | Concentration SWCNTs in solution ( $\text{mg mL}^{-1}$ ) |
|--------------------|--|
| C0.1, 10h          | 0.10   |
| C1.25, 10h         | 0.19   |
| C0.1, 20h          | 0.10   |
| C0.1, 10h, Triton  | 0.08   |
| C1.25, 10h, Triton | 0.27   |
| C0.1, 20h, Triton  | 0.09   |
| C1.25, 20h, PVP    | 0.17   |

As seen in Table 25, the most stable solutions contain  $0.1 \text{ mg mL}^{-1}$  when the same amount of starting SWCNTs were used and  $0.19 \text{ mg mL}^{-1}$  for a starting concentration of  $1.25 \text{ mg mL}^{-1}$  SWCNTs in neat Cyrene (C1.25, 10h). SWCNTs dispersed in Cyrene and Triton used as dispersant were stable when a concentration of a minimum of  $0.08 \text{ mg mL}^{-1}$  was achieved for a starting concentration of SWCNTs in a solution of  $0.1 \text{ mg mL}^{-1}$ . A higher concentration of starting nanotubes in a solution of Cyrene and Triton reached maximum stability when  $0.27 \text{ mg mL}^{-1}$  was obtained. When PVP was applied as a dispersant, only one concentration of dispersed SWCNT in Cyrene has shown a high potential. A concentration of  $0.17 \text{ mg mL}^{-1}$  was stable for six months. The results demonstrate that a higher concentration of SWCNTs is obtained after sonication and

centrifugation in pure Cyrene, and adding surfactants is not necessary to be added as stabilisation agents in Cyrene-based solutions.

## 5.7. Chapter conclusion

Carbon nanotubes have gained huge interest due to their excellent mechanical, thermal and electric properties. However, due to their hydrophobic characteristics and strong Van der Waals attraction, the dispersion of carbon nanotubes in neat solvents and polymer matrices is generally poor. In this work, their dispersion using ultrasonication, followed by centrifugation and decanting the supernatant. The ultrasonic baths used to disperse carbon nanotubes present a major drawback; the ultrasound waves in the bath create a nonhomogeneous energy dissipation pattern which affects the uniform dispersion. However, good dispersion of nanotubes in aqueous solutions and other solvents is not always achieved. Dispersions of pristine single-walled carbon nanotubes in neat Cyrene and surfactant and polymer assisted methods were used: in this work: ultrasonication followed by centrifugation and decanting of the supernatant. Generally, non-functionalised nanotubes have shown no stability in pure solvents. In this work, the viscosity of Cyrene has proven to be a good factor in dispersing the nanotubes. Due to the higher viscosity of Cyrene than of NMP the sedimentation velocity decreased when compared to the latter and the solutions were more stable. This explained why the sedimentation of SWCNT was faster in NMP than in Cyrene and are stable for a longer time in the latter fluid than the former. Overall, Cyrene was a better medium to disperse carbon nanotubes than NMP, with concentrations up to  $0.9 \text{ mg mL}^{-1}$ , compared to a maximum of  $0.1 \text{ mg mL}^{-1}$  for NMP-based fluids. In Cyrene, hardly any nanotube bundles as can be seen in the TEM image, indicating that almost all the SWCNTs are highly exfoliated at both low and concentration ( $0.1$  and  $1.25 \text{ mg mL}^{-1}$ ). When Triton X-100 is used in Cyrene-based solutions, well dispersed nanotubes can be observed; however small bundles can be observed too, due to possible  $\pi$ -stacking between the nanotubes or between the nanotubes with the surfactant. A lower concentration of SWCNTs is desired to avoid saturation and re-aggregation. The wrapping effect of PVP around of SWCNTs in this work has been efficient in a solution based on Cyrene, yielding highly dispersed nanotubes, which increases with the sonication time and the starting concentration. Overall, the  $\pi$ -stacking behaviour between the SWCNTs in pure Cyrene or between SWCNTs and surfactant in Cyrene/Triton solutions has a greater influence than the polymer wrapping mechanism related to Cyrene/PVP-based dispersion. Only the samples with a concentration of at least  $0.08 \text{ mg mL}^{-1}$  SWCNTs in neat Cyrene or with the aid of dispersants were stable for six months. However, NMP-based solutions presented bundles

when dispersed in neat solvent. Dispersion of SWCNTs is more efficient when Triton surfactant and the commonly used polymer PVP has been used to un-zip the individual nanotubes from existing bundles. Cyrene-based fluids have shown higher stability, with samples stable up to six months, while all NMP-based fluids, in a pure solvent or with aid of dispersants, were short-lived, no longer than one day. Small SWCNTs are present in the residual solvent after sonication, centrifugation, and filtration of a Cyrene-based solution, wherever pure solvent was used, or with surfactant or polymer assisted dispersion.



# Chapter VI

## 6. Cyrene in membrane technology<sup>7 8 9 10</sup>

---

<sup>7</sup> This chapter is adapted from the article: *"Fabrication of PES/PVP water filtration membranes using Cyrene<sup>®</sup>, a safer bio-based polar aprotic solvent"* submitted to *Advances in Polymer Technology*

R.A. Milescu has produced the filtration membranes and has tested the water filtration with help from Matthew J. Walters. Also, R. A. Milescu has performed the IR analyses, thermal stability, contact angle experiments, SEM images and porosity experiments by gravimetric method. Dr Carlos Grattoni from Leeds University has performed mercury porosimetry measurements and low-field NMR spectroscopy. Dr C. R. McElroy, Thomas J. Farmer, Paul M. Williams and James H. Clark supervised the work and participated to writing of the article.

<sup>8</sup> This chapter is adapted from the article *"A Family of Water-Immiscible, Dipolar Aprotic, Diamide Solvents from Succinic Acid"* submitted to *ChemSusChem*

R.A. Milescu has produced filtration membranes using the new solvent and wrote the corresponding section.

<sup>9</sup> This chapter is adapted from the article *"Polymer chemistry applications of bio-based Cyrene and its derivative Cygnet 0.0 as safer replacements for polar aprotic solvents"* submitted to *ChemSusChem*.

R.A. Milescu has produced filtration membranes using three solvent/solvent systems, four different polymers and two temperatures of casting solutions, has synthesised Cygnet 0.0 and Cygnet-Cyrene mixture using new methodologies. She also has performed the thermal stability, SEM images of the new membranes and HSP predictions. Dr Con R. McElroy developed *in-situ* synthesis method of Cygnet-Cyrene mixture. Alessandro Pellis and Marco Vastano have realised bio-catalysed polycondensation reactions and Anna Zhenova contributed to the ethanol recrystallisation of Cygnet 0.0. All authors contributed to the writing of the article.

<sup>10</sup> This chapter is adapted from the article, *"Greener solvents and their role in PVDF dissolution"*. Manuscript in preparation.

R.A. Milescu has performed the initial solvent screening and HSP predictions, has produced the PVDF membranes and performed SEM analysis of the membranes with Anna Zhenova.



## 6.1. Introduction

Population growth and water pollution increased the demand for clean water in the 21<sup>st</sup> century and the access to it requires improvements of present water filtration technology.<sup>589-591</sup> According to Goal 6 of UN Sustainable Development Goals regarding the clean water and sanitation, “one in three people do not have access to safe drinking water, two out of five people do not have a basic hand-washing facility”.<sup>592</sup> Conventional processes of water cleaning include filtration, distillation, sedimentation, biological (sand filters or activated carbons) or chemical treatment such as chlorination, precipitation, oxidation, coagulation/flocculation, ion-exchange.<sup>593, 594</sup> Membrane technologies are widely applied in wastewater reuse and seawater desalination, which are some of the most promising solutions to meet the demand for clean water resources.<sup>595, 596</sup> Membranes used in water filtration account for the largest share of the commercial market for membranes worldwide, due to the increasing attention paid to environmental problems linked to the growing demand for clean water.<sup>597-600</sup> Membrane separation process has many advantages: high water quality, ease of use in clean technology, less energy demand, environmentally benign, greater flexibility in the designing system and easy maintenance.<sup>591</sup>

Membranes' preparation involves generally large amount of solvents, especially in a non-solvent induced phase separation (NIPS) process. Polar aprotic solvents such as NMP, DMAc, DMF and DMSO are generally involved in casting solution.<sup>601-604</sup> They are associated with severe health and safety issues. Herein, Cyrene has been assessed in this work for its suitability in substituting these solvents in the fabrication of filtration membranes.

## 6.2. Filtration membranes - Background

A membrane is a thin layer of semi-permeable material which acts as a selective barrier between two systems (*i.e.*, removal of solid particles suspended in a fluid medium). The skin provides the permeability and selectivity of the membrane, whilst the substrate assures its mechanical strength.<sup>605</sup> The membranes can be selectively permeable or semi-permeable. A permeable membrane refers to a biological membrane in most cases which is selective in what passes through and where size is not the determining factor. A semi-permeable membrane depends on pore size and acts as a barrier which retains larger particles (concentrate) and allows smaller molecules to pass through the membrane (permeate) by diffusion.

## 6.2.1. Types of membranes

### 6.2.1.1. Membranes classified based on their morphology

Membranes can be symmetrical and asymmetrical, homogenous or heterogenous, solid or liquid, porous or dense (non-porous) and their structures can be observed in Figure 90:

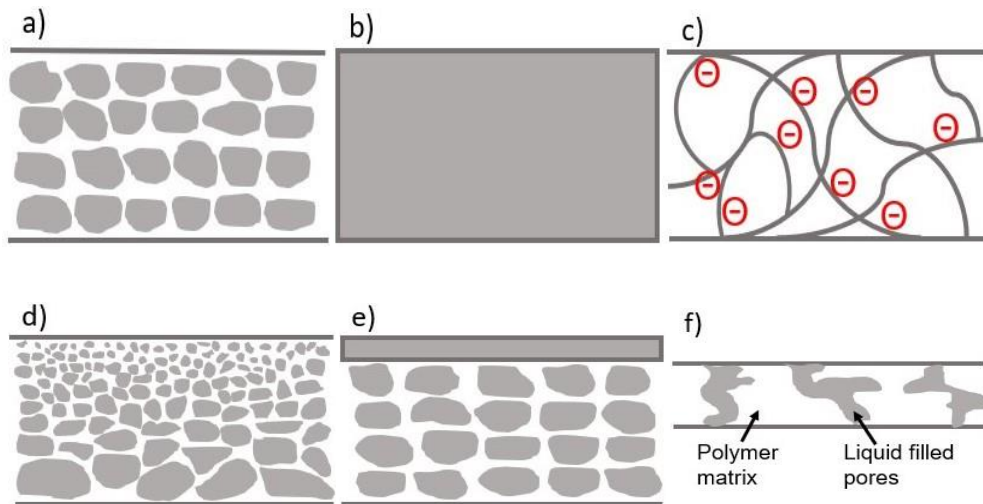


Figure 90: Symmetrical membranes: (a) microporous, (b) nonporous dense and (c) electrically charged. Asymmetrical membranes: (d) Loeb-Sourirajan structure, (e) thin-film composite and (f) supported liquid. Adapted from reference.<sup>591</sup>

- Symmetrical microporous membrane presents pores smaller (pore size  $0.1-5 \mu\text{m}$ ) than the conventional liquid filtration ( $1-10 \mu\text{m}$ ) and is formed either by phase inversion or by heating the polymer above its melting point prior to extrusion into thin films followed by stretching techniques.<sup>591</sup> This type of membranes have symmetric pore structures where the voids are similar in size throughout their thickness.
- Non-porous membranes are dense and commonly used for reverse osmosis, nanofiltration or gas separation and the separation of solutes is achieved by diffusion.<sup>591</sup>
- Electrically charged membranes are either non-porous or microporous. The negative or positive fixed ions are present in the walls of the membrane (*e.g.* anion-exchange membranes contain positive ions, while a cation-exchange membrane has negative fixed ions). In case of positive and negative ions present in the same membrane, it is called "mosaic membranes". The separation occurs through ion exchange membranes by applying an electric field; hence these membranes are electrically conductive. (Figure 91).<sup>591</sup> This type of separation employs ion exchange membranes and is used in applications such as water desalination, lithium extraction from brines or extraction of salts from seawater.<sup>606-608</sup>



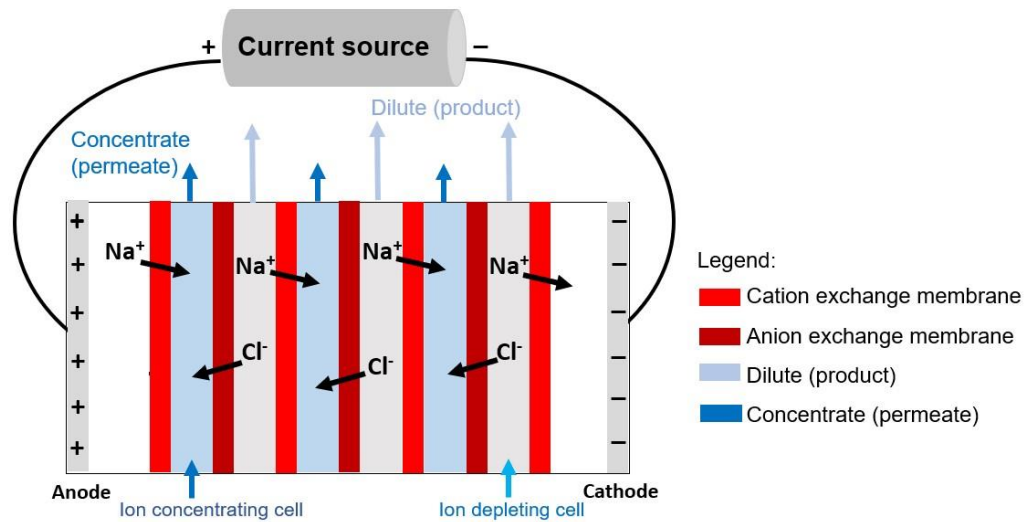


Figure 91: Electrically charged membranes packed in an electrodedialysis system. Adapted from reference.<sup>609</sup>

- d) Loeb-Sourirajan structure has asymmetric pore size and porosity through the thickness of the membrane; the voids are smaller near one surface and bigger on the other surface. This type of membranes was developed in the 1960s and represent the most common asymmetric membranes.<sup>610</sup>
- e) Thin-film composite membranes present a thin surface layer supported by a much thicker, porous structure. Surface layer permits the separation of solutes, whilst the porous structure acts as a support layer. Both layers are generally made of different polymeric materials and are prepared by interfacial polymerization, solution coating, and plasma polymerisation.
- f) Supported liquid membranes are formed from a thin layer of organic phase immobilised onto an inert microporous support (usually with dissolved reagents) within the membrane and sits between two aqueous phases of different compositions. The analytes (*i.e.*, metal ions) are extracted from an aqueous sample through an organic liquid phase into another usually temporally stagnant, aqueous phase.<sup>611</sup>

### 6.2.1.2. Types of filtrations based on pore size

Membrane can be divided based upon the size of the component in the feed solution that can pass through them: microfiltration, ultrafiltration, nanofiltration and reverse osmosis (Figure 92):

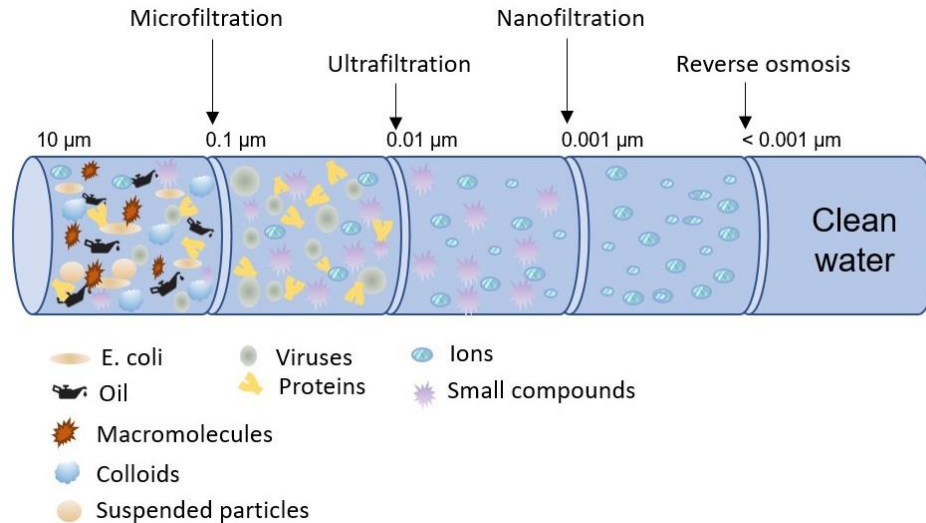


Figure 92: Types of filtration membranes based on size of the analyte. Adapted from reference.<sup>612</sup>

- Microfiltration (MF) membranes have pore size ranging from 0.1 to 10 μm and are used to remove large particles, colloids, and bacteria from feed streams in applications such as the food and beverage industry and treating the wastewater. A membrane with bigger pores than 10 μm is used for “macrofiltration” of beach sand, pollen, some paint pigments, red blood cell or yeast cell.<sup>613</sup>
- Ultrafiltration (UF) membranes have a pore size from 0.01 to 0.1 μm, falling in the range between nanofiltration and microfiltration. They are used in wastewater treatment, chemical recovery, food industry or medical usage.<sup>614</sup>
- Nanofiltration (NF) membranes are pressure-driven with pores between 0.001 to 0.01 μm. This membrane rejects multivalent salts and uncharged solutes, while allowing some salts to pass through.<sup>615</sup> They are similar to reverse osmosis membranes, but they use lower pressure and are less energy intensive to run. The most effective method to fabricate NF membrane is the composite membrane technique, where an ultrathin dense layer is formed on an existing porous substrate to obtain a composite membrane.<sup>616-618</sup>
- Reverse osmosis (RO) membranes have the smallest pore size and generally requires a high pressure to reject all monovalent ions and viruses while allowing water molecules to pass through in clean aqueous solutions. This technology is extensively used in desalination and industrial water treatment.<sup>619, 620</sup>

### 6.2.1.3. Other types of membranes

Membranes can separate solutes based on principles other than size:

- a) Pervaporation is a process to separate liquids based on their boiling points using a vacuum on the gaseous side of the membrane.
- b) Dialysis is a clinically membrane-based treatment in which an artificial kidney or haemodialyser assures the metabolic functions of a failing kidney. The metabolic waste (solutes and water) products from the kidney are removed by using different mass separation mechanisms (diffusion, convection and adsorption).<sup>621-624</sup>
- c) Electrodialysis is an electrochemical process used to separate charged particles from a raw solution (retentate) into a more concentrated solution (permeate) and relies on electrically conductive membranes, discussed in Section 6.2.1.1.

## 6.2.2. Properties of filtration membranes

Filtration membranes present high separation efficiency, low energy consumption and are simple in operation, making them a sustainable approach to replace traditional separation processes.<sup>625</sup> Membranes used in industrial separation processes need to have high permeability and selectivity, resistant to fouling, cheap, mechanically and thermally resistant and sustainable.

### 6.2.2.1. High permeability and selectivity

The quality of water passing through the membrane is crucial; hence the increased water-solute selectivity and not permeability is needed for desalination applications.<sup>626</sup> Selectivity plays a vital role in desalination of water, rejecting the salts and other solutes and finally providing clean water. Reverse osmosis membranes (RO) and thin-film composites (TFC) lie in this category. The selective-layer performance of current TFC membranes generally consists of a crosslinked polyamide layer formed through interfacial polymerisation supported by a polymeric ultrafiltration (UF) porous support.<sup>627</sup> TFC represents the benchmark for new desalination membranes.<sup>626</sup> The transport of water and solutes is made by the solution-diffusion model of the selective layer (dense film). Generally, a selectivity-permeability trade-off needs to be in place, TFC forward osmosis (FO) membranes have been tailored in order to achieve both selectivity and permeability by a post-annealing approach.<sup>628</sup> RO are generally highly permeable membranes; to

achieve an extremely high selectivity, membranes with uniform-diameter nanochannels are created which retain solutes by size exclusion. Carbon nanotubes (CNTs) have been employed in membranes for a high selectivity with diameters small enough to reject salt and small solutes. However, they need to be aligned in a thin membrane to achieve water permeability of a THF membrane.<sup>626</sup>

### 6.2.2.2. Resistant to fouling

Fouling of the membrane is a process resulting in loss of flux due to the deposition of suspended or dissolved substances on top or inside the membranes. Maintenance and operation cost are increased by fouling due to shortening of membrane life, limiting their utilisation.<sup>590, 629, 630</sup> The membrane fouling represents both clogging of membrane pores and deposition of sludge cake on the membrane (Figure 93):

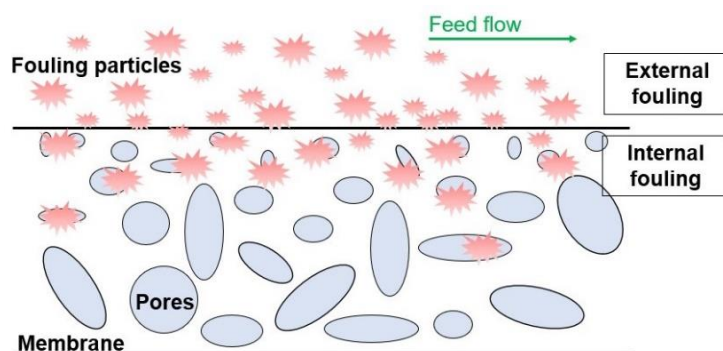


Figure 93: Membranes fouling phenomenon. Adapted from reference.<sup>615</sup>

The formation of membrane fouling starts with the adsorption of foulants and their build-up.<sup>629</sup> This initial adsorption of foulants onto membrane is a critical process that precedes the formation of membrane fouling.<sup>631</sup> Membrane fouling can be influenced by various factors:

- The interactions between membranes and the feed. The hydrophobic membranes are more prone to fouling than the hydrophilic membranes due to the hydrophobic interactions between solutes, microbial cells and membrane material.<sup>632, 633</sup>
- Characteristics of membrane (pore size, hydrophilicity, zeta potential, and surface roughness, structure, and chemical properties). Sponge-like microstructures are more prone than finger-like structures due to pore fouling due to their highly porous network.<sup>634</sup> Membrane with rough surface are more prone to fouling layers, the membranes with a smooth surface due to the presence of large "filling-in points" from their surface.<sup>635</sup>

- The size of the particles from the feed solution. Activated sludge biomass (suspended solids, colloids and solutes) Soluble and colloidal materials can block internal pores of the membrane, whilst the suspended solids are responsible for the “cake layer” formation on the surface.<sup>636</sup>
- Conditions of separation process. Variations in operating conditions (*e.g.* flow input, organic load) can change the nature and/or structure of the feed and its fouling tendency.<sup>637</sup>

The types of fouling and the pollutants responsible with the pore clogging are:

- Biofouling: this is mainly caused by microorganisms such as fungi or bacteria,
- Colloidal fouling agents: metal oxides, suspended matter, clay minerals and salt precipitates,
- Organic fouling: this is caused by the dissolved organic matter such as proteins or polysaccharides,
- Scaling: inorganic precipitation fouling such as calcium sulphate or calcium carbonate are the most common pollutants in this form of membrane fouling.

Membrane fouling can be reversible or irreversible based on the attachment strength of the particulates to the membrane. Cleaning of the membranes after their use in filtration processes can be physically, biologically, and chemically accomplished. The reversible fouling can be done by physical cleaning where the pollutants are loosely attached to the membrane surface (“cake layer formation”). This layer can be easily removed by mechanical cleaning, which can apply the use of high-pressure water jets, abrasion or backflushing by using permeate.<sup>638</sup> Irreversible fouling cannot be removed by physical cleaning. In biological cleaning, the microorganisms are removed using biocides. Chemical cleaning includes the use of bases and acids to remove impurities and foulants. Solutes, colloids, and microbial cells pass through membrane pores and precipitate inside, blocking internal pores. In some cases, it is impossible to fully remove the fouling using any method, even chemically cleaning. In such cases the pores are permanently blocked. Membranes’ fouling makes the separation unpredictable and shortens its lifetime due to a higher energy demand to push the water through the pores.<sup>639, 640</sup> Hence, the characteristics of the membranes are tailored to lower the fouling and improve the filtration efficiency. Hydrophilic homopolymers such as polyvinylpyrrolidone (PVP) or poly(ethylene glycol) (PEG), silver, titanium-based nanoparticles or polysaccharides are ideal for incorporation into the membranes in order to reduce the fouling of the polymeric membranes.<sup>63, 641-643</sup>

### 6.2.2.3. Mechanical strength

The first polymeric membranes were from cellulose; they were not mechanically resistant and collapsed under high pressure. Mechanical strength is important in filtration applications where a high pressure is necessary. Today's polymeric membranes have improved; the synthetic novel polymers have been tailored to have high mechanical strength and flexibility; advanced surface functionalisation or different functionalisation of different layers of the same membrane, higher porosity.<sup>644</sup> However, a challenge to improve at the same time the permeability and retention capacity of the membranes remains. Metal/metal oxides nanoparticles, carbon nanotubes or graphene are incorporated currently in membranes for higher strength.<sup>476, 641, 645</sup>

### 6.2.2.4. High temperature resistance

Thermal stability represents the capacity of a membrane to resist to harsh high temperatures which could ultimately destroy them. Heat resistance of a membrane is important in applications where heat treatment is applied to kill microbial organisms in food products or medical diagnosis and to enhance the desalination performance.<sup>646</sup> Polymeric membranes with high temperature resistance are used in areas of extreme environmental conditions. For this purpose, metal oxides, carbon nanotubes or graphene are added in membrane composition to increase their thermal stability.<sup>646, 647</sup>

### 6.2.2.5 Manufacturing reproducibility, low price

Polymeric membranes are largely used for applications where a low-cost filtration is desirable.<sup>641</sup> The most common membranes are easily prepared using low-cost materials and simple processes; hence they are easy to reproduce. Ceramic membranes, however, are used in water filtration; they have high fouling resistance and are chemically stable, but they are currently only applied in small scale processes because of their high cost.<sup>648</sup> Hence, when deciding the type of membrane for a specific application, the cost of the manufacturing process is to be considered.

### 6.2.2.6. Sustainability

The ideal membrane is robust, resistant to harsh conditions and long-lasting. Moreover, the demands of membrane applications generally require them to be toxicologically benign. As the majority of carbon footprint for membrane separation comes from its fabrication stage, the longevity of the membrane contributes to the “greenness” of the process in comparison with other energy-intensive filtration techniques. Hence, the longer a membrane can function, the greener the process is, as the carbon footprint of the fabrication and disposal of the membranes will become negligible in comparison with the carbon footprint of processing.<sup>649</sup> A process should comply with green principles and consider waste prevention, better atom economy, the use of safe chemicals and solvents and higher energy efficiency.<sup>650</sup> Sustainable fabrication is continuously sought by replacing membrane materials with biodegradable alternatives, replacing the toxic solvents involved in the process with safer alternatives and minimising waste generation.<sup>164</sup> In drinking water application, the toxicity of the materials used is very important; release of materials and solvents from membranes during their casting need to be monitored to minimise toxicity effects. The solvents used in casting gel preparation are generally toxic and their replacement is crucial especially in a non-solvent induced phase (NIPS) process, where solvent loading is high. Researchers became very interested in replacing the toxic solvents with safer alternatives such as ionic liquids, or greener polar aprotic solvents (DMSO, MBSA, CP, GVL) have been successfully applied in this process, to minimise the problems of toxic solvent release to the environment.<sup>164, 651-653</sup> Methyl and ethyl lactate, dimethyl isosorbide, triethyl-phosphate and even water are nontoxic and biodegradable solvents and have been used to prepare membranes.<sup>654-659</sup>

### 6.2.3. Membrane preparation by Non-Solvent Induced Phase Separation (NIPS)

Preparation of membranes relies on phase separation process, in which a solid phase separates from a polymer solution. The main separation processes are NIPS (non-solvent induced phase separation), PIPS (polymerisation induced phase separation) and TIPS (thermal induced evaporation).<sup>660-662</sup> NIPS, or immersion precipitation, is the most used thanks to its versatility and variety in terms of broad membranes composition and application. In NIPS process, a thin film polymer solution is immersed in a coagulation bath containing a non-solvent, where the exchange of solvent and non-solvent takes place (Figure 94). The non-solvent causes the polymer to precipitate as the solvent diffuses into the casting bath.

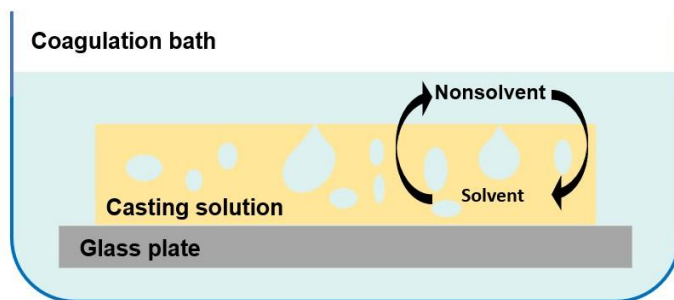


Figure 94: Schematic non-solvent induced phase separation process.

Additionally, a sacrificial polymer with broad solubility (in both the solvent and non-solvent) may be incorporated to increase both porosity and hydrophilicity within the membrane. Some of the parameters affecting the structure of the membrane are the composition of the casting solution, thickness of the casting solution, the type of the non-solvent and its temperature, the exposure time, the humidity and the temperature of the air.

## 6.2.4. Demixing processes during NIPS

### 6.2.4.1. Liquid-liquid demixing

Non-solvent induced separation (NIPS) is a widely used process to create a porous microstructure.<sup>94, 648, 658, 663-665</sup> In the NIPS process, a polymer solution is cast as a thin film on a suitable support and immersed in a coagulation bath containing a nonsolvent, where the polymer precipitation occurs.<sup>666-668</sup> The membrane's porosity has been described as water entering the cast film and the solvent leaving.<sup>669</sup> The immersion precipitation method creates change in the polymer concentration, leading to two phases, polymer-rich and polymer-poor. The stability of the solution changes, and hence, the phase inversion occurs.<sup>670</sup> The phase inversion involves mass transfer between solvent and nonsolvent by diffusion.<sup>671</sup> Membranes formation mechanism by the diffusional exchange of solvent and nonsolvent was predicted using the mass transfer modelling and phase behaviour.<sup>672-674</sup> During the diffusion induced phase separation, two types of demixing can occur: 1) liquid-liquid and 2) solid-liquid.

The liquid-liquid demixing is strongly influenced by the thermodynamic and kinetic property of the membrane system. Generally, three components are involved in the phase separation (solvent/polymer/nonsolvent). Hence a ternary phase diagram is the most useful tool to describe the thermodynamic behaviour of these systems. A ternary diagram based on Flory-Huggins theory is commonly used as a tool to analyse the thermodynamic and kinetic behaviour of the membrane



system in a phase inversion process. The Flory-Huggins model uses concentration and interaction between the components of the membrane solution to calculate the composition of membrane solution at equilibrium (the three components' interactions are polymer-solvent, polymer-nonsolvent and solvent-nonsolvent and are considered constant).<sup>675-678</sup> A binodal curve (or cloud point curve) is plotted in the ternary diagram. It is used to determine the type of demixing of the polymeric membrane solution and to predict the membrane's structure. The polymer precipitation kinetics are characterised by the solvent/non-solvent exchange rate and the additive loss.<sup>605, 679-681</sup> Changes in composition, binodal curve and precipitation path result in different membrane structure and performances.<sup>682</sup> Liquid-liquid demixing is generally associated with a low polymer concentration in the casting solution,<sup>683</sup> whilst high polymer concentration in casting solution can generate solid-liquid demixing.<sup>683</sup> Liquid-liquid demixing can determine the formation of two different morphologies:<sup>684</sup>

- Delayed precipitation results in membranes with dense skin and a porous sub-layer with isolated pores (sponge-like configurations),
- High precipitation rates (or instantaneous demixing) can produce membranes with large finger-like pores and porous skin.<sup>667</sup>

The moment of onset of the demixing process depends on the thickness of the film.<sup>684</sup> It was found that the macrovoids do not appear unless the dope's thickness exceeds a critical value.<sup>685, 686</sup> Macrovoids are larger than the rest of the pore network and are considered defects frequently present in membranes. Researchers try to eliminate them from membranes destined for gas separation and reverse osmosis applications, where small pores and a mechanically strong sponge-like structure are desired.<sup>687-689</sup> Macrovoids form as a result of fast demixing, and their formation was associated with thermodynamic solvent–nonsolvent exchange rate (or mass transfer) in the membrane solution,<sup>668, 690</sup> or as a result of the mechanical stresses at the film/ bath interface that results in weak points and induces solvent intrusion,<sup>667, 691, 692</sup> based on Marangoni effects<sup>693, 694</sup> and osmosis pressure.<sup>695</sup>

Sponge-like structures (or cellular structures) form due to a slow demixing. In this case the polymer precipitation is slow, and a dense top layer with sponge-like membranes is obtained.<sup>696</sup> Two types of sponge-like structures can form with 1) interconnected pores or 2) closed pores. However, an interconnected is desired for gas filtration.

#### 6.2.4.2. Solid-liquid demixing

When the film of casting solution is immersed in the coagulation bath containing a non-solvent, a liquid-liquid phase equilibrium is present at the interface, whilst the solid-liquid phase separation takes moments later.<sup>697</sup> This type of demixing is seen in semicrystalline polymers (*i.e.*, polyamide) or a high concentration of a polymer in the casting solution.<sup>697</sup> High polymer concentration in casting solution can generate spherulitic (spherical) or axialitic structures (multilayer aggregates) in the membrane.<sup>683, 697</sup> Crystallisation requires an induction time and a nucleus must be created for the solid-liquid to take place, which then can grow into spherulites.<sup>669, 698</sup> The pores of such membranes are represented by the voids from between the partly crystalline units.

### 6.3. Materials used in membrane technology

Polymer selection is based on compatibility with membrane fabrication technology and the end application. Organic, porous, polymeric membranes for water and wastewater treatment have traditionally been produced from cellulose acetate (CA),<sup>699</sup> polysulfone (PSf),<sup>700</sup> polyvinylidene difluoride (PVDF),<sup>630, 701</sup> polyacrylonitrile (PAN),<sup>702</sup> polytetrafluoroethylene (PTFE) and polyvinyl alcohol (PVA).<sup>703</sup> Inorganic membranes are made from metal (aluminium or titanium), ceramic, carbon, silica, zeolites and oxides. They are used for water treatment and desalination<sup>704</sup> due to their resisting to harsh chemical cleaning, high temperature and wear resistance, high chemical stability and long lifetime. However, they have a high cost of production, are very rigid which can lead to cracking (ceramic membranes) and can even be poisonous (metallic membranes).

In this work, only the polymeric flat sheet membranes were discussed.

### 6.3.1. Polyethersulfone (PES)

Polyethersulfone (PES) (Figure 95) is one of the most used polymers in membrane science due to its excellent performance and high thermal, chemical, and mechanical stability.

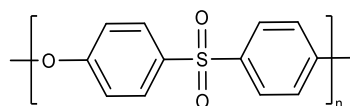


Figure 95: Chemical structure of polyethersulfone.

PES membranes are suitable for water purification from heavy metals, dyes or oils<sup>705-706-709</sup> and thin-film composites for gas separation.<sup>710</sup> PES polymers are recently manufactured using green solvents such as methyl lactate, dimethyl isosorbide, Polarclean™, DMSO Evol and ionic liquids.<sup>94, 651, 652, 654, 658, 711-713</sup> In this project, sustainable dialysis and water filtration membranes have been produced using the new, safer, bio-based solvents, Cyrene<sup>63</sup> and MBSA<sup>39</sup> and Cygnet 0.0 in place of toxic polar aprotic solvents, most commonly NMP.

### 6.3.2. Polyvinylidene difluoride (PVDF)

Polyvinylidene difluoride (PVDF) (Figure 96) is a semi-crystalline polymer with repeating unit of  $-(CH_2CF_2)_n-$  and is one of the most used membrane materials with increased interest from researchers and manufacturers in recent years.<sup>714</sup>

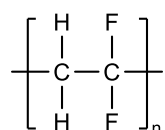


Figure 96: Chemical structure of polyvinylidene difluoride.

This type of membrane exhibits high mechanical strength, good chemical resistance, thermal stability and ageing resistance and are used in water treatment,<sup>715, 716</sup> membrane distillation,<sup>717, 718</sup> gas separation,<sup>719, 720</sup> pollutants removal from water (boron, VOCs, ammonia),<sup>553, 721-723</sup> ethanol recovery from an ethanol-water mixture by pervaporation,<sup>724, 725</sup> separator for lithium-ion battery<sup>726</sup> and ion exchange process.<sup>727, 728</sup> The antifouling performance of this class of membranes can be improved by hydrophilic modification *via* both physical and chemical methods.<sup>716, 729</sup>

### 6.3.3. Polysulfone (PSf)

Polysulfone (PSf) (Figure 97) is used for polymeric membranes with high thermal stability (150–170 °C), chemical inertness over the whole pH range, mechanical strength (fracture toughness, flexion and torsion) and processability.<sup>73, 730-733</sup>

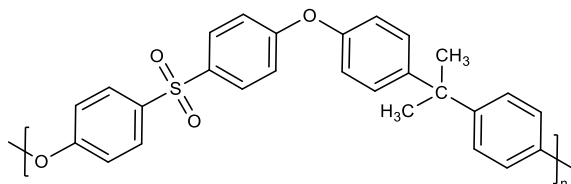


Figure 97: Chemical structure of polysulfone.

This type of membranes is used in haemodialysis application, due to a higher biocompatibility than other materials, high permeability for low-molecular weight proteins and high resistance during sterilisation.<sup>734</sup>

### 6.3.4. Cellulose acetate (CA)

Cellulose acetate (CA) (Figure 98) is the acetate ester of cellulose, a renewable and biodegradable resource.

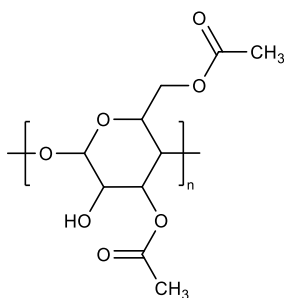


Figure 98: Chemical structure of cellulose acetate.

Cellulose acetate-based membranes were the first generation of filtration membranes<sup>610</sup> and are still used for water treatment,<sup>735-738</sup> haemodialysis<sup>739-741</sup> and gas separation.<sup>742-744</sup> CA membranes are durable and resistant to chlorine; they have outstanding desalination efficiency and are widely used in RO process.<sup>745, 746</sup>

### 6.3.5. Polyimide (PI)

Polyimides (PIs) (Figure 99) are stiff polymeric materials due to their aromatic backbone, making them ideal for membranes with excellent thermal stability, chemical resistance, mechanical strength and electrical properties.<sup>360, 747</sup>

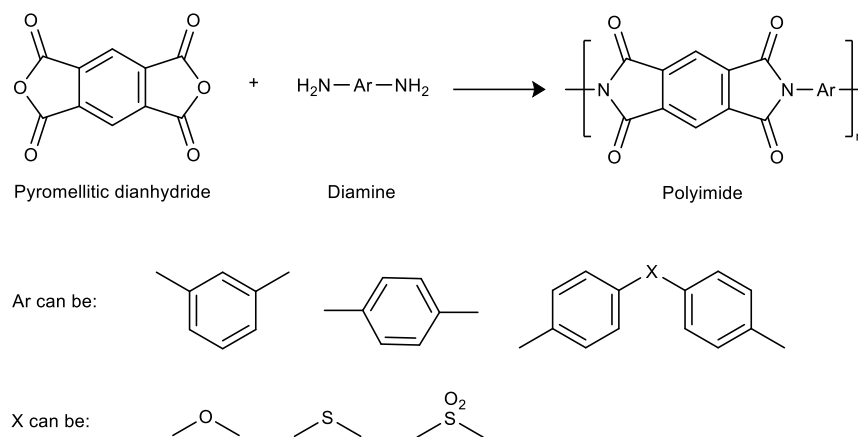


Figure 99: Synthesis of polyimide membranes from a diamine and a dianhydride. Adapted from reference.<sup>360</sup>

PI membranes are commonly synthesised from diamine and dianhydride or a combination between NIPS and imidisation leading to sponge-type polyimide membranes.<sup>748</sup> PI membranes are used for gas separation applications<sup>749</sup> or thin-film composite for desalination processes.<sup>750</sup> In this work, a thermoplastic polyimide has been used to produce PI membranes using a simple NIPS method.

## 6.4. Solvents and mixtures of solvents used to produce membranes

### 6.4.1. Cyrene and NMP

Repro-toxic solvents such as NMP,<sup>602, 751, 752</sup> DMF<sup>751</sup> or DMAc<sup>75</sup> or combinations of them<sup>604, 753</sup> and the much safer, but still problematic DMSO<sup>599, 754, 755</sup> are generally used in membrane technology. Recently NMP was added to REACH's restricted substances list,<sup>83</sup> and its replacement is crucial in membrane technology where large volumes of it is used. DMF and DMAc are also on the Substances of Very High Concern (SVHC) list as toxic for reproduction (may damage the unborn

child). Hence, the list of available and safe polar aprotic solvents is currently very small. In this work, Cyrene was used in membranes preparation to replace these toxic solvents. However, NMP was used in this work as a benchmark for the novel technology using Cyrene.

### 6.4.2. Cygnet 0.0-Cyrene mixture (Cg:Cy)

By combining Cyrene (liquid) with Cygnet 0.0 (needle-like crystalline solid at room temperature), new binary solvent systems are formed; liquid at room temperature until it reaches a proportion of 50 wt% of Cyrene in Cygnet 0.0, and more solid with the increase of Cygnet's concentration (Figure 100):

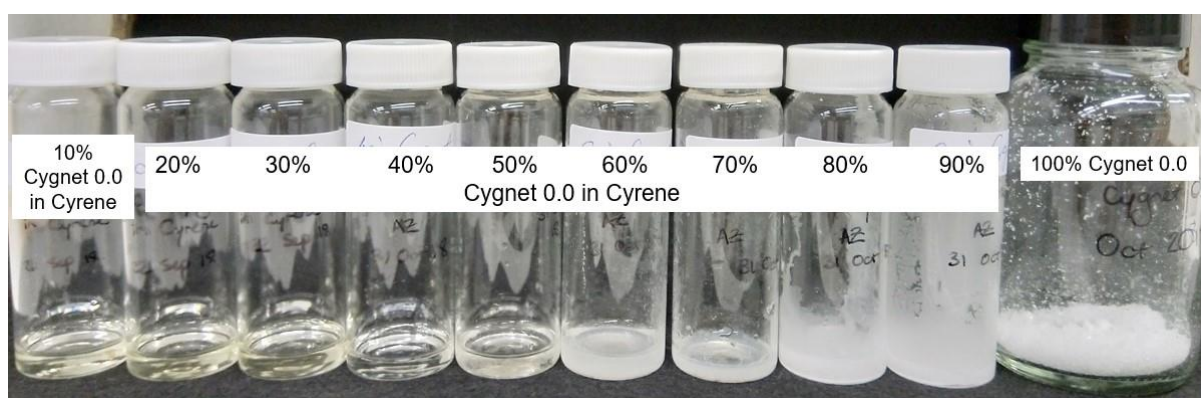


Figure 100: Mixtures of Cg:Cy at different concentrations and pure Cygnet 0.0.

For ease of handling in both laboratory and industrial settings, only 50% Cg:Cy (noted as "Cg:Cy") was used to prepare CA, PSf, PES and PI filtration membranes. Up to this date, only PES was previously used in the preparation of membranes using Cyrene,<sup>63</sup> none of the polymers were used to prepare membranes using any of the Cygnet-Cyrene mixtures.

### 6.4.3. Cygnet 0.0

Cygnet 0.0 is a ketal derivative of Cyrene, which is solid at room temperature, an unusual characteristic for an industrial solvent which are usually required to be in liquid form at ambient temperatures. Cygnet 0.0 is a needle-like crystalline solid at room temperature (Figure 100), with a melting point of 71 °C. Polyimide, polysulfone, polyethersulfone and cellulose acetate membranes were produced in this study for the first time using pure Cygnet 0.0 by a NIPS process.

#### **6.4.4. *N,N'*-Dimethyl-*N,N'*-dibutylsuccinamide (MBSA)**

*N,N'*-dimethyl-*N,N'*-dibutylsuccinamide (MBSA), another polar aprotic solvent synthesised at GCCE, University of York was used for the first time in membrane technology and the results published.<sup>39</sup> In the NIPS process, the miscibility of the solvent with the non-solvent (usually water) is very important in membranes forming; MBSA is immiscible with water and this phenomenon was studied in this work.

#### **6.4.5. $\gamma$ -Valerolactone (GVL)**

$\gamma$ -Valerolactone (GVL) can be synthesised from cellulose waste, is water-miscible and has very low toxicity.<sup>101</sup> Common membranes (PES, PI, PSf, CA) were produced using GVL *via* NIPS.<sup>756</sup> In this work, PVDF membranes were manufactured using GVL and compared to the bio-based Cyrene and the commonly used solvents such as NMP and DMSO.

#### **6.4.6. Cyclopentanone (CP)**

Only recently, cyclopentanone has been used for the preparation of membranes. Hansen solubility approach was used to identify less harmful and less toxic solvents for membrane technology. Microporous PVDF-based membranes were obtained using this solvent.<sup>757</sup> In this work, PVDF membranes have been manufactured using cyclopentanone and compared to other greener solvents, including Cyrene.

### **6.5. Additives used in membranes preparation**

#### **6.5.1. Polyvinyl pyrrolidone (PVP)**

PVP is a non-toxic hydrophilic homopolymer used as hydrophilicity additive and pore-forming agent in membrane fabrication for water purification and treatment, food processing (*i.e.*, beer and wine filtration), gas separation, haemodialysis etc.<sup>554, 604, 751, 758</sup> In NIPS process, PVP is part of the polymer casting solution and, due to its solubility in the non-solvent, it leaves the system with

the solvent and the non-solvent. Some of the PVP remains in the precipitated polymer, increasing its hydrophilicity.

### 6.5.2. Single-walled carbon nanotubes (SWCNTs)

Carbon nanotubes are widely used in membranes technology for water treatment due to their thermal and mechanical stability, conductivity, antimicrobial and antifouling properties.<sup>467, 468, 476,</sup>

<sup>477</sup> The bacterial action of CNTs involves a combination of chemical and physical mechanisms: physical (damaging the cell wall and membrane of microorganism by membrane punching) and chemical (interaction between CNT and microorganism surface lead to generation of toxic substances such a reactive oxygen species, which places the cell under oxidative stress and then biological death). The short CNTs are effective when in a membrane as they can puncture the microorganisms (cells lose their cellular integrity); conversely, in a liquid media, longer CNTs form aggregates that act like needles surrounding the cells.

Two different categories of carbon nanotubes membranes were produced in this work: Bucky paper membranes and nanocomposite CNT membranes; however only the nanocomposites containing SWCNTs were studied in this work.

#### a) "Bucky paper"

Carbon nanotubes are randomly entangled of CNTs dispersed in a large porous 3D network with used for water treatment.<sup>476, 759, 760</sup> In this work, a Bucky paper was obtained from 1mL of a solution of SWNT dispersed in Cyrene after 20h sonicating; the filtrate was then recovered after centrifugation. The filtrate was collected and filtered through a 0.22  $\mu\text{m}$  pore size membrane. CNTs purification step (removing of metal catalyst particles or amorphous carbon) has not been realised in this work. However, these impurities could affect the structure and properties of a Bucky paper. The obtained paper was dried by flushing ethanol for faster drying and remove all the solvent residue left in the pores (Figure 101).



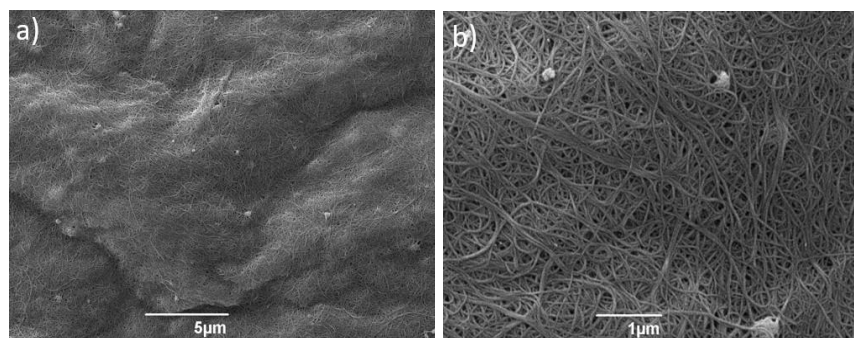


Figure 101: (a) Low and (b) high magnifications of top surface SEM images of a Bucky paper obtained from single-walled carbon nanotubes dispersed in Cyrene.

Bucky-papers were the first macroscopic structures obtained from carbon nanotubes due to the simplicity of their preparation.<sup>759, 760</sup> The carbon nanotubes have a strong tendency to aggregate due to van der Waals interactions and  $\pi$ - $\pi$  interactions holding them together into a cohesive Bucky-paper. The small and large pores in the Bucky paper correspond to the spaces within and between bundles of CNT's.<sup>467</sup>

#### b) Nanocomposite CNT membranes

Composite membranes containing carbon nanotubes incorporated in the solution have superior mechanical, thermal, antimicrobial and antifouling properties than pristine membranes.<sup>476</sup> However, one of the limiting factors for incorporation of nanotubes into polymeric membranes is their high aggregation, resulting in a low dispersability in the casting solution. The incorporation of CNTs is realised by phase inversion, interfacial polymerisation, layer-by-layer.<sup>469, 761, 762</sup>

In this work, single-walled carbon nanotubes (SWCNTs) were incorporated in PES membranes by phase inversion (Section 6.6).

### 6.5.3. Natural polysaccharides

Natural polysaccharides such as alginic acid, chitosan, cellulose, dextrans, lignins, gum Arabic from wild trees or polysaccharides-based materials (activated carbon) have been successfully incorporated in membranes for various separations.<sup>642, 763, 764</sup> The advantages offered by these additives for membrane-based separation include:

- Biocompatibility and biodegradability,
- Hydrophilicity due to the hydroxyl, carboxyl, amine, and hydroxyl groups,

- Abundance in nature,
- Low cost, and
- Chemical reactivity.

These materials are used in filtration primarily for nano-filtration and pervaporation applications like dehydration of organic solvents, in particular ethanol dehydration.<sup>763</sup> The membranes prepared from the pristine sodium alginate form of alginic acid are not mechanically strong enough and they are usually cross-linked by blending it with some other polymers, or by incorporating some particulate matrix (*e.g.* glutaraldehyde, chitosan) for applications such as dye removal, dehydration of ethanol.<sup>765-768</sup> Chitosan is resistant to most organic solvents<sup>769-772</sup> and it exhibits high hydrophilicity and good film-forming capabilities being used in applications from separation membranes to biomedical membranes, due to its antimicrobial properties<sup>773</sup> and wound-healing activity.<sup>774</sup> Acacia gum has been used in membranes preparation as an efficient hydrophilic additive to enhance the antifouling, mechanical and rejection properties membranes.<sup>642, 775</sup> Starch has been used as pore forming in membrane technology in the development of low-cost ceramic membranes used to treat wastewater from textile industry.<sup>776-778</sup> The pores are formed in starch by its burning at sintering temperature between 300 and 1600 °C.<sup>778, 779</sup> Starch is preferred to calcium carbonate because starch is very cheap, is easily processed and is environmentally friendly. The preparation of porous materials with starch is based on “starch consolidation casting”, based on the starch properties of gelling in warm water, which allows its use as consolidator and pore producer.<sup>780, 781</sup> Better porosity has been reported when chemically or physically modified starches were used and controlled porous microstructures were developed.<sup>780, 782</sup>

#### 6.5.4. Polysaccharides-based Starbon™ materials

Activated carbon has been used in membrane technology on ceramic support in wastewater treatment<sup>783-787</sup> or gas separation mixed matrix membranes.<sup>788</sup> Around 2006, polysaccharide-derived Starbons™ were discovered and first reported by the York Green Chemistry Centre of Excellence. Starbons are a new class of bio-based mesoporous carbonaceous materials, similar to activated carbon, made from waste biomass including food peelings and seaweed which is both mesoporous (containing pores with diameters between 2 and 50 nm) and microporous, and tuneable surface functionality.<sup>789</sup> The functionality of these materials can be easily controlled by their carbonisation temperature. The hydrophilicity/hydrophobicity of the surface plays a vital role in adsorption of gasses; acidic gasses such as carbon dioxide, hydrogen sulphide and sulphur

dioxide adsorb better onto a hydrophobic surface. This type of Starbon materials are carbonised at high temperature (800-1200 °C).<sup>790</sup> Ammonia, which is basic, was best adsorbed onto a hydrophilic surface of low temperature-carbonised (300 °C) Starbons due to their acidic functional groups from the surface.<sup>791</sup> In this work, S300 was used as additive in PES membranes, replacing PVP as hydrophilic agent and pore forming. Starbon materials could potentially be good candidates as an additive in gas and water filtration, due to their porosity and tunable functionality.

## 6.6. Polyethersulfone (PES) membranes

### 6.6.1. HSPiP's predictive role in polymer dissolution

Over thirty solvents were used in this work to test the dissolution of polyethersulfone (PES) 3020 from INGE.BASF. A 3D representation (Figure 102a) shows the distance of the solvents which dissolved the polymer:

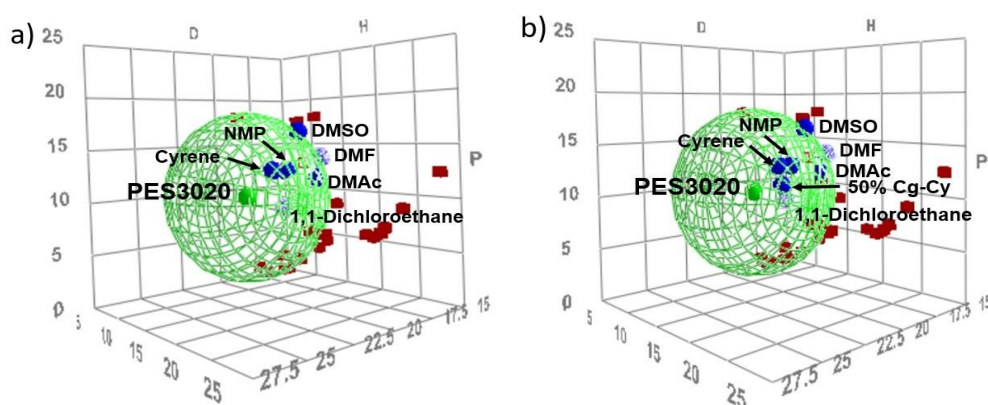


Figure 102: (a) Neat solvents used to dissolve the polymer PES3020 and (b) mixtures of Cygnel in Cyrene were mapped in Hansen space with solubility sphere for PES3020. Hansen solubility parameters are given here in units of  $\text{MPa}^{1/2}$ . Only the good solvents (blue spheres) are named here.

A bad solvent will have a  $R_a$  larger than the sphere's  $R_o$ , making  $RED > 1$ , while solvents likely to affect the material will have a  $RED < 1$ . A solvent with a  $RED < 1$  and closer to the polymer's centre is predicted to perform well. The Hansen sphere for PES3020 was created, which had  $\delta_D=20.42$ ,  $\delta_P=9.89$  and  $\delta_H=6.55 \text{ MPa}^{1/2}$ , a radius=8.5, fit=0.969 and core = [0.10, 0.20, 0.55]. In Hansen sphere, Cyrene has the smallest distance from polymer in the Hansen space ( $RED$  value of 0.468),

suggesting the greatest affinity to PES3020 (Table 26), followed by NMP with 0.64 value for RED and DMAc with RED value of 0.934.

Table 26: Hansen Solubility Parameters of different solvents and RED calculated for PES polymer

| Solvent                | $\delta_D$ | $\delta_P$ | $\delta_H$ | Score | RED    |
|------------------------|------------|------------|------------|-------|--------|
| Cyrene                 | 18.9       | 12.4       | 7.1        | 1     | 0.468  |
| N-Methyl-2-pyrrolidone | 18         | 12.3       | 7.2        | 1     | 0.64   |
| N,N'-Dimethylacetamide | 16.8       | 11.5       | 9.4        | 1     | 0.934  |
| Dimethyl sulfoxide     | 18.4       | 16.4       | 10.2       | 1     | 0.998  |
| N,N'-Dimethylformamide | 17.4       | 13.7       | 11.3       | 1     | 1.008* |
| 1,1-Dichloroethane     | 16.5       | 7.8        | 3          | 1     | 1.041* |

\* Wrongly positioned solvents outside the Hansen space. Only the good solvents are shown in this table. Hansen solubility parameters of the solvents are sourced from HSPiP database and expressed in  $MPa^{1/2}$ .

Table 27: Hansen Solubility Parameters of different solvents and RED calculated for PES3020 dissolution

| Solvent/mixture        | $\delta_D$ | $\delta_P$ | $\delta_H$ | Score | RED    |
|------------------------|------------|------------|------------|-------|--------|
| 40 wt% Cg:Cy           | 18.7       | 10.7       | 7          | -     | 0.422  |
| 30 wt% Cg:Cy           | 18.7       | 11.1       | 7          | -     | 0.435  |
| 50 wt% Cg:Cy           | 18.6       | 10.3       | 7          | 1     | 0.437  |
| 20 wt% Cg:Cy           | 18.8       | 11.6       | 7.1        | -     | 0.438  |
| 60 wt% Cg:Cy           | 18.5       | 9.9        | 7          | -     | 0.458  |
| 70 wt% Cg:Cy           | 18.5       | 9.5        | 7          | -     | 0.46   |
| 10 wt% Cg:Cy           | 18.8       | 12         | 7.1        | -     | 0.462  |
| Cyrene                 | 18.9       | 12.4       | 7.1        | 1     | 0.471  |
| 80 wt% Cg:Cy           | 18.4       | 9          | 6.9        | -     | 0.491  |
| 90 wt% Cg:Cy           | 18.4       | 8.6        | 6.9        | -     | 0.503  |
| Cygnat 0.0             | 18.3       | 8.2        | 6.9        | -     | 0.541  |
| N-Methyl-2-pyrrolidone | 18         | 12.3       | 7.2        | 1     | 0.643  |
| N,N'-Dimethylacetamide | 16.8       | 11.5       | 9.4        | 1     | 0.935  |
| Dimethyl sulfoxide     | 18.4       | 16.4       | 10.2       | 1     | 0.997  |
| N,N'-Dimethylformamide | 17.4       | 13.7       | 11.3       | 1     | 1.006* |
| 1,1-Dichloroethane     | 16.5       | 7.8        | 3          | 1     | 1.050* |

\* Wrongly positioned solvents outside the Hansen space. Only the good solvents and the new Cg:Cy are shown in this table. Hansen solubility parameters of the solvents are sourced from HSPiP database and expressed in  $MPa^{1/2}$ .

As seen in Table 27, HSPiP predicted the solubility parameters of Cygnet:Cyrene mixtures as a linear combination of the parameters for each individual component. Only 50 wt% Cygnet:Cyrene was tested; the blend dissolved the polymer and a score of “1” was given. The input of additional good solvents has resulted in the sphere slightly changing its parameters to  $\delta_D=20.43$ ,  $\delta_P=9.89$  and  $\delta_H=6.60 \text{ MPa}^{1/2}$  and a core of [0.10, 0.20, 0.60], a radius  $R=8.5$  and a  $\text{Fit}=0.970$ . A mixture of 40 wt% Cg:Cy was predicted the best to dissolve PES 3020 followed by mixtures containing 30 and 50 wt% Cygnet in Cyrene. This new sphere results in Cyrene moving marginally further from the centre with a different RED value, of 0.471. Less polar Cygnet 0.0 was predicted to perform less well than Cyrene or any Cg:Cy mixtures.

## 6.6.2. Polyethersulfone (PES) membranes preparation

### 6.6.2.1. PES membranes using Cyrene (PES/C) and NMP (PES/N) as solvents

In this study, the polyethersulfone membranes (PES/C and PES/N) with highly asymmetrical pore structure were fabricated from hot (70 °C) and cold (17 °C) casting solutions of PES, PVP, and solvent (Cyrene or NMP) using a non-solvent phase inversion technique. The composition of Cyrene- and NMP-based PES casting solutions can be seen in Table 28. The membranes were coded based on the solvent used (PES/C are the membranes cast from a solution containing Cyrene whilst PES/N represents membranes in NMP) and the concentration of PVP used, *e.g.* “0” means a membrane produced with no PVP, whilst “0.1” through to “10” means a membrane produced with 0.1% through to 10% PVP respectively. For example, a PES membrane produced with Cyrene® and 0.1% PVP will be referred to as “PES/C0.1” while the same membrane produced in NMP would be denoted “PES/N0.1”.

Table 28: Composition of casting solutions (wt%)

| Membrane type | PES/N solution (wt%) |      |      | PES/C solution (wt%) |      |        |
|---------------|----------------------|------|------|----------------------|------|--------|
|               | PES                  | PVP  | NMP  | PES                  | PVP  | Cyrene |
| PES/0         | 16.7                 | 0    | 83.3 | 16.7                 | 0    | 83.3   |
| PES/0.1       | 16.7                 | 0.08 | 83.3 | 16.7                 | 0.08 | 83.3   |
| PES/0.5       | 16.6                 | 0.4  | 83.0 | 16.6                 | 0.4  | 83.0   |
| PES/1         | 16.5                 | 0.8  | 82.6 | 16.5                 | 0.8  | 82.6   |
| PES/5         | 16                   | 4    | 80   | 16                   | 4    | 80     |
| PES/10        | 15.4                 | 7.7  | 76.9 | 15.4                 | 7.7  | 76.9   |

The casting solution was prepared by dissolving 20 wt% of PES pellets (as compared to the mass of solvent) into Cyrene or NMP at a temperature of 70 °C for 4h. Different concentrations of PVP were added under continuous stirring. The casting solution was degassed and then placed on an acrylic plate for PES/N or on a Polyester (PET) non-woven fabric CraneMat CU632 (Neehan Technical Materials, USA) for PES/C. The casting solution was cast using a RK Print K101 bench casting machine (RK Print, UK) at a speed of 3 cm s<sup>-1</sup> for the membranes produced in NMP and 2 cm s<sup>-1</sup> for membranes produced in Cyrene. The thickness of all membranes was controlled at 500 µm. The casting film was submerged in a coagulation bath containing deionised water at RT. Membranes were then washed three times in distilled water for 10 minutes while under sonication to wash out the residual solvent. The fabricated membranes were then stored in deionised water until further use. The membranes were prepared at RT of 17 °C and a humidity of 74-78%. The temperature of the water bath was 12 °C and the time from casting the gel to placing it in a water bath was limited to a maximum of 5 seconds. To characterise the prepared membranes, they were first washed with deionised water and dried in a vacuum oven at 80 °C for 12 hours.

#### 6.6.2.2. PES membranes using Cyrene (PES/C), 50 wt% Cygnet 0.0-Cyrene blend (PES/Cg-Cy) and pure Cygnet 0.0 (PES/Cg)

PES filtration membranes were manufactured in this work using both hot (100 °C) and cold (RT) casting gels containing different solvents: neat Cyrene, Cygnet 0.0 and a mixture of Cyrene and its derivative Cygnet 0.0 (50 wt%) using a non-solvent phase inversion technique (NIPS). The membranes prepared using 50 wt% Cygnet in Cyrene were coded as "PES/Cg:Cy". The composition of the casting gels can be seen in Table 29:

Table 29: Composition of casting solutions of PES/C, PES/Cg:Cy and PES/Cg (wt%)

| Membrane code | Polymer (wt%) |        | Solvent/mixture (wt%) |            |
|---------------|---------------|--------|-----------------------|------------|
|               | PES           | Cyrene | Cygnet: Cyrene        | Cygnet 0.0 |
| PES/Cyrene    | 15            | 85     |                       |            |
| PES/Cg: Cy    | 15            |        | 85                    |            |
| PES/Cygnet    | 15            |        |                       | 85         |

15% of each polymer was immersed in 85% solvent and heated up to 100 °C for 3-4h. Each polymer solution was cast onto a glass plate using a steel blade, using a thickness of 200 µm. The casting film was submerged in a coagulation bath containing deionised water at RT. Hot casting was

achieved by pre-heating a quartz glass sheet (200x200 mm) in an oven at 100 °C for 20 minutes. The time from removing the quartz glass to NIPS casting bath, the membrane was kept to a maximum of 3 minutes to limit cooling. Membranes were then washed in distilled water and stored in deionised water until further use. To characterise the prepared membranes, they were dried in vacuum oven at 80 °C for 12 hours.

### 6.6.2.3. PES membranes prepared with *N,N'*-dimethyl-*N,N'*-dibutylsuccinamide (PES/MBSA)

Traditionally, water is used as on-solvent in NIPS process. As MBSA is considered immiscible with water, a reversed approach was adapted for this work. Three membranes were manufactured from PES and MBSA as solvent. The glass plate with the casting solution was quickly immersed in the coagulation bath. Water and two non-polar solvents were used in this work as non-solvents: hexane and 2,2,5,5-tetramethyloxolane (TMO), as both are miscible with MBSA. The casting solution and the non-solvents are shown in Table 30:

Table 30: Composition of casting solutions of PES/MBSA and the non-solvents used

| Membrane code | Casting solution (wt%) |      | Non-solvent (in excess) |
|---------------|------------------------|------|-------------------------|
|               | PES                    | MBSA |                         |
| PES/MBSA      |                        |      | Water                   |
| PES/MBSA      | 10                     | 90   | Hexane                  |
| PES/MBSA      |                        |      | TMO                     |

The casting solution was prepared by dissolving 10 wt% of PES pellets (as compared to the mass of solvent) into MBSA at a temperature of 100 °C for 6h. The casting solution was degassed, then placed on a glass plate and immersed in a bath of solvent, *via* a non-solvent phase inversion technique (NIPS). The thickness of all membranes was controlled at 150 µm using a manual casting knife. The casting film was submerged in a coagulation bath containing solvent at RT, causing the PES to precipitate. MBSA is only partially miscible with water (Figure B 18). As the water as non-solvent is in excess in NIPS process, the miscibility of MBSA with water is very important. The polar aprotic solvents such as NMP, DMAc, DMF are miscible with water. The newly discovered bio-based Cyrene reacts chemically with the water and leads to the formation of geminal diol.<sup>52</sup> The miscibility of MBSA in water shows a very interesting behaviour with only partially solubility and stability of the new binary system (Figure B 19). When the water is in excess (in an attempt to copy

the conditions of NIPS process), MBSA becomes miscible with water giving a pale yellow colour, which is stable, which could represent the hydration of MBSA (Figure B 19).

#### 6.6.2.4. PES membranes prepared with Cyrene or NMP and carbon nanotubes

The mixed (nanocomposite) carbon nanotubes (CNT) membranes have been manufactured *via* the phase inversion process, using water as a coagulant. The main aim of introducing carbon nanotubes into the membrane's matrix is to improve the performance of existing membranes by including surface hydrophilicity (chemically surface functionalisation), thermal and mechanical stability, antimicrobial and antifouling properties and improved salt rejection capability.<sup>792, 793</sup> In this project, four membranes have been prepared. The casting solution composition can be seen in Table 31:

Table 31: Casting solution composition (wt%) of PES membranes produced with carbon nanotubes and NMP or Cyrene

| Membrane type | Polymer and additive (wt%) |     |       | Solvent (wt%) |        |
|---------------|----------------------------|-----|-------|---------------|--------|
|               | PES                        | PVP | SWCNT | NMP           | Cyrene |
| PES/CNT/N0    | 15                         | 0   | 0.1   | 84.9          | 0      |
| PES/CNT/C0    | 15                         | 0   | 0.1   | 0             | 84.9   |
| PES/CNT/C3    | 12                         | 3   | 0.1   | 0             | 84.9   |
| PES/CNT/C5    | 10                         | 5   | 0.1   | 0             | 84.9   |

The membranes are coded based on the additive used: "PES/C0" is the membrane produced with Cyrene and no additive, while "PES/N" is manufactured using NMP as a solvent. PES/C3 and PES/C5 means a membrane produced with 3% and 5% PVP respectively. All membranes have been produced using 0.1% pristine single-walled carbon nanotubes (SWCNTs) and noted as "PES/CNT". The SWCNT were dispersed first in the solvent by sonicating for 10 minutes. This solution was used to dissolve PES by dissolving 10-15 wt% of PES pellets at a temperature of 70 °C for 4h. Then concentrations of 3% PVP or 5% PVP were added under continuous stirring. The casting solution was degassed and then placed on a glass plate and a film of thickness of 150 µm was obtained using a manual casting knife. The casting film was submerged in a coagulation bath containing deionised water at RT. Membranes were then washed three times in distilled water for 10 minutes while under sonication in order to wash out the residual solvent. The fabricated membranes were



then stored in deionised water until further use. To characterise the prepared membranes, they were first washed with deionised water and dried in a vacuum oven at 80 °C overnight.

### 6.6.2.5. PES membranes prepared with Cyrene and Starbon™ materials as a bio-based additive

The membranes are coded based on the additive used: PES is the membrane produced with Cyrene and no additive, while PES/PVP and PES/S300 mean a membrane produced with 1% PVP and 1% S300 respectively (Table 32). All membranes have been produced using Cyrene in this study.

Table 32: Composition of casting solutions (wt%)

| Membrane type | Polymer and additive (wt%) |     |      | Solvent (wt%) |
|---------------|----------------------------|-----|------|---------------|
|               | PES                        | PVP | S300 | Cyrene        |
| PES           | 15                         | 0   | 0    | 85            |
| PES/PVP       | 15                         | 1   | 0    | 84            |
| PES/S300      | 15                         | 0   | 1    | 84            |

The casting solution was prepared by dissolving 15 wt% of PES pellets into Cyrene at a temperature of 70 °C for 4h. A concentration of 1% PVP or 1% S300 were added under continuous stirring. The casting solution was degassed and then placed on a glass plate and a film of thickness of 150 µm was obtained using a manual casting knife. The casting film was submerged in a coagulation bath containing deionised water at RT. Membranes were then washed and dried at 80 °C overnight. The fabricated membranes were then stored in deionised water until further use.

### 6.6.3. Viscosity of PES/C and PES/N casting solutions

The viscosity of the casting solutions impacted the permeability of membranes morphologies in previous work.<sup>63</sup> The casting solutions of polyethersulfone dissolved in Cyrene or NMP were used to measure their dynamic viscosities (Figure 103). Six types of membranes were analysed for each solvent, depending on the amount of additive PVP used: no additive (PES/C0 and PES/N0), 0.1% PVP (PES/C0.1 and PES/N0.1), 0.5% PVP (PES/C0.5 and PES/N0.5), 1% PVP (PES/C1 and PES/N1), 5% PVP (PES/C5 and PES/N5) and 10% PVP (PES/C10 and PES/N10).

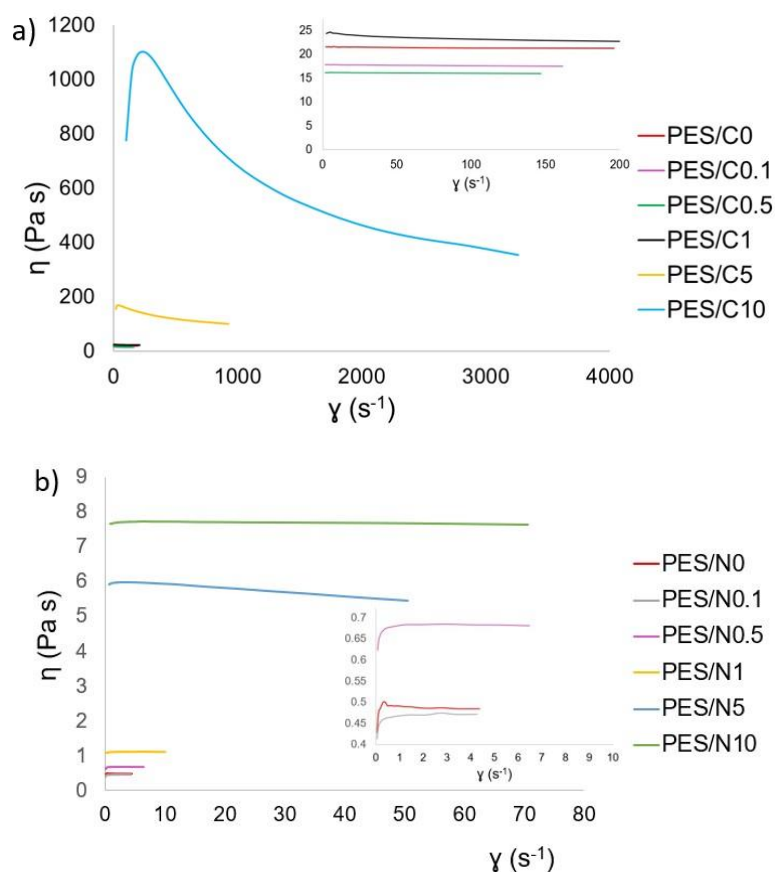


Figure 103: (a) Variation of the dynamic viscosity versus shear rate of polyethersulfone casting solutions in Cyrene and (b) NMP.

Generally, PES showed a typical pseudo-plastic (or shear thinning) behaviour; the viscosity decreases with the shear rate and temperature.<sup>794</sup> PES consists of semi-rigid chains, which have a strong effect on its rheological behaviour. At lower viscosities, the polymer backbone is less rigid. Later, this “flexible” state was explained by “disentanglement” inside the polymer, permitting it to flow.<sup>353</sup> During the shear thinning, the macromolecules flow in the shear direction. This phenomenon is described by the disentanglement, when the flow resistance of the macromolecules is lowered by increasing of the shear stress.<sup>353</sup> The shear rates (speed) destroy the structure to some degree, which then leads to the lower viscosity.<sup>795</sup> At rest, PES solutions are highly entangled and shear thinning as these interactions are reduced. All PES/C samples (Figure 103a) have higher dynamic viscosities than PES/N samples, which have shown a nearly linear, Newtonian-like behaviour (Figure 103b). A range between 0.45 and 8 Pa s can be observed for NMP-based casting solutions, whilst viscosities between 15 and 400 Pa s are observed in case of Cyrene-based solutions. Viscosities increase with increasing loadings of PVP in both solvent systems. Viscosity ratio between PES/C1 and PES/C10 (*approx.* 25 to 400 Pa s) is much higher than between PES/N1 and PES/N10 (*approx.* 1 to 7.5 Pa s), which could indicate stronger interactions

(*i.e.*, hydrogen bonding) between the Cyrene and polymers (PES or/and PVP) than between NMP and the respective polymers. Dynamic viscosities of PES/C0, PES/0.1 and PES/C0.5 did not increase with the increase of PVP loading probably due to the small amount of PVP which did not disperse uniformly in the solutions, affecting the disentanglement of the polymer in bulk. This phenomenon can be seen for PES/N0 and PES/N0.1. In this work, at a low shear rate, the viscosity is not stable and high values can be seen because the fluid does not have enough time to respond; the measurement is occurring in the transitional zone and not at a steady state. A steady state is reached after a certain length of time, the time is dependent on the speed disentanglement. The highly viscous solution of PES/C10 needs longer time to reach a steady state; hence the high curve seen at a low shear rate.

#### **6.6.4. Scanning Electron Microscopy (SEM) analyses of PES membranes**

##### **6.6.4.1. SEM analyses of PES/C and PES/N membranes**

All membranes produced herein (except for PES/C10) present a typical Loeb-Sourirajan structure with pores which increase in diameter from the top to the bottom surface of the membrane. Top layer is supported by a sponge-like substructure (important for the mechanical resistance of the membranes), and macrovoids, due to the instantaneous demixing during the phase inversion.<sup>667</sup> The casting solution has a high affinity for water which can cause changes in morphology and performance.<sup>651</sup> Finger-like structures can be seen near the top layer of the membrane which formed due to a fast demixing between the solvent and non-solvent. In some cases, a sponge structure can be seen in the centre of membrane due to slow demixing of relatively thick casting solution (500  $\mu\text{m}$ ). When the polymer starts to precipitate in the water from the casting bath, the first layer to come in contact with the water is the top layer (generally the external sides of the gel); then the precipitation advances slowly through the thickness of the membrane until it reaches the last layer which is supported by the glass plate. However, in some cases, when the water penetrates the layer between the glass plate and the precipitated membrane, fast demixing occurs detaching the membrane from the glass plate. Increasing the PVP content in the casting solution led to slower demixing, especially towards the bottom layer of the membrane (closest to the glass slide). When the exchange from solvent to anti-solvent occurs, it starts at the surface, where finger voids are observed and slows as it approaches the bottom layer, when more sponge-like structures are seen.

It has been generally accepted that instantaneous demixing leads to macrovoidic structure and delayed demixing leads to a sponge-like structure.<sup>554, 667</sup> While the sponge-like structure looks the same for membranes produced in both Cyrene and NMP, Figure 104 indicates differences between pore size and morphology in a macrovoidic layer at the same magnification:

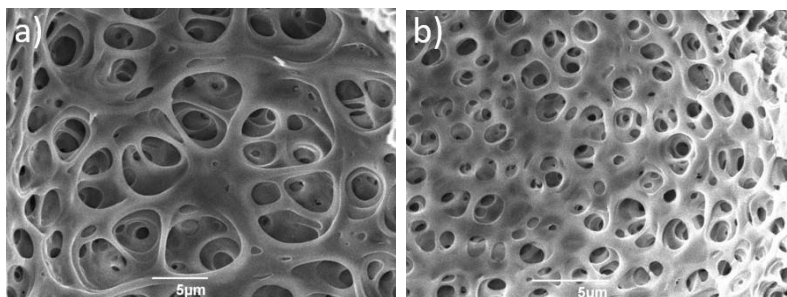


Figure 104: Detail of cross-sectional SEM images of (a) PES/C0.1 and (b) PES/N0.1.

During the demixing between the solvent (Cyrene) from a PES/C and the non-solvent (water), a geminal diol is formed; hence the tertiary solvent system (Cyrene/diol/water) is responsible for membranes morphology.<sup>52</sup> When pure PES is used, the phase separation of polymer solution occurs immediately, due to low viscosity of the casting solution. The higher viscosity of Cyrene (discussed in Chapter 1) adds to the solution's viscosity leading to a slower demixing process and hence to a more visible sponge-like structure (Figure 105) than in PES/N membranes (Figure 106). The modification of polymer solution (by adding PVP) changes the pore structure of the membrane.<sup>663</sup> Also, different temperatures of the casting solution lead to differences in their morphology (Figure 105):

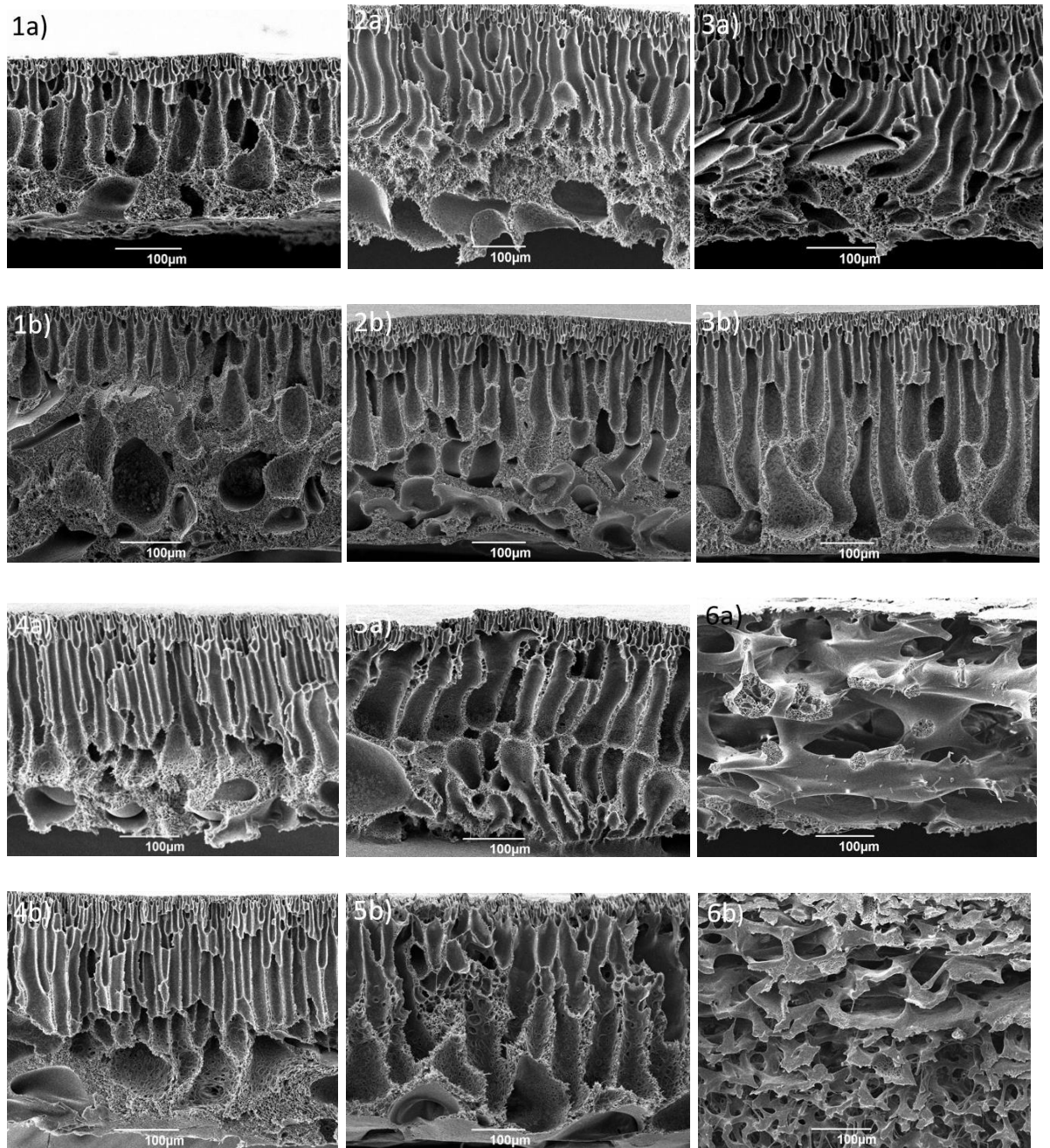


Figure 105: Cross-sectional SEM images of PES membranes produced from Cyrene and different concentrations of PVP: (1) 0%, (2) 0.1%, (3) 0.5%, (4) 1%, (5) 5% and (6) 10% in cold (a) and hot solutions (b). All membranes have a thickness of 500  $\mu\text{m}$ .

The membranes cast from Cyrene hot solutions showed more sponge-like structure, with macro-voids all the way through the membrane. A greater difference in morphology starts from a concentration of 5% PVP, with the greatest at a concentration of 10% PVP. PES/C10 has developed a completely different surface morphology, with big voids (Figure 105 6a and Figure 105 6b). This could be caused by a large amount of PVP which dissolved in water and left big voids in the membrane or the solid-liquid demixing of a high polymer concentration in the casting solution (20% PES and 10% PVP).

The rheology of the casting solution of PES/C10 and PES/N10 was studied, with a decrease in viscosity with increasing temperature clearly visible (Figure B 20 in Appendix B). It was previously found that the higher viscosity solution will change with temperature to a greater extent than a low viscosity solution.<sup>796</sup> In the present work, both PES/C10 and PES/N casting solutions decrease with temperature. Moreover, a bigger difference in morphology is seen when comparing a membrane with high viscosity (PES/C10) when casting from a solution at room temperature with a hot one cast from a hot solution, where the viscosity decreased substantially. A lower viscosity allows faster demixing; faster interaction between the solvent and non-solvent takes place in these solutions. The membranes cast from hot/cold solutions in NMP's showed different morphologies (red circle in Figure 106 b and e) where PES/N0.1 cast from a hot casting solution presents a middle sponge layer (Figure 106 2b), while PES/N0.1 cast from a cold solution clearly shows the finger layer all the way through the membrane (Figure 106 2a):

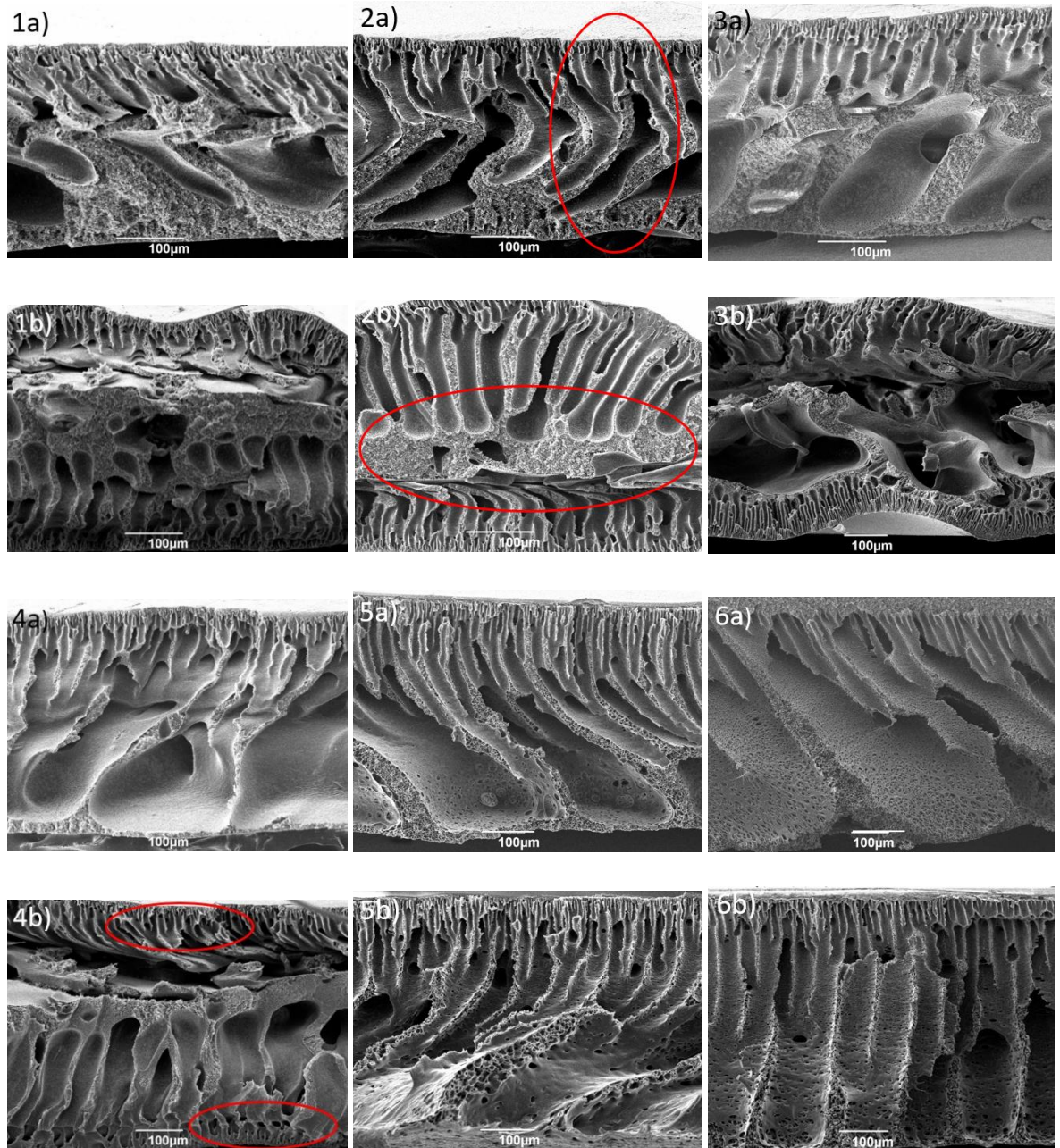


Figure 106: Cross-sectional SEM images of PES membranes produced from NMP and different concentrations of PVP: (1) 0%, (2) 0.1%, (3) 0.5%, (4) 1%, (5) 5% and (6) 10% in cold (a) and hot solutions (b). All membranes have a thickness of 500  $\mu\text{m}$ .

In the case of PES/N1 cast from a hot solution (Figure 106 4b, red circle) the demixing happened on top layer and also penetrated the space between the glass plate and hot gel, leading to fast demixing and detaching the membrane from the glass plate, forming two active porous layers and a sponge layer in the middle where the demixing happened slower. In case of a cold casting solution PES/N1 did not detach from the glass plate during demixing and the process of demixing between the solvent and non-solvent happened from the top to the bottom layer

(close to the glass plate); hence the finger layers on top supported on a sponge layer (Figure 106 4a).

#### 6.6.4.2. SEM analyses of PES/Cyrene, PES/Cg:Cy and PES/Cygnnet membranes

Different morphologies can be easily seen when changing the solvent and the temperature of the casting gel. Polyethersulfones (PES) membranes (Figure 107) manufactured using Cyrene and cast from a casting solution at room temperature or a hot solution are typical asymmetrical membranes with Loeb-Sourirajan structure (Figure 107 a and b).<sup>610</sup> Loeb-Sourirajan membranes present asymmetric pore size and porosity through the thickness of the membrane; the voids are smaller near one surface and bigger on the other surface.

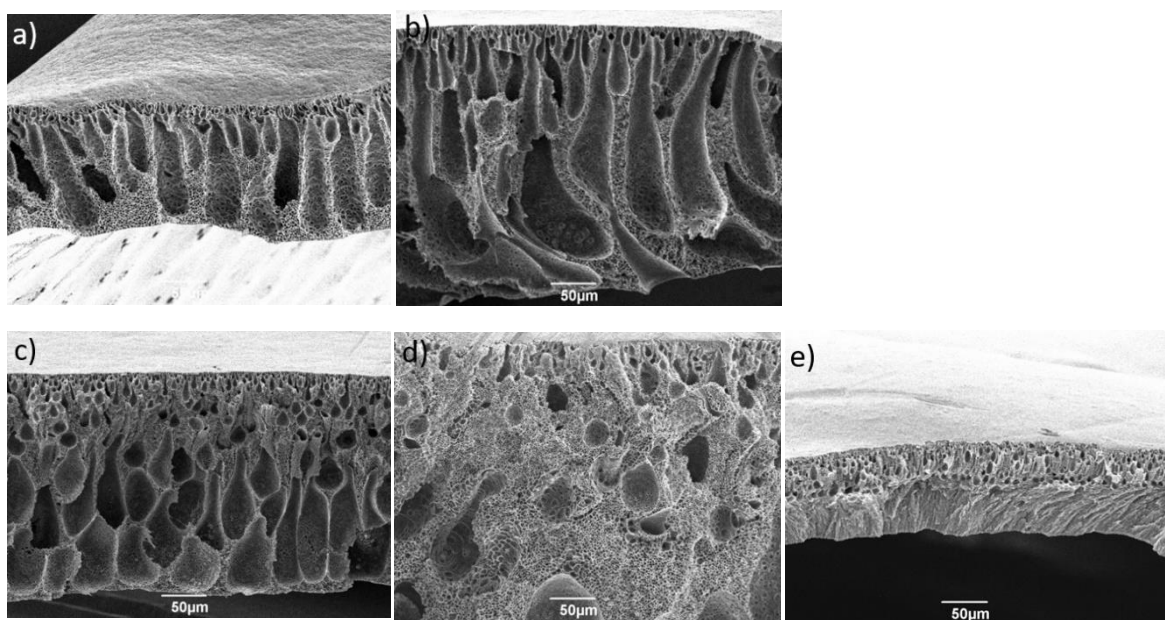


Figure 107: Cross-sectional SEM images of PES membranes using Cyrene and cast from a gel at (a) room temperature and from (b) a hot gel, using (c) Cygnnet 0.0/Cyrene blend at room temperature and (d) hot solution and from (e) pure Cygnnet 0.0. All membranes have a thickness of 200  $\mu\text{m}$ .

A PES membrane cast from a solution at room temperature (Figure 107 a) shows more non-interconnected finger-layers. The demixing inside the solution happens slower especially towards the bottom layer of membrane (closest to the glass slide). A hot casting solution of PES leads to a faster de-mixing due to a lower viscosity and faster solvent-water interaction, generating more macrovoids and less sponge-like structure. Membranes prepared using Cg:Cy showcases more non-interconnected finger-layers, when cast from a solution at RT (Figure 107 c) due to the solubility of both Cyrene and Cygnnet 0.0 from the mixture Cg:Cy with the anti-solvent (water); no



sponge-like can be seen in this case. When using pure Cygnet 0.0 was used in the casting solution, a top active porous layer is formed due to the de-mixing between the solvent and the anti-solvent (Figure 107 e).<sup>755</sup> The porous layer is a mixture of macrovoid and sponge-like structures supported on a dense layer. This dense layer is formed due to the cooling down of the solution and crystallisation of the solvent; no demixing was possible in this layer. The combination of a porous, permeable layer with a non-permeable layer originated from the same casting solution and formed without any crosslinking with another layer, which is generally another polymeric film, could be a step forward in replacing the traditional thin-film composite membranes with a simple, one-step production process.

An important factor to be considered in the solvent/non-solvent demixing represents the mixture between Cyrene and water. They form a geminal diol when mixed and different proportions of Cyrene-geminal diol-water can be involved in the liquid-liquid demixing. This phenomenon can be partially involved in demixing when Cg:Cy is used, but not responsible for the demixing when Cygnet is employed.

#### 6.6.4.3. SEM analysis of PES/MBSA membranes

A typical non-solvent is water since it is inexpensive and environmentally benign; however, other non-solvents such as methanol, ethanol, isopropanol, glycerol, hexane, acetone, and xylene have been also used, leading to different morphological zones in the generated membranes.<sup>260, 681, 797-799</sup> In this work, PES-based membranes were produced using MBSA as a solvent and three different non-solvents to cast the membranes: water, hexane and TMO. As MBSA was found to be able to dissolve PES, it was tested for its ability to fabricate a filtration membrane. The varying affinities of MBSA/PES casting solutions for non-solvents cause changes in membranes morphologies (Figure 108). The porosity of the PES/MBSA membranes produced using water and TMO as non-solvents were comparable to those previously reported in the literature with Loeb-Sourirajan structure and provide a fully bio-based solvent system for their production. The membranes cast in the water showed a dense skin and finger-like structures through the thickness of the membrane (Figure 108 1a-c).

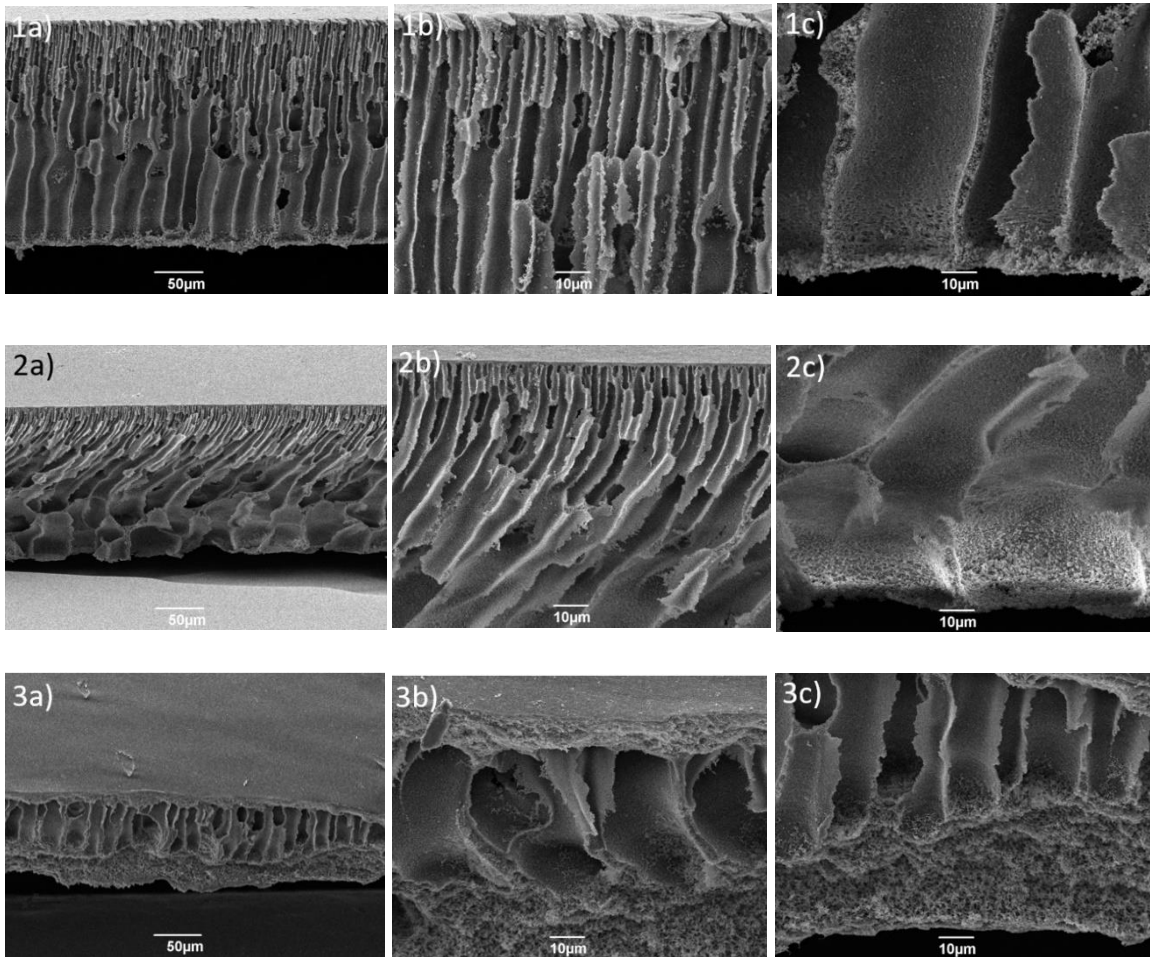


Figure 108: Scanning Electron Microscopy images of (a) cross-section, (b), top side and (c) bottom side of PES membranes using MBSA as solvent and (1) water, (2) TMO and (3) hexane as non-solvent. All membranes have a thickness of 150  $\mu\text{m}$ .

During liquid-liquid demixing between the solvent (MBSA) and non-solvent (water) the exchange has happened fast, leading to the formation of macrovoids in the membrane. A toxic solvent (hexane) and a greener alternative (TMO) (Figure 108 2a-c) have been used as non-solvent, being compared to water, which is mostly used for this purpose. They allowed demixing of the mutually soluble MBSA, generating a finger-like porous structure with large macrovoids at the bottom. Using TMO as the non-solvent generated a similar morphology to when water was used, but with larger macrovoids at the bottom surface (Figure 108 2c). PES/MBSA cast in hexane (Figure 108 3a-c) resulted in a partial dissolution (Figure B 21) of the polymer-poor phase of the casting solution in the nonsolvent due to the miscibility of the solvent and nonsolvent. As a result, the morphology of the membrane was negatively affected, with dense regions at the surfaces (Figure 108 3b, c). A dense skin and finger-like morphology can be seen, supported on a thick, dense layer due to a slow demixing of the layer closest to the glass plate. The bottom layer of the membrane cast in hexane present a new morphology, between a dense and a sponge-like layer due to a very slow

demixing process. During precipitation of the casting solution in the bath of hexane is believed that the demixing of non-polar hexane with the polar aprotic solvent from the casting gel (MBSA) happens very slow, taking hours for the PES/MBSA to fully precipitate. This could be due to the density of the solvents involved (Table 33) or the some loss of the polymer into the casting bath which potentially increased the viscosity of the casting gel and demixing happened slower.

Table 33: The density of the solvents used in PES membranes cast using MBSA as solvent and water, TMO and hexane as non-solvents

| Solvent name | Density (g mL <sup>-1</sup> ) |
|--------------|-------------------------------|
| MBSA         | 0.99                          |
| Water        | 1                             |
| TMO          | 0.802                         |
| Hexane       | 0.659                         |

#### 6.6.4.4. SEM of membranes using singled-walled carbon nanotubes (SWCNTs)

SEM was used to observe the surface and cross-sectional morphology of membranes containing single-walled carbon nanotubes. As all membranes were produced using 0.1% compared to the mass of solvent, the differences occur when changing the solvent and varying the amount of PVP. Membrane produced with Cyrene (Figure 109 1a) is different from the one manufactured with NMP (Figure 109 4a):

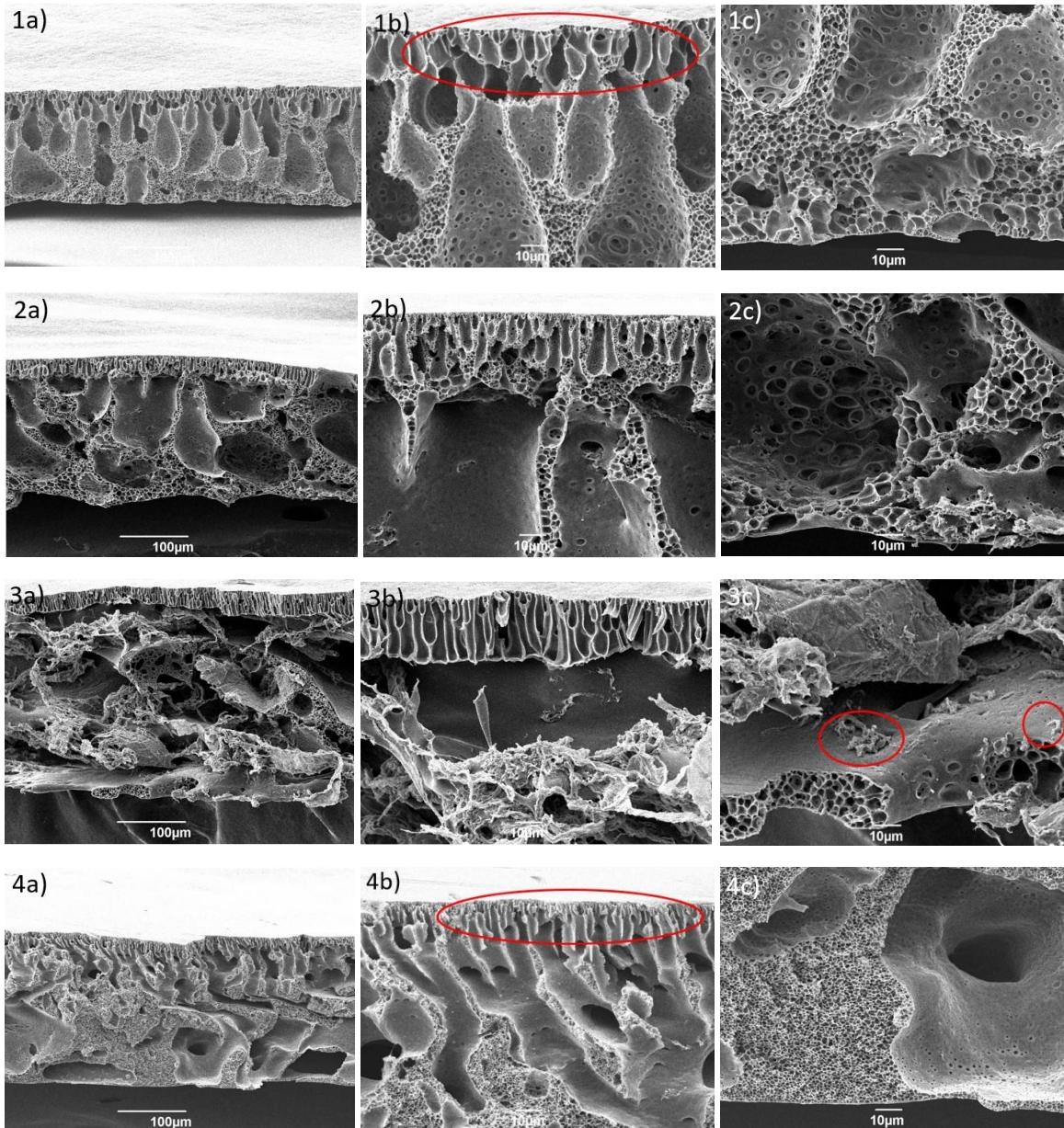


Figure 109: Scanning Electron Microscopy images of (a) cross-section, (b), top side and (c) bottom side of membranes of (1) PES and Cyrene, (2) PES, Cyrene and 3% PVP and (3) PES, Cyrene and 5% PVP and (4) NMP. All membranes contain 0.1% single-walled carbon nanotubes (SWCNTs) and a thickness of 150  $\mu\text{m}$ .

Bigger pores are seen in the Cyrene-based membrane, with more finger-like layers and different shape of the pores, due to the demixing between water and Cyrene, and formation of a solvent system containing Cyrene/geminal diol/water. In the NMP-derived membranes, the sponge layer is more visible, but with smaller pores than Cyrene-derived ones, observation previously highlighted.<sup>63</sup> There are fewer macrovoids in NMP-based membranes, but they are larger, due to a fast demixing. In Cyrene-based membranes, the same macrovoids are smaller, but more frequently seen. PVP behaves as an antisolvent agent in the demixing step due to its high solubility in water and the casting solution has a high affinity for water which can cause changes in

morphology and performance when the amount of the additive is increased in the Cyrene-based membranes (Figure 109 1c, 2c,3c). Also, PVP plays a stabilisation role for the carbon nanotubes in the solution. The literature suggest PVP wraps around CNT tubes by double and triple helix (middle) or multiple parallel wrapping strands from the same polymer chain.<sup>557, 562, 583</sup> The more PVP is added to the casting solution, the bigger change in the morphology is seen and clusters of CNT and possibly with PVP can be seen in Figure 109 3c (red circle) and Figure B 22.

When using an optical microscope, larger pores emerged of the hybrid membrane PES/Cyrene (Figure 110 1b) compared with NMP-derived membrane (Figure 110 3b), favourable to membrane flux. Both membranes were cast without the pore-forming additive, PVP,<sup>63</sup> which means no additive is necessary to form pores. This phenomenon was also observed in a previous work.<sup>63</sup>

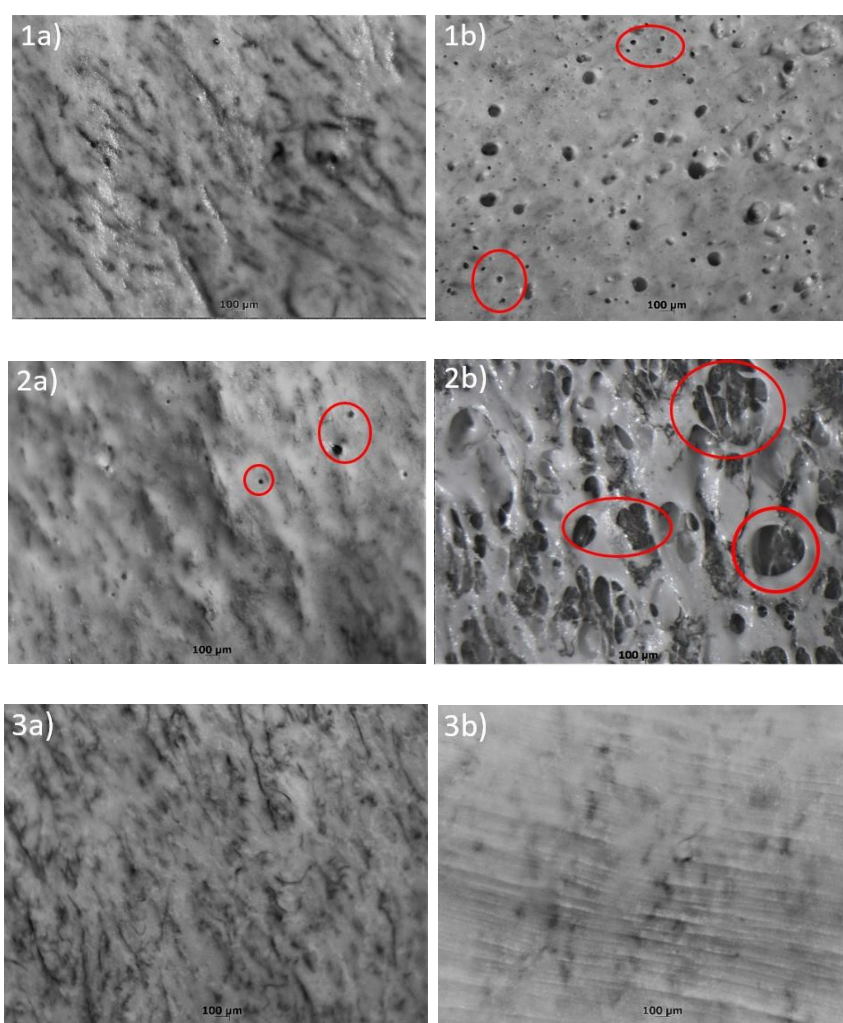


Figure 110: Stereo (optical) microscope images of (a) the top surface and (b) bottom surface of a PES membrane produced with (1) Cyrene, (2) Cyrene and 5% PVP or (3) NMP. All membranes contain 0.01% SWCNT.

Pores can be seen onto both surfaces of Cyrene-derived membranes, less onto the top surface of a PES/C and no additive (Figure 110 1a). Both Cyrene-based membranes (Figure 110 1 and 2) developed pores on the bottom layer, increased in size with the pore-forming additive PVP addition. The latter membrane shows pores onto top surface too. On the other hand, no pores can be seen on both the top and bottom surfaces of an NMP-derived membrane (Figure 110 3). The presence of pores onto membranes produced with Cyrene, with and without PVP, could represent an advantage in antimicrobial membranes for a better access to the nanotubes inside the porous membrane or membranes with high flux. The antibacterial performance of nanotubes is as a result of them damaging the outer membrane of bacteria and releasing the intracellular content (cells lose their cellular integrity) or by the capacity of the nanotubes aggregates to act like needles surrounding the cells. The access of the bacteria to the nanotubes inside the membrane is possible through the pores, the bigger the pores, the better the antibacterial activity.

#### 6.6.4.5. SEM images of PES/C/S300 membranes

All membranes were produced using Cyrene as the solvent and polyethersulfone as the main polymer. Two membranes were manufactured using different additives: PVP (Figure 111 2) and S300 (Figure 111 3). Both pristine and PES/ PVP membranes were characterised in section 3.3.3.1. of this study.

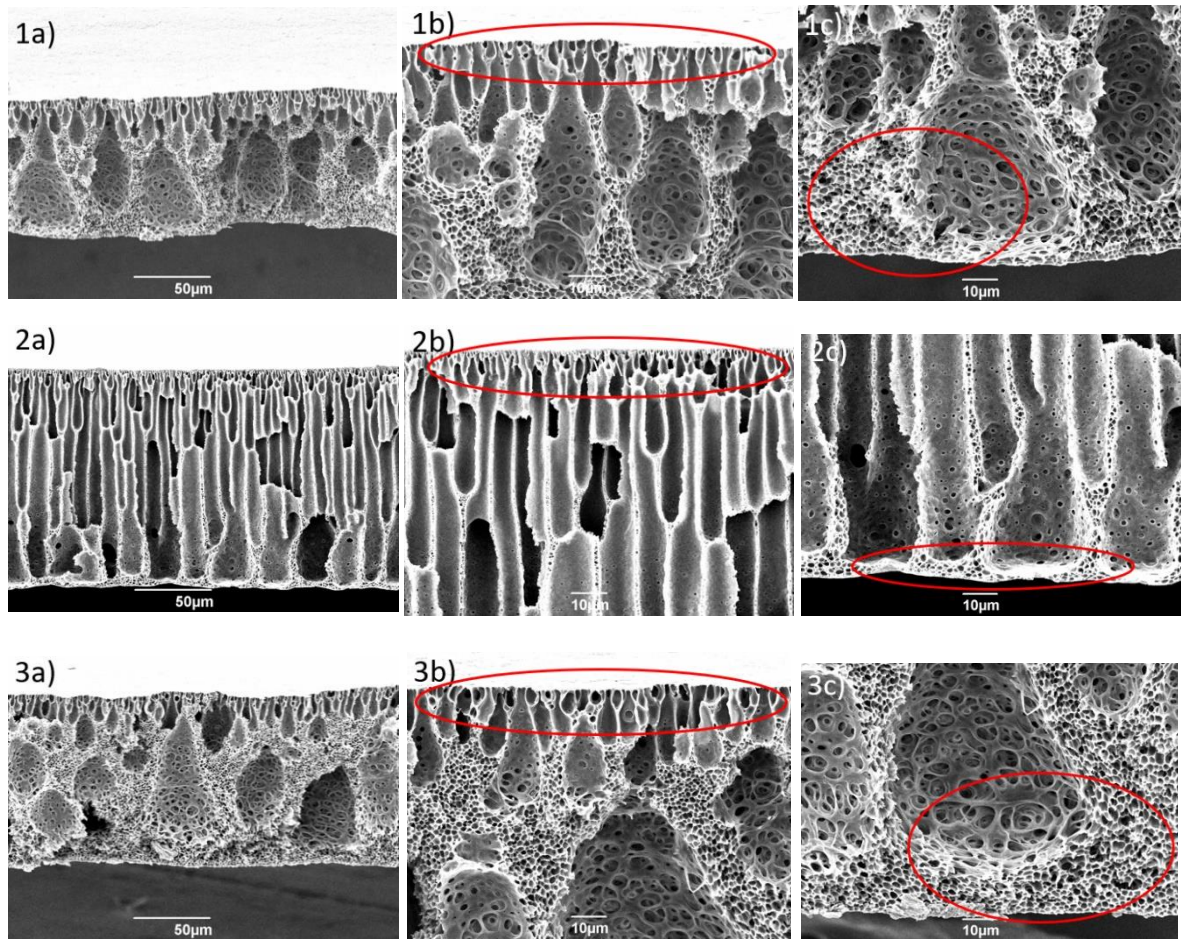


Figure 111: Scanning Electron Microscopy images of (a) cross-section, (b) top side and (c) bottom side of membranes produced from (1) pristine PES, (2) PES and 1% PVP and (3) PES and 1% S300. All membranes have been produced using Cyrene as a solvent and have a thickness of 150  $\mu\text{m}$ .

The novel membrane using starch-derived S300 as additive looks very similar to the pristine PES membrane, with macrovoids and sponge-like structures (Figure 111 1 and 3). Both PES and PES/S300 (Figure 111 1 and 3) are very porous, with visible larger pores, compared to PES/PVP (Figure 111 2). The lower side of the cross-section of the PES/S300 presents a sponge-like layer, bigger than in the other membranes (Figure 111 3c). This adds more mechanical strength to this type of membrane.<sup>667, 800</sup> PES/PVP presents finger-like structures through the thickness of the membrane (Figure 111 2a) and almost no sponge-like can be observed. Membranes manufactured using Cyrene are more sustainable, with less loss of polymeric material (Figure B 23a), unlike NMP-based membranes (Figure B 23b).<sup>63</sup> In this work, no loss of black powdered S300 or polymers can be observed (Figure B 23c).

#### 6.6.4.6. Influence of membranes thickness on morphology

As seen previously in this Section 6.6.3., the solvent and the temperature of the casting solution have changed the morphology of the membranes. In this work, PES membranes were cast using different thickness; hence their morphology was studied. In a previous work, it has been shown how thickness of a membrane not only changes the morphology, but also has a great influence on the filtration efficiency.<sup>63</sup> In this work, only pristine PES membranes cast from casting solutions at room temperature were considered to compare different morphologies when the thickness is changed (Figure 112):

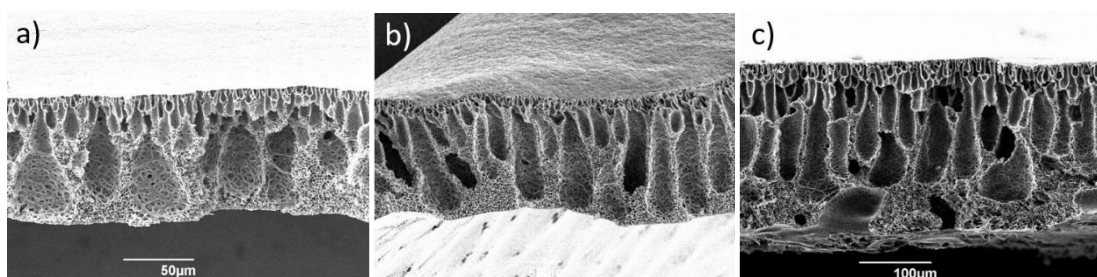


Figure 112: Influence of the thickness of flat sheet membrane on PES membranes morphology with a thickness of (a) 150, (b) 200 and (c) 500  $\mu\text{m}$ .

As observed in Figure 112, the cast solution's thickness changes the morphology of a flat sheet membrane. A membrane with a thickness of 150  $\mu\text{m}$  (Figure 112 a) presents macrovoids and a very porous sponge-like structure due to a fast demixing between the solvent and non-solvent. When the thickness of the membrane is increased to 200  $\mu\text{m}$ , demixing occurs slower (Figure 112 b) and finger-like can be observed supported on a larger sponge-like layer. When the thickness reaches 500  $\mu\text{m}$  (Figure 112 c), demixing is slowed down, influencing the morphology greatly. In this membrane, macrovoids and finger-like structures can be seen, supported on a larger sponge-like layer. This type of membrane showed previously inefficient water filtration because the finger-like layers are not interconnected.<sup>63</sup> This could mean that a thin membrane is more efficient for liquid filtration, whilst membranes with the more sponge-like structure are mechanically stronger and efficient for filtration where great pressure is needed (*i.e.*, gas membranes).



## 6.6.5. Porosity of PES membranes

### 6.6.5.1. Mercury Intrusion Porosimetry (MICP) analysis of PES/C and PES/N membranes

As seen in Figure 113a, the Cyrene-based membranes presented higher porosity in comparison to NMP (Figure 113b and Table A 21) in all cases, with a maximum of 79% and 78.8% for PES/CO.1 and PES/C1 respectively. The membrane prepared with Cyrene developed porosity even when not using pore-forming PVP (PES/CO with 76.7% total porosity), which demonstrates superior porosity than an NMP-based membrane using pore-forming additive (PES/NO.1) with 76.3% porosity.

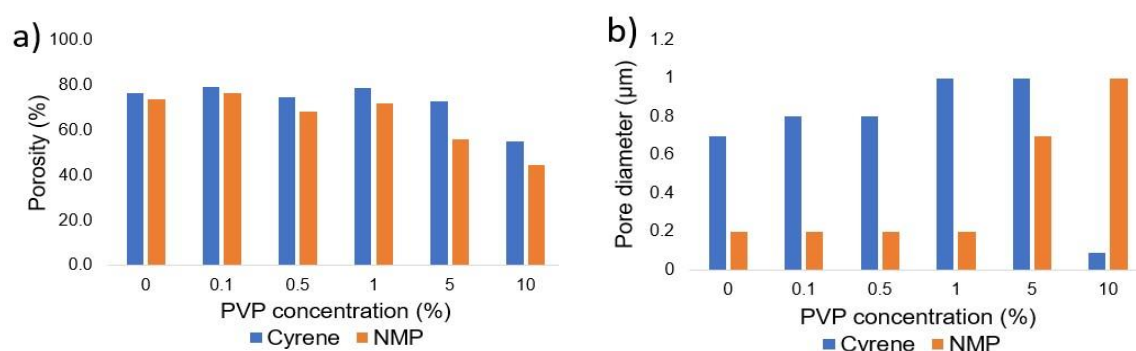


Figure 113: (a) Overall porosity and (b) pore size distribution of PES membranes prepared with Cyrene (in blue) and NMP (in orange).

The membrane with 10% PVP has the lowest total porosity (54.9%), and at this point, the membrane exhibits a different morphology (phenomenon seen in SEM images). On the other hand, the highest porosity (76.3%), for the membranes produced with NMP is obtained with a PVP concentration of 0.1%. The lowest porosity for the membranes produced using NMP occurs for PES/N10 (44.6%). It is also significant that 0.1% PVP is enough to produce good quality PES/C membranes, lowering the amount of sacrificial polymer represents an important starting point for the sustainable membrane fabrication together with substitution of a toxic petroleum-derived solvent with a safe, bio-based alternative. Both Cyrene- and NMP-based membranes present a slightly decreasing porosity when 0.5% PVP is used (PES/CO.5 and PES/NO.5) and decrease when using a higher concentration of PVP (PES/C5 and PES/N5). This decrease in porosity is more visible in the case of NMP-based membranes. However, this means that 1% of additive is sufficient to give the maximum porosity in both types of membranes, with Cyrene-based membranes more superior than the NMP equivalents.

Figure 113b shows the pore diameter of membranes produced with Cyrene and NMP. PES/C membranes developed bigger pores than PES/N, except for PES/C10, which has a different morphology. Pore size of a Cyrene-based membrane with no additive (PES/C0) has a similar pore diameter to that obtained in NMP-based membrane using at 5% PVP (PES/N5). This means that no additive is necessary to form pores when using Cyrene as a solvent. Similarly, a membrane produced using Cyrene and 1% PVP (PES/C1) shows the same pore diameter as an NMP-based membrane when using 10% (PES/N10) of the same pore-forming agent. That means that less sacrificial pore-forming agent is required when using Cyrene as solvent compared to NMP based systems. Membranes prepared with Cyrene have pore diameters from 0.09  $\mu\text{m}$  (PES/C10) to 1  $\mu\text{m}$  (PES/C1 and PES/C5), while the membranes prepared with NMP range between 0.2  $\mu\text{m}$  (PES/N0, 0.1, 0.5, 1 $\mu\text{m}$ ) to 1  $\mu\text{m}$  (PES/N10). Figure 113b shows the similarity between PES/C1 and PES/C5 to PES/N10 in pore size and pore distribution. The membranes made using Cyrene need 1% PVP to develop the biggest pores (PES/C1), while the membranes produced with NMP need twice as much PVP to develop the same pore diameter. A high degree of variation in the pore system is seen when PVP concentration is increased. This is observed by the greater decrease in total porosity and an increase of pore diameters in the range between 0.5 and 1  $\mu\text{m}$  for PES/C0-PES/C5, followed by a dramatic decrease of pore diameter for PES/C10. The Cyrene-based membranes pore diameter follows a trend from a minimum with PES/C0 to a maximum with PES/C5. Above a 5% PVP loading, this type of membranes drops drastically in pore diameter. This is as a result of the morphology of the membrane changing significantly, with large cavities containing very small pores on the walls. This morphology is seen in PES/C10 where a "diffusion membrane" has been formed, at which point it is believed that the pores of 0.09  $\mu\text{m}$  are incorporated in the walls of cavities, replacing the classical macro-voids. The asymmetric membranes have variable pore diameters, from 0.001 to 10  $\mu\text{m}$  while the symmetric one (PES/C10) present more uniform pores, with the majority of pores of 1  $\mu\text{m}$  diameter. PES/C0 presents a small number of pores of 0.1  $\mu\text{m}$ ; the quantity of this type of pores increases with increasing of PVP in casting solution and their presence is exclusively in PES/C10. Membranes made using NMP increase their pore diameters with increasing PVP concentration from PES/N0 to PES/N10. The NMP-based membranes present the same small pore diameter until a concentration of 5% of pore-forming additive is added to the casting gel, leading to a bigger pore diameter with a maximum for PES/N10.

The results from NMR spectroscopy are consistent with the previously reported MICP results (Figure 114):

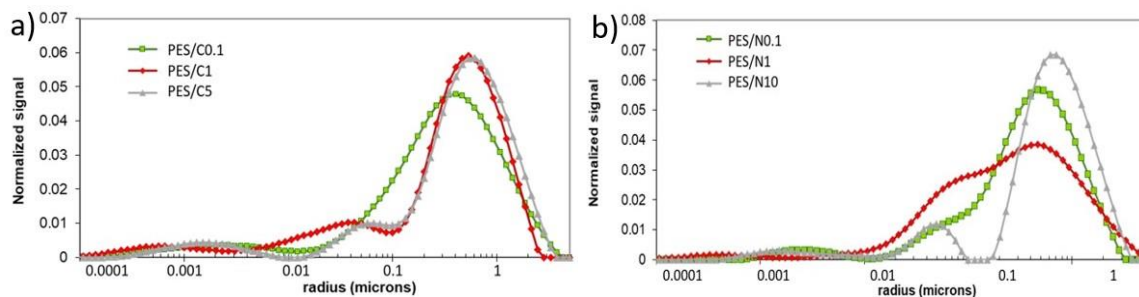


Figure 114: (a) Pore size distribution of PES produced with Cyrene and (b) NMP using relaxation NMR.

The largest pores (around 10  $\mu\text{m}$ ) can be seen in the membranes produced with Cyrene, increasing in line with the concentration of PVP used, with a maximum in PES/C5. For PES/N the number of larger pores increases with increasing PVP concentration, while smaller pores are no longer seen (*i.e.*, pores in the range 0.001 to 0.01 microns are only observed for PES/N0.1).

#### 6.6.5.2. Gravimetric determination of the porosity of PES/C and PES/N membranes

Although less precise than other methodologies applied in this research, gravimetric method is a widely used to calculate the porosity of filtration membranes due to their simplicity and use of water as filling media.<sup>74, 653, 775</sup> This method was used in this work to calculate the total porosity of PES membranes, in addition to the MICP and NMR methods. Figure 115 shows the absorption capacity of PES/C (in blue) and PES/N (in orange) to retain pure water in their pores. Full data is presented in Table A 22 in Appendix A.

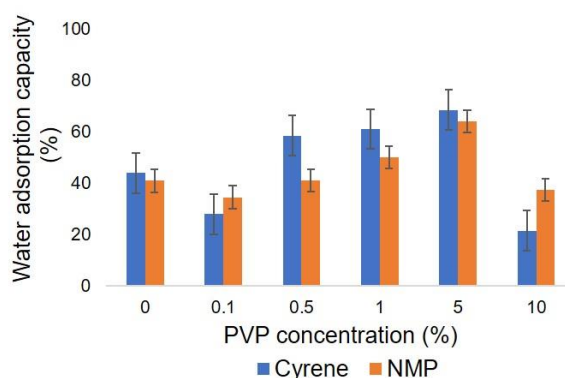


Figure 115: Gravimetric analysis of PES/C (in blue) and PES/N (in orange).

PES/C consistently developed a greater water retention capacity than the respective PES/N membrane (consistent with MICP, relaxation NMR and SEM data). MICP and gravimetric data present differences between the samples generated using the same solvent. For example, gravimetrically PES/C5 presents the biggest capacity of water absorption, while for MICP data, PES/C0.1 has the biggest total porosity. However, PES/C10 showed the smallest capacity to retain water, which is entirely consistent with MICP and SEM data.

### 6.6.6. PES membranes characterisation by infrared spectroscopy

In this work, infrared spectra of PES/C0 and PES/C10 membranes were screened to determine the increasing of hydrophilicity when PVP was added. PES membranes present functional groups specific to PES (Figure 116), S=O symmetric stretch at  $1149\text{ cm}^{-1}$ , C-SO<sub>2</sub>-C asymmetric stretch at  $1320\text{ cm}^{-1}$ , C-O asymmetric stretch at  $1240\text{ cm}^{-1}$ , C<sub>6</sub>H<sub>6</sub> ring stretch at  $1578$  and  $1486\text{ cm}^{-1}$ , C-H stretch at  $3096$ - $3094\text{ cm}^{-1}$ , in addition to the residual PVP as indicated by a C=O stretch at  $1667$ - $1662\text{ cm}^{-1}$ , pyrrolidinyl radical at  $1462$  and  $1423\text{ cm}^{-1}$ , C-N vibration at  $1072\text{ cm}^{-1}$  and C-H asymmetric stretch at  $2950\text{ cm}^{-1}$ .

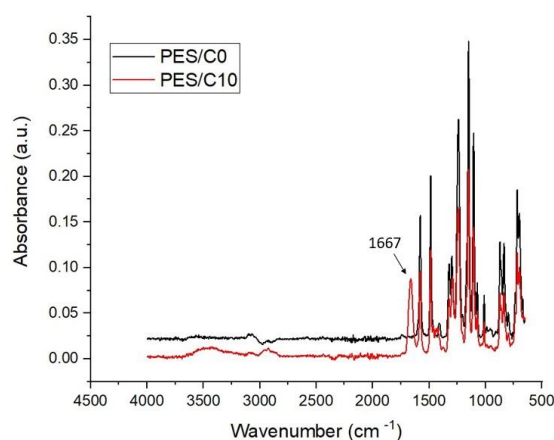


Figure 116: Infrared spectra of PES/C0 and PES/C10.

During membrane precipitation step, some of the PES from the surface leaves the membrane together with most of the water-soluble PVP polymer. However, enough PVP remains, with its presence confirmed by the signal at  $1667\text{ cm}^{-1}$ , allowing greater hydrophilic interactions at the polymer surface than observed with PES alone. In the case of PES/Cyrene, clouding due to release of PES into the gelation media (Figure B 23a) was less apparent than in the PES/NMP system (Figure B 23b).

## 6.6.7. Thermal stability of PES membranes

### 6.6.7.1. Thermal stability of PES/C and PES/N membranes

The results of thermogravimetric analysis (TGA) on the membranes prepared here are shown in Table 34. TGA and DTG curves can be seen in Figure B 26. PVP has a decomposition temperature ( $T_d$ ) around 440 °C, while PES3020 decomposes at 580-600 °C, which means that mass losses arising from PVP would be apparent before PES began to decompose.

Table 34: Thermogravimetric (TGA) analysis measurements of PES membranes produced with Cyrene (PES/C) and NMP (PES/N)

| C/Samples | $T_d$ (°C) | Residue (%) | N/Samples | $T_d$ (°C) | Residue (%) |
|-----------|------------|-------------|-----------|------------|-------------|
| PES3020   | 589.7      | 38          |           |            |             |
| PVP K90   | 443.2      | 5.3         |           |            |             |
| PES/C0    | 588.7      | 30.6        | PES/N0    | 572.9      | 30.4        |
| PES/C0.1  | 577.2      | 32.3        | PES/N0.1  | 564.8      | 24.1        |
| PES/C0.5  | 588.5      | 30.2        | PES/N0.5  | 569.2      | 25.3        |
| PES/C1    | 580.5      | 30.2        | PES/N1    | 576.2      | 30.5        |
| PES/C5    | 568.2      | 41.9        | PES/N5    | 546.7      | 23.5        |
| PES/C10   | 580.7      | 39.8        | PES/N10   | 561.7      | 22.8        |

The first degradation took place below 120 °C due to moisture loss, followed by Cyrene volatilisation at around 170 °C (or 140 °C for NMP), followed by PVP decomposition at *ca.* 420 °C and PES decomposition at *ca.* 580-600 °C. The differential thermogravimetric data shows a greater amount of residual PVP in PES/C membranes than in their NMP counterparts. As seen in Table 34, PES/C membranes consistently show higher thermal stability than PES/N equivalents. PES/C0 has a thermal decomposition of 588.7 °C, while PES/N0 decomposes at 578.4 °C, which means that greater energy is required to break the bonds of PES/C membrane. The addition of PVP to the membranes decreases the thermal stability, due to a lower decomposition temperature of PVP than of PES, but the miscibility of both polymers has been confirmed by thermal analysis. The differences between the concentration of PVP and the TGA residue may be due to PVP being retained within the membranes after washing with water, depending on the membranes' porosity and pore size. It was observed that PES/N membranes lose some PES from the membrane surface when casting the film. PES/N membranes lost more PES and PVP than PES/C, which means that Cyrene makes a better media for type of membranes as well as being more hydrophilic.

### 6.6.7.2. Thermal stability of PES/C, PES/Cg:Cy and PES/Cg membranes

The polyethersulfone (PES) membranes are coded based on the solvent used. For example, a membrane coded as "PES/Cg:Cy" will be referred to as PES membrane produces using 50 wt% Cygnet:Cyrene mixture, while "PES/Cyrene" refers to PES membranes produced using pure Cyrene as solvent. No difference was seen in the TGA data between membranes cast from hot or room temperature solutions; hence only membranes cast from a room temperature casting solution have been shown. Membranes manufactured using pure Cygnet 0.0 were only cast at 100 °C due to the melting point of the solvent. As such, only hot casting solutions-based membranes were used for thermogravimetric analyses for PES/Cygnet. Full thermogravimetric (TGA) and differential thermogravimetric (DTG) analyses can be seen in Figure B 27 and the results summarised in Table 35:

Table 35: Thermogravimetric (TGA) and differential thermogravimetric (DTG) analyses measurements of PES membranes

| Membrane code | T <sub>d</sub> (°C) | Residue (%) |
|---------------|---------------------|-------------|
| PES/Cyrene    | 554.9               | 32.8        |
| PES/Cg:Cy     | 577.1               | 33.8        |
| PES/Cygnet    | 570.1               | 41.1        |

PES membranes show thermal decomposition between 566 °C when using pure Cygnet 0.0 (the lowest temperature) and the highest temperature (577 °C) when Cg:Cy is used. The degradation temperature of Cyrene is of 165°C while Cygnet 0.0 degrades at 210 °C (Figure B 28). No residues can be seen after carbonisation of Cyrene under a flow of nitrogen, while Cygnet 0.0 shows 8.8% residue. A membrane produced with Cygnet 0.0 was expected to have a higher degradation temperature. However, in this study PES/Cg:Cy and PES/Cygnet have higher degradation temperatures than PES/Cyrene due to the presence of Cygnet 0.0, which has a higher degradation temperature than Cyrene. PES/Cygnet has a T<sub>d</sub> lower than PES/Cg:Cy probably due to the Cygnet's leaving the casting solution during the demixing at the top side of the membrane.

## 6.6.8. Surface wetting property of PES membranes

Surface hydrophilicity of membranes is generally characterised by the contact angle measurements between water and membrane surface. As shown in Figure 117a and Table A 23 (Appendix A), the static water contact angle of the new PES films produced with Cyrene decreased from 73.1° for PES/C0 to 37.5° for PES/C10, with a hydrophilic character in all cases. This decreasing of the contact angle indicates increasing in hydrophilicity of these membranes with increasing residual PVP content.

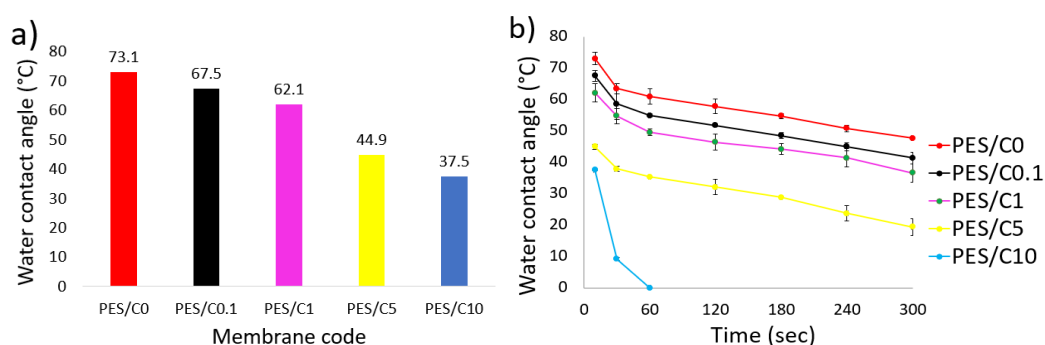


Figure 117: (a) Static water contact angle and (b) the time-dependent values for a sessile drop spreading over a range of PES membranes produced with Cyrene.

The wetting changes were recorded over time employing of the same methodology used for static contact angle, but with values taken over a 300-second range. It can be seen in Figure 117b how the droplets change in a reproducible manner and reduce their contact angle. A larger initial drop in contact angle occurs as water rapidly fills pores at the surface of the membrane, until locally saturated. This phenomenon was found to be due to a result of the advancing angle (higher angle which relies on the hydrophobic surface component) changing into a receding angle (low contact angle of the hydrophilic component) upon a decrease in droplet volume and is due to imbibition and evaporation.<sup>801</sup> The contact angle of PES/C0 recorded the smallest change during the test time, due to a less hydrophilic character and the tendency of the droplet to be repulsed by the membrane surface at least at the beginning. Over time, when the membrane is locally saturated, the droplet moves into the porous membrane and the contact angle changes. On the other side, PES/C10 membrane was found to have the most dramatic change in its contact angle, due to the most hydrophilic character and its porosity. The SEM images of the PES/C10 demonstrated a very porous membrane which would allow the droplet of water to be completely absorbed in under 60 seconds during the experiment.

## 6.6.9. Pure water permeability of PES/C and PES/N

Pure water permeability (PWP) testing was evaluated based on water flux (Table A 24). Evidence in the literature indicates that the sponge layer filters slower than the finger layer of a membrane.<sup>667</sup> Based on these criteria, the permeate flux seen in Figure 118 shows differences between the membranes depending on the solvent used, the concentration of PVP used and the temperature of the casting solution:

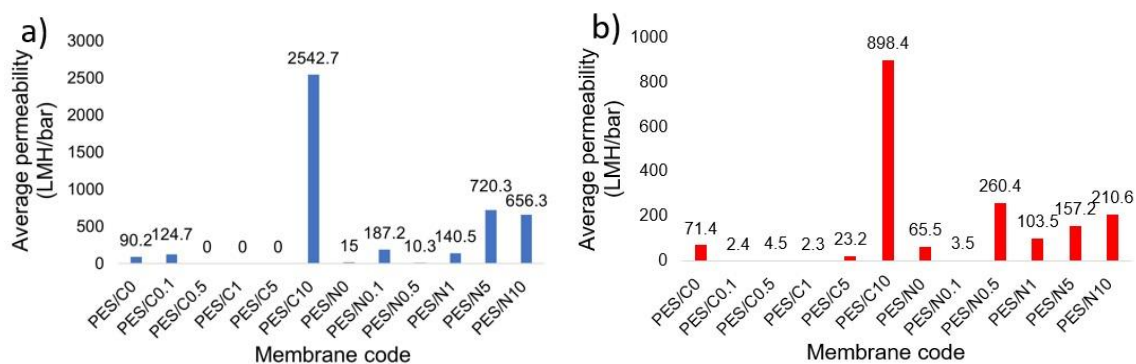


Figure 118: (a) Pure water permeability of membranes cast from cold (room temperature) and (b) hot casting solution.

The membranes produced using Cyrene and cast from a cold casting solution show an increasing permeability when PVP is added with a maximum at 10% PVP, but with no permeability when using 0.5, 1 and 5% PVP. This is explained by the morphology of the membrane, with more finger-layers on top of the membrane a dense sponge layer at the bottom of the membrane. This is due to the thickness of the membrane chosen in this study (500  $\mu\text{m}$ ) which results in different morphologies most likely depending on the speed of exchange between the solvent and water. At the top surface, this is rapid, with the polymer precipitating out and voids forming as a result of water displacement. At the bottom, crystallisation has dominated, with fewer voids. This results in low permeability as the finger regions are not interconnected. The loading of PVP employed had a great impact of permeability. When using over 0.1% PVP, the produced membranes showed no flux, due to the presence of dead ends of the finger layers presented in their morphologies. The new membranes PES/C0 and PES/C0.1 cast from cold solution together with PES/C0 from a hot solution are believed to be suitable for ultrafiltration (UF), while a permeability lower than 20 LMH/bar for a nanofiltration/reverse osmosis (NF/RO), while the PES/C10 membrane showed greater fluxes more in keeping of a microfiltration membrane (MF). Instead, when the same membranes are cast from a hot solution, the produced membranes showed a permeability with a



maximum at 10% PVP, but with a smaller permeate flux than the corresponding cold solution membrane. The membranes produced from a cold casting solution using Cyrene and a PVP concentration above 0.1%, developed a morphology with finger layers in the middle of the membrane but are not interconnected to the surface, thus registering no permeate flux. When adding PVP, the permeability also increased in PES/N, with a maximum flux at 10% PVP and when the membrane was cast from a cold casting solution. When cast from a hot solution, the membrane produced from the same concentration of PVP showed a higher flux of water due to a void in the middle of the membrane which permitted a higher permeability. Looking at Figure 106 2a and Figure 106 2b relating to PES/N0.1, the hot cast seems to have a layer in which all the pores appear blocked about halfway through the membrane (red circle in Figure 106 2b). However, in the cold cast, the pores appear to traverse the membrane (red circle in Figure 106 2a). The presence of the middle sponge layer in PES/N membranes which were hot cast showed a lower permeability than the ones coming from a cold solution, except for PES/N0.5, where the morphology shows a thicker sponge layer, which would generally slow the flux down.

## **6.7. Polyvinylidene difluoride (PVDF) filtration membranes**

### **6.7.1. HSPiP's predictive role in polymer dissolution**

Computational modelling was used in combination with empirical solubility tests to identify which candidates from a green solvent database were most likely to dissolve polyvinylidene difluoride (PVDF). First, twenty-nine randomly chosen solvents were tested for PVDF dissolution by mixing them for three days at room temperature. Only NMP and DMAc were able to dissolve it, and this data has created a very small sphere, with  $\delta_D=17.40$ ,  $\delta_P=12.05$  and  $\delta_H=8.33 \text{ MPa}^{1/2}$ , a radius of 1.7, and a core= $\pm[0.30, 0.75, 0.60]$  and a fit of 1. Hansen sphere obtained for PVDF5130 is presented in Figure 119 and full data can be found in Table A 25.

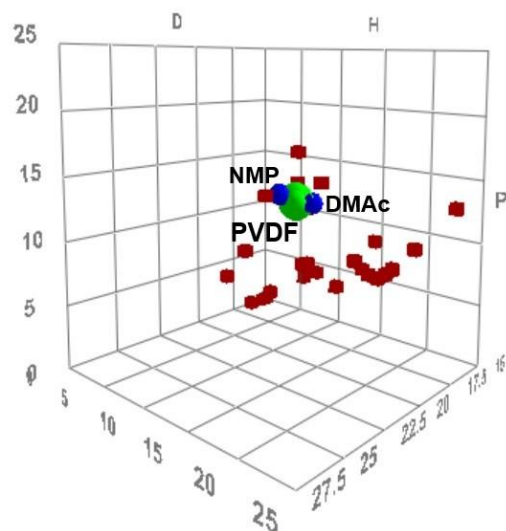


Figure 119: Recommended solvents mapped in Hansen space with solubility sphere for PVDF polymer. Only the good solvents (blue spheres) were named here.

Next, combinations of three solvents in various proportions was used to more precisely determine the boundaries of the sphere at RT.<sup>802</sup> Because the sphere was still small, heating the solvent-polymer mixtures to 60 °C gave a reasonable sphere of 3.8 with single solvents dissolving the polymer. Following these conditions, four bio-based solvent candidates such as DMSO, Cyrene,  $\gamma$ -valerolactone (GVL), and cyclopentanone (CP) were correctly predicted to dissolve PVDF (Table 36):

Table 36: Solvents predicted by HSPiP as good solvents for PVDF dissolution and their Hansen Solubility Parameters

| Solvent                        | $\delta_D$ | $\delta_P$ | $\delta_H$ | Score | RED    |
|--------------------------------|------------|------------|------------|-------|--------|
| Cyrene                         | 18.9       | 12.4       | 7.1        | 5     | 1.898  |
| <i>N</i> -Methyl-2-pyrrolidone | 18         | 12.3       | 7.2        | 1     | 0.995  |
| <i>N,N'</i> -Dimethylacetamide | 16.8       | 11.5       | 9.4        | 1     | 0.986  |
| Dimethyl sulfoxide             | 18.4       | 16.4       | 10.2       | 5     | 3.012  |
| $\gamma$ -Valerolactone        | 16.9       | 11.5       | 6.3        | -     | 1.350* |
| Cyclopentanone                 | 17.9       | 11.9       | 5.2        | 5     | 1.946  |

\*- \* Proposed solvent. Hansen solubility parameters of the solvents are sourced from HSPiP database and expressed in MPa<sup>1/2</sup>.

These solvents were used in this project and compared to the industry standard solvent to produce PVDF membranes: NMP (the NMP-based PVDF membrane was used as benchmark). The solvents screened in HSPiP were sourced from the Chem21 Solvent Selection Guide,<sup>38</sup> Moity's research paper,<sup>803</sup> Jessop's research on solvatochromic parameters for solvents of interest in

green chemistry<sup>804</sup> and the Inkemia catalogue of green solvents.<sup>805</sup> Each of the solvents within the HSP sphere can dissolve 10% w/v PVDF: NMP and DMSO at room temperature over several hours and GVL, Cyrene, and CP with heating to 60-100 °C.

## 6.7.2. Preparation of PVDF membranes

PVDF casting solutions were prepared using the traditional NMP and DMSO, compared to the bio-based Cyrene and other green solvents such as GVL and CP (Figure 120d, e). Figure 120a, b shows how NMP and DMSO solutions form clumps when mixing with PVDF, while the rest of the samples disperse uniform during the stirring and dissolve fast at temperatures of 60-100 °C.

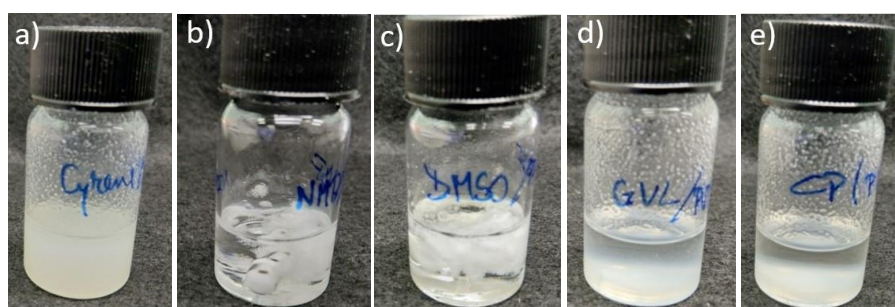


Figure 120: PVDF dissolution in (a) Cyrene, (b) NMP, (c) DMSO, (d) GVL and (e) CP at the beginning of stirring.

Of these four candidates, DMSO was the only one to behave similarly to NMP, dissolving PVDF at RT under stirring, causing clumping of the PVDF powder and reduced dissolution speed. It also remains liquid at room temperature, with no gelation occurring. The other three green solvents (GVL, Cyrene, and CP) readily disperse PVDF at room temperature, with no clumping problem and reducing dissolution time. When cooled to room temperature, these solutions form strong gels, with Cyrene and CP gels happening almost immediately upon cooling (Figure 121a, e). PVDF/GVL gel takes at least 24h to fully set (Figure 121d):

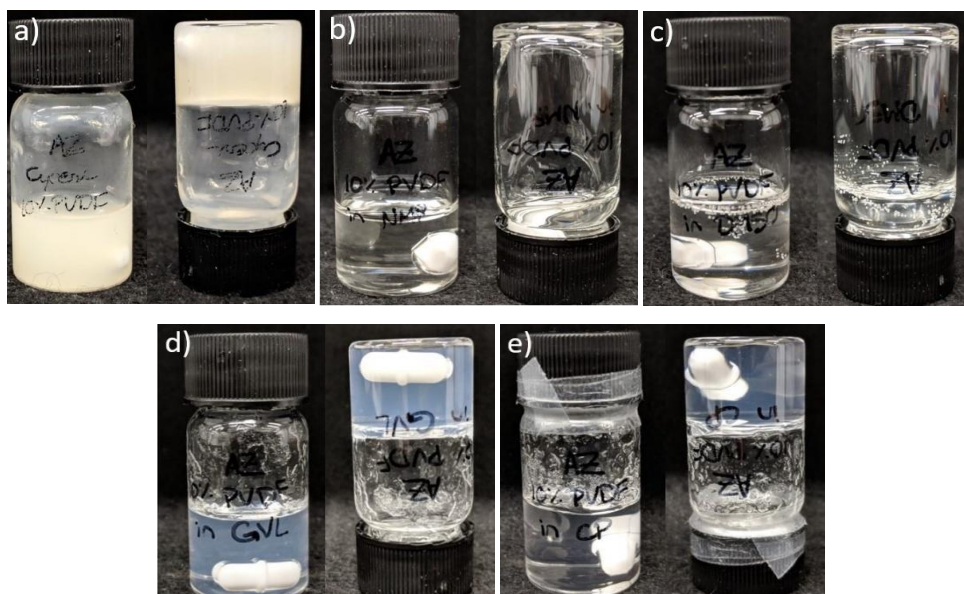


Figure 121: PVDF dissolution in (a) Cyrene, (b) NMP, (c) DMSO, (d) GVL and (e) CP at the end of casting gel producing. NMP and DMSO solutions are viscous liquids, while GVL, Cyrene, and CP form strong gels.

PVDF membranes were prepared with 10% w/v solutions of PVDF in each of the five solvents via NIPS; the composition of the casting solutions can be seen in Table 37:

Table 37: Composition of the casting solutions (%w/v) of PVDF membranes produced with different solvents

| Membrane type | PVDF (%w/v) | Solvent used                   |
|---------------|-------------|--------------------------------|
| PVDF/Cyrene   |             | Cyrene                         |
| PVDF/NMP      |             | <i>N</i> -Methyl-2-pyrrolidone |
| PVDF/DMSO     | 10          | Dimethyl sulfoxide             |
| PVDF/GVL      |             | $\gamma$ -Valerolactone        |
| PVDF/CP       |             | Cyclopentanone                 |

DMSO and NMP solutions precipitated fast when the solution was immersed in the water bath, CP and Cyrene were slow to precipitate while GVL is somewhere in between. NMP, GVL, and DMSO-based membranes are opaque white with wrinkled surfaces. CP and Cyrene formed translucent, almost colourless membranes with smooth, glassy surfaces. NMP, DMSO, and GVL-based membranes were cast from a solution at room temperature, whilst CP and GVL-based solution were cast when hot (100 °C). Films of 500  $\mu$ m were immersed in the coagulation bath containing water at room temperature and left until the precipitation was complete.

### 6.7.3. SEM images of PVDF membranes

The membranes are coded depending on the solvent used. *i.e.*, PVDF/Cyrene represents a PVDF-based membrane manufactured using Cyrene as solvent. The structure of PVDF membrane surfaces has changed depending on the solvent used. A top-surface for PVDF/NMP (Figure 122 2c) and PVDF/DMSO (Figure 122 3c) are dense; a skinless, porous top surface<sup>806, 807</sup> can be observed in case of PVDF/Cyrene (Figure 122 1c), PVDF/CP (Figure 122 5c) and PVDF/GVL (Figure 122 4c):

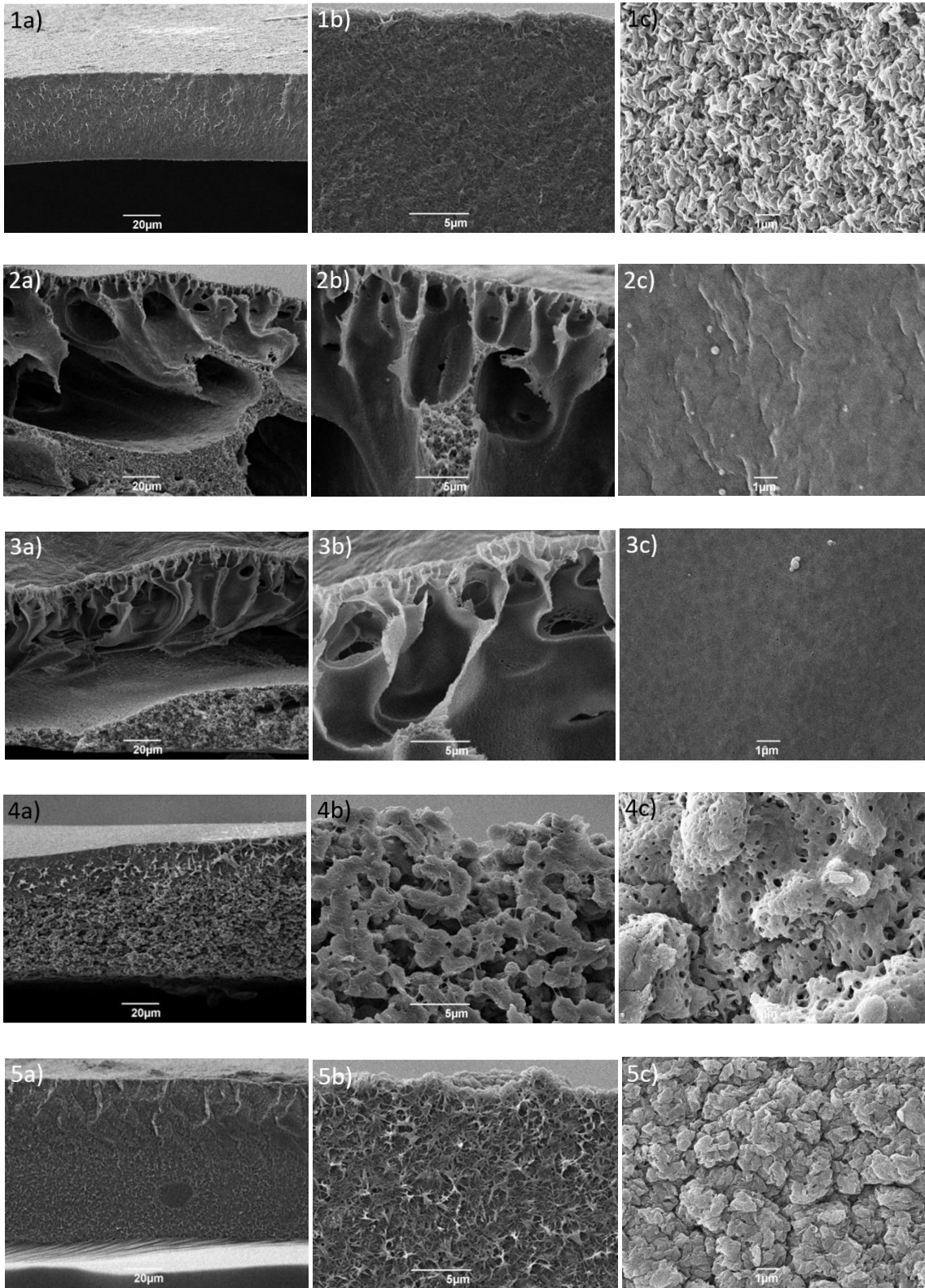


Figure 122: SEM micro-images of cross-section (a), top side detail of the same cross-section (b) and the top surface of membranes produced from Cyrene (1), NMP (2), DMSO (3), GVL (4) and CP (5), All membranes were cast at 500 μm.

The PVDF/NMP and PVDF/DMSO membranes prepared *via* NIPS instantaneously precipitated after casting due to fast liquid-liquid demixing (solvent-nonsolvent) and membranes with a dense top layer and macro-voids supported on sponge-like structure visible in the cross-section images (Figure 122 2c and 3c). A greater difference in morphology starts when changing the solvent. Cyrene, GVL and CP-based membranes are manufactured from gels, making the de-mixing process and a dense (Figure 122 1 and 5) or granular structures (Figure 122 4) are obtained. PVDF/Cyrene and PVDF/CP showcase bi-continuous morphology, composed of small crystallite particles (Figure 122 1 and 5). This type of morphology showed previously a higher water flux than the globular with the top dense top layer (PVDF/GVL-like membrane).<sup>807</sup> Both CP- and Cyrene-based membranes in this work were cast when hot solutions to prevent gelation. The GVL-based membrane (Figure 122 4a-c) developed a granular, spherulitic morphology, under a top dense top-surface similarly described in the literature.<sup>806, 807</sup> In this case, two membrane formation mechanisms can occur in the dope solution simultaneously: solid-liquid demixing (crystallisation) and liquid-liquid demixing.<sup>808, 809</sup> However, in the case of solid-liquid demixing, crystallisation occurs and forms granular membranes with a bi-continuous structure composed of globules joined together.<sup>799</sup> When crystallisation takes place simultaneously with solvent-nonsolvent demixing, membranes with crystalline particles and macrovoids can form (seen at the layer close to the casting plate) in Figure 122 4a.<sup>806</sup>

PVDF is a semi-crystalline polymer and has demonstrated both liquid-liquid and solid-liquid demixing consistent with the literature.<sup>674, 799, 810</sup> For demixing for a semicrystalline polymer such as PVDF, it was found that the equilibrium thermodynamic considerations are not enough to explain the membrane formation.<sup>799</sup> The equilibrium crystallization lines are located at higher solvent concentrations than the binodal boundaries.<sup>799</sup> Moreover, the degree of supersaturation necessary to form nuclei increases with increasing polymer concentration. The system's kinetics is an important factor deciding the type of demixing for this type of polymer and the membrane formation system can be related to the rate of solvent/nonsolvent exchange.<sup>799</sup>

## 6.8. Polysulfone (PSf), cellulose acetate (CA), and polyimide (PI) filtration membranes

### 6.8.1. Preparation of PSf, CA and PI membranes

In this study, cellulose acetate (CA), polyimide (PI) and polysulfone (PSf) filtration membranes were fabricated from hot (100 °C) and cold (RT) casting solutions using two neat solvents and a mixture of them (Cyrene, Cg:Cy and neat Cygnet 0.0). 15% of each polymer was immersed in 85% solvent and heated up to 100 °C for 3-4h. The casting solutions composition (Table 38) were degassed and cast at 200 µm.

Table 38: Casting solutions of CA, PSf and PI membranes produced using Cyrene, pure Cygnet 0.0 and 50% Cyrene-50% Cygnet (wt%)

|            | Polymer (wt%) |                   |           | Solvent (wt%) |                   |            |
|------------|---------------|-------------------|-----------|---------------|-------------------|------------|
|            | Polysulfone   | Cellulose acetate | Polyimide | Cyrene        | Cyrene-Cygnet 0.0 | Cygnet 0.0 |
| PSf/Cyrene | 15            |                   |           | 85            |                   |            |
| PSf/Cg:Cy  | 15            |                   |           |               | 85                |            |
| PSf/Cygnet | 15            |                   |           |               |                   | 85         |
| CA/Cyrene  |               | 15                |           | 85            |                   |            |
| CA/Cg/Cy   |               | 15                |           |               | 85                |            |
| CA/Cygnet  |               | 15                |           |               |                   | 85         |
| PI/Cyrene  |               |                   | 15        | 85            |                   |            |
| PI/Cg:Cy   |               |                   | 15        |               | 85                |            |
| PI/Cygnet  |               |                   | 15        |               |                   | 85         |

Each polymer solution was cast at ambient temperature onto a glass plate using a steel blade, using a thickness of 200 µm. The casting film was submerged in a coagulation bath containing deionised water at RT, causing the polymers to precipitate. Membranes were then washed three times in distilled water for 10 minutes while under sonication in order to wash out the residual solvent and then stored in deionised water until further use. The process of casting a gel when hot was previously reported.<sup>63</sup> To characterise the prepared membranes, they were washed with deionised water and dried in a vacuum oven at 80 °C for 12 hours. The hot casting was possible due to keeping a quartz glass in an oven at 100 °C for 20 minutes. A maximum of 3 minutes and a

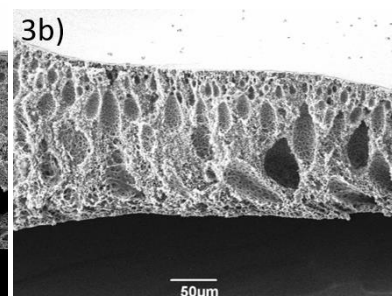
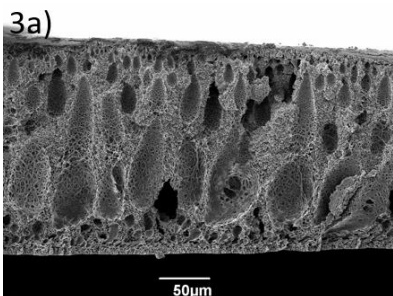
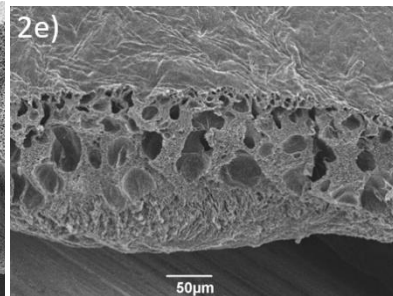
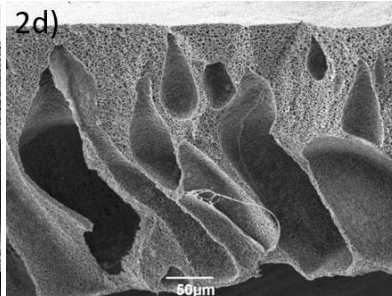
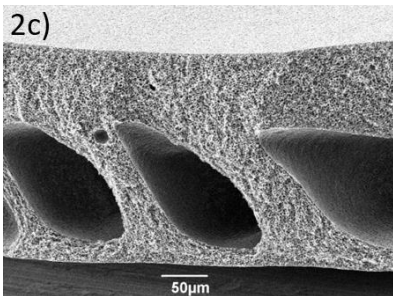
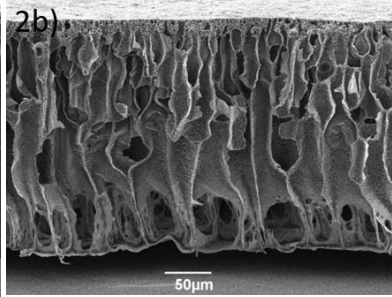
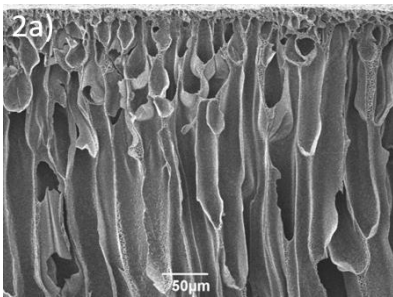
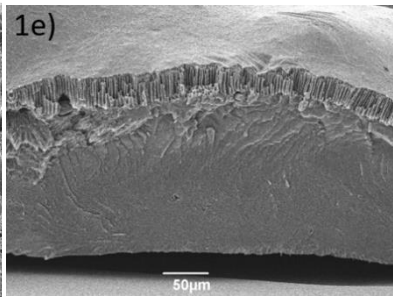
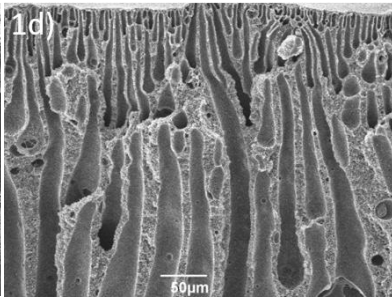
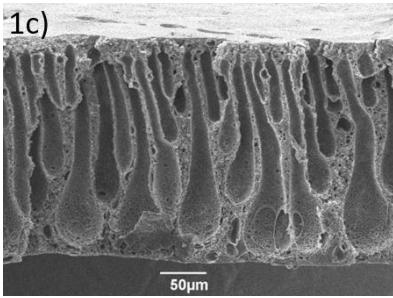
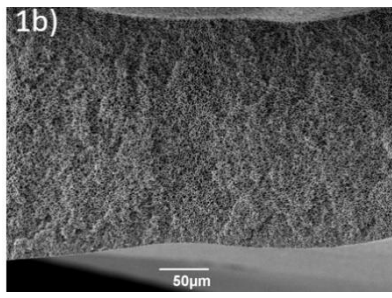
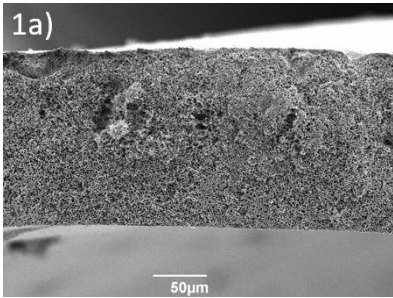


loss of few degrees were taken into account from the moment the quartz plate is taken from the oven to the moment the casting gel is placed onto it and the film cast in the water.

## 6.8.2. SEM analyses of the produced membranes

In this study, three solvents (pure Cyrene, pure Cygnet 0.0 and 50 wt% Cygnet-Cyrene (noted as "Cg:Cy") and three different polymers were used to prepare filtration membranes. Cellulose acetate, polysulfone and polyimide have not been fabricated using Cyrene until this point. Also, Cygnet in Cyrene blend and Cygnet 0.0 was never used before in membrane technology. The SEM images of the produced membranes show differences in the morphology of the membranes when using three different solvents or blend of solvents. The scanning electron microscopy (SEM) images of the produced membranes show differences in the membranes' morphology when solvent and polymer change (Figure 123). The membranes prepared using pure Cyrene and Cg:Cy via NIPS process, precipitated after casting due to the immersion in the bath containing water as nonsolvent. Rapid solvent/non-solvent exchange results in the formation of macro-voids and finger-like, while a slow resulted in a sponge-like or dense structures.<sup>660, 663</sup>

**Polysulfone (PSf)** membranes produced with Cyrene (Figure 123 1a, b) developed a full sponge layer morphology. The temperature of the casting solution does not make a big difference in morphology in this case. During the de-mixing between the solvent (Cyrene) and non-solvent (water) a mixture of pure water, pure Cyrene and a geminal diol can coexist<sup>52</sup> and are involved in the formation of the porous structures. As reported in previous studies sponge morphology is associated with greater mechanical strength compared to macrovoidic morphology and is useful for gas filtration.<sup>667</sup> When the mixture Cg:Cy is used, the cross-sectional morphology obtained is significantly different (Figure 123 1c, d) showing a typical Loeb-Sourirajan structure with a thin top layer supported on finger-like layer present through all the membrane thickness and small sponge-like layer, very similar to PES/Cyrene membranes, reported previously.<sup>63</sup>



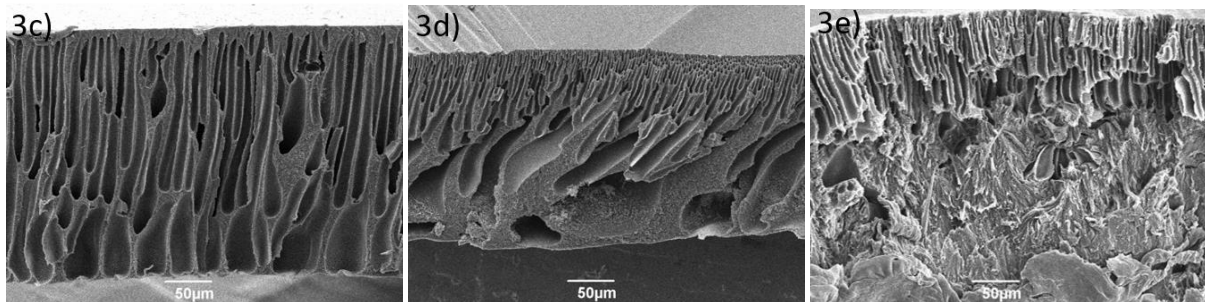


Figure 123: Scanning electron microscopy images of membranes produced from (1) polysulfone, (2) cellulose acetate and (3) polyimide using Cyrene (a,b), Cg:Cy (c,d) and pure Cygnnet 0.0 (e) as solvents. The membranes were cast from solutions at room temperature (a, c) and from a hot solution at 100 °C (b, d, e). All membranes have a thickness of 200 μm.

**Cellulose acetate (CA)** membranes produced using Cyrene as solvent and cast from a gel at RT or from a hot gel (Figure 123 2a, b) display finger-like layer all the way through the membrane due to the instantaneous solvent-nonsolvent demixing during the phase inversion. A Cg:Cy-based membrane exhibits a completely different morphology when cast from a solution at room temperature (Figure 123 2c); mostly a sponge-like structure with large macro-voids, probably due to the air bubbles which did not collapse during the degassing.<sup>667</sup> This sponge-like layer could resolve the issue of this type of membrane, offering more mechanical strength, often related to high-pressure filtration applications. In case of CA membrane cast from a hot solution (Figure 123 2d), the viscosity of the solution is lowered with the temperature, hence the demixing happens faster and more macrovoids can be seen through the thickness of the membrane while the less sponge-like structure was observed.

**Polyimide (PI)** membranes are generally generated from a thermal imidisation between a diamine and a dianhydride at high temperature (>250 °C)<sup>811</sup> or a combination between NIPS and imidisation leading to sponge-type polyimide membranes.<sup>748</sup> In this study, a straightforward approach was taken; the PI membranes were produced by simply dissolving the thermoplastic polyimide polymer in a solvent, followed by NIPS casting in water (Figure 123 3a-e). When casting polyimide membranes in Cyrene, the dissolved polymer solution is a less viscous solution with two top active porous layers on top and close to the glass plate (bottom layer). The active porous layer from the bottom layer could result from the fast demixing between the solvent and the non-solvent which has entered the space between the casting gel and the casting plate, detaching the membrane. Between the two top active porous layers, big finger layers can be seen due to the instantaneous de-mixing. For a Cg:Cy-based membrane, the morphology changes. When cast from a gel at room temperature, the de-mixing is instantaneous, forming non-interconnected finger-like layers all the way through the membrane. It was shown before that these non-interconnected layers could lead to a slow or non-permeable membrane.<sup>63</sup> When the same membrane is cast from

a hot solution, more sponge-like structure can be seen at the bottom of the membrane, which indicated a slower demixing at the bottom layer (close to the glass plate).

The casting of membranes in pure Cygnet 0.0 was only possible from a solution at 100 °C, due to the solid state of the solvent at room temperature. When using pure Cygnet 0.0 (Figure 123 1-3e) in the casting gel of all polymers, a top active porous layer is formed due to the demixing between the solvent and the anti-solvent.<sup>755</sup> The porous layer is a mixture of macrovoid and sponge-like structures in case of CA (Figure 123 2e) or finger-like structure for PSf (Figure 123 1e) and PI (Figure 123 3e). The porous layers are supported by a dense layer, bigger in case of PSf and PI, which is seen due to the cooling down of the solution and crystallisation of the solvent Cygnet 0.0; no demixing was possible in this layer. The combination of a porous, permeable layer with a non-permeable layer could be useful for coatings with waterproof, windproof and heat resistance properties.<sup>812</sup>

### 6.8.3. Thermal stability of the produced membranes

Thermogravimetric analyses were performed to determine the thermal decomposition.

The membranes are coded based on the polymer and the solvent used. For example, a membrane coded as "PSf/Cg:Cy" will be referred to as polysulfone membrane produced using Cg:Cy mixtures, while "CA/Cyrene" is referred to as a cellulose acetate membrane produced using pure Cyrene as a solvent. No difference was seen between membranes cast from hot and room temperature casting gels; hence only membranes cast from a gel at room temperature were tested. However, since the membranes manufactured using pure Cygnet 0.0 were only cast at 100 °C for this solvent, hot solutions were used for thermogravimetric analyses. Full thermogravimetric (TGA) and differential thermogravimetric (DTG) analyses can be seen in Figure B 30 and the results summarised in Table 39:

Table 39: TGA and DTG measurements of PSf, CA and PI membranes

| Membrane code | T <sub>d</sub> (°C) | Residue (%) |
|---------------|---------------------|-------------|
| PSf/Cyrene    | 518.6               | 36.2        |
| PSf/Cg:Cy     | 526.1               | 31.5        |
| PSf/Cygnet    | 528.0               | 34.4        |
| CA/Cyrene     | 365.1               | 23.9        |
| CA/Cg:Cy      | 355.6               | 19.1        |
| CA/Cygnet     | 371.9               | 10.1        |
| PI/Cyrene     | >600                | 66.7        |
| PI/Cg:Cy      | >600                | 67.1        |
| PI/Cygnet     | 518.2               | 59.4        |

As seen in Table 39, the most thermally stable membranes are produced from polyimide, with high degradation temperature (518-600 °C), while cellulose acetate-based membranes have the lowest degradation temperatures (355-372 °C). The degradation temperature of Cyrene is of 165°C while Cygnet 0.0 degrades at 210 °C (Figure B 28). No residues can be seen after carbonisation of Cyrene under a flow of nitrogen, while Cygnet 0.0 shows 8.8% residue. Cg:Cy mixture produced PES and PSf membranes with high degradation temperatures of 577.1 and 526.1 °C respectively, higher than Cyrene-based membranes, due to a higher degradation temperature of Cygnet from the mixture. In case of CA, Cygnet 0.0 produced highest thermally stable membranes, with a degradation temperature of 371.9 °C. PI-based membranes have high degradation temperature, at around 600 °C, but higher than PI-based membrane produced using pure Cygnet 0.0 (518.2 °C). CA-based membranes produced the smallest residual material, while PI-based the highest yield (over 59%). This means that PI membranes are most thermally stable, while CA-based filtration membranes have the lowest thermal stability.

## 6.9. Chapter conclusion

At present, 2.2 billion people do not have access to drinking water, and 3 billion people worldwide lack basic handwashing facilities at home, which is necessary to stop coronavirus (COVID-19) from spreading. Goal 6 of the United Nations proposes to “ensure availability and sustainable management of water and sanitation for all”. Hence, membranes science attracted huge interest from scientists. Filtration membranes represent a sustainable approach to replace traditional separation processes, assuring high separation efficiency while they are easy to use and need low energy consumption. To produce green and sustainable filtration membranes, the materials and the solvents used in the process should be safer, with a lower environmental impact. Changing the solvent, which makes up the casting solution’s biggest part, is a big step to a sustainable membrane.

In this work, Cyrene was used as an alternative solvent to traditional, yet toxic polar aprotic solvents commonly used in membrane science, such as NMP, DMF and DMAc. Polyethersulfone, polyvinylidene fluoride, polysulfone, cellulose acetate and polyimide membranes were produced in this work using Cyrene, its ketal derivative Cygnet 0.0 or a mixture of the two. They were compared to the traditionally produced version using NMP. Polyethersulfone membrane morphology and performance were tailored, acting on the casting solution composition and temperature. The new membranes produced with Cyrene are more sustainable, with less of both polymers’ loss and tunable pore size and contact angles, from a less hydrophilic PES/C0 to a more hydrophilic PES/C10 membranes. The membranes prepared with the bio-based solvent Cyrene showed greater porosity, bigger pore-size and higher thermal stability, than the PES membranes produced with NMP. It was found in this work that no additive is necessary to form pores when Cyrene is applied as a solvent, PES/C0 having the same pore diameter as NMP-based membranes produced with 5% PVP (PES/N5), meaning that no additive may not be necessary for the role of pore-forming when using Cyrene. The permeability of the new membranes produced with Cyrene was easily tailored in the range between NF/RO to MF, by changing the temperature of the casting solution. In contrast, only slightly small changes were observed when using NMP. Polymer solution viscosity is a key parameter in membrane formation, affecting the morphology and transport properties. In general, they showed that higher viscosity solutions prevent macrovoid formation and vice versa. The morphology of the membranes cast from a higher viscosity casting solution showed a more dramatic change as a function of temperature. The morphology was different for the two casting solutions when using Cyrene, with a symmetrical one observed when hot cast. This is less obvious when casting from a cold solution. Heating allowed the solvent-polymer interactions to dominate over the polymer-polymer interactions. However, this trend is less

observed for NMP-based membranes, probably because NMP evaporated quicker than Cyrene at elevated temperatures. New additives such as carbon nanotubes and polysaccharide-derived mesoporous materials were used in this project to improve the hydrophilicity, mechanical strength, porosity and conductive properties.

The type of solvent used for coagulation is another important factor to control membrane morphology. New PES membranes were produced in this work using a new bio-based solvent, MBSA. Water, TMO and hexane were used as non-solvents. MBSA is partially soluble in water, which is in excess in the NIPS process, allowing an effective solvent-nonsolvent demixing in this system. The membranes produced with MBSA were successfully cast in water and TMO. Demixing PES/MBSA in hexane as non-solvent led to the formation of a membrane with a large dense layer due to crystallisation.

Four bio-based solvents were used to produce polyvinylidene fluoride separation membranes and were compared to a "reference", manufactured from NMP. Various membrane morphologies can be obtained by changing the solvent from casting solution resulting in a different induced factor in the phase separation process. A typical liquid-liquid demixing between the solvent and non-solvent is seen in PVDF/NMP and PVDF/DMSO leading to membranes with a dense top-layer and macrovoidic layer supported by sponge-like morphology. Cyrene and CP-based membranes presented a bi-continuous morphology composed of crystallite particles, very efficient for water filtration. GVL-based PVDF membrane showcases a globular morphology supported by a dense layer.

This study explored a binary solvent system of bio-based Cyrene and one of its derivatives, Cygnet 0.0, with potentially novel solvent properties in membranes technology applications. The addition of 50% of the Cygnet to Cyrene made a practical difference in solvent behaviour with polymers, water filtration membranes were cast with polyimide, polysulfone, polyethersulfone and cellulose acetate using the NIPS casting process. Cygnet 0.0 and 50 wt% Cygnet-Cyrene mixture were used for the first time in membranes preparation. The membranes were produced without the aid of additives. The morphology of the new membranes was dependent on the polymer and casting solution temperature, resulting in different morphologies. Interestingly, pure solid Cygnet 0.0 generated soft membranes with a) a permeable layer supported on b) a dense layer from a single casting solution layer, generally obtained in thin-film composites.

This work has demonstrated the applicability of Cyrene in membranes science and identified many important aspects of membranes uses in strategic industrial sectors, where sustainability is crucial.





# Chapter VII

## 7. Conclusion and further work



## 7.1. Conclusion

The objectives of this thesis were to use the bio-based solvent Cyrene as a replacement to the toxic polar aprotic solvents such as NMP, DMF and DMAc in polymer dissolution for graffiti removal, poly (amido-imide) wire enamels, filtration membranes, extractions of polyphenols and carbon nanotubes dispersions. Overall, the work presented in this thesis demonstrates that there is extensive scope for the use of Cyrene in the chemical industry by means of proof of principle demonstrated by results and safety screening. A detailed summary of conclusions is discussed at the end of each chapter.

In this study, the cleaning efficiency of Cyrene was studied and compared to over thirty solvents as a neat solvent or used in poultices. Cyrene has been shown to be advantageous for paint removal applications, removing layers of paint from surfaces and minimising stains and residues. New sustainable Cyrene-water based formulations could be viable future paint stripping solutions. The low human and environmental toxicity of Cyrene makes it a more sustainable alternative to the existent conventional paint removal products, including for outdoor use of graffiti.

In poly(amide imide) enamels, Cyrene was employed prior to this work, and the results showed superior characteristics than when synthesised using NMP. Moreover, in this study, the use of HSPiP facilitated the formation of new solvent systems based on Cyrene and carbonates or DMSO. Ethylene carbonate-Cyrene mixture demonstrated superior chemical properties, high flexibility, adhesion and hardness strength to the traditional NMP-based PAIs. Even though the preliminary investigation carried some limitations involving the uniformity and thickness of the film coatings, these results were comparable with PAI synthesised when Cyrene was used as a solvent.

Cyrene created new solvent systems with distinct properties in mixtures with water, expanding the potential of Cyrene as a green solvent. The solvent systems containing Cyrene-water-geminal diol have shown increased solubility and extraction of natural flavonoids from orange skin and tea leaves, up to ten times higher than neat Cyrene. Hesperidin and rutin were extracted using a new and simple process involving a minimum amount of solvent. The new solvent system becomes cheaper due to water dilution and could be preferred in future extractions. Heating up Cyrene has improved the capacity of the solvent for extracting hesperidin and rutin; the diffusion into the sample matrices was improved by lowering the solvent viscosity. Although improving the process's energy efficiency is important, the new solid-liquid extraction method using Cyrene demonstrated simplicity and good use of time and resources.

Cyrene was also used as a dispersion media for carbon nanotubes dispersions by ultrasonication, followed by centrifugation and decanting the supernatant. Cyrene showed variations in the number of nanotubes dispersed by sonication, being strongly influenced by the sample vial position in the ultrasonic bath. Overall results showed a higher dispersion ability of Cyrene and longer stability, up to six months. This was explained by Cyrene's viscosity, higher than traditional solvents, which decreased the sedimentation velocity. Triton showed selectivity for Cyrene solutions, whilst PVP has dispersed nanotubes in NMP more efficiently than in neat solvent.

In membrane technology, Cyrene was used as an alternative solvent to NMP, DMF and DMAc for membrane preparation. Polyethersulfone, polyvinylidene fluoride, polysulfone, cellulose acetate and polyimide membranes were produced in this work using Cyrene, its ketal derivative, Cygnet 0.0, or a mixture of the two. Cyrene-derived membranes demonstrated superior properties to those obtained using NMP: more porous membranes were obtained; no additive was needed to form pores when Cyrene is employed, and no leaching of the additive PVP was observed during the phase inversion. Cyrene enabled easy tailoring of the membrane's properties with the change of its viscosity. For the first time discussed in this work, increasing the temperature of Cyrene has showed that different viscosities of the solvent make a difference in the membrane's morphology and filtration efficiency. Importantly in this application, any accidental spills of Cyrene in the environment would not lead to long-term hazards because it was found to be biodegradable and non-toxic to aquatic life. Also, new solvents and additives were used in membrane technology for sustainable membranes. Polysaccharide-derived Starbon materials were employed as hydrophilic agents in PES/Cyrene-based membranes. They could represent a step forward in creating more sustainable membranes due to the bio-based solvent and bio-derived additive in the casting solution.

## 7.2. Further work

The work presented in this thesis has demonstrated the investigation of the application of Cyrene in various sectors. However, some further work is still needed:

Cyrene has proven to be a promising solvent as a paint stripper; it showed good cleaning results, is not toxic to the user and does not contaminate the substrate as much as other organic solvents. However, its high viscosity and high surface tension made the cleaning process longer than other cleaning agents. This could be resolved by lowering its surface tension by adding surfactants or by

simply mixing Cyrene with water or other green solvents. Moreover, Cyrene could be tested in cleaning other substrates and other types of paint.

Cyrene is a very promising solvent for wire enamels. Other coatings are also worth trying with Cyrene as the solvent in their syntheses.

Research in the extraction of bioactive compounds is a large area, and other polyphenols could be extracted using Cyrene and Cyrene-based solvent systems, especially Cyrene-water blends.

Regarding carbon nanotubes, measurements of pulses generated in different areas of the ultrasonic bath should be studied to measure the dispersion ability of Cyrene more accurately. Also, the order of destruction of the nanotubes' walls needs to be considered as future work.

It was well demonstrated in this work that Cyrene-based membranes can be easily tailored for various types of filtrations. Membranes produced during this work are currently being tested to determine the type of filtration they are best suitable for. However, membrane science is a huge area where safe solvents need to be used and more research could be done in this area. Cyrene could be tested as a solvent for gas membranes, food processing and other applications. Also, more research could be done around non-toxic polymers, especially polyesters.



# Chapter VIII

## 8. Experimental section





## 8.1. Chemicals

The main solvent, Cyrene, used in this study was kindly provided by Circa Group. Deionised water was provided in-house by the lab using an ELGA CENTRA® system.

### 8.1.1. Chemicals - Chapter 2

- Tiles of 5 x 10 cm<sup>3</sup> and of 2 mm thickness of aluminium foil were used from Amazon. The 5 x 5 x 1 cm<sup>3</sup> white gloss ceramic wall tiles were purchased from a local B&Q store. Both non-porous and porous substrates were painted and left to dry for a week.
- Fast-drying Kobra HP250 400ml Aerosol Spray Paint - Red Orange, 100% acrylic formulation (from Kobrapaint.co.uk) with a high "solid" content (to ensure great coverage on any surface) was used as received for removal tests. The solvents used in this formulation are acetone, n-butyl acetate, 1-methoxy-2-propanol.
- Clostermann Aerosol Honda Repsol Racing Red High Gloss spray paint can from Advanced Paints.co.uk and contains butanol and acetone.
- Two acrylic binders (Viacryl SC 134/50WS165 and Viacryl SC 166/45BAC) were kindly donated by Allnex, Germany.
- Non-porous aluminium foil and porous ceramic tiles were sprayed (Figure 36 c) with commercially available red graffiti paint and left to dry for a week.
- Solvents were purchased from Merck or Alfa Aesar, with a typical purity of ≥99%.

### 8.1.2. Chemicals - Chapter 3

- Torlon AI10 was provided by Solvay, containing 90-99.9% PAI, 0.1-0.2% 4,4'-methylenedianiline and 3-6% NMP.
- Trimellitic acid anhydride (TMA) with 97% purity and 4,4'-methylenediphenyl diisocyanate (4,4'-MDI) having 98% purity were purchased from Merck.
- Solvents were purchased from Merck or Alfa Aesar, with a typical purity of ≥99%.

### 8.1.3. Chemicals - Chapter 4

- Pure standards of hesperidin and rutin were purchased from Merck.
- Oranges were obtained from a local producer in São Paulo, Brasil. The fruits were unpeeled with a sharp knife, dried, milled and stored in a jar protected from the light and humidity.
- Black tea was purchased from a local supermarket, milled and stored until extraction.
- Solvents were provided by UFSCar, Brasil.

### 8.1.4. Chemicals – Chapter 5

- Single-walled carbon nanotubes (SWCNTs) Tuball with <2nm diameter and >5um length were kindly offered by OCSiAl, of is  $\geq 80\%$  and impurities  $\leq 15\%$ . They were used as received, without further purification.
- PVP Luvitek K-90 Pulver was obtained from INGE.BASF, Germany
- Triton™ X-100 was purchased from Merck.
- Solvents were purchased from Merck or Alfa Aesar, with a typical purity of  $\geq 99\%$ .

### 8.1.5. Chemicals - Chapter 6

- Ultrason E3020 P Polyarylethersulfone and PVP Luvitek K-90 Pulver were obtained from INGE.BASF, Germany. Both polymers were solvent exchanged in ethanol and ethyl acetate respectively and dried in vacuum oven overnight.
- PVDF 5130 was obtained from project partners at Warwick, dried under vacuum overnight, and stored in desiccator.
- Cellulose acetate, polysulfone and polyimide polymers were purchased from Merck
- Solvents were purchased from Merck or Alfa Aesar, with a typical purity of  $\geq 99\%$ .

## 8.2. Experimental – Chapter 1

### *Thermogravimetric analysis*

Thermogravimetric analysis was performed on a PL Thermal Sciences STA 625. Samples of 9 mg of Cyrene were weighed into an aluminium TGA pan and heated under the nitrogen flow to avoid the oxidation of the samples. A temperature ramp of 10 °C/min was used to heat the samples from room temperature to 625 °C.

### *Viscosity*

The dynamic viscosity of Cyrene was analysed using a Malvern Kinexus pro+ rotational rheometer with a 40 mm diameter 4° angle cone over a 61mm plate (CP4/40 SR2013 SS: PL61 ST S1540 SS). One millilitre solvent as used for each test and in triplicate. A single frequency strain-controlled temperature ramp was performed from 10 to 50 °C, at a ramp rate of 1 °C.

## 8.3. Experimental – Chapter 2

### *Graffiti painting*

Non-porous aluminium foils were one-coat painted (one side only) in a fume-hood with the commercially available red graffiti aerosols described above and left to dry for a week (Figure 124). The porous ceramic tiles were coated on the glazed side up and left to air-dry under laboratory conditions for one week. The tiles were then rotated to the glazed side down and the porous surface coated and left to dry for one week.

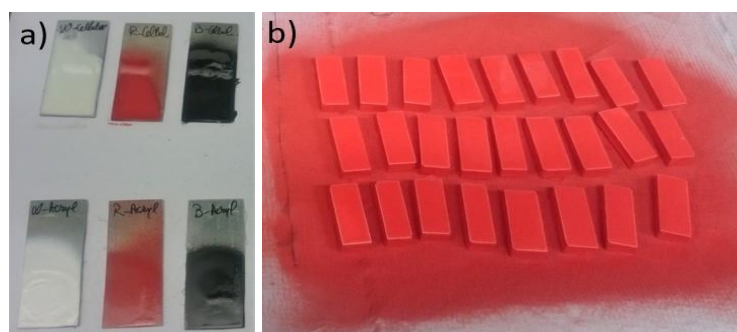


Figure 124: (a) Painted aluminium slides and (b) ceramic tiles using different colours from both acrylic and cellulose-based graffiti aerosols.

### ***Infrared Spectroscopy***

The functional groups present in samples were investigated using PerkinElmer Spectrum 400 ATR-FTIR Spectrometer with transmittance peaks in 4000-450  $\text{cm}^{-1}$  region, with rapid scanning (4 scans) and resolution 4  $\text{cm}^{-1}$  at room temperature. The obtained data was analysed using the OriginPro 2019 software.

### ***Graffiti removal from aluminium slides using immersion tests***

In this study, a direct interaction between pure solvents and polymer films has been used to assess the dissolution of polymeric coatings in different individual solvents. The one-side painted aluminium slides were dried for a week (Figure 125a). They In a simple test, the coated aluminium slides were partly immersed in beakers containing 20 ml of the selected pure solvents (Figure 125b):

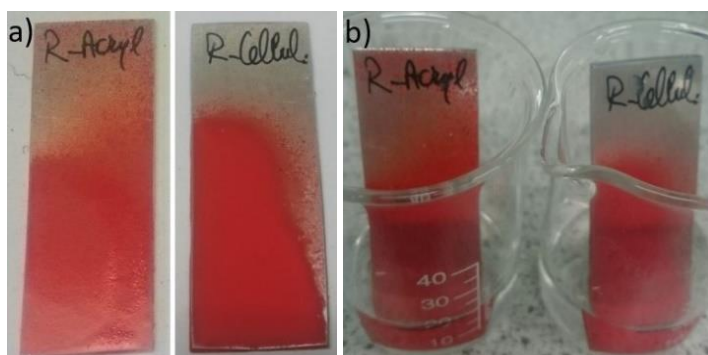


Figure 125: Red graffiti paint removal from non-porous aluminium slides. (a) The slides were painted using graffiti aerosol and left to dry and (b) immersed in beakers containing different solvents

### ***Graffiti removal from porous ceramic tiles using immersion tests***

The dried, painted porous ceramic tiles were then immersed in vials with 20 mL solvent and rolled (using Stuart analogue tube rollers) for three days to ensure uniform contact with the solvents. (Figure 126). After three days, the tiles were removed from the solvent and a gentle mechanical action was performed using roll paper to remove any residues; no rinsing was performed afterwards.

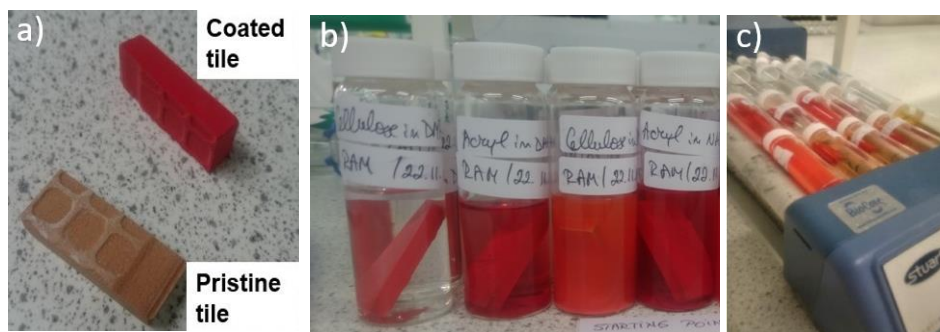


Figure 126: (a) Pristine and painted tiles, (b) dip-in test of graffiti paint removal from the stained ceramic tiles using (c) Stuart rollers.

### ***Graffiti removal using poultices***

This test shows the best reality of cleaning materials, using a paste formed out talc and solvent, followed by scraping this off after one day (Figure 127). Small spots of polymeric coatings were applied to the substrate and left to dry (Figure 127a). Poultices were obtained from 2 g of talc and 5 mL of individual solvents. The obtained poultices were applied on the painted spots and covered with a plastic film to prevent the solvent from evaporating (Figure 127b). The next day, the plastic foil was removed from treated spots (Figure 127c) and the residues were removed from the surface using roll paper.



Figure 127: Poultice test: (a) the stained surface was covered by (b) poultices made of solvent and talc and covered using plastic foil. After 24 hours, (c) the plastic foil was removed, and results were assessed.

### ***Hansen Solubility Parameters and laboratory cleaning tests***

For this test, the results of “Graffiti removal using immersion tests” were used to assess the graffiti paint removal. Solubility was assessed based on visual inspection and ranking scores were given from 1 to 5, “1” meaning fully dissolved, “4” only the glazed side was cleaned and “5” where the solvent did not clean the painted ceramic tiles in any way. The obtained solubility scores are inserted into the HSPiP software to generate an empirical Hansen Solubility Parameters sphere for each commercial graffiti paint, and their RED,  $\delta_D$ ,  $\delta_P$  and  $\delta_H$  are calculated. This is based on a

spherical model (Hansen solubility sphere) where the good solvents are inside and the bad ones out of the sphere. The relative energy distance (RED) values determine the ability of a solvent to dissolve a solute. A RED < 1 suggests a high solvent–solute affinity, a RED > 1 suggests a low affinity, and a RED = 1 suggests the boundary condition.

### ***Inductively Coupled Plasma-Mass Spectrometry (ICP-MS) analysis***

The ICP-MS analyses were realised by John Angus from the Biorenewables Development Centre (BDC). ICP-MS was performed to identify the chemical elements present in the acrylic graffiti paint and ceramic tiles using an Agilent 7700x ICP-MS.

### ***Optical microscopy***

A Leica S6D Microscope with 6.3x-40x magnification and flat image field was employed to visualise the showing effect after the acrylic paint removal using Cyrene and NMP. The working distance is 110 mm, from microscope to specimen, providing space for manipulation. A typical image of the object and the parameters used can be seen in Figure 128:

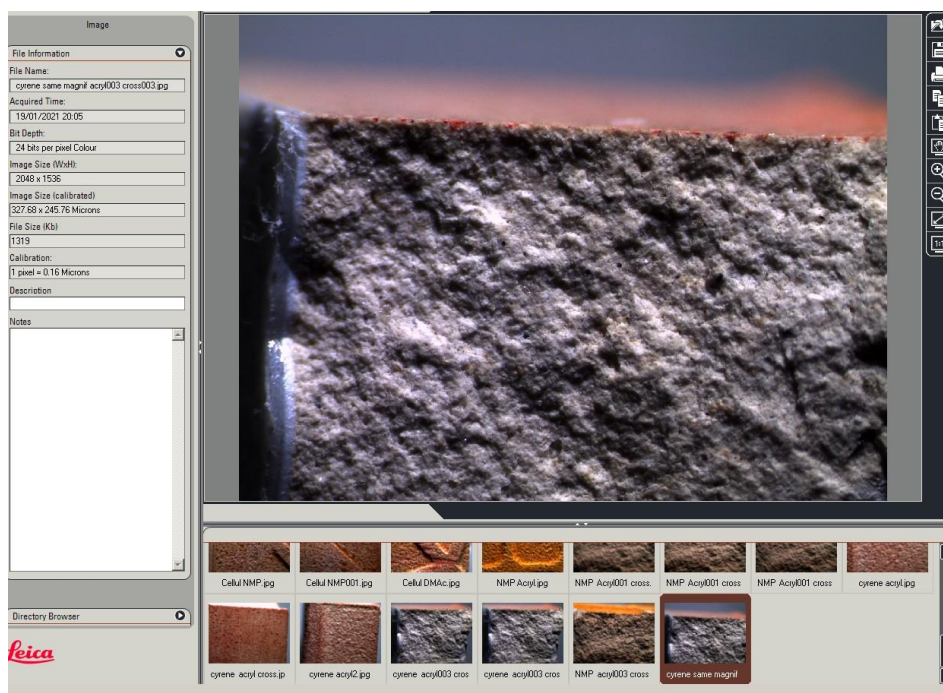


Figure 128: Cross-sectional optical microscope image of a ceramic tile cleaned by Cyrene.

## 8.4. Experimental – Chapter 3

### *PAIs synthesis*

The solvent/solvent system was placed in a round bottom flask with a reflux condenser and nitrogen inlet. Trimellitic acid anhydride (TMA) was added under stirring and mixture heated to 65 °C, when it dissolves. The mixture was further heated to 89 °C when 4,4'-methylenediphenyl diisocyanate (4,4'-MDI) was added (the monomer dissolves at 85 °C). The solvent or solvent system and the monomers were heated up under stirring at 145 °C for four hours and the obtained solution was cooled down to room temperature.

### *Viscosity analysis*

Dynamic viscosities of PES casting solutions were measured by a Malvern Kinexus pro+ rotational rheometer with a plate CP4/40 SR2013 SS: PL61 ST S1540 SS (40 mm diameter 4° angle cone over a 61 mm plate). Samples of 1 mL were used to test PAIs viscosity. All measurements in this study were performed at 1 atm and 298.15 K. The experiment sequence "Shear stress ramp with yield stress analysis" of "rSpace" software was run for the dynamic viscosity of the polymer solutions as function for shear rate determination.

### *Thermal curing of PAI*

PAI films were cured in a curing equipment seen in Figure 129 and contained: 1) a heating source, 2) round bottom flask, 3) substrate containing PAI film, 4) adapter, 5) nitrogen inlet, 6) condenser, 7) adapter and 8) receiving flask.

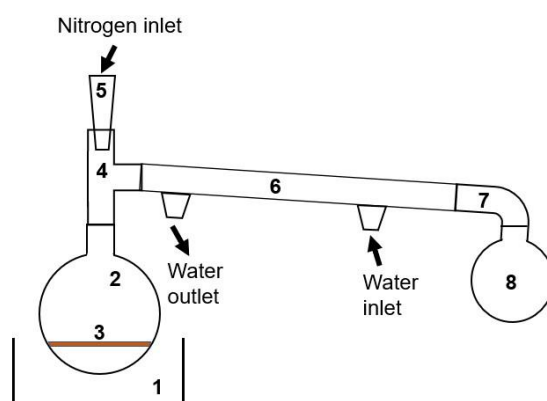


Figure 129: Schematic diagram of PAIs curing system.

PAI films were applied onto an aluminium substrate and heated up to 220 or 240 °C and maintained for 2 hours. The heating rate was fast at the beginning of the curing 10 °C min<sup>-1</sup> from RT to 120 °C and then slow (2 °C min<sup>-1</sup>) until it reached the curing temperature.

### ***Thermogravimetric analysis of PAIs***

Thermogravimetric analyses were performed on a PL Thermal Sciences STA 625. 5 mg of cured PAIs cured at 240 °C were weighed into an aluminium TGA pan and heated under the nitrogen flow to 625 °C at a rate of 10 °C/min. The glass transition temperatures of the obtained PAIs are obtained from the differential scanning calorimeter DSC and the char yield percentage at 625 °C are obtained from the TGA curves.

### ***NMR Spectroscopy***

NMR samples were prepared by dissolving 5-40 mg material in DMSO-d<sub>6</sub>. <sup>1</sup>H NMR and <sup>13</sup>C NMR spectra were carried out by a Bruker 300 MHz spectrometer. NMR data was analysed using ACD Labs 2020 LSM and signals were calibrated against the residual solvent peak.

### ***Solvent resistance test***

PAI resins with Cyrene, NMP and blends with ethylene carbonate and with DMSO were cured at temperatures between 220 and 240 °C. The slides containing one-layer cured PAIs were immersed in vials containing NMP and left for 24h, when the results were registered.

### ***Adhesion strength - peel test***

For this test, the PAI resins were cured on Al foil first and one of the ends was clamped. Force was applied to assure a better adhesion of the tape (Scapa 3159) onto coating. The tape was peeled off at an angle of 90° manually and the results were registered.

### ***Abrasion resistance test***

PAI films were cured on an aluminium foil surface. Before testing, the cured film was placed on a firm horizontal surface and tested for scratches or gouges that may prevent an accurate test. During the test, different pencils (Figure 130 b) are scratched along the surface of the coating to determine which one is hard enough to gouge the coating. The hardness tester (Figure 130 a) holds the pencil at 45° angle and pushed forward against the film using a pressure.





Figure 130: (a) Hardness tester and (b) the pencils used in the abrasion test of PAI wire enamels.

The force of 1 Kg was applied one time and the results recorded. The pencil rating is this level of hardness which does not scratch the surface. A B pencil is soft, with 9B, the softest. The pencils increase in hardness as they go from 9B to a single B. The hardness continues as the pencils go from HB to F (intermediate) to H all the way up to 9H, which is the hardest in the set of pencils used in this work. Only three pencils were chosen for this test to be used onto the same surface: 9B which is the softest, 9H (the sharpest), and F (intermediate). The results were recorded using a Leica S6D microscope too for a deeper analysis.

## 8.5. Experimental – Chapter 4

### *Hesperidin and rutin extraction from plant-derived sources*

For hesperidin extraction in this study, a sample of 250 mg of orange peel waste was dispersed in 5 mL of the solvent and then stirred using a homogenizer (IKA Ultra-Turrax T10 basic) for 2 minutes at 14,450 rpm and room temperature (RT extraction). The same procedure was used for rutin extraction from black tea, with 500 mg of biomass homogenised in 5 mL of solvent.

Hot extraction was performed by heating the solid-solvent mixture at 65 °C for 2 hours, then homogenised for 2 minutes at 14,450 rpm. The amounts of sample and solvent are as used above (250 mg of dried orange peel in 5 mL of the solvent for hesperidin and 500 mg of dried tea leaves in 5 mL of solvent for rutin).

A less energy-consuming technique was also tested for some of the solvent mixtures (fast-hot extraction), by heating the solvent up to 65 °C and then adding it to the sample, followed by the same homogenisation procedure (2 minutes at 14,450 rpm). The sample-solvent mixtures were centrifuged at 3100 g-force and 10 °C for 10 minutes and filtered using a 0.45 µm PTFE filter for further analysis.

### Quantitative characterisation by UH-PLC

Liquid chromatography was used to detect and quantify the analytes hesperidin and rutin in extracts from orange waste and black tea, respectively. UHPLC (Ultra-High-Performance Liquid Chromatography) system Waters ACQUITY H-class UPLC coupled with Photodiode Array UV (PDA) set to 280 nm (hesperidin) and 355 nm (rutin) was used with CSH C18 column (Waters, 1.7  $\mu\text{m}$ , 2.1x100 mm) and water (A) and methanol (B) mobile phase at 0.3 mL/min, column temperature of 35 °C (hesperidin) and 40°C (rutin) and injection of 1  $\mu\text{L}$ . The gradient elution for hesperidin was: 90% A, 0 min; 80% A, 2min; 72.5% A, 7min; 0% A, 8 min. The gradient elution for rutin was: 85% A, 0 min; 82.9% A, 7 min; 0% A, 8 min.

The extraction yield was calculated using the following equation:

$$Y = Cx \frac{V}{M} \quad (\text{eq. 15})$$

where "Y" is the extraction yield in  $\text{mg g}^{-1}$ , "C" is the concentration in  $\text{mg L}^{-1}$ , "V" is the extraction volume in litres and "M" is the sample mass in milligrams. Waters Acquity UPLC equipped with QDa and PDA detectors. The retention time of hesperidin standard can be seen at minute 6.357:

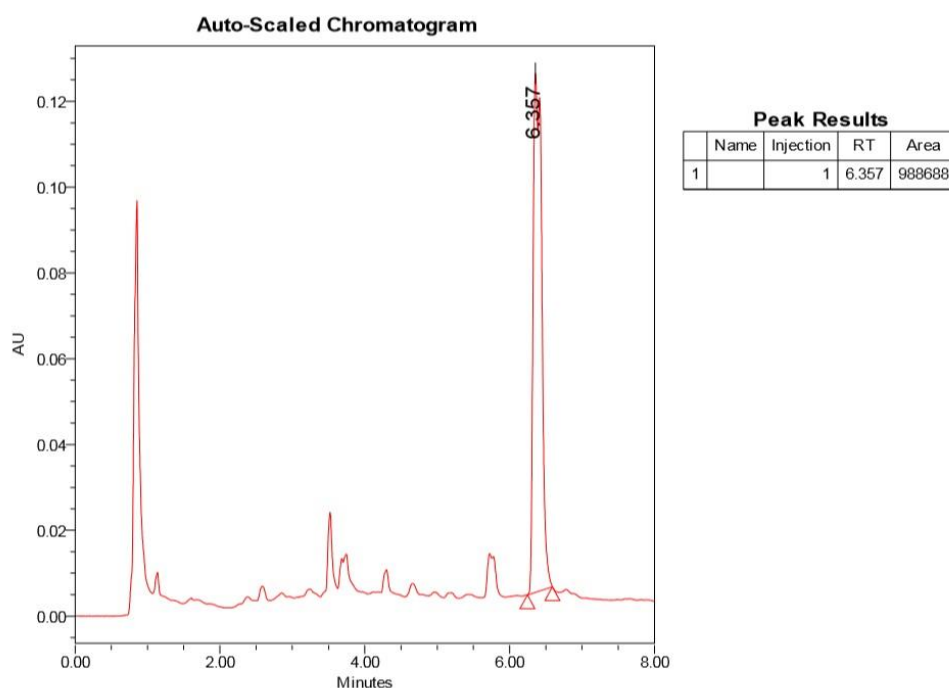


Figure 131: UH-PLC chromatogram of hesperidin standard.

UH-PLC chromatogram of hesperidin standard can be seen in Figure 131 and an example of hesperidin extraction from orange peel using Cyrene is given in Figure 132:

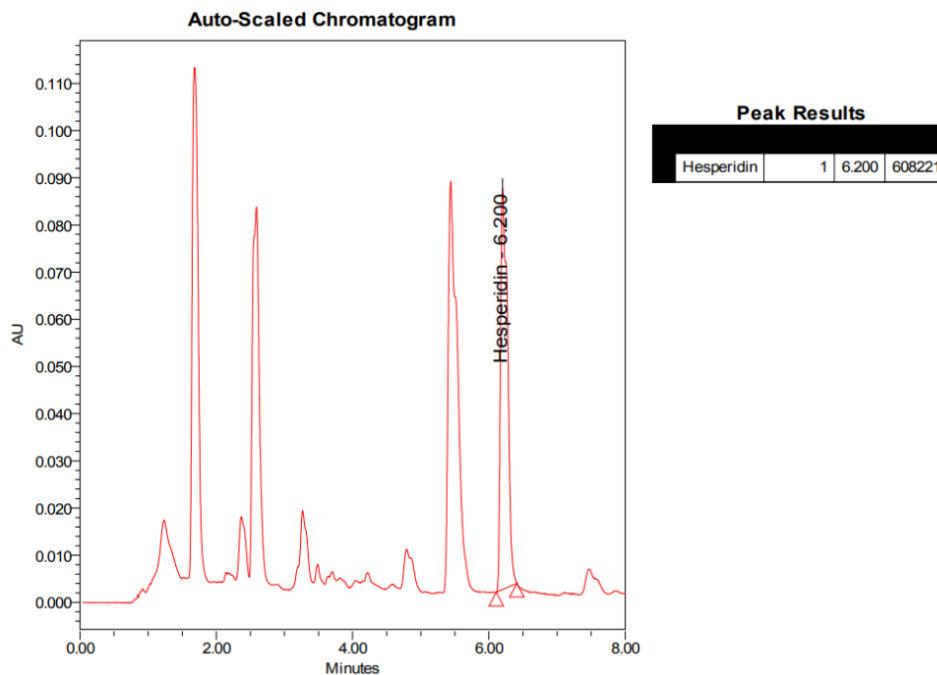


Figure 132: UH-PLC chromatogram of hesperidin extracted by 70% Cyrene-30% H<sub>2</sub>O mixture.

## 8.6. Experimental – Chapter 5

### *Ultrasonication experiments for dispersion of SWCNTs*

SWCNTs were dispersed in the three solvents using an ultrasonic bath for different periods of time (1, 5, 10 and 20 hours) in 1.5-hour intervals (Figure 133). 15 mL centrifuge tubes containing the solution were placed in a beaker and placed into the ultrasonic bath. At the end of sonication, the solution was kept at room temperature overnight.

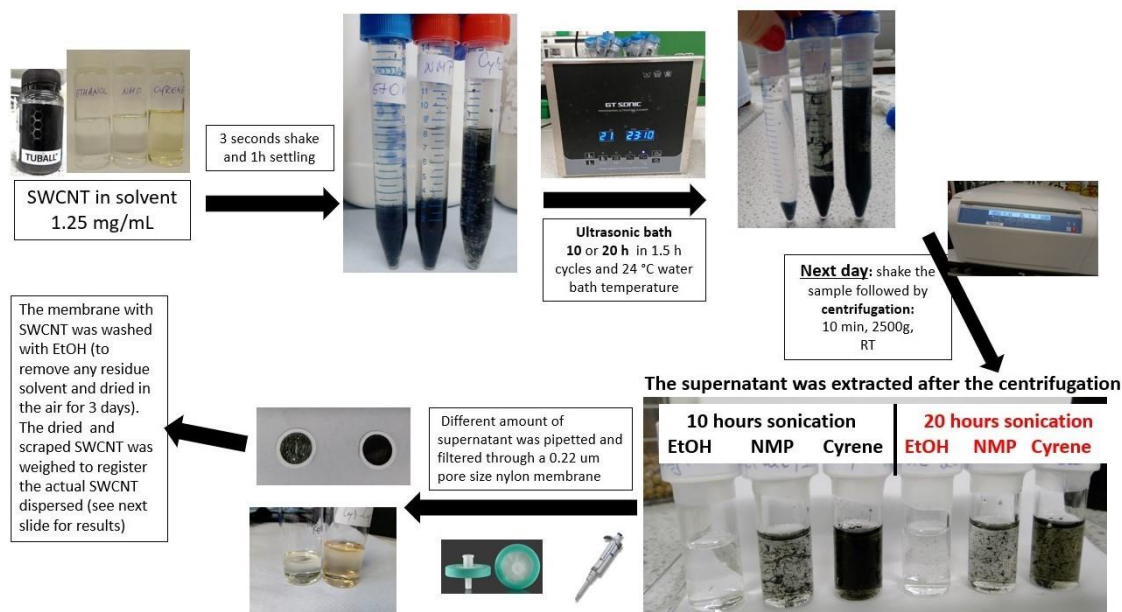


Figure 133: The description of the single-walled carbon nanotubes (SWCNTs) dispersion in Cyrene, NMP and ethanol used in this project.

On the next day, the samples were centrifuged for 10 minutes at 2500 g, at room temperature followed using a Biofuge Primo centrifuge with an angle of 90 degrees and 17 cm rotor. The upper 80% of the supernatant was then carefully decanted. The supernatant was then collected and filtrate through a 0.22  $\mu\text{m}$  pore size nylon membranes (pastel green P/N: FIL-S-NY-022-13-100 from Chromatography Direct). The nanotubes deposited onto membrane were washed several times with ethanol to remove any residual solvent and left to dry in the air for a few days. The dried and scraped SWCNTs from the membrane were weighed and the actual concentration registered.

The ultrasonic bath used in this work GT SONIC-D3 (3L), with overall size of 275x170x240 mm and internal dimensions the tank 240x140x100 mm. An ultrasonic power of 100 Watt has been used to disperse the carbon nanotubes in solutions and 1 h sonication stages. The bath was operated at 40 kHz after being filled with 1200 mL water. The temperature of the water in the bath was kept at 25 °C ice was added time to time to avoid the rise in the temperature in the bath during the experiments.

### **Standard deviation and Z-score**

Standard deviation ( $\sigma$ ) reflects the amount of variability within a data set and is calculated from:

$$\sigma = \sqrt{\frac{\sum(x_i - \mu)^2}{N}} \quad (\text{eq. 16})$$

Where " $\sum$ " is the sum of " $x_i$ ", which means the values from the data set, " $\mu$ " is the mean of all numbers from the data set and " $N$ " represents the total of the values from data set.

Z-score ( $z$ ), or standard score, is the number of standard deviations a data point is lower or higher than the mean. This score is calculated from the equation below:

$$z = \frac{x - \mu}{\sigma} \quad (\text{eq. 17})$$

Where " $x$ " is the raw score (a value of the data set), " $\mu$ " is the mean of all numbers from data set and " $\sigma$ " represents the standard deviation of the sample.

### ***Scanning Electron Microscopy (SEM) analysis***

Scanning Electron Microscopy (SEM) micrographs were carried out with the assistance of Dr Meg Stark and Karen Hodgkinson at the Department of Biology, University of York. The membranes were dried and frozen in liquid nitrogen followed by Au/Pd coating. SEM images of the coated membranes were recorded using a JEOL JSM-6490LV Scanning Electron Microscope.

### ***Transmission Electron Microscopy (TEM) analysis***

TEM images were taken by Dr Meg Stark and Karen Hodgkinson from the Biology department at the University of York. 200 mesh formvar/carbon copper grids were pre-treated by glow discharge in Polaron E6000 vacuum coating unit to make them hydrophilic. 5  $\mu$ L of each sample were loaded onto these pre-treated grids and left to dry for 48 hours in a fume hood before analysis. The grids were analysed on FEI Tecnai 12 BioTwin G2 Transmission Electron Microscope operating at 120kV. The images were collected on a SIS CCD camera at magnifications of 6.8k and 98k. Only samples sonicated for 1 and 20 hours were analysed in this work.

## **8.7. Experimental – Chapter 6**

### ***Membranes preparation***

All membranes produced in this work have been prepared using a NIPS process (Figure 134). The casting solution was prepared by dissolving the main polymer (PES, CA, PVDF, PSf or PI) into solvent at a temperature of 70°C for 4h. Additives were added into the solution, *e.g.* PVP, CNTs or Starbon materials. SWCNTs were added in the solvent and the polymers added in this solution. The casting solutions were degassed and cast from a room temperature or hot solutions. The thickness of membranes varied between 150-500  $\mu$ m. The casting film was submerged in a coagulation bath containing deionised water at room temperature, causing the polymers to precipitate. Membranes were then washed and stored in deionised water until further use.

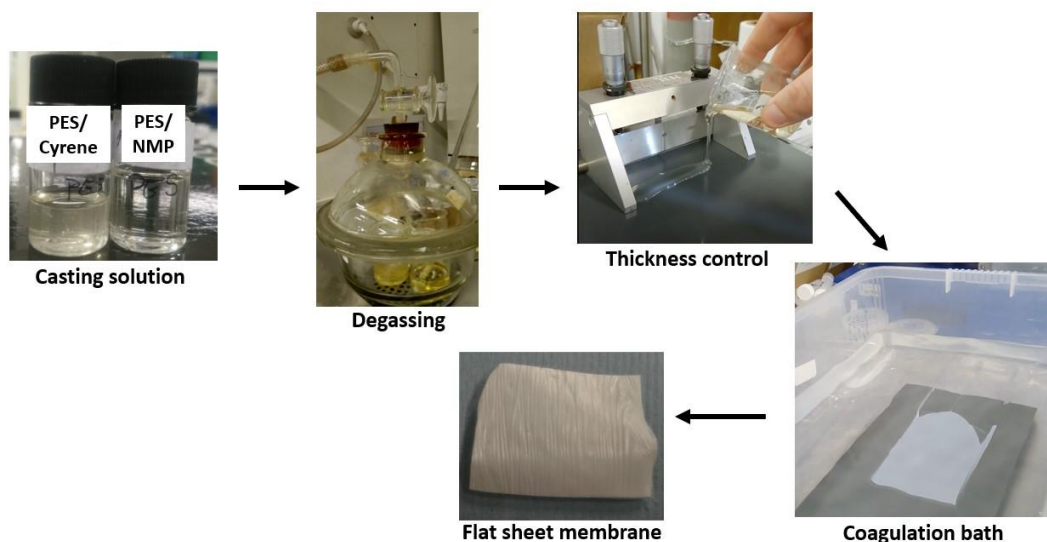


Figure 134: The schematic illustration of membrane preparation using NIPS process.

### ***Viscosity analysis***

Dynamic viscosities of PES casting solutions were measured by a Malvern Kinexus pro+ rotational rheometer with a rSpace software interface and a plate CP4/40 SR2013 SS: PL61 ST S1540 SS (40 mm diameter 4° angle cone over a 61 mm plate). 1 mL of sample was used to perform viscosity tests. All measurements in this study were performed at 1 atm and 298.15 K. The program used for viscosity testing is ‘Viscometry shear stress ramp’.

### ***Porosity and pore size distribution of the produced membranes***

#### ***a) Mercury Intrusion Porosimetry (MICP) and NMR methods***

Porosity and pore size distribution test were determined using Mercury Intrusion Porosimetry (MIP) using a Micromeritics Autopore IV instrument located in the University of Leeds. This method is based on the behaviour of “nonwetting” liquids in capillary which cannot be absorbed by the pores of a solid itself but requires an external pressure to be applied. By measuring the volume of mercury that intrudes into the sample material with each pressure change, the volume of pores in the corresponding size class can be obtained. MIP only shows accessible interconnected pores (if the closed pores are incompressible). The applied mercury pressure is inversely proportional to the size of the pores. A lower pressure is needed to penetrate large pores, while a greater pressure is needed to access smaller pores. From the pressure versus intrusion data, the instrument generates volume and size distributions using the Washburn equation:

$$D = - \frac{4\gamma\cos\theta}{P} \quad (\text{eq.18})$$

where “D” stands for pore diameter ( $\mu\text{m}$ ), “P” is the applied pressure (psi), “ $\gamma$ ” represents Hg-air surface tension ( $484 \text{ mN m}^{-1}$ ) and “ $\theta$ ” is Hg-air-porous material contact angle ( $140^\circ$ ).

**NMR spectroscopy** was used as supporting evidence of the pore size distributions and was considered a more sustainable and less toxic method compared to the MIP method, which can distort the skeletal porous structure of a sample. However, this method was used previously to characterise porosity, pore geometry, connectivity and permeability of sandstones and carbonates. In this project, the NMR was used to confirm the volume of fluid filling the pore space and a T2 distribution (equivalent to a pore size distribution, PSD) is obtained after deconvolution of magnetization relaxation (Figure 135):

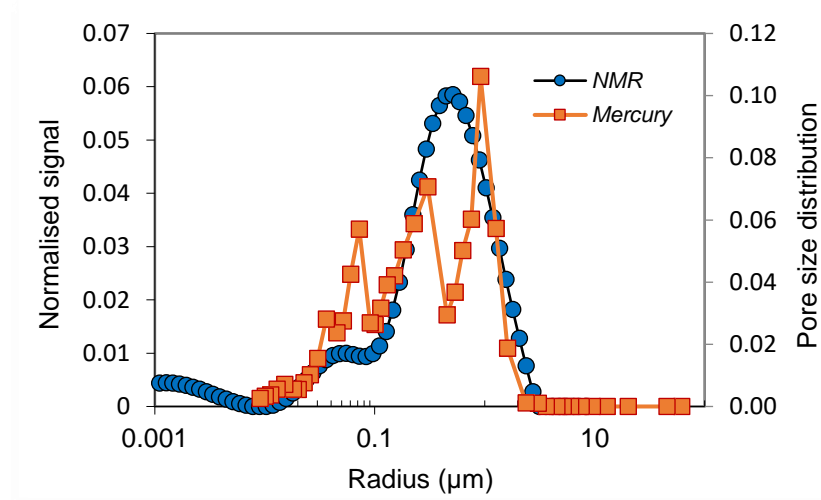


Figure 135: MIP and NMR methods of porosity using a PES/C5.

As a measure of membrane’s hydrophilicity, the water contact angle (WCA) was measured *via* the sessile drop method using a Theta Lite optical tensiometer at a room temperature of  $22^\circ\text{C}$ . A range of  $0.5\text{--}1.5 \mu\text{L}$  droplet sizes of water were placed on the membrane surface and the images were recorded using the automated OneAttension software. The static contact angles were measured at a minimum of three random locations and the mean values reported to minimize experimental error.

### **b) Gravimetric method**

This method is repeatedly used in literature to evaluate the porosity of the membranes *via* determining take up of water. The membranes were vacuum dried at 80 °C, before being weighed and their size and thickness measured. They were then immersed in distilled water at RT for 24h, before being weighed again, and the increase in mass registered. The %water retained in pores was calculated using the following equation:

$$\varepsilon = \frac{W_w - W_d}{A l \rho} \times 100 \quad (\text{eq. 19})$$

where “ $W_w$ ” and “ $W_d$ ” represent wet and dry masses (g) of the membranes, respectively, “ $A$ ” is the membrane surface area ( $\text{m}^2$ ), “ $l$ ” is thickness of membrane (m) and “ $\rho$ ” is density of water at RT ( $998 \text{ Kg m}^{-3}$ ).

### **Contact angle (CA) determination**

As a measure of membrane’s hydrophilicity, the water contact angle (WCA) was measured *via* the sessile drop method<sup>813</sup> using a Theta Lite optical tensiometer at a room temperature of 22 °C. A range of 0.5–1.5  $\mu\text{L}$  droplet sizes of water were placed on the membrane surface and the images were recorded using the automated OneAttension software. The static contact angles were measured at a minimum of three random locations and the mean values reported to minimize experimental error.

### **Pure water permeability (PWP) test**

Membrane permeability (flux) was determined by University of Swansea, by measuring the pure water fluxes using a stirred cell (Sterlitech HP4750). The filtration solutions were stirred magnetically at 300 rpm and a constant temperature of  $25 \pm 0.5$  °C. Rates of filtration were determined by continuously weighing the filtrate on an electronic balance connected to a data logger. A digital electronic balance from Ohaus (Scout Pro Range), with an accuracy of 0.01 g was used to continuously measure the weight of the permeate. Recording the weight at certain time intervals also allows the calculation of the permeate flux:

$$J_w = \frac{m(t+\Delta t) - m(t)}{\rho A_m \Delta t} \quad (\text{eq. 20})$$

where “ $J_w$ ” is the water flux ( $\text{L m}^{-2} \text{ h}^{-1}$  (LMH)), “ $m$ ” is the mass at a given time, “ $\rho$ ” is the density of water, “ $A_m$ ” is the area of the membrane ( $\text{m}^2$ ) and “ $t$ ” is the time (s).



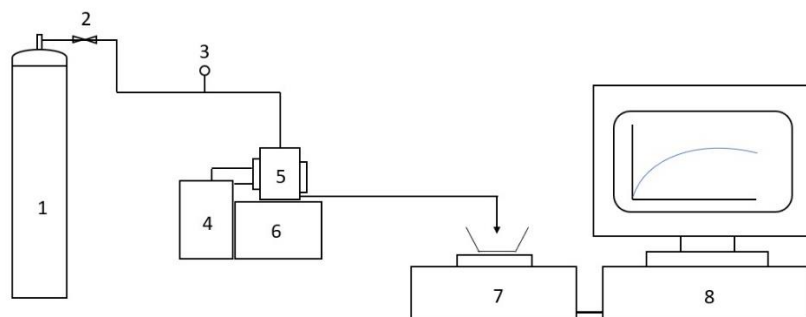


Figure 136: A schematic diagram of the frontal filtration equipment. (1) nitrogen cylinder, (2) valve, (3) pressure sensor, (4) water bath, (5) membrane cell, (6) magnetic stirrer, (7) electronic balance, (8) PC.

Figure 136 shows schematically the arrangement of the membrane filtration and flux measurement equipment. The filtration cell was pressurised using nitrogen gas (oxygen free) with pressure controlled by means of a regulator on the cylinder. The 50 mm diameter membranes were first subject to an initial pressure of 1 bar until a stable flux was evident, then the pressure increased to 5 and 10 bar.

#### ***Cygnat 0.0 synthesis***

Cyrene (0.12 moles) and ethylene glycol (0.21 moles) were added in a round bottom flask with 0.75 g acid catalyst (KSF200). The mixture was heated under stirring to 100 °C for one hour. After one hour, the mixture was cooled down to room temperature, and the catalyst was removed by vacuum filtration. Magnesium sulfate was added to remove any water traces, and the mixture filtrate once more.  $^{13}\text{C}$  NMR spectrum of Cygnat 0.0 has been previously reported.<sup>126</sup>  $^1\text{H}$  NMR spectra of the reactants and the mixture at the beginning and the end of the reaction can be seen in Figure 137:

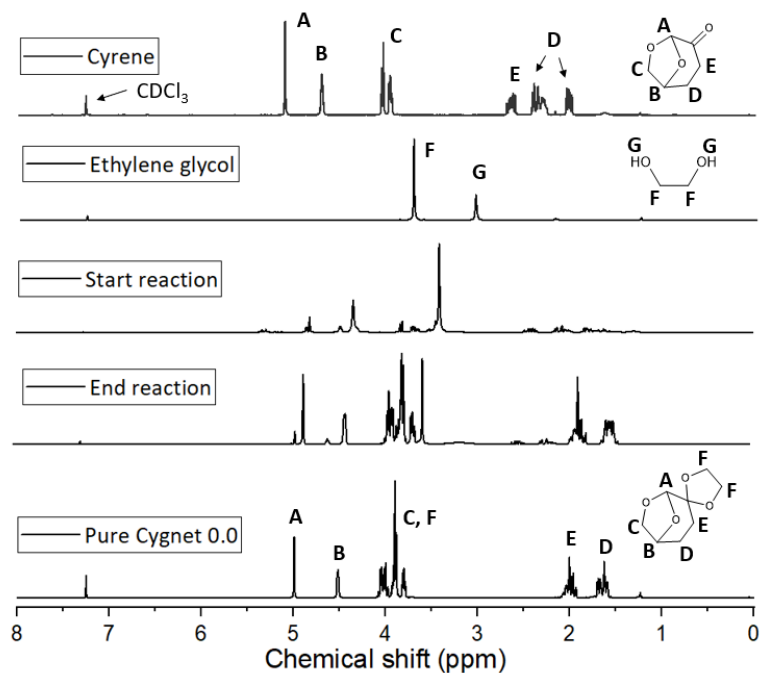


Figure 137:  $^1\text{H-NMR}$  Spectra of Cygnet 0.0 and the reactants leading to its formation

The solution was stored in the fridge overnight. Cygnet 0.0 was recrystallised from ethanol, aligning well with green chemistry principles and no toluene was employed in the mechanism. The filtrate containing ethylene glycol and ethanol is separate by removing the ethanol first using a rota evaporator. The catalyst was washed and reactivated by carbonisation at  $200\text{ }^\circ\text{C}$  for 3 hours. A yield of 85% Cygnet 0.0 has been obtained.

#### ***Cygnet 0.0: Cyrene 50-50 (Cg: Cy) synthesis***

Because Cyrene is the precursor for Cygnet 0.0 Cg: Cy blend could be conveniently synthesised by using ethylene glycol as limiting reagent (0.08 moles ethylene glycol and 0.12 moles Cyrene).

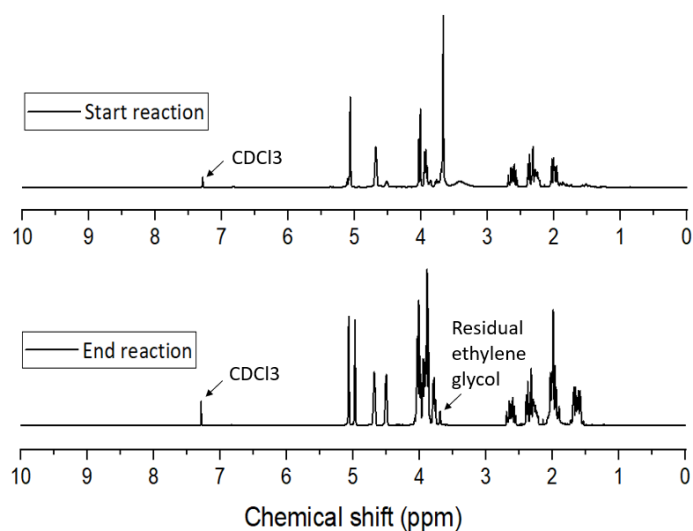


Figure 138:  $^1\text{H-NMR}$  spectrum of Cg:Cy from the reaction between Cyrene and ethylene glycol

Removal of water with a drying agent, followed by filtration to remove drying agent and catalyst, presents an attractive single-step synthetic option, which requires no further purification. Residual ethylene glycol can be observed in Figure 138 and a yield of 86% Cygnet 0.0 was achieved in this case.

## 8.8. Computational methodologies

### 8.8.1. Hansen Solubility Parameters in Practice (HSPiP)

Hansen Solubility Parameters (HSPs) are extensively used to predict solubility and search for solvent alternatives by investigating the similarity of solvency between the bio-based solvent and the traditional ones. HSPs have been used for the research of polymer solubility in solvents and surface science,<sup>127-129</sup> to predict the dispersion of nanoparticles (cellulose nanoparticles) in polymeric films<sup>130</sup> drug-nail interaction,<sup>131</sup> solubility behaviour of globular plant proteins,<sup>132</sup> solubility of liquid crystals in solvents<sup>133</sup> and solubility of carbon nanotubes and fullerenes in solvents, polymers and aqueous surfactant emulsions.<sup>134-138</sup> Hansen Solubility Parameters (HSP)<sup>139</sup> were chosen to predict molecular affinities, solubility, and solubility-related phenomena of polymers in different solvents by mapping the three values (dispersion interactions  $\delta_D$ , dipolarity  $\delta_P$  and hydrogen bonding ability  $\delta_H$ ) in a three-dimensional “Hansen space”, using 5<sup>th</sup> edition 5.0.03 of HSPiP. These three terms, when combined, can predict the behavior of solvents more accurately than the Hildebrand solubility parameters, where the materials with similar

values of Hildebrand solubility parameter “ $\delta$ ” are likely to be miscible and the hydrogen bonding and polar interactions are not considered.<sup>814</sup>

The universal principle “like dissolves like” is widely employed for solubility parameters. In some cases, solubility parameters are also defined as “cohesion energy parameters” since they are obtained from the energy needed to transform a liquid into a gas. The energy of vaporisation can be a direct measure of the total cohesion energy as all types of bonds assembling the liquid together can be broken by evaporation. Therefore, the total cohesive energy is identical to the energy of vaporisation. Historically, the term “solubility parameter” was first proposed by Hildebrand and Scott. The Hildebrand solubility parameter “ $\delta$ ” is defined as the square root of the cohesive energy density, which is the energy required to remove a unit volume of molecules from their neighbours to be separated infinitely and is equal to  $E/V$ :

$$\delta = \frac{E^{1/2}}{V} \quad (\text{eq. 21})$$

where “ $V$ ” is the molar volume of the pure solvent and “ $E$ ” is its energy of vaporisation.

$$\delta^2 = \frac{E}{V} \quad (\text{eq. 22})$$

Hansen proposed that the total energy of vaporisation or cohesive energy “ $E$ ” could be separated into at least 3 different parts:  $E_D$ ,  $E_P$ ,  $E_H$ .

“ $E_D$ ” is dispersion cohesive energy, which comes from the nonpolar (dispersion) atomic forces, “ $E_P$ ” is the polar cohesive energy produced by the permanent dipole-permanent dipole molecular forces and “ $E_H$ ” is the electron exchange energy obtained from the hydrogen bonding molecular forces.

The total cohesive energy “ $E_{\text{Tot}}$ ” becomes:

$$E_{\text{Tot}} = E_D + E_P + E_H \quad (\text{eq. 23})$$

which divided by molar volume “ $V$ ” will give:

$$\frac{E}{V} = \frac{E_D}{V} + \frac{E_P}{V} + \frac{E_H}{V} \quad (\text{eq. 24})$$

And then combining  $\delta^2 = \frac{E}{V}$  and  $\frac{E}{V} = \frac{E_D}{V} + \frac{E_P}{V} + \frac{E_H}{V}$  the total solubility parameter “ $\delta$ ” is defined by a sum of squares of dispersion, polar, and hydrogen bond contributions:

$$\delta_{\text{Tot}}^2 = \delta_D^2 + \delta_P^2 + \delta_H^2 \quad (\text{eq. 25})$$

where “ $\delta$ ” is the Hildebrand solubility parameter and “ $\delta_D$ ,  $\delta_P$  and  $\delta_H$ ” stand for Hansen dispersion cohesion solubility parameter, polar cohesion solubility parameter and hydrogen bonding cohesion solubility parameter, respectively. These 3 parameters can be used as coordinates to establish a 3D dimension Hansen space (Figure 139):

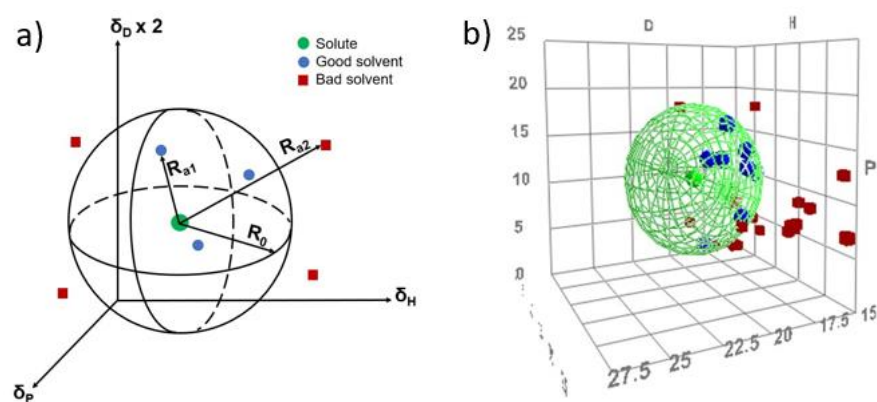


Figure 139: (a) Hansen Solubility Parameters 3D diagram and (b) an example from the present work with  $R_0$  (interaction radius) and  $R_a$  (Hansen distance).  $R_{a1}$  and  $R_{a2}$  are examples of Hansen distances between the solute and a good and a bad solvent, respectively.

“ $\delta_D$ ” is Van der Waals, polarisability, the number of electrons/random molecules. Solvents such as propylene carbonate or chlorobenzene and even Cyrene and DMSO have a big value due to their large aromatic groups, sulfoxide groups, generally with a lot of free electrons. Even the smallest molecules such as diethyl ether and acetic acid have big values, *ca.* 14.5 because Van der Waals is what keeps solvents together. “ $\delta_P$ ” is polarity and so hexane and heptane have no polarity and their value is “0”, while molecules such as acetonitrile, which has the polar C-N in a straight line. The large DMSO is also polar. “ $\delta_H$ ” is hydrogen bonding and hexane and heptane have none of it, while water has lots of it (42.3 Mpa<sup>1/2</sup>). Between ethanol and methanol, the extra CH<sub>2</sub> of the first one dilutes the amount of hydrogen bonding.

The Hansen distance ( $R_a$ ) in Hansen space is defined by the following equation:

$$R_a^2 = 4(\delta_D^{\text{solvent}} - \delta_D^{\text{solute}})^2 + (\delta_P^{\text{solvent}} - \delta_P^{\text{solute}})^2 + (\delta_H^{\text{solvent}} - \delta_H^{\text{solute}})^2 \quad (\text{eq. 26})$$

Equation 26 can also be written as:

$$R_a = \sqrt{4(\delta_D^{\text{solvent}} - \delta_D^{\text{solute}})^2 + (\delta_P^{\text{solvent}} - \delta_P^{\text{solute}})^2 + (\delta_H^{\text{solvent}} - \delta_H^{\text{solute}})^2} \quad (\text{eq. 27})$$

In general, the lower the value of  $R_a$  the two chemicals have, the more similar solubility they will possess.  $R_0$  is defined as “interaction radius”. If the solubility of the solvent for the solute needs

to be retained,  $R_a$  cannot exceed  $R_0$ . The units of  $R_a$  and  $R_0$  are both  $\text{Mpa}^{1/2}$ . To compare  $R_a$  and  $R_0$ , the relative energy difference (RED) was proposed:

$$\text{RED} = \frac{R_a}{R_0} \quad (\text{eq. 28})$$

The relative energy difference (RED) represents the position of a solvent in solubility space and three cases can occur:  $\text{RED} < 1$  the molecules are alike and will dissolve,  $\text{RED} = 1$  the system will partially dissolve,  $\text{RED} > 1$  the system will not dissolve.

For ternary solvent systems,  $\delta_x$  is calculated for each Hansen parameter taking in account the % (v/v) of substances, according to the following equation:

$$\delta_x = (\delta_x^{\text{solvent A}} \times \varphi^{\text{solvent A}}) + (\delta_x^{\text{solvent B}} \times \varphi^{\text{solvent B}}) + (\delta_x^{\text{solvent C}} \times \varphi^{\text{solvent C}}) \quad (\text{eq. 29})$$

where " $\delta_x$ " represents Hansen parameters ( $\delta_D$ ,  $\delta_P$  or  $\delta_H$ ) of the new solvent system; " $\varphi$ " is the volumetric fraction of each solvent and solvents "A, B and C" stand for the solvents from the ternary system. Microsoft Excel 2016's "Solver" tool was used to determine the parameters to minimize  $R_a$  between the tested combination and the solute's empirical Hansen Solubility Parameters, thus giving the optimal theoretical concentration of each solvent utilised in each mixture.

## 8.8.2. COSMOtherm modelling

COSMOtherm was used to calculate the chemical potential of a molecule in pure or mixed liquid at variable temperature. This software predicts thermodynamic properties such as solubilities, activity coefficients and phase diagrams, free energies of solvation or vapour pressures in liquid mixtures and requires no experimental data. The properties of liquids are predicted using three programs: ArgusLabX, COSMOconfX and COSMOthermX. Cyrene is given as example here (Figure 140) for showing a COSMO surface, where green to yellow represents the weakly polar surfaces ( $\text{CH}_2$ ), blue represents positive polarity (hydrogen) and red codes strongly negative polar surfaces or electron rich (oxygen). The molecule appears mostly in blue (electron deficient), so positively polar, phenomenon explained by the presence of the high intensity, sharp peak at around  $-0.01 \delta$  ( $\text{e}/\text{\AA}^2$ ) in Figure 140c of  $\delta$ -profile. The other peak at around  $0.01 \delta$  ( $\text{e}/\text{\AA}^2$ ) is allocated to the negative polarity (oxygen).

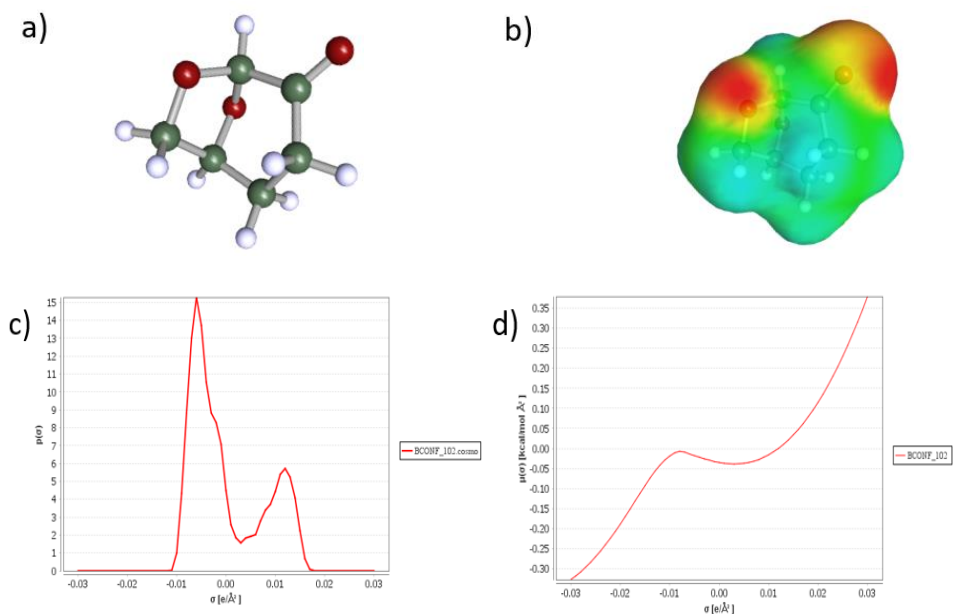


Figure 140: (a) Cosmo geometry, (b)  $\delta$ -surface, (c)  $\delta$ -profile and (d)  $\delta$ -potential of Cyrene.

### ArgusLab

ArgusLab (version 4.0.1. from Mark Thompson and Planaria Software LLC, 2004, USA) was used in this work for molecular modelling.<sup>41</sup> The molecular geometry was optimised using the Austin Model 1 (AM1) and a restricted Hartree-Fock (RHF) calculation.

### COSMOconfX

COSMOconfX (version 4.0., COSMOlogic GmbH & Co. KG, Germany) was used to calculate the conformations of the molecules obtained from ArgusLab (Figure 141):

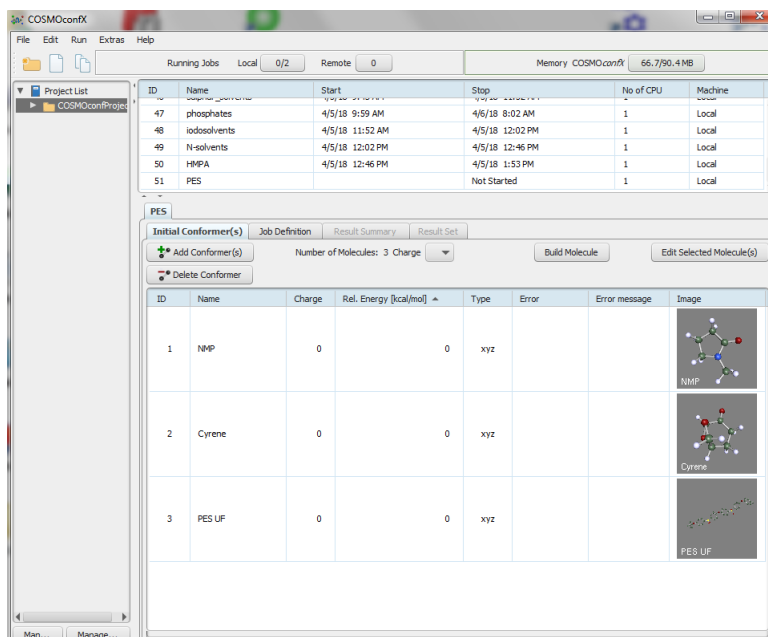


Figure 141: COSMOconfX interface.

A typical workflow of a single structure contains the following steps:

- 1- **Conformer generation**, which can be done by COSMOfrag and MOPAC or by Balloon<sup>42</sup> and can be used with the BP-TZVP parametrisation of COSMOtherm. BP-TZVP COSMO optimisation offers a full geometry optimisation with density functional theory and a medium sized basis set. BALLOON\_CONF\_GEN was used for the conformer generation; the molecule set obtained contains MMFF94 structures and energies. This step requires a single molecular conformation and generates different structures using single bond rotations, each of them having different energy, polarity, and hydrogen bonding capacity.
- 2- **Check and reduction**, when the conformer with the lowest COSMO energy has been used and higher energy conformers are eliminated together with conformers with wrong stereochemistry.
- 3- **Quantum Chemistry calculations**. COSMOconfx uses a single point or geometry optimisation to find a better atomic arrangement which makes the molecule most stable.
- 4- **Clustering**, when the only conformations that show a different physical behaviour are selected. Using only a single conformation can cause significant errors.

The name of the job will be used will contain the name of conformer files and “cosmo” as for COSMO conformers, the numbers “1, 2” are in order of ascending energies, the lowest one will be designed for the lowest energy.



## COSMOthermX

COSMOthermX (version C3.0\_1501, COSMOlogic GmbH & Co. KG, Germany, with TZVP basis set level) was used in this work to obtain the molecular surface charges,  $\delta$ -profiles" (Figure 140c) and  $\delta$ -potential (Figure 140d) of the solvents used in dissolution of various polymers. COSMOtherm is based on "Conductor-like Screening MOdel for Real Solvents" (COSMO-RS) theory of interacting molecular surface charges.<sup>43,44</sup> COSMO-RS is a predictive method for thermodynamic equilibria of fluids and liquid mixtures, where the solvents are considered in their liquid state and all parts of the molecular surfaces can be in contact with each other. In COSMO calculations a solute molecule is calculated in a virtual conductor environment, where it induces a polarisation charge density on the molecular surface of the solute (surface between the solute molecule and conductor). During the quantum chemical self-consistency algorithm, the solute molecule is converged to its energetically optimal state in a conductor depending on its electron density. A COSMOtherm calculation involves two steps: compound selection and property input.

- 1- **Compound selection.** A COSMOtherm calculation requires screening charge density  $\delta$  of the molecules and transforms the screening charge surface into a screening charge distribution, called " $\delta$ -profile".  $\delta$ -profiles for conformers are calculated individually in a quantum chemical COSMO calculation and stored in a COSMO file with the extension ".cosmo" or ".ccf". COSMO files were generated using a TZVP level, based on molecular structures retrieved from DFT (Density Functional Theory) calculations. For COSMO-RS, only conformers with different  $\delta$ -profiles are relevant. If a compound has multiple conformers, they will be combined into a single compound. The  $\delta$ -profile of a mixture is the weighted sum of the profiles of all its components.
- 2- **Property input.** The compounds selected for a property are shown in Figure 142, where a polymer and numerous solvents are listed.

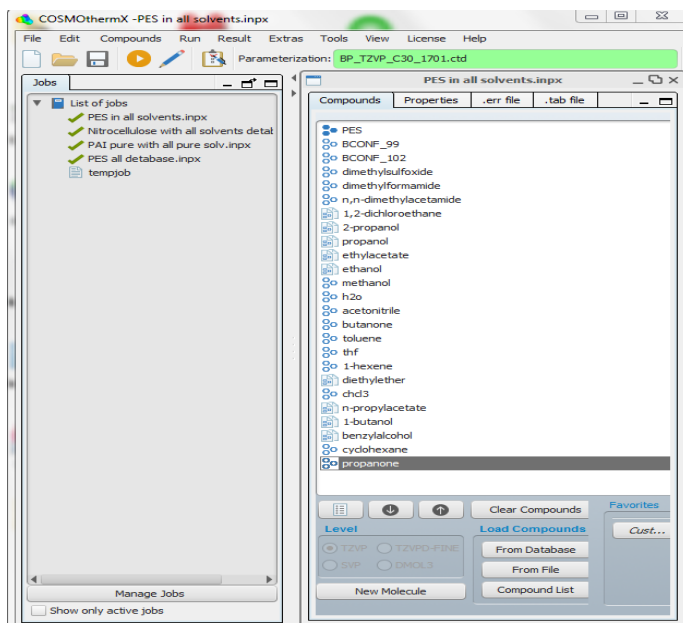


Figure 142: List of compounds and polymer selected for a property calculation.

Once the compounds are selected, the properties with adjustable settings (e.g. temperature, composition of the system) are added to the system (Figure 143), which can contain one or several compounds represented in mole or mass fraction numbers. Several COSMO calculations can be run in a single job. When a job has finished, calculation results are displayed.

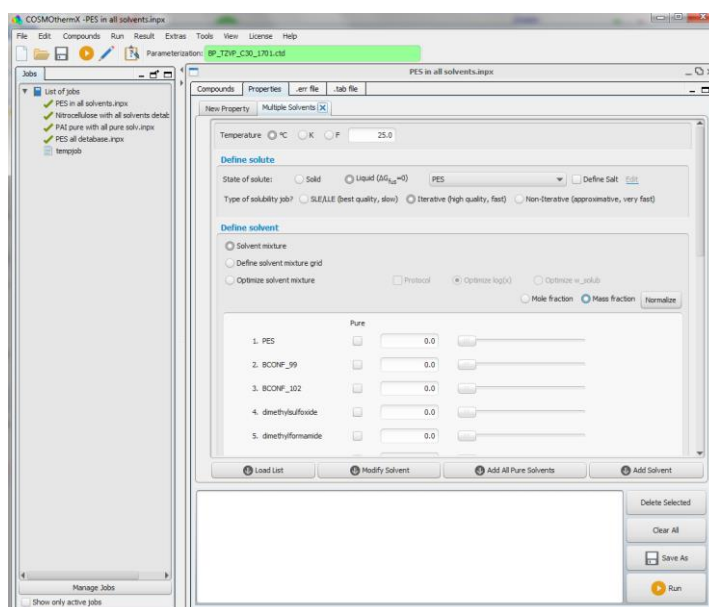


Figure 143: Composition of COSMOtherm system.

At the end of calculations, COSMOtherm states that the closer to value “0” the better solvent will be, and an example is seen in Figure 29 (Section 1.5.4.).

### 8.8.3. CHEM21 green metrics toolkit

Chemical Manufacturing Methods for the 21st Century Pharmaceutical Industries (CHEM21), a consortium of six pharmaceutical companies, thirteen universities and four small to medium enterprises from across Europe, work together to develop sustainable biological and chemical alternatives to finite materials technologies for the pharmaceutical industry. The most used metrics (set of statistics that measure results) were yield, followed by conversion and selectivity. The CHEM21 project has developed unified “metrics toolkit” to monitor, measure, compare and evaluate new methodologies in terms of their “green credentials”.<sup>44</sup> When producing a toolkit, compromises will have to be made it won’t be able to cover everything. The mass itself doesn’t give a true picture of the greenness of a reaction and the health and safety and the elemental sustainability don’t have simple metrics associated with them and the chemist should be aware of “the big picture” when they use them. The key parameters of the metrics toolkit are: life cycle assessment (LCA), solvents, renewability, health and safety, critical elements, catalysis, chemical of concern, waste, efficiency and energy.<sup>44</sup> A flag based system was used to score of acceptability: green flag means “preferred”, amber is “acceptable-some issues” and red is “undesirable”.

The toolkit allows the user to a) assess/demonstrate the “green credentials” of their research, b) benchmark by giving a baseline to compare their results to, and c) monitor, measure and evaluate new methodologies to ensure that solving one problem does not give rise to others in the process.<sup>44</sup> A series of green metrics covered by CHEM21 are seen below:

$$\% \text{ yield} = \frac{\text{moles of product}}{\text{moles of limiting reactant}} \times 100 \quad (\text{eq. 30})$$

$$\text{AE} = \frac{\text{molecular weight of product}}{\text{total molecular weight of reactants}} \times 100 \quad (\text{eq.3})$$

$$\% \text{ conversion} = 100 - \frac{\text{final mass of limiting reactant}}{\text{initial mass of limiting reactant}} \times 100 \quad (\text{eq. 31})$$

$$\% \text{ selectivity} = \frac{\% \text{ yield}}{\% \text{ conversion}} \times 100 \quad (\text{eq. 32})$$

A mass-based yield is determined from the reaction mass efficiency (RME):<sup>44</sup>

$$\text{RME} = \frac{\text{mass of isolated product}}{\text{total mass of reactants}} \times 100 \quad (\text{eq. 4})$$

MI/PMI (mass intensity/process mass intensity) is a metric based on all mass based inputs, such as solvents, catalysts, reagents, work up etc.<sup>44</sup> This metric is important to assess efficiency of a process step-by-step (MI) and cumulatively, of the entire process (PMI):

$$\text{MI/PMI} = \frac{\text{total mass in a process}}{\text{mass of product}} \quad (\text{eq. 33})$$

# Appendix A

Table A 1: Greener solvents used in this work

| Recommended solvents from<br>CHEM21 <sup>38</sup> | Problematic solvents from<br>CHEM21 <sup>38</sup> | Green solvents from references         |
|---|---|--|
| Acetone   | Acetonitrile                                      | MBSA <sup>39</sup>                     |
| <i>i</i> -Amyl alcohol                            | Acetic acid                                       | OME <sub>(3-5)</sub> <sup>269</sup>    |
| Anisole   | Acetic anhydride                                  | TMO <sup>40</sup>                      |
| 1-Butanol   | Benzyl alcohol                                    | Cygnat 0.0 <sup>126</sup>              |
| <i>i</i> -Butanol                                 | Chlorobenzene                                     | $\gamma$ -Valerolactone <sup>101</sup> |
| Butyl acetate                                     | Cyclohexane                                       | Cyclopentanone <sup>102</sup>          |
| <i>t</i> -Butanol                                 | <i>Me</i> -cyclohexane                            |  |
| Dimethyl carbonate                                | Cyclohexanone                                     |  |
| Ethylene glycol                                   | Cyclopentyl methyl ether                          |  |
| Ethanol   | <i>p</i> -Cymene                                  |  |
| Ethyl acetate                                     | Cyrene  |  |
| Ethylene glycol                                   | Diethyl succinate                                 |  |
| Glycol diacetate                                  | DMSO  |  |
| Isoamyl acetate                                   | <i>N,N'</i> -Dimethylpropyleneurea                |  |
| Isopropyl acetate                                 | <i>Me</i> -THF                                    |  |
| <i>i</i> -Butyl acetate                           | Ethyl lactate                                     |  |
| Isobutyl alcohol                                  | Ethylene carbonate                                |  |
| Methanol  | Ethyl tert-butyl ether (ETBE)                     |  |
| Methyl ethyl ketone (MEK)                         | Formic acid                                       |  |
| Methyl isobutyl ketone<br>(MIBK)                  | Glycerol  |  |
| 1-Propanol  | Heptane   |  |
| 2-Propanol  | Lactic acid                                       |  |
| TAME  | <i>d</i> -Limonene                                |  |
| Water   | Methyl acetate                                    |  |
|   | 1,3-Propanediol                                   |  |
|   | Propylene carbonate                               |  |

Table A 2: Hansen solubility parameters, the scores given, relative energy distance (RED) and molar volume of the solvents used to test acrylic graffiti paint dissolution

| Solvent                              | $\delta_D$ | $\delta_P$ | $\delta_H$ | Score | RED    | Mvol  |
|--------------------------------------|------------|------------|------------|-------|--------|-------|
| Cyrene                               | 18.9       | 12.4       | 7.1        | 1     | 0.546  | 102.5 |
| <i>N</i> -Methyl-2-pyrrolidone (NMP) | 18         | 12.3       | 7.2        | 2     | 0.722  | 96.6  |
| Methylene chloride (DCM)             | 17         | 7.3        | 7.1        | 3     | 0.936* | 64.4  |
| <i>N,N'</i> -Dimethylacetamide       | 16.8       | 11.5       | 9.4        | 2     | 0.984  | 93    |
| Benzyl alcohol                       | 18.4       | 6.3        | 13.7       | 4     | 0.999* | 103.8 |
| Chlorobenzene                        | 19         | 4.3        | 2          | 3     | 1.005  | 102.1 |
| Dimethyl sulfoxide (DMSO)            | 18.4       | 16.4       | 10.2       | 2     | 1.014* | 71.3  |
| <i>N,N'</i> -Dimethylformamide (DMF) | 17.4       | 13.7       | 11.3       | 5     | 1.023  | 77.4  |
| Tetrahydrofuran (THF)                | 16.8       | 5.7        | 8          | 2     | 1.051* | 81.9  |
| Propylene carbonate                  | 20         | 18         | 4.1        | 4     | 1.071  | 85.2  |
| 2-Methylfuran                        | 17.3       | 2.8        | 7.4        | 4     | 1.155  | 89.7  |
| 1,1-Dichloroethane                   | 16.5       | 7.8        | 3          | 4     | 1.163  | 84.7  |
| Acetone                              | 15.5       | 10.4       | 7          | 3     | 1.247  | 73.8  |
| OME <sub>(3-5)</sub>                 | 15.6       | 7.1        | 6.1        | 3     | 1.269  | -     |
| Ethyl acetate                        | 15.8       | 5.3        | 7.2        | 3     | 1.283  | 98.6  |
| Toluene                              | 18         | 1.4        | 2          | 2     | 1.347* | 106.6 |
| 2-Pinene                             | 16.9       | 1.8        | 3.1        | 5     | 1.406  | 159   |
| Cyclohexene                          | 17.2       | 1          | 2          | 4     | 1.48   | 101.9 |
| 1-Butanol                            | 16         | 5.7        | 15.8       | 3     | 1.559  | 92    |
| 2,2,5,5-tetramethyloxolane (TMO)     | 15.6       | 2.3        | 2.4        | 4     | 1.618  | 159.9 |
| Acetonitrile                         | 15.3       | 18         | 6.1        | 3     | 1.625  | 52.9  |
| Propionic acid                       | 14.7       | 5.3        | 12.4       | 3     | 1.626  | 75    |
| 2-Propanol                           | 15.8       | 6.1        | 16.4       | 3     | 1.624  | 76.9  |
| $\alpha$ -pinene                     | 16.2       | 1          | 1.8        | 4     | 1.635  | 159   |
| Acetic acid                          | 14.5       | 8          | 13.5       | 4     | 1.648  | 57.6  |
| 1-Propanol                           | 16         | 6.8        | 17.4       | 4     | 1.651  | 75.1  |
| Diethyl ether                        | 14.5       | 2.9        | 4.6        | 4     | 1.717  | 104.7 |
| Ethanol                              | 15.8       | 8.8        | 19.4       | 3     | 1.824  | 58.6  |
| Heptane                              | 15.3       | 0          | 0          | 5     | 1.94   | 147   |
| Hexane                               | 14.9       | 0          | 0          | 5     | 2.003  | 131.4 |
| Methanol                             | 14.7       | 12.3       | 22.3       | 5     | 2.269  | 40.6  |
| Lactic acid                          | 17         | 8.3        | 28.4       | 5     | 2.614  | 73.8  |
| Water                                | 15.5       | 16         | 42.3       | 5     | 4.336  | 18    |

\* represents solvents wrongly positioned in or out of Hansen sphere.

Table A 3: Hansen solubility parameters, the scores given, relative energy distance (RED) and molar volume of the solvents used for the cellulose-based paint dissolution

| Solvent                              | $\delta_D$ | $\delta_P$ | $\delta_H$ | Score | RED    | MVol  |
|--------------------------------------|------------|------------|------------|-------|--------|-------|
| <i>N</i> -Methyl-2-pyrrolidone (NMP) | 18         | 12.3       | 7.2        | 1     | 0.422  | 96.6  |
| Cyrene                               | 18.9       | 12.4       | 7.1        | 1     | 0.528  | 102.5 |
| <i>N,N</i> -Dimethylacetamide        | 16.8       | 11.5       | 9.4        | 1     | 0.855  | 93    |
| Dimethyl sulfoxide (DMSO)            | 18.4       | 16.4       | 10.2       | 1     | 0.903  | 71.3  |
| Nitrobenzene                         | 20         | 10.6       | 3.1        | 5     | 0.981* | 102.7 |
| Propylene carbonate                  | 20         | 18         | 4.1        | 2     | 0.983  | 85.2  |
| Dimethylformamide (DMF)              | 17.4       | 13.7       | 11.3       | 5     | 0.988* | 77.4  |
| Acetone                              | 15.5       | 10.4       | 7          | 3     | 1.008  | 73.8  |
| Acetonitrile                         | 15.3       | 18         | 6.1        | 3     | 1.059  | 52.9  |
| Methylene dichloride (DCM)           | 17         | 7.3        | 7.1        | 5     | 1.176  | 64.4  |
| 1,1-Dichloroethane                   | 16.5       | 7.8        | 3          | 5     | 1.179  | 84.7  |
| OME <sub>(3-5)</sub>                 | 15.6       | 7.1        | 6.1        | 4     | 1.36   | 100   |
| Dimethyl carbonate                   | 15.5       | 8.6        | 9.7        | 3     | 1.376  | 84.7  |
| Fluorobenzene                        | 18.1       | 6.1        | 2          | 5     | 1.418  | 94.3  |
| Tetrahydrofuran (THF)                | 16.8       | 5.7        | 8          | 4     | 1.476  | 81.9  |
| Ethyl acetate                        | 15.8       | 5.3        | 7.2        | 3     | 1.611  | 98.6  |
| Chlorobenzene                        | 19         | 4.3        | 2          | 5     | 1.734  | 102.1 |
| Benzyl alcohol                       | 18.4       | 6.3        | 13.7       | 4     | 1.878  | 103.8 |
| 2-Methylfuran                        | 17.3       | 2.8        | 7.4        | 5     | 1.884  | 89.7  |
| Acetic acid                          | 14.5       | 8          | 13.5       | 2     | 1.991* | 57.6  |
| Propionic acid                       | 14.7       | 5.3        | 12.4       | 5     | 2.11   | 75    |
| 2,2,5,5-tetramethyloxolane (TMO)     | 15.6       | 2.3        | 2.4        | 5     | 2.117  | 159.9 |
| Diethyl ether                        | 14.5       | 2.9        | 4.6        | 5     | 2.134  | 104.7 |
| Toluene                              | 18         | 1.4        | 2          | 5     | 2.147  | 106.6 |
| Cyclohexene                          | 17.2       | 1          | 2          | 5     | 2.219  | 101.9 |
| 1-Butanol                            | 16         | 5.7        | 15.8       | 5     | 2.274  | 92    |
| 2-Propanol                           | 15.8       | 6.1        | 16.4       | 5     | 2.33   | 76.9  |
| Benzene                              | 18.4       | 0          | 2          | 5     | 2.376  | 89.5  |
| 1-Propanol                           | 16         | 6.8        | 17.4       | 5     | 2.383  | 75.1  |
| Ethanol                              | 15.8       | 8.8        | 19.4       | 5     | 2.548  | 58.6  |
| Heptane                              | 15.3       | 0          | 0          | 5     | 2.601  | 147   |
| Hexane                               | 14.9       | 0          | 0          | 5     | 2.646  | 131.4 |
| Methanol                             | 14.7       | 12.3       | 22.3       | 5     | 2.977  | 40.6  |
| Lactic acid                          | 17         | 8.3        | 28.4       | 5     | 3.905  | 73.8  |
| Water                                | 15.5       | 16         | 42.3       | 5     | 6.114  | 18    |

\* represents solvents wrongly positioned in or out of Hansen sphere.

Table A 4: Hansen solubility parameters, the scores given, relative energy distance (RED) and molar volume of neat solvents and Cyrene-water mixtures used to test acrylic graffiti paint dissolution

| Solvent                              | $\delta_D$ | $\delta_P$ | $\delta_H$ | Score | RED    | MVol  |
|--------------------------------------|------------|------------|------------|-------|--------|-------|
| Cyrene                               | 18.9       | 12.4       | 7.1        | 1     | 0.534  | 102.5 |
| <i>N</i> -Methyl-2-pyrrolidone (NMP) | 18         | 12.3       | 7.2        | 2     | 0.714  | 96.6  |
| Methylene dichloride (DCM)           | 17         | 7.3        | 7.1        | 3     | 0.942* | 64.4  |
| <i>N,N'</i> -Dimethylacetamide       | 16.8       | 11.5       | 9.4        | 2     | 0.979  | 93    |
| Dimethyl sulfoxide (DMSO)            | 18.4       | 16.4       | 10.2       | 2     | 0.998  | 71.3  |
| Benzyl alcohol                       | 18.4       | 6.3        | 13.7       | 4     | 1.008  | 103.8 |
| <i>N,N'</i> -Dimethylformamide (DMF) | 17.4       | 13.7       | 11.3       | 5     | 1.013  | 77.4  |
| Chlorobenzene                        | 19         | 4.3        | 2          | 3     | 1.018  | 102.1 |
| Propylene carbonate                  | 20         | 18         | 4.1        | 4     | 1.052  | 85.2  |
| Tetrahydrofuran (THF)                | 16.8       | 5.7        | 8          | 2     | 1.060* | 81.9  |
| 1,1-Dichloroethane                   | 16.5       | 7.8        | 3          | 4     | 1.167  | 84.7  |
| 2-Methylfuran                        | 17.3       | 2.8        | 7.4        | 4     | 1.17   | 89.7  |
| 75% Cyrene-25% H <sub>2</sub> O      | 18.1       | 13.3       | 15.9       | -     | 1.233  | 81.4  |
| Acetone                              | 15.5       | 10.4       | 7          | 3     | 1.245  | 73.8  |
| OME <sub>(3-5)</sub>                 | 15.6       | 7.1        | 6.1        | 3     | 1.274  | 100   |
| Ethyl acetate                        | 15.8       | 5.3        | 7.2        | 3     | 1.291  | 98.6  |
| Toluene                              | 18         | 1.4        | 2          | 2     | 1.362* | 106.6 |
| 2-Pinene                             | 16.9       | 1.8        | 3.1        | 5     | 1.42   | 159   |
| Cyclohexene                          | 17.2       | 1          | 2          | 4     | 1.494  | 101.9 |
| 1-Butanol                            | 16         | 5.7        | 15.8       | 3     | 1.565  | 92    |
| Acetonitrile                         | 15.3       | 18         | 6.1        | 3     | 1.612  | 52.9  |
| TMO                                  | 15.6       | 2.3        | 2.4        | 4     | 1.628  | 159.9 |
| 2-Propanol                           | 15.8       | 6.1        | 16.4       | 3     | 1.629  | 76.9  |
| Propionic acid                       | 14.7       | 5.3        | 12.4       | 3     | 1.632  | 75    |
| Beta Pinene                          | 16.2       | 1          | 1.8        | 4     | 1.648  | 100   |
| Acetic acid                          | 14.5       | 8          | 13.5       | 4     | 1.65   | 57.6  |
| 1-Propanol                           | 16         | 6.8        | 17.4       | 4     | 1.655  | 75.1  |
| Diethyl ether                        | 14.5       | 2.9        | 4.6        | 4     | 1.727  | 104.7 |
| Ethanol                              | 15.8       | 8.8        | 19.4       | 3     | 1.825  | 58.6  |
| Heptane                              | 15.3       | 0          | 0          | 5     | 1.951  | 147   |
| Hexane                               | 14.9       | 0          | 0          | 5     | 2.015  | 131.4 |
| 50% Cyrene-50% H <sub>2</sub> O      | 17.2       | 14.2       | 24.7       | -     | 2.244  | 60.3  |
| Methanol                             | 14.7       | 12.3       | 22.3       | 5     | 2.266  | 40.6  |
| Lactic acid                          | 17         | 8.3        | 28.4       | 5     | 2.615  | 73.8  |
| 25% Cyrene-75% H <sub>2</sub> O      | 16.4       | 15.1       | 33.5       | -     | 3.279  | 39.1  |
| Water                                | 15.5       | 16         | 42.3       | 5     | 4.332  | 18    |

\* represents solvents wrongly positioned in or out of Hansen sphere.



Table A 5: Hansen solubility parameters, the scores given, relative energy distance (RED) and molar volume of neat solvents and Cyrene-water mixtures used to test cellulose-based graffiti paint dissolution

| Solvent                              | $\delta_D$ | $\delta_P$ | $\delta_H$ | Score | RED    | MVol  |
|--------------------------------------|------------|------------|------------|-------|--------|-------|
| <i>N</i> -Methyl-2-pyrrolidone (NMP) | 18         | 12.3       | 7.2        | 1     | 0.464  | 96.6  |
| Cyrene                               | 18.9       | 12.4       | 7.1        | 1     | 0.595  | 102.5 |
| <i>N,N'</i> -Dimethylacetamide       | 16.8       | 11.5       | 9.4        | 1     | 0.861  | 93    |
| Dimethyl sulfoxide (DMSO)            | 18.4       | 16.4       | 10.2       | 1     | 0.936  | 71.3  |
| Acetone                              | 15.5       | 10.4       | 7          | 3     | 0.977* | 73.8  |
| Acetonitrile                         | 15.3       | 18         | 6.1        | 3     | 1.003  | 52.9  |
| <i>N,N'</i> -Dimethylformamide (DMF) | 17.4       | 13.7       | 11.3       | 5     | 1.009  | 77.4  |
| Propylene carbonate                  | 20         | 18         | 4.1        | 2     | 1.017* | 85.2  |
| Nitrobenzene                         | 20         | 10.6       | 3.1        | 5     | 1.028  | 102.7 |
| 1,1-Dichloroethane                   | 16.5       | 7.8        | 3          | 5     | 1.161  | 84.7  |
| Methylene dichloride (DCM)           | 17         | 7.3        | 7.1        | 5     | 1.184  | 64.4  |
| OME <sub>(3-5)</sub>                 | 15.6       | 7.1        | 6.1        | 4     | 1.342  | 100   |
| Dimethyl Carbonate                   | 15.5       | 8.6        | 9.7        | 3     | 1.365  | 84.7  |
| Fluorobenzene                        | 18.1       | 6.1        | 2          | 5     | 1.427  | 94.3  |
| Tetrahydrofuran (THF)                | 16.8       | 5.7        | 8          | 4     | 1.485  | 81.9  |
| Ethyl acetate                        | 15.8       | 5.3        | 7.2        | 3     | 1.604  | 98.6  |
| Chlorobenzene                        | 19         | 4.3        | 2          | 5     | 1.755  | 102.1 |
| 75% Cyrene-25% H <sub>2</sub> O      | 18.1       | 13.3       | 15.9       | -     | 1.769  | 81.4  |
| 2-Methylfuran                        | 17.3       | 2.8        | 7.4        | 5     | 1.898  | 89.7  |
| Benzyl alcohol                       | 18.4       | 6.3        | 13.7       | 4     | 1.915  | 103.8 |
| Acetic acid                          | 14.5       | 8          | 13.5       | 2     | 1.982* | 57.6  |
| TMO                                  | 15.6       | 2.3        | 2.4        | 5     | 2.103  | 159.9 |
| Propionic acid                       | 14.7       | 5.3        | 12.4       | 5     | 2.104  | 75    |
| Diethyl ether                        | 14.5       | 2.9        | 4.6        | 5     | 2.112  | 104.7 |
| Toluene                              | 18         | 1.4        | 2          | 5     | 2.157  | 106.6 |
| Cyclohexene                          | 17.2       | 1          | 2          | 5     | 2.222  | 101.9 |
| 1-Butanol                            | 16         | 5.7        | 15.8       | 5     | 2.288  | 92    |
| 2-Propanol                           | 15.8       | 6.1        | 16.4       | 5     | 2.342  | 76.9  |
| Benzene                              | 18.4       | 0          | 2          | 5     | 2.39   | 89.5  |
| 1-Propanol                           | 16         | 6.8        | 17.4       | 5     | 2.398  | 75.1  |
| Ethanol                              | 15.8       | 8.8        | 19.4       | 5     | 2.562  | 58.6  |
| Heptane                              | 15.3       | 0          | 0          | 5     | 2.585  | 147   |
| Hexane                               | 14.9       | 0          | 0          | 5     | 2.627  | 131.4 |
| Methanol                             | 14.7       | 12.3       | 22.3       | 5     | 2.982  | 40.6  |
| 50% Cyrene-50% H <sub>2</sub> O      | 17.2       | 14.2       | 24.7       | -     | 3.203  | 60.3  |
| Lactic acid                          | 17         | 8.3        | 28.4       | 5     | 3.931  | 73.8  |
| 25% Cyrene-50% H <sub>2</sub> O      | 16.4       | 15.1       | 33.5       | -     | 4.663  | 39.1  |
| Water                                | 15.5       | 16         | 42.3       | 5     | 6.133  | 18    |

\* represents solvents wrongly positioned in or out of Hansen sphere.

Table A 6: Hansen solubility parameters, the scores given, relative energy distance (RED) and molar volume of the neat solvents used for Torlon AI10 dissolution

| Solvent                              | $\delta_D$ | $\delta_P$ | $\delta_H$ | Score | RED   | MVol  |
|--------------------------------------|------------|------------|------------|-------|-------|-------|
| Cyrene                               | 18.9       | 12.4       | 7.1        | 1     | 0.337 | 102.5 |
| Pyridine                             | 19         | 8.8        | 5.9        | 1     | 0.5   | 80.9  |
| <i>N</i> -Methyl-2-pyrrolidone (NMP) | 18         | 12.3       | 7.2        | 1     | 0.505 | 96.6  |
| <i>N,N'</i> -Dimethylacetamide       | 16.8       | 11.5       | 9.4        | 1     | 0.822 | 93    |
| <i>N,N'</i> -Dimethylformamide (DMF) | 17.4       | 13.7       | 11.3       | 1     | 0.899 | 77.4  |
| Dimethyl sulfate                     | 16.5       | 13         | 7          | 2     | 0.976 | 95.5  |
| Dimethyl sulfoxide (DMSO)            | 18.4       | 16.4       | 10.2       | 1     | 0.982 | 71.3  |
| Quinoline                            | 20.5       | 5.6        | 5.7        | 2     | 0.996 | 118.5 |
| Benzyl benzoate                      | 20         | 5.1        | 5.2        | 5     | 1.051 | 190.3 |
| Tetrahydrofuran (THF)                | 16.8       | 5.7        | 8          | 5     | 1.136 | 81.9  |
| Benzyl alcohol                       | 18.4       | 6.3        | 13.7       | 5     | 1.158 | 103.8 |
| Piperidine                           | 17.3       | 4.5        | 8.2        | 5     | 1.186 | 99.3  |
| Acetone                              | 15.5       | 10.4       | 7          | 5     | 1.225 | 73.8  |
| Dimethyl carbonate                   | 15.5       | 8.6        | 9.7        | 5     | 1.277 | 84.7  |
| Furfuryl alcohol                     | 17.4       | 7.6        | 15.1       | 5     | 1.343 | 87.1  |
| Chloroform                           | 17.8       | 3.1        | 5.7        | 5     | 1.374 | 80.5  |
| Ethyl acetate                        | 15.8       | 5.3        | 7.2        | 5     | 1.424 | 98.6  |
| 1-Hexanol                            | 15.9       | 5.8        | 12.5       | 5     | 1.501 | 125.2 |
| Acetonitrile                         | 15.3       | 18         | 6.1        | 5     | 1.742 | 52.9  |
| OME <sub>(3-5)</sub>                 | 15.6       | 7.1        | 6.1        | 5     | 1.768 | 100   |
| Acetic acid                          | 14.5       | 8          | 13.5       | 5     | 1.793 | 57.6  |
| Toluene                              | 18         | 1.4        | 2          | 5     | 1.84  | 106.6 |
| 1-Propanol                           | 16         | 6.8        | 17.4       | 3     | 1.9   | 75.1  |
| Cyclohexene                          | 17.2       | 1          | 2          | 5     | 1.963 | 101.9 |
| Diethyl ether                        | 14.5       | 2.9        | 4.6        | 5     | 2.058 | 104.7 |
| Ethanol                              | 15.8       | 8.8        | 19.4       | 5     | 2.113 | 58.6  |
| Heptane                              | 15.3       | 0          | 0          | 5     | 2.505 | 147   |
| Hexane                               | 14.9       | 0          | 0          | 5     | 2.571 | 131.4 |
| Methanol                             | 14.7       | 12.3       | 22.3       | 5     | 2.676 | 40.6  |
| Water                                | 15.5       | 16         | 42.3       | 5     | 5.598 | 18    |

Table A 7: Hansen solubility parameters, the scores given, relative energy distance (RED) and molar volume of the neat solvents and solvent systems used for Torlon AI10 dissolution

| Solvent/mixture solvents             | $\delta_D$ | $\delta_P$ | $\delta_H$ | Score | RED    | MVol  |
|--------------------------------------|------------|------------|------------|-------|--------|-------|
| Cyrene                               | 18.9       | 12.4       | 7.1        | 1     | 0.454  | 102.5 |
| 51% DMSO-49% Cyrene                  | 18.6       | 14.4       | 8.7        | 1     | 0.514  | 86.6  |
| 51% Propylene C-49% Cyrene           | 19.5       | 15.3       | 5.6        | 5     | 0.533* | 93.7  |
| <i>N</i> -Methyl-2-pyrrolidone (NMP) | 18         | 12.3       | 7.2        | 1     | 0.662  | 96.6  |
| Dimethyl sulfoxide (DMSO)            | 18.4       | 16.4       | 10.2       | 1     | 0.711  | 71.3  |
| Pyridine                             | 19         | 8.8        | 5.9        | 1     | 0.732  | 80.9  |
| 51% EC-49% Cyrene                    | 18.4       | 17.1       | 6.1        | 1     | 0.799  | 83.9  |
| <i>N,N'</i> -Dimethylformamide (DMF) | 17.4       | 13.7       | 11.3       | 1     | 0.86   | 77.4  |
| 51% Dimethyl C-49% Cyrene            | 17.2       | 10.5       | 8.4        | 5     | 0.892* | 93.4  |
| <i>N,N'</i> -Dimethylacetamide       | 16.8       | 11.5       | 9.4        | 1     | 0.959  | 93    |
| Quinoline                            | 20.5       | 5.6        | 5.7        | 2     | 0.994  | 118.5 |
| Dimethyl sulfate                     | 16.5       | 13         | 7          | 2     | 1.027* | 95.5  |
| 75% EC-25% Cyrene                    | 18.2       | 19.4       | 5.6        | 1     | 1.055* | 75.1  |
| 51% Diethyl C-49% Cyrene             | 17         | 9.3        | 5.3        | 5     | 1.078  | 112.3 |
| Benzyl benzoate                      | 20         | 5.1        | 5.2        | 5     | 1.084  | 190.3 |
| Benzyl alcohol                       | 18.4       | 6.3        | 13.7       | 5     | 1.185  | 103.8 |
| Tetrahydrofuran (THF)                | 16.8       | 5.7        | 8          | 5     | 1.309  | 81.9  |
| Acetone                              | 15.5       | 10.4       | 7          | 5     | 1.315  | 73.8  |
| Furfuryl alcohol                     | 17.4       | 7.6        | 15.1       | 5     | 1.32   | 87.1  |
| Piperidine                           | 17.3       | 4.5        | 8.2        | 5     | 1.338  | 99.3  |
| Dimethyl carbonate                   | 15.5       | 8.6        | 9.7        | 5     | 1.382  | 84.7  |
| Chloroform                           | 17.8       | 3.1        | 5.7        | 5     | 1.461  | 80.5  |
| Acetonitrile                         | 15.3       | 18         | 6.1        | 5     | 1.481  | 52.9  |
| Ethyl acetate                        | 15.8       | 5.3        | 7.2        | 5     | 1.537  | 98.6  |
| 1-Hexanol                            | 15.9       | 5.8        | 12.5       | 5     | 1.55   | 125.2 |
| Acetic Acid                          | 14.5       | 8          | 13.5       | 5     | 1.747  | 57.6  |
| 1-Propanol                           | 16         | 6.8        | 17.4       | 3     | 1.764  | 75.1  |
| Toluene                              | 18         | 1.4        | 2          | 5     | 1.784  | 106.6 |
| Ethanol                              | 15.8       | 8.8        | 19.4       | 5     | 1.876  | 58.6  |
| Cyclohexene                          | 17.2       | 1          | 2          | 5     | 1.904  | 101.9 |
| Diethyl ether                        | 14.5       | 2.9        | 4.6        | 5     | 2.03   | 104.7 |
| Methanol                             | 14.7       | 12.3       | 22.3       | 5     | 2.256  | 40.6  |
| Heptane                              | 15.3       | 0          | 0          | 5     | 2.346  | 147   |
| Hexane                               | 14.9       | 0          | 0          | 5     | 2.404  | 131.4 |
| Water                                | 15.5       | 16         | 42.3       | 5     | 4.418  | 18    |

\* solvents wrongly positioned inside the Hansen sphere.

Table A 8: Solvents employed in the extraction of hesperidin and rutin and their classification according to Chem21 green solvent guide.<sup>38</sup>

| Solvents' polarity       |             |                           |                      |
|--------------------------|-------------|---------------------------|----------------------|
| Polar protic             |             | Polar aprotic             | Non-polar            |
| Butanol (BuOH)           |             | Ethyl acetate             | Cyclohexane          |
| Ethanol (EtOH)           |             | Methyl ethyl ketone (MEK) | Heptane              |
| Methanol (MeOH)          |             | Cyrene                    | <i>d</i> -Limonene   |
| 2-Propanol               |             | Acetonitrile (MeCN)       | Toluene              |
| Water (H <sub>2</sub> O) |             | Dimethyl sulfoxide (DMSO) | $\alpha$ -Pinene     |
| Acetic acid              |             | Methylene chloride (DCM)  | Hexane               |
| Acetic anhydride         |             | Tetrahydrofuran (THF)     | 1,4-Dioxana          |
| Ethylene glycol (EG)     |             | Acetone                   | Carbon tetrachloride |
| Formic acid              |             | Dimethylacetamide (DMAc)  | Chloroform           |
|                          |             | Dimethylformamide (DMF)   | Diethyl ether        |
|                          |             |                           | Benzene              |
| Recommended              | Problematic | Hazardous                 | Highly hazardous     |

Table A 9: Hansen solubility parameters, the scores given, relative energy distance (RED) and molar volume of the solvents used to test hesperidin dissolution

| Solvent                               | $\delta_D$ | $\delta_P$ | $\delta_H$ | Score | RED    | MVol  |
|---------------------------------------|------------|------------|------------|-------|--------|-------|
| Dimethyl sulfoxide (DMSO)             | 18.4       | 16.4       | 10.2       | 1     | 0.713  | 71.3  |
| <i>N,N'</i> -Dimethylformamide (DMF)  | 17.4       | 13.7       | 11.3       | 1     | 0.778  | 77.4  |
| Methanol                              | 14.7       | 12.3       | 22.3       | 2     | 0.891  | 40.6  |
| Acetic anhydride                      | 16         | 11.7       | 10.2       | 5     | 0.979* | 95    |
| Acetonitrile                          | 15.3       | 18         | 6.1        | 5     | 1      | 52.9  |
| <i>N,N'</i> -Dimethylacetamide (DMAc) | 16.8       | 11.5       | 9.4        | 1     | 1.005* | 93    |
| Ethylene glycol                       | 17         | 11         | 26         | 1     | 1.008* | 55.9  |
| Ethanol                               | 15.8       | 8.8        | 19.4       | 5     | 1.009  | 58.6  |
| Formic acid                           | 14.6       | 10         | 14         | 1     | 1.030* | 37.9  |
| Cyrene                                | 18.9       | 12.4       | 7.1        | 4     | 1.09   | 102.5 |
| Acetic acid                           | 14.5       | 8          | 13.5       | 5     | 1.178  | 57.6  |
| 2-Propanol                            | 15.8       | 6.1        | 16.4       | 5     | 1.206  | 76.9  |
| Acetone                               | 15.5       | 10.4       | 7          | 5     | 1.225  | 73.8  |
| 1-Butanol                             | 16         | 5.7        | 15.8       | 5     | 1.234  | 92    |
| Methylene chloride (DCM)              | 17         | 7.3        | 7.1        | 5     | 1.358  | 64.4  |
| Methyl ethyl ketone (MEK)             | 16         | 9          | 5.1        | 5     | 1.381  | 90.2  |
| Tetrahydrofuran (THF)                 | 16.8       | 5.7        | 8          | 3     | 1.421  | 81.9  |
| Ethyl acetate                         | 15.8       | 5.3        | 7.2        | 5     | 1.5    | 98.6  |
| 1,4-Dioxane                           | 17.5       | 1.8        | 9          | 4     | 1.64   | 85.7  |
| Chloroform                            | 17.8       | 3.1        | 5.7        | 5     | 1.676  | 80.5  |
| Diethyl ether                         | 14.5       | 2.9        | 4.6        | 5     | 1.799  | 104.7 |
| <i>d</i> -Limonene                    | 17.2       | 1.8        | 4.3        | 5     | 1.818  | 162.9 |
| $\alpha$ -Pinene                      | 16.9       | 1.8        | 3.1        | 5     | 1.873  | 159   |
| Water                                 | 15.5       | 16         | 42.3       | 5     | 1.919  | 18    |
| Toluene                               | 18         | 1.4        | 2          | 5     | 1.946  | 106.6 |
| Benzene                               | 18.4       | 0          | 2          | 4     | 2.032  | 89.5  |
| Carbon tetrachloride                  | 17.8       | 0          | 0.6        | 5     | 2.094  | 97.1  |
| Cyclohexane                           | 16.8       | 0          | 0.2        | 5     | 2.117  | 108.9 |
| Heptane                               | 15.3       | 0          | 0          | 5     | 2.152  | 147   |
| Hexane                                | 14.9       | 0          | 0          | 5     | 2.163  | 131.4 |

\* solvents wrongly positioned inside the Hansen sphere.

Table A 10: Hansen solubility parameters, the scores given, relative energy distance (RED) and molar volume of the solvents used to test the dissolution of rutin

| Solvent                               | $\delta_D$ | $\delta_P$ | $\delta_H$ | Score | RED    | MVol  |
|---------------------------------------|------------|------------|------------|-------|--------|-------|
| <i>N,N'</i> -Dimethylformamide (DMF)  | 17.4       | 13.7       | 11.3       | 1     | 0.768  | 77.4  |
| Dimethyl sulfoxide (DMSO)             | 18.4       | 16.4       | 10.2       | 1     | 0.795  | 71.3  |
| Ethanol                               | 15.8       | 8.8        | 19.4       | 1     | 0.864  | 58.6  |
| Ethylene glycol                       | 17         | 11         | 26         | 1     | 0.886  | 55.9  |
| <i>N,N'</i> -Dimethylacetamide (DMAc) | 16.8       | 11.5       | 9.4        | 1     | 0.972  | 93    |
| Cyrene                                | 18.9       | 12.4       | 7.1        | 1     | 0.98   | 102.5 |
| 2-Propanol                            | 15.8       | 6.1        | 16.4       | 5     | 0.998* | 76.9  |
| 1-Butanol                             | 16         | 5.7        | 15.8       | 2     | 1.004* | 92    |
| Acetic anhydride                      | 16         | 11.7       | 10.2       | 5     | 1.01   | 95    |
| Methanol                              | 14.7       | 12.3       | 22.3       | 1     | 1.013* | 40.6  |
| Formic acid                           | 14.6       | 10         | 14         | 5     | 1.072  | 37.9  |
| Acetic acid                           | 14.5       | 8          | 13.5       | 5     | 1.159  | 57.6  |
| Methylene chloride (DCM)              | 17         | 7.3        | 7.1        | 5     | 1.217  | 64.4  |
| Tetrahydrofuran (THF)                 | 16.8       | 5.7        | 8          | 5     | 1.242  | 81.9  |
| Acetone                               | 15.5       | 10.4       | 7          | 5     | 1.281  | 73.8  |
| 1,4-Dioxane                           | 17.5       | 1.8        | 9          | 5     | 1.349  | 85.7  |
| Methyl ethyl ketone (MEK)             | 16         | 9          | 5.1        | 5     | 1.386  | 90.2  |
| Acetonitrile                          | 15.3       | 18         | 6.1        | 5     | 1.389  | 52.9  |
| Ethyl acetate                         | 15.8       | 5.3        | 7.2        | 5     | 1.393  | 98.6  |
| Chloroform                            | 17.8       | 3.1        | 5.7        | 5     | 1.444  | 80.5  |
| <i>d</i> -Limonene                    | 17.2       | 1.8        | 4.3        | 5     | 1.63   | 162.9 |
| $\alpha$ -Pinene                      | 16.9       | 1.8        | 3.1        | 5     | 1.721  | 159   |
| Toluene                               | 18         | 1.4        | 2          | 5     | 1.76   | 106.6 |
| Diethyl ether                         | 14.5       | 2.9        | 4.6        | 5     | 1.764  | 104.7 |
| Benzene                               | 18.4       | 0          | 2          | 5     | 1.819  | 89.5  |
| Carbon tetrachloride                  | 17.8       | 0          | 0.6        | 5     | 1.93   | 97.1  |
| Cyclohexane                           | 16.8       | 0          | 0.2        | 5     | 2      | 108.9 |
| Heptane                               | 15.3       | 0          | 0          | 5     | 2.102  | 147   |
| Hexane                                | 14.9       | 0          | 0          | 5     | 2.13   | 131.4 |
| Water                                 | 15.5       | 16         | 42.3       | 5     | 2.203  | 18    |

\* represents solvents wrongly positioned in or out of Hansen sphere.

Table A 11: Binary mixtures and their optimised Ra and composition for hesperidin and rutin

| Hesperidin                     |                |                     | Rutin                          |                |                     |
|--------------------------------|----------------|---------------------|--------------------------------|----------------|---------------------|
| Binary mixtures                | R <sub>a</sub> | Composition (A%/B%) | Binary mixtures                | R <sub>a</sub> | Composition (A%/B%) |
| DMSO/H <sub>2</sub> O          | 4.97           | 76/24               | Cyrene/H <sub>2</sub> O        | 4.87           | 70/30               |
| DMSO/Ethylene glycol (EG)      | 7.2            | 62/38               | DMSO/EG                        | 5.17           | 54/46               |
| MeOH/DMSO                      | 7.48           | 57/43               | EG/Cyrene                      | 5.28           | 53/47               |
| Cyrene/H <sub>2</sub> O        | 7.7            | 70/33               | DMSO/H <sub>2</sub> O          | 5.89           | 78/22               |
| DMSO/EtOH                      | 9.01           | 56/44               | DMSO/EtOH                      | 7.32           | 55/45               |
| MeOH/Cyrene                    | 9.38           | 74/26               | DMSO/MeOH                      | 7.60           | 62/38               |
| EG/Cyrene                      | 9.65           | 56/44               | Cyrene/MeOH                    | 7.95           | 51/49               |
| DMSO/Acetone                   | 9.68           | 96/4                | EG/MEK                         | 7.96           | 68/32               |
| Acetone/H <sub>2</sub> O       | 9.75           | 69/31               | EG/Acetone                     | 8.18           | 66/34               |
| MEK/H <sub>2</sub> O           | 10/13          | 64/36               | EtOH/Cyrene                    | 8.22           | 57/43               |
| DMSO/Acetic acid               | 10.42          | 62/38               | EG/d- Limonene                 | 8.39           | 74/26               |
| MeOH/Acetone                   | 10.56          | 72/28               | EG/Ethyl acetate               | 8.69           | 71/29               |
| MeOH/MEK                       | 10.68          | 79/21               | MEK/H <sub>2</sub> O           | 9.17           | 64/36               |
| EG/Acetone                     | 10.83          | 50/50               | DMSO/Acetic acid               | 9.23           | 85/15               |
| MeOH/d-Limonene                | 11.12          | 97/3                | EG/Acetic acid                 | 9.63           | 71/29               |
| MeOH/Ethyl acetate             | 11.13          | 91/9                | EtOH/EG                        | 9.64           | 54/46               |
| EG/MEK                         | 11.13          | 59/41               | Acetone/H <sub>2</sub> O       | 9.68           | 67/33               |
| MeOH/Acetic acid               | 11.27          | 85/15               | d- Limonene/H <sub>2</sub> O   | 9.73           | 59/41               |
| EtOH/Cyrene                    | 11.68          | 73/27               | EtOH/MEK                       | 10.11          | 90/10               |
| EG/Ethyl acetate               | 12.31          | 66/34               | EtOH/Acetone                   | 10.13          | 90/10               |
| Acetic acid/EG                 | 12.53          | 60/40               | EtOH/d-Limonene                | 10.20          | 97/3                |
| Ethyl Acetate/H <sub>2</sub> O | 12.54          | 63/37               | EtOH/H <sub>2</sub> O          | 10.21          | 99/1                |
| EG/d-Limonene                  | 12.57          | 80/20               | Ethyl acetate/H <sub>2</sub> O | 10.30          | 65/35               |
| EtOH/Acetone                   | 12.61          | 67/33               | EG/MeOH                        | 10.44          | 96/4                |
| EtOH/H <sub>2</sub> O          | 11.74          | 96/04               | EG/H <sub>2</sub> O            | 10.45          | 99/1                |
| Acetic Acid/H <sub>2</sub> O   | 12.71          | 79/21               | MeOH/d-Limonene                | 10.67          | 75/25               |
| EtOH/MEK                       | 12.77          | 82/18               | MeOH/MEK                       | 10.71          | 70/30               |
| EtOH/EG                        | 12.78          | 98/2                | MeOH/Acetone                   | 10.88          | 68/32               |
| EtOH/Acetic acid               | 13.23          | 68/32               | Cyrene/Acetic acid             | 11.03          | 69/31               |
| d-Limonene/H <sub>2</sub> O    | 13.5           | 54/46               | MeOH/Ethyl acetate             | 11.05          | 73/27               |
| Cyrene/Ethyl acetate           | 13.53          | 97/3                | EtOH/Ethyl acetate             | 11.66          | 57/43               |
| Acetic Acid/Cyrene             | 14.11          | 78/22               | MeOH/Acetic acid               | 11.67          | 73/27               |
| Acetic acid/Acetone            | 14.98          | 87/13               | Acetic acid/H <sub>2</sub> O   | 11.87          | 77/23               |
| Acetone/Cyrene                 | 15.62          | 90/10               | Acetic acid/Acetone            | 13.69          | 90/10               |
|                                |                |                     | MEK/Ethyl acetate              | 16.29          | 58/42               |

Table A 12: Tertiary mixtures with Cyrene and their optimised R<sub>a</sub> and composition

| Hesperidin                          |                |                        | Rutin             |                |                        |
|-------------------------------------|----------------|------------------------|-------------------|----------------|------------------------|
| Tertiary mixtures                   | R <sub>a</sub> | Composition (A%/B%/C%) | Tertiary mixtures | R <sub>a</sub> | Composition (A%/B%/C%) |
| Acetone/H <sub>2</sub> O/Cyrene     | 8.33           | 68/31/1                | EC/DMSO/Cyrene    | 5.10           | 48/34/18               |
| MeOH/Cyrene/Acetone                 | 8.37           | 72/18/10               | DMSO/MeOH/Cyrene  | 7.60           | 58/38/4                |
| MEK/H <sub>2</sub> O/Cyrene         | 9.09           | 44/35/21               |                   |                |                        |
| Cyrene/H <sub>2</sub> O/Acetic acid | 9.37           | 49/29/22               |                   |                |                        |
| Ethylene/Cyrene/Acetic acid         | 10.73          | 44/29/27               |                   |                |                        |
| Ethylene/MEK/Cyrene                 | 10.81          | 57/26/17               |                   |                |                        |
| Ethylene/Cyrene/EtOH                | 10.96          | 45/40/15               |                   |                |                        |
| EtOH/Acetone/Cyrene                 | 11.18          | 67/26/7                |                   |                |                        |



Table A 13: Hansen solubility parameters, the scores given and relative energy distance (RED) of the pure solvents, mixtures, and Cyrene's geminal diol used to test the dissolution of hesperidin

| Solvent/mixture solvents                        | $\delta_D$ | $\delta_P$ | $\delta_H$ | Score | RED    |
|---|------------|------------|------------|-------|--------|
| 62% DMSO-38% Ethylene glycol (EG)               | 17.9       | 14.4       | 16.2       | 1     | 0.548  |
| Dimethyl sulfoxide (DMSO)                       | 18.4       | 16.4       | 10.2       | 1     | 0.599  |
| 56% DMSO-44% EtOH                               | 17.3       | 13.1       | 14.2       | 1     | 0.641  |
| 43% DMSO-57% MeOH                               | 16.3       | 14.1       | 17.1       | 1     | 0.645  |
| <i>N,N'</i> -Dimethylformamide (DMF)            | 17.4       | 13.7       | 11.3       | 1     | 0.673  |
| 70% Cyrene-30% H <sub>2</sub> O                 | 17.9       | 13.5       | 17.7       | 2     | 0.708  |
| 50% Cyrene-20% H <sub>2</sub> O-30% EtOH        | 17.3       | 12         | 17.8       | 3     | 0.848* |
| 49% Cyrene-22% Acetic acid-29% H <sub>2</sub> O | 16.9       | 12.4       | 18.6       | 3     | 0.857* |
| 21% Cyrene-35% H <sub>2</sub> O-44% MEK         | 16.4       | 12.1       | 18.5       | 5     | 0.898* |
| 50% Cyrene-50% EtOH                             | 17.4       | 10.6       | 13.3       | 1     | 0.927  |
| 31% H <sub>2</sub> O-69% Acetone                | 15.5       | 12.2       | 18.1       | 5     | 0.934* |
| 70% Cyrene-30% EtOH                             | 18         | 11.3       | 10.8       | 1     | 0.946  |
| Acetic anhydride                                | 16         | 11.7       | 10.2       | 5     | 0.971* |
| Cyrene's geminal diol                           | 19.4       | 11.2       | 15.9       | 1     | 0.983  |
| 64% MEK-36% H <sub>2</sub> O                    | 15.8       | 11.6       | 18.6       | 5     | 0.987* |
| <i>N,N'</i> -Dimethylacetamide                  | 16.8       | 11.5       | 9.4        | 1     | 0.999  |
| 30% Cyrene-70% EtOH                             | 16.7       | 9.9        | 15.7       | 1     | 1.014* |
| 72% MeOH-28% Acetone                            | 14.9       | 11.8       | 18         | 1     | 1.027* |
| Acetonitrile                                    | 15.3       | 18         | 6.1        | 5     | 1.035  |
| 79% MeOH-21% MEK                                | 15         | 11.6       | 18.7       | 3     | 1.065  |
| 20% Cyrene-70% EtOH-10% H <sub>2</sub> O        | 16.4       | 10.2       | 19.2       | 5     | 1.115  |
| Cyrene  | 18.9       | 12.4       | 7.1        | 4     | 1.145  |
| Formic acid                                     | 14.6       | 10         | 14         | 1     | 1.155* |
| 20% Cyrene-60% EtOH-20% H <sub>2</sub> O        | 16.4       | 11         | 21.5       | 4     | 1.189  |
| 50% Cyrene-50% H <sub>2</sub> O                 | 17.2       | 14.2       | 24.7       | 5     | 1.25   |
| Methanol (MeOH)                                 | 14.7       | 12.3       | 22.3       | 2     | 1.275* |
| Ethanol (EtOH)                                  | 15.8       | 8.8        | 19.4       | 5     | 1.289  |
| Acetone   | 15.5       | 10.4       | 7          | 5     | 1.316  |
| 20% Cyrene-50% EtOH-30% H <sub>2</sub> O        | 16.3       | 11.7       | 23.8       | 4     | 1.326  |
| Acetic acid                                     | 14.5       | 8          | 13.5       | 5     | 1.363  |
| 2-Propanol                                      | 15.8       | 6.1        | 16.4       | 5     | 1.473  |
| 1-Butanol                                       | 16         | 5.7        | 15.8       | 5     | 1.498  |
| Methylene chloride (DCM)                        | 17         | 7.3        | 7.1        | 5     | 1.525  |
| Methyl ethyl ketone (MEK)                       | 16         | 9          | 5.1        | 5     | 1.539  |
| Ethylene glycol (EG)                            | 17         | 11         | 26         | 1     | 1.552* |
| 70% EtOH-30% H <sub>2</sub> O                   | 15.7       | 11         | 26.3       | 5     | 1.618  |
| Tetrahydrofuran (THF)                           | 16.8       | 5.7        | 8          | 3     | 1.633  |
| Ethyl acetate                                   | 15.8       | 5.3        | 7.2        | 5     | 1.742  |
| 30% Cyrene-70% H <sub>2</sub> O                 | 16.5       | 14.9       | 31.7       | 5     | 1.973  |
| 1,4-Dioxane                                     | 17.5       | 1.8        | 9          | 4     | 1.991  |
| 50% EtOH-50% H <sub>2</sub> O                   | 15.7       | 12.4       | 30.9       | 4     | 1.994  |
| Chloroform                                      | 17.8       | 3.1        | 5.7        | 5     | 2.007  |
| Diethyl ether                                   | 14.5       | 2.9        | 4.6        | 5     | 2.176  |

|                               |      |      |      |   |       |
|-------------------------------|------|------|------|---|-------|
| <i>d</i> -Limonene            | 17.2 | 1.8  | 4.3  | 5 | 2.207 |
| 2-Pinene                      | 16.9 | 1.8  | 3.1  | 5 | 2.28  |
| Toluene                       | 18   | 1.4  | 2    | 5 | 2.389 |
| 30% EtOH-70% H <sub>2</sub> O | 15.6 | 13.8 | 35.4 | 5 | 2.423 |
| Benzene                       | 18.4 | 0    | 2    | 4 | 2.524 |
| Carbon tetrachloride          | 17.8 | 0    | 0.6  | 5 | 2.603 |
| Cyclohexane                   | 16.8 | 0    | 0.2  | 5 | 2.63  |
| Heptane                       | 15.3 | 0    | 0    | 5 | 2.678 |
| Hexane                        | 14.9 | 0    | 0    | 5 | 2.695 |
| Water                         | 15.5 | 16   | 42.3 | 5 | 3.135 |

\* represents solvents wrongly positioned in or out of Hansen sphere.

Table A 14: Hansen solubility parameters, the scores given and relative energy distance of the pure solvents, mixtures, and Cyrene's geminal diol used to test the dissolution of rutin

| Solvent/mixture solvents             | $\delta_D$ | $\delta_P$ | $\delta_H$ | Score | RED    |
|--------------------------------------|------------|------------|------------|-------|--------|
| 70% Cyrene-30% H <sub>2</sub> O      | 17.9       | 13.5       | 17.7       | 1     | 0.105  |
| 33% DMSO-48% EG-19% Cyrene           | 17.8       | 13.1       | 17.3       | 1     | 0.129  |
| 46% EG-54% DMSO                      | 17.8       | 13.9       | 17.5       | 1     | 0.149  |
| 47% Cyrene-53% EG                    | 17.9       | 11.7       | 17.2       | 1     | 0.195  |
| Cyrene's geminal diol                | 19.4       | 11.2       | 15.9       | 1     | 0.381  |
| 43% DMSO-57% EtOH                    | 16.9       | 12         | 15.5       | 1     | 0.424  |
| 49% MeOH-51% Cyrene                  | 16.9       | 12.4       | 14.5       | 1     | 0.489  |
| 62% DMSO-38% MeOH                    | 17         | 14.9       | 14.7       | 1     | 0.493  |
| 34% Acetone-66% EG                   | 16.5       | 10.8       | 19.6       | 1     | 0.523  |
| 57% EtOH-43% Cyrene                  | 17.1       | 10.3       | 14.2       | 1     | 0.575  |
| 26% Limonene-74% EG                  | 17.1       | 8.6        | 20.3       | 1     | 0.637  |
| 70% EG-30% Ethyl acetate             | 16.6       | 9.3        | 20.5       | 1     | 0.648  |
| <i>N,N'</i> -Dimethylformamide (DMF) | 17.4       | 13.7       | 11.3       | 1     | 0.751  |
| Ethanol (EtOH)                       | 15.8       | 8.8        | 19.4       | 1     | 0.761  |
| 50% H <sub>2</sub> O-50% Cyrene      | 17.2       | 14.2       | 24.7       | 4     | 0.819* |
| Dimethyl sulfoxide (DMSO)            | 18.4       | 16.4       | 10.2       | 1     | 0.917  |
| Methanol (MeOH)                      | 14.7       | 12.3       | 22.3       | 1     | 0.955  |
| 2-Propanol                           | 15.8       | 6.1        | 16.4       | 5     | 0.973* |
| Ethylene glycol (EG)                 | 17         | 11         | 26         | 1     | 0.99   |
| Formic acid                          | 14.6       | 10         | 14         | 5     | 0.991* |
| 1-Butanol                            | 16         | 5.7        | 15.8       | 2     | 0.998  |
| Acetic Anhydride                     | 16         | 11.7       | 10.2       | 5     | 1      |
| <i>N,N'</i> -Dimethylacetamide       | 16.8       | 11.5       | 9.4        | 1     | 1.006* |
| Acetic acid                          | 14.5       | 8          | 13.5       | 5     | 1.128  |
| 70% EtOH-30% H <sub>2</sub> O        | 15.7       | 11         | 26.3       | 2     | 1.138* |
| Cyrene                               | 18.9       | 12.4       | 7.1        | 2     | 1.195* |
| Methylene chloride (DCM)             | 17         | 7.3        | 7.1        | 5     | 1.382  |
| Acetone                              | 15.5       | 10.4       | 7          | 5     | 1.385  |
| Tetrahydrofuran (THF)                | 16.8       | 5.7        | 8          | 5     | 1.405  |
| Acetonitrile                         | 15.3       | 18         | 6.1        | 5     | 1.558  |
| Ethyl acetate                        | 15.8       | 5.3        | 7.2        | 5     | 1.565  |
| Methyl ethyl ketone (MEK)            | 16         | 9          | 5.1        | 5     | 1.568  |
| 50% EtOH-50% H <sub>2</sub> O        | 15.7       | 12.4       | 30.9       | 2     | 1.574* |
| 1,4-Dioxane                          | 17.5       | 1.8        | 9          | 5     | 1.602  |
| 30% Cyrene-70% H <sub>2</sub> O      | 16.5       | 14.9       | 31.7       | 5     | 1.613  |
| Chloroform                           | 17.8       | 3.1        | 5.7        | 5     | 1.747  |
| <i>d</i> -Limonene                   | 17.2       | 1.8        | 4.3        | 5     | 1.971  |
| Diethyl ether                        | 14.5       | 2.9        | 4.6        | 5     | 2.038  |
| 30% EtOH-70% H <sub>2</sub> O        | 15.6       | 13.8       | 35.4       | 4     | 2.052  |
| $\alpha$ -Pinene                     | 16.9       | 1.8        | 3.1        | 5     | 2.083  |
| Toluene                              | 18         | 1.4        | 2          | 5     | 2.184  |
| Benzene                              | 18.4       | 0          | 2          | 5     | 2.279  |
| Carbon tetrachloride                 | 17.8       | 0          | 0.6        | 5     | 2.404  |

---

|             |      |    |      |   |       |
|-------------|------|----|------|---|-------|
| Cyclohexane | 16.8 | 0  | 0.2  | 5 | 2.46  |
| Heptane     | 15.3 | 0  | 0    | 5 | 2.545 |
| Hexane      | 14.9 | 0  | 0    | 5 | 2.57  |
| Water       | 15.5 | 16 | 42.3 | 5 | 2.816 |

---

*\* represents solvents wrongly positioned in or out of Hansen sphere.*

Table A 15: Hansen solubility parameters, the scores given and relative energy distance (RED) of the pure solvents, mixtures, Cyrene's geminal diol and ternary Cyrene/geminal diol/water mixtures used to test the dissolution of hesperidin

| Solvent/mixture solvents   | $\delta_D$ | $\delta_P$ | $\delta_H$ | Score | RED    |
|--|------------|------------|------------|-------|--------|
| 62% DMSO-38% Ethylene glycol   | 17.9       | 14.4       | 16.2       | 1     | 0.783  |
| Dimethyl sulfoxide (DMSO)  | 18.4       | 16.4       | 10.2       | 1     | 0.783  |
| 70% Cyrene-30% H <sub>2</sub> O  | 17.9       | 13.5       | 17.7       | 2     | 0.817  |
| 43% DMSO-57% MeOH  | 16.3       | 14.1       | 17.1       | 1     | 0.869  |
| 50% Cyrene-50% H <sub>2</sub> O  | 17.2       | 14.2       | 24.7       | 5     | 0.875* |
| 56% DMSO-44% EtOH  | 17.3       | 13.1       | 14.2       | 1     | 0.887  |
| Cyrene's geminal diol  | 19.4       | 11.2       | 15.9       | 1     | 0.896  |
| <i>N,N'</i> -Dimethylformamide (DMF)   | 17.4       | 13.7       | 11.3       | 1     | 0.905  |
| 49% Cyrene-22% Acetic acid-29% H <sub>2</sub> O                              | 16.9       | 12.4       | 18.6       | 3     | 0.910* |
| 50% Cyrene-20 % H <sub>2</sub> O-30% EtOH                                    | 17.3       | 12         | 17.8       | 3     | 0.912* |
| 21% Cyrene-35% H <sub>2</sub> O-44% MEK                                      | 16.4       | 12.1       | 18.5       | 5     | 0.948* |
| 31% H <sub>2</sub> O-69% Acetone   | 15.5       | 12.2       | 18.1       | 5     | 0.992* |
| 70% Cyrene-30% EtOH  | 18         | 11.3       | 10.8       | 1     | 0.997  |
| 64% MEK-36% H <sub>2</sub> O   | 15.8       | 11.6       | 18.6       | 5     | 1.001  |
| Acetonitrile   | 15.3       | 18         | 6.1        | 5     | 1.003  |
| 50% Cyrene-50% EtOH  | 17.4       | 10.6       | 13.3       | 1     | 1.008* |
| 20% Cyrene-60% EtOH-20% H <sub>2</sub> O                                     | 16.4       | 11         | 21.5       | 4     | 1.009  |
| 20% Cyrene-50% EtOH-30% H <sub>2</sub> O                                     | 16.3       | 11.7       | 23.8       | 4     | 1.009  |
| Cyrene   | 18.9       | 12.4       | 7.1        | 4     | 1.018  |
| 20% Cyrene-70% EtOH-10% H <sub>2</sub> O                                     | 16.4       | 10.2       | 19.2       | 5     | 1.034  |
| 30% Cyrene-70% EtOH  | 16.7       | 9.9        | 15.7       | 1     | 1.043* |
| 72% MeOH-28% Acetone   | 14.9       | 11.8       | 18         | 1     | 1.044* |
| Ethylene Glycol (EG)   | 17         | 11         | 26         | 1     | 1.044* |
| 79% MeOH-21% MEK   | 15         | 11.6       | 18.7       | 3     | 1.047  |
| Methanol (MeOH)  | 14.7       | 12.3       | 22.3       | 2     | 1.055* |
| New Geminal diol (GD) ternary mixture<br>for 70% Cyrene-30% H <sub>2</sub> O | 16.8       | 14.5       | 31.5       | 1     | 1.058* |
| <i>N,N'</i> -Dimethylacetamide   | 16.8       | 11.5       | 9.4        | 1     | 1.062* |
| 30% Cyrene-70% H <sub>2</sub> O  | 16.5       | 14.9       | 31.7       | 5     | 1.064  |
| Acetic anhydride   | 16         | 11.7       | 10.2       | 5     | 1.072  |
| 70% EtOH-30% H <sub>2</sub> O  | 15.7       | 11         | 26.3       | 5     | 1.108  |
| New GD ternary mixture for 50% Cyrene-<br>50% H <sub>2</sub> O               | 16.1       | 25.1       | 37.8       | 5     | 1.117  |
| Ethanol (MeOH)   | 15.8       | 8.8        | 19.4       | 5     | 1.126  |
| Formic acid  | 14.6       | 10         | 14         | 1     | 1.159* |
| 50% EtOH-50% H <sub>2</sub> O  | 15.7       | 12.4       | 30.9       | 4     | 1.162  |
| Acetone  | 15.5       | 10.4       | 7          | 5     | 1.218  |
| Acetic acid  | 14.5       | 8          | 13.5       | 5     | 1.253  |
| 2-Propanol   | 15.8       | 6.1        | 16.4       | 5     | 1.253  |
| 30% EtOH-70% H <sub>2</sub> O  | 15.6       | 13.8       | 35.4       | 5     | 1.263  |
| 1-Butanol  | 16         | 5.7        | 15.8       | 5     | 1.266  |
| Methylene chloride (DCM)   | 17         | 7.3        | 7.1        | 5     | 1.283  |

|  |      |      |      |   |       |
|--|------|------|------|---|-------|
| Methyl ethyl ketone (MEK)                                      | 16   | 9    | 5.1  | 5 | 1.299 |
| Tetrahydrofuran (THF)  | 16.8 | 5.7  | 8    | 3 | 1.339 |
| New GD ternary mixture for 30% Cyrene-<br>70% H <sub>2</sub> O | 15.8 | 15.6 | 40.2 | 5 | 1.389 |
| Ethyl acetate  | 15.8 | 5.3  | 7.2  | 5 | 1.408 |
| Chloroform   | 17.8 | 3.1  | 5.7  | 5 | 1.476 |
| Water  | 15.5 | 16   | 42.3 | 5 | 1.478 |
| 1,4-Dioxane  | 17.5 | 1.8  | 9    | 4 | 1.478 |
| <i>d</i> -Limonene   | 17.2 | 1.8  | 4.3  | 5 | 1.579 |
| $\alpha$ -Pinene   | 16.9 | 1.8  | 3.1  | 5 | 1.616 |
| Diethyl ether  | 14.5 | 2.9  | 4.6  | 5 | 1.616 |
| Toluene  | 18   | 1.4  | 2    | 5 | 1.636 |
| Benzene  | 18.4 | 0    | 2    | 4 | 1.69  |
| Carbon tetrachloride   | 17.8 | 0    | 0.6  | 5 | 1.737 |
| Cyclohexane  | 16.8 | 0    | 0.2  | 5 | 1.769 |
| Heptane  | 15.3 | 0    | 0    | 5 | 1.817 |
| Hexane   | 14.9 | 0    | 0    | 5 | 1.831 |

\* represents solvents wrongly positioned in or out of Hansen sphere.

Table A 16: Hansen solubility parameters, the scores given and relative energy distance (RED) of the pure solvents, mixtures, Cyrene's geminal diol and ternary Cyrene/geminal diol/water mixtures used to test the dissolution of rutin

| Solvent/mixture solvents                                       | $\delta_D$ | $\delta_P$ | $\delta_H$ | Score | RED    |
|--|------------|------------|------------|-------|--------|
| Cyrene's geminal diol  | 19.4       | 11.2       | 15.9       | 1     | 0.559  |
| 70% Cyrene-30% H <sub>2</sub> O                                | 17.9       | 13.5       | 17.7       | 1     | 0.66   |
| 46% EG-54% DMSO  | 17.8       | 13.9       | 17.5       | 1     | 0.674  |
| 33% DMSO-48% EG-19% Cyrene                                     | 17.8       | 13.1       | 17.3       | 1     | 0.678  |
| 47% Cyrene-53% EG  | 17.9       | 11.7       | 17.2       | 1     | 0.678  |
| 50% H <sub>2</sub> O-50% Cyrene                                | 17.2       | 14.2       | 24.7       | 4     | 0.754* |
| 26% Limonene-74% EG  | 17.1       | 8.6        | 20.3       | 1     | 0.784  |
| 43% DMSO-57% EtOH  | 16.9       | 12         | 15.5       | 1     | 0.812  |
| Ethylene glycol (EG)   | 17         | 11         | 26         | 1     | 0.814  |
| 62% DMSO-38% MeOH  | 17         | 14.9       | 14.7       | 1     | 0.816  |
| 34% Acetone-66% EG   | 16.5       | 10.8       | 19.6       | 1     | 0.816  |
| 70% EG-30% Ethyl acetate                                       | 16.6       | 9.3        | 20.5       | 1     | 0.824  |
| 49% MeOH-51% Cyrene  | 16.9       | 12.4       | 14.5       | 1     | 0.832  |
| 57% EtOH-43% Cyrene  | 17.1       | 10.3       | 14.2       | 1     | 0.838  |
| Dimethyl sulfoxide (DMSO)                                      | 18.4       | 16.4       | 10.2       | 1     | 0.844  |
| <i>N,N'</i> -Dimethylformamide (DMF)                           | 17.4       | 13.7       | 11.3       | 1     | 0.874  |
| Ethanol (EtOH)   | 15.8       | 8.8        | 19.4       | 1     | 0.921  |
| Cyrene   | 18.9       | 12.4       | 7.1        | 2     | 0.932  |
| 70% EtOH-30% H <sub>2</sub> O                                  | 15.7       | 11         | 26.3       | 2     | 0.955  |
| New GD ternary mixture for 70% Cyrene and 30% H <sub>2</sub> O | 16.8       | 14.5       | 31.5       | 1     | 0.979  |
| <i>N,N'</i> -Dimethylacetamide (DMAc)                          | 16.8       | 11.5       | 9.4        | 1     | 1.001* |
| 1-Butanol  | 16         | 5.7        | 15.8       | 2     | 1.004* |
| 2-Propanol   | 15.8       | 6.1        | 16.4       | 5     | 1.005  |
| Methanol   | 14.7       | 12.3       | 22.3       | 1     | 1.008* |
| 30% Cyrene-70% H <sub>2</sub> O                                | 16.5       | 14.9       | 31.7       | 5     | 1.014  |
| Acetic anhydride   | 16         | 11.7       | 10.2       | 5     | 1.044  |
| 50% EtOH-50% H <sub>2</sub> O                                  | 15.7       | 12.4       | 30.9       | 2     | 1.062* |
| Formic acid  | 14.6       | 10         | 14         | 5     | 1.099  |
| Methylene dichloride (DCM)                                     | 17         | 7.3        | 7.1        | 5     | 1.125  |
| Tetrahydrofuran (THF)  | 16.8       | 5.7        | 8          | 5     | 1.139  |
| Acetic acid  | 14.5       | 8          | 13.5       | 5     | 1.146  |
| 1,4-Dioxane  | 17.5       | 1.8        | 9          | 5     | 1.163  |
| Acetone  | 15.5       | 10.4       | 7          | 5     | 1.208  |
| Chloroform   | 17.8       | 3.1        | 5.7        | 5     | 1.223  |
| 30% EtOH-70% H <sub>2</sub> O                                  | 15.6       | 13.8       | 35.4       | 4     | 1.225  |
| Ethyl Acetate  | 15.8       | 5.3        | 7.2        | 5     | 1.253  |
| Methyl ethyl ketone (MEK)                                      | 16         | 9          | 5.1        | 5     | 1.254  |
| Acetonitrile   | 15.3       | 18         | 6.1        | 5     | 1.267  |
| <i>d</i> -Limonene   | 17.2       | 1.8        | 4.3        | 5     | 1.35   |
| Toluene  | 18         | 1.4        | 2          | 5     | 1.41   |

|   |      |      |      |   |       |
|---|------|------|------|---|-------|
| New Gd ternary mixture for 30% Cyrene-70% | 15.8 | 15.6 | 40.2 | 5 | 1.413 |
| H <sub>2</sub> O                          |      |      |      |   |       |
| α-Pinene                                  | 16.9 | 1.8  | 3.1  | 5 | 1.415 |
| Benzene                                   | 18.4 | 0    | 2    | 5 | 1.432 |
| New GD ternary mixture for 50% Cyrene-50% | 16.1 | 25.1 | 37.8 | 5 | 1.436 |
| H <sub>2</sub> O                          |      |      |      |   |       |
| Diethyl ether                             | 14.5 | 2.9  | 4.6  | 5 | 1.497 |
| Carbon tetrachloride                      | 17.8 | 0    | 0.6  | 5 | 1.519 |
| Water                                     | 15.5 | 16   | 42.3 | 5 | 1.529 |
| Cyclohexane                               | 16.8 | 0    | 0.2  | 5 | 1.587 |
| Heptane                                   | 15.3 | 0    | 0    | 5 | 1.683 |
| Hexane                                    | 14.9 | 0    | 0    | 5 | 1.708 |

\* represents solvents wrongly positioned in or out of Hansen sphere

Table A 17: Solubility of polyvinyl pyrrolidone PVP K90 in various solvents

| Solvent                       | Solubility result   |
|-------------------------------|---------------------|
| Cyrene                        | Yes                 |
| Water                         | Yes                 |
| Ethanol                       | Yes                 |
| Methanol                      | Yes                 |
| N-Methyl-2-pyrrolidone (NMP)  | Yes                 |
| N,N'-Dimethylformamide (DMF)  | Yes                 |
| Dimethyl sulfoxide (DMSO)     | Yes                 |
| N,N'-Dimethylacetamide (DMAc) | Yes                 |
| Benzyl alcohol                | Yes                 |
| Dimethyl carbonate            | No                  |
| 1-Propanol                    | Yes                 |
| Hexanoic acid                 | Yes                 |
| Tetrahydrofuran (THF)         | Yes                 |
| Acetone                       | Yes                 |
| OME <sub>(3-5)</sub>          | No                  |
| Cyclopentanone                | No                  |
| Ethyl acetate                 | No                  |
| 2-Propanol                    | Yes                 |
| Octanoic acid                 | Yes                 |
| Acetonitrile                  | Yes                 |
| Propylene carbonate           | Yes                 |
| Chloroform                    | Yes                 |
| 1,1-Dichloroethane            | Yes                 |
| Diethyl ether                 | No                  |
| Toluene                       | No                  |
| Cyclohexene                   | Partially dissolved |
| β-Pinene                      | No                  |
| Heptane                       | No                  |
| Hexane                        | No                  |



Table A 18: Concentrations, average and standard deviation of single-walled carbon nanotubes (SWCNTs) dispersed in pure solvents (Cyrene and NMP) and with the aid of additives (Triton X-100 and PVP)

| Sample            | Concentration of SWCNTs dispersed (mg mL <sup>-1</sup> ) |        |        |        |        | Mean  | Standard deviation | Confidence level for mean (99%) |
|-------------------|--|--------|--------|--------|--------|-------|--------------------|---------------------------------|
|                   | Test 1   | Test 2 | Test 3 | Test 4 | Test 5 |       |                    |                                 |
| C0.1, 1h          | 0.067  | 0.02   | 0.054  | 0.011  |        | 0.038 | 0.027              | 0.078                           |
| C0.1, 5h          | 0.09   | 0.075  | 0.06   | 0.05   |        | 0.069 | 0.018              | 0.051                           |
| C0.1, 10h         | 0.07   | 0.07   | 0.08   | 0.1    |        | 0.08  | 0.014              | 0.041                           |
| C0.1, 20h         | 0.06   | 0.09   | 0.09   |        |        | 0.08  | 0.017              | 0.099                           |
| N0.1, 1h          | 0.012  | 0.014  |        |        |        | 0.013 | 0.001              | 0.064                           |
| N0.1, 5h          | 0.013  | 0.018  |        |        |        | 0.016 | 0.004              | 0.159                           |
| N0.1, 10h         | 0.006  | 0.01   |        |        |        | 0.008 | 0.003              | 0.127                           |
| N0.1, 20h         | 0.005  | 0.02   |        |        |        | 0.013 | 0.011              | 0.477                           |
| C1.25, 1h         | 0.135  | 0.004  | 0.017  |        |        | 0.052 | 0.072              | 0.414                           |
| C1.25, 5h         | 0.84   | 0.37   | 0.13   | 0.13   | 0.99   | 0.492 | 0.402              | 0.828                           |
| C1.25, 10h        | 0.11   | 0.06   |        |        |        | 0.085 | 0.035              | 1.591                           |
| C1.25, 20h        | 0.084  | 0.03   |        |        |        | 0.057 | 0.038              | 1.719                           |
| N 1.25, 1h        | 0.02   | 0.01   |        |        |        | 0.015 | 0.007              | 0.318                           |
| N 1.25, 5h        | 0.036  | 0.03   |        |        |        | 0.033 | 0.004              | 0.191                           |
| N 1.25, 10h       | 0.1  | 0.08   |        |        |        | 0.090 | 0.014              | 0.637                           |
| N 1.25, 20h       | 0.03   | 0.01   |        |        |        | 0.020 | 0.014              | 0.637                           |
| C0.1, 1h, Triton  | 0.06   | 0.02   |        |        |        | 0.040 | 0.028              | 1.273                           |
| C0.1, 5h, Triton  | 0.09   | 0.08   |        |        |        | 0.085 | 0.007              | 0.318                           |
| C0.1, 10h, Triton | 0.05   | 0.09   | 0.08   |        |        | 0.073 | 0.028              | 0.119                           |
| C0.1, 20h, Triton | 0.089  | 0.09   |        |        |        | 0.090 | 0.001              | 0.032                           |
| N0.1, 1h, Triton  | 0.022  | 0.04   |        |        |        | 0.031 | 0.013              | 0.573                           |
| N0.1, 5h, Triton  | 0.02   | 0.01   |        |        |        | 0.015 | 0.007              | 0.318                           |

|                       |       |       |      |       |       |       |
|-----------------------|-------|-------|------|-------|-------|-------|
| N0.1, 10h,<br>Triton  | 0.01  | 0.01  |      | 0.010 | 0.000 | 0.000 |
| N0.1, 20h,<br>Triton  | 0.03  | 0.04  |      | 0.035 | 0.007 | 0.318 |
| C1.25, 1h,<br>Triton  | 0.01  | 0.03  |      | 0.020 | 0.014 | 0.637 |
| C1.25, 5h,<br>Triton  | 0.06  | 0.023 |      | 0.042 | 0.026 | 1.178 |
| C1.25, 10h,<br>Triton | 0.55  | 0.27  |      | 0.410 | 0.198 | 8.912 |
| C1.25, 20h,<br>Triton | 0.33  | 0.4   |      | 0.365 | 0.050 | 2.228 |
| N1.25, 1h,<br>Triton  | 0.013 | 0.03  |      | 0.022 | 0.012 | 0.541 |
| N1.25, 5h,<br>Triton  | 0.01  | 0.04  |      | 0.025 | 0.021 | 0.955 |
| N1.25, 10h,<br>Triton | 0.01  | 0.06  |      | 0.035 | 0.035 | 1.591 |
| N1.25, 20h,<br>Triton | 0.07  | 0.07  |      | 0.070 | 0.000 | 0.000 |
| C0.1, 1h, PVP         | 0.03  | 0.019 |      | 0.025 | 0.008 | 0.350 |
| C0.1, 5h, PVP         | 0.08  | 0.023 |      | 0.052 | 0.040 | 1.814 |
| C0.1, 10h,<br>PVP     | 0.06  | 0.05  | 0.01 | 0.040 | 0.027 | 0.191 |
| C0.1, 20h,<br>PVP     | 0.07  | 0.08  |      | 0.075 | 0.007 | 0.318 |
| N0.1, 1h, PVP         | 0.031 | 0.016 |      | 0.024 | 0.011 | 0.477 |
| N0.1, 5h, PVP         | 0.03  | 0.018 |      | 0.024 | 0.009 | 0.382 |
| N0.1, 10h,<br>PVP     | 0.02  | 0.017 |      | 0.019 | 0.002 | 0.095 |
| N0.1, 20h,<br>PVP     | 0.08  | 0.096 |      | 0.088 | 0.011 | 0.509 |
| C1.25, 1h,<br>PVP     | 0.017 | 0.022 |      | 0.020 | 0.004 | 0.159 |
| C1.25, 5h,<br>PVP     | 0.06  | 0.03  | 0.04 | 0.043 | 0.015 | 0.088 |
| C1.25, 10h,<br>PVP    | 0.08  | 0.056 |      | 0.068 | 0.017 | 0.764 |
| C1.25, 20h,<br>PVP    | 0.11  | 0.17  |      | 0.140 | 0.042 | 1.910 |

|                    |       |       |       |       |       |
|--------------------|-------|-------|-------|-------|-------|
| N1.25, 1h,<br>PVP  | 0.027 | 0.018 | 0.023 | 0.006 | 0.286 |
| N1.25, 5h,<br>PVP  | 0.03  | 0.022 | 0.026 | 0.006 | 0.255 |
| N1.25, 10h,<br>PVP | 0.04  | 0.034 | 0.037 | 0.004 | 0.191 |
| N1.25, 20h,<br>PVP | 0.07  | 0.054 | 0.062 | 0.011 | 0.509 |

---

Table A 19: Hansen solubility parameters, the scores given and relative energy distance (RED) of the solvents used to test the dissolution of PES3020

| Solvent                              | $\delta_D$ | $\delta_P$ | $\delta_H$ | Score | RED   |
|--------------------------------------|------------|------------|------------|-------|-------|
| Cyrene                               | 18.9       | 12.4       | 7.1        | 1     | 0.468 |
| <i>N</i> -Methyl-2-pyrrolidone (NMP) | 18         | 12.3       | 7.2        | 1     | 0.64  |
| <i>N,N'</i> -Dimethylacetamide       | 16.8       | 11.5       | 9.4        | 1     | 0.934 |
| Dimethyl sulfate                     | 16.5       | 13         | 7          | 5     | 0.993 |
| Dimethyl sulfoxide (DMSO)            | 18.4       | 16.4       | 10.2       | 1     | 0.998 |
| Tetrahydrofuran (THF)                | 16.8       | 5.7        | 8          | 5     | 0.998 |
| Propylene carbonate                  | 20         | 18         | 4.1        | 4     | 1.002 |
| <i>N,N'</i> -Dimethylformamide (DMF) | 17.4       | 13.7       | 11.3       | 1     | 1.008 |
| Chloroform                           | 17.8       | 3.1        | 5.7        | 4     | 1.013 |
| 1,1-Dichloroethane                   | 16.5       | 7.8        | 3          | 1     | 1.041 |
| Benzyl alcohol                       | 18.4       | 6.3        | 13.7       | 4     | 1.054 |
| Sulfolane                            | 17.8       | 17.4       | 8.7        | 5     | 1.106 |
| 2-Methylfuran                        | 17.3       | 2.8        | 7.4        | 5     | 1.115 |
| Acetone                              | 15.5       | 10.4       | 7          | 4     | 1.159 |
| Ethyl acetate                        | 15.8       | 5.3        | 7.2        | 5     | 1.215 |
| Dimethyl carbonate                   | 15.5       | 8.6        | 9.7        | 5     | 1.224 |
| TMO                                  | 15.5       | 8.6        | 9.7        | 5     | 1.224 |
| Toluene                              | 18         | 1.4        | 2          | 5     | 1.268 |
| <i>p</i> -Xylene                     | 17.8       | 1          | 3.1        | 5     | 1.279 |
| Propyl acetate                       | 15.3       | 4.3        | 7.6        | 5     | 1.377 |
| Acetonitrile                         | 15.3       | 18         | 6.1        | 5     | 1.537 |
| 1-Butanol                            | 16         | 5.7        | 15.8       | 5     | 1.583 |
| Propionic acid                       | 14.7       | 5.3        | 12.4       | 5     | 1.604 |
| Cyclohexane                          | 16.8       | 0          | 0.2        | 5     | 1.623 |
| Diethyl ether                        | 14.5       | 2.9        | 4.6        | 5     | 1.633 |
| 2-Propanol                           | 15.8       | 6.1        | 16.4       | 5     | 1.65  |
| 1-Propanol                           | 16         | 6.8        | 17.4       | 5     | 1.685 |
| Heptane                              | 15.3       | 0          | 0          | 5     | 1.843 |
| OME <sub>(3-5)</sub>                 | 15.6       | 7.1        | 6.1        | 5     | 1.859 |
| Ethanol                              | 15.8       | 8.8        | 19.4       | 5     | 1.866 |
| Hexane                               | 14.9       | 0          | 0          | 5     | 1.906 |
| Methanol                             | 14.7       | 12.3       | 22.3       | 5     | 2.307 |
| Water                                | 15.5       | 16         | 42.3       | 5     | 4.421 |

Table A 20: Hansen solubility parameters, the scores given, and relative energy distance (RED) of the solvents and Cygnet-Cyrene mixtures proposed to dissolve polyethersulfone PES3020

| Solvent/mixture                      | $\delta_D$ | $\delta_P$ | $\delta_H$ | Score | RED    |
|--------------------------------------|------------|------------|------------|-------|--------|
| 40 wt% Cg:Cy                         | 18.7       | 10.7       | 7          | -     | 0.422  |
| 30 wt% Cg:Cy                         | 18.7       | 11.1       | 7          | -     | 0.435  |
| 50 wt% Cg:Cy                         | 18.6       | 10.3       | 7          | 1     | 0.437  |
| 20 wt% Cg:Cy                         | 18.8       | 11.6       | 7.1        | -     | 0.438  |
| 60 wt% Cg:Cy                         | 18.5       | 9.9        | 7          | -     | 0.458  |
| 70 wt% Cg:Cy                         | 18.5       | 9.5        | 7          | -     | 0.46   |
| 10 wt% Cg:Cy                         | 18.8       | 12         | 7.1        | -     | 0.462  |
| Cyrene                               | 18.9       | 12.4       | 7.1        | 1     | 0.471  |
| 80 wt% Cg:Cy                         | 18.4       | 9          | 6.9        | -     | 0.491  |
| 90 wt% Cg:Cy                         | 18.4       | 8.6        | 6.9        | -     | 0.503  |
| Cygnnet 0.0                          | 18.3       | 8.2        | 6.9        | -     | 0.541  |
| <i>N</i> -Methyl-2-pyrrolidone (NMP) | 18         | 12.3       | 7.2        | 1     | 0.643  |
| <i>N,N'</i> -Dimethylacetamide       | 16.8       | 11.5       | 9.4        | 1     | 0.935  |
| Dimethyl sulfoxide (DMSO)            | 18.4       | 16.4       | 10.2       | 1     | 0.997  |
| Dimethyl sulfate                     | 16.5       | 13         | 7          | 5     | 0.997* |
| Tetrahydrofuran (THF)                | 16.8       | 5.7        | 8          | 5     | 1.000* |
| Propylene carbonate                  | 20         | 18         | 4.1        | 4     | 1.006  |
| <i>N,N'</i> -Dimethylformamide (DMF) | 17.4       | 13.7       | 11.3       | 1     | 1.006* |
| Chloroform                           | 17.8       | 3.1        | 5.7        | 4     | 1.017  |
| Benzyl alcohol                       | 18.4       | 6.3        | 13.7       | 4     | 1.047  |
| 1,1-Dichloroethane                   | 16.5       | 7.8        | 3          | 1     | 1.050* |
| Sulfolane                            | 17.8       | 17.4       | 8.7        | 5     | 1.107  |
| 2-Methylfuran                        | 17.3       | 2.8        | 7.4        | 5     | 1.117  |
| Acetone                              | 15.5       | 10.4       | 7          | 4     | 1.164  |
| Ethyl acetate                        | 15.8       | 5.3        | 7.2        | 5     | 1.219  |
| TMO                                  | 15.5       | 8.6        | 9.7        | 5     | 1.225  |
| Dimethyl carbonate                   | 15.5       | 8.6        | 9.7        | 5     | 1.225  |
| Toluene                              | 18         | 1.4        | 2          | 5     | 1.274  |
| <i>p</i> -Xylene                     | 17.8       | 1          | 3.1        | 5     | 1.285  |
| <i>n</i> -Propyl acetate             | 15.3       | 4.3        | 7.6        | 5     | 1.38   |
| Acetonitrile                         | 15.3       | 18         | 6.1        | 5     | 1.542  |
| 1-Butanol                            | 16         | 5.7        | 15.8       | 5     | 1.579  |
| Propionic acid                       | 14.7       | 5.3        | 12.4       | 5     | 1.604  |
| Cyclohexane                          | 16.8       | 0          | 0.2        | 5     | 1.63   |
| Diethyl ether                        | 14.5       | 2.9        | 4.6        | 5     | 1.638  |
| 2-Propanol                           | 15.8       | 6.1        | 16.4       | 5     | 1.645  |
| 1-Propanol                           | 16         | 6.8        | 17.4       | 5     | 1.68   |
| Heptane                              | 15.3       | 0          | 0          | 5     | 1.85   |
| Ethanol                              | 15.8       | 8.8        | 19.4       | 5     | 1.86   |
| Hexane                               | 14.9       | 0          | 0          | 5     | 1.913  |
| Methanol                             | 14.7       | 12.3       | 22.3       | 5     | 2.302  |
| Water                                | 15.5       | 16         | 42.3       | 5     | 4.412  |

\* represents solvents wrongly positioned in or out of Hansen sphere.

Table A 21: Overall porosity (%) and pore diameter ( $\mu\text{m}$ ) of PES membranes prepared with Cyrene (PES/C) and NMP (PES/N)

| Membrane code | Porosity (%) | Pore diameter ( $\mu\text{m}$ ) |
|---------------|--------------|---------------------------------|
| PES/C0        | 76.7         | 0.7                             |
| PES/C0.1      | 79           | 0.8                             |
| PES/C0.5      | 74.6         | 0.8                             |
| PES/C1        | 78.8         | 1                               |
| PES/C5        | 72.7         | 1                               |
| PES/C10       | 54.9         | 0.09                            |
| PES/N0        | 73.6         | 0.2                             |
| PES/N0.1      | 76.3         | 0.2                             |
| PES/N0.5      | 68.4         | 0.2                             |
| PES/N1        | 72.1         | 0.2                             |
| PES/N5        | 56.1         | 0.7                             |
| PES/N10       | 44.6         | 1                               |

Table A 22: Gravimetric analysis of PES membranes prepared with Cyrene (PES/C) and NMP (PES/N)

| Membrane code | Test 1 | Test 2 | Average | Standard deviation |
|---------------|--------|--------|---------|--------------------|
| PES/C0        | 40.6   | 47.3   | 43.95   | 4.74               |
| PES/C0.1      | 24.4   | 31.5   | 27.95   | 5.02               |
| PES/C0.5      | 54.8   | 62.2   | 58.5    | 12.87              |
| PES/C1        | 70.2   | 52     | 61.1    | 12.87              |
| PES/C5        | 75     | 62.1   | 68.55   | 9.12               |
| PES/C10       | 20.1   | 23     | 21.55   | 2.05               |
| PES/N0        | 46.8   | 35.1   | 40.95   | 8.27               |
| PES/N0.1      | 32.6   | 36.4   | 34.5    | 2.69               |
| PES/N0.5      | 35.8   | 46.2   | 41      | 7.35               |
| PES/N1        | 50     | 50     | 50      | 0                  |
| PES/N5        | 56.3   | 71.8   | 64.05   | 10.96              |
| PES/N10       | 30.8   | 44.1   | 37.45   | 9.4                |

Table A 23: Static contact angle of PES/C and PES/N membranes

| Membrane code | Static contact angle (°C) |
|---------------|---------------------------|
| PES/C0        | 73.1                      |
| PES/C0.1      | 67.5                      |
| PES/C1        | 62.1                      |
| PES/C5        | 44.9                      |
| PES/C10       | 37.5                      |

Table A 24: Pure water permeability of membranes casted from cold and hot casting solutions

| Membranes cast from a cold casting solution | Permeability (LMH/bar) | Membranes cast from a hot casting solution | Permeability (LMH/bar) |
|---|------------------------|--|------------------------|
| PES/C0                                      | 90.2                   | PES/C0                                     | 71.4                   |
| PES/C0                                      | 124.7                  | PES/C0.1                                   | 2.4                    |
| PES/C0.5                                    | 0                      | PES/C0.5                                   | 4.5                    |
| PES/C1                                      | 0                      | PES/C1                                     | 2.3                    |
| PES/C5                                      | 0                      | PES/C5                                     | 23.2                   |
| PES/C10                                     | 2542.7                 | PES/C10                                    | 898.4                  |
| PES/N0                                      | 15                     | PES/N0                                     | 65.5                   |
| PES/N0.1                                    | 187.2                  | PES/N0.1                                   | 3.5                    |
| PES/N0.5                                    | 10.3                   | PES/N0.5                                   | 260.4                  |
| PES/N1                                      | 140.5                  | PES/N1                                     | 103.5                  |
| PES/N5                                      | 720.3                  | PES/N5                                     | 157.2                  |
| PES/N10                                     | 656.3                  | PES/N10                                    | 210.6                  |

Table A 25: Hansen solubility parameters, the scores given and relative energy distance (RED) of the solvents used to test the dissolution of PVDF 5130

| Solvent                              | $\delta_D$ | $\delta_P$ | $\delta_H$ | Score | RED    | MVol  |
|--------------------------------------|------------|------------|------------|-------|--------|-------|
| <i>N,N'</i> -Dimethylacetamide       | 16.8       | 11.5       | 9.4        | 1     | 0.99   | 93    |
| <i>N</i> -Methyl-2-pyrrolidone (NMP) | 18         | 12.3       | 7.2        | 1     | 0.999  | 96.6  |
| Dimethyl sulfate                     | 16.5       | 13         | 7          | 5     | 1.375  | 95.5  |
| Cyclopentanone                       | 17.9       | 11.9       | 5.2        | 5     | 1.854  | 89.1  |
| Cyrene                               | 18.9       | 12.4       | 7.1        | 5     | 1.97   | 102.5 |
| <i>N,N'</i> -Dimethylformamide (DMF) | 17.4       | 13.7       | 11.3       | 5     | 2.163  | 77.4  |
| Acetone                              | 15.5       | 10.4       | 7          | 5     | 2.41   | 73.8  |
| Dimethyl sulfoxide (DMSO)            | 18.4       | 16.4       | 10.2       | 5     | 3.206  | 71.3  |
| Tetrahydrofuran (THF)                | 16.8       | 5.7        | 8          | 5     | 3.658  | 81.9  |
| Benzaldehyde                         | 19.4       | 7.4        | 5.3        | 5     | 3.934  | 101.9 |
| Ethyl acetate                        | 15.8       | 5.3        | 7.2        | 5     | 4.278  | 98.6  |
| Furfuryl alcohol                     | 17.4       | 7.6        | 15.1       | 5     | 4.79   | 87.1  |
| Propyl acetate                       | 15.3       | 4.3        | 7.6        | 5     | 5.042  | 115.8 |
| Hexanoic acid                        | 16.3       | 4.2        | 11.5       | 5     | 5.05   | 126.3 |
| Acetic acid                          | 14.5       | 8          | 13.5       | 5     | 5.111  | 57.6  |
| Chloroform                           | 17.8       | 3.1        | 5.7        | 5     | 5.357  | 80.5  |
| Methoxycyclopentane                  | 15.8       | 5.7        | 14.5       | 5     | 5.499  | 92    |
| 2-Butanol                            | 15.8       | 5.7        | 14.5       | 5     | 5.499  | 92    |
| Propionic acid                       | 14.7       | 5.3        | 12.4       | 5     | 5.533  | 75    |
| 1-Butanol                            | 16         | 5.7        | 15.8       | 5     | 5.979  | 92    |
| Chlorobenzene                        | 19         | 4.3        | 2          | 5     | 6.04   | 102.1 |
| 2-Propanol                           | 15.8       | 6.1        | 16.4       | 5     | 6.181  | 76.9  |
| 1-Propanol                           | 16         | 6.8        | 17.4       | 5     | 6.393  | 75.1  |
| Diethyl ether                        | 14.5       | 2.9        | 4.6        | 5     | 6.559  | 104.7 |
| Ethanol                              | 15.8       | 8.8        | 19.4       | 5     | 7.092  | 58.6  |
| Cyclohexene                          | 17.2       | 1          | 2          | 5     | 7.323  | 101.9 |
| Heptane                              | 15.3       | 0          | 0          | 5     | 8.777  | 147   |
| Methanol                             | 14.7       | 12.3       | 22.3       | 5     | 8.892  | 40.6  |
| Hexane                               | 14.9       | 0          | 0          | 5     | 8.917  | 131.4 |
| Water                                | 15.5       | 16         | 42.3       | 5     | 20.239 | 18    |



# Appendix B

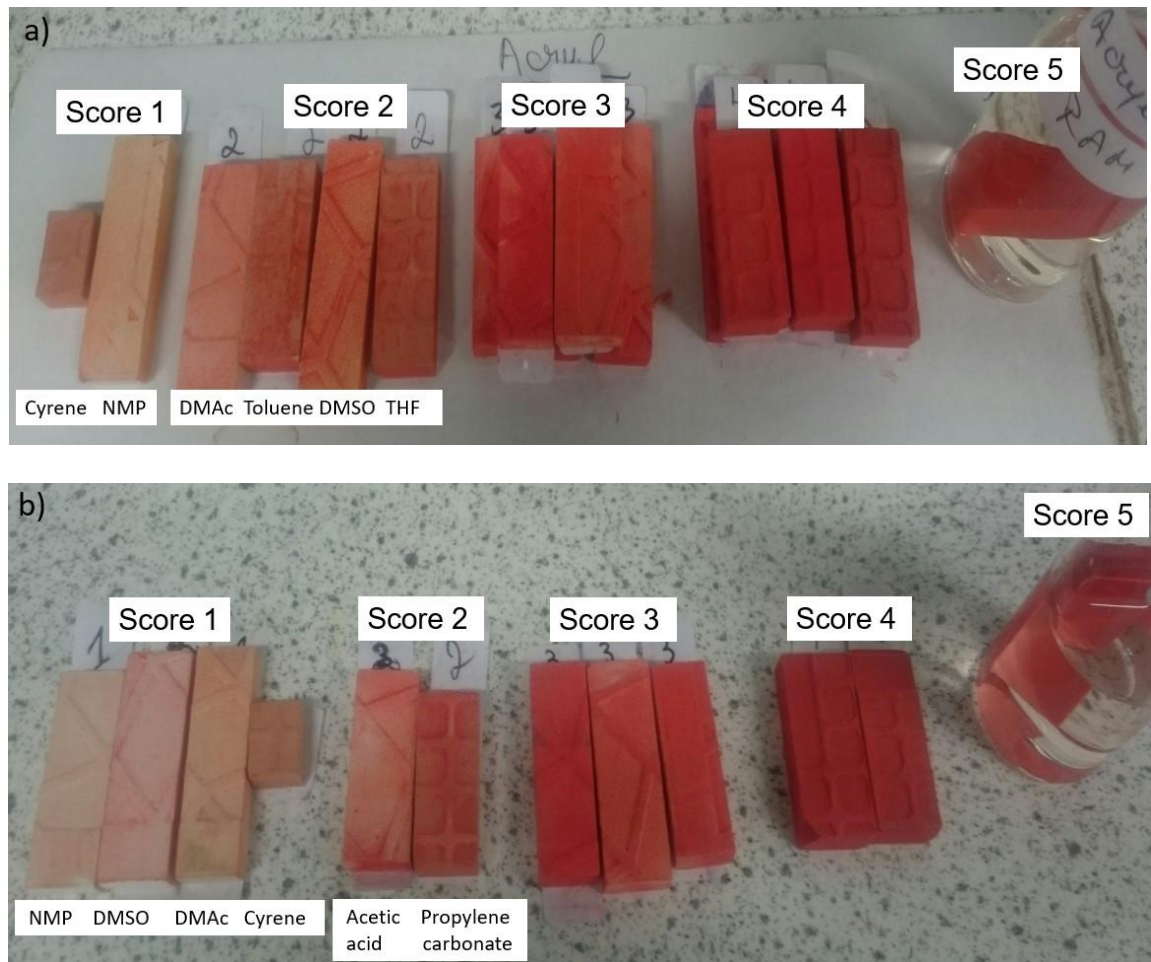


Figure B 1: Scores from 1 (good cleaning) to 5 (no change) given to the cleaned tiles of (1) acrylic and (2) cellulose nitrate paint.

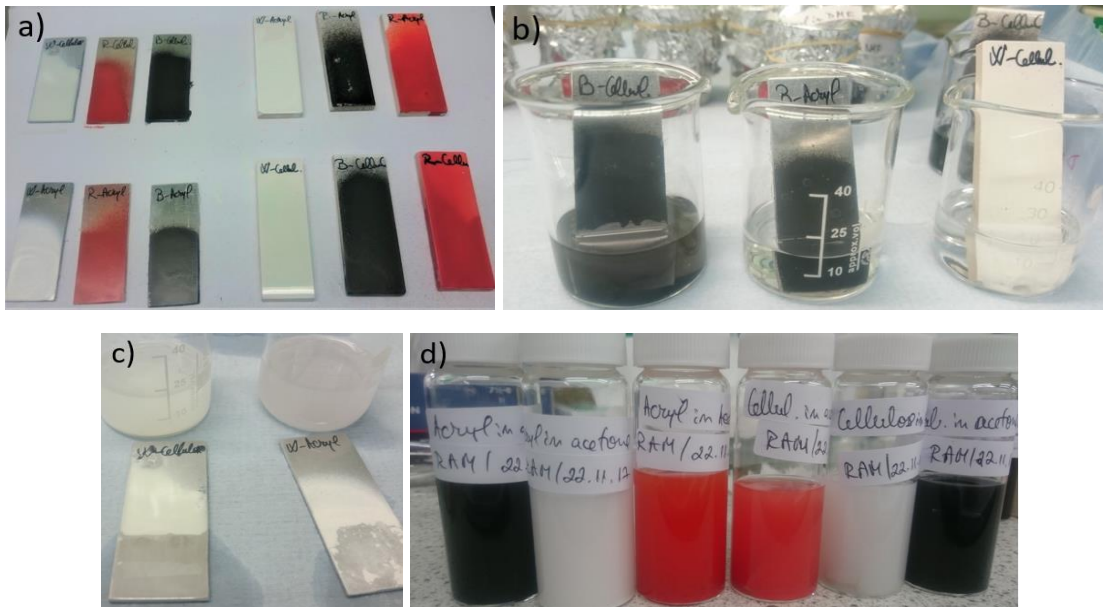


Figure B 2: (a) Porous and non-porous substrates were painted on *approx.* 70% of the surface, (b) were dried and immersed in (b, c) beakers or (d) vials containing individual solvents.

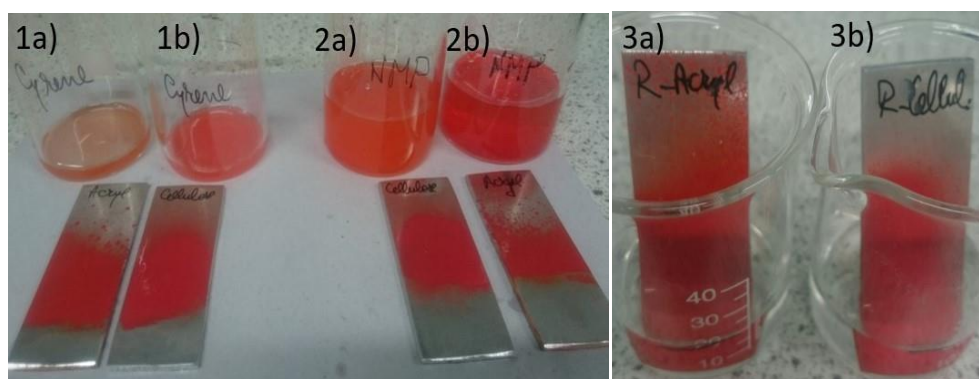


Figure B 3: Results of the graffiti cleaning from the aluminium slides using (1) Cyrene, (2) NMP and (3) DMF of cleaning (1a, 2b, 3a) acrylic and (1b, 2a, 3b) cellulose-based paints.

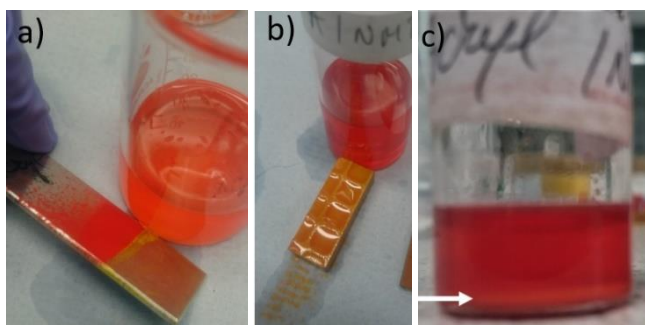


Figure B 4: Effect of NMP on cellulose and acrylic paint. (a) A yellow residue can be seen onto aluminium slide, (b) ceramic tile and (c) on the bottom of the vial.

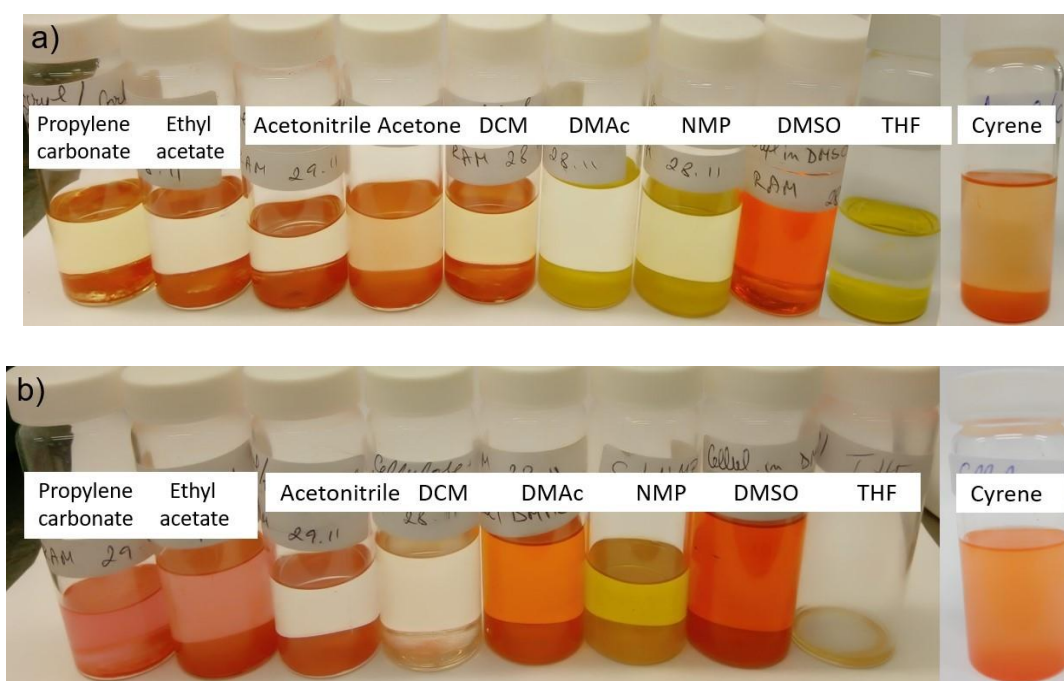


Figure B 5: (a) Solvent residues from acrylic and (b) cellulose nitrate graffiti removal by various polar aprotic solvents, including Cyrene. THF has evaporated after a while.

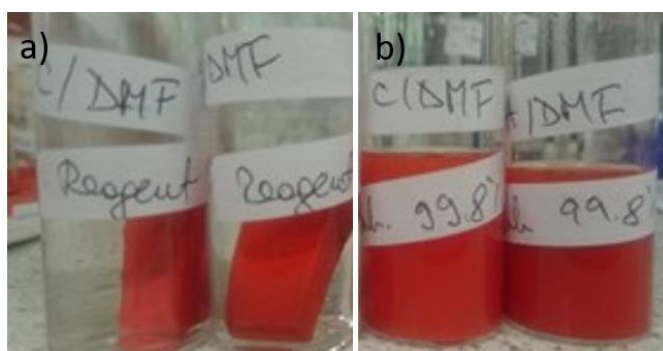


Figure B 6: (a) DMF reagent of 99% purity and (b) DMF anhydrous (99.8%) used as cleaning agent for acrylic and cellulose-based paints.

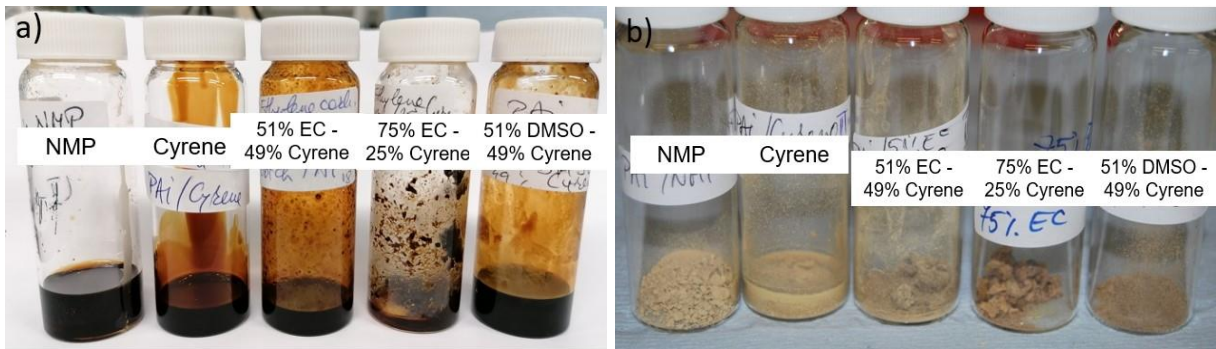


Figure B 7: (a) Solutions of PAIs produced using NMP, Cyrene and mixtures of Cyrene with EC or DMSO and (b) PAIs resins.



Figure B 8: PAI/Cyrene cured at 220 °C.

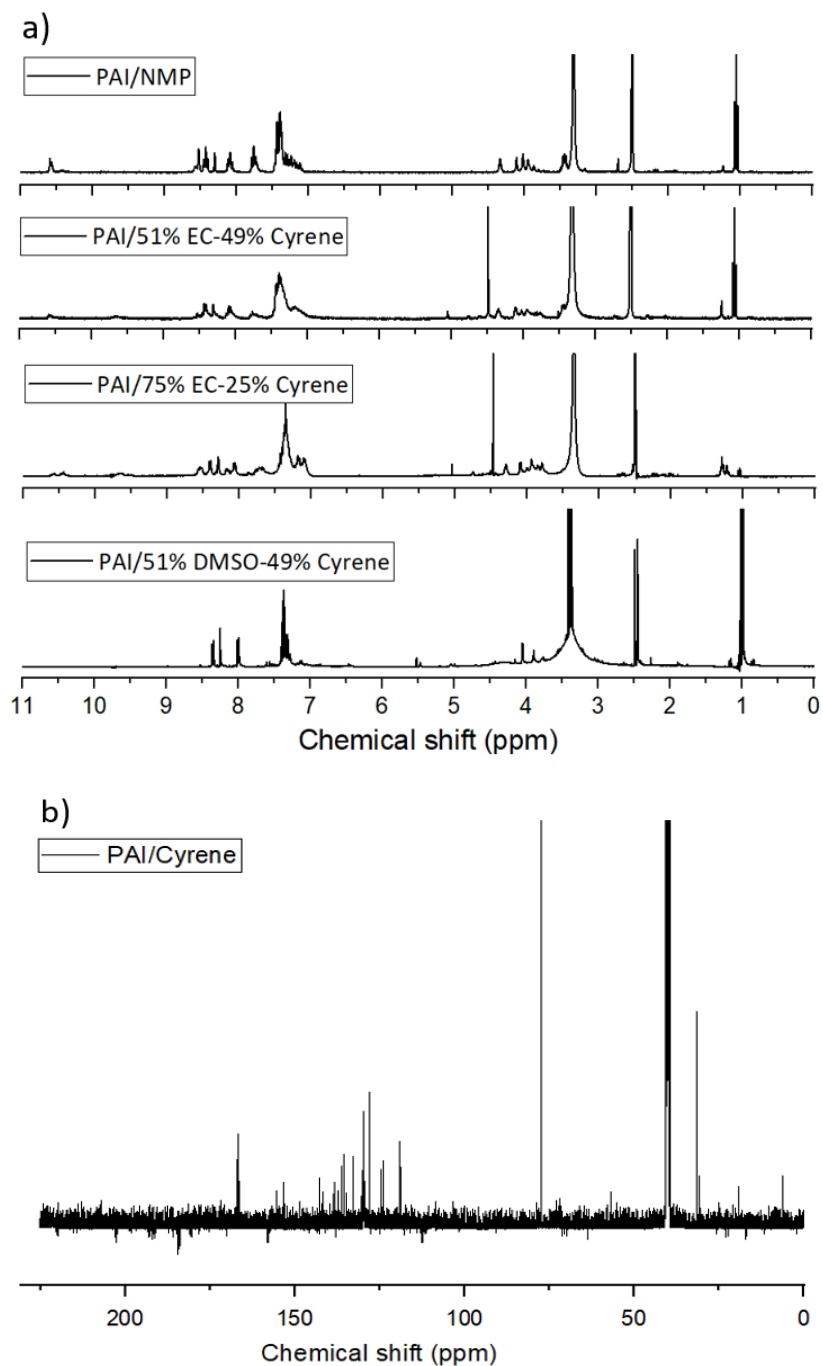


Figure B 9: (a)  $^1\text{H}$ -NMR spectra of PAI/NMP, PAI/51% EC-49% Cyrene, PAI/75% EC-49% Cyrene and PAI/51% DMSO-49% Cyrene. All PAIs were cured at 240 °C. (b)  $^{13}\text{C}$  NMR spectrum of PAI/Cyrene.

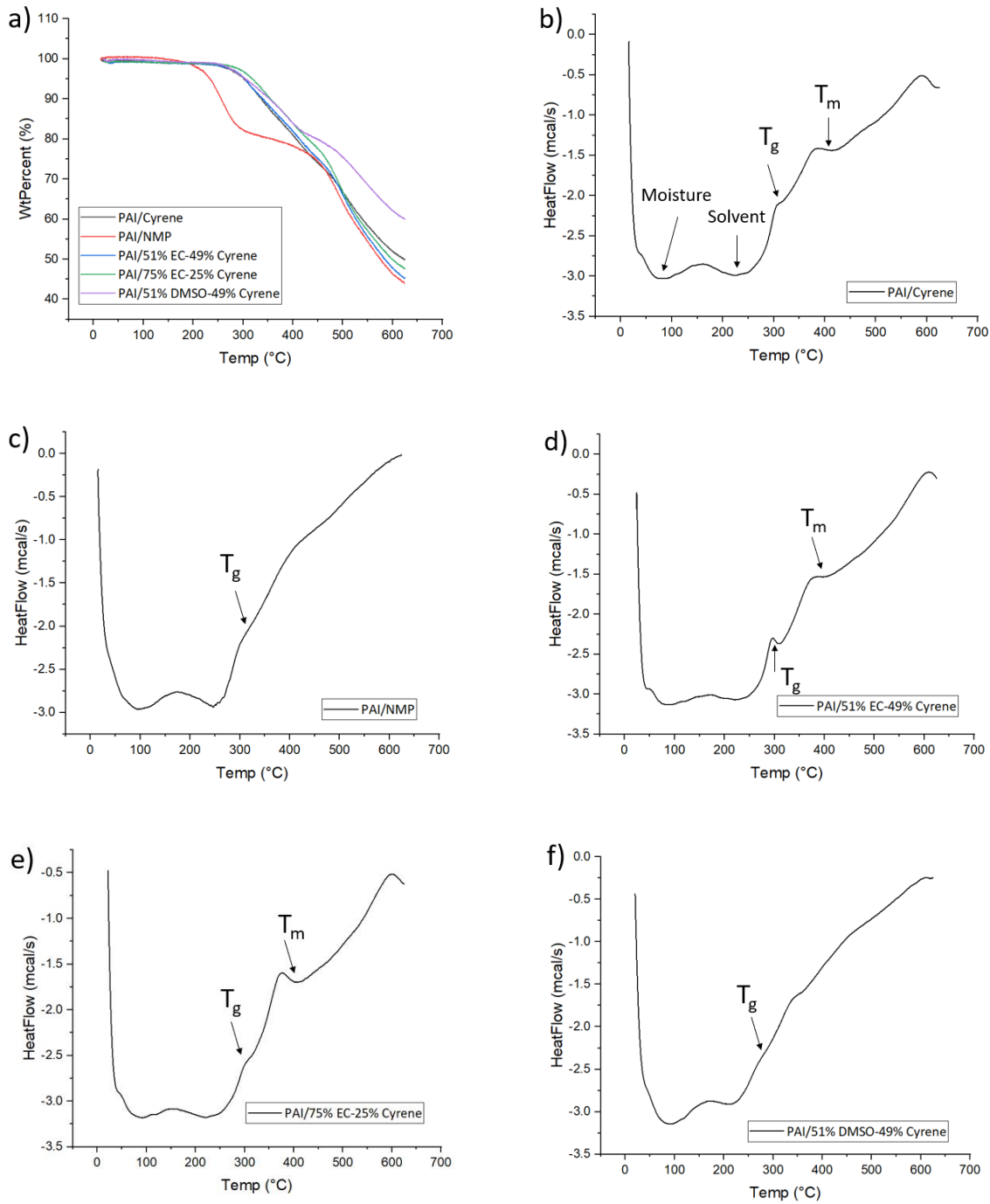


Figure B 10: (a) Thermogravimetric analysis (TGA) and differential scanning calorimeter (DSC) measurements of (b) PAI/Cyrene, (c) PAI/NMP, (d) PAI/51% EC-49% Cyrene, (e) PAI/75% EC-49% Cyrene and (f) PAI/51% DMSO-49% Cyrene. All PAI films were cured at 240 °C.

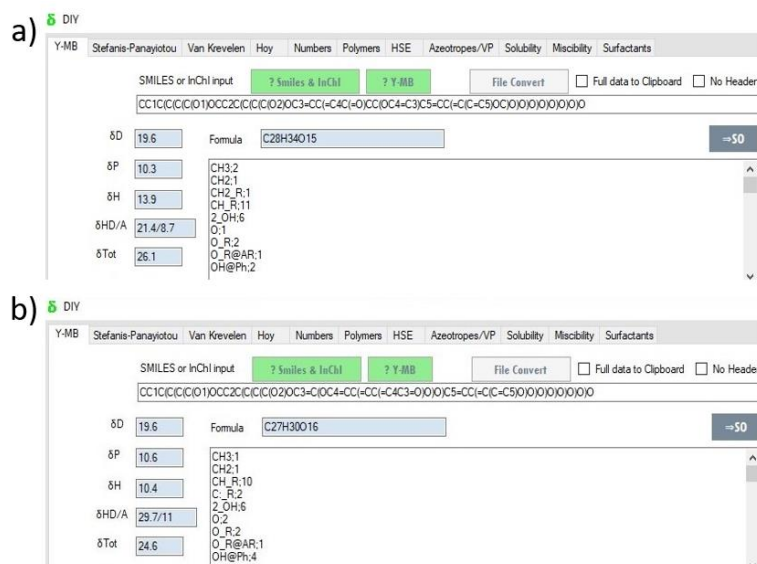


Figure B 11: (a) Partial solubility parameters of hesperidin and (b) rutin calculated using DIY 5.03 version of Hansen Solubility Parameters in Practice (HSPiP).

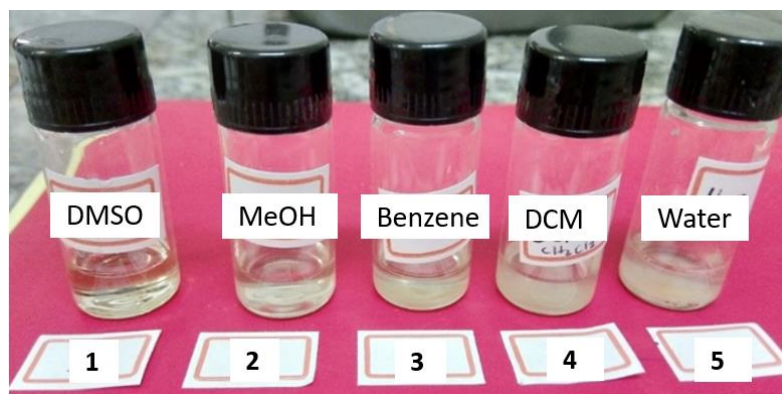


Figure B 12: In vitro dissolution test of hesperidin and the scores given by visual inspection.

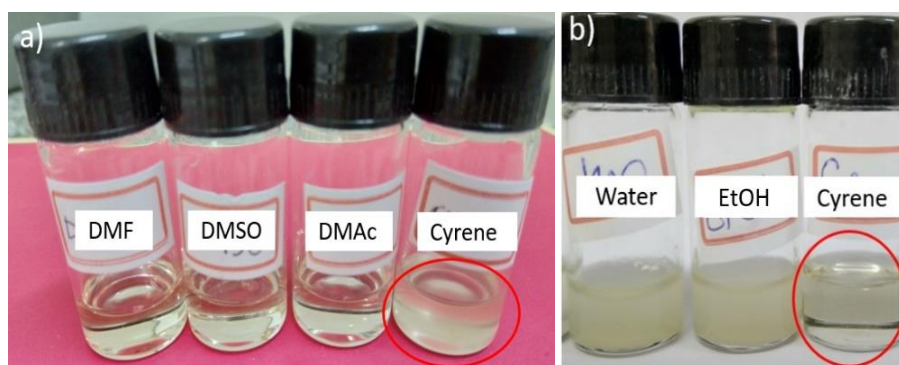
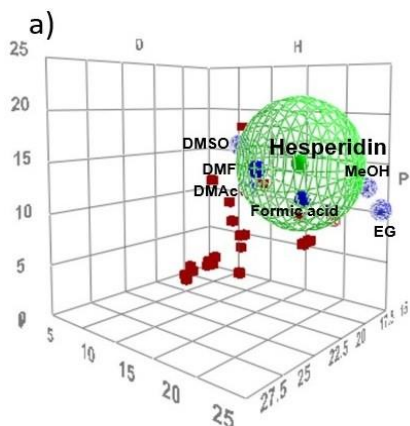


Figure B 13: (a) Dissolution of hesperidin in Cyrene (red circle) at room temperature (b) and at 65 °C.



b)

| Solvent                      | $\delta D$ | $\delta P$ | $\delta H$ | Score | RED    | MVol  |
|------------------------------|------------|------------|------------|-------|--------|-------|
| Dimethyl Fomamide (DMF)      | 17.4       | 13.7       | 11.3       | 1     | 0.753  | 77.4  |
| Formic Acid                  | 14.6       | 10         | 14         | 1     | 0.989* | 37.9  |
| Ethanol                      | 15.8       | 8.8        | 19.4       | 5     | 0.989* | 58.6  |
| Acetic Anhydride             | 16         | 11.7       | 10.2       | 5     | 1.009  | 95    |
| Dimethyl Sulfoxide (DMSO)    | 18.4       | 16.4       | 10.2       | 1     | 1.016* | 71.3  |
| N,N-Dimethyl Acetamide       | 16.8       | 11.5       | 9.4        | 1     | 1.093* | 93    |
| Methanol                     | 14.7       | 12.3       | 22.3       | 2     | 1.102* | 40.6  |
| Acetic Acid                  | 14.5       | 8          | 13.5       | 5     | 1.237  | 57.6  |
| 2-Propanol                   | 15.8       | 6.1        | 16.4       | 5     | 1.259  | 76.9  |
| 1-Butanol                    | 16         | 5.7        | 15.8       | 5     | 1.305  | 92    |
| Ethylene Glycol              | 17         | 11         | 26         | 1     | 1.470* | 55.9  |
| Cyrene                       | 18.9       | 12.4       | 7.1        | 4     | 1.481  | 102.5 |
| Acetone                      | 15.5       | 10.4       | 7          | 5     | 1.522  | 73.8  |
| Acetonitrile                 | 15.3       | 18         | 6.1        | 5     | 1.609  | 52.9  |
| Methylene Dichloride (Dic... | 17         | 7.3        | 7.1        | 5     | 1.691  | 64.4  |

Figure B 14: (a) Forced fit for hesperidin using HSPiP and (b) the new RED values of the solvents after the changes in software.

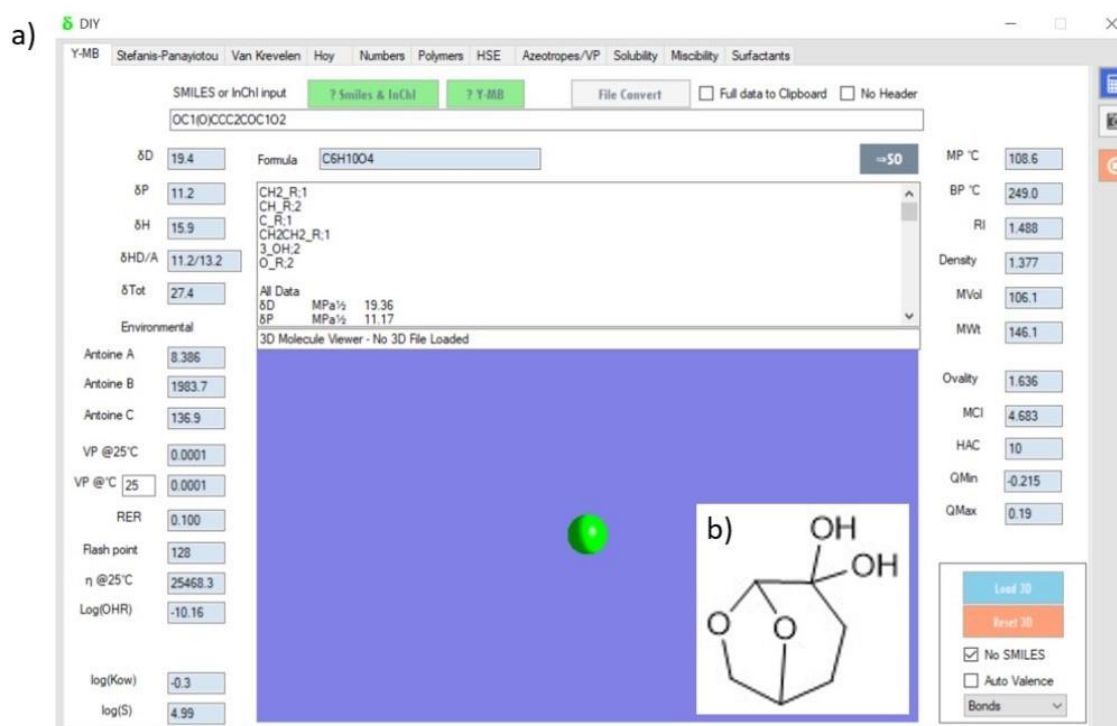


Figure B 15: (a) Hansen Solubility Parameters (HSPs) calculated for (b) Cyrene's hydrate using DIY 5.03 version of HSPiP.



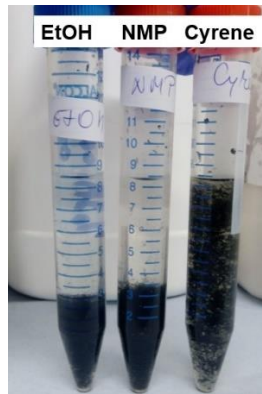


Figure B 16: (a) Solution of  $1.25 \text{ mg mL}^{-1}$  SWCNTs dispersion on ethanol, (b) NMP and (c) Cyrene after shaking the tube for 10 seconds and left to settle for one hour.

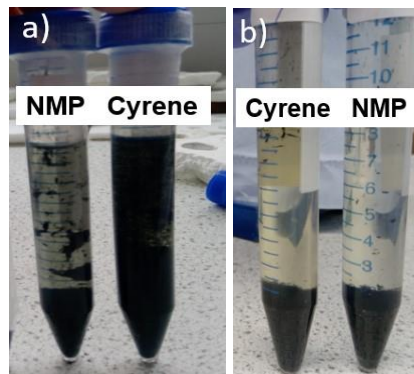


Figure B 17: (a) Solution of  $1.25 \text{ mg mL}^{-1}$  SWCNTs in NMP and Cyrene after 10 hours of sonication and centrifugation at  $10^\circ\text{C}$  and (b)  $20^\circ\text{C}$  immediately after sonication.

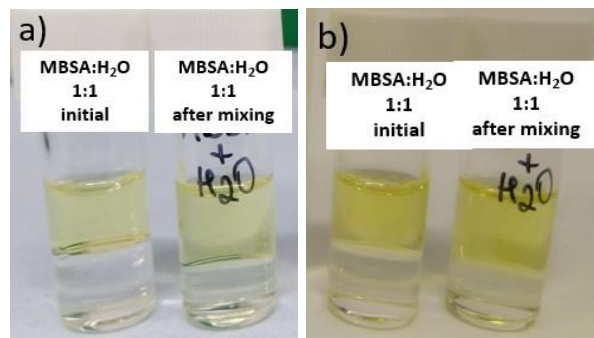


Figure B 18: (a) Miscibility of MBSA and water 1:1 after 1 hour and (b) after 3 days.

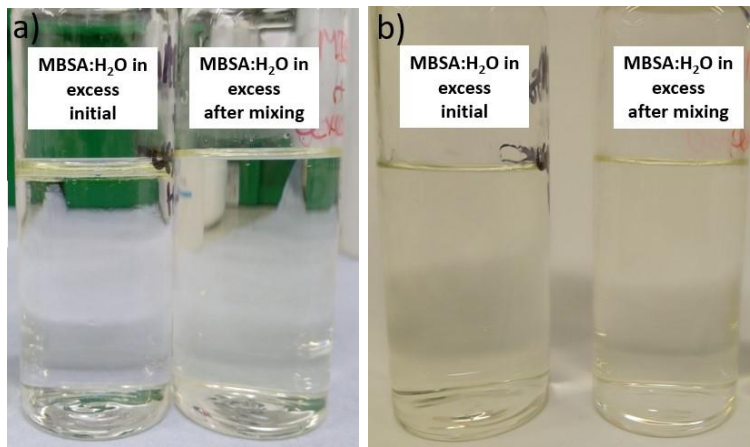


Figure B 19: (a) Miscibility of MBSA and excess of water after 1hour and (b) after 3 days.

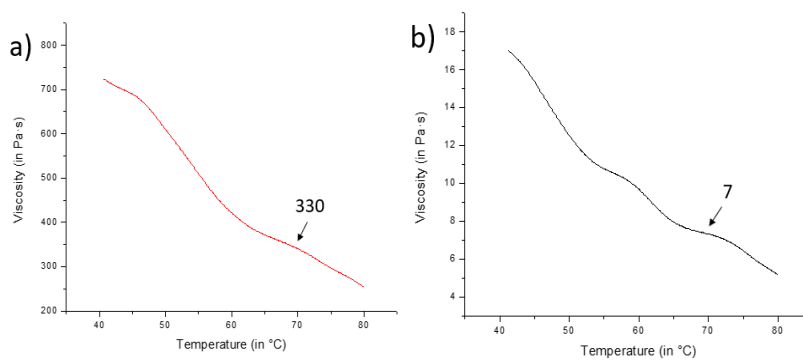


Figure B 20: Change in viscosity with temperature of PAI/C10 and PES/N10 casting solutions.



Figure B 21: Casting bath in which the PES membrane was produced with MBSA (PES/MBSA) and casted in hexane. The red rails are showing the residue of PES remaining after the casting process.

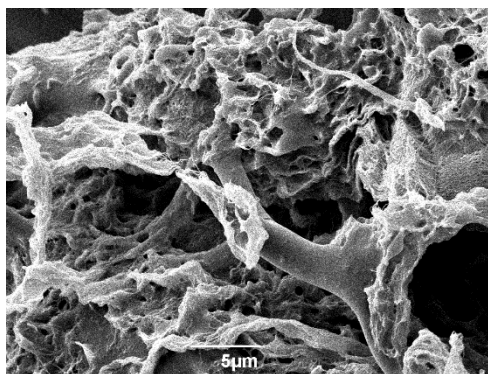


Figure B 22: Cross-sectional SEM figure of PES membranes produced using Cyrene and 5% PVP and 0.1% SWCNTs.

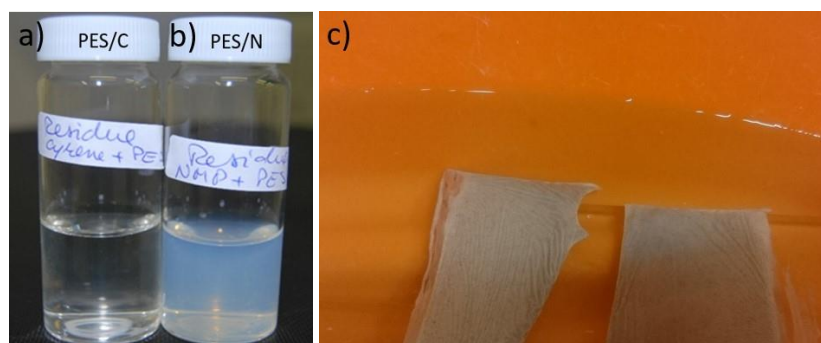


Figure B 23: (a) Coagulation bath of PES/PVP membranes in Cyrene and (b) NMP after membrane casting. (c) shows PES membranes produced with Cyrene and S300 after casting.

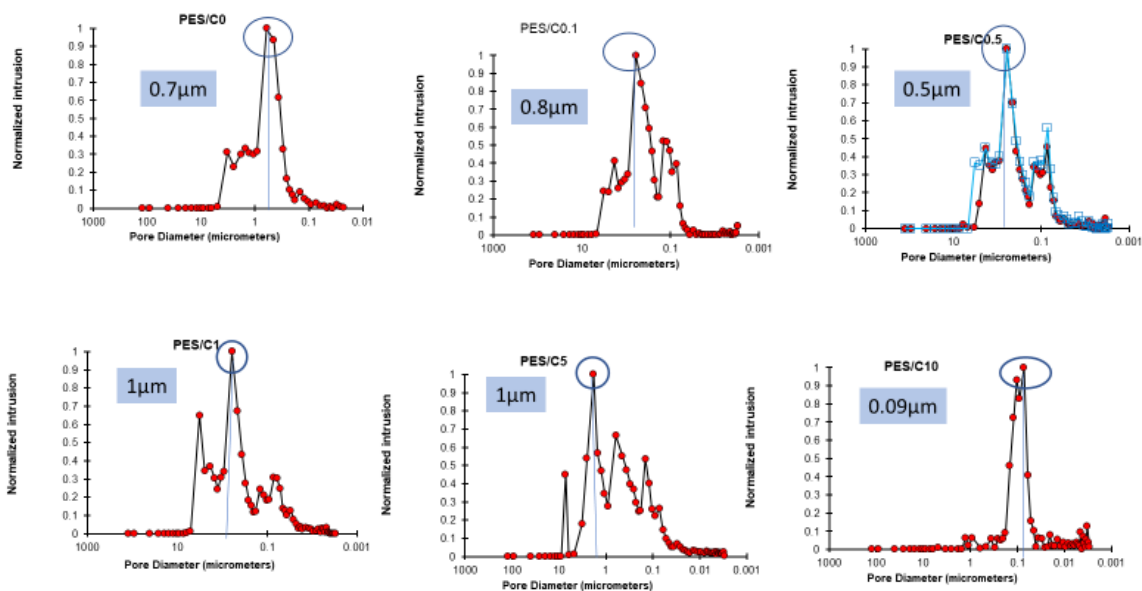


Figure B 24: Pore diameters of Cyrene-based PES membranes.

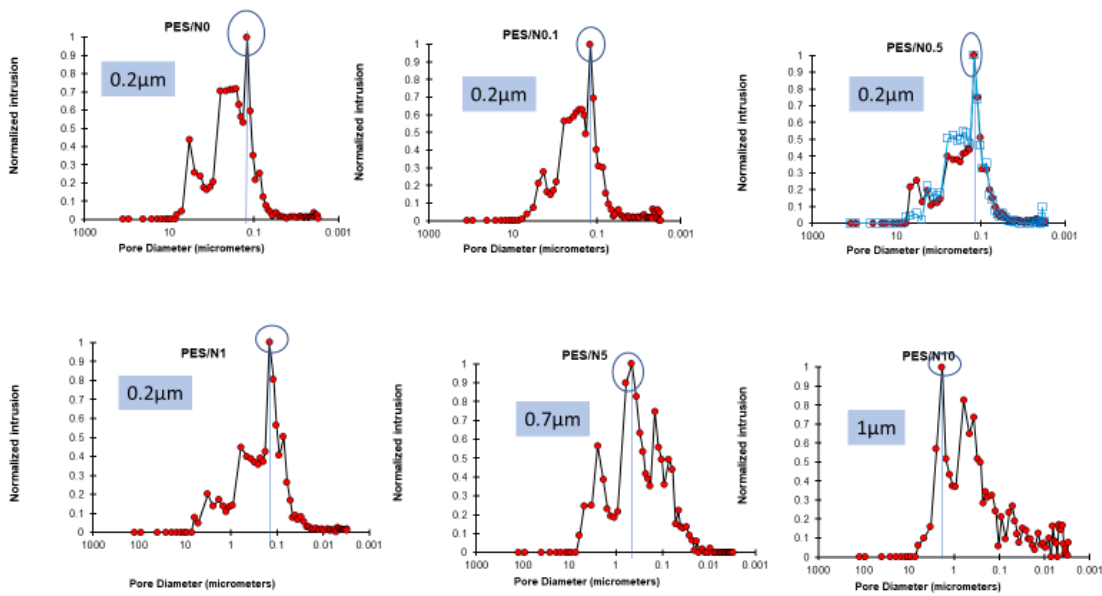


Figure B 25: Pore diameter of NMP-based PES membranes.

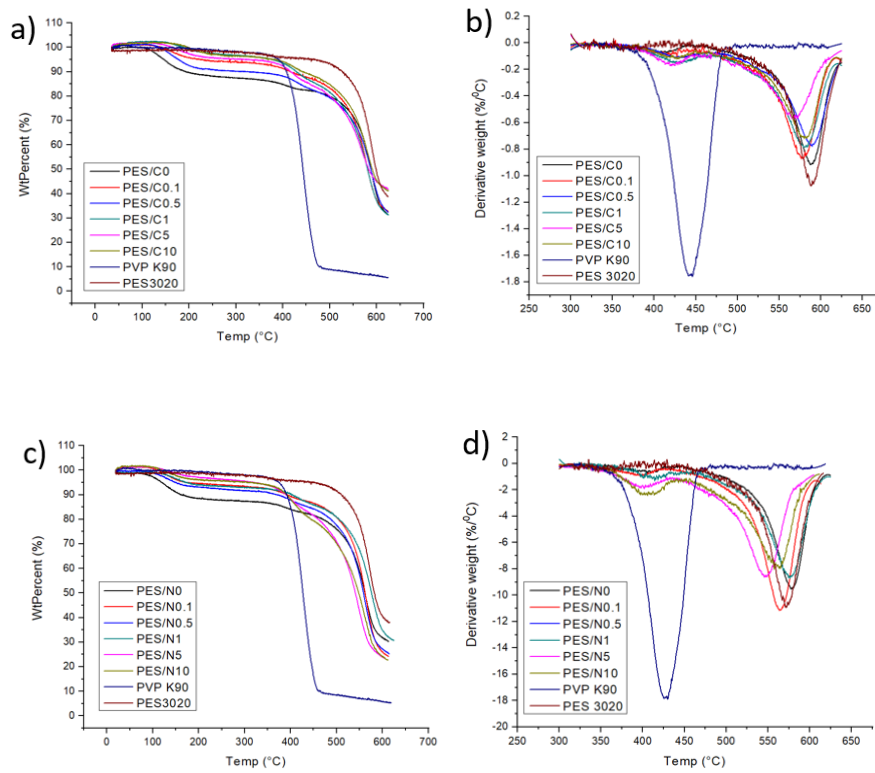


Figure B 26: (a-b) Thermogravimetric analysis (TGA) and differential thermogravimetric (DTG) measurements of PES/C and (c-d) PES/N membranes.

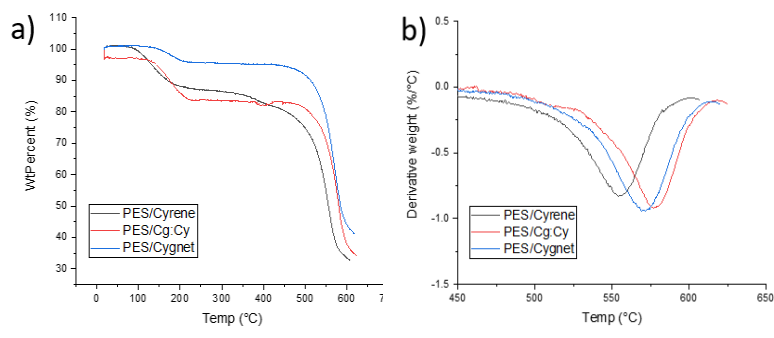


Figure B 27: (a) Thermogravimetric (TGA) and (b) differential thermogravimetric (DTG) measurements of PES-based membranes and pure Cyrene and Cygnnet 0.0.

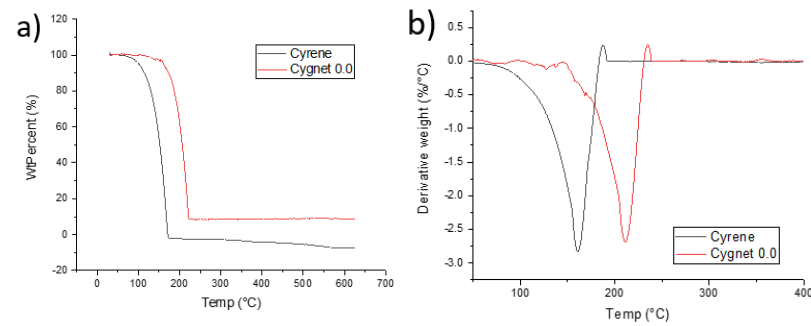


Figure B 28: (a) Thermogravimetric (TGA) and (b) differential thermogravimetric (DTG) measurements of Cyrene and Cygnnet 0.0.

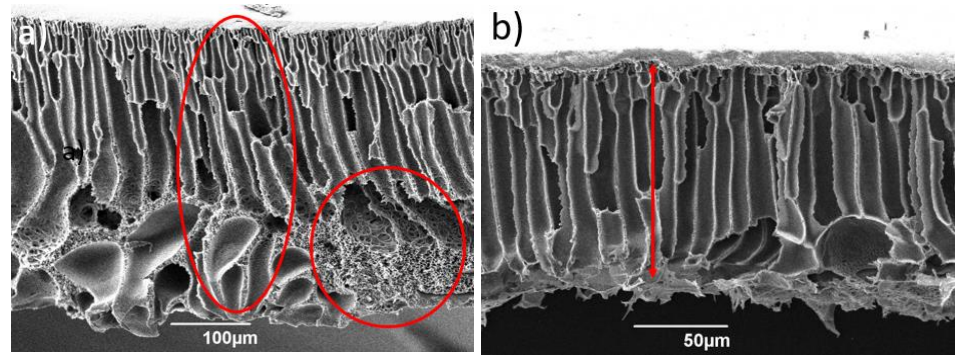


Figure B 29: PES/C1 membrane cast using different thickness: (a) 500 μm and (b) 250 μm.

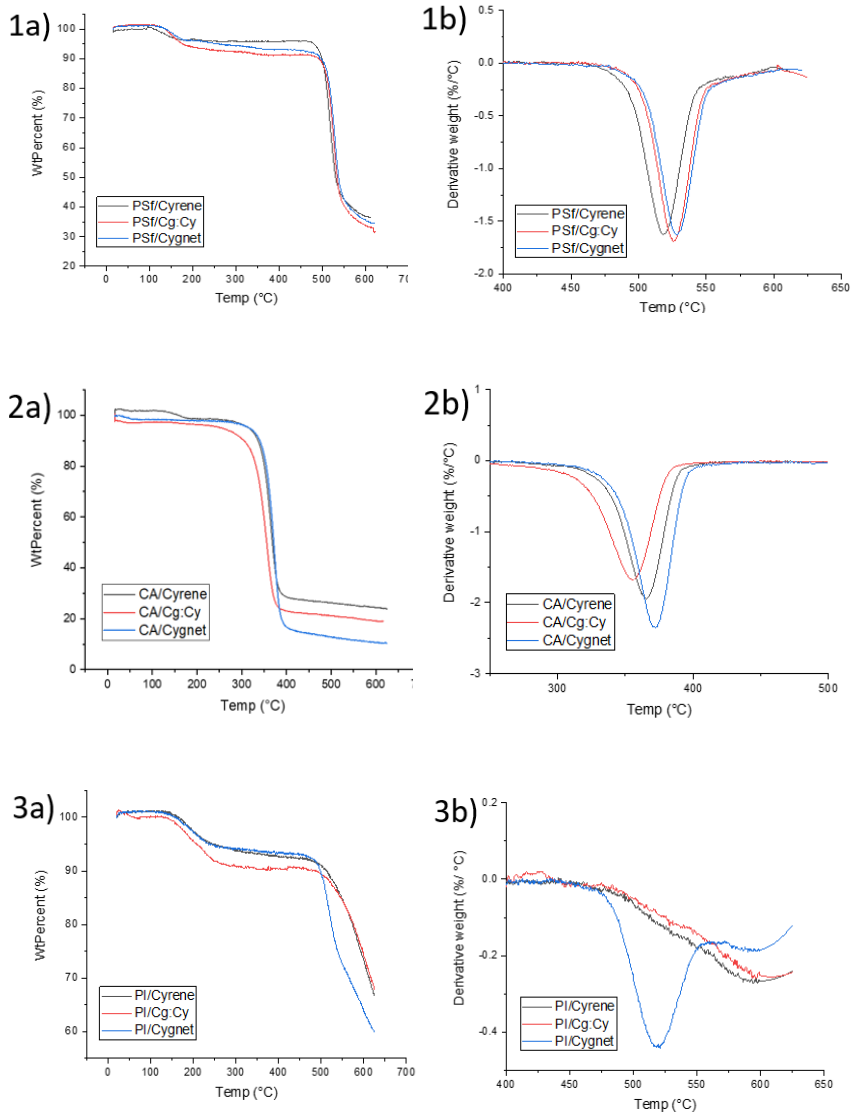


Figure B 30: (a) Thermogravimetric (TGA) and (b) differential thermogravimetric (DTG) measurements of PSf (1), CA (2) and PI (3)-based membranes and neat Cyrene and Cygnnet 0.0.

# Appendix C

Summary of First Pass Metrics Toolkit BASELINE (Ethanol-water mixture)

| Reactant (Limiting Reactant First) | Mass (g)    | Mol    | MW          | Mass (g) | Catalyst | Reagent | Mass (g)    | Reaction solvent | Volume (cm <sup>3</sup> ) | Density (g ml <sup>-1</sup> ) | Mass (g)     | Workup chemical | Mass (g)    | Workup solvent | Volume (cm <sup>3</sup> ) | Density (g ml <sup>-1</sup> ) | Mass (g) |             |
|------------------------------------|-------------|--------|-------------|----------|----------|---------|-------------|------------------|---------------------------|-------------------------------|--------------|-----------------|-------------|----------------|---------------------------|-------------------------------|----------|-------------|
| Wet lime peel                      | 5.00        |        |             |          |          |         |             | Ethanol          | 30.00                     | 0.79                          | 23.70        |                 |             |                |                           |                               |          | 0.00        |
|                                    |             | #DV/OI |             |          |          | Water   |             |                  | 20.00                     | 1.00                          | 20.00        |                 |             |                |                           |                               |          | 0.00        |
|                                    |             | #DV/OI |             |          |          |         |             |                  |                           |                               | 0.00         |                 |             |                |                           |                               |          | 0.00        |
|                                    |             | #DV/OI |             |          |          |         |             |                  |                           |                               | 0.00         |                 |             |                |                           |                               |          | 0.00        |
|                                    |             | #DV/OI |             |          |          |         |             |                  |                           |                               | 0.00         |                 |             |                |                           |                               |          | 0.00        |
|                                    |             | #DV/OI |             |          |          |         |             |                  |                           |                               | 0.00         |                 |             |                |                           |                               |          | 0.00        |
| <b>Total</b>                       | <b>5.00</b> |        | <b>0.00</b> |          |          |         | <b>0.00</b> |                  |                           |                               | <b>43.70</b> |                 | <b>0.00</b> |                |                           |                               |          | <b>0.00</b> |

| Yield       | #DV/OI | Flag   |
|-------------|--------|--------|
| Conversion  | 100.0  | #DV/OI |
| Selectivity | #DV/OI | #DV/OI |
| AE          | #DV/OI | #DV/OI |
| RME         | 0.270  | OE     |

$$RME = \frac{\text{mass of isolated product}}{\text{total mass of reactants}} \times 100$$

$$AE = \frac{\text{molecular weight of product}}{\text{total molecular weight of reactants}} \times 100$$

$$\text{mass intensity} = \frac{\text{total mass in a process or process step}}{\text{mass of product}}$$

$$OE = \frac{RME}{AE} \times 100$$

| Product                     | Mass (g) | MW  | Mol    |
|-----------------------------|----------|-----|--------|
|                             | 0.01350  |     | #DV/OI |
| Unreacted limiting reactant |          | MBS |        |

**Experimental:** Extraction was performed in 250 mL Erlenmeyer flasks at 50 °C for 4 h, with 120 rpm agitation in an orbital shaking incubator. 5 g of fresh peel was used as the extraction material, and the solvent volume was 50 mL. At this stage of the process, 2 kg of Mexican limes were washed to remove impurities. They were then squeezed, and the seeds were manually removed. Finally, the peel was ground up in a blender, until the particle size was less than 1 cm. The extract was concentrated in a rotavapor. The concentration of hesperidin in the extracts was determined by HPLC, and the yields were calculated as "mg of hesperidin per gram of fresh peel". The solid-to-solvent ratio and the solvent composition were varied according to the experimental design and they were duplicated we use here 0.1 g/mL ratio and 60-40% EtOH-water. An SSR of 0.1 g/cm<sup>3</sup> and 60% ethanol maximized the extraction yield, thereby obtaining a value of 2.7 mg g<sup>-1</sup> (average from 2 extractions).

## Solvents (First Pass)

| Preferred solvents   | water, EtOH, nBuOH, AcOPr, AcONBu, PhOMe, MeOH, TBUOH, BrOH, ethylene glycol, acetone, MEK, MBK, AcOEt, sulfolane  |
|--|--|
| Problematic solvents: (acceptable only if substitution does not offer advantages)          | DMSO, cyclohexanone, DMPU, AcOH, Ac2O, Acetonitrile, AcOMe, THF, heptane, Me-cyclohexane, toluene, xylene, MTBE, cyclohexane, chlorobenzene, formic acid, pyridine, Me-THF |
| Hazardous solvents: These solvents have significant health and/or safety concerns          | dioxane, pentane, TEK, diisopropyl ether, DCE, DCM, DMF, DMA, MAP, methoxyethanol, hexane  |
| Highly hazardous solvents: The solvents which are agreed not to be used, even in screening | Et <sub>2</sub> O, Benzene, CCl <sub>4</sub> , chloroform, DCE, nitromethane, CS <sub>2</sub> , HMPA   |

| Catalyst/enzyme (First Pass)  | Tick       |
|---|------------|
| Catalyst or enzyme used, or reaction takes place without any catalyst/reagents. | Green Flag |
| Use of stoichiometric quantities of reagents                                    | Amber Flag |
| Use of reagents in excess   | Red Flag   |

| Facile recovery of catalyst/enzyme | Tick       |
|------------------------------------|------------|
| catalyst/enzyme not recovered      | Green Flag |
|                                    | Amber Flag |

**Instructions for use:** Enter your data into the tables above to automatically calculate yield, AE, RME, MI/PMI and OE. Use the blank boxes in the tables to enter experimental data and note the flags for each Key Parameter. **Printing tips:** This spreadsheet is designed to be printed with 'landscape', 'narrow margin' and 'fit all columns on one page' settings

| Critical elements | Supply remaining | Flag colour | Note element |
|-------------------|------------------|-------------|--------------|
| 5-50 years        | Red Flag         | Red         |              |
| 50-500 years      | Amber Flag       | Amber       |              |
| +500 years        | Green Flag       | Green       |              |

Remaining years until depletion of known reserves  
Based on current rate of use

50-500 years  
5-50 years  
>500 years

Lanthanides\*  
Actinides †

| Energy (First Pass)                          | Tick         |
|--|--------------|
| Reaction run between 0 to 70°C               | Green Flag ✓ |
| Reaction run between -20 to 0 or 70 to 140°C | Amber Flag   |
| Reaction run below -20 or above 140°C        | Red Flag     |

|  | Tick         |
|--|--------------|
| Reaction run at reflux                                   | Red Flag     |
| Reaction run 5°C or more below the solvent boiling point | Green Flag ✓ |

| Batch/flow | Tick       |
|------------|------------|
| Flow       | Green Flag |
| Batch      | Amber Flag |

| Work Up   | List         |
|---|--------------|
| quenching<br>filtration<br>centrifugation<br>crystallisation<br>Low temperature distillation/evaporation/<br>sublimation (<140 °C at atmospheric pressure)<br>solvent exchange, quenching into aqueous<br>solvent | Green Flag ✓ |
| chromatography/ion exchange<br>high temperature<br>multiple recrystallisation   | Amber Flag   |
|   | Red Flag     |

| Health & safety            | Red Flag                     | Amber Flag                   | Green Flag | List substances and H-codes  | List substances and H-codes                        |
|----------------------------|------------------------------|------------------------------|------------|--|--|
| Highly explosive           | H200, H203, H202, H203       | H205, H220, H224             | ✓          | List substances and H-codes<br>H225 Highly flammable liquid and vapour | List substances and H-codes<br>H319 Eye irritation |
| Explosive thermal runaway  | H230, H240, H250             | H241                         |            |  |  |
| Toxic                      | H300, H310, H330             | H301, H311, H331             |            |  |  |
| Long Term toxicity         | H340, H350, H360, H370, H372 | H341, H351, H361, H371, H373 |            |  |  |
| Environmental implications | H400, H410, H411, H420       | H401, H412                   |            |  |  |

| Use of chemicals of environmental concern  | List substances of very high concern |
|--|--------------------------------------|
| Chemical identified as Substances of Very High Concern by ChemSec which are utilised | Red Flag                             |

Figure C 1: Summary of first pass metrics toolkit “baseline” for old method of extraction using a mixture between ethanol and water.



Summary of First Pass Metrics Toolkit NEW METHOD (Cyrene/water)

| Reactant (Limiting Reactant First) | Mass (g)    | MW          | Mol     | Catalyst | Mass (g)    | Reagent | Mass (g) | Reaction solvent | Volume (cm <sup>3</sup> ) | Density (g ml <sup>-1</sup> ) | Mass (g)    | Work up chemical | Mass (g)    | Workup solvent | Volume (cm <sup>3</sup> ) | Density (g ml <sup>-1</sup> ) | Mass (g) |             |
|------------------------------------|-------------|-------------|---------|----------|-------------|---------|----------|------------------|---------------------------|-------------------------------|-------------|------------------|-------------|----------------|---------------------------|-------------------------------|----------|-------------|
| Orange peel                        | 0.25        |             |         |          |             |         |          | Cyrene           | 3.50                      | 1.25                          | 4.38        |                  |             |                |                           |                               |          | 0.00        |
|                                    |             |             | #DIV/0! |          |             |         |          | Water            | 1.50                      | 1.00                          | 1.50        |                  |             |                |                           |                               |          | 0.00        |
|                                    |             |             | #DIV/0! |          |             |         |          |                  |                           |                               | 0.00        |                  |             |                |                           |                               |          | 0.00        |
|                                    |             |             | #DIV/0! |          |             |         |          |                  |                           |                               | 0.00        |                  |             |                |                           |                               |          | 0.00        |
|                                    |             |             | #DIV/0! |          |             |         |          |                  |                           |                               | 0.00        |                  |             |                |                           |                               |          | 0.00        |
|                                    |             |             | #DIV/0! |          |             |         |          |                  |                           |                               | 0.00        |                  |             |                |                           |                               |          | 0.00        |
| <b>Total</b>                       | <b>0.25</b> | <b>0.00</b> |         |          | <b>0.00</b> |         |          |                  |                           |                               | <b>5.88</b> |                  | <b>0.00</b> |                |                           |                               |          | <b>0.00</b> |

Flag

|                                 |         |         |
|---------------------------------|---------|---------|
| Yield                           | #DIV/0! | 100.0   |
| Conversion                      | #DIV/0! | 100.0   |
| Selectivity                     | #DIV/0! |         |
| AE                              | #DIV/0! |         |
| RME                             | 2.926   | OE      |
| PMI total                       | 839.0   | #DIV/0! |
| PMI Reaction reagents, catalyst | 839.0   |         |
| PMI reaction solvents           | 34.2    |         |
| PMI Workup                      | 804.8   |         |
| PMI Workup chemical             | 0.0     |         |
| PMI workup solvents             | 0.0     |         |

$$RME = \frac{\text{mass of isolated product}}{\text{total mass of reactants}} \times 100$$

$$AE = \frac{\text{molecular weight of product}}{\text{total molecular weight of reactants}} \times 100$$

$$\text{mass intensity} = \frac{\text{total mass in a process or process step}}{\text{mass of product}}$$

$$OE = \frac{RME}{AE} \times 100$$

**Experimental:**  
This method involves 5 mL mixture Cyrene-water (70:30) and 250 mg of dried orange peel in a single-stage extraction. The solid-solvent mixture before homogenisation at 65 °C for 2 hours, followed by extraction for 2 minutes at 14,450 rpm.  
The compounds were identified by ultra high-pressure liquid chromatography (UH-PLC), a less solvent intensive method, with a 1 µL injection volume in 80% water and 20% methanol. At the end of both processes, the solvent was concentrated in a rotary evaporator for ethanol and vacuum distillation for Cyrene. A maximum yield of 29.21 mg g<sup>-1</sup> was obtained in a single-stage extraction.

Solvents (First Pass)

|   |   |                     |
|---|---|---------------------|
| <b>Preferred solvents</b>   | water, EtOH, nBuOH, AcOPr, AcONBu, PhOMe, MeOH, tBuOH, BrOH, ethylene glycol, acetone, MEK, MIBK, AcOEt, sulfolane  | List solvents below |
| <b>Problematic solvents:</b> (acceptable only if substitution does not offer advantages)            | DMSO, cyclohexanone, DMPU, AcOH, Ac <sub>2</sub> O, Acetonitrile, AcOMe, THF, heptane, Me-cyclohexane, toluene, xylene, MTBE, cyclohexane, chlorobenzene, formic acid, pyridine, Me-THF | Water               |
| <b>Hazardous solvents:</b> (these solvents have significant health and/or safety concerns)          | hexane, pentane, TKA, diisopropyl ether, DMF, DCM, DMF  | Cyrene              |
| <b>Highly hazardous solvents:</b> (The solvents which are agreed not to be used, even in screening) | Et <sub>2</sub> O, Benzene, CCl <sub>4</sub> , chloroform, DCE, nitromethane, CS <sub>2</sub> , HMPA  |                     |

Catalyst/enzyme (First Pass)

|   |            |   |      |
|---|------------|---|------|
| Catalyst or enzyme used, or reaction takes place without any catalyst/reagents. | Green Flag | ✓ | Tick |
| Use of stoichiometric quantities of reagents                                    | Amber Flag |   |      |
| Use of reagents in excess   | Red Flag   |   |      |

|                                    |            |      |
|------------------------------------|------------|------|
| Facile recovery of catalyst/enzyme | Green Flag | Tick |
| catalyst/enzyme not recovered      | Amber Flag |      |

**Instructions for use:** Enter your data into the tables above to automatically calculate yield, AE, RME, MI/PMI and OE.  
Use the blank boxes in the tables to enter experimental data and note the flags for each Key Parameter.  
**Printing tips:** This spreadsheet is designed to be printed with 'landscape', 'narrow margin' and 'fit all columns on one page' settings



Figure C 2: Summary of first pass metrics toolkit using a mixture between Cyrene and water.

# Abbreviations

|                   |  |
|-------------------|--|
| 4,4' MDI          | 4,4'-Methylenebis (phenyl isocyanate)  |
| A                 | Membrane surface area (in water permeability) or shear stress (in rheology)                      |
| AIT               | Auto-ignition temperature  |
| ASTM              | American Society for Testing and Materials   |
| ATR-FTIR          | Attenuated Total Reflection Fourier Transform Infrared Spectroscopy                              |
| BAS               | Bile acid salts  |
| BP                | Boiling point  |
| C                 | Speed of light in a medium   |
| C <sub>0</sub>    | Speed of light in vacuum   |
| CA                | Cellulose acetate  |
| CEN               | European Committee for Standardisation   |
| CHEM21            | Chemical Manufacturing Methods for the 21st Century Pharmaceutical Industries                    |
| CDCl <sub>3</sub> | Chloroform   |
| CP                | Cyclopentanone   |
| COSMO-RS          | Conductor-like Screening Model for Real Solvents   |
| CST               | Corresponding State Theory   |
| D                 | Pore diameter or dipole moment   |
| DMAc              | <i>N,N'</i> -Dimethylacetamide   |
| DMF               | <i>N,N'</i> -Dimethylformamide   |
| DMSO              | Dimethyl sulfoxide   |
| E                 | Strength of the electric field applied   |
| E <sub>D</sub>    | Dispersion cohesive energy which comes from the nonpolar (dispersion) atomic forces              |
| E <sub>H</sub>    | Hildebrand electron exchange energy obtained from the hydrogen bonding molecular forces          |
| E <sub>P</sub>    | Hildebrand polar cohesive energy produced by the permanent dipole moment dipole molecular forces |
| EC                | Ethylene carbonate   |
| EG                | Ethylene glycol  |
| EHS               | Environmental, Health and Safety   |
| Et <sub>3</sub> N | Triethylamine  |

|                      |   |
|----------------------|---|
| F                    | Force   |
| FP                   | Flash Point                                       |
| G'                   | Store modulus of mechanical energy                |
| G''                  | Loss modulus                                      |
| GHG                  | Greenhouse gas                                    |
| GVL                  | $\gamma$ -valerolactone                           |
| GWP                  | Global Warming Potential                          |
| HMF                  | Hydroxymethylfurfural                             |
| HSPiP                | Hansen's Solubility Parameters in Practice        |
| <sup>1</sup> H-NMR   | Proton Nuclear Magnetic Resonance                 |
| H <sub>v</sub>       | Heat of vaporisation                              |
| ICP -MS              | Inductively Coupled Plasm-Mass Spectrometry       |
| InChi                | IUPAC International Chemical Identifier           |
| IUPAC                | International Union of Pure and Applied Chemistry |
| J <sub>w</sub>       | Water flux  |
| l                    | Thickness of membrane                             |
| LCA                  | Life Cycle Assessment                             |
| M                    | Mass  |
| MEK                  | Methyl Ethyl Ketone                               |
| M                    | Molar mass  |
| NMP                  | 1-Methyl-2-pirrolidinone                          |
| P                    | Pressure or polarisation                          |
| Pa                   | Pascal  |
| PAI                  | Poly(amido-imide)                                 |
| PAN                  | Polyacrylonitrile                                 |
| P <sub>c</sub>       | Critical pressure                                 |
| PC                   | Propylene carbonate                               |
| PDA                  | Photo Diode Array detector                        |
| Pd(OAc) <sub>2</sub> | Palladium (II) acetate                            |
| PES                  | Polyethersulfone                                  |
| PI                   | Polyimide   |
| ppb                  | Parts per billion                                 |
| ppm                  | Parts per million                                 |

|        |  |
|--------|--|
| PSD    | Pore size distribution   |
| PSf    | Polysulfone  |
| PTFE   | Polytetrafluoroethylene  |
| PVDF   | Polyvinylidene fluoride  |
| PVP    | Polyvinylpyrrolidone   |
| QC     | Quantum chemical   |
| QDa    | Mass detector  |
| QM     | Quantum mechanics  |
| QSPR   | Quantitative Structure Property Relationships                        |
| REACH  | Registration, Evaluation, Authorisation and Restriction of Chemicals |
| $R_0$  | Radius of the Hansen sphere  |
| $R_a$  | Distance between the solute and the solvent                          |
| RED    | Relative energy difference   |
| RER    | Relative Evaporation Rate  |
| RT     | Room temperature   |
| S4     | Sustainable Solvent Selection Service                                |
| SEM    | Scanning electron microscopy   |
| SMILES | Simplified Molecular-Input Line Entry System                         |
| T      | Time   |
| TBL    | Triple bottom line   |
| $T_c$  | Critical temperature   |
| TEP    | Triethyl phosphate   |
| THF    | Tetrahydrofuran  |
| TG     | Thermogravimetry   |
| TMA    | Trimellitic anhydride  |
| T/yr   | Tonnes per year  |
| UHPLC  | Ultra-High Performance Liquid Chromatography                         |
| UNEP   | United Nations Environment Programme                                 |
| $V_m$  | Molar volume   |
| $V_p$  | Vapour pressure  |
| WCA    | Water contact angle  |
| $W_d$  | Dry mass of a membrane   |
| $W_w$  | Wet mass of a membrane   |

|                        |   |
|------------------------|---|
| $\gamma$ -MB           | Yamamoto-molecular break                                    |
| $\delta_D$             | Hansen dispersion cohesion solubility parameter             |
| $\delta_H$             | Hansen hydrogen bonding cohesion solubility parameter       |
| $\delta_P$             | Hansen polar cohesion solubility parameter                  |
| $\gamma$               | Hg-air surface tension (in MIP) or shear rate (in rheology) |
| $\theta$               | Hg-air-porous material contact angle                        |
| $\rho$                 | Density   |
| $\eta$                 | Dynamic viscosity   |
| $\sigma$               | Shear stress  |
| $\Delta H_v$           | Heat of vaporisation  |
| $\epsilon, \epsilon_r$ | Dielectric constant or relative electric permittivity       |

# References

1. P. T. Anastas and T. C. Williamson (eds.), in: *Green Chemistry: Designing Chemistry for the Environment*, ACS Symposium Series 626, Washington, D.C., 1996, ch. 1, 1-17.
2. P. Anastas and N. Eghbali, *Chem. Soc. Rev.*, 2010, **39**, 301-312.
3. R. A. Sheldon, *Green Chem.*, 2007, **9**, 1273-1283.
4. E. S. Beach, Z. Cui and P. T. Anastas, *Energy Environ. Sci.*, 2009, **2**, 1038-1049.
5. Registration, Evaluation, Authorisation and Restriction of Chemicals (REACH) regulation. Available at: <https://echa.europa.eu/regulations/reach/legislation>, Accessed 14.03.2020.
6. Chemicals Classification, Labelling and Packaging (CLP) legislation. Available at: <https://echa.europa.eu/regulations/clp/legislation>. Accessed 14.03.2020.
7. Chemicals industry: prepare for after the transition period. Available at: <https://www.hse.gov.uk/brexit/chemicals-brexit-guidance.htm>. Accessed 11.11.2020.
8. Registration, Evaluation, Authorisation and Restriction of Chemicals regulation after Brexit. Available at: <https://www.hse.gov.uk/brexit/reach-guidance.htm>. Accessed 11.11.2020.
9. J. Philp, *Energy Environ. Sci.*, 2015, **8**, 3063-3068.
10. S. Sauve, S. Bernard and P. Sloan, *Environ. Dev.*, 2016, **17**, 48-56.
11. J. H. Clark, T. J. Farmer, L. Herrero-Davila and J. Sherwood, *Green Chem.*, 2016, **18**, 3914-3934.
12. S. V. Mohan, G. N. Nikhil, P. Chiranjeevi, C. N. Reddy, M. V. Rohit, A. N. Kumar and O. Sarkar, *Bioresour. Technol.*, 2016, **215**, 2-12.
13. M. Eissen, J. O. Metzger, E. Schmidt and U. Schneidewind, *Angew. Chem., Int. Ed.*, 2002, **41**, 414-436.
14. Brundtland Report of United Nations, World Commission on Environment and Development in *Our Common Future*, Oxford University Press, Oxford, 1987.
15. J. Elkington, in: *The Triple Bottom Line- Does it all add up?*, A. Henriques, J. Richardson (eds.), London, 2013, ch. 1, 1-17.
16. The United Nations Environment Programme (UNEP), *Towards a Green Economy: Pathways to Sustainable Development and Poverty Eradication*. Available at: [https://www.cbd.int/financial/doc/green\\_economyreport2011.pdf](https://www.cbd.int/financial/doc/green_economyreport2011.pdf). Accessed 09.08.2018.
17. F. Chemat, M. A. Vian and G. Cravotto, *International Journal of Molecular Sciences*, 2012, **13**, 8615-8627.

18. "Bio-based" definition. Available at: <https://www.cen.eu/work/areas/chemical/biobased/Pages/default.aspx>, EN 16575. Accessed 09.08.2018.
19. M. Bandres, P. de Caro, S. Thiebaud-Roux and M. E. Borredon, *C. R. Chim.*, 2011, **14**, 636-646.
20. S. J. F. Byrne, J. Sherwood, C. R. McElroy, T. J. Farmer, J. H. Clark, A. J. Hunt, in *Bio-Based Solvents*, F. Jerome, R. Luque (eds.), Wiley, 2017, ch. 3, 49-82.
21. Y. L. Gu and F. Jerome, *Chem. Soc. Rev.*, 2013, **42**, 9550-9570.
22. C. Capello, U. Fischer and K. Hungerbuhler, *Green Chem.*, 2007, **9**, 927-934.
23. P. T. Anastas and M. M. Kirchhoff, *Acc. Chem. Res.*, 2002, **35**, 686-694.
24. P. S. Bauerlein, T. L. ter Laak, P. de Voogt, C. Muller, D. Vogt, I. J. S. Fairlamb, J. M. Slattery, A. C. Whitwood and A. F. Lee, *Abstr. Pap. Am. Chem. Soc.*, 2010, **240**, -.
25. R. L. Vekariya, *J. Mol. Liq.*, 2017, **227**, 44-60.
26. H. Vanda, Y. T. Dai, E. G. Wilson, R. Verpoorte and Y. H. Choi, *C. R. Chim.*, 2018, **21**, 628-638.
27. A. S. Khan, T. H. Ibrahim, N. A. Jabbar, M. I. Khamis, P. Nancarrow and F. S. Mjalli, *RSC Adv.*, 2021, **11**, 12398-12422.
28. S. Y. Tan, F. E. Bedoya-Lora, J. P. Hallett and G. H. Kelsall, *Electrochim. Acta*, 2021, **376**. 1-9.
29. J. Q. Chen, Y. Yu, B. J. Zhu, J. G. Han, C. Liu, C. G. Liu, L. Y. Miao and S. Fakudze, *Sci. Total Environ.*, 2021, **765**, 142754-142764.
30. D. B. Zhao, Y. C. Liao and Z. D. Zhang, *Clean-Soil Air Water*, 2007, **35**, 42-48.
31. C. Bakirtzi, K. Triantafyllidou and D. P. Makris, *J. Appl. Res. Med. Aromat. Plants*, 2016, **3**, 120-127.
32. S. Gore, S. Baskaran and B. Koenig, *Green Chem.*, 2011, **13**, 1009-1013.
33. C. A. Nkuku and R. J. LeSuer, *J. Phys. Chem. B*, 2007, **111**, 13271-13277.
34. F. Ilgen and B. Konig, *Green Chem.*, 2009, **11**, 848-854.
35. R. K. Henderson, C. Jimenez-Gonzalez, D. J. C. Constable, S. R. Alston, G. G. A. Inglis, G. Fisher, J. Sherwood, S. P. Binks and A. D. Curzons, *Green Chem.*, 2011, **13**, 854-862.
36. A. Valavanidis, T. Vlachogianni, in *Green chemistry and green Engineering, from theory to practice for the protection of the environment and sustainable development*, Synchrone Themata Publs, Athens, 1<sup>st</sup> edn., 2012, ch. 1, 1-16.
37. Sustainable Solvent Selection Service (S4). Available at: <https://www.york.ac.uk/res/s4/about.html>. Accessed 09.08.2018.



38. D. Prat, A. Wells, J. Hayler, H. Sneddon, C. R. McElroy, S. Abou-Shehada and P. J. Dunn, *Green Chem.*, 2016, **18**, 288-296.
39. F. P. Byrne, C. M. Nussbaumer, E. J. Savin, R. A. Milesco, C. R. McElroy, J. H. Clark, B. M. A. van Vugt-Lussenburg, B. van der Burg, M. Y. Meima, H. E. Buist, E. D. Kroese, A. J. Hunt and T. J. Farmer, *Chemsuschem*, 2020, **13**, 3212-3221.
40. F. Byrne, T. Farmer, A. Hunt and J. Clark, *ECO-BIO*, 2018.
41. B. M. Trost, *Science*, 1991, **254**, 1471-1477.
42. A. D. Curzons, D. J. C. Constable, D. N. Mortimer and V. L. Cunningham, *Green Chem.*, 2001, **3**, 1-6.
43. A. D. Kreuder, T. House-Knight, J. Whitford, E. Ponnusamy, P. Miller, N. Jesse, R. Rodenborn, S. Sayag, M. Gebel, I. Aped, I. Sharfstein, E. Manaster, I. Ergaz, A. Harris and L. N. Grice, *ACS Sus. Chem. & Eng.*, 2017, **5**, 2927-2935.
44. C. R. McElroy, A. Constantinou, L. C. Jones, L. Summerton and J. H. Clark, *Green Chem.*, 2015, **17**, 3111-3121.
45. R. M. F. Kerton, R. Mariott, *Alternative Solvents for Green Chemistry*, R. Soc. Chem., R. M. F. Kerton, R. Mariott, A. Stankiewicz, G. Kraus, P. Seidl, Y. Kou, J. Clark (eds.), 2<sup>nd</sup> ed., 2013.
46. "Solvent" definition by the International Union of Pure and Applied Chemistry (IUPAC). A.D. McNaught, A. Wilkinson, *IUPAC Compendium of Chemical Terminology*, Blackwell Scientific Publications, Oxford, 1997, **2**. Accessed 04.04.2021.
47. J. H. Clark, T. J. Farmer, A. J. Hunt and J. Sherwood, *International Journal of Molecular Sciences*, 2015, **16**, 17101-17159.
48. "Miscibility" definition by the International Union of Pure and Applied Chemistry. A.D. McNaught, A. Wilkinson, *IUPAC Compendium of Chemical Terminology*, 2<sup>nd</sup> ed. (the "Gold Book"), 1997. Accessed 03.07.2020.
49. H. Gamsjager, J. W. Lorimer, P. Scharlin and D. G. Shaw, *Pure Appl. Chem.*, 2008, **80**, 233-276.
50. J. Clayden, N. Greeves, S. Warren, *Organic chemistry*, OUP Oxford, 2<sup>nd</sup> ed., 2012, 249.
51. A. Rashid, E. T. White, T. Howes, J. D. Litster and I. Marziano, *J. Chem. Eng. Data*, 2014, **59**, 2699-2703.
52. M. De Bruyn, V. L. Budarin, A. Misefari, S. Shimizu, H. Fish, M. Cockett, A. J. Hunt, H. Hofstetter, B. M. Weckhuysen, J. H. Clark and D. J. Macquarrie, *ACS Sus. Chem. Eng.*, 2019, **7**, 7878-7883.
53. B. A. Miller-Chou and J. L. Koenig, *Prog. Polym. Sci.*, 2003, **28**, 1223-1270.
54. G. R. Guillen, Y. J. Pan, M. H. Li and E. M. V. Hoek, *Ind. Eng. Chem. Res.*, 2011, **50**, 3798-3817.
55. A. P. Srivastava and E. B. Nauman, *Polym. Mater. Sci. Eng. Proceed.*, 1993, **69**, 307-308.

56. K. Ueberreiter in: *Diffusion in polymers*, J. Crank, G. S. Park (eds.), Academic Press, London and New York, 1968, **14**, The solution process, 219-257.
57. D. F. Stamatialis, M. Sanopoulou and I. Raptis, *J. Appl. Polym. Sci.*, 2002, **83**, 2823-2834.
58. J. Manjkow, J. S. Papanu, D. W. Hess, D. S. Soane and A. T. Bell, *J. Electrochem. Soc.*, 1987, **134**, 2003-2007.
59. E. E. Parsonage, N. A. Peppas and P. I. Lee, *J. Vac. Sci. Technol., B*, 1987, **5**, 538-545.
60. E. Gipstein, A. C. Ouano, D. E. Johnson and O. U. Need, *Polym. Eng. Sci.*, 1977, **17**, 396-401.
61. A. C. Ouano and J. A. Carothers, *Polym. Eng. Sci.*, 1980, **20**, 160-166.
62. W. J. Cooper, P. D. Krasicky and F. Rodriguez, *J. Appl. Polym. Sci.*, 1986, **31**, 65-73.
63. R. A. Milesco, C. R. McElroy, T. J. Farmer, P. M. Williams, M. J. Walters and J. H. Clark, *Adv. Polym. Technol.*, 2019, **2019**, 1-15.
64. I. P. Beletskaya and A. V. Cheprakov, *Chem. Rev.*, 2000, **100**, 3009-3066.
65. R. B. Merrifield, *J. Am. Chem. Soc.*, 1963, **85**, 2149-2154.
66. C. B. Chen, J. Li, R. Li, G. Y. Xiao and D. Y. Yan, *New J. Chem.*, 2013, **37**, 2778-2783.
67. Y. Xu, H. Z. Cao, Y. Q. Xue, B. Li and W. H. Cai, *Nanomaterials*, 2018, **8**, 942-974.
68. K. D. Ausman, R. Piner, O. Lourie, R. S. Ruoff and M. Korobov, *J. Phys. Chem., B*, 2000, **104**, 8911-8915.
69. S. Giordani, S. D. Bergin, V. Nicolosi, S. Lebedkin, M. M. Kappes, W. J. Blau and J. N. Coleman, *J. Phys. Chem., B*, 2006, **110**, 15708-15718.
70. T. Otsuka and Y. Chujo, *Polymer*, 2009, **50**, 3174-3181.
71. *US Pat.*, US4360633A, 1982.
72. P. W. A. Fessler, *US3975345A.*, 1978.
73. A. Abdelrasoul, H. Doan, A. Lohi and C. H. Cheng, *ChemBioEng Rev.*, 2015, **2**, 22-43.
74. M. Amirilargani, M. Sadrzadeh and T. Mohammadi, *J. Polym. Res.*, 2010, **17**, 363-377.
75. M. Khorsand-Ghayeni, J. Barzin, M. Zandi and M. Kowsari, *Polym. Bull.*, 2017, **74**, 2081-2097.
76. D. J. Tranchemontagne, J. R. Hunt and O. M. Yaghi, *Tetrahedron*, 2008, **64**, 8553-8557.
77. NMP for paint removal. Available at: <https://www.eastman.com/Pages/ProductHome.aspx?product=71103627>, Accessed 21.03.2020.
78. P. Karande and S. Mitragotri, *Biochim. Biophys. Acta, Biomembr.*, 2009, **1788**, 2362-2373.
79. H. Marwah, T. Garg, A. K. Goyal and G. Rath, *Drug Delivery*, 2016, **23**, 564-578.
80. *US Pat.*, US4150038A, 1977.
81. O. Ferreira and S. P. Pinho, *Ind.Eng. Chem. Res.*, 2012, **51**, 6586-6590.
82. C. D. Stalikas, *J. Sep. Sci.*, 2007, **30**, 3268-3295.

83. NMP added to REACH restricted substance list. Available at: <https://chemicalwatch.com/66647/nmp-added-to-reach-restricted-substances-list>. Accessed 13.01.2018.
84. European Chemicals Agency (ECHA) committees conclude on two restrictions and 15 harmonised classification and labelling opinions. Available at: <https://echa.europa.eu/-/echa-s-committees-conclude-on-two-restrictions-and-15-harmonised-classification-and-labelling-opinions>. Accessed 08.05.2020.
85. DMAc ECHA infocard. Available at: <https://echa.europa.eu/substance-information/-/substanceinfo/100.004.389> Accessed 28.06.2020.
86. DMSO ECHA infocard. Available at: <https://echa.europa.eu/substance-information/-/substanceinfo/100.000.604>. Accessed 28.06.2020.
87. *US Pat.*, US6987191B1, 2000.
88. *Eur. Pat.*, EP1489067A1, 2003.
89. J. L. Liu, C. K. Guo, Z. F. Zhang, T. Jiang, H. Z. Liu, J. L. Song, H. L. Fan and B. X. Han, *Chem. Commun.*, 2010, **46**, 5770-5772.
90. *World Pat.*, WO2000073251A1, 2000.
91. *Eur. Pat.*, EP1828102B1, 2006.
92. P. E. Correa and D. P. Riley, *J. Org. Chem.*, 1985, **50**, 1787-1788.
93. Q. Yang, M. Sheng, X. Y. Li, C. Tucker, S. V. Cespedes, N. J. Webb, G. T. Whiteker and J. Yu, *Org. Process Res. Dev.*, 2020, **24**, 916-939.
94. T. Marino, F. Galiano, S. Simone and A. Figoli, *Environ. Sci. Pollut. Res.*, 2019, **26**, 14774-14785.
95. Global Green and bio-based solvent market. Available at: <https://www.energyglobal.com/>. Accessed 09.08.2018.
96. B. H. Lipshutz, F. Gallou and S. Handa, *ACS Sus. Chem. Eng.*, 2016, **4**, 5838-5849.
97. Cyrene ECHA infocard. Available at: <https://echa.europa.eu/substance-information/-/substanceinfo/100.234.612>. Accessed 23.08.2018.
98. Ethylene carbonate ECHA infocard. Available at: <https://echa.europa.eu/substance-information/-/substanceinfo/100.002.283> Accessed 28.06.2020.
99. Propylene carbonate ECHA infocard. Available at: <https://echa.europa.eu/substance-information/-/substanceinfo/100.003.248> Accessed 28.06.2020.
100. Gamma-valerolactone ECHA infocard. Accesible at: <https://echa.europa.eu/substance-information/-/substanceinfo/100.003.245> Accessed 28.06.2020.
101. X. R. Shen, D. Z. Xia, Y. X. Xiang and J. G. Gao, *E-Polymers*, 2019, **19**, 323-329.
102. Cyclopentanone ECHA infocard. Available at: <https://echa.europa.eu/substance-information/-/substanceinfo/100.004.033>. Accessed 11.11.2020.

103. J. Sherwood, T. J. Farmer and J. H. Clark, *Chem*, 2018, **4**, 2010-2012.
104. P. Tundo and M. Selva, *Acc. Chem. Res.*, 2002, **35**, 706-716.
105. S. Y. Huang, B. Yan, S. P. Wang and X. B. Ma, *Chem. Soc. Rev.*, 2015, **44**, 3079-3116.
106. F. Doro, P. Winnertz, W. Leitner, A. Prokofieva and T. E. Muller, *Green Chem.*, 2011, **13**, 292-295.
107. H. C. Genuino, H. H. V. de Bovenkamp, E. Wilbers, J. G. M. Winkelman, A. Goryachev, J. P. Hofmann, E. J. M. Hensen, B. M. Weckhuysen, P. C. A. Bruijninx and H. J. Heeres, *ACS Sus. Chem. Eng.*, 2020, **8**, 5903-5919.
108. M. Dohade and P. L. Dhepe, *Catal. Sci. Technol.*, 2018, **8**, 5259-5269.
109. T. Shen, R. J. Hu, C. J. Zhu, M. Li, W. Zhuang, C. L. Tang and H. J. Ying, *RSC Adv.*, 2018, **8**, 37993-38001.
110. Moving beyond drop-in replacements: Performance-Advantaged Biobased Chemicals. Available at: <https://www.energy.gov/sites/prod/files/2018/06/f53/Performance-Advantaged%20Biobased%20Chemicals%20Workshop%20Report.pdf>. Accessed 09.08.2018.
111. A. A. M. Peru, A. L. Flourat, C. Gunawan, W. Raverty, M. Jevric, B. W. Greatrex and F. Allais, *Molecules*, 2016, **21**, 988-997.
112. J. Sherwood, M. De Bruyn, A. Constantinou, L. Moity, C. R. McElroy, T. J. Farmer, T. Duncan, W. Raverty, A. J. Hunt and J. H. Clark, *Chem. Commun.*, 2014, **50**, 9650-9652.
113. F. Eiden and F. Denk, *Arch. Pharm.*, 1991, **324**, 353-354.
114. F. Shafizadeh, R.H. Fumeaux, T.T. Stevenson, *Carbohydr. Res.*, 1979, **71**, 169-191.
115. D. E. Richardson and W. D. Raverty, *Appita*, 2016, **69**, 344-351.
116. Non-Petroleum Based Solvent Could Come to Tasmania. Available at: <http://www.abc.net.au/news/2015-11-13/tasmanias-new-multi-billion-dollar-green-chemical-and-industry/6939522>. Accessed 16.02.2020.
117. New plant in France to produce Cyrene as part of ReSolute project. Available at: <https://bioenergyinternational.com/biochemicals-materials/circa-group-to-head-resolute-to-resolve-commercial-bio-based-solvent-production>. Accessed 28.03.2021.
118. V. K. Brel, A. V. Samet, L. D. Konyushkin, A. I. Stash, V. K. Belsky and V. V. Semenov, *Mendeleev Commun.*, 2015, **25**, 44-46.
119. A. L. Flourat, A. A. M. Peru, A. R. S. Teixeira, F. Brunissen and F. Allais, *Green Chem.*, 2015, **17**, 404-412.
120. S. H. Krishna, D. J. McClelland, Q. A. Rashke, J. A. Dumesic and G. W. Huber, *Green Chem.*, 2017, **19**, 1278-1285.
121. J. Mazario, M. P. Romero, P. Concepcion, M. Chavez-Sifontes, R. A. Spanevello, M. B. Comba, A. G. Suarez and M. E. Domine, *Green Chem.*, 2019, **21**, 4769-4785.

122. L. M. M. Mouterde, F. Allais and J. D. Stewart, *Green Chem.*, 2018, **20**, 5528-5532.
123. K. L. Wilson, A. R. Kennedy, J. Murray, B. Greatrex, C. Jamieson and A. J. B. Watson, *Beilstein J. Org. Chem.*, 2016, **12**, 2005-2011.
124. J. Zhang, G. B. White, M. D. Ryan, A. J. Hunt and M. J. Katz, *ACS Sustainable Chem. Eng.*, 2016, **4**, 7186-7192.
125. SigmaAldrich.com. Available at: <https://www.sigmaaldrich.com/united-kingdom.html>. Accessed 02.07.2020.
126. A. A. C. Pacheco, J. Sherwood, A. Zhenova, C. R. McElroy, A. J. Hunt, H. L. Parker, T. J. Farmer, A. Constantinou, M. De Bruyn, A. C. Whitwood, W. Raverty and J. H. Clark, *ChemSusChem*, 2016, **9**, 3503-3512.
127. C. M. Hansen, *J. Paint Technol.*, 1967, **511**, 505-510.
128. C. M. Hansen, P. E. Pierce, *Ind. Eng. Chem. Prod. Res. Dev.*, 1974, **13**, 218-225.
129. C. M. Hansen, E. Wallström, *J. Adhesion*, 1983, **15**, 275-286.
130. S. Gardebjer, M. Andersson, J. Engstrom, P. Restorp, M. Persson and A. Larsson, *Polym. Chem.*, 2016, **7**, 1756-1764.
131. B. Hossin, K. Rizi and S. Murdan, *Eur. J. Pharm. Biopharm.*, 2016, **102**, 32-40.
132. J. C. Serrano-Ruiz, R. Luque and A. Sepulveda-Escribano, *Chem. Soc. Rev.*, 2011, **40**, 5266-5281.
133. S. M. Pestov and S. Yaghoubpour, *Liq. Cryst. Their Appl.*, 2018, **18**, 95-102.
134. S. Detriche, G. Zorzini, J. F. Colomer, A. Fonseca and J. B. Nagy, *J. Nanosci. Nanotechnol.*, 2008, **8**, 6082-6092.
135. C. M. Hansen and A. L. Smith, *Carbon*, 2004, **42**, 1591-1597.
136. J. Ma and R. M. Larsen, *J. Thermoplast. Compos. Mater.*, 2014, **27**, 801-815.
137. J. Ma and R. M. Larsen, *ACS Appl. Mater. Interfaces*, 2013, **5**, 1287-1293.
138. H. T. Ham, Y. S. Choi and I. J. Chung, *J. Colloid Interface Sci.*, 2005, **286**, 216-223.
139. C. M. Hansen, *Ind. Eng. Chem. Prod. Res. Dev.*, 1969, **8**, 2-11.
140. Pirika software. Available at: <http://pirika.com/ENG/HSP/HelperApp.html>. Accessed 14.02.2019.
141. InChi software version 1.04. Available at: <https://www.inchi-trust.org/>. Accessed 16.02.2018.
142. Hansen Solubility Parameters in Practice 5.0.03 version. Available at: <https://www.hansen-solubility.com/downloads.php>. Accessed 02.11.2017.
143. Joback method from Pirika. Available at: <https://www.pirika.com/ENG/TCPE/HTML5/Joback/index.html>, Accessed 05.03.2019.
144. K. G. Joback and R. C. Reid, *Chem. Eng. Commun.*, 1987, **57**, 233-243.
145. M. Durand, V. Molinier, W. Kunz and J. M. Aubry, *Chem. Eur. J.*, 2011, **17**, 5155-5164.

146. A. Benazzouz, L. Moity, C. Pierlot, V. Molinier and J. M. Aubry, *Colloids Surf., A*, 2014, **458**, 101-109.
147. L. Mistry, K. Mapesa, T. W. Bousfield and J. E. Camp, *Green Chem.*, 2017, **19**, 2123-2128.
148. H. J. Salavagione, J. Sherwood, M. De Bruyn, V. L. Budarin, G. J. Ellis, J. H. Clark and P. S. Shuttleworth, *Green Chem.*, 2017, **19**, 2550-2560.
149. K. L. Wilson, J. Murray, C. Jamieson and A. J. B. Watson, *Org. Biomol. Chem.*, 2018, **16**, 2851-2854.
150. K. L. Wilson, J. Murray, C. Jamieson and A. J. B. Watson, *Synlett*, 2018, **29**, 650-654.
151. L. Hughes, C. R. McElroy, A. C. Whitwood and A. J. Hunt, *Green Chem.*, 2018, **20**, 4423-4427.
152. T. W. Boustietd, K. P. R. Pearce, S. B. Nyamini, A. Angelis-Dimakis and J. E. Camp, *Green Chem.*, 2019, **21**, 3675-3681.
153. M. Vastano, A. Pellis, C. B. Machado, R. Simister, S. J. McQueen-Mason, T. J. Farmer and L. D. Gomez, *Macromol. Rapid Commun.*, 2019, **40**, 1900361-1900371.
154. P. Ray, T. Hughes, C. Smith, M. Hibbert, K. Saito and G. P. Simon, *Polym. Chem.*, 2019, **10**, 3334-3341.
155. T. Marino, F. Galiano, A. Molino and A. Figoli, *J. Membr. Sci.*, 2019, **580**, 224-234.
156. C. A. Carner, C. F. Croft, S. D. Kolev and M. Almeida, *Sep. Purif. Technol.*, 2020, **239**, 116486-116513.
157. X. Z. Meng, Y. Q. Pu, M. Li and A. J. Ragauskas, *Green Chem.*, 2020, **22**, 2862-2872.
158. R. A. Milescu, M. L. Segatto, A. Stahl, C. R. McElroy, T. J. Farmer, J. H. Clark and V. G. Zuin, *ACS Sus. Chem. Eng.*, 2020, **8**, 18245-18257.
159. T. Brouwer and B. Schuur, *ACS Sus. Chem. Eng.*, 2020, **8**, 14807-14817.
160. D. H. Gharib, F. Malherbe and S. E. Moulton, *Langmuir*, 2018, **34**, 12137-12144.
161. K. W. Pan, Y. Y. Fan, T. Leng, J. S. Li, Z. Y. Xin, J. W. Zhang, L. Hao, J. Gallop, K. S. Novoselov and Z. R. Hu, *Nat. Commun.*, 2018, **9**, 5197-5207.
162. *World Pat.*, WO2017050541A1, 2017.
163. J. E. Camp, *ChemSusChem*, 2018, **11**, 3048-3055.
164. H. Y. N. Thi, B. T. D. Nguyen and J. F. Kim, *Membranes*, 2021, **11**, 19-39.
165. Chemical safety report for Cyrene. Available at: <https://echa.europa.eu/registration-dossier/-/registered-dossier/16252/10>. Accessed 08.02.2021.
166. J. Mellentine, A. DeVierno, L. N. Grice and J. Whitford, *Turning lignocellulose waste into solvent with lower carbon footprint, 252th American Chemical Society National Meetings & Exposition*, 2016.
167. *US Pat.*, US20120111714, 2012.

168. Global Warming Potential (GWP), Available at: <https://www.epa.gov/ghgemissions/understanding-global-warming-potentials>, Accessed 05.07.2020.
169. The history of graffiti from ancient times to modern days. Available at: <https://www.thevintagenews.com/2016/11/17/the-history-of-graffiti-from-ancient-times-to-modern-days/>. Accessed 05.07.2020.
170. M. J. Whitford, History and trends in graffiti, in *Getting rid of graffiti: A practical guide to graffiti removal and anti-graffiti protection*, 1992, 1-7.
171. Famous graffiti artists Available at: <https://www.timeout.com/newyork/art/top-famous-street-artists> Accessed 18.07.2020.
172. Graffiti movement in Romania. Accessible at: <https://www.urbanadventures.com/blog/supporting-street-artists-in-bucharest/>. Accessed 18.07.2020.
173. R. Giorgi, M. Baglioni and P. Baglioni, *Anal. Bioanal. Chem.*, 2017, **409**, 3707-3712.
174. O. Garcia and K. Malaga, *J. Cult. Heritage*, 2012, **13**, 77-82.
175. Criminal Damage Act 1971. Accessible at: [https://www.legislation.gov.uk/ukpga/1971/48/pdfs/ukpga\\_19710048\\_en.pdf](https://www.legislation.gov.uk/ukpga/1971/48/pdfs/ukpga_19710048_en.pdf). Accessed 18.07.2020.
176. P. Sanmartin, F. Cappitelli and R. Mitchell, *Constr. Build. Mater.*, 2014, **71**, 363-374.
177. V. Gomes, A. Dionisio and J. S. Pozo-Antonio, *Sci. Total Environ.*, 2018, **625**, 233-245.
178. S. J. Haneef, J. B. Johnson, C. Dickinson, G. E. Thompson and G. C. Wood, *Atmos. Environ., Part A*, 1992, **26**, 2963-2974.
179. T. Grontoft, D. Thickett, P. Lankester, S. Hackney, J. H. Townsend, K. Ramsholt and M. Garrido, *Stud. Conserv.*, 2016, **61**, 70-82.
180. G. Germinario, I. D. van der Werf, G. Palazzo, J. L. R. Ros, R. M. Montes-Estelles and L. Sabbatini, *Prog. Org. Coat.*, 2017, **110**, 162-171.
181. C. Jost, C. Muehlethaler and G. Massonnet, *Forensic Sci. Int.*, 2016, **258**, 32-40.
182. P. Sanmartin and F. Cappitelli, *Coatings*, 2017, **7**, 180-196.
183. M. Baglioni, M. Alterini, D. Chelazzi, R. Giorgi and P. Baglioni, *Front. Mater.*, 2019, **6**, 311-328.
184. V. Gomes, A. Dionisio and J. S. Pozo-Antonio, *Prog. Org. Coat.*, 2017, **113**, 90-109.
185. M. M. Mueller, J. W. Moore, R. A. Doggett and D. H. Tingstrom, *J. Appl. Behavior Anal.*, 2000, **33**, 89-92.
186. M. Carvalho and A. Dionisio, *J. Cult. Heritage*, 2015, **16**, 579-590.
187. J. S. Pozo-Antonio, T. Rivas, M. P. Fiorucci, A. J. Lopez and A. Ramil, *Microchem. J.*, 2016, **125**, 1-9.

188. P. Ortiz, V. Antunez, R. Ortiz, J. M. Martin, M. A. Gomez, A. R. Hortal and B. Martinez-Haya, *Appl. Surf. Sci.*, 2013, **283**, 193-201.
189. P. Barreiro, A. Andreotti, M. P. Colombini, P. Gonzalez and J. S. Pozo-Antonio, *Coatings*, 2020, **10**, 196-213.
190. V. Atanassova, I. Kostadinov, P. Zahariev, M. Grozeva and I. Miloushev, *19<sup>th</sup> International Conference and School on Quantum Electronics: Laser Physics and Applications*, Sozopol, 2016.
191. P. Pouli, C. Fotakis, B. Hermosin, C. Saiz-Jimenez, C. Domingo, M. Oujja and M. Castillejo, *Spectrochim. Acta, Part A*, 2008, **71**, 932-945.
192. D. Anglos, S. Couris and C. Fotakis, *Appl. Spectrosc.*, 1997, **51**, 1025-1030.
193. A. Costela, I. Garcia-Moreno, C. Gomez, O. Caballero and R. Sastre, *Appl. Surf. Sci.*, 2003, **207**, 86-99.
194. C. Gomez, A. Costela, I. Garcia-Moreno and R. Sastre, *Appl. Surf. Sci.*, 2006, **252**, 2782-2793.
195. P. Sanjeevan, A. J. Klemm and P. Klemm, *Appl. Surf. Sci.*, 2007, **253**, 8543-8553.
196. T. Rivas, S. Pozo, M. P. Fiorucci, A. J. Lopez and A. Ramil, *Appl. Surf. Sci.*, 2012, **263**, 563-572.
197. V. Zafirooulos, C. Balas, A. Manousaki, Y. Marakis, P. Maravelaki-Kalaitzaki, K. Melesanaki, P. Pouli, T. Stratoudaki, S. Klein, J. Hildenhagen, K. Dickmann, B. S. Luk'Yanchuk, C. Mujat and A. Dogariu, *J. Cult. Heritage*, 2003, **4**, 249S-256S.
198. V. Verges-Belmin and C. Dignard, *J. Cult. Heritage*, 2003, **4**, 238S-244S.
199. R. W. Eck, D. R. Martinelli and Nrc, *Maint. Manage. Bridge Struct.*, 1998, **1642**, 35-42.
200. T. K. Nowotny, S. A. Velinsky, T. A. Lasky and S. P. Donohoe, *Mech. Based Des. Struct. Mach.*, 2012, **40**, 366-379.
201. G. Lustrato, G. Alfano, A. Andreotti, M. P. Colombini and G. Ranalli, *Int. Biodeterior. Biodegrad.*, 2012, **69**, 51-61.
202. R. Bellucci, P. Cremonesi and G. Pignagnoli, *Stud. Conserv.*, 1999, **44**, 278-281.
203. A. Webster and E. May, *Trends in Biotechnol.*, 2006, **24**, 255-260.
204. F. Troiano, S. Vicini, E. Gioventu, P. F. Lorenzi, C. M. Improta and F. Cappitelli, *Polym. Degrad. Stab.*, 2014, **107**, 321-327.
205. C. Saiz-Jimenez, *Int. Biodeterior. Biodegrad.*, 1997, **40**, 225-232.
206. F. Cappitelli, S. Vicini, P. Piaggio, P. Abbruscato, E. Princi, A. Casadevall, J. D. Nosanchuk and E. Zanardini, *Macromol. Biosci.*, 2005, **5**, 49-57.
207. C. J. McNamara, M. Breuker, M. Helms, T. D. Perry and R. Mitchell, *J. Cult. Heritage*, 2004, **5**, 361-364.



208. M. Salem, H. Brim, S. Hussain, M. Arshad, M. B. Leigh and h. Zia ul, *Biotechnol. Adv.*, 2008, **26**, 151-161.
209. M. Musolino, F. Arico and P. Tundo, *J. Cult. Heritage*, 2019, **36**, 268-274.
210. S. Samolik, M. Walczak, M. Plotek, A. Sarzynski, I. Pluska and J. Marczak, *Stud. Conserv.*, 2015, **60**, 58-64.
211. D. Urquhart, The treatment of graffiti on historic surfaces. Advice on graffiti removal procedures, anti-graffiti coatings and alternative strategies. Historic Scotland Technical Advice Note No.18. Historic Scotland, Edinburgh, 1999.
212. J. D. Rodrigues, D. Costa, M. Mascalchi, I. Osticioli and S. Siano, *Appl. Phys. A: Mater. Sci. Process.*, 2014, **117**, 365-370.
213. J. S. Pozo-Antonio, T. Rivas, A. J. Lopez, M. P. Fiorucci and A. Ramil, *Sci. Total Environ.*, 2016, **571**, 1017-1028.
214. C. Rodriguez-Navarro, A. Rodriguez-Navarro, K. Elert and E. Sebastian, *Journal of Applied Physics*, 2004, **95**, 3350-3357.
215. C. M. Grossi, P. Brimblecombe, R. M. Esbert and F. J. Alonso, *Color Res. Appl.*, 2007, **32**, 320-331.
216. F. Bonini, S. Piletsky, A. P. F. Turner, A. Speghini and A. Bossi, *Biosens. Bioelectron.*, 2007, **22**, 2322-2328.
217. Shadow and ghosting remover. Available at: <https://www.specifiedby.com/urban-hygiene-ltd/graffiti-shadow-ghosting-remover>. Accessed 27.08.2020.
218. C. Burns, G. Lott, C. Wood, *Stone*, 2012.
219. A. Moura, I. Flores-Colen, J. de Brito and A. Dionisio, *J. Cult. Heritage*, 2017, **24**, 31-44.
220. M. Lettieri. M. Masieri, *Appl. Surf. Sci.*, 2014, **288**, 466-477.
221. P. M. Carmona-Quiroga, R. M. J. Jacobs and H. A. Viles, *Coatings*, 2017, **7**, 1-11.
222. F. Cazaux and X. Coqueret, *Surf. Coat. Int., Part B*, 2001, **84**, 127-134.
223. K. H. Haas, S. Amberg-Schwab and K. Rose, *Thin Solid Films*, 1999, **351**, 198-203.
224. P. Adapala, S. Gaur, R. G. Puri, A. S. Khanna, *Open J. Appl. Sci.*, 2015, **5**, 808-818.
225. M. Masieri, M. Lettieri, *Coatings*, 2017, **7**, 18-31.
226. M. Bader, R. Wrbitzky, M. Blaszkewicz, M. Schaper and C. van Thriel, *Arch. Toxicol.*, 2008, **82**, 13-20.
227. *World Pat.*, WO2013107822A1, 2017.
228. *US Pat.*, US8361948B2, 2011.
229. *Aust. Pat.*, AU2010305318A1, 2010.
230. *Br. Pat.*, GB2191501A, 1987.
231. *Slovakia Pat.*, SK50982007A3, 2007.

232. H. Anundi, S. Langworth, G. Johanson, M. L. Lind, B. Akesson, L. Friis, N. Itkes, E. Soderman, B. A. G. Jonsson and C. Edling, *Int. Arch. Occup. Environ. Health*, 2000, **73**, 561-569.
233. C. Ursin, C. M. Hansen, J. W. Vandyk, P. O. Jensen, I. J. Christensen and J. Ebbehøj, *Am. Ind. Hyg. Assoc. J.*, 1995, **56**, 651-660.
234. R. Wrbitzky and J. Angerer, *Int. Arch. Occup. Environ. Health*, 1998, **71**, 309-316.
235. S. Kezic, K. Mahieu, A. C. Monster and F. A. deWolff, *Occup. Environ. Med.*, 1997, **54**, 38-43.
236. G. Korinth, T. Goen, M. Lakemeyer, H. C. Broding and H. Drexler, *Contact Dermatitis*, 2003, **49**, 248-254.
237. S. Langworth, H. Anundi, L. Friis, G. Johanson, M. L. Lind, E. Soderman and B. A. Akesson, *Int. Arch. Occup. Environ. Health*, 2001, **74**, 213-218.
238. *US Pat.*, US5015410A, 1990.
239. Regulations GOV - Docket Folder Summary. Available at: <https://www.regulations.gov/docket?D=EPA-HQ-OPPT-2016-0231>, 2018. Accessed 05.06.2020.
240. NMP restricted by REACH. Annex XVII – the restricted substances list. Accessible at: <https://echa.europa.eu/substances-restricted-under-reach//dislist/details/0b0236e1827f617f>. Accessed 25.07.2018.
241. B. Akesson and B. A. G. Jonsson, *Drug Metab. Dispos.*, 1997, **25**, 267-269.
242. H. L. Leira, A. Tiltnes, K. Svendsen and L. Vetlesen, *Contact Dermatitis*, 1992, **27**, 148-150.
243. U. Hass, S. P. Lund and J. Elsner, *Neurotoxicol. Teratol.*, 1994, **16**, 241-249.
244. A. M. Saillenfait, F. Gallissot, I. Langonne and J. P. Sabate, *Food Chem. Toxicol.*, 2002, **40**, 1705-1712.
245. A. M. Saillenfait, F. Gallissot and G. Morel, *Food and Chemical Toxicology*, 2003, **41**, 583-588.
246. G. D. Loizou, K. Jones, P. Akrill, D. Dyne and J. Cocker, *Toxicol. Sci.*, 1999, **48**, 170-179.
247. V. Riihimäki and P. Pfaffli, *Scand. J. Work, Environ. Health*, 1978, **4**, 73-85.
248. Safety of laser products –Part 1:Equipment classification, requirements and user's guide Available at: [https://shop.textalk.se/shop/ws26/40626/files/full\\_size\\_-\\_for\\_start\\_page\\_banner/iec60825-1%7Bed1.2%7Den.pdf](https://shop.textalk.se/shop/ws26/40626/files/full_size_-_for_start_page_banner/iec60825-1%7Bed1.2%7Den.pdf) Accessed 17.07.2020.
249. *US Pat.*, US2438038A, 1948.
250. C. Ricci, F. Gambino, M. Nervo, A. Piccirillo, A. Scarcella, F. Zenucchini and J. S. Pozo-Antonio, *Coatings*, 2020, **10**, 466-487.
251. *US Pat.*, US6673157B1, 2000.
252. *Aust. Pat.*, AU2015278250B2, 2015
253. *World Pat.*, WO2011018366A1, 2009.
254. *US Pat.*, US8222194B2, 2008.

255. W. Leidl and W. Biergert, *J. Reprod. Fertil.*, 1968, **15**, 177-180.
256. E. Krainer, J. M. Becker and F. Naider, *J. Med. Chem.*, 1991, **34**, 174-180.
257. T. Durrani, R. Clapp, R. Harrison and D. Shusterman, *J. Appl. Toxicol.*, 2020, **40**, 1325-1341.
258. W. Scholz in *Surface Coatings*, P. Parsons et al. (eds.), Chapman & Hall, Dordrecht, 1993, ch. 31, 539-580.
259. T. Learner, *The Conservator*, 2010, **24**, 96-103.
260. G. J. Dahe, R. P. Singh, K. W. Dudeck, D. L. Yang and K. A. Berchtold, *J. Membr. Sci.*, 2019, **577**, 91-103.
261. C. W. Saunders, *J. Energ. Mater.*, 1990, **8**, 149-203.
262. D. Stoye, W. Freitag (eds.) in *Paints, Coatings and Solvents*, Wiley, Weinheim, New York, Chichester, Brisbane, Singapore, Toronto, 2<sup>nd</sup> ed., ch. 2, 1998, 11-96.
263. ASTM C242—19a Standard Terminology of Ceramic White Wares and Related Products. Available at: <https://www.astm.org/DATABASE.CART/HISTORICAL/C242-19A.htm>. Accessed 18.10.2020.
264. CTIOA Tile Institute of America Ceramic, Tile and Stone Standards. Available at: <http://ctioa.org/> Accessed 18.10.2020.
265. L. Reclaru, L. C. Ardelean, C. A. Miu and A. F. Grecu, *Materials*, 2020, **13**, 1697-1721.
266. K. K. Kommanapalli, P. Lyot, J. R. Sunkara and P. Checule, *J. Korean Ceram. Soc.*, 2018, **55**, 126-134.
267. F. Pacheco-Torgal and S. Jalali, *Constr. Build. Mater.*, 2010, **24**, 832-838.
268. M. Baglioni, G. Poggi, Y. J. Benavides, F. M. Camacho, R. Giorgi and P. Baglioni, *J. Cult. Heritage*, 2018, **34**, 218-226.
269. A. Zhenova, A. Pellis, R. A. Milescu, C. R. McElroy, R. J. White and J. H. Clark, *ACS Sus. Chem. Eng.*, 2019, **7**, 14834-14840.
270. F. Govaert and M. Bernard, *Forensic Sci. Int.*, 2004, **140**, 61-70.
271. V. I. Kovalenko, R. M. Mukhamadeeva, L. N. Maklakova and N. G. Gustova, *J. Struct. Chem.*, 1993, **34**, 540-547.
272. S. Segalini, A. D. Chirico, G. Depinto, M. Pegoraro, *XXV Fatippec Congress*, Turin, 2000.
273. P. Sanmartin and J. S. Pozo-Antonio, *Constr. Build. Mater.*, 2020, **236**, 117736-117748.
274. *US Pat.*, US5006279A, 1988.
275. *US Pat.*, US4927556A, 1987.
276. *US Pat.*, US518661A, 1993.
277. P. Baglioni, D. Berti, M. Bonini, E. Carretti, L. Dei, E. Fratini and R. Giorgi, *Adv. Colloid Interface Sci.*, 2014, **205**, 361-371.
278. Fundamentals of Paint Adhesion. Available at: <https://www.materialstoday.com/metal-finishing/features/fundamentals-of-paint-adhesion/>. Accessed 18.09.2020.

279. N. Teo and S. C. Jana, *Langmuir*, 2018, **34**, 8581-8590.
280. *US Pat.*, US4749510A, 1987.
281. W. C. Walsh, in: *Reducing Risk in Paint Stripping*, Washington D.C., 1991, 177-184.
282. P. Pouli, D. C. Emmony, C. E. Madden and I. Sutherland, *J. Cult. Heritage*, 2003, **4**, 271S-275S.
283. P. Plagemann, J. Weise and A. Zockoll, *Prog. Org. Coat.*, 2013, **76**, 616-625.
284. J. M. Dodda and P. Belsky, *Eur. Polym. J.*, 2016, **84**, 514-537.
285. H. Kikuchi, H. Hanawa and Y. Honda, *Electron. Commun. in Japan*, 2013, **96**, 41-48.
286. F. S. Li, W. L. Qiu, R. P. Lively, J. S. Lee, A. A. Rownaghi and W. J. Koros, *ChemSusChem*, 2013, **6**, 1216-1223.
287. S. Mallakpour, M. Dinari and M. Hatami, *J. Mater. Sci.*, 2015, **50**, 2759-2767.
288. K. Faghihi, M. Hajibeygi and M. Shabanian, *Macromol. Res.*, 2009, **17**, 739-745.
289. S. H. Lee, S. H. Choi, S. Y. Kim and J. R. Youn, *J. Appl. Polym. Sci.*, 2010, **117**, 3170-3180.
290. G. G. Duan, S. W. Liu, S. H. Jiang and H. Q. Hou, *J. Mater. Sci.*, 2019, **54**, 6719-6727.
291. *World Pat.*, WO2017050541A1, 2017.
292. *US Pat.*, US2421024A1, 1947.
293. Torlon from Solvay. Available at: <https://www.solvay.com/en/brands/torlon-ai>. Accessed 26.07.2020.
294. X. M. Zhang, J. G. Liu and S. Y. Yang, *Rev. Adv. Mater. Sci.*, 2016, **46**, 22-38.
295. R. J. Canto-Acosta, M. I. Loria-Bastarrachea, H. J. Carrillo-Escalante, E. Hernandez-Nunez, M. Aguilar-Vega and J. L. Santiago-Garcia, *RSC Adv.*, 2018, **8**, 284-290.
296. *US Pat.*, US2512606A, 1945.
297. C. J. Billerbeck, S. J. Henke, in: *Engineering Thermoplastics. Properties and applications*, J. M. Margolis (ed.), Taylor & Francis, New York and Basel, 1985, ch. 15, 373-383.
298. G. P. Robertson, M. D. Guiver, M. Yoshikawa and S. Brownstein, *Polymer*, 2004, **45**, 1111-1117.
299. S. Diaham and M. L. Locatelli, *J. Phys. D: Appl. Phys.*, 2013, **46**, 185302-185310.
300. H. J. Lao, N. Mushtaq, G. F. Chen, H. Y. Jiang, Y. Jiao, A. J. Zhang and X. Z. Fang, *Polymer*, 2020, **206**, 122889-122922.
301. L. Bai, L. Zhai, M. H. He, C. O. Wang, S. Mo and L. Fan, *Chin. J. Polym. Sci.*, 2020, **38**, 748-758.
302. X. L. Li, H. Y. Lei, J. C. Guo, J. H. Wang, S. L. Qi, G. F. Tian and D. Z. Wu, *J. Appl. Polym. Sci.*, 2019, **136**, 47989-47998.
303. T. Matsuura, Y. Hasuda, S. Nishi and N. Yamada, *Macromolecules*, 1991, **24**, 5001-5005.
304. S. Dal Kim, S. Y. Kim and I. S. Chung, *J. Polym. Sci., Part A: Polym. Chem.*, 2013, **51**, 4413-4422.

305. L. Yi, W. Huang and D. Y. Yan, *J. Polym. Sci., Part A: Polym. Chem.*, 2017, **55**, 533-559.
306. M. Hasegawa, Y. Watanabe, S. Tsukuda and J. Ishii, *Polym. Int.*, 2016, **65**, 1063-1073.
307. L. Bai, L. Zhai, M. H. He, C. G. Wang, S. Mo and L. Fan, *React. Funct. Polym.*, 2019, **141**, 155-164.
308. T. J. Murray, *Macromol. Mater. Eng.*, 2008, **293**, 350-360.
309. W. Wrasidlo and J. M. Augl, *J. Polym. Sci., Part A-1: Polym. Chem.*, 1969, **7**, 321-332.
310. H. Behniafar and S. Haghghat, *Eur. Polym. J.*, 2006, **42**, 3236-3247.
311. C. P. Yang, R. S. Chen and C. S. Wei, *Eur. Polym. J.*, 2002, **38**, 1721-1729.
312. S. H. Lee, S. H. Choi, J. I. Choi, J. R. Lee and J. R. Youn, *Korean Journal of Chemical Engineering*, 2010, **27**, 658-665.
313. D. J. Liaw, B. Y. Liaw and J. M. Tseng, *J. Polym. Sci., Part A: Polym. Chem.*, 1999, **37**, 2629-2635.
314. D. J. Liaw and W. H. Chen, *Polymer*, 2003, **44**, 3865-3870.
315. E. Hamciuc, I. Sava, M. Bruma, T. Kopnick, B. Schulz, B. Sapich, J. Wagner and J. Stumpe, *Polym. Adv. Technol.*, 2006, **17**, 641-646.
316. H. Behniafar, A. Beit-Saleed and A. Hadian, *Polym. Degrad. Stab.*, 2009, **94**, 1991-1998.
317. S. H. Hsiao, W. J. Guo, W. F. Lee, Y. C. Kung and Y. J. Lee, *Mater. Chem. Phys.*, 2011, **130**, 1086-1093.
318. H. Behniafar and A. Abedini-pozveh, *Polym. Degrad. Stab.*, 2011, **96**, 1327-1332.
319. S. Mallakpour and F. Rafiemanzelat, *Eur. Polym. J.*, 2005, **41**, 2945-2955.
320. Z. Rasheva, L. Soroachynska, S. Grishchuk and K. Friedrich, *Express Polym. Lett.*, 2015, **9**, 196-210.
321. M. Xiaokun Ma, Sun-Jae Kim, in: *Scanning Electron Microscopy*, V. Kazmiruk (ed), IntechOpen, Croatia, 2012, ch. 21, 557-576.
322. K. Faghihi and M. Hajibeygi, *Polym. Sci., Ser. B*, 2011, **53**, 137-143.
323. J. Hoekstra, *Philips Tech. Rev.*, 1938, **3**, 40-47.
324. M. G. Danikas and S. Morsalin, *Eng. Technol. Appl. Sci. Res.*, 2019, **9**, 4079-4084.
325. R. H. Kienle and L. V. Adams, *Ind. Eng. Chem.*, 1929, **21**, 1279-1282.
326. J. Heighes, *Electr. Insul.*, 1983, 130-146.
327. D. Kind, D. Karner (eds.), in: *High-Voltage Insulation Technology*, Springer, Vieweg, Germany, 1985, ch. 1, 1-60.
328. T. Tanaka, *IEEE Trans. Dielectr. Electr. Insul.*, 2005, **12**, 914-928.
329. F. Guastavino, C. Gianoglio, E. Torello, M. Ferraris, W. Gianelli, *IEEE 2nd International Conference on Dielectrics (Icd)*, Budapest, 2018.
330. D. E. Selvaraj, S. Usa, C. P. Sugumaran, *Int. J. Sci. Eng. Appl.*, 2012, **1**, 51-55.
331. M. Mesaki, H. Goda, *Furukawa Rev.*, 2002, **22**, 1-4.

332. Y. W. Fang, H. Yu, Y. B. Wang, Z. H. Zhang, C. L. Zhuang, G. Fang, Z. L. Luo, B. Zhang and B. Wang, *J. Polym. Eng.*, 2020, **40**, 806-814.
333. *US Pat.*, US4048144, 1977.
334. *US Pat.*, US 3541038, 1970.
335. *US Pat.*, US4048144, 1977.
336. 4-chloroformylphthalic anhydride ECHA infocard. Available at: <https://echa.europa.eu/substance-information/-/substanceinfo/100.013.522>. Accessed 01.05.2021.
337. 4,4'-methylenedianiline ECHA infocard. Available at: <https://echa.europa.eu/substance-information/-/substanceinfo/100.002.705>. Accessed 01.05.2021.
338. K. S. Ho and L. W. Chen, *J. Polym. Sci., Part A: Polym. Chem.*, 1997, **35**, 1703-1710.
339. L. W. Chen and K. S. Ho, *J. Polym. Sci., Part A: Polym. Chem.*, 1997, **35**, 1711-1717.
340. S. Y. Tsay, M. F. Tsai and B. K. Chen, *J. Appl. Polym. Sci.*, 2005, **95**, 321-327.
341. Z. X. Li, L. Fan, Z. Y. Ge, J. T. Wu and S. Y. Yang, *J. Polym. Sci., Part A: Polym. Chem.*, 2003, **41**, 1831-1840.
342. C. Hamciuc, E. Hamciuc, T. Pakula and L. Okrasa, *Polym. Plast. Technol. Eng.*, 2006, **45**, 143-148.
343. J. T. Vaughn, W. J. Koros, J. R. Johnson and O. Karvan, *J. Membr. Sci.*, 2012, **401**, 163-174.
344. Benzene-1,2,4-tricarboxylic acid 1,2-anhydride ECHA infocard. Available at: <https://echa.europa.eu/substance-information/-/substanceinfo/100.008.190>. Accessed 09.08.2018.
345. 4,4'-methylenediphenyl diisocyanate Infocard. Available at: <https://echa.europa.eu/substance-information/-/substanceinfo/100.002.697>. Accessed 25.10.2020.
346. T. Weiss, H. Schuster, J. Muller, K. H. Schaller, H. Drexler, J. Angerer and H. U. Kafferlein, *Ann. Occup. Hyg.*, 2011, **55**, 886-892.
347. X. Y. Zhang, J. C. Lambert, M. A. Doll, J. M. Walraven, G. E. Arteel and D. W. Hein, *J. Pharmacol. Exp. Ther.*, 2006, **316**, 289-294.
348. B. G. Harvey, G. R. Yandek, J. T. Lamb, W. S. Eck, M. D. Garrison and M. C. Davis, *RSC Adv.*, 2017, **7**, 23149-23156.
349. P. Jeandet, C. Clement and E. Courrot, *Eng. Life Sci.*, 2014, **14**, 622-632.
350. M. D. Garrison, M. A. Savolainen, A. P. Chafin, J. E. Baca, A. M. Bons and B. G. Harvey, *Accs Sus. Chem. Eng.*, 2020, **8**, 14137-14149.
351. F. Gharagheizi, *J. Appl. Polym. Sci.*, 2007, **103**, 31-36.
352. F. Duan, T. F. Wong and A. Crivoi, *Nanoscale Res. Lett.*, 2012, **7**, 360-366.

353. C. N. Cheaburu, O. N. Ciocoiu, G. Staikos and C. Vasile, *J. Appl. Polym. Sci.*, 2013, **127**, 3340-3348.
354. S. Q. Zhou, R. Ni and D. Funfschilling, *J. Appl. Phys.*, 2010, **107**, 54317-54323.
355. D. Abliz, Y. G. Duan, L. Steuernagel, L. Xie, D. C. Li and G. Ziegmann, *Polym. Polym. Compos.*, 2013, **21**, 341-348.
356. C. Ageorges and L. Ye, *Composites, Part A*, 2001, **32**, 1603-1612.
357. R. Pitchumani, J. W. Gillespie and M. A. Lamontia, *J. Compos. Mater.*, 1997, **31**, 244-275.
358. J. Tierney and J. W. Gillespie, *J. Compos. Mater.*, 2006, **40**, 1487-1506.
359. Z. B. Zhang, X. D. Wang, Y. Luo, Z. Q. Zhang and L. D. Wang, *J. Thermoplast. Compos. Mater.*, 2010, **23**, 647-664.
360. K. Vanherck, G. Koeckelberghs and I. F. J. Vankelecom, *Prog. Polym. Sci.*, 2013, **38**, 874-896.
361. Y. J. Kim, T. E. Glass, G. D. Lyle and J. E. McGrath, *Macromolecules*, 1993, **26**, 1344-1358.
362. S. Mallakpour and E. Khadem, *High Perform. Polym.*, 2014, **26**, 392-400.
363. S. H. Hsiao, H. M. Wang, J. S. Chou, W. J. Guo, T. M. Lee, C. M. Leu and C. W. Su, *J. Polym. Res.*, 2012, **19**, 9757-9769.
364. Y. Yoshioka and K. Tashiro, *Polymer*, 2003, **44**, 7007-7019.
365. S. Diahm and M. L. Locatelli, *IEEE Trans. Dielectr. Electr. Insul.*, 2015, **22**, 3053-3058.
366. *US Pat.*, US4742150A, 1986.
367. J. F. Dezern and C. R. Gautreaux, *Polym. Eng. Sci.*, 1991, **31**, 860-866.
368. E. Grabiec, E. Schab-Balcerzak, W. Domagala and M. Kurcok, *High Perform. Polym.*, 2009, **21**, 265-281.
369. C. P. Yang and S. H. Hsiao, *Makromol. Chem.*, 1989, **190**, 2119-2131.
370. Standard Test Method for Film Hardness by Pencil Test, ASTM D3363-2005 R, 2011.
371. ASTM Definition of Term Relating to Adhesion D 907-70, Philadelphia, PA, 1970.
372. J. J. Chen and S. J. Bull, *J. Phys. D: Appl. Phys.*, 2011, **44**, 34001-34020.
373. T. Hata, *J. Adhes.*, 1972, **4**, 161-170.
374. *Rom. Pat.*, RO9801014, 1998.
375. B.S. Paulsen, 2010. Highlights through the history of plant medicine. In: Proceedings from a Symposium Held at The Norwegian Academy of Science and Letters, Norway, 2010.
376. M. Vinatoru, *Ultrason. Sonochem.*, 2001, **8**, 303-313.
377. M. J. R. Desborough and D. M. Keeling, *Br. J. Haematol.*, 2017, **177**, 674-683.
378. A. Shevchuk, L. Jayasinghe and N. Kuhnert, *Food Res. Int.*, 2018, **109**, 387-402.
379. S. V. Luca, I. Macovei, A. Bujor, A. Miron, K. Skalicka-Wozniak, A. C. Aprotosoiaie and A. Trifan, *Crit. Rev. Food Sci. Nutr.*, 2020, **60**, 626-659.
380. E. Shawky, A. A. Nada and R. S. Ibrahim, *RSC Adv.*, 2020, **10**, 27961-27983.

381. P. Das, R. Majumder, M. Mandal and P. Basak, *J. Biomol. Struct. Dyn.*, 2020, **39**, 6265-6280.
382. A. Montero-Calderon, C. Cortes, A. Zulueta, A. Frigola and M. J. Esteve, *Sci. Rep.*, 2019, **9**, 16120-16127.
383. M. D. Coll, L. Coll, J. Laencina and F. A. Tomas-Barberan, *Z. Lebensm. -Unters. -Forsch., A Food Res. Technol.*, 1998, **206**, 404-407.
384. M. Hajialyani, M. H. Farzaei, J. Echeverria, S. M. Nabavi, E. Uriarte and E. Sobarzo-Sanchez, *Molecules*, 2019, **24**, 648-665.
385. X. Gao, A. Cassidy, M. A. Schwarzschild, E. B. Rimm and A. Ascherio, *Neurology*, 2012, **78**, 1138-1145.
386. C. Y. Li and H. Schluesener, *Crit. Rev. Food Sci. Nutr.*, 2017, **57**, 613-631.
387. I. C. W. Arts and P. C. H. Hollman, *Am. J. Clin. Nutr.*, 2005, **81**, 317S-325S.
388. F. Meneguzzo, R. Ciriminna, F. Zabini and M. Pagliaro, *Processes*, 2020, **8**, 549-567.
389. M. Grosse, N. Ruetalo, M. Layer, D. Hu, R. Businger, S. Rheber, C. Setz, P. Rauch, J. Auth, M. Froba, E. Brysch, M. Schindler and U. Schubert, *Viruses-Basel*, 2021, **13**, 647-663.
390. S. Yasri and V. Wiwanitkit, *J. Acute Dis.*, 2016, **5**, 77-78.
391. C. B. Samaranayake and E. Yap, *Intern. Med. J.*, 2014, **44**, 423-425.
392. C. R. Wu, Y. Liu, Y. Y. Yang, P. Zhang, W. Zhong, Y. L. Wang, Q. Q. Wang, Y. Xu, M. X. Li, X. Z. Li, M. Z. Zheng, L. X. Chen and H. Li, *Acta Pharm. Sin. B*, 2020, **10**, 766-788.
393. S. Singh, M. Fulbabu Sk, A. Sonawane, P. Kar and S. Sadhukhan, *J. Biomol. Struct. Dyn.*, 2021, **39**, 6249-6264.
394. S. Mahdian, A. Ebrahim-Habibi and M. Zarrabi, *J. Diabetes Metab. Disord.*, 2020, **19**, 1-9.
395. Y. D. Singh, B. Jena, R. Ningthoujam, S. Panda, P. Priyadarsini, S. Pattanayak, M. K. Panda, M. C. Singh and K. B. Satapathy, *Adv. Tradit. Med.*, 2020, **20**, 496-507.
396. Y. S. Li, A. D. Kandhare, A. A. Mukherjee and S. L. Bodhankar, *Regul. Toxicol. Pharmacol.*, 2019, **105**, 77-85.
397. B. Gullon, T. A. Lu-Chau, M. T. Moreira, J. M. Lema and G. Eibes, *Trends Food Sci. Technol.*, 2017, **67**, 220-235.
398. M. K. Anwer, R. Al-Shdefat, S. Jamil, P. Alam, M. S. Abdel-Kader and F. Shakeel, *J. Chem. Eng. Data*, 2014, **59**, 2065-2069.
399. N. Mahato, M. Sinha, K. Sharma, R. Koteswararao and M. H. Cho, *Foods*, 2019, **8**, 523-603.
400. Zuin, V.G., L. Z. Ramin, M. L. Segatto, A. S. Stahl, K. Zanotti, M. R. Forim, M. F. F. Silva and J. B. Fernandes, *Pure Appl. Chem.*, 2020, **92**, 1-14.
401. J. A. Kruse, *Crit. Care Clin.*, 2012, **28**, 661-711.
402. L. Panzella, F. Moccia, R. Nasti, S. Marzorati, L. Verotta and A. Napolitano, *Front. Nutr.*, 2020, **7**, 60-86.
403. V. G. Zuin and L. Z. Ramin, *Top. Curr. Chem.*, 2018, **376**, 3-56.



404. F. Girotto, L. Alibardi and R. Cossu, *Waste Manage.*, 2015, **45**, 32-41.
405. The 17 UN sustainable development. Available at: <https://sustainabledevelopment.un.org/>. Accessed 15.05.2020.
406. H. C. J. Godfray, J. R. Beddington, I. R. Crute, L. Haddad, D. Lawrence, J. F. Muir, J. Pretty, S. Robinson, S. M. Thomas and C. Toulmin, *Science*, 2010, **327**, 812-818.
407. K. Kummerer, J. H. Clark and V. G. Zuin, *Science*, 2020, **367**, 369-370.
408. A. S. Matharu, E. M. de Melo and J. A. Houghton, *Bioresour. Technol.*, 2016, **215**, 123-130.
409. V. G. Zuin, M. L. Segatto and L. Z. Ramin, *Curr. Opin. Green Sustain. Chem.*, 2018, **9**, 1-7.
410. C. S. K. Lin, L. A. Pfaltzgraff, L. Herrero-Davila, E. B. Mubofu, S. Abderrahim, J. H. Clark, A. A. Koutinas, N. Kopsahelis, K. Stamatelatou, F. Dickson, S. Thankappan, Z. Mohamed, R. Brocklesby and R. Luque, *Energy Environ. Sci.*, 2013, **6**, 426-464.
411. J. A. S. Lopez, Q. Li and I. P. Thompson, *Crit. Rev. Biotechnol.*, 2010, **30**, 63-69.
412. A. Chanet, D. Milenkovic, C. Manach, A. Mazur and C. Morand, *J. Agric. Food Chem.*, 2012, **60**, 8809-8822.
413. C. Morand, C. Dubray, D. Milenkovic, D. Lioger, J. F. Martin, A. Scalbert and A. Mazur, *Am. J. Clin. Nutr.*, 2011, **93**, 73-80.
414. Food and Agriculture Organization of the United Nations (FAO), in: *Crops*, 2018.
415. A. Gil-Izquierdo, M. I. Gil, F. A. Tomas-Barberan and F. Ferreres, *J. Agric. Food Chem.*, 2003, **51**, 3024-3028.
416. M. Ligor, O. Kornysova, A. Maruska and B. Buszewski, *JPC-J PLANAR CHROMAT*, 2008, **21**, 355-360.
417. L. Chebil, C. Humeau, J. Anthoni, F. Dehez, J. M. Engasser and M. Ghoul, *J. Chem. Eng. Data*, 2007, **52**, 1552-1556.
418. M. M. Victor, J. M. David, M. V. M. Cortez, J. L. Leite and G. S. B. da Silva, *Waste and Biomass Valorization*, 2021, **12**, 313-320.
419. L. S. Chua, *J. Ethnopharmacol.*, 2013, **150**, 805-817.
420. A. Ciric, H. Prosen, M. Jelkic-Stankov and P. Durdevic, *Talanta*, 2012, **99**, 780-790.
421. L. Angiolillo, M. A. Del Nobile and A. Conte, *Curr. Opin. Food Sci.*, 2015, **5**, 93-98.
422. B. Nayak, F. Dahmoune, K. Moussi, H. Remini, S. Dairi, O. Aoun and M. Khodir, *Food Chem.*, 2015, **187**, 507-516.
423. K. Ameer, H. M. Shahbaz and J. H. Kwon, *Compr. Rev. Food Sci. Food Saf.*, 2017, **16**, 295-315.
424. S. Hilali, A. S. Fabiano-Tixier, K. Ruiz, A. Hejjaj, F. A. Nouh, A. Idlimam, A. Bily, L. Mandi and F. Chemat, *ACS Sus. Chem. Eng.*, 2019, **7**, 11815-11822.
425. M. Puri, D. Sharma and C. J. Barrow, *Trends Biotechnol.*, 2012, **30**, 37-44.

426. M. S. Liza, R. A. Rahman, B. Mandana, S. Jinap, A. Rahmat, I. S. M. Zaidul and A. Hamid, *Food Bioprod. Process.*, 2010, **88**, 319-326.
427. A. R. Toledo-Guillen, I. Higuera-Ciapara, G. Garcia-Navarrete and J. C. de la Fuente, *J. Biotechnol.*, 2010, **150**, 313-314.
428. J. Azmir, I. S. M. Zaidul, M. M. Rahman, K. M. Sharif, A. Mohamed, F. Sahena, M. H. A. Jahurul, K. Ghafoor, N. A. N. Norulaini and A. K. M. Omar, *J. Food Eng.*, 2013, **117**, 426-436.
429. Z. Berk, in: *Food Process Engineering and Technology*, Academic Press, Israel, 3<sup>rd</sup> ed., 2018, ch. 11, 289-308.
430. B. S. Belleste, L. Z. Ramin, D. Porto, A. I. Ribeiro, M. R. Forim, V. G. Zuin, J. B. Fernan des and M. Silva, *J. Braz. Chem. Soc.*, 2018, **29**, 1123-1129.
431. J. D. P. de la Rosa, P. Ruiz-Palomino, E. Arriola-Guevara, J. Garcia-Fajardo, G. Sandoval and G. M. Guatemala-Morales, *Processes*, 2018, **6**, 266-278.
432. L. X. Liu and J. Chen, *J. Chem. Eng. Data*, 2008, **53**, 1649-1650.
433. Circa Group wins environmental leader's top product. Available at: <https://sustainabilityconsult.com/news/385-press-release-circa-group-s-renewable-solvent-wins-environmental-leader-s-top-product-2019-award>. Accessed 26.03.2020.
434. M. J. Raymond, C. S. Slater and M. J. Savelski, *Green Chem.*, 2010, **12**, 1826-1834.
435. ATEX directive. Explosive atmospheres in the workplace. Available at: <https://www.hse.gov.uk/fireandexplosion/atex.htm#whatatex>. Accessed 20.08.2020.
436. A. G. Mamalis, L. O. G. Voglander and A. Markopoulos, *Precision Engineering-Journal of the International Societies for Precision Engineering and Nanotechnology*, 2004, **28**, 16-30.
437. D. Tasis, N. Tagmatarchis, A. Bianco and M. Prato, *Chem. Rev.*, 2006, **106**, 1105-1136.
438. S. Iijima, *Nature*, 1991, **354**, 56-58.
439. S. Iijima and T. Ichihashi, *Nature*, 1993, **363**, 603-605.
440. H. Y. Miao, J. T. Lue and M. S. Ouyang, *J. Nanosci. Nanotechnol.*, 2006, **6**, 1375-1380.
441. W. P. Jiang, P. Molian and H. Ferkel, *J. Manuf. Sci. Eng.-T ASME*, 2005, **127**, 703-707.
442. S. E. Iyuke, T. A. Mamvura, K. Liu, V. Sibanda, M. Meyyappan and V. K. Varadan, *Nanotechnology*, 2009, **20**, 375602-375612.
443. H. He, L. A. Pham-Huy, P. Dramou, D. L. Xiao, P. L. Zuo and C. Pham-Huy, *Biomed. Res. Int.*, 2013, **2013**, 1-12.
444. S. Iijima, *Phys. B*, 2002, **323**, 1-5.
445. A. Hirsch, *Angew. Chem., Int. Ed.*, 2002, **41**, 1853-1859.
446. M. L. Minus and S. Kumar, *Jom-U.S.*, 2005, **57**, 52-58.
447. F. Hussain, M. Hojjati, M. Okamoto and R. E. Gorga, *J. Compos. Mater.*, 2006, **40**, 1511-1575.

448. M. S. Han, Y. K. Lee, W. N. Kim, H. S. Lee, J. S. Joo, M. Park, H. J. Lee and C. R. Park, *Macromol. Res.*, 2009, **17**, 863-869.
449. S. H. Lee, M. W. Kim, S. H. Kim and J. R. Youn, *Eur. Polym. J.*, 2008, **44**, 1620-1630.
450. A. Star and J. F. Stoddart, *Macromolecules*, 2002, **35**, 7516-7520.
451. S. H. Lee, E. Cho, S. H. Jeon and J. R. Youn, *Carbon*, 2007, **45**, 2810-2822.
452. N. B. Saleh, L. D. Pfefferle and M. Elimelech, *Environ. Sci. Technol.*, 2008, **42**, 7963-7969.
453. C. Pramanik, J. R. Gissinger, S. Kumar and H. Heinz, *ACS Nano*, 2017, **11**, 12805-12816.
454. V. C. Moore, M. S. Strano, E. H. Haroz, R. H. Hauge, R. E. Smalley, J. Schmidt and Y. Talmon, *Nano Lett.*, 2003, **3**, 1379-1382.
455. J. C. Charlier, P. Lambin and T. W. Ebbesen, *Phys. Rev. B*, 1996, **54**, 8377-8380.
456. J. N. Coleman, U. Khan and Y. K. Gun'ko, *Adv. Mater.*, 2006, **18**, 689-706.
457. A. B. Dalton, S. Collins, E. Munoz, J. M. Razal, V. H. Ebron, J. P. Ferraris, J. N. Coleman, B. G. Kim and R. H. Baughman, *Nature*, 2003, **423**, 703-703.
458. Y. L. Li, I. A. Kinloch and A. H. Windle, *Science*, 2004, **304**, 276-278.
459. A. Thess, R. Lee, P. Nikolaev, H. J. Dai, P. Petit, J. Robert, C. H. Xu, Y. H. Lee, S. G. Kim, A. G. Rinzler, D. T. Colbert, G. E. Scuseria, D. Tomanek, J. E. Fischer and R. E. Smalley, *Science*, 1996, **273**, 483-487.
460. C. Journet, W. K. Maser, P. Bernier, A. Loiseau, M. L. delaChapelle, S. Lefrant, P. Deniard, R. Lee and J. E. Fischer, *Nature*, 1997, **388**, 756-758.
461. L. A. Girifalco, M. Hodak and R. S. Lee, *Phys. Rev. B*, 2000, **62**, 13104-13110.
462. W. Dai, J. Wang, X. H. Gan, H. Wang, X. G. Su and C. Xi, *Colloids Surf., A*, 2020, **589**, 124369-124399.
463. L. Y. Liang, W. Y. Xie, S. X. Fang, F. He, B. H. Yin, C. Tlili, D. Q. Wang, S. Qiu and Q. W. Li, *J. Mater. Chem., C*, 2017, **5**, 11339-11368.
464. M. S. Ata, R. Poon, A. M. Syed, J. Milne and I. Zhitomirsky, *Carbon*, 2018, **130**, 584-598.
465. W. R. Yang, P. Thordarson, J. J. Gooding, S. P. Ringer and F. Braet, *Nanotechnology*, 2007, **18**, 412001-412013.
466. N. L. W. Septiani and B. Yulianto, *J. Electrochem. Soc.*, 2016, **163**, 97-106.
467. M. H. O. Rashid and S. F. Ralph, *Nanomaterials*, 2017, **7**, 99-127.
468. J. H. Choi, J. Jegal, W. N. Kim and H. S. Choi, *J. Appl. Polym. Sci.*, 2009, **111**, 2186-2193.
469. J. N. Shen, C. C. Yu, H. M. Ruan, C. J. Gao and B. Van der Bruggen, *J. Membr. Sci.*, 2013, **442**, 18-26.
470. E. W. Wong, P. E. Sheehan and C. M. Lieber, *Science*, 1997, **277**, 1971-1975.
471. T. W. Odom, J. L. Huang, P. Kim and C. M. Lieber, *ACS Abstr. Pap.*, 1998, **216**, 77-78.
472. C. Dekker, *Phys. Today*, 1999, **52**, 22-28.
473. P. L. McEuen, *Phys. World*, 2000, **13**, 31-36.

474. L. M. Peng, Z. Y. Zhang and S. Wang, *Mater. Today*, 2014, **17**, 433-442.
475. Y. Y. Huang and E. M. Terentjev, *Polymers*, 2012, **4**, 275-295.
476. Ihsanullah, *Sep. Purif. Technol.*, 2019, **209**, 307-337.
477. C. F. de Lannoy, D. Jassby, D. D. Davis and M. R. Wiesner, *J. Membr. Sci.*, 2012, **415**, 718-724.
478. N. W. S. Kam, M. O'Connell, J. A. Wisdom and H. J. Dai, *Proc. Natl. Acad. Sci. USA*, 2005, **102**, 11600-11605.
479. M. F. Islam, E. Rojas, D. M. Bergey, A. T. Johnson and A. G. Yodh, *Nano Lett.*, 2003, **3**, 269-273.
480. M. Zheng, A. Jagota, E. D. Semke, B. A. Diner, R. S. McLean, S. R. Lustig, R. E. Richardson and N. G. Tassi, *Nature Mater.*, 2003, **2**, 338-342.
481. K. Chiou, S. Byun, J. Kim and J. X. Huang, *P. Natl. Acad. Sci. USA*, 2018, **115**, 5703-5708.
482. L. Vaisman, G. Marom and H. D. Wagner, *Adv. Funct. Mater.*, 2006, **16**, 357-363.
483. S. Niyogi, M. A. Hamon, H. Hu, B. Zhao, P. Bhowmik, R. Sen, M. E. Itkis and R. C. Haddon, *Acc. Chem. Res.*, 2002, **35**, 1105-1113.
484. V. Georgakilas, K. Kordatos, M. Prato, D. M. Guldi, M. Holzinger and A. Hirsch, *J. ACS*, 2002, **124**, 760-761.
485. C. A. Furtado, U. J. Kim, H. R. Gutierrez, L. Pan, E. C. Dickey and P. C. Eklund, *J. ACS*, 2004, **126**, 6095-6105.
486. P. J. Boul, J. Liu, E. T. Mickelson, C. B. Huffman, L. M. Ericson, I. W. Chiang, K. A. Smith, D. T. Colbert, R. H. Hauge, J. L. Margrave and R. E. Smalley, *Chem. Phys. Lett.*, 1999, **310**, 367-372.
487. J. Liu, M. J. Casavant, M. Cox, D. A. Walters, P. Boul, W. Lu, A. J. Rimberg, K. A. Smith, D. T. Colbert and R. E. Smalley, *Chem. Phys. Lett.*, 1999, **303**, 125-129.
488. S. D. Bergin, V. Nicolosi, P. V. Streich, S. Giordani, Z. Y. Sun, A. H. Windle, P. Ryan, N. P. P. Niraj, Z. T. T. Wang, L. Carpenter, W. J. Blau, J. J. Boland, J. P. Hamilton and J. N. Coleman, *Adv. Mater.*, 2008, **20**, 1876-1881.
489. L. T. Cai, J. L. Bahr, Y. X. Yao and J. M. Tour, *Chem. Mater.*, 2002, **14**, 4235-4241.
490. S. D. Bergin, Z. Y. Sun, P. Streich, J. Hamilton and J. N. Coleman, *J. Phys. Chem., C*, 2010, **114**, 231-237.
491. R. Poon and I. Zhitomirsky, *Colloid Interface Sci. Commun.*, 2020, **34**, 100226-100229.
492. J. Chen, M. A. Hamon, H. Hu, Y. S. Chen, A. M. Rao, P. C. Eklund and R. C. Haddon, *Science*, 1998, **282**, 95-98.
493. J. E. Riggs, Z. X. Guo, D. L. Carroll and Y. P. Sun, *J. ACS*, 2000, **122**, 5879-5880.
494. J. L. Bahr, J. P. Yang, D. V. Kosynkin, M. J. Bronikowski, R. E. Smalley and J. M. Tour, *J. ACS*, 2001, **123**, 6536-6542.

495. S. B. Sinnott, *J. Nanosci. Nanotechnol.*, 2002, **2**, 113-123.
496. M. Prato, K. Kostarelos and A. Bianco, *Acc. Chem. Res.*, 2008, **41**, 60-68.
497. E. T. Mickelson, C. B. Huffman, A. G. Rinzler, R. E. Smalley, R. H. Hauge and J. L. Margrave, *Chem. Phys. Lett.*, 1998, **296**, 188-194.
498. K. F. Kelly, I. W. Chiang, E. T. Mickelson, R. H. Hauge, J. L. Margrave, X. Wang, G. E. Scuseria, C. Radloff and N. J. Halas, *Chem. Phys. Lett.*, 1999, **313**, 445-450.
499. J. I. H. Touhara, T. Mizuno, *Fluorine Chem.*, 2002, **114**, 181-188.
500. J. L. Stevens, A. Y. Huang, H. Q. Peng, L. W. Chiang, V. N. Khabashesku and J. L. Margrave, *Nano Lett.*, 2003, **3**, 331-336.
501. H. Hu, B. Zhao, M. A. Hamon, K. Kamaras, M. E. Itkis and R. C. Haddon, *J. ACS*, 2003, **125**, 14893-14900.
502. E. Unger, A. Graham, F. Kreupl, M. Liebau and W. Hoenlein, *Curr. Appl. Phys.*, 2002, **2**, 107-111.
503. K. S. Kim, D. J. Bae, J. R. Kim, K. A. Park, S. C. Lim, J. J. Kim, W. B. Choi, C. Y. Park and Y. H. Lee, *Adv. Mater.*, 2002, **14**, 1818-1821.
504. K. Esumi, M. Ishigami, A. Nakajima, K. Sawada and H. Honda, *Carbon*, 1996, **34**, 279-281.
505. R. C. Haddon, J. Sippel, A. G. Rinzler and F. Papadimitrakopoulos, *MRS Bull.*, 2004, **29**, 252-259.
506. R. Q. Yu, L. W. Chen, Q. P. Liu, J. Y. Lin, K. L. Tan, S. C. Ng, H. S. O. Chan, G. Q. Xu and T. S. A. Hor, *Chem. Mater.*, 1998, **10**, 718-722.
507. M. L. Sham and J. K. Kim, *Carbon*, 2006, **44**, 768-777.
508. S. C. Wang, K. S. Chang and C. J. Yuan, *Electrochim. Acta*, 2009, **54**, 4937-4943.
509. P. C. Ma, J. K. Kim and B. Z. Tang, *Carbon*, 2006, **44**, 3232-3238.
510. H. Kong, C. Gao and D. Y. Yan, *J. ACS*, 2004, **126**, 412-413.
511. J. Liu, A. G. Rinzler, H. J. Dai, J. H. Hafner, R. K. Bradley, P. J. Boul, A. Lu, T. Iverson, K. Shelimov, C. B. Huffman, F. Rodriguez-Macias, Y. S. Shon, T. R. Lee, D. T. Colbert and R. E. Smalley, *Science*, 1998, **280**, 1253-1256.
512. M. J. O'Connell, S. M. Bachilo, C. B. Huffman, V. C. Moore, M. S. Strano, E. H. Haroz, K. L. Rialon, P. J. Boul, W. H. Noon, C. Kittrell, J. P. Ma, R. H. Hauge, R. B. Weisman and R. E. Smalley, *Science*, 2002, **297**, 593-596.
513. M. Kozłowska, B. Meyer and P. Rodziewicz, *J. Mol. Model.*, 2019, **25**, 206-219.
514. A. P. Yu, E. Bekyarova, M. E. Itkis, D. Fakhrutdinov, R. Webster and R. C. Haddon, *J. ACS*, 2006, **128**, 9902-9908.
515. J. U. Lee, J. Huh, K. H. Kim, C. Park and W. H. Jo, *Carbon*, 2007, **45**, 1051-1057.
516. N. Grossiord, P. van der Schoot, J. Meuldijk and C. E. Koning, *Langmuir*, 2007, **23**, 3646-3653.

517. L. M. Woods, S. C. Badescu and T. L. Reinecke, *Phys. Rev., B*, 2007, **75**, 155415-155423.
518. D. H. Lin and B. S. Xing, *Environ. Sci. Technol.*, 2008, **42**, 7254-7259.
519. Q. X. Li, J. S. Church, A. Kafi, M. Naebe and B. L. Fox, *J. Nanopart. Res.*, 2014, **16**, 2513-2524.
520. E. Ramos, W. A. Pardo, M. Mir and J. Samitier, *Nanotechnology*, 2017, **28**, 135702-135728.
521. T. Hasan, V. Scardaci, P. H. Tan, A. G. Rozhin, W. I. Milne and A. C. Ferrari, *Phys. E*, 2008, **40**, 2414-2418.
522. T. V. Plisko and A. V. Bilyukevich, *Colloid Polym. Sci.*, 2014, **292**, 2571-2580.
523. S. M. Fatemi and M. Foroutan, *J. Iran. Chem. Soc.*, 2015, **12**, 1905-1913.
524. R. M. F. Fernandes, B. Abreu, B. Claro, M. Buzaglo, O. Regev, I. Furo and E. F. Marques, *Langmuir*, 2015, **31**, 10955-10965.
525. F. Tournus, S. Latil, M. I. Heggie and J. C. Charlier, *Phys. Rev. B*, 2005, **72**, 75431-75435.
526. H. Hyung and J. H. Kim, *Environ. Sci. Technol.*, 2008, **42**, 4416-4421.
527. M. A. Chappell, A. J. George, K. M. Dontsova, B. E. Porter, C. L. Price, P. H. Zhou, E. Morikawa, A. J. Kennedy and J. A. Steevens, *Environ. Pollut.*, 2009, **157**, 1081-1087.
528. D. H. Marsh, G. A. Rance, M. H. Zaka, R. J. Whitby and A. N. Khlobystov, *Phys. Chem. Chem. Phys.*, 2007, **9**, 5490-5496.
529. S. Yoshio, J. Tatami, T. Yamakawa, T. Wakihara, K. Komeya, T. Meguro, K. Aramaki and K. Yasuda, *Carbon*, 2011, **49**, 4131-4137.
530. S. M. Sabet, H. Mahfuz, J. Hashemi, M. Nezakat and J. A. Szpunar, *J. Mater. Sci.*, 2015, **50**, 4729-4740.
531. C. Park, Z. Ounaies, K. A. Watson, R. E. Crooks, J. Smith, S. E. Lowther, J. W. Connell, E. J. Siochi, J. S. Harrison and T. L. S. Clair, *Chem. Phys. Lett.*, 2002, **364**, 303-308.
532. V. S. Moholkar, S. P. Sable and A. B. Pandit, *Aiche J.* 2000, **46**, 684-694.
533. A. Sesis, M. Hodnett, G. Memoli, A. J. Wain, I. Jurewicz, A. B. Dalton, J. D. Carey and G. Hinds, *J. Phys. Chem. B*, 2013, **117**, 15141-15150.
534. T. G. Leighton, *Prog. Biophys. Mol. Biol.*, 2007, **93**, 3-83.
535. H. X. Xu, B. W. Zeiger and K. S. Suslick, *Chem. Soc. Rev.*, 2013, **42**, 2555-2567.
536. K. S. Suslick and G. J. Price, *Annu. Rev. Mater. Sci.*, 1999, **29**, 295-326.
537. F. Contamine, F. Faid, A. M. Wilhelm, J. Berlan and H. Delmas, *Chem. Eng. Sci.*, 1994, **49**, 5865-5873.
538. H. J. Park, M. Park, J. Y. Chang and H. Lee, *Nanotechnology*, 2008, **19**, 335702-335709.
539. P. Garg, J. L. Alvarado, C. Marsh, T. A. Carlson, D. A. Kessler and K. Annamalai, *Int. J. Heat Mass Transfer*, 2009, **52**, 5090-5101.
540. J. I. Paredes and M. Burghard, *Langmuir*, 2004, **20**, 5149-5152.

541. V. Datsyuk, P. Landois, J. Fitremann, A. Peigney, A. M. Galibert, B. Soula and E. Flahaut, *J. Mater. Chem.*, 2009, **19**, 2729-2736.
542. P. Keinanen, S. Siljander, M. Koivula, J. Sethi, E. Sarlin, J. Vuorinen and M. Kanerva, *Heliyon*, 2018, **4**, 787-801.
543. R. Rastogi, R. Kaushal, S. K. Tripathi, A. L. Sharma, I. Kaur and L. M. Bharadwaj, *J. Colloid Interface Sci.*, 2008, **328**, 421-428.
544. C. Klumpp, K. Kostarelos, M. Prato and A. Bianco, *Biochim. Biophys. Acta, Biomembr.*, 2006, **1758**, 404-412.
545. ECHA included Triton X-100 in the Authorisation List (Annex XIV). Available at: <https://echa.europa.eu/authorisation-list>. Accessed 10.11.2020.
546. X. L. Xie, Y. W. Mai and X. P. Zhou, *Mater. Sci. Eng., R*, 2005, **49**, 89-112.
547. D. Qian, E. C. Dickey, R. Andrews and T. Rantell, *Appl. Phys. Lett.*, 2000, **76**, 2868-2870.
548. T. Fukumaru, F. Toshimitsu, T. Fujigaya and N. Nakashima, *Nanoscale*, 2014, **6**, 5879-5886.
549. X. Xin, G. Y. Xu, T. T. Zhao, Y. Y. Zhu, X. F. Shi, H. J. Gong and Z. Q. Zhang, *J. Phys. Chem. C*, 2008, **112**, 16377-16384.
550. B. T. Raimi-Abraham, S. Mahalingam, M. Edirisinghe and D. Q. M. Craig, *Mater. Sci. Eng., C*, 2014, **39**, 168-176.
551. M. Teodorescu and M. Bercea, *Polym. Plast. Technol. Eng.*, 2015, **54**, 923-943.
552. K. Halake, M. Birajdar, B. S. Kim, H. Bae, C. Lee, Y. J. Kim, S. Kim, H. J. Kim, S. Ahn, S. Y. An and J. Lee, *J. Ind. Eng. Chem.*, 2014, **20**, 3913-3918.
553. M. O. Mavukkandy, Q. Zaib and H. A. Arafat, *J. Environ. Chem. Eng.*, 2018, **6**, 6733-6740.
554. E. Saljoughi, M. Amirilargani and T. Mohammadi, *J. Appl. Polym. Sci.*, 2009, **111**, 2537-2544.
555. X. Zhi, H. L. Fang, C. C. Bao, G. X. Shen, J. L. Zhang, K. Wang, S. W. Guo, T. Wan and D. X. Cui, *Biomaterials*, 2013, **34**, 5254-5261.
556. T. Hasan, V. Scardaci, P. H. Tan, A. G. Rozhin, W. I. Milne and A. C. Ferrari, *J. Phys. Chem. C*, 2007, **111**, 12594-12602.
557. M. Namasivayam, M. R. Andersson and J. Shapter, *Polymers*, 2019, **11**, 162-173.
558. K. M. Liew, M. F. Kai and L. W. Zhang, *Compos. Struct.*, 2017, **160**, 81-88.
559. M. D. Vo and D. V. Papavassiliou, *Carbon*, 2016, **100**, 291-301.
560. A. Abdullah, I. S. Mohamad, A. Y. B. Hashim, N. Abdullah and S. Z. Abidin, in: *Proceedings of Mechanical Engineering Research Day 2016*, M. A. B. Salim, M. F. B. Abdollah, T. B. Tuan (eds.), 2016, 171-172.
561. W. B. Kong, L. Sun, Y. Wu, K. L. Jiang, Q. Q. Li, J. P. Wang and S. S. Fan, *Carbon*, 2016, **96**, 1053-1059.

562. Y. Boguslavsky, T. Fadida, Y. Talyosef and J. P. Lellouche, *J. Mater. Chem.*, 2011, **21**, 10304-10310.
563. Y. L. Li, J. Yang, Q. H. Zhao and Y. Li, *Langmuir*, 2013, **29**, 13527-13534.
564. W. Wenseleers, Vlasov, II, E. Goovaerts, E. D. Obratsova, A. S. Lobach and A. Bouwen, *Adv. Funct. Mater.*, 2004, **14**, 1105-1112.
565. T. Matsuda, D. Minami, F. Khoerunnisa, M. Sunaga, M. Nakamura, S. Utsumi, T. Itoh, T. Fujimori, T. Hayashi, Y. Hattori, M. Endo, H. Isobe, H. Onodera and K. Kaneko, *Langmuir*, 2015, **31**, 3194-3202.
566. A. Star, D. W. Steuerman, J. R. Heath and J. F. Stoddart, *Angew. Chem., Int. Ed.*, 2002, **41**, 2508-2512.
567. Y. L. Zhao and J. F. Stoddart, *Acc. Chem. Res.*, 2009, **42**, 1161-1171.
568. N. Sohrabi, A. Alihosseini, V. Pirouzfard and M. Z. Pedram, *Membranes*, 2020, **10**, 283-298.
569. S. Marchesan and M. Prato, *Chem. Commun.*, 2015, **51**, 4347-4359.
570. M. Zheng, A. Jagota, M. S. Strano, A. P. Santos, P. Barone, S. G. Chou, B. A. Diner, M. S. Dresselhaus, R. S. McLean, G. B. Onoa, G. G. Samsonidze, E. D. Semke, M. Usrey and D. J. Walls, *Science*, 2003, **302**, 1545-1548.
571. O. V. Kharissova, B. I. Kharisov and E. G. D. Ortiz, *RSC Adv.*, 2013, **3**, 24812-24852.
572. A. Henni, J. J. Hromek, P. Tontiwachwuthikul and A. Chakma, *J. Chem. Eng. Data*, 2004, **49**, 231-234.
573. B. Garcia, R. Alcalde, J. M. Leal and J. S. Matos, *J. Phys. Chem. B*, 1997, **101**, 7991-7997.
574. H. Yu, Y. Qu, Z. Dong, W. J. Li, Y. Wang, W. Ren, Z. Cui, *2007 7th IEEE Conference on Nanotechnology (IEEE NANO)*, 2007, 1212-1216.
575. A. P. Yu, C. C. L. Su, I. Roes, B. Fan and R. C. Haddon, *Langmuir*, 2010, **26**, 1221-1225.
576. M. Yudasaka, R. Yamada, N. Sensui, T. Wilkins, T. Ichihashi and S. Iijima, *J. Phys. Chem. B*, 1999, **103**, 6224-6229.
577. T. Zhao, Q. Tang, Y. Liu, C. Zhu and X. Zhao, *J. Nanomater.*, 2007, **2007**, 1-4.
578. R. L. Vander Wal and L. J. Hall, *Chem. Phys. Lett.*, 2001, **349**, 178-184.
579. J. W. Jang, K. W. Lee, C. E. Lee, B. Kim and C. J. Lee, *Curr. Appl. Phys.*, 2013, **13**, 1069-1074.
580. Y. Li, X. B. Zhang, J. H. Luo, W. Z. Huang, J. P. Cheng, Z. Q. Luo, T. Li, F. Liu, G. L. Xu, X. X. Ke, L. Li and H. J. Geise, *Nanotechnology*, 2004, **15**, 1645-1649.
581. A. G. Rinzler, J. Liu, H. Dai, P. Nikolaev, C. B. Huffman, F. J. Rodriguez-Macias, P. J. Boul, A. H. Lu, D. Heymann, D. T. Colbert, R. S. Lee, J. E. Fischer, A. M. Rao, P. C. Eklund and R. E. Smalley, *Appl. Phys. A: Mater. Sci. Process.*, 1998, **67**, 29-37.
582. H. Hu, A. P. Yu, E. Kim, B. Zhao, M. E. Itkis, E. Bekyarova and R. C. Haddon, *J. Phys. Chem. B*, 2005, **109**, 11520-11524.
583. T. Fujigaya and N. Nakashima, *Sci. Technol. Adv. Mater.*, 2015, **16**, 24802-24823.



584. B. Koh, J. B. Park, X. M. Hou and W. Cheng, *J. Phys. Chem. B*, 2011, **115**, 2627-2633.
585. H. Ramaraj, J. Madiga, H. Elangovan, P. Haridoss and C. P. Sharma, *Trans. Indian Inst. Met.*, 2017, **70**, 2629-2639.
586. X. X. Wang, J. N. Wang, H. Chang and Y. F. Zhang, *Adv. Funct. Mater.*, 2007, **17**, 3613-3618.
587. V. Sa and K. G. Kornev, *Langmuir*, 2011, **27**, 13451-13460.
588. J. A. Rojas, L. A. Ardila-Rodriguez, M. F. Diniz, M. Goncalves, B. Ribeiro and M. C. Rezende, *Mater. Des.*, 2019, **166**, 107612-107648.
589. D. Gielen, F. Boshell and D. Saygin, *Nat. Mater.*, 2016, **15**, 117-120.
590. A. Bogler, S. Lin and E. Bar-Zeev, *J. Membr. Sci.*, 2017, **542**, 378-398.
591. A. Lee, J. W. Elam and S. B. Darling, *Environ. Sci. Water Res. Technol.*, 2016, **2**, 17-42.
592. Goal 6 UN Sustainable Development Goals Available at: <https://www.un.org/sustainabledevelopment/water-and-sanitation/> Accessed 24.11.2020.
593. B. Hua, H. X. Xiong, Z. Y. Wang, J. T. Hill, S. Buckler, S. Gao, J. Yang and B. L. Deng, *Water Environ. Res.*, 2015, **87**, 912-945.
594. E. G. Filatova, *Izvestiya Vuzov-Prikladnaya Khimiya I Biotekhnologiya*, 2015, **2**, 97-109.
595. Z. Y. Liu, H. W. Bai, J. Lee and D. D. Sun, *Energy Environ. Sci.*, 2011, **4**, 2582-2585.
596. M. J. Park, S. Phuntsho, T. He, G. M. Nisola, L. D. Tijing, X. M. Li, G. Chen, W. J. Chung and H. K. Shon, *J. Membr. Sci.*, 2015, **493**, 496-507.
597. J. S. Ho, Z. Ma, J. J. Qin, S. H. Sim and C. S. Toh, *Desalination*, 2015, **365**, 242-249.
598. S. Al Aani, C. J. Wright and N. Hilal, *Desalination*, 2018, **432**, 115-127.
599. Y. L. Thuyavan, N. Anantharaman, G. Arthanareeswaran and A. F. Ismail, *J. Chem. Technol. Biotechnol.*, 2016, **91**, 2568-2581.
600. M. Omidvar, M. Soltanieh, S. M. Mousavi, E. Saljoughi, A. Moarefian and H. Saffaran, *J. Environ. Health Sci. Eng.*, 2015, **13**, 42-50.
601. N. Evenepoel, S. F. Wen, M. T. Tsehaye and B. Van der Bruggen, *J. Appl. Polym. Sci.*, 2018, **135**, 46494-46503.
602. N. Maximous, G. Nakhla, W. Wan and K. Wong, *J. Membr. Sci.*, 2009, **341**, 67-75.
603. R. M. Boom, I. M. Wienk, T. Vandenboomgaard and C. A. Smolders, *J. Membr. Sci.*, 1992, **73**, 277-292.
604. A. Rahimpour and S. S. Madaeni, *J. Membr. Sci.*, 2007, **305**, 299-312.
605. A. C. Sun, W. Kosar, Y. F. Zhang and X. S. Feng, *Desalination*, 2013, **309**, 156-164.
606. N. Ul Afsar, M. A. Shehzad, M. Irfan, K. Emmanuel, F. Sheng, T. T. Xu, X. M. Ren, L. Ge and T. W. Xu, *Desalination*, 2019, **458**, 25-33.
607. X. Y. Nie, S. Y. Sun, Z. Sun, X. F. Song and J. G. Yu, *Desalination*, 2017, **403**, 128-135.
608. Z. X. Wang, Y. B. Luo and P. Yu, *J. Membr. Sci.*, 2006, **280**, 134-137.

609. M. Tedesco, H. V. M. Hamelers and P. M. Biesheuvel, *J. Membr. Sci.*, 2016, **510**, 370-381.
610. S. Loeb and S. Sourirajan, Sea water demineralization by means of an osmotic membrane, *Adv. Chem. Ser.*, **38**, 117-132.
611. P. K. Parhi, *J. Chem.*, 2013, **2013**, 1-11.
612. Types of filtration membranes based on size of the analyte. Available at: <https://www.protecind.com/solutions/water-treatment/filtration/membrane-filtration>. Accessed 04.03.2020.
613. S. F. Anis, R. Hashaikeh and N. Hilal, *J. Water Process. Eng.*, 2019, **32**, 100941-100952.
614. S. Al Aani, T. N. Mustafa and N. Hilal, *J. Water Process. Eng.*, 2020, **35**, 101241-101254.
615. S. T. Muntha, A. Kausar and M. Siddiq, *Polym.-Plast. Technol. Eng.*, 2017, **56**, 841-856.
616. Y. Zhu, P. J. Dou, H. L. He, H. L. Lan, S. S. Xu, Y. B. Zhang, T. He and J. S. Niu, *Sep. Purif. Technol.*, 2020, **239**, 116528-116559.
617. N. N. Gumbi, J. X. Li, B. B. Mamba and E. N. Nxumalo, *Desalination*, 2020, **474**, 114176-114189.
618. M. B. He, T. Li, M. L. Hu, C. Chen, B. C. Li, J. Crittenden, L. Y. Chu and H. Y. Ng, *Sep. Purif. Technol.*, 2020, **230**, 115855-115891.
619. L. Weinrich, C. N. Haas and M. W. LeChevallier, *J. Water Reuse Desalin.*, 2013, **3**, 85-101.
620. G. D. Kang and Y. M. Cao, *Water Res.*, 2012, **46**, 584-600.
621. R. M. Hakim, D. T. Fearon and J. M. Lazarus, *Kidney Int.*, 1984, **26**, 194-200.
622. M. Kohlova, C. G. Amorim, A. Araujo, A. Santos-Silva, P. Solich and M. Montenegro, *J. Artif. Organs*, 2019, **22**, 14-28.
623. S. K. Patnaik, *Pediatr. Nephrol.*, 2013, **28**, 1680-1681.
624. C. Ronco and W. R. Clark, *Nature Reviews Nephrology*, 2018, **14**, 394-410.
625. S. S. Hosseini, E. Bringas, N. R. Tan, I. Ortiz, M. Ghahramani and M. A. A. Shahmirzadi, *J. Water Proc. Eng.*, 2016, **9**, 78-110.
626. J. R. Werber, A. Deshmukh and M. Elimelech, *Environ. Sci. Technol. Lett.*, 2016, **3**, 112-120.
627. N. Y. Yip, A. Tiraferri, W. A. Phillip, J. D. Schiffman and M. Elimelech, *Environ. Sci. Technol.*, 2010, **44**, 3812-3818.
628. X. C. An, Y. X. Hu, N. Wang, T. Wang and Z. Y. Liu, *NPG Asia Mater.*, 2019, **11**, 13-24.
629. A. Drews, *J. Membr. Sci.*, 2010, **363**, 1-28.
630. Z. H. Wang, H. R. Yu, J. F. Xia, F. F. Zhang, F. Li, Y. Z. Xia and Y. H. Li, *Desalination*, 2012, **299**, 50-54.
631. Q. Y. Wang, Z. W. Wang, C. W. Zhu, X. J. Mei and Z. C. Wu, *J. Membr. Sci.*, 2013, **446**, 154-163.
632. S. S. Madaeni, A. G. Fane and D. E. Wiley, *J. Chem. Technol. Biotechnol.*, 1999, **74**, 539-543.
633. I. S. Chang, C. H. Lee and K. H. Ahn, *Sep. Purif. Technol.*, 1999, **34**, 1743-1758.

634. P. Le-Clech, V. Chen and T. A. G. Fane, *J. Membr. Sci.*, 2006, **284**, 17-53.
635. Y. L. He, P. Xu, C. J. Li and B. Zhang, *Water Res.*, 2005, **39**, 4110-4118.
636. T. Itonaga, K. Kimura and Y. Watanabe, *Water Sci. Technol.*, 2004, **50**, 301-309.
637. H. Evenblij, B. Verrecht, J. van der Graaf and B. Van der Bruggen, *Desalination*, 2005, **178**, 193-201.
638. Z. A. Bhatti, Q. Mahmood, I. A. Raja, A. H. Malik, M. S. Khan and D. L. Wu, *Phys. Chem. Earth*, 2011, **36**, 465-469.
639. M. Koh, M. A. Clark and K. J. Howe, *J. Membr. Sci.*, 2005, **256**, 169-175.
640. X. L. Ma, Y. L. Su, Q. Sun, Y. Q. Wang and Z. Y. Jiang, *J. Membr. Sci.*, 2007, **300**, 71-78.
641. L. Y. Ng, A. W. Mohammad, C. P. Leo and N. Hilal, *Desalination*, 2013, **308**, 15-33.
642. Y. Manawi, V. Kochkodan, E. Mahmoudi, D. J. Johnson, A. W. Mohammad and M. A. Atieh, *Sci. Rep.*, 2017, **7**, 15831-15842.
643. J. H. Kim and K. H. Lee, *J. Membr. Sci.*, 1998, **138**, 153-163.
644. M. Ulbricht, *Polymer*, 2006, **47**, 2217-2262.
645. H. W. Yoon, Y. H. Cho and H. B. Park, *Philos. Trans. R. Soc., A*, 2016, **374**, 24-46.
646. C. Boo and M. Elimelech, *Nat. Nanotechnol.*, 2017, **12**, 500-503.
647. H. Y. Liao, H. Y. Zhang, G. Qin, Z. H. Li, L. Q. Li and H. Q. Hong, *RSC Adv.*, 2017, **7**, 22112-22120.
648. M. M. Pendergast and E. M. V. Hoek, *Energy Environ. Sci.*, 2011, **4**, 1946-1971.
649. G. Szekely, M. F. Jimenez-Solomon, P. Marchetti, J. F. Kim and A. G. Livingston, *Green Chem.*, 2014, **16**, 4440-4473.
650. J. H. Zhu, Q. F. Zhang, J. F. Zheng, S. H. Hou, H. C. Mao and S. B. Zhang, *J. Membr. Sci.*, 2016, **517**, 39-46.
651. T. Marino, E. Blasi, S. Tornaghi, E. Di Nicolo and A. Figoli, *J. Membr. Sci.*, 2018, **549**, 192-204.
652. D. S. Lakshmi, T. Cundari, E. Furia, A. Tagarelli, G. Fiorani, M. Carraro and A. Figoli, *Macromol. Symp.*, 2015, **357**, 159-167.
653. D. T. T. Nu, N. P. Hung, C. V. Hoang and B. Van der Bruggen, *Appl. Sci.-Basel*, 2019, **9**, 3347-3361.
654. M. A. Rasool, C. Van Goethem and I. F. J. Vankelecom, *Sep. Purif. Technol.*, 2020, **232**, 115903-115930.
655. C. S. M. Pereira, V. Silva and A. E. Rodrigues, *Green Chem.*, 2011, **13**, 2658-2671.
656. T. Marino, S. Blefari, E. Di Nicolo and A. Figoli, *Green Process. Synth.*, 2017, **6**, 295-300.
657. S. Fadhil, T. Marino, H. F. Makki, Q. F. Alsalhy, S. Blefari, F. Macedonio, E. Di Nicolo, L. Giorno, E. Drioli and A. Figoli, *Chem. Eng. Process.*, 2016, **102**, 16-26.

658. F. Russo, F. Galiano, F. Pedace, F. Arico and A. Figoli, *ACS Sus. Chem. Eng.*, 2020, **8**, 659-668.
659. A. Hanafia, C. Faur, A. Deratani, P. Guenoun, H. Garate, D. Quemener, C. Pochat-Bohatier and D. Bouyer, *J. Membr. Sci.*, 2017, **526**, 212-220.
660. F. Tasselli, in: *Encyclopedia of membranes*, Springer Berlin Heidelberg, Berlin, 2015, 1-3.
661. R. Pervin, P. Ghosh and M. G. Basavaraj, *RSC Adv.*, 2019, **9**, 15593-15605.
662. F. Wang, L. Ratke, H. D. Zhang, P. Altschuh and B. Nestler, *J. Sol-Gel Sci. Technol.*, 2020, **94**, 356-374.
663. N. Arahman, T. Maimun, Mukramah and Syawaliah, *International Conference on Engineering, Science and Nanotechnology*, Solo, Indonesia, 2016.
664. Q. Zhang, Y. Liu, Y. Su, R. N. Zhang, L. Fan, Y. N. Liu, T. Y. Ma and Z. Y. Jiang, *RSC Adv.*, 2016, **6**, 35532-35538.
665. B. S. Lalia, V. Kochkodan, R. Hashaikeh and N. Hilal, *Desalination*, 2013, **326**, 77-95.
666. A. M. W. Bulte, M. H. V. Mulder, C. A. Smolders and H. Strathmann, *J. Membr. Sci.*, 1996, **121**, 37-49.
667. H. Strathmann, K. Kock, P. Amar and R. W. Baker, *Desalination*, 1975, **16**, 179-203.
668. H. Strathmann and K. Kock, *Desalination*, 1977, **21**, 241-255.
669. H. Strathmann, P. Scheible and R. W. Baker, *J. Appl. Polym. Sci.*, 1971, **15**, 811-828.
670. P. S. T. Machado, A. C. Habert and C. P. Borges, *J. Membr. Sci.*, 1999, **155**, 171-183.
671. M. Di Luccio, R. Nobrega and C. P. Borges, *J. Appl. Polym. Sci.*, 2002, **86**, 3085-3096.
672. C. S. Tsay and A. J. McHugh, *J. Polym. Sci., Part B: Polym. Phys.*, 1990, **28**, 1327-1365.
673. P. Radovanovic, S. W. Thiel and S. T. Hwang, *J. Membr. Sci.*, 1992, **65**, 213-229.
674. L. P. Cheng, D. J. Lin, C. H. Shih, A. H. Dwan and C. C. Gryte, *J. Polym. Sci., Part B: Polym. Phys.*, 1999, **37**, 2079-2092.
675. M. Metze, S. Barbe, A. Reiche, D. Melzner and T. Scheper, *Euromembrane Conference 2012*, London, 2012, **44**, 1460-1460.
676. P. T. P. Aryanti, S. R. Joscarita, A. K. Wardani, S. Subagjo, D. Ariono, I. G. Wenten, *J. Eng. Technol. Sci.*, 2016, **48**, 135-149.
677. A. Laxminarayan and G. T. Caneba, *Polym. Eng. Sci.*, 1991, **31**, 1597-1603.
678. L. Xu and F. Qiu, *Polymer*, 2014, **55**, 6795-6802.
679. A. K. Holda and I. F. J. Vankelecom, *J. Appl. Polym. Sci.*, 2015, **132**, 42130-42146.
680. H. Matsuyama, M. Nishiguchi and Y. Kitamura, *J. Appl. Polym. Sci.*, 2000, **77**, 776-783.
681. Y. S. Kang, H. J. Kim and U. Y. Kim, *J. Membr. Sci.*, 1991, **60**, 219-232.
682. M. Sadrzadeh and S. Bhattacharjee, *J. Membr. Sci.*, 2013, **441**, 31-44.
683. A. M. W. Bulte, E. M. Naafs, F. vanEeten, M. H. V. Mulder, C. A. Smolders and H. Strathmann, *Polymer*, 1996, **37**, 1647-1655.

684. A. J. Reuvers and C. A. Smolders, *J. Membr. Sci.*, 1987, **34**, 67-86.
685. N. Vogrin, C. Stropnik, V. Musil and M. Brumen, *J. Membr. Sci.*, 2002, **207**, 139-141.
686. D. F. Li, T. S. Chung, J. Z. Ren and R. Wang, *Ind. Eng. Chem. Res.*, 2004, **43**, 1553-1556.
687. V. A. Kosma and K. G. Beltsios, *J. Membr. Sci.*, 2012, **407**, 93-107.
688. M. A. Frommer and R. M. Messalem, *Ind. Eng. Chem. Prod. Res. Dev.*, 1973, **12**, 328-333.
689. M. R. Pekny, A. R. Greenberg, V. Khare, J. Zartman, W. B. Krantz and P. Todd, *J. Membr. Sci.*, 2002, **205**, 11-21.
690. C. A. Smolders, A. J. Reuvers, R. M. Boom and I. M. Wienk, *J. Membr. Sci.*, 1992, **73**, 259-275.
691. S. S. Shojaie, W. B. Krantz and A. R. Greenberg, *J. Membr. Sci.*, 1994, **94**, 281-298.
692. M. R. Pekny, J. Zartman, W. B. Krantz, A. R. Greenberg and P. Todd, *J. Membr. Sci.*, 2003, **211**, 71-90.
693. D. R. Tree, T. Iwama, K. T. Delaney, J. Lee and G. H. Fredrickson, *ACS Macro Lett.*, 2018, **7**, 582-586.
694. V. G. Levich and V. S. Krylov, *Annu. Rev. Fluid Mech.*, 1969, **1**, 293-316.
695. S. A. McKelvey and W. J. Koros, *J. Membr. Sci.*, 1996, **112**, 29-39.
696. T. H. Young and L. W. Chen, *Desalination*, 1995, **103**, 233-247.
697. A. M. W. Bulte, B. Folkers, M. H. V. Mulder and C. A. Smolders, *J. Appl. Polym. Sci.*, 1993, **50**, 13-26.
698. H. D. Keith and F. J. Padden, *J. Appl. Phys.*, 1963, **34**, 2409-2421.
699. M. Elimelech, X. H. Zhu, A. E. Childress and S. K. Hong, *J. Membr. Sci.*, 1997, **127**, 101-109.
700. K. S. Kim, K. H. Lee, K. Cho and C. E. Park, *J. Membr. Sci.*, 2002, **199**, 135-145.
701. S. Ayyaru and Y. H. Ahn, *J. Membr. Sci.*, 2017, **525**, 210-219.
702. I. Sentana, M. A. De La Rubia, M. Rodriguez, E. Sentana and D. Prats, *Sep. Purif. Technol.*, 2009, **68**, 305-311.
703. E. L. Yang, X. H. Qin and S. Y. Wang, *Mater. Lett.*, 2008, **62**, 3555-3557.
704. A. K. Fard, G. McKay, A. Buekenhoudt, H. Al Sulaiti, F. Motmans, M. Khraisheh and M. Atieh, *Materials*, 2018, **11**, 74-120..
705. A. A. R. Abdel-Aty, Y. S. A. Aziz, R. M. G. Ahmed, I. M. A. ElSherbiny, S. Panglisch, M. Ulbricht and A. S. G. Khalil, *Sep. Purif. Technol.*, 2020, **253**, 117467-117487.
706. M. R. Ganjali, A. Badiei, A. Mouradzadegan, V. Vatanpour, H. Rezanian, S. S. M. Khadem, F. Shamiry, M. T. Munir, S. Habibzadeh and M. R. Saeb, *Polym. Test.*, 2020, **91**, 106796-106838.
707. H. Patil, V. Shanmugam and K. Marathe, *Indian Chem. Eng.*, 2020, 1-10.
708. S. Ansari, A. Moghadassi and S. M. Hosseini, *Korean J. Chem. Eng.*, 2020, **20**, 618-626.

709. M. Peydayesh, T. Mohammadi and S. K. Nikouzad, *J. Membr. Sci.*, 2020, **611**, 118205-118242.
710. R. Z. Pang, K. K. Chen, Y. Han and W. S. W. Ho, *J. Membr. Sci.*, 2020, **612**, 118443-118452.
711. D. Kim, H. Vovusha, U. Schwingenschlogl and S. P. Nunes, *J. Membr. Sci.*, 2017, **539**, 161-171.
712. D. Kim, O. R. Salazar and S. P. Nunes, *Green Chem.*, 2016, **18**, 5151-5159.
713. S. Zulfiqar, U. Rafique and M. J. Akhtar, *Environ. Sci. Pollut. Res.*, 2019, **26**, 15795-15802.
714. G. D. Kang and Y. M. Cao, *J. Membr. Sci.*, 2014, **463**, 145-165.
715. N. A. Ibrahim, M. D. H. Wirzal, N. A. H. Nordin, N. S. Abd Halim and Iop, Malaysia, 2017.
716. J. P. Mericq, J. Mendret, S. Brosillon and C. Faur, *Chem. Eng. Sci.*, 2015, **123**, 283-291.
717. F. A. AlMarzooqi, M. R. Bilad and H. A. Arafat, *Eur. Polym. J.*, 2016, **77**, 164-173.
718. C. Boo, J. Lee and M. Elimelech, *Environ. Sci. Technol.*, 2016, **50**, 12275-12282.
719. J. Duarte, C. C. Cherubini, V. dos Santos, A. Schneider and M. Zeni, *Euromembrane Conference 2012*, London, 2012, **44**, 1146-1149.
720. N. A. Ahmad, C. P. Leo, A. L. Ahmad and A. W. Mohammad, *Int. J. Hydrogen Energy*, 2016, **41**, 4855-4861.
721. K. P. Ramaiah, D. Satyasri, S. Sridhar and A. Krishnaiah, *J. Hazard. Mater.*, 2013, **261**, 362-371.
722. D. Y. Hou, J. Wang, X. C. Sun, Z. K. Luan, C. W. Zhao and X. J. Ren, *J. Hazard. Mater.*, 2010, **177**, 613-619.
723. X. Y. Tan, S. P. Tan, W. K. Teo and K. Li, *J. Membr. Sci.*, 2006, **271**, 59-68.
724. P. Sukitpaneemit and T. S. Chung, *Ind. Eng. Chem. Res.*, 2012, **51**, 978-993.
725. A. Karanasiou, M. Kostoglou and A. Karabelas, *Water*, 2018, **10**, 947-962.
726. X. Li, J. H. Tao, D. H. Hu, M. H. Engelhard, W. G. Zhao, J. G. Zhang and W. Xu, *J. Mater. Chem. A*, 2018, **6**, 5006-5015.
727. Y. L. Lei, Y. J. Luo, F. Chen and L. H. Mei, *Polymers*, 2014, **6**, 1914-1928.
728. X. T. Zuo, W. X. Shi, S. L. Yu and J. J. He, *Water Sci. Technol.*, 2012, **66**, 2343-2348.
729. E. A. Feijani, A. Tavasoli and H. Mahdavi, *Ind. Eng. Chem. Res.*, 2015, **54**, 12124-12134.
730. I. C. Kim and K. H. Lee, *J. Appl. Polym. Sci.*, 2003, **89**, 2562-2566.
731. B. Hu, L. Y. Miao, Y. X. Zhao and C. L. Lu, *J. Membr. Sci.*, 2017, **530**, 84-94.
732. S. Kheirieh, M. Asghari and M. Afsari, *Rev Chem Eng*, 2018, **34**, 657-693.
733. Y. F. Zhao, L. P. Zhu, Z. Yi, B. K. Zhu and Y. Y. Xu, *J. Membr. Sci.*, 2013, **440**, 40-47.
734. S. K. Bowry, *Int. J. Artif. Organs*, 2002, **25**, 447-460.
735. D. D. Fazullin and G. V. Mavrin, *Chem. Pet. Eng.*, 2019, **55**, 649-656.
736. H. Y. Kim, Y. Cho and S. W. Kang, *J. Ind. Eng. Chem*, 2019, **78**, 421-424.
737. L. P. Pena, M. Betancourt, J. Herrera and E. Nicolau, *Abstr. Pap. Am. Chem. Soc.*, 2019, **257**.

738. S. M. Ghaseminezhad, M. Barikani and M. Salehirad, *Composites, Part B*, 2019, **161**, 320-327.
739. M. Faria, C. Moreira, T. Eusebio, P. Brogueira and M. N. de Pinho, *Cellulose*, 2020, **27**, 3847-3869.
740. S. Senthilkumar, S. Rajesh, D. Mohan and P. Soundararajan, *Sep. Sci. Technol.*, 2013, **48**, 66-75.
741. C. M. Kee and A. Idris, *Sep. Purif. Technol.*, 2010, **75**, 102-113.
742. A. Khakpay, P. Scovazzo and S. Nouranian, *J. Membr. Sci.*, 2019, **589**, 117228-117264.
743. A. Y. Tremblay, A. Fouda, A. Lui, T. Matsuura and S. Sourirajan, *Can. J. Chem. Eng.*, 1988, **66**, 1027-1030.
744. B. S. Minhas, T. Matsuura and S. Sourirajan, *Ind. Eng. Chem. Res.*, 1987, **26**, 2344-2348.
745. S. A. F. Ali, L. A. William, S. M. Ebrahim and E. A. Fadl, *Cellulose*, 2020, **27**, 9545-9545.
746. I. Ali, M. A. Raza, R. Mehmood, A. Islam, A. Sabir, N. Gull, B. Haider, S. H. Park and R. U. Khan, *Int. J. Mol. Sci.*, 2020, **21**, 7338-7351.
747. G. F. Zhao, T. Ishizaka, H. Kasai, H. Oikawa and H. Nakanishi, *Chem. Mater.*, 2007, **19**, 1901-1905.
748. M. Kim, G. Kim, J. Kim, D. Lee, S. Lee, J. Kwon and H. Han, *Microporous and Mesoporous Mater.*, 2017, **242**, 166-172.
749. S. Neyertz and D. Brown, *J. Membr. Sci.*, 2020, **614**, 118478-118532.
750. C. Y. Yang, W. X. Xu, Y. Nan and Y. G. Wang, *J. Membr. Sci.*, 2020, **616**, 118603-118610.
751. S. Zhao, W. T. Yan, M. Q. Shi, Z. Wang, J. X. Wang and S. C. Wang, *J. Membr. Sci.*, 2015, **478**, 105-116.
752. S. Alibakhshi, M. Youssefi, S. S. Hosseini and A. Zadhoush, *Mater. Res. Express*, 2019, **6**, 125326-125340.
753. K. Yoon, B. S. Hsiao and B. Chu, *Polymer*, 2009, **50**, 2893-2899.
754. I. Sadeghi, A. Aroujalian, A. Raisi, B. Dabir and M. Fathizadeh, *J. Membr. Sci.*, 2013, **430**, 24-36.
755. G. Arthanareeswaran and V. M. Starov, *Desalination*, 2011, **267**, 57-63.
756. M. A. Rasool and I. F. J. Vankelecom, *Green Chem.*, 2019, **21**, 1054-1064.
757. A. Hofmann, E. Thissen, M. Migeot, N. Bohn, S. Dietrich and T. Hanemann, *Polymers*, 2017, **9**, 489-500.
758. A. Pagidi, R. Saranya, G. Arthanareeswaran, A. F. Ismail and T. Matsuura, *Desalination*, 2014, **344**, 280-288.
759. Y. A. Kim, H. Muramatsu, T. Hayashi, M. Endo, M. Terrones and M. S. Dresselhaus, *Chem. Vapor Depos.*, 2006, **12**, 327-330.

760. M. Endo, H. Muramatsu, T. Hayashi, Y. A. Kim, M. Terrones and N. S. Dresselhaus, *Nature*, 2005, **433**, 476-476.
761. S. Majeed, D. Fierro, K. Buhr, J. Wind, B. Du, A. Boschetti-De-Fierro and V. Abetz, *J. Membr. Sci.*, 2012, **403**, 101-109.
762. J. Park, W. Choi, J. Cho, B. H. Chun, S. H. Kim, K. B. Lee and J. Bang, *Desalin. Water Treat.*, 2010, **15**, 76-83.
763. I. T. Meireles, R. M. Huertas, C. A. V. Torres, I. M. Coelho and J. G. Crespo, *Carbohydr. Polym.*, 2018, **191**, 216-224.
764. S. Spirk, G. Findenig, A. Doliska, V. E. Reichel, N. L. Swanson, R. Kargl, V. Ribitsch and K. Stana-Kleinschek, *Carbohydr. Polym.*, 2013, **93**, 285-290.
765. P. Kanti, K. Srigowri, J. Madhuri, B. Smitha and S. Sridhar, *Sep. Purif. Technol.*, 2004, **40**, 259-266.
766. S. D. Bhat and T. M. Aminabhavi, *Sep. Purif. Rev.*, 2007, **36**, 203-229.
767. B. V. K. Naidu, K. Rao and T. M. Aminabhavi, *J. Membr. Sci.*, 2005, **260**, 131-141.
768. X. L. Chen, X. L. Gao, W. W. Wang, D. Wang and C. J. Gao, *Desalin. Water Treat.*, 2010, **18**, 198-205.
769. K. Kurita, M. Hirakawa, S. Kikuchi, H. Yamanaka and J. Yang, *Carbohydr. Polym.*, 2004, **56**, 333-337.
770. J. Miao, L. C. Zhang and H. C. Lin, *Chemical Engineering Science*, 2013, **87**, 152-159.
771. K. R. Holme and A. S. Perlin, *Carbohydr. Polym.*, 1997, **302**, 7-12.
772. A. Domard, M. Rinaudo and C. Terrassin, *Int. J. Biol. Macromol.*, 1986, **8**, 105-107.
773. T. Tanigawa, Y. Tanaka, H. Sashiwa, H. Saimoto and Y. Shigemasa, *Adv. Chitin Chitosan*, 1992, 206-215.
774. D. K. Kweon, S. B. Song and Y. Y. Park, *Biomaterials*, 2003, **24**, 1595-1601.
775. Y. Manawi, V. Kochkodan, A. F. Ismail, A. W. Mohammad and M. A. Atieh, *Membranes*, 2019, **9**, 30-46.
776. H. Elomari, B. Achiou, A. Karim, M. Ouammou, A. Albizane, J. Bennazha, S. A. Younssi and I. Elamrani, *J. Asian Ceram. Soc.*, 2017, **5**, 313-319.
777. G. C. C. Yang and C. M. Tsai, *Desalination*, 2008, **233**, 129-136.
778. F. A. Almeida, E. C. Botelho, F. C. L. Melo, T. M. B. Campos and G. P. Thim, *J. Eur. Ceram. Soc.*, 2009, **29**, 1587-1594.
779. R. D. Sahnoun and S. Baklouti, *Appl. Clay Sci.*, 2013, **83**, 399-404.
780. M. H. Talou and M. A. Camerucci, *J. Eur. Ceram. Soc.*, 2015, **35**, 1021-1030.
781. O. Lyckfeldt and J. M. F. Ferreira, *J. Eur. Ceram. Soc.*, 1998, **18**, 131-140.
782. R. Barea, M. I. Osendi, P. Miranzo and J. M. F. Ferreira, *J. Am. Ceram. Soc.*, 2005, **88**, 777-779.



783. B. Jafari, M. Abbasi and S. A. Hashemifard, *J. Cleaner Prod.*, 2020, **244**, 118720-118734.
784. A. Sakoda, T. Nomura and M. Suzuki, *Adsorption*, 1996, **3**, 93-98.
785. S. Wang, C. Ma, C. Pang, Z. H. Hu and W. Wang, *Environ. Sci. Pollut. Res.*, 2019, **26**, 34167-34176.
786. X. Y. Zhao, C. Huang, S. Zhang and C. Y. Wang, *J. Macromol. Sci., Part B: Phys.*, 2019, **58**, 909-920.
787. P. Ramadoss, T. Regi, M. I. Rahman and D. Arivuoli, *J. Appl. Polym. Sci.*, 2019, **137**, 48746-48756.
788. J. Lewis, M. A. Q. Al-sayaghi, C. Buelke and A. Alshami, *Sep. Purif. Rev.*, 2019, **50**, 1-31.
789. R. J. White, V. Budarin, R. Luque, J. H. Clark and D. J. Macquarrie, *Chem. Soc. Rev.*, 2009, **38**, 3401-3418.
790. G. Dura, V. L. Budarin, J. A. Castro-Osma, P. S. Shuttleworth, S. C. Z. Quek, J. H. Clark and M. North, *Angew. Chem., Int. Ed.*, 2016, **55**, 9173-9177.
791. P. S. Shuttleworth, J. Parker, V. L. Budarin, S. W. Breeden, D. J. Macquarrie, R. L. Luque, R. White and J. H. Clark, *Clean Technology 2011: Bioenergy, Renewables, Storage, Grid, Waste and Sustainability*, 2011, 267-270.
792. H. D. Wagner, O. Lourie, Y. Feldman and R. Tenne, *Appl. Phys. Lett.*, 1998, **72**, 188-190.
793. O. Lourie, D. M. Cox and H. D. Wagner, *Phys. Rev. Lett.*, 1998, **81**, 1638-1641.
794. K. Qi and R. Huang, *Int. J. Polym. Mater.*, 1995, **29**, 157-164.
795. S. P. Li, G. Zhao and H. Y. Chen, *J. Dispersion Sci. Technol.*, 2005, **26**, 415-419.
796. L. F. Padilha and C. P. Borges, *Braz. J. Chem. Eng.*, 2019, **36**, 497-509.
797. S. Mazinani, S. Darvishmanesh, M. Ehsanzadeh and B. Van der Bruggen, *J. Membr. Sci.*, 2017, **526**, 301-314.
798. S. Y. P.J. Brown, J. Yang, *Autex Res. J.*, 2002, **2**, 101-108.
799. L. P. Cheng, T. H. Young, W. Y. Chuang, L. Y. Chen and L. W. Chen, *Polymer*, 2001, **42**, 443-451.
800. E. Elele, Y. Shen, J. Tang, Q. Lei, B. Khusid, G. Tkacik and C. Carbrello, *J. Membr. Sci.*, 2019, **591**, 117351-117380.
801. T. H. Muster and C. A. Prestidge, *Int. J. Pharm.*, 2002, **234**, 43-54.
802. F. Machui, S. Langner, X. D. Zhu, S. Abbott and C. J. Brabec, *Sol. Energy Mater. Sol. Cells*, 2012, **100**, 138-146.
803. L. Moity, M. Durand, A. Benazzouz, C. Pierlot, V. Molinier and J. M. Aubry, *Green Chem.*, 2012, **14**, 1132-1145.
804. P. G. Jessop, D. A. Jessop, D. B. Fu and L. Phan, *Green Chem.*, 2012, **14**, 1245-1259.
805. InKemiagreenchemicals.com. Available at: <https://www.inkemia.com/en/>. Accessed 09.08.2018.

806. M. M. Tian, S. S. Yuan, F. Decaesstecker, J. Y. Zhu, A. Voiodine and B. Van der Bruggen, *Desalination*, 2020, **477**, 114265-114272.
807. X. F. Li, Y. G. Wang, X. L. Lu and C. F. Xiao, *J. Membr. Sci.*, 2008, **320**, 477-482.
808. D. J. Lin, K. Beltsios, C. L. Chang and L. P. Cheng, *J. Polym. Sci., Part B: Polym. Phys.*, 2003, **41**, 1578-1588.
809. D. J. Lin, K. Beltsios, T. H. Young, Y. S. Jeng and L. P. Cheng, *J. Membr. Sci.*, 2006, **274**, 64-72.
810. P. Sukitpaneenit and T. S. Chung, *J. Membr. Sci.*, 2009, **340**, 192-205.
811. Y. X. Xu, C. X. Chen, P. X. Zhang, B. H. Sun and J. D. Li, *J. Chem. Eng. Data*, 2006, **51**, 1841-1845.
812. Bi-component PTFE membranes. Available at: <http://www.porellemembranes.co.uk/en/membranes/ptfe-membranes/>. Accessed 08.12.2020.
813. M. Peydayesh, M. Bagheri, T. Mohammadi and O. Bakhtiari, *RSC Adv.*, 2017, **7**, 24995-25008.
814. J. H. Hildebrand and R. L. Scott, *Annu. Rev. Phys. Chem.*, 1950, **1**, 75-92.